Publication Date (Web): June 18, 2015 | doi: 10.1021/bk-2015-1192.fw001

Green Polymer Chemistry: Biobased Materials and Biocatalysis

In Green Polymer Chemistry: Biobased Materials and Biocatalysis; Smith, et al.;
ACS Symposium Series; American Chemical Society: Washington, DC, 2015.

Publication Date (Web): June 18, 2015 | doi: 10.1021/bk-2015-1192.fw001

Publication Date (Web): June 18, 2015 | doi: 10.1021/bk-2015-1192.fw001

ACS SYMPOSIUM SERIES **1192**

Green Polymer Chemistry: Biobased Materials and Biocatalysis

H. N. Cheng, Editor
Southern Regional Research Center
Agricultural Research Service
U.S. Department of Agriculture
New Orleans, Lousiana

Richard A. Gross, Editor
Rensselaer Polytechnic Institute
Troy, New York

Patrick B. Smith, Editor
Michigan Molecular Institute
Midland, Michigan

Sponsored by the
ACS Division of Polymer Chemistry, Inc.

American Chemical Society, Washington, DC

Distributed in print by Oxford University Press

Library of Congress Cataloging-in-Publication Data

Green polymer chemistry : biobased materials and biocatalysis / H.N. Cheng, editor, Southern Regional Research Center, Agricultural Research Service, U.S. Department of Agriculture, New Orleans, Louisiana, Richard A. Gross, editor, Rensselaer Polytechnic Institute, Troy, New York, Patrick B. Smith, editor, Michigan Molecular Institute, Midland, Michigan ; sponsored by the ACS Division of Polymer Chemistry, Inc.
pages cm1. -- (ACS symposium series ; 1192)
Includes bibliographical references and index.
ISBN 978-0-8412-3065-1 -- ISBN 978-0-8412-3066-8 1. Polymers. 2. Polymerization. 3. Green chemistry. I. Cheng, H. N., editor. II. Gross, Richard A., 1957- editor. III. Smith, Patrick B. (Materials scientist), editor. IV. American Chemical Society. Division of Polymer Chemistry.
QD381.G726 2015
547′.28--dc23

2015022683

The paper used in this publication meets the minimum requirements of American National Standard for Information Sciences—Permanence of Paper for Printed Library Materials, ANSI Z39.48n1984.

Distributed in print by Oxford University Press

PRINTED IN THE UNITED STATES OF AMERICA

Publication Date (Web): June 18, 2015 | doi: 10.1021/bk-2015-1192.fw001

Foreword

The ACS Symposium Series was first published in 1974 to provide a mechanism for publishing symposia quickly in book form. The purpose of the series is to publish timely, comprehensive books developed from the ACS sponsored symposia based on current scientific research. Occasionally, books are developed from symposia sponsored by other organizations when the topic is of keen interest to the chemistry audience.

Before agreeing to publish a book, the proposed table of contents is reviewed for appropriate and comprehensive coverage and for interest to the audience. Some papers may be excluded to better focus the book; others may be added to provide comprehensiveness. When appropriate, overview or introductory chapters are added. Drafts of chapters are peer-reviewed prior to final acceptance or rejection, and manuscripts are prepared in camera-ready format.

As a rule, only original research papers and original review papers are included in the volumes. Verbatim reproductions of previous published papers are not accepted.

ACS Books Department

Publication Date (Web): June 18, 2015 | doi: 10.1021/bk-2015-1192.fw001

Publication Date (Web): June 18, 2015 | doi: 10.1021/bk-2015-1192.pr001

Preface

Green chemistry is the design of chemical products and processes that reduce or eliminate the use or generation of hazardous substances. Green polymer chemistry is an extension of green chemistry to polymer science and engineering. Developments in this area have been stimulated by health and environmental concerns, interest in sustainability, desire to decrease the dependence on petroleum, and opportunities to design and produce "green" products and processes. It has become an active and viable field in its own right and continues to attract attention from researchers and manufacturers.

A current feature of green polymer chemistry is that it is both global and multidisciplinary. Thus, publications in this field are spread out over different journals in different countries. Moreover, a successful research effort may involve collaborations of people in various disciplines, such as organic chemistry, polymer chemistry, material science, chemical engineering, biochemistry, molecular biology, microbiology, enzymology, toxicology, environmental science, and analytical chemistry. It is important for workers in this field to communicate and share information through meetings, symposia, and books.

In view of the trends and the advances in this field, we organized an international symposium on "Green Polymer Chemistry: Biobased Materials and Biocatalysis" at the American Chemical Society (ACS) National Meeting in San Francisco, California, in August 2014. The symposium was very successful, with a total of 77 presentations and 23 posters. Most of the leading researchers in this field attended the symposium. Many exciting findings and techniques were reported in numerous areas, including new uses of biobased feedstock, green reactions, green processing methodologies, and green polymeric products.

In view of the success of the San Francisco symposium, we asked many of the symposium participants to contribute chapters to this book, where they either reported original results or wrote special reviews of their ongoing work. Because this field covers many disciplines, we believe there is value in having a book that pulls together all relevant topics in one place. Whereas almost all aspects of green polymer chemistry are included in this book, a particular emphasis has been placed on biobased materials and biocatalysis. We hope this book provides a good representation of what is happening in the forefront of research in green polymer chemistry.

This book is targeted for scientists, engineers, and students, who are involved or interested in green polymer chemistry. These may include chemists, biochemists, material scientists, chemical engineers, microbiologists, molecular biologists, enzymologists, toxicologists, environmental scientists, and analytical chemists. It can be a textbook for a course on green chemistry and also a reference

In Green Polymer Chemistry: Biobased Materials and Biocatalysis; Smith, et al.;
ACS Symposium Series; American Chemical Society: Washington, DC, 2015.

book for people who need information on specific topics involving biocatalysis and biobased materials.

We thank the authors for preparing their manuscripts and the reviewers for their patience during the peer review process. Assistance from the ACS Books staff (particularly Caitlyn Matuska, Tim Marley, Arlene Furman, and Bob Hauserman) is gratefully acknowledged. Thanks are also due to the ACS Division of Polymer Chemistry, Inc., for sponsoring the 2014 symposium.

H. N. Cheng
Southern Regional Research Center
USDA – Agricultural Research Service
1100 Robert E. Lee Blvd.
New Orleans, Louisiana 70124

Richard A. Gross
Department of Chemistry and Chemical Biology
Rensselaer Polytechnic Institute
110 8th Street
Troy, New York 12180

Patrick B. Smith
Michigan Molecular Institute
1910 West St Andrews Road
Midland, Michigan 48640

Publication Date (Web): June 18, 2015 | doi: 10.1021/bk-2015-1192.pr001

Editors' Biographies

H. N. Cheng

H. N. Cheng (Ph.D., University of Illinois) is currently a research chemist at the Southern Regional Research Center of the U.S. Department of Agriculture in New Orleans, where he works on projects involving improved utilization of commodity agricultural materials, green chemistry, and polymer reactions. Prior to 2009, he worked for Hercules Incorporated where he was involved at various times with new product development, team and project leadership, new business evaluation, pioneering research, and supervision of analytical research. Over the years, his research interests have included green polymer chemistry, biocatalysis and enzymatic reactions, pulp and paper chemistry, functional foods, polymer characterization, and NMR spectroscopy. He is an ACS Fellow and a POLY Fellow and has authored or co-authored 192 papers, 25 patent publications, co-edited 11 books, and organized or co-organized 25 symposia at national ACS meetings since 2003.

Richard A. Gross

Richard A. Gross (Ph.D., Polytechnic University) holds the Constellation Chaired Professorship at Rensselaer Polytechnic Institute (RPI) and is also a member of RPI's Departments of Chemistry and Biology as well as Biomedical Engineering. Previously, he was on the faculty of University of Massachusetts (Lowell) (1988−1998) and occupied the Herman F. Mark Chair Professorship at Polytechnic University (1998–2013). His research is focused on developing biocatalytic routes to biobased materials, combining chemical methods with cell-free and whole-cell biocatalytic systems to produce a large number of new biobased materials. He has over 400 publications in peer-reviewed journals with approximately 7,000 citations, has edited six books, and has been granted or filed 26 patents. He has received numerous awards, including the Presidential Green Chemistry Award in the academic category (2003) and induction into the American Institute for Medical and Biological Engineering (2007), and is Turner Alfrey Visiting Professor (2010), and a POLY Fellow (2015). He founded SyntheZyme, LLC, (where he serves as Chief Technology Officer) in 2009 to commercialize technologies developed in his laboratory.

Publication Date (Web): June 18, 2015 | doi: 10.1021/bk-2015-1192.ot001

In Green Polymer Chemistry: Biobased Materials and Biocatalysis; Smith, et al.;
ACS Symposium Series; American Chemical Society: Washington, DC, 2015.

Patrick B. Smith

Patrick B. Smith (Ph.D, Michigan State University) currently serves as a research scientist at Michigan Molecular Institute. He had a productive and distinguished career at The Dow Chemical Company, rising to the rank of Fellow prior to his retirement in 2007. During his time at Dow, he served with Cargill Dow Polymers, which launched the Ingeo™ line of poly(lactic acid) products. He consulted for Archer Daniels Midland (ADM) between 2007 and 2010 as their R&D leader for the Telles joint venture that commercialized poly(hydroxyalkanoates) and on ADM's biobased propylene glycol effort. He was elected as an ACS Fellow in 2013. He has co-authored nearly 500 Dow technical reports, over 75 publications, and has been granted two patents.

Publication Date (Web): June 18, 2015 | doi: 10.1021/bk-2015-1192.ot001

Publication Date (Web): June 18, 2015 | doi: 10.1021/bk-2015-1192.ch001

Chapter 1

Green Polymer Chemistry: Some Recent Developments and Examples

H. N. Cheng,[1] Richard A. Gross,[2] and Patrick B. Smith[3]

[1]Southern Regional Research Center, USDA/Agriculture Research Service, 1100 Robert E. Lee Boulevard, New Orleans, Louisiana 70124
[2]Department of Chemistry and Chemical Biology, Rensselaer Polytechnic Institute, 110 8th Street, Troy, New York 12180-3590
[3]Michigan Molecular Institute, 1910 West Street Andrews Road, Midland, Michigan 48640
***E-mail: hn.cheng@ars.usda.gov.**

Green polymer chemistry continues to be a popular field, with many books and publications in print. Research is being conducted in several areas within this field, including: 1) green catalysis, 2) diverse feedstock base, 3) degradable polymers and waste minimization, 4) recycling of polymer products and catalysts, 5) energy generation or minimization during use, 6) optimal molecular design and activity, 7) benign solvents, and 8) improved syntheses or processes in order to achieve atom economy, reaction efficiency, and reduced toxicity. Advances have been made in many areas, including new uses of biobased feedstock, green reactions, green processing methodologies, and green products. A selected review is made in this article, focusing particularly on biobased materials and biocatalysis. Some recent developments and examples are provided, taken particularly from the presentations made at the American Chemical Society (ACS) national meeting in San Francisco in August 2014 and the articles included in this symposium volume.

In Green Polymer Chemistry: Biobased Materials and Biocatalysis; Smith, et al.;
ACS Symposium Series; American Chemical Society: Washington, DC, 2015.

Publication Date (Web): June 18, 2015 | doi: 10.1021/bk-2015-1192.ch001

Introduction

Green Chemistry is the design of chemical products and processes that reduce or eliminate the use or generation of hazardous substances (*1*, *2*). Green polymer chemistry is an extension of green chemistry to polymer science and engineering. It has become an active and viable field in its own right and continues to be popular with many polymer scientists, with several books and review articles already published in this field (*3–11*). For convenience, we have previously (*8*) grouped the developments in green polymer chemistry in eight categories (Table 1). These categories also seem to be consistent with the themes discussed in earlier articles and books in this field (*1–11*).

Table 1. Major Categories for Green Polymer Chemistry, Adapted from Reference (*12*)

Major Pathways	*Examples*
Green catalysts	Biocatalysts, such as enzymes and whole cells
Diverse feedstock base	Biobased building blocks and agricultural feedstock (sugars, peptides, triglycerides, lignin, ferulic acid). Natural fillers in composites. CO_2 as monomer.
Degradable polymers and waste minimization	Agri-based renewable materials. Some polyesters and polyamides.
Recycling of polymer products and catalysts	Many degradable polymers can potentially be recycled. Immobilized enzymes may be reused.
Energy generation or minimization of use	Biofuels. Energy-saving processes (e.g., reactive extrusion, jet cooking, microwave).
Optimal molecular design and activity	Polymers with designed structures or functions. Improved biocatalysts. Protein synthesis. Genetic/metabolic engineering.
Benign solvents	Water, ionic liquids, or reactions without solvents
Improved syntheses and processes	Atom economy, reaction efficiency, decreased byproducts, toxicity reduction.

The present article provides a selective review of this field, focusing particularly on biobased materials and biocatalysis. Biocatalysis usually involves enzymes, micro-organisms, and even higher organisms to catalyze or promote reactions. Most biocatalytic reactions are done in water or in the absence of a solvent, involving lower temperatures (60ºC or lower), with the generation of reduced byproducts. Thus, biocatalysis represents an exemplary green method to carry out polymerization and polymer reactions. This is an area of active research, and several reviews (*12–15*) and books (*16–19*) are available.

In Green Polymer Chemistry: Biobased Materials and Biocatalysis; Smith, et al.;
ACS Symposium Series; American Chemical Society: Washington, DC, 2015.

Biobased materials entail the use of natural or agri-based building blocks and polymers, and derivatives of these materials. There are also many reviews (*20–25*) and books (*26–30*) on this topic. The popularity of these materials is reinforced by several factors including: 1) decreased dependence on petroleum as raw material; 2) relative price stability of agri-based products in comparison to petrochemical-based polymers; 3) sustainability, biodegradability, and environmental benefits of bio-based materials; 4) increased economic opportunities for farmers and rural communities through value-added products from agricultural commodities (*31*).

Some recent developments and examples are provided below (*32–58*), taken primarily from the presentations made at the ACS national meeting in San Francisco in August 2014 and the articles included in this symposium volume.

Publication Date (Web): June 18, 2015 | doi: 10.1021/bk-2015-1192.ch001

Recent Developments and Examples

Biocatalysis and Chemo-enzymatic Approaches

An example of biocatalysis in this book is given by Puskas et al (*32*), who carried out the synthesis of symmetric and asymmetric telechelic polymers using *Candida antarctica* lipase B. Quantitative functionalization of polyisobutylenes, polysiloxane, and poly(ethylene glycol)s (PEGs) was achieved. Controlled polycondensation of tetra(ethylene glycol) and divinyl benzene yielded symmetric and asymmetric telechelic PEGs with high efficiency.

Barrera-Rivera et al (*33*) synthesized oligomeric polycaprolactone diol (DEG1) using immobilized *Yarrowia lipolytica* lipase (YLL) and diethylene glycol as initiator. A series of linear polyester-urethanes were then prepared chemically from DEG1, a diisocyanate and an amino acid. The resulting products were found to have rather different thermal, mechanical, solubility and hydrolytic behavior.

Pion et al (*34*) utilized a chemo-enzymatic method to synthesize ferulic acid derivatives. These materials then became new platforms used as A_2-type monomers for the preparation of renewable aliphatic-aromatic copolyesters and poly(ester-urethane)s, and as precursors for the synthesis of α,ω-dienes monomers leading to poly(ester-alkenamer)s.

Maloney et al (*35*) provided an overview of the state-of-the-art technologies currently used for wastewater treatment and proposed developing novel solutions using enzymes and enzyme-based conjugates to remediate active chemicals and their metabolic products by ensuring water reusability.

Kodokawa (*36*) carried out enzymatic synthesis of non-natural oligo- and polysaccharides by phosphorylase-catalyzed glycosylations using substrates that were analogous to natural ones as glycosyl donor. Thus, they employed potato phosphorylase-catalyzed xylosylation, (N-formyl)glucosaminylation, and mannosylation of maltooligosaccharides with α-D-xylose, (N formyl)-α-D-glucosamine, and α-D-mannose 1-phosphates to obtain nonnatural oligosaccharides. Through the use of phosphorylase from other organisms, additional new structures were obtained.

In Green Polymer Chemistry: Biobased Materials and Biocatalysis; Smith, et al.;
ACS Symposium Series; American Chemical Society: Washington, DC, 2015.

Cote and Skory (*37*) studied the factors affecting the structures and yields of insoluble glucans produced from sucrose by lactic acid bacteria. These authors showed that the addition of soluble dextran or an enzyme that produced a soluble dextran to the reaction increased the yield of insoluble glucan. However, the insoluble glucan product contained a lower proportion of α(1→3) linkages. They also showed that the yield was drastically affected by substrate and enzyme concentrations.

Nduko et al (*38*) reviewed the production of lactic acid (LA)-based polymers via a one-step metal-free system, using a lactate-polymerizing enzyme. Included in their chapter were the production of LA-enriched and PLA-like polymers in bacteria from glucose and xylose, metabolic/genetic engineering for polymer yield enhancement, and studies of the properties and the biodegradability of the LA-based polymers.

Publication Date (Web): June 18, 2015 | doi: 10.1021/bk-2015-1192.ch001

Other Catalysts and Functional Peptides

Romain and Williams (*39*) reported that a single catalyst might be applied for both ring-opening polymerization (ROP) and ring-opening copolymerization (ROCOP) of oxygenated cyclic monomers via a "one-pot" procedure that resulted in various copolymers. They also uncovered a novel chemoselective catalyst control pathway, whereby the nature of the metal chain-end group controlled the polymerization cycle and thereby the composition of the copolymer.

MacDonald and Shaver (*40*) used specially designed aluminum complexes as catalysts for the synthesis of highly isotactic or heterotactic poly(lactic acid), β-lactone, δ-valerolactone, lactide, ε-caprolactones and macrolactones, with a significant level of control over molecular weight and dispersity. Macrostructures synthesized included random copolymers, AB diblock and ABA triblock copolymers and polymer stars.

Tada et al (*41*) employed molecular evolutionary engineering to evolve aptamers through the development of *in vitro* selection. In particular, they synthesized new aptamers selected from libraries containing unnatural components to generate new, artificial aptamer functions.

Biobased Materials from Triglyceride Feedstock

Hernandez et al (*42*) discovered that under certain reaction conditions controlled radical polymerization, such as RAFT (reversible addition−fragmentation chain-transfer polymerization) could limit the number of initiation sites and drastically reduce the rate of chain transfers and termination reactions. This discovery facilitated the synthesis of customized chain architectures such as block copolymers from vegetable oils. Through this method, they produced poly(styrene-b-AESO-b-styrene) triblock copolymers with properties similar to petroleum based thermoplastic elastomers.

In their chapter Havelka and Gerhardt (*43*) reviewed Elevance's approach to use cross-metathesis reactions between plant oils and olefins to generate new families of specialty monomers. Two examples are functionalized poly-α-olefin

(used in synthetic lubricants) and octadecanedioic acid (which shows improved chemical resistance versus shorter chain alternatives).

Hong et al (*44*) polymerized epoxidized corn oil with BF_3-etherate and hydrolyzed the product to form a polyacid with an acid value of 158 mg KOH/g. The hydrolyzed products were then used as curing agents for epoxy resins.

Cheng and Biswas (*45*) provided an overview of the various structural modifications made on plant oils in their laboratories The reactions included Diels-Alder, ene reaction, transesterification, acid or enzymatic hydrolysis, heat-bodying reaction, hydrogenation, epoxidation, formation of acetonide, aminohydrin and azidohydrin, click reaction, and polymerization.

Mannari et al (*46*) developed soybean oil-based building blocks and demonstrated their suitability as alternative raw materials in advanced UV-curing coating compositions. An example was a hyper-branched soy urethane acrylate (HSPU), used as the primary component of a UV-curable composition. Another example was a group of soy-based, low-viscosity, and high-functionality acrylate monomers that were designed and utilized as reactive diluent in UV-cure formulations.

Kim et al (*47*) made solid lipid nanoparticles (SLN), which were biocolloidal dispersions that could be loaded with hydrophilic or hydrophobic ingredients, such as drug molecules or lipase enzyme. An example was the meso-macroporous material made from SLN dispersions through a dual templating mechanism combining self-assembling of micelles and imprinting of soft nanoparticles.

Publication Date (Web): June 18, 2015 | doi: 10.1021/bk-2015-1192.ch001

Biobased Materials from Carbohydrate Feedstock

Lo Re at al (*48*) carried out metal-free synthesis of enantiomeric PLA/clay nanohybrids through in-situ intercalative ring-opening polymerization (ROP) of lactide. They employed different techniques to quench the polymerization reaction in order to overcome extensive degradation on further melt-processing. They also prepared stereocomplexed polylactide/nanoclays bionanocomposites and studied their thermal properties.

In their article, Luebben and Raebiger (*49*) presented the first reported synthesis of poly(2,5-dihydroxy-1,4-dioxane), a novel renewable thermoplastic polyacetal prepared by polymerization of glycolaldehyde dimer, 2,5-dihydroxy-1,4-dioxane via a catalytic process. The monomer can be obtained in high purity and large quantities from the fast pyrolysis of lignocellulosic feedstock at a reasonable cost.

Toyama et al (*50*) synthesized a high-strength and heat-resistant novel bioplastic by derivatizing cellulose with acetic and a long chain acid (3-pentadecylphenoxy acetic acid (a derivative of cardanol, from cashew nut shell) through an efficient process. The properties of the bioplastic were further improved by adding poly(butylene succinate adipate) and glass fiber.

Organophosphorus compounds can serve as replacements for organo-halogen flame retardants. Howell and Daniel (*51*) synthesized a series of phosphorus-containing compounds derived from esters of isosorbide (from starch) and 10-undecenoic acid (from castor oil). Several of these compounds displayed good

flame-retarding behavior when incorporated into a cured DGEBA (diglycidyl ether of bisphenol A) epoxy resin at levels sufficient to introduce 1-2% phosphorus.

Materials from Other Biobased Resources

Maiorana et al (*52*) synthesized bio-based epoxy monomers from diphenolic acid (DPA) with the goal of producing a drop-in replacement for the diglycidyl ether of bisphenol A (DGEBA). A series of resins was prepared from alkyl DPA esters and cured under identical conditions using the same crosslinker. The properties were tested; the thermal behavior was found to be tunable through the length of the ester chain.

Hu et al (*53*) developed furan-based structures as a potential replacement for phenyl building blocks in epoxy systems. In a comparison of epoxy-amine cure kinetics of furanyl and phenyl building blocks, they suggested that hydrogen bonding on the furanyl ring potentially affected reactivity and reactivity ratios, thus impacting processing characteristics, thermal, and mechanical properties of furan-based epoxy systems relative to phenyl analogues. Nguyen et al (*54*) made a number of polyesters from bio-aromatics such as acetylferulic and acetyldihydroxyferulic acid. The copolymers from these monomers can have tunable thermal and physical properties and may possibly be sustainable replacements for a variety of non-renewable and non-degradable commodity plastics. As noted above, Pion et al (A3) also made derivatives of ferulic acid, which were then used to make other products.

Li and Li (*55*) developed new pressure-sensitive adhesives (PSAs) from renewable dimer acid (DA) and epoxides. Upon evaluation, only the polymer from the DA and trimethylolpropane triglycidyl ether could serve as a PSA. Structural modifications improved the properties even further. The preparation of the new PSAs did not require any organic solvent or toxic chemicals.

Guenthner et al (*56*) synthesized a wide variety of cyanate ester monomers derived from renewable resources. In their chapter, they studied the structure-property relationships for monomer melting point, glass transition temperature at full conversion, and char yields at 600 °C under nitrogen and air. The quantitative correlations enabled the predictions of the properties of two as-yet unsynthesized monomers.

There is a significant market demand for bio-based PET due to the "Plant PET Technology Collaborative" made up of Coca Cola, Ford, Heinz, Nike and Procter & Gamble. This consortium and other retailers are assisting several pre-commercial enterprises to develop commercial processes for bio-based terephthalic acid. Smith (*57*) gave an up-to-date review of this development. Techno-economic evaluations have shown that some of the companies have achieved economics that are competitive with those of the petro-based material.

Schiraldi (*58*) provided a detailed review of aerogels. A wide range of sustainable, bio-based polymers can be converted essentially quantitatively into low density aerogels. The freeze drying process employed is somewhat energy intensive but generates no appreciable chemical waste. These aerogels exhibit useful mechanical properties, including low flammability and are promising targets for commercialization.

Publication Date (Web): June 18, 2015 | doi: 10.1021/bk-2015-1192.ch001

Pipeline to Green Polymers

Another way to approach green polymer chemistry is to conceive this field as a pipeline to green polymers. A schematic is shown in Figure 1.

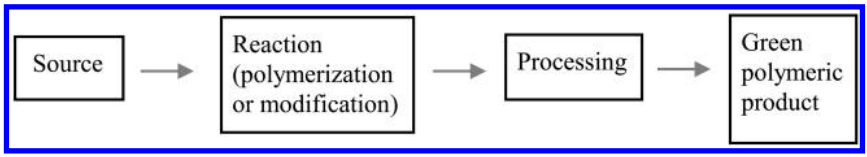

Figure 1. Schematic showing the pipeline to green polymeric products.

Publication Date (Web): June 18, 2015 | doi: 10.1021/bk-2015-1192.ch001

In Figure 1 the source can be a monomer or an agricultural raw material (e.g., cellulose, starch, and triglyceride). Polymerization can take place with or without catalyst and with or without a solvent. The catalyst may be acid/base, metal-containing, organic, or biocatalysts. The solvent may be aqueous, organic, supercritical CO_2, perfluorinated medium, ionic liquid, or simply absent. Processing may involve extraction, separation, purification, waste removal, and many other operations. In processing, yield, efficiency, environmental compliance and energy utilization are some of the key considerations. Finally, product development may comprise many activities such as compounding, formulation, stabilization, packaging, and evaluations.

Biobased Feedstock

The biobased feedstock may include monomers and other building blocks, and agricultural raw materials. Examples of biobased monomers include terephthalic acid as discussed by Smith (*57*) and a family of monomers from the cross-metathesis reaction between plant oils and olefins as discussed by Havelka and Gerhardt (*43*).

Many polymeric products are made from biobased starting materials. In this book, triglycerides were used as raw materials by Hernandez et al (*42*), Havelka and Gerhardt (*43*), Hong et al (*44*), Cheng and Biswas (*45*), Mannari et al (*46*), and Kim et al (*47*). Dimer acids were formulated into pressure sensitive adhesives by Li and Li (*55*).

Carbohydrate feedstock was engaged for the production of PLA (*38–40*, *48*), poly(2,5-dihydro-1,4-dioxane) (*49*), modified cellulose (*50*), and phosphorus –containing isosorbide esters (*51*).

Levulinic acid can be derived from cellulose. Condensation of levulinic acid with two equivalents of phenol yields diphenolic acid, which can possibly replace bisphenol A diglycidyl ether (*52*). Furanyl chemicals can also be produced from cellulose and hemicellulose, and they were used as building block in epoxy systems (*53*).

In Green Polymer Chemistry: Biobased Materials and Biocatalysis; Smith, et al.;
ACS Symposium Series; American Chemical Society: Washington, DC, 2015.

Ferulic acid, an abundant material found in plant cell wall components, is often utilized in the synthesis of other aromatic compounds. For example, it was employed as the starting material by Pion et al (*34*) and Nguyen et al (*54*). A large number of polycyanurates from phenolic structures from renewable resources were studied in the chapter by Guenthner et al (*56*).

Green Reactions

Under this category can be included conventional and bio-catalysis, green or solvent-free media, and other highly efficient reactions. As noted earlier, biocatalysis is a good illustration of green reactions. In this book, Puskas et al (*32*) and Barrera-Rivera et al (*33*) used lipases, Kadokawa (*36*) phosphorylase, Cote and Skory (*37*) glucansucrase, and Nduko et al (*38*) lactate polymerizing enzyme for various polymerization and modification reactions. For wastewater treatment, the chapter by Maloney et al (*35*) used oxidase and peroxidase.

The application of non-biocatalytic catalysts was discussed in several chapters, e.g., Romain and Williams (*39*), MacDonald and Shaver (*40*), Hernandez et al (*42*), Havelka and Gerhardt (*43*), Hong et al (*44*), Cheng and Biswas (*45*), Lo Re et al (*48*), and others.

The synthesis of proteins through "evolutionary molecular engineering" can also be considered a green reaction. Tada et al (*41*) demonstrating the ability to produce functional proteins using such *in vitro* selection methods.

Green Processing

Because of environmental and energy considerations, industry is paying increased attention to improved processes that aim to minimize energy and chemical waste, to increase yield, and to decrease safety and toxicity hazards. As such, improved reaction planning and process design can facilitate greener processing and reduce logistical problems. In this regard, the use of agriculturally based starting materials, e.g., carbohydrates, triglycerides, lignin and other natural phenolics, has the inherent advantage of reduced toxicity and safer handling of reactants and products.

Three papers in this book may be highlighted in this regard. The paper by Toyama et al (*50*) to synthesize a novel cellulosic derivative is a good example of process studies designed to decrease solvent and energy use without sacrificing product properties. The preparation of the dimer acid-epoxide adhesive by Li and Li (*55*) appears not to involve organic solvents or toxic chemicals and is more environmentally friendly. Furthermore, the use of single-step metal-free system for the synthesis of PLA (*38*) has the potential of being a more eco-friendly process.

Green Products

In general, the polymeric products made from natural agri-based sources are more likely to be degradable and possibly recyclable, thereby being more "green" and eco-friendly. Two specific examples of green products could be pointed out.

In Green Polymer Chemistry: Biobased Materials and Biocatalysis; Smith, et al.;
ACS Symposium Series; American Chemical Society: Washington, DC, 2015.

PLA is well known as a biodegradable and bioresorbable product that has a large number of applications. Several chapters in this book deal with PLA (*38–40*, *48*). Enzymes and enzyme-based conjugates were proposed to be useful products for the treatment of wastewater (*35*).

In addition, many biobased materials are specifically mentioned to have beneficial product functions or market niches. For example, insoluble glucans may possibly be used for enhanced oil recovery, encapsulation and production of biocompatible films and fibers (*37*). Solid-lipid nanoparticles are possible carriers for drug molecules or enzymes (*47*). Phosphorus-containing isosorbide esters are possible flame retardants (*51*). Dimer-epoxy resins are noted as pressure sensitive adhesives (*55*). Aerogels, which can be made from biobased polymers, are shown to have excellent properties (*58*).

Obviously during the course of a research project, the project members usually have some products in mind. Thus, many more examples of current and potential products can be found in virtually all the chapters in this book. Interested readers are encouraged to study the individual chapters in detail and find out more about the latest developments in this field.

Publication Date (Web): June 18, 2015 | doi: 10.1021/bk-2015-1192.ch001

Acknowledgments

Thanks are due to the chapter authors of this symposium volume for their contributions and for their cooperation during the peer review process. Mention of trade names or commercial products in this publication is solely for the purpose of providing specific information and does not imply recommendation or endorsement by the U.S. Department of Agriculture (USDA). USDA is an equal opportunity provider and employer.

References

1. Horvath, I. T.; Anastas, P. T. *Chem. Rev.* **2007**, *107*, 2169–2173.
2. *Green Chemistry: Challenging Perspectives*; Tundo, P., Anastas, P. T., Eds.; Oxford University Press: Oxford, U.K., 2000.
3. Stevens, E. S. *Green Plastics: An Introduction to the New Science of Biodegradable Plastics*; Princeton University Press: Princeton, NJ, 2002.
4. *Green Polymer Chemistry: Biocatalysis and Biomaterials*; Cheng, H. N., Gross, R. A., Eds.; ACS Symposium Series 1043; American Chemical Society: Washington, DC, 2010.
5. *Green Polymerization Methods: Renewable Starting Materials, Catalysis and Waste Reduction*; Mathers, R. T., Meier, M. A. R., Eds.; Wiley-VCH: Weinheim, Germany, 2011.
6. *Green Polymer Chemistry: Biocatalysis and Materials II*; Cheng, H. N., Gross, R. A., Smith, P. B., Eds.; ACS Symposium Series 1144; American Chemical Society: Washington, DC, 2013.
7. Williams, C. K.; Hillmyer, M. A. *Polym. Rev.* **2008**, *48*, 1–10.
8. Cheng, H. N.; Gross, R. A. *ACS Symp. Ser.* **2010**, *1043*, 1–14.
9. Gandini, A. *Green Chem.* **2011**, *13*, 1061–1083.

10. Mulhaupt, R. *Macromol. Chem. Phys.* **2013**, *214*, 159–174.
11. Cheng, H. N.; Smith, P. B.; Gross, R. A. *ACS Symp. Ser.* **2013**, *1144*, 1–12.
12. Gross, R. A.; Kumar, A.; Kalra, B. *Chem. Rev.* **2001**, *101*, 2097–2124.
13. Kobayashi, S.; Uyama, H.; Kimura, S. *Chem. Rev.* **2001**, *101*, 3793–3818.
14. Kobayashi, S.; Makino, A. *Chem. Rev.* **2009**, *109*, 5288–5353.
15. Cheng, H. N.; Gu, Q.-M. *Polymers* **2012**, *4*, 1311–1330 (Special Issue on Enzymes in Monomer and Polymer Synthesis).
16. *Biocatalysis in Polymer Chemistry*; Loos, K., Ed.; Wiley-VCH: Weinheim, Germany, 2011.
17. *Polymer Biocatalysis and Biomaterials II*; Cheng, H. N., Gross, R. A., Eds.; ACS Symposium Series 999; American Chemical Society: Washington, DC, 2008.
18. *Polymer Biocatalysis and Biomaterials*; Cheng, H. N., Gross, R. A., Eds.; ACS Symposium Series 900; American Chemical Society: Washington, DC, 2005.
19. *Biocatalysis in Polymer Science*; Gross, R. A., Cheng, H. N., Eds.; ACS Symposium Series 840; American Chemical Society: Washington, DC, 2003.
20. Roach, P.; Eglin, D.; Rohde, K.; Perry, C. C. *J. Mater. Sci.: Mater. Med.* **2007**, *18*, 1263.
21. Meier, M. A. R.; Metzgerb, J. O.; Schubert, U. S. *Chem. Soc. Rev.* **2007**, *36*, 1788–1802.
22. Bhardwaj, R.; Mohanty, A. K. *J. Biobased Mater. Bioenergy* **2007**, *1* (2), 191–209.
23. Raquez, J.-M.; Deléglise, M.; Lacrampe, M.-F.; Krawczak, P. *Progr. Polym. Sci.* **2010**, *35*, 487–509.
24. Cheng, H. N. *ACS Symp. Ser.* **2012**, *1114*, xiii–xiv.
25. Khemani, K.; Scholz, C. *ACS Symp. Ser.* **2012**, *1114*, 3–10.
26. *Natural Fibers, Biopolymers, and Biocomposites*; Mohanty, A. K., Misra, M., Drzal, L. T., Eds.; CRC Press: Boca Raton, FL, 2005.
27. Wool, R.; Sun, X. S. *Bio-Based Polymers and Composites*; Elsevier: Burlington, MA, 2005.
28. *Biobased Monomers, Polymers, and Materials*; Smith, P. B., Gross, R. A., Eds.; ACS Symposium Series 1105; American Chemical Society: Washington, DC, 2012.
29. *Degradable Polymers and Materials: Principles and Practice*, 2nd ed; Khemani; K., Scholz, C., Eds.; ACS Symposium Series 1114; American Chemical Society: Washington, DC, 2012.
30. Greene, J. P. *Sustainable Plastics*; Wiley: Hoboken, NJ, 2014.
31. Roland-Holst, D.; Triolo, R.; Heft-Neal, S.; Bayrami, B. 2013; http://www.bearllc.net/Files/BEAR_ResearchPaper_0012100_11.2013.pdf.
32. Puskas, J. E.; Castano, M.; Gergely, A. L. Green Polymer Chemistry: Enzyme-catalyzed Polymer Functionalization. In *Green Polymer Chemistry: Biobased Materials and Biocatalysis III*; Cheng, H. N., Gross, R. A., Smith. P. B., Eds.; ACS Symposium Series 1192; American Chemical Society: Washington, DC, 2015; Chapter 2.

33. Barrera-Rivera, K. A.; Marcos-Fernandez, A.; Martinez-Richa, A. Chemo-enzymatic Synthesis and Characterization of Polyester-urethanes Bearing Amino-acid Moieties. In *Green Polymer Chemistry: Biobased Materials and Biocatalysis III*; Cheng, H. N., Gross, R. A., Smith. P. B., Eds.; ACS Symposium Series 1192; American Chemical Society: Washington, DC, 2015; Chapter 3.
34. Pion, F.; Reano, A. F.; Oulame, M. Z.; Barbara, I.; Flourat, A. L.; Ducrot, P.-H.; Allais. F. Chemo-enzymatic Synthesis, Derivatizations and Polymerizations of Renewable Phenolic Monomers Derived from Ferulic Acid and Biobased Polyols: An Access to Sustainable Copolyesters, Poly(ester-urethane)s and Poly(ester-alkenamer)s. In *Green Polymer Chemistry: Biobased Materials and Biocatalysis III*; Cheng, H. N., Gross, R. A., Smith. P. B., Eds.; ACS Symposium Series 1192; American Chemical Society: Washington, DC, 2015; Chapter 4.
35. Maloney, A. J.; Dong, C.; Campbell, A. S.; Dinu, C. Z. Emerging Enzyme-based Technologies for Wastewater Treatment. In *Green Polymer Chemistry: Biobased Materials and Biocatalysis III*; Cheng, H. N., Gross, R. A., Smith. P. B., Eds.; ACS Symposium Series 1192; American Chemical Society: Washington, DC, 2015; Chapter 5.
36. Kadokawa, J. Enzymatic Synthesis of Non-natural Oligo- and Polysaccharides by Phosphorylase-catalyzed Glycosylations Using Analogue Substrates. In *Green Polymer Chemistry: Biobased Materials and Biocatalysis III*; Cheng, H. N., Gross, R. A., Smith. P. B., Eds.; ACS Symposium Series 1192; American Chemical Society: Washington, DC, 2015; Chapter 6.
37. Cote, G. L.; Skory, C. D. Water-Insoluble Glucans from Sucrose via Glucansucrases. Factors Influencing Structures and Yields. In *Green Polymer Chemistry: Biobased Materials and Biocatalysis III*; Cheng, H. N., Gross, R. A., Smith. P. B., Eds.; ACS Symposium Series 1192; American Chemical Society: Washington, DC, 2015; Chapter 7.
38. Nduko, J. M.; Sun, J.; Taguchi, S. Biosynthesis, Properties and Biodegradation of Lactate-based Polymers. In *Green Polymer Chemistry: Biobased Materials and Biocatalysis III*; Cheng, H. N., Gross, R. A., Smith. P. B., Eds.; ACS Symposium Series 1192; American Chemical Society: Washington, DC, 2015; Chapter 8.
39. Romain, C.; Williams, C. K. Combining Sustainable Polymerization Routes for the Preparation of Polyesters, Polycarbonates and Copolymers. In *Green Polymer Chemistry: Biobased Materials and Biocatalysis III*; Cheng, H. N., Gross, R. A., Smith. P. B., Eds.; ACS Symposium Series 1192; American Chemical Society: Washington, DC, 2015; Chapter 9.
40. MacDonald, J. P.; Shaver, M. P. Aluminum Salen and Salan Polymerization Catalysts: From Monomer Scope to Macrostructure Control. In *Green Polymer Chemistry: Biobased Materials and Biocatalysis III*; Cheng, H. N., Gross, R. A., Smith. P. B., Eds.; ACS Symposium Series 1192; American Chemical Society: Washington, DC, 2015; Chapter 10.
41. Tada, S.; Uzawa, T.; Ito, Y. Creation of Functional Peptides by Evolutionary Engineering with Bioorthogonal Incorporation of Artificial Components. In

Green Polymer Chemistry: Biobased Materials and Biocatalysis III; Cheng, H. N., Gross, R. A., Smith. P. B., Eds.; ACS Symposium Series 1192; American Chemical Society: Washington, DC, 2015; Chapter 11.
42. Hernandez, N.; Yan, M.; Williams, R. C.; Cochran, E. Thermoplastic Elastomers from Vegetable Oils via Reversible Addition-Fragmentation Chain Transfer Polymerization. In *Green Polymer Chemistry: Biobased Materials and Biocatalysis III*; Cheng, H. N., Gross, R. A., Smith. P. B., Eds.; ACS Symposium Series 1192; American Chemical Society: Washington, DC, 2015; Chapter 12.
43. Havelka, K. O.; Gerhardt, G. E. From Biorefinery to Performance Technology: Transforming Renewable Olefinic Building Blocks into Lubricants and Other High-Value Products. In *Green Polymer Chemistry: Biobased Materials and Biocatalysis III*; Cheng, H. N., Gross, R. A., Smith. P. B., Eds.; ACS Symposium Series 1192; American Chemical Society: Washington, DC, 2015; Chapter 13.
44. Hong, J.; Hairabedian, D.; Petrovic, Z. S.; Myers, A. Polyacids from Corn Oil as Curing Agents for Epoxy Resins. In *Green Polymer Chemistry: Biobased Materials and Biocatalysis III*; Cheng, H. N., Gross, R. A., Smith. P. B., Eds.; ACS Symposium Series 1192; American Chemical Society: Washington, DC, 2015; Chapter 14.
45. Cheng, H. N.; Biswas, A. Modifications of Plant Oils for Value-Added Uses. In *Green Polymer Chemistry: Biobased Materials and Biocatalysis III*; Cheng, H. N., Gross, R. A., Smith. P. B., Eds.; ACS Symposium Series 1192; American Chemical Society: Washington, DC, 2015; Chapter 15.
46. Mannari, V.; Patel, C.; Li, W.; Kiamanesh. A. Soy-based Building Blocks for Advanced Photo-cure Coating Systems. In *Green Polymer Chemistry: Biobased Materials and Biocatalysis III*; Cheng, H. N., Gross, R. A., Smith. P. B., Eds.; ACS Symposium Series 1192; American Chemical Society: Washington, DC, 2015; Chapter 16.
47. Kim, S.; Jacoby, J.; Stebe, M.-J.; Canilho, N.; Pasc, A. Solid Lipid Nanoparticle - Functional Template of Meso-macrostructured Silica Materials. In *Green Polymer Chemistry: Biobased Materials and Biocatalysis III*; Cheng, H. N., Gross, R. A., Smith. P. B., Eds.; ACS Symposium Series 1192; American Chemical Society: Washington, DC, 2015; Chapter 17.
48. Lo Re, G.; Dubois, P.; Raquez, J.-M. In Situ Metal-free Synthesis of Polylactide Enantiomers Grafted from Nanoclays of High Thermostability. In *Green Polymer Chemistry: Biobased Materials and Biocatalysis III*; Cheng, H. N., Gross, R. A., Smith. P. B., Eds.; ACS Symposium Series 1192; American Chemical Society: Washington, DC, 2015; Chapter 18.
49. Luebben, S. D.; Raebiger, J. W. A Novel Renewable Thermoplastic Polyacetal by Polymerization of Glycolaldehyde Dimer, a Major Product of the Fast Pyrolysis of Cellulosic Feedstock. In *Green Polymer Chemistry: Biobased Materials and Biocatalysis III*; Cheng, H. N., Gross, R. A., Smith. P. B., Eds.; ACS Symposium Series 1192; American Chemical Society: Washington, DC, 2015; Chapter 19.

Publication Date (Web): June 18, 2015 | doi: 10.1021/bk-2015-1192.ch001

50. Toyama, K.; Soyama, M.; Tanaka, S.; Iji, M. Development of Cardanol-bonded Cellulose Resin with Non-food Plant Resources: Low Energy Heterogeneous Synthesis Process. In *Green Polymer Chemistry: Biobased Materials and Biocatalysis III*; Cheng, H. N., Gross, R. A., Smith. P. B., Eds.; ACS Symposium Series 1192; American Chemical Society: Washington, DC, 2015; Chapter 20.
51. Howell, B. A.; Daniel, Y. G. Phosphorus Flame Retardants from Esters of Isosorbide and 10-Undecenoic Acid. In *Green Polymer Chemistry: Biobased Materials and Biocatalysis III*; Cheng, H. N., Gross, R. A., Smith. P. B., Eds.; ACS Symposium Series 1192; American Chemical Society: Washington, DC, 2015; Chapter 21.
52. Maiorana, A.; Spinella, S.; Gross, R. A. Bio-Based Epoxy Resins from Diphenolate Esters--Replacing the Diglycidyl Ether of Bisphenol A. In *Green Polymer Chemistry: Biobased Materials and Biocatalysis III*; Cheng, H. N., Gross, R. A., Smith. P. B., Eds.; ACS Symposium Series 1192; American Chemical Society: Washington, DC, 2015; Chapter 22.
53. Hu, F.; Sharifi, M.; Palmese, G. Influence of Furanyl Building Blocks on the Cure Kinetics of a Renewable Epoxy-Amine System. In *Green Polymer Chemistry: Biobased Materials and Biocatalysis III*; Cheng, H. N., Gross, R. A., Smith. P. B., Eds.; ACS Symposium Series 1192; American Chemical Society: Washington, DC, 2015; Chapter 23.
54. Nguyen, H. T. H.; Suda, E. R.; Bradic, E. M.; Hvozdovich, J. A.; Miller, S. A. Polyesters from Bio-Aromatics. In *Green Polymer Chemistry: Biobased Materials and Biocatalysis III*; Cheng, H. N., Gross, R. A., Smith. P. B., Eds.; ACS Symposium Series 1192; American Chemical Society: Washington, DC, 2015; Chapter 24.
55. Li, A.; Li, K. Development and Characterization of Pressure-Sensitive Adhesives from Dimer Acid and Epoxides. In *Green Polymer Chemistry: Biobased Materials and Biocatalysis III*; Cheng, H. N., Gross, R. A., Smith. P. B., Eds.; ACS Symposium Series 1192; American Chemical Society: Washington, DC, 2015; Chapter 25.
56. Guenthner, A. J.; Harvey, B. G.; Davis, M. C.; Ford, M. D.; Meylemans, H. A.; Wright, M. E.; Chafin, A. P.; Mabry, J. M. Structure-Property Relationships for Polycyanurate Networks Derived from Renewable Resources. In *Green Polymer Chemistry: Biobased Materials and Biocatalysis III*; Cheng, H. N., Gross, R. A., Smith. P. B., Eds.; ACS Symposium Series 1192; American Chemical Society: Washington, DC, 2015; Chapter 26.
57. Smith, P. B. Bio-based Sources for Terephthalic Acid. In *Green Polymer Chemistry: Biobased Materials and Biocatalysis III*; Cheng, H. N., Gross, R. A., Smith. P. B., Eds.; ACS Symposium Series 1192; American Chemical Society: Washington, DC, 2015; Chapter 27.
58. Schiraldi, D. Green Polymer Aerogels. In *Green Polymer Chemistry: Biobased Materials and Biocatalysis III*; Cheng, H. N., Gross, R. A., Smith. P. B., Eds.; ACS Symposium Series 1192; American Chemical Society: Washington, DC, 2015; Chapter 28.

Publication Date (Web): June 18, 2015 | doi: 10.1021/bk-2015-1192.ch002

Chapter 2

Green Polymer Chemistry: Enzyme-Catalyzed Polymer Functionalization

Judit E. Puskas,[*,1] Marcela Castano,[1,2] and Attila L. Gergely[1]

[1]Department of Chemical & Biomolecular Engineering, The University of Akron, 264 Wolf Ledges, Akron, Ohio 44325
[2]Present address: Avery Dennison, 15939 Industrial Parkway, Cleveland, Ohio 44135
[*]E-mail: jpuskas@uakron.edu.

Enzymes are "green" alternative to conventional chemical catalysts offering several advantages including high selectivity, high efficiency, ability to operate under mild conditions, recyclability and biocompatibility. This paper will first give an overview of the functionalization of natural and synthetic polymers. Subsequently our work related to the synthesis of symmetric and asymmetric telechelic polymers using *Candida antarctica* lipase B will be discussed. Quantitative functionalization of polyisobutylenes, polysiloxanes and poly(ethylene glycol)s (PEGs) was achieved. Multifunctional PEGs were also successfully produced. Controlled polycondensation of tetraethylene glycol and divinyl benzene yielded symmetric and asymmetric telechelic PEGs with high efficiency.

Introduction

Green Chemistry is a relatively new emerging field that focuses on achieving sustainability to meet environmental and economic goals by developing chemical processes that follow the 12 basic principles of sustainable chemistry (*1*). Enzymes are an environmentally friendly alternative to conventional chemical catalysts (*2*). Specifically, lipases are widely used in esterification, transesterification, aminolysis, and Michael addition reactions in organic syntheses (*2*, *3*). Enzymes can also catalyze polymer synthesis – this area of research has extensively

In Green Polymer Chemistry: Biobased Materials and Biocatalysis; Smith, et al.;
ACS Symposium Series; American Chemical Society: Washington, DC, 2015.

been reviewed (*3*–*7*). Our group has been concentrating on the quantitative end-functionalization of synthetic polymers (*8*–*15*). This paper will give an overview of our work after reviewing prior representative work related to polymer functionalization.

Functionalization of Natural Polymers

Several research groups reported work related to enzyme-catalyzed functionalization of natural polymers. Some interesting examples are given below.

The CALB-catalyzed acylation of cellulose acetate (*16*) and hydroxypropyl cellulose (*17*) yielded various ester side groups with high efficinecy. In the case of the acylation of cellulose acetate with lauric and oleic acids (Figure 1), the final conversion of both fatty acids was about 35% after 96 h of incubation at 50 °C. In the case of hydroxypropyl cellulose the final ester content was about 11% after 6-day incubation at 50°C.

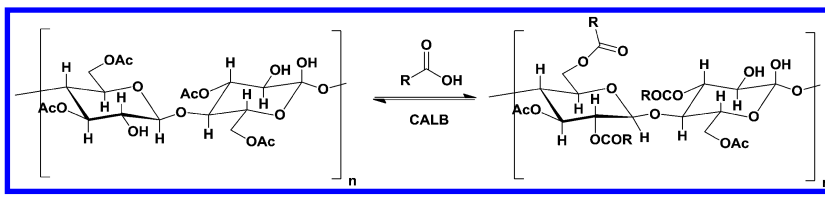

Figure 1. CALB-catalyzed acylation of cellulose acetate.

Starch nanoparticles in microemulsions were reacted with vinyl stearate, -caprolactone, and maleic anhydride in the presence of CALB at 40 °C for 48 h to give esters with degrees of substitution (DS) of 0.8, 0.6, and 0.4, respectively. Substitution occurred regioselectively at the C-6 position of the glucose repeat units (Figure 2) (*18*).

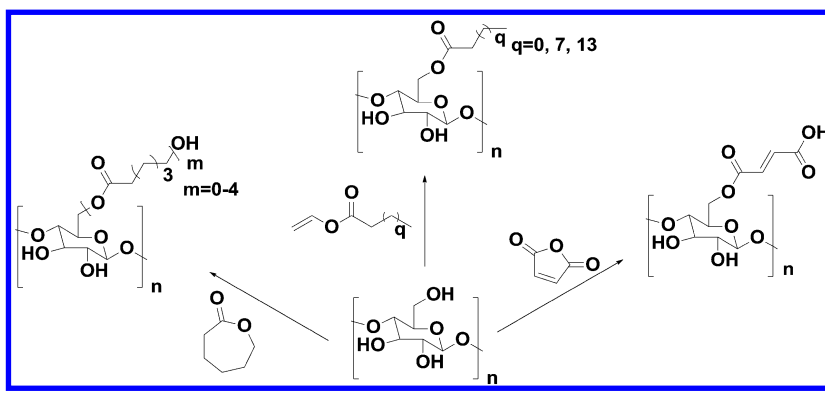

Figure 2. CALB-catalyzed functionalization of starch nanoparticles.

In Green Polymer Chemistry: Biobased Materials and Biocatalysis; Smith, et al.;
ACS Symposium Series; American Chemical Society: Washington, DC, 2015.

Publication Date (Web): June 18, 2015 | doi: 10.1021/bk-2015-1192.ch002

Another example is a novel regioselective strategy for the transesterification of Konjac glucomannan (KGM) with vinyl acetate using CALB in a solvent-free system. KGM is an abundant, naturally occurring polysaccharide isolated from the tubers of the *Amorphophallus konjac* plant. It consists of β-1,4-linked D-glucose and D-mannose units, and the molar ratio of glucose to mannose has been reported to be around 1 to 1.60. The degree of substitution (DS) was 0.34 and 0.58 at 30 and 60ºC, respectively. It was also found that the DS decreased with increasing KGM molecular weight (from 114,000 to 980,000 g/mol) (*19*).

Functionalization of Synthetic Polymers

Enzymes have also been employed for the functionalization of synthetic polymers. CALB-catalyzed modification of pendant ester groups of a polystyrene is a good example of a clear-cut regioselective transesterification reaction (*20*). From the two ester groups present, only the ester group distant from the polymer backbone was involved in the reaction. It is possible that due to the proximity of the acyl (ester) group (A) to the bulk of the polymer backbone, the enzyme is incapable of coordinating to the acyl group, but the more distant group (B) is available to the enzyme (Figure 3).

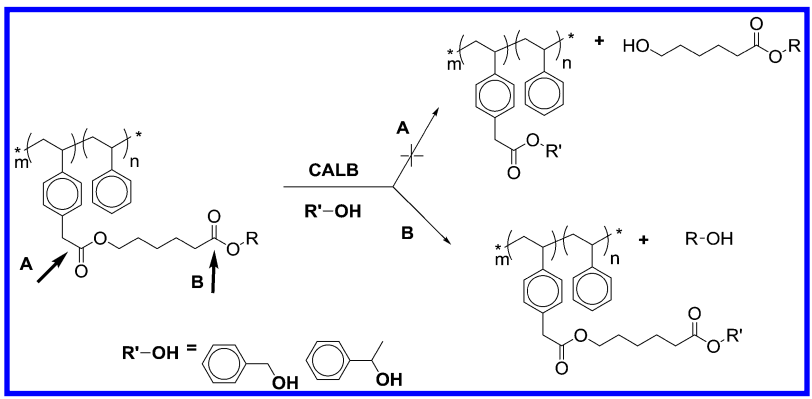

Figure 3. CALB-catalyzed modification of pendant ester groups of a polystyrene.

Jarvie, Overton and Pourçain showed that CALB was able to catalyze the selective epoxidation of polybutadiene (M_n=1,300 g/mol) (35% *trans*, 20% *cis*, 45% vinyl) in organic solvents in the presence of hydrogen peroxide and catalytic quantities of acetic acid (Figure 4). The *cis* and *trans* alkene bonds of the backbone were epoxidised in yields of up to 60% while the pendant vinyl groups remained untouched (*21*).

Publication Date (Web): June 18, 2015 | doi: 10.1021/bk-2015-1192.ch002

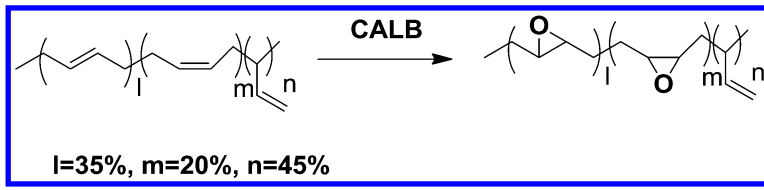

Figure 4. CALB-catalyzed epoxidation of polybutadiene.

The enantioselective enzymatic transesterification of copolymers of *R*-isomers and *S*-isomers of styrene and *p*-vinylphenylethanol by CALB using vinyl acetate was investigated (Figure 5) (*22*). When a backbone contained 100% *S* groups no acetylation was detected. By contrast, when the backbone contained 100% *R* groups, 75% of the alcohol groups was converted into ester groups within 24 h.

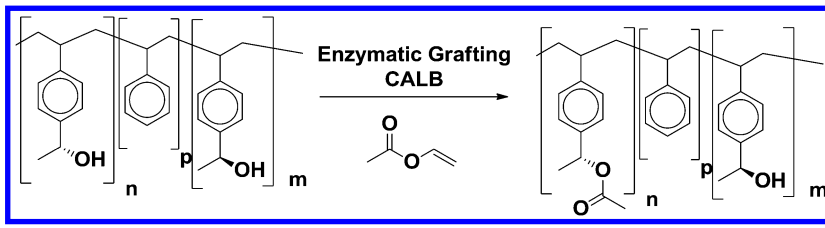

*Figure 5. Enzymatic transesterification of vinyl acetate with copolymers of **R**- and **S**-isomers of styrene and p-vinlyphenylethanol by CALB.*

CALB-catalyzed acylation of comb-like methacrylamide polymers was induced by reacting the OH groups in the side chains with vinyl acetate, phenyl acetate, 4-fluorophenyl acetate, and phenyl stearate in THF at an ambient temperature for 6 days (Figure 6). Conversions varied from 20% to 93%, depending on the acylating agent (*23*).

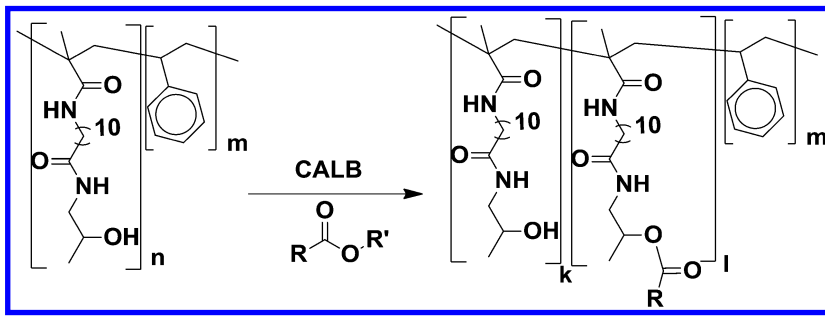

Figure 6. CALB-catalyzed acylation of comb-like methacrylamide polymers.

In Green Polymer Chemistry: Biobased Materials and Biocatalysis; Smith, et al.;
ACS Symposium Series; American Chemical Society: Washington, DC, 2015.

Publication Date (Web): June 18, 2015 | doi: 10.1021/bk-2015-1192.ch002

Telechelic carboxylic acid functionalized poly(dimethyl siloxanes) (PDMSs) were reacted with α,β-ethylglucoside at 70 °C under vacuum for 34 hours in the presence of CALB. The product was a mixture of mono- and difunctional esters (Figure 7) (*24*).

These examples demonstrate chemo- and regioselectivity, but tend to be less than quantitative.

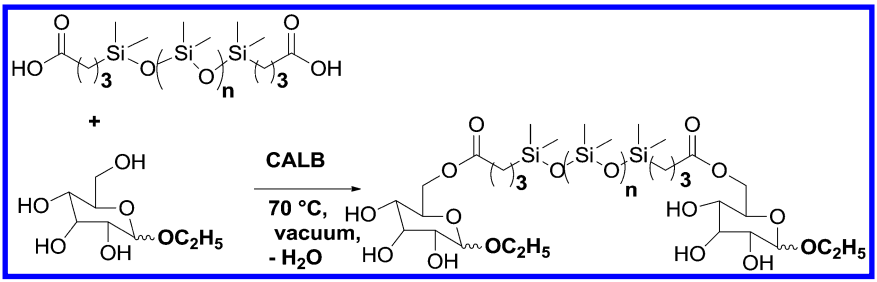

Figure 7. Esterification of telechelic carboxylic acid functionalized PDMSs with α,β-ethylglucoside in the presence of CALB.

Quantitative End-Functionalization of Synthetic Polymers

Despite all the advantages that the enzymatic catalysis offers, the area of end-functionalization of pre-formed synthetic symmetric or asymmetric telechelic polymers has not been fully developed yet. Our group reported the first examples of quantitative functionalization of synthetic polymers using CALB-catalyzed reactions with and without organic solvents (*8–10*). For example, Figure 8 shows the quantitative methacrylation by transesterification of vinyl methacrylate with hydroxy-functionalized polyisobutylenes (PIBs) in the presence of CALB within 24h in hexane and 2h in bulk, respectively. The last example demonstrates regioselective transesterification, leaving the sterically hindered hydroxyl group intact (*9*). Additionally, commercially available polydimethylsiloxanes (PDMS), PDMS-monocarbinol and PDMS-dicarbinols were also methacrylated with vinyl methacrylate under solventless conditions within 2 hours in the presence of CALB (*10*, *11*). *Primary* hydroxy-functionalized polystyrene (PS-$(CH_3)_2$Si-CH_2-OH, M_n=2600 g/mol; M_w/M_n =1.06) was quantitatively methacrylated by transesterification of vinyl methacrylate within 48 hours (*11*). PEGs were also effectively functionalized (*8*, *10–15*).

PEG is a particularly important polymer since it is non-toxic, hydrophilic polymer that is used widely for biomedical applications (*25*, *26*). One applications is to enhance the circulation time and blood half-life for cell imaging, drug delivery, and antibody-based therapy (*27–31*). However, the HO-end groups that are available for chemical derivatization are only a small fraction of the molecular mass of the polymer, and chemistries utilized for end-group modification must be of high fidelity in nature and leave few or ideally no residuals (*32–34*). Since

Publication Date (Web): June 18, 2015 | doi: 10.1021/bk-2015-1192.ch002

CALB is immobilized on a resin, it can conveniently be separated from the product, yielding very pure compounds for potential pre-clinical and clinical applications (*35–37*).

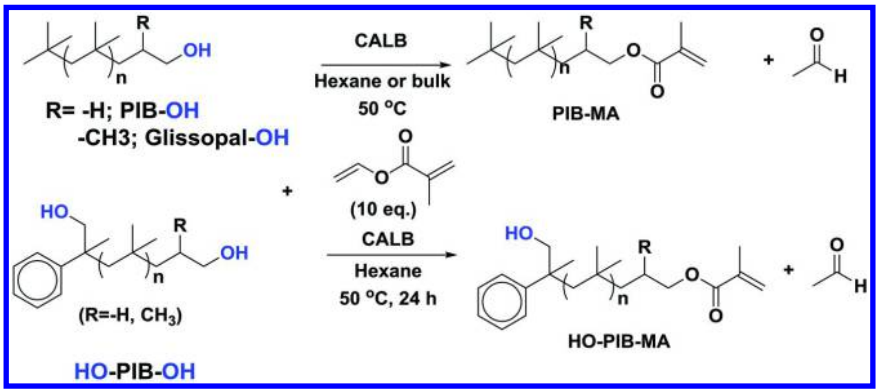

Figure 8. CALB-catalyzed methacrylation of PIB-OHs. PIB-OH (M_n=5200 g/mol; M_w/M_n=1.09), Glissopal-OH (M_n=3600 g/mol; M_w/M_n=1.34), and asymmetric telechelic HO-PIB-OH (M_n=7200 g/mol; M_w/M_n=1.04).

PEGs were effectively functionalized under solvent-free conditions within 4 h by dissolving low molecular weight liquified HO–PEG–OH (M_n = 1050 and 2000 g/mol) in the corresponding acyl donors (vinyl methacrylate, vinyl acrylate and vinyl crotonate) at 50 ºC (Figure 9). ^{1}H and ^{13}C NMR along with MALDI-ToF confirmed quantitative conversion with the expected structures (*14*).

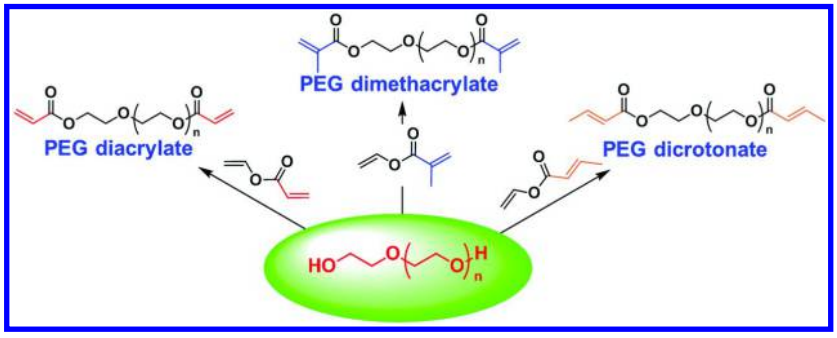

Figure 9. Functionalized PEGs via CALB-catalyzed transesterification.

In Green Polymer Chemistry: Biobased Materials and Biocatalysis; Smith, et al.;
ACS Symposium Series; American Chemical Society: Washington, DC, 2015.

Publication Date (Web): June 18, 2015 | doi: 10.1021/bk-2015-1192.ch002

Multifunctional structures such as $(HO)_2$–TEG–$(OH)_2$ and $(HO)_2$–PEG–$(OH)_2$ were also successfully synthesized using sequential CALB-catalyzed transesterification and Michael addition of diethanolamine to the acrylate double bonds (Figure 10) (*12*). These structures will be used as cores of novel dendrimers. Both transesterification and Michael addition reactions were successful as quantitative conversions were reached within 24 h and 2 h, respectively.

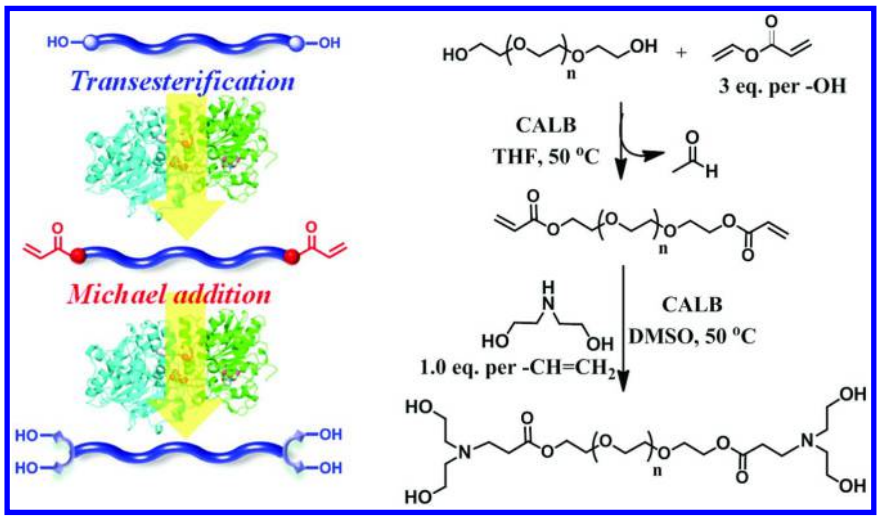

Figure 10. Synthesis of $(HO)_2$–PEG–$(OH)_2$ via sequential CALB-catalyzed transesterification and Michael addition.

Subsequently $(HO)_4$–TEG–$(OH)_4$ and $(HO)_4$–PEG–$(OH)_4$ have also been made by repeating the reaction sequence shown in Figure 10.

Synthesis of Asymmetric and Symmetric Vinyl-Functionalized PEG Oligomers

In order to be able to synthesize asymmetric and symmetric telechelic PEGs we investigated the kinetics of the transesterification of divinyl adipate (DVA) with tetraethylene glycol (TEG). We found conditions under which polycondensation was minimized and symmetric and asymmetric telechelic TEGs were obtained with M_n = 700 – 1700 g/mol and M_w/M_n = 1.1-1.3. Specifically, at DVA/TEG=1.5 molar ratio 100% of the oligomers had divinyl end groups after 20 minutes reaction time. At DVA/TEG = 3 only vinyl end groups were detected after 5 minutes. HO-$(TEG)_n$-Vinyl was maximized at 70% at DVA/TEG 1/1.5 molar ratio at 10 minutes reaction time (Figure 11), while ~90% HO-$(TEG)_n$-OH was obtained in 20 minutes with TEG excess (*15*).

In Green Polymer Chemistry: Biobased Materials and Biocatalysis; Smith, et al.;
ACS Symposium Series; American Chemical Society: Washington, DC, 2015.

Publication Date (Web): June 18, 2015 | doi: 10.1021/bk-2015-1192.ch002

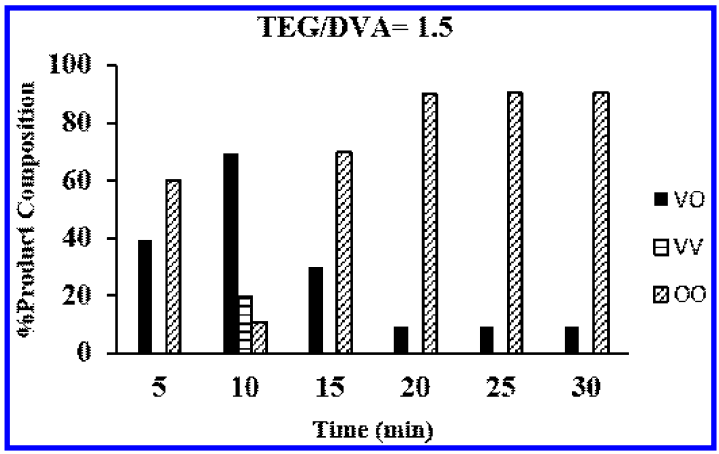

Figure 11. Kinetics of the polycondensation of TEG with DVA.

Thus with the judicious selection of reaction conditions and time symmetric and asymmetric telechelic oligomers can be synthesized with high efficiency.

Conclusion

In summary, CALB was shown to be an effective catalyst for selective end-functionalization of polymers. The end functionalization is still an ongoing work in our laboratories and there are many opportunities for new applications.

References

1. Anastas, P.; Eghbali, N. *Chem. Soc. Rev.* **2010**, *39*, 301–312.
2. Faber, K. *Biotransformations in Organic Chemistry*, 5th ed.; Springer-Verlag: New York, 2004.
3. Kobayashi, S.; Makino, A. *Chem. Rev.* **2009**, *109*, 5288–5353.
4. Gross, R.; Kumar, A.; Kalra, B. *Chem. Rev.* **2001**, *101*, 2097–2124.
5. Uyama, H.; Kobayashi, S. *Adv. Polym. Sci.* **2006**, *194*, 133–158.
6. Kobayashi, S.; Uyama, H.; Kimura, S. *Chem. Rev.* **2001**, *101*, 3793–3818.
7. Varma, I. K.; Albertsson, A.-C.; Rajkhowa, R.; Srivastava, R. K. *Prog. Polym. Sci.* **2005**, *30*, 949–981.
8. Puskas, J. E.; Sen, M. Y.; Kasper, J. R. *J. Polym. Sci., Part A: Polym. Chem.* **2008**, *46*, 324–327.
9. Sen, M. Y.; Puskas, J. E.; Ummadisetty, S.; Kennedy, J. P. *Macromol. Rapid Comm.* **2008**, *29*, 1598–1602.
10. Puskas, J. E.; Sen, M. Process of Preparing Functionalized Polymers via Enzyme Catalysis. U.S. Patent 12/732,467, September 23, 2010.
11. Puskas, J. E.; Sen, M. Y.; Seo, K. S. *J. Polym. Sci., Part A: Polym. Chem.* **2009**, *47*, 2959–2976.
12. Puskas, J. E.; Seo, K. S.; Sen, M. Y. *Eur. Polym. J.* **2011**, *47*, 524–534.

Publication Date (Web): June 18, 2015 | doi: 10.1021/bk-2015-1192.ch002

13. Castano, M.; Seo, K. S.; Kim, G.; Becker, M. L.; Puskas, J. E. *Macromol. Rapid Commun.* **2013**, *34*, 1375–1380.
14. Seo, K. S.; Castano, M.; Casiano, M; Wesdemiotis, C.; Becker, M. L.; Puskas, J. E. *RSC Adv.* **2014**, *4*, 1683–1688.
15. Castano, M.; Seo, K. S.; Guo, K.; Becker, M. L.; Wesdemiotis, C.; Puskas, J. E. *Polym. Chem.* **2015** DOI:0.1039/C4PY01223B.
16. Sereti, V.; Stamatis, H.; Koukios, E.; Kolisis, F. *J. Biotechnol.* **1998**, *66*, 219–223.
17. Sereti, V.; Stamatis, H.; Pappas, C.; Polissiou, M.; Kolisis, F. *Biotechnol. Bioeng.* **2001**, *72*, 495–500.
18. Chakraborty, S.; Sahoo, B.; Teraoka, I.; Miller, L. M.; Gross, R. A. *Macromolecules* **2005**, 61–68.
19. Chen, Z.-G.; Zong, M.-H.; Li, G.-J. *J. Appl. Polym. Sci.* **2006**, *102*, 1335–1340.
20. Padovani, M.; Hilker, I.; Duxbury, C. J.; Heise, A. *Macromolecules* **2008**, *41*, 2439–2444.
21. Jarvie, A. W. P.; Overton, N.; Pourçain, C. B. S. *J. Chem. Soc., Perkin Trans.* **1999**, *1*, 2171–2176.
22. Duxbury, C. J.; Hilker, I.; Wildeman, S. M.; Heise, A. *Angew. Chem., Int. Ed.* **2007**, *46*, 8452–8454.
23. Pavel, K.; Ritter, H. *Makromol. Chem.* **1992**, *328*, 323–328.
24. Sahoo, B.; Brandstadt, K. F.; Lane, T. H.; Gross, R. *Org. Lett.* **2005**, *7*, 3857–3860.
25. Kukula, H.; Schlaad, H.; Antonietti, M.; Förster, S. *J. Am. Chem. Soc.* **2002**, *124*, 1658–1663.
26. Lin, L. Y.; Karwa, A.; Kostelc, J. G.; Lee, N. S.; Dorshow, R. B.; Wooley, K. L. *Mol. Pharm.* **2012**, *9*, 2248–2255.
27. Shrestha, R.; Shen, Y.; Pollack, K.; Taylor, J.-S.; Wooley, K. L. *Bioconjugate Chem.* **2012**, *23*, 574–585.
28. Sun, X.; Rossin, R.; Turner, J. L.; Becker, M. L.; Joralemon, M. J.; Welch, M. J.; Wooley, K. L. *Biomacromolecules* **2005**, *6*, 2541–2554.
29. Duncan, R.; Vicent, M. J. *Adv. Drug Delivery Rev.* **2013**, *65*, 60–70.
30. Marcano, D. C.; Bitner, B. R.; Berlin, J. M.; Jarjour, J.; Lee, J. M.; Jacob, A.; Fabian, R. H.; Kent, T. A.; Tour, J. M. *J. Neurotrauma* **2013**, *30*, 789–796.
31. Muthiah, M.; Vu-Quang, H.; Kim, Y. K.; Rhee, J. H.; Kang, S. H.; Jun, S. Y.; Choi, Y. J.; Jeong, Y. Y.; Cho, C. S.; Park, I. K. *Carbohydr. Polym.* **2013**, *92*, 1586–1595.
32. Jevsevar, S.; Kunstelj, M.; Porekar, V. G. *Biotechnol. J.* **2010**, *5*, 113–128.
33. Jacob, M. K.; Leena, S.; Kumar, K. S. *Biopolymers* **2008**, *90*, 512–525.
34. Kochling, J. D.; Miao, H.; Young, C. R.; Looker, A. R.; Shannon, M.; Montgomery, E. R. *J. Pharm. Biomed. Anal.* **2007**, *43*, 1638–1646.
35. Leung, M. K. M.; Hagemeyer, C. E.; Johnston, A. P. R.; Gonzales, C.; Kamphuis, M. M. J.; Ardipradja, K.; Such, G. K.; Peter, K.; Caruso, F. *Angew. Chem., Int. Ed.* **2012**, *51*, 7132–7136.
36. Fang, Y.; Xu, W.; Wu, J.; Xu, Z.-K. *Chem. Commun. (Cambridge, U.K.)* **2012**, *48*, 11208–11210.
37. Fang, Y.; Huang, X.-J.; Chen, P.-C.; Xu, Z.-K. *BMB Rep.* **2011**, *44*, 87–95.

Publication Date (Web): June 18, 2015 | doi: 10.1021/bk-2015-1192.ch003

Chapter 3

Chemoenzymatic Synthesis and Characterization of Polyester-Urethanes Bearing Amino-Acids Moieties

Karla A. Barrera-Rivera,[1] Ángel Marcos-Fernández,[2] and Antonio Martínez Richa*,[1]

[1]Departamento de Química, División de Ciencias Naturales y Exactas, Universidad de Guanajuato, Noria Alta S/N, Guanajuato, Guanajuato 36050, México
[2]Departamento de Física de Polímeros, Elastómeros y Aplicaciones Energéticas, Instituto de Ciencia y Tecnología de Polímeros (CSIC), Juan de la Cierva No. 3, 28006 Madrid, España
***E-mail: richa@ugto.mx.**

Oligomeric polycaprolactone diol (DEG1) was synthesized using biocatalysis with immobilized *Yarrowia lipolytica* lipase (YLL) and diethyleneglycol as initiator. A series of linear poly ester-urethanes were prepared from synthesized PCL diol, hexamethylenediisocyanate (HDI) and (i) L-lysine ethyl ester dihydrochloride, (ii) L-cysteine hydrochloride, (iii) L-histidine monohydrochloride monohydrate and (iv) L-ornithine hydrochloride. Characterization of prepared polyurethanes by different techniques (FT-IR, solid-state NMR. DSC, solubility in different solvents, mechanical properties and hydrolytic behavior) shows striking differences in their properties.

In Green Polymer Chemistry: Biobased Materials and Biocatalysis; Smith, et al.;
ACS Symposium Series; American Chemical Society: Washington, DC, 2015.

Publication Date (Web): June 18, 2015 | doi: 10.1021/bk-2015-1192.ch003

Introduction

In the field of biomaterials, there is a great interest in the development of degradable polymers. Synthetic biodegradable polymers can be used as materials for temporary scaffolds for tissue engineering purposes, as sutures, drug delivery devices, orthopedic fixation devices or temporary vascular grafts. These polymers need to possess the desired biocompatibility, suitable mechanical properties and predictable biodegradability. For application in the body, materials with a high water affinity offer the added advantage of compatibility with the internal environment of the body, which has high water content (*1*). Biodegradable polyurethanes (PUs) are generally prepared by using easily hydrolyzable polyols, such as polycaprolactone diol (PCL), polyacrylic acid (PAA), polylactic acid (PLA), and polyglycolic acid (PGA), as soft segments. Biodegradable polymers also are commonly biocompatible, water soluble, low crystalline or having low melting point (*2*). Biodegradation of PCL films by pure strains of microorganisms isolated from industrial compost induces a weight loss of 95 wt% (with respect to the initial mass) after 200 h of incubation. It is expected that derivatives obtained by chain extension reactions of PCL also show similar biodegradable properties. Most of these derivatives have also potential uses in surgery as drug delivery agents. One of the more important factors to consider for PCL chain extension reactions is the chemical nature of the polyester end groups. Diol derivatives (--telechelic diols) are specially targeted, due to the feasibility of the hydroxyl end-groups to react with different functional groups (*3*).

Enzyme-catalyzed polymerization may become a versatile method for the production of sustainable polyurethanes, as lipase, for example, is a renewable catalyst with high catalytic activities. The most prominent advantage of using a hydrolytic enzymes for the production of polymers is the reversible polymerization-degradation reaction that allows chemical recycling. Polymer chains that contain enzymatically hydrolyzable moieties can be specifically cleaved by a hydrolytic enzyme to produce potentially repolymerizable low-molecular-weight fragments that can be recycled (*4*). Lipases emerged as one of the leading biocatalysts with proven potential for contributing to the multibillion-dollar lipid technology bio-industry. In particular, *Yarrowia lipolytica* has been considered an industrial workhorse because of its ability to produce important metabolites and intense secretory activity. One of the most important products secreted by this microorganism is lipase. *Yarrowia lipolytica* lipases are attracting the interest of scientists and industrial researchers due to their ability to catalyze important high-value applications in the food, pharmaceutical, fine chemicals and environmental industries (*5*).

In this work, we have synthesized and characterized a series of biodegradable non-toxic polyester-urethanes based on polycaprolactone diol obtained via enzymatic polymerization, HDI and four different amino acid chain extenders, namely L-lysine ethyl ester dihydrochloride, L-cysteine hydrochloride, L-histidine monohydrochloride monohydrate, and L-ornithine hydrochloride. With this approach, we intend (i) to produce biocompatible materials with novel biological functions and (b) to obtain polymers with unique architectures with potential biomedical applications.

Experimental

Materials

ε-caprolactone (ε-CL) 97 %, was dried over calcium hydride and distilled under reduced pressure before use. Diethylene glycol (DEG) 99 %, Lewatit VP OC 1026 beads, stannous 2-ethylhexanoate ~95 %, hexamethylenediisocyanate (HDI) ≥98 %, , L-lysine ethyl ester dihydrochloride (L-Lys) puriss ≥99 %, , L-cysteine hydrochloride (L-Cys) ≥98 %, L-histidine monohydrochloride monohydrate (L-Hist) ≥98 %, and L-ornithine hydrochloride (L-Orn) 99 %, triethylamine 99% and 1,2-dichloroethane anhydrous 99.8 % were purchased from Sigma Aldrich and used as received. *Yarrowia lipolytica* lipase (YLL) was obtained and immobilized according to the procedure described in the literature (*6*, *7*).

Publication Date (Web): June 18, 2015 | doi: 10.1021/bk-2015-1192.ch003

Instrumentation

Solution ^{1}H spectra were recorded at room temperature on a Varian Gemini 2000. Chloroform-*d* ($CDCl_3$) was used as solvent. Solid-state ^{13}C NMR spectra were recorded under proton decoupling on a Bruker Avance 400 operating at 100.613 MHz for ^{13}C. A Bruker probe equipped with 4 mm rotors was used. CP-MAS spectra were obtained under Hartmann-Hahn matching conditions and a spinning rate of 6.0 kHz was used. A contact time of 2.5 ms and a repetition time of 4 s were used. The measurements were made using spin-lock power in radiofrequency units of 60 kHz and typically 4,000 transients were recorded. Chemical shifts were externally referenced to tetramethylsilane (TMS) using adamantane.

FT-IR spectra were obtained with the ATR technique on films deposited over a diamond crystal on a Perkin-Elmer two spectrometer in the 4000-650 cm^{-1} range with an average of 4 scans at 4 cm^{-1} resolution. Gel permeation chromatography multi-angle light scattering. (GPC-MALLS) was used to determine molecular weights and molecular weight distributions, M_w/M_n, of macrodiols samples. The chromatographic set-up used consists of an Alliance HPLC Waters 2695 Separation Module having a vacuum degassing facility on online, an auto sampler, a quaternary pump, a columns thermostat, and a Waters 2414 Differential Refractometer for determining the distribution of molecular weight. The temperature of the columns was controlled at 33 ºC by the thermostat. Tensile properties were measured in a MTS Synergie 200 testing machine equipped with a 100 N load cell. Type 3 dumbbell test pieces (according to ISO 37) were cut from film. A crosshead speed of 200 mm/min was used. Strain was measured from crosshead separation and referred to 12 mm initial length. Five samples were tested for each polymer composition. For thermal analysis samples were conducted on a Mettler Toledo differential scanning calorimetry (DSC)-822e using heating and cooling rates of 10 °C/min. Thermal scans were performed from 25 °C to 80 ºC, 80 °C to -90 °C, -90 °C to 80 °C.

In Green Polymer Chemistry: Biobased Materials and Biocatalysis; Smith, et al.;
ACS Symposium Series; American Chemical Society: Washington, DC, 2015.

Publication Date (Web): June 18, 2015 | doi: 10.1021/bk-2015-1192.ch003

Synthesis of α,ω-Telechelic poly(ε-caprolactone) Diol (HOPCLOH)

PCL diols were prepared according to the literature (*6*, *7*). DEG1 (10 mmol of -CL, 1 mmol of DEG and 12 mg YLL-1026). Vials were stoppered with a teflon silicon septum and placed in a thermostated bath at 120 ºC for 6 h. No inert atmosphere was used. After the reaction was stopped, the enzyme was filtered off and the PCL diol was dried at room temperature for 12 h, and stored at ambient temperature in a dessicator until used.

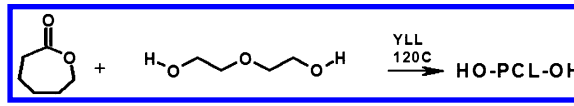

Figure 1. Synthesis of α,ω-telechelic poly (ε-caprolactone) diol via enzymatic polymerization.

Chemical Synthesis of Polyester-Urethane with Aminoacids

Dry PCL diol (2.5 g) and HDI in the appropriate amount (OH:NCO ratio = 1:1) and 15 mL of 1,2-dichloroethane were charged in a round bottom flask. The catalyst, stannous 2-ethylhexanoate (1% mol by PCL diol moles) was added, and stirred for 1 h and 30 minutes at 80 ºC; after that time, 0.3498 mmoles of aminoacid and 1.046 mmole of triethylamine were added to the reaction mixture and allowed 5 hours for reaction. The resulting solution was poured over a Teflon petri dish (*d*-10 cm). The solution was allowed to stand at ambient temperature for 24 h for solvent evaporation. The film was then released and dried at room temperature. Samples for physical characterization were cut from films, film thickness ranged from 30-50 m.

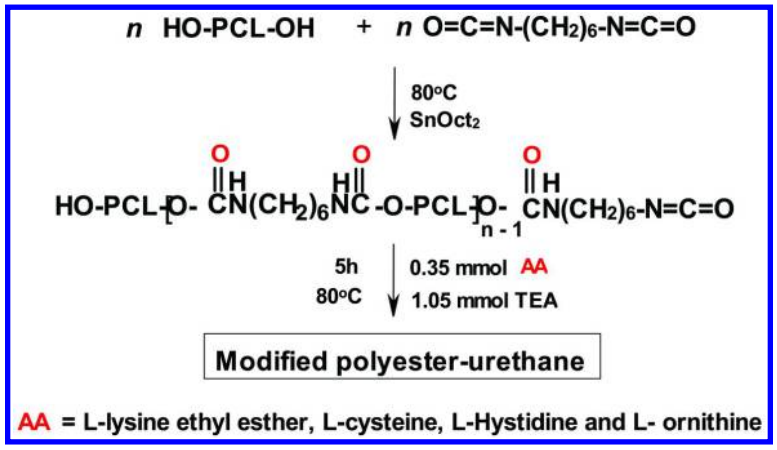

Figure 2. Chemical synthesis of polyester-urethanes bearing aminoacids.

In Green Polymer Chemistry: Biobased Materials and Biocatalysis; Smith, et al.;
ACS Symposium Series; American Chemical Society: Washington, DC, 2015.

Hydrolytic Degradation

Hydrolytic degradation was carried out in NaOH 1M solution pH 13, ammonium bicarbonate solution 5mM (ABC) pH 8, Ringer I solution (NaCl, $CaCl_2$, KCl) pH 7 and -toluenesulfonic acid solution 0.5M pH 0.5. The PUs films (1 cm x 1 cm) were placed into an individual glass vials containing 10 mL of each solution, and then incubated at 90 °C for two hours. When -toluenesulfonic acid solution was used, the incubation time was for 30 minutes. After incubation samples were rinsed by deonized water, vaccum dried for 24 h, and reweighed to determine weight loss using the following equation:

$$\text{Weight loss (\%)} = (W_o\text{-}W_t)/W_o \text{ X } 100\%$$

Where W_o and W_t are the dry weight of the sample before and after degradation, respectively.

Publication Date (Web): June 18, 2015 | doi: 10.1021/bk-2015-1192.ch003

Results and Discussion

Synthesis of α,ω-Telechelic poly(ε-caprolactone) Diol (HOPCLOH)

Synthesis of PCL diol by biocatalysis with immobilized *Yarrowia lipolytica* lipase (YLL) was performed in the presence of diethylene glycol (DEG) as initiator/chain-transfer agent (Figure 1). Bulk polymerization of ε-CL was carried out at 120 °C for 6 h. ε-CL was quantitatively incorporated into the polymer chains and 100% ε-CL conversion was achieved. Analysis of molecular weight distribution curve of final polymers obtained by GPC revealed that unimodal distribution was present. In Table 1 we report the molecular weights. The ^{1}H-NMR spectrum analysis showed the existence of three different chemical species: those formed by bisubstitution of DEG with PCL, those formed by monosubstitution of DEG with PCL and unreacted DEG. These species are also obtained when organometallic catalyst is used for ring-opening polymerization of ε-CL (*8*). In the last column of Table 1, we report the percentage of HAPCLOH present in our sample (8%). This means that some additional water molecules are present in the reaction, and they can come from lipase, DEG, ε-CL, and/or humidity present in the air.

Chemical Synthesis of Polyester-Urethane with Aminoacids

An oligomer with reactive hydroxyl end groups was used as precursor of polyester-urethanes. Polyurethanes with reactive end groups were treated with α-amino acids under mild conditions (Figure 2). Typically, DEG1 and HDI were reacted with a molar ratio of 1:1, respectively, in the presence of tin (II) 2-ethylhexanoate [$Sn(Oct)_2$] as catalyst in 1,2-dichloroethane as solvent at 80 °C for 1 h and 30 minutes; after that time, 0.35 mmoles of aminoacid and 1.05 mmole of triethylamine were added to the reaction mixture and allowed 5 hours for reaction. Condensation reactions between polymer end-groups and reactive groups of α-aminoacid occurs, leading to the formation of a polymer with complex morphology.

In Green Polymer Chemistry: Biobased Materials and Biocatalysis; Smith, et al.;
ACS Symposium Series; American Chemical Society: Washington, DC, 2015.

Publication Date (Web): June 18, 2015 | doi: 10.1021/bk-2015-1192.ch003

Table 1. Molecular Weight, Percent of Bisubstitution, Monosubstitution and α-Hydroxyl-ω-(carboxylic acid) poly(ε-caprolactone) (HAPCLOH) in the Synthesized PCL-Diol

PCLdiol	*Mn (GPC)*	*MW/Mn (GPC)*	*Mn (MALDI)*	*Mn (^{1}H-NMR)*	*%Mono (OH)*	*%Bi (OH)*	*HAPCLOH (%)*
DEG1	4321	1.181	1363	836	34	66	8

Publication Date (Web): June 18, 2015 | doi: 10.1021/bk-2015-1192.ch003

Table 2. Solubilities for the Synthesized Polyester-Urethanes at Room Temperature

PUR	*THF*	*Chloroform*	*1,2-dichloroethane*	*Toluene*	*DMSO*	*Acetone*	*Ethyl acetate*
DEG1 HDI	*	+	*	/	/	/	-
DEG1 L-Hist HDI	/	+ after 24 hrs	/	/	/	/	/
DEG1 L-Orn HDI	*	+	/	/	/	/	/
DEG1 L-Cys HDI	/	*	/	/	-	/	/
DEG1 L-Lys HDI	+ after 24 hrs	+	*	/	-	/	/

(*) partially soluble, some gel; (+) soluble, (-) insoluble, (/) insoluble, it swells.

Publication Date (Web): June 18, 2015 | doi: 10.1021/bk-2015-1192.ch003

After casting from the reaction solution and drying, the resulting polymeric films were in general very insoluble in the solvents tested (see Table 2). Only DEG1HDI, DEG1 L-Orn HDI, and DEG1 L-Lys HDI were soluble at room temperature in chloroform; DEG1 L-Hist HDI was soluble in chloroform after 24 hrs. In THF DEG1HDI and DEG1 l-Orn HDI were partially soluble, a gel was formed during reaction, probably due to cross-linking reactions through allophanate groups (reaction of isocyanate with urethane groups). This particular case was seen when DEG1 L-Cys HDI was dissolved in chloroform; DEG1 HDI and when DEG1 L-Lys HDI were dissolved in 1,2-dichloroethane.

Final polyurethanes containing aminoacids were analyzed by FT-IR spectroscopy (Figure 3). In the case of α,ω-telechelic poly(ε-caprolactone) diol (DEG1) a single band of carbonyl stretching vibrations at 1722 cm^{-1} corresponding to ester group [-(C=O)-O-] was observed in the FTIR spectrum. For the polyurethanes, two pairs of bands could be seen: (1) the first assigned to urethane group at 1627 cm^{-1} and 1535 cm^{-1} due to carbonyl C=O stretching vibration and N-H stretching vibration, respectively (Amide I), and (2) the second pair corrresponding to amide II 1618 cm^{-1} and 1532 cm^{-1}.

The IR peak pattern in polyester-urethanes with amino acids tends to broaden, probably because of amido acid-urethane interactions through hydrogen bonding. Other important vibrations present in the spectrum are: N-H stretching and CH_2 symmetrical stretching at 3344 cm^{-1}, 2938 cm^{-1} and 2865 cm^{-1}, respectively. Similar peak patterns were observed in all analyzed polyester-urethanes samples.

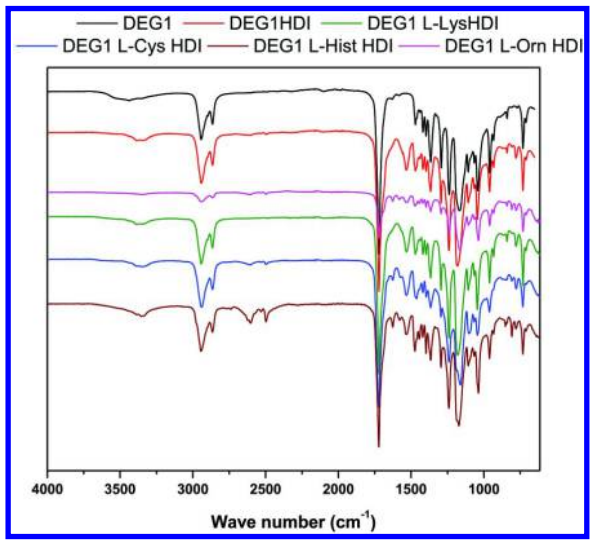

Figure 3. FT-IR spectra of the synthesized polyester-urethanes.

Solid-state NMR spectra of polyurethanes DEG1HDI and DEG1 L-LysHDI are shown in Figure 4. Assigments were made based on the chemical shifts observed in solution for a similar polyurethane (*9*). The same peak pattern is observed in both spectra. However, some differences in peak shapes are evident:

In Green Polymer Chemistry: Biobased Materials and Biocatalysis; Smith, et al.;
ACS Symposium Series; American Chemical Society: Washington, DC, 2015.

carboxyl peak is broader for DEG1HDI sample, whereas peaks adscribed to PCL component are narrower. Also, peaks for carbons *c* and *d* of PCL component are well resolved in the DEG1HDI spectrum. These differences indicate that the presence of L-lysine induce the formation of different types of phases, not present in the PUR sample without aminoacid.

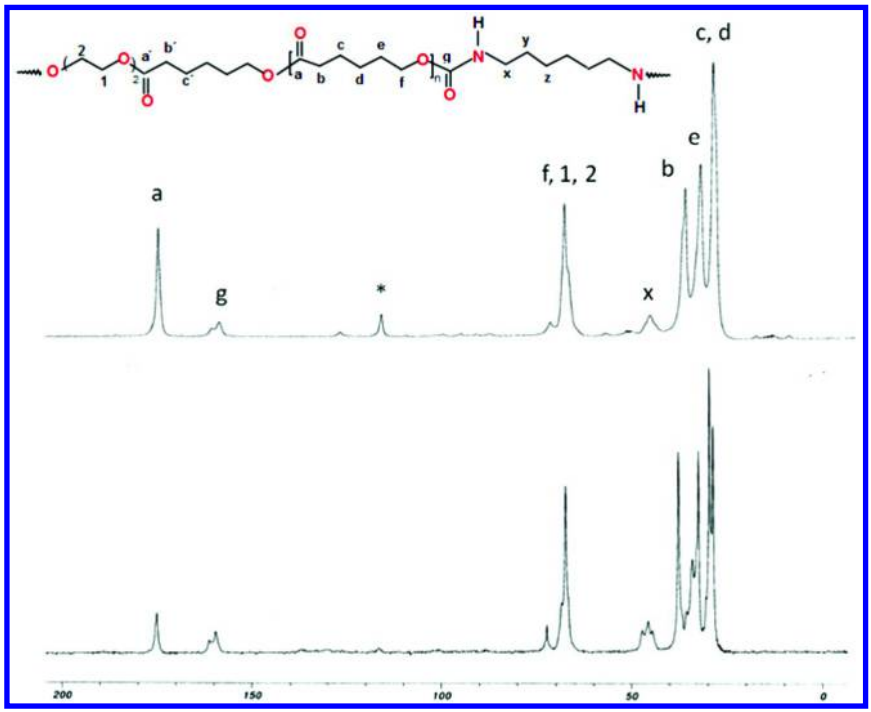

*Figure 4. Solid state CP-MAS ^{13}C NMR(100.6 MHz) spectra: top PURDEG1 L-LysHDI, bottom PURDEG1HDI, * = spinning sideband.*

In Table 3, the mechanical properties of the prepared polyester-urethanes are listed. Strain-stress curves are shown in Figure 5. Two different behaviors were found due to crystallinity of polymer samples. On one side, DEG1HDI and DEG1 L-Hist behaved as elastomers, with a low modulus and increasing growth of stress with strain until chains aligned and reached their maximum extension before breaking. At very high extension, above 400%, whitening of the neck zone is observed. This behavior could be due to strain-induced crystallization, similar to that observed for natural rubber, where an increment in the slope of the curve in the final part is observed. After rupture, polymer recovered almost completely its initial shape. On the other side, semicrystalline polymers (DEG1 L-Orn HDI, DEG1 L-Cys HDI and DEG1 L-Lys HDI) behaved as tough plastics. After a very stepped stress growth at low strain, they went through a yielding point. At this point, it could visually be observed the formation of a neck on the narrow part of the test specimen.

In Green Polymer Chemistry: Biobased Materials and Biocatalysis; Smith, et al.;
ACS Symposium Series; American Chemical Society: Washington, DC, 2015.

Publication Date (Web): June 18, 2015 | doi: 10.1021/bk-2015-1192.ch003

Publication Date (Web): June 18, 2015 | doi: 10.1021/bk-2015-1192.ch003

Table 3. Mechanical Properties of the Synthesized Polyester-Urethanes Obtained from PCL-Diol, Amino-Acids and HDI

PUR	*Strain at yield (MPa)*	*Stress at break (MPa)*	*Strain at break (%)*	*Modulus (MPa)*	*Hard segment (%)*	*Soft segment (%)*
DEG1HDI	60±8	45±6	1430±130	11±2	24	76
DEG1 L-ORN HDI	4.0±0.5	6.8±0.3	27±5	93±11	39	61
DEG1 L-CYS HDI	3.9±0.3	7.0±0.4	62±54	53±8	38	62
DEG1 L-HIST HDI	12.0±1.1	21±3	1750±170	23±1	45	55
DEG1 L-LYS HDI	4.0±0.5	7.0±0.6	820±150	66±4	46	54

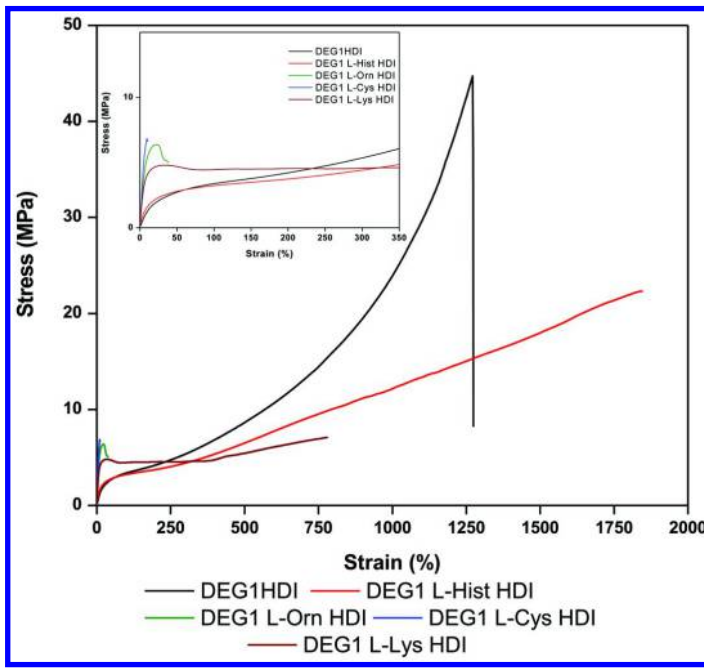

Figure 5. Stress-strain graph of the synthesized polyester-urethanes.

The modulus increased when the hard segment (HS) increased, compared with the PUR without amino acid. The modulus increased and the strain at break decreased when the HS content on the polymer increased. Polymer with lowest HS content (DEG1 L-Cys HDI) showed a slightly higher value for the modulus and smaller values for strain at break than those expected by the content of crystalline PCL present in this polymer.

In Green Polymer Chemistry: Biobased Materials and Biocatalysis; Smith, et al.;
ACS Symposium Series; American Chemical Society: Washington, DC, 2015.

Thermal properties for polyester-urethanes were registered from 25 to 80 °C followed by cooling and reheating from -90 to 80 °C. In Table 4, the results from DSC measurements are listed. In the first heating (25-80°C), DEG1 HDI and DEG1 L-Cys HDI showed a flat baseline, whereas DEG1 L-Hist HDI, DEG1 L-Orn HDI and DEG1 L-Lys HDI displayed a transition due to pure PCL phase melting (Figure 6).

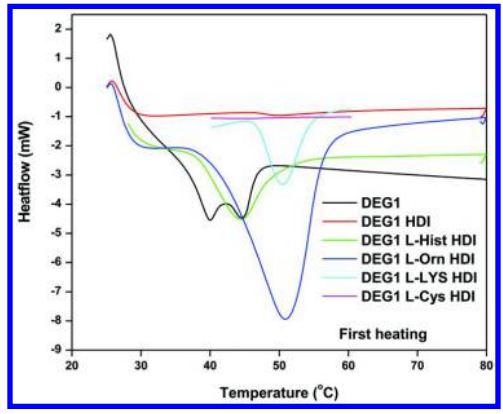

Figure 6. First heating DSC curves of the synthesized polyester-urethanes.

In the second heating (Figure 7), crystallinity decreased for DEG1 L-Hist HDI, DEG1 L-Orn HDI and DEG1 L-Lys HDI samples. For DEG1 HDI and DEG1 L-Cys HDI only a marginal crystallinity was recovered. This reduction on crystallinity could be due to the mixing of pure PCL phase and mixed PCL-hard segment phase or to the slow recrystallization rate of pure PCL phase, or both.

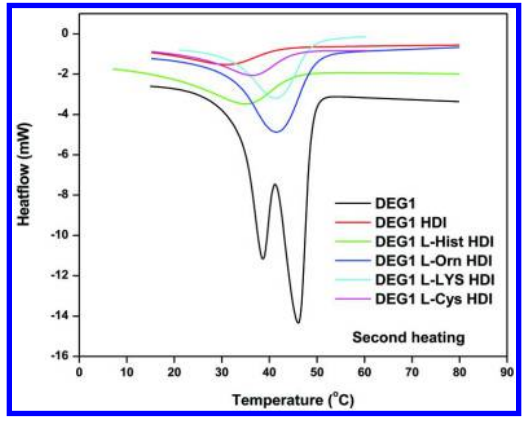

Figure 7. Second heating DSC curves of the synthesized polyester-urethanes.

In Green Polymer Chemistry: Biobased Materials and Biocatalysis; Smith, et al.;
ACS Symposium Series; American Chemical Society: Washington, DC, 2015.

Publication Date (Web): June 18, 2015 | doi: 10.1021/bk-2015-1192.ch003

Table 4. Thermal Properties of the Synthesized Polyester-Urethanes Obtained from PCL-Diol, Amino-Acids and HDI Obtained by DSC

Sample	*T_m (°C) First heating*	*ΔH_m (J/mol) First heating*	*T_m (°C) Second heating*	*ΔH_m (J/mol) Second heating*	*T_c (°C)*
DEG1	40.0	14.3	46.1	75.8	13.0
DEG1HDI	31.0	31.5	30.8	23.8	-25.1
DEG1 L-ORN HDI	44.4	48.6	34.9	35.2	-21.10
DEG1 L-CYS HDI	-	-	36.3	29.1	-17.3
DEG1 L-HIST HDI	51.0	29.3	41.5	25.2	-6.1
DEG1 L-LYS HDI	50.6	9.7	41.4	32.8	-2.5

Publication Date (Web): June 18, 2015 | doi: 10.1021/bk-2015-1192.ch003

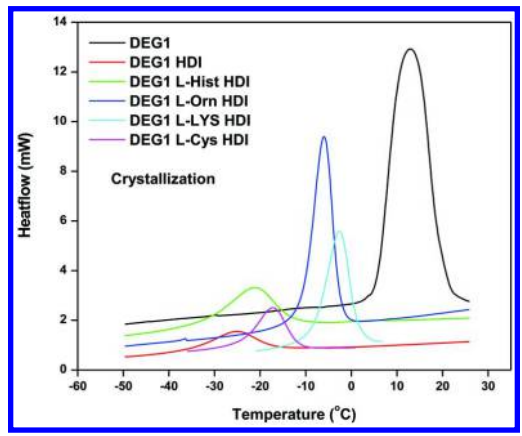

Figure 8. Crystallization DSC curves of the synthesized polyester-urethanes.

Figure 8 shows the crystallization patterns (from 80 to -90 °C) of all the synthesized polyester-utethanes. In the first heating (25-80°C), DEG1 HDI and DEG1 L-Cys HDI showed a flat baseline, after this heating all the samples presented crystallization of PCL.

In Green Polymer Chemistry: Biobased Materials and Biocatalysis; Smith, et al.;
ACS Symposium Series; American Chemical Society: Washington, DC, 2015.

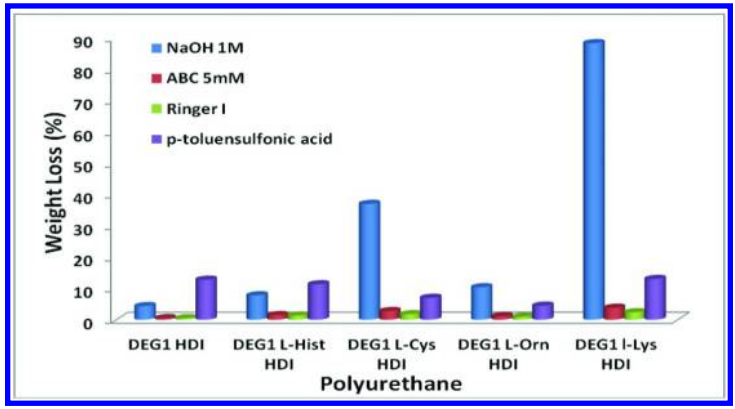

Figure 9. Hydrolytic degradation results of the PURs at 90 °C.

Publication Date (Web): June 18, 2015 | doi: 10.1021/bk-2015-1192.ch003

Figure 9 shows the hydrolytic degradation behavior of the PURs at 90°C. For DEG1 L-Lys HDI, DEG1 L-Orn HDI and DEG1 L-Cys HDI the degradation is faster in NaOH solution. This is due to the volume expansion of PUR at higher temperatures so alkaline water molecules could diffuse more easily into de PUR. However, DEG1 L-Hist HDI and DEG1HDI samples were more susceptible to hydrolysis under acidic conditions. This is probably due to the higher rate of proton exchange in an acid environment for this samples.

Conclusion

A series of biodegradable, non-toxic polyester-urethanes were synthesized from well characterized polycaprolactone diol, L-lysine ethyl ester dihydrochloride, L-cysteine hydrochloride, L-histidine monohydrochloride monohydrate and L-ornithine hydrochloride. Pure PCL crystallinity strongly affected the mechanical properties and the water absorption behavior. Amorphous polymers were elastomeric, with shape recovery after rupture, whereas semicrystalline polymers behave as tough plastics, with a yielding point, and with higher modulus at higher hard segment content. The polyester-urethanes described in this work are materials of good processability and good mechanical properties with a potential use as biodegradable materials for applications requiring long degradations times.

Acknowledgments

Financial support by Consejo Nacional de Ciencia y Tecnología (CONACyT) Grant 153922 and 196921 are acknowledged. We also thank Laboratorio Nacional UG-CONACYT for performing solid-state NMR measurements.

References

1. Loh, X. J.; Colin Sng, K. B.; Li, J. *Biomaterials* **2008**, *29*, 3185–3194.
2. Tsou, C-H.; Lee, H-T.; Tsai, H-A.; Cheng, H-J.; Suen, M-Ch. *Polym. Degrad. Stab.* **2013**, *98*, 643–650.
3. Báez, J. E.; Marcos-Fernández, A.; Lebrón-Aguilar, R.; Martínez-Richa, A. *Polymer* **2006**, *47*, 8420–8429.
4. Yanagishita, Y.; Kato, M.; Toshima, K.; Matsumura, S. *ChemSusChem* **2008**, *1*, 133–142.
5. Brígida, A. I. S.; Amaral, P. F. F.; Coelho, M. A. Z.; Gonçalves, L. R. B. *J. Mol. Catal. B: Enzym.* **2014**, *101*, 149–158.
6. Barrera-Rivera, K. A.; Marcos-Fernández, A.; Martínez-Richa, A. In *Green Polymer Chemistry: Biocatalysis and Biomaterials*; Cheng, H. N.; Gross, R. A., Eds.; ACS Symposium Series 1043; American Chemical Society: Washington DC, 2010; Vol. 1, pp 227−235.
7. Barrera-Rivera, K. A.; Flores-Carreón, A.; Martínez-Richa, A. *Lipases and Phospholipases: Methods and Applications*; Sandoval G., Ed.; Humana Press: New York, 2012; Vol. 861, pp. 485−493.
8. Marcos-Fernández, A.; Abraham, G. A.; Valentín, J. L.; San Román, J. *Polymer* **2006**, *47*, 785–798.
9. Barrera-Rivera, K. A.; Peponi, L.; Marcos-Fernández, A.; Kenny, J. M.; Martínez-Richa, A. *Polym. Degrad. Stab.* **2014**, *108*, 188–194.

Publication Date (Web): June 18, 2015 | doi: 10.1021/bk-2015-1192.ch003

Publication Date (Web): June 18, 2015 | doi: 10.1021/bk-2015-1192.ch004

Chapter 4

Chemo-enzymatic Synthesis, Derivatizations, and Polymerizations of Renewable Phenolic Monomers Derived from Ferulic Acid and Biobased Polyols: An Access to Sustainable Copolyesters, Poly(ester-urethane)s, and Poly(ester-alkenamer)s

Florian Pion,[1,2] Armando Félix Reano,[1,2,3] Mouandhoime Zahahe Oulame,[1,2] Imane Barbara,[3] Amandine Léa Flourat,[1,2,3] Paul-Henri Ducrot,[1,2] and Florent Allais[*,1,2,3,4,5]

[1]AgroParisTech, UMR 1318 IJPB, Route de Saint-Cyr, F-78026 Versailles, France
[2]INRA, UMR 1318 IJPB, Route de Saint-Cyr, F-78026 Versailles, France
[3]AgroParisTech, Chaire Agro-Biotechnologies Industrielles (ABI), 247 rue Paul Vaillant Couturier, F-51100 Reims, France
[4]AgroParisTech, UMR 782 GMPA, Avenue Lucien Brétignières, F-78850 Thiverval-Grignon, France
[5]INRA, UMR 782 GMPA, Avenue Lucien Brétignières, F-78850 Thiverval-Grignon, France
[*]E-mail: florent.allais@agroparistech.fr.

The synthesis of monomers as well as polymers from plant fats, oils, and sugars has already found some industrial application and recent developments in this field offer promising new opportunities. In this field, many bio-based aliphatic polymers, exhibiting smooth biodegradability, have been developed. Nevertheless, the applications of these polymers are limited because of their poor thermal properties and durability. In order to alleviate these drawbacks, introduction of aromatic subunits is an efficient method for improving the performances of this type of materials. Nevertheless, many key commercial aromatics are derived from petrochemical feedstocks.

In Green Polymer Chemistry: Biobased Materials and Biocatalysis; Smith, et al.; ACS Symposium Series; American Chemical Society: Washington, DC, 2015.

Therefore, most recently, much focus has been placed on bio-based aromatic compounds to replace monomers and polymers such as bisphenol A, styrene, methylene diisocyanate, phenol resins, aromatic polyesters. In this context, we put a great deal of effort into developing new aromatic chemical platforms from ferulic acid, a natural *p*-hydroxycinnamic acid found in lignocellulose. Obtained through a chemo-enzymatic synthetic process, these phenolic platforms have been used as A_2-type monomers for the preparation of renewable aliphatic-aromatic copolyesters and poly(ester-urethane)s, and as precursors for the synthesis of α,ω-dienes monomers leading to poly(ester-alkenamer)s. The structure and thermal properties of these novel bio-based polymers deriving from ferulic acid were studied in order to evaluate their potential in industrial applications.

Publication Date (Web): June 18, 2015 | doi: 10.1021/bk-2015-1192.ch004

Introduction

Nowadays in industrial chemical processes, whatever the specialties (e.g., drugs, polymers, materials), use of renewable molecules derived from biomass and development of eco-friendly processes are probably two of the greatest challenges that scientists have to face. To be competitive, bio-based products must exhibit functionalities at least equivalent to those of the petroleum-based products. Thus, research should not be limited to pure and simple substitution of existing products, but they must also propose innovative molecules and materials with new valued-added features.

Many research programs on new bio-based monomers/additives and polymers are already investigated in large public and private research institutions (*1*). They all aim at producing innovative and eco-friendly biomaterials from renewable raw plant materials or biorefineries by-products. Especially plant derived fats and oils bear a great potential for the substitution of currently used petrochemicals, since monomers, fine chemicals and polymers can be derived from these resources in a straightforward fashion. The synthesis of monomers as well as polymers from plant fats, oils and sugars has already found some industrial application and recent developments in this field offer promising new opportunities (*2–5*). More recently, scientists got interested in the use of a new bio-based industrial platform using microalgae as raw material for the sustainable production and recovery of hydrocarbons and (exo)polysaccharides, and their further conversion to renewable polymers (*6*). In this field, many bio-based aliphatic polyesters have been developed (*7–10*). Made of bio-based raw materials and exhibiting smooth biodegradability, these structures received important attention. However, despite these attractive points, bio-based aliphatic polyesters applications are limited because of their poor thermal properties and durability. In order to alleviate these drawbacks, introduction of aromatic subunits into a thermoplastic polyester backbone is an efficient method for intrinsically improving the performances of

In Green Polymer Chemistry: Biobased Materials and Biocatalysis; Smith, et al.;
ACS Symposium Series; American Chemical Society: Washington, DC, 2015.

this type of materials (*11*, *12*). Nevertheless, many key commercial chemicals are based on aromatic structures, ultimately derived from petrochemical feedstocks (*13*). Therefore, most recently, much focus has been placed on bio-based aromatic compounds to replace monomers and polymers such as phenol, bisphenol A, styrene, methylene diisocyanate, phenol resins, aromatic polyesters and their biocomposites (*14*). Some literature reports described some very interesting works based on natural flavonoids (*15*) or cardanol (*16*), but these resources are available in limited quantities. On the other hand, the lignocellulosic biomass represents more than 30% of non-fossil-carbon on earth. Lignin is a unique aromatic raw material (phenolics) and the only durable alternative to substitute oil-based aromatic compounds (*17*). Lignins are mainly available as byproduct of pulp and paper industry, the quality and the chemical structure of these so-obtained lignins highly depend on the processes used for the separation of the different plant biopolymers. Nowadays, Kraft process, used in paper industry, represents the major process for lignin production. However, the resulting lignin derivatives incorporate a significant amount of sulphur salts and are quite difficult to use as starting material for polymer chemistry. On the other hand, the development of second generation biofuels will readily provide new types of industrial lignins that could prove themselves as renewable sources of phenolic molecules for polymer and material chemistry. Lignins are formed through oxidative polymerization of three *p*hydroxycinnamic alcohols (aka monolignols) exhibiting different substitution patterns (*p*-coumaryl, coniferyl and sinapyl alcohols) (*18*). Even if depolymerization of lignin (*19*) is an alluring route to give access to bio-based aromatics needed by chemical industry, this route remains perfectible.

Meanwhile, another approach consisting on the preparation of new bio-based materials using monomeric phenolics originating from this biomass appears to be a more viable and relevant alternative. In this context, ferulic acid, one of the most abundant cinnamic acid in lignocellulose, present in relatively large quantities in beetroot pulp as well as rice and wheat bran, has been identified as a promising bio-based platform molecule for the preparation of innovative polymers and materials (*20*, *21*). Its production at industrial scale from these biorefineries and food industries byproducts is being investigated. According to the best estimates, prices could be as low as $3 per kg, which puts it at a reasonable price for a monomer. It is noteworthy that ferulic acid can also be readily synthesized from vanillin, a phenolic compound industrially produced from lignins (sale price ca. $6-15 per kg), but this requires extra synthetic/purifications step leading to higher production cost.

Many research groups have recently demonstrated the great potential of ferulic acid-derived AB-type monomers through the development of new homopolyesters exhibiting appealing thermal properties through either metal-catalyzed polycondensation (*22–25*), oxalyl- (*26*) or thionyl-chloride- (*27*) activated polycondensations. Other homo- and copolyesters of natural *p*-hydroxycinnamic acids showing remarkable liquid–crystal (*28–35*), biodegradability (*36*, *37*) or biocompatibility (*30*) properties were also reported. However, they are often hard to process because of a too high melting temperature (T_m). To lower the T_m, *p*-hydroxycinnamic acids were copolymerized with aliphatic monomer to increase the structural flexibility of the resulting polymers (*38–40*). Another

In Green Polymer Chemistry: Biobased Materials and Biocatalysis; Smith, et al.;
ACS Symposium Series; American Chemical Society: Washington, DC, 2015.

Publication Date (Web): June 18, 2015 | doi: 10.1021/bk-2015-1192.ch004

approach, recently applied for the synthesis of bisphenols from vanillin (*41*), is to prepare A_2-type bisphenols from these *p*-hydroxycinnamic acids and aliphatic moieties then polymerize them with B_2-type monomers for the preparation of alternating copolymers.

Having developed expertise in lignin related phenol compounds chemistry (*42–47*), we recently put a great deal of effort into developing new valorizations of ferulic acid. In this context, we first devised and designed a new class of bio-based polyfunctional molecules incorporating ferulic acid moieties through the development of an enzymatic process involving polystyrene supported *Candida antarctica* lipase B (aka CAL-B or Novozyme®435) (*48*). This strategy allowed the incorporation of both aromatic and aliphatic segments into renewable A_2-type bisphenolic structures to be used as monomers in various types of polymerization systems. With these new bisphenols in hand, we then studied their copolymerization with activated biobased diacids and characterized the thermomechanical properties of the resulting aliphatic-aromatic copolyesters (*49*). In parallel, these bisphenols were also reacted with two of the most widely used isocyanates (*50*) to provide poly(ester-urethane)s (aka PEUs) with aromatic urethane bonding structures. Such polymers are known to exhibit high thermal degradation and mechanical properties and are expected to be good candidates as protective coatings (*51*). Finally, bisphenols have been used as precursors for the synthesis of novel α,ω-dienes monomers which were then submitted to ADMET polymerization. The structure and thermal properties of the novel poly(ester-alkenamer)s obtained through this method were studied in order to evaluate their potential in industrial applications (*52*).

Publication Date (Web): June 18, 2015 | doi: 10.1021/bk-2015-1192.ch004

Experimental

Materials and Methods

All reagents and *Candida antarctica* lipase B immobilized on Immobeads (Ref: L4777-10G, recombinant, expressed from *Aspergillus niger*, ≥5000 propyl laurate units.g^{-1}, batch numbers: 071M1351 and SLBB9500) were purchased from Aldrich Chemical Co. and were used as received. Dichloromethane was distilled under argon over CaH_2. *o*-dichlorobenzene was distilled over $CaCl_2$ under vacuum and stored under argon prior to use. Dimethylformamide (DMF) was dried using a mBraun Solvent System. Compounds were purified on a Puriflash 430 purchased from Interchim, using Si-OH phase columns. Melting points were measured with a Büchi 510. Melting points were measured with a Büchi 510. ^{1}H and ^{13}C NMR spectra have been recorded at 400.16 and 100.62 MHz, respectively, to check compounds structure and purity. The most representative NMR data have been reported in previous publications (*48–50*, *52*) Thermo-Gravimetric analyses (TGA) were recorded using a Q-500 from TA. The samples were dried in a vacuum-oven at 50 °C for 18 h prior to analysis. About 5-10 mg of each sample were heated from 25 to 600 °C at 10 °C.min^{-1} under inert atmosphere (nitrogen). Differential Scanning Calorimetry (DSC) analyses were performed under inert atmosphere on a DSC 6000 from Perkin Elmer. About

5-10 mg of each sample were weighted in an open pan that went to heat/cool/heat cycle at 10 °C.min^{-1}; data are given from the second heating scan. Size exclusion chromatography (SEC) were performed:

- for bis/trisphenols, polyesters and poly(ester-urethane)s: in chloroform (flow rate 1 mL.min^{-1}) with a HPLC system equipped with a Gilson 305 pump, an UltiMate 3000 Autosampler from Dionex, a Mixed-B column (600 mm x 7.5 mm, 10 µm) from PL calibrated with polystyrene standards (400-2,000,000 Da purchased from Aldrich Chemical) at 25 °C, using UV detection at 254 nm with an Ultimate 3000 PDA from Dionex. Results were calculated with Cirrus GPC 3.0.
- for poly(ester-alkenamer)s: in THF (flow rate 1 mL.min^{-1}) with an Infinity 1260 system, Agilent Technologies with a quadruple detection (IR, UV, LS, viscosimetry) and two PL-Gel 5mm Mixed D column (300 mm × 7.5 mm) with polystyrene standards (400-2,000,000 Da purchased from Aldrich Chemical Co) at 40 °C.

Publication Date (Web): June 18, 2015 | doi: 10.1021/bk-2015-1192.ch004

Preparation of Ethyl Dihydroferulate (2)

Ferulic acid (**1**) (250 g, 1.29 mol, 1 eq) was dissolved in ethanol (900 mL, 250 g.L^{-1}) in presence of few drops of concentrated hydrochloric acid and heated at reflux for 2 days. The reaction mixture was then cooled to RT and put under argon before adding Pd/C 10%w (4.5 g, 5%w). Mixture was stirred 18 h at RT under H_2 flow and the reaction monitored by TLC until complete conversion of the starting material. The solution was filtered on Celite and the solvent was removed under vacuum and the resulting crude product was filtrated over a pad of celite and silica gel to afford **2** as a white powder (277 g, 96%, m.p. 42 °C).

*Enzymatic Preparation in Bulk of Bis-O-dihydroferuloyl Isosorbide (**IDF**)*

Isosorbide (1 eq) and **2** (3 eq) were melted and magnetically stirred at 75 °C before adding CAL-B (10% by weight relative to the total weight of isosorbide and **2**). The reaction mixture was kept under reduced pressure for 3 days. The reaction mixture was then dissolved in ethyl acetate (or acetone) and filtered to remove CAL-B beads. The solvent was then evaporated under vacuum and the crude product was purified by flash chromatography on silica gel eluted with cyclohexane:AcOEt 70:30 until affording unreacted **2**, then 45:55 to provide *bis*-O-*dihydroferuloyl isosorbide* (85%, **IDF**).

Synthesis of Acrylates Monomers

Bisphenol (1 eq) was dissolved in anhydrous dichloromethane (C = 0.5 M) and the solution was put under argon prior to adding triethylamine (2.2 eq). The reaction mixture was cooled to 0 °C and acryloyl chloride (2.2 eq) was added

dropwise. Temperature was allowed to rise to room temperature, and the reaction was stirred for an extra 18 h before being washed with water. The organic layer was dried over $MgSO_4$, filtered and then concentrated under vacuum and the crude product was purified by flash chromatography on silica gel eluted with cyclohexane:AcOEt 75:25 to afford the desired bisacrylate as a colorless oil.

Synthesis of α,ω-Diene Monomers

Bisphenol (1 equiv) and K_2CO_3 (3 equiv) were dissolved in dry DMF (C = 2.5 M) under nitrogen. Bromo-alkene (2.5 equiv) was then added, and the mixture was stirred and heated at 80 °C for 12 h. Reaction was quenched with water (v(H_2O) = v(DMF)) and the aqueous layer was extracted three times with ethyl acetate (3 x v(H_2O)). Organic layers were combined, washed with brine, dried over anhydrous $MgSO_4$, filtered and concentrated. Crude product was purified by flash chromatography on silica gel Cyclohexane:AcOEt 75:25 to yield the corresponding α,ω-diene monomer.

General Procedure for Polycondensations/Polymerizations

Bulk Polymerization for Polyesters

In a round-bottom flask under argon were successively added bisphenol (1 eq.) and diacyl chloride (succinic or azelaic) (1 eq.). The reaction mixture was magnetically stirred under argon and heated (100-180 °C) for the given time. The resulting polymer was dissolved in chloroform, precipitated in cold methanol and recovered by filtration.

General Procedures for Polyurethanes Preparation

In a round-bottom flask under argon were successively added bisphenol (1 eq), solvent ($CHCl_3$, MEK, MIBK or 1,4-dioxane) and diisocyanate (HDI or TDI) (1 eq). The reaction mixture was magnetically stirred under argon and heated (100-140 °C) for the given time. The resulting polymer was precipitated in cold methanol and recovered by filtration.

ADMET in Mass Polymerization

α,ω-diene monomer (1 eq.) and *p*-benzoquinone (2 eq. relative to Hoveyda-Grubbs II catalyst) were stirred at 80 °C, under vacuum for 5 min. Hoveyda-Grubbs II catalyst (1-10 mol%) was added and the reaction was continued, under vacuum, for 4 h. Reaction was quenched with 1 mL of THF and 4 drops of vinyl ethyl ether. Product was concentrated and a sample was taken for GPC analyses. The remainder was dissolved in THF (1 mL) and precipitated in cold methanol (10 mL).

Publication Date (Web): June 18, 2015 | doi: 10.1021/bk-2015-1192.ch004

In Green Polymer Chemistry: Biobased Materials and Biocatalysis; Smith, et al.;
ACS Symposium Series; American Chemical Society: Washington, DC, 2015.

Publication Date (Web): June 18, 2015 | doi: 10.1021/bk-2015-1192.ch004

Results and Discussion

Chemo-enzymatic Synthesis of a New Class of Renewable Polyphenols from Ferulic Acid

The chemical esterification of *p*-hydroxycinnamic acids with alcohols is difficult due to heat sensitivity and to the susceptibility of oxidation of phenolic acids in alkaline media. Furthermore, chemical reactions are unselective, resulting in unwanted side reactions and byproducts that need to be removed by purification steps generating extra wastes to dispose of. On the other hand, the lipase-mediated enzymatic synthesis offers many advantages: milder reaction conditions, minimization of side reactions and byproducts, a selective specificity, fewer intermediary and purification steps, and a more environmentally friendly process (lower energy consumption and waste materials production).

Efforts were rapidly turned to the use of *Candida antarctica* lipase B supported on lmmobead 150 (aka CAL-B), a promising biocatalyst for polyol esterification. Lipases are indeed becoming increasingly attractive in the pharmaceutical, cosmetic and oil industry due to their chemical and thermal stability in either aqueous or non-aqueous solvents and their high substrate selectivities. They are also known for giving high yield transformations (*53–55*), and have been used to produce renewable and biodegradable polyesters such as PLA (*56*, *57*). Moreover immobilized biocatalysts offer, from an industrial point of view, ease of handling, easy recovery and recycling (*58*, *59*). However, lipase-mediated direct esterification of *p*-hydroxycinnamic acids (*60–70*) with alcohols generally suffers from long reaction time and/or low yields. To improve the efficiency of this reaction, one can either reduce the conjugated unsaturation (*via* catalytic hydrogenation) (*65*, *70–75*), use alkyl *p*-hydroxycinnamates (e.g., ethyl, *n*-octyl) (*70*, *73*, *75–83*) or ionic liquids as solvents (*68*, *84*, *85*). Therefore, to warrant high yields transesterifications with the selected primary and/or secondary alcohols (i.e., ethylene glycol, 1,3-propanediol, 1,4-butanediol, isosorbide, and glycerol), the initial step of our synthetic approach was the production of ethyl dihydroferulate (**2**). Apart from its higher reactivity of lipase toward ferulic acid, **2** is a liquid at 75 °C under atmospheric pressure (reaction conditions) and can serve as a solvent when ferulic acid (**1**) is a solid and needs to be dissolved in organic solvents. As depicted in Scheme 1, **1** was subjected to a one-pot two-step process (Fischer esterification and palladium-catalyzed hydrogenation) allowing the formation of the desired ethyl dihydroferulate (**2**) in 96% yield.

With ethyl dihydroferulate in hands, the lipase-catalyzed transesterification of **2** with the chosen bio-based polyols was performed to produce the corresponding bis- and trisphenols (**3-7**) (Scheme 1). It is noteworthy that one of the main advantages of using CAL-B in this synthesis is its inactivity towards phenols. Indeed, no side-products originating from phenol esterification were ever observed. This remarkable selectivity renders unnecessary the protection of the phenols for the enzymatic transesterification step (atom economy). In addition, the lipase-catalyzed transesterification can be conducted either solvent-free under reduced pressure (ethanol removal) or in solvent with azeotropic removal of ethanol.

In Green Polymer Chemistry: Biobased Materials and Biocatalysis; Smith, et al.;
ACS Symposium Series; American Chemical Society: Washington, DC, 2015.

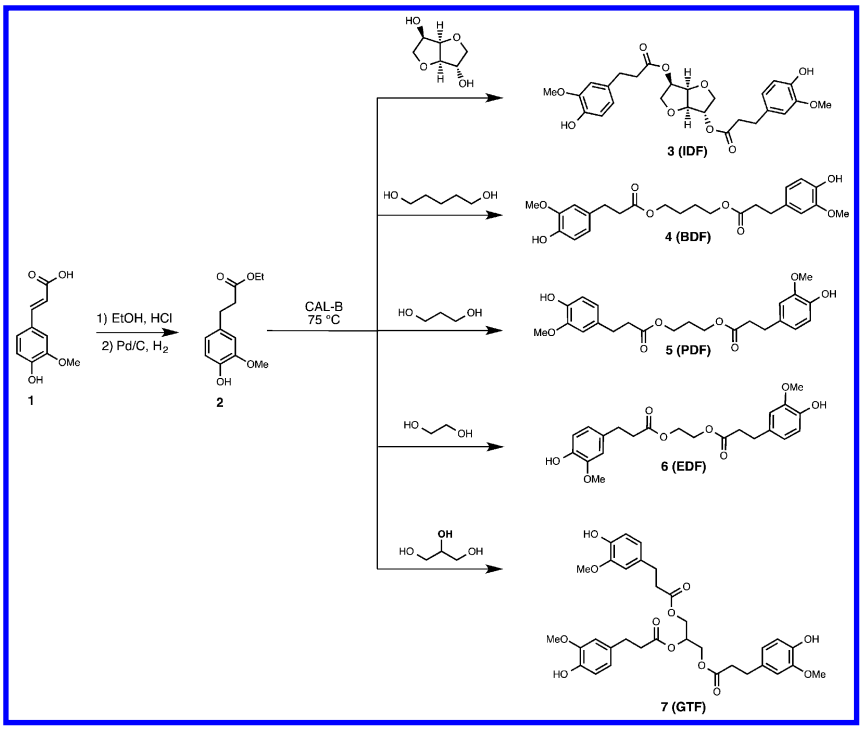

*Scheme 1. Lipase-Catalyzed Transesterification of **2** with Bio-based Polyols. (Adapted with permission from reference (48). Copyright 2013 The Royal Society of Chemistry)*

Isosorbide, readily obtained from corn (*86*) was first chosen for its robust bicyclic structure (*87*), potentially providing high thermal and mechanical properties to the resulting polymers (*88*, *89*). Classified by the US Food and Drugs Administration as a "generally recognized as safe" (aka GRAS) material (*90*), isosorbide was previously employed as a generic diol monomer in several polymer systems like polyester (*91–94*), polyether (*94*, *95*), polycarbonate (*94*, *96*) and polyurethane (*94*, *97*), among others. The synthesis of isosorbide-derived polyesters could be realized using activated diacid derivatives, Lewis acid catalysts or lipase-biocatalysis coupled with the removal of low mass condensation products. Moreover, when incorporated into polyesters, the ester link of isosorbide is easily degraded by esterases (*98*), enhancing the potential biodegradability of the materials. These promising features prompted us to investigate its association with ferulic acid to prepare macromonomers. Furthermore the influence of its bicyclic structure on the final properties of the resulting polymers was compared to those of aliphatic segments by using ethylene glycol, 1,3-propanediol and 1,4-butanediol three readily available bio-based diols that can be efficiently obtained via fermentation of sugars (*99–101*). By using these four diols, the impact of the aliphatic chain length on the physico-chemical properties of the

Publication Date (Web): June 18, 2015 | doi: 10.1021/bk-2015-1192.ch004

polymers will be investigated. Finally, glycerol, which is produced in large scale from bio-based triglycerides (plant oils) (*102*), was also employed to prepare a trisphenol macromonomer following a similar process.

In accordance with previously published works on lipase-catalyzed transesterifications (*103*), whatever the transesterification procedure, CAL-B load was systematically 10% by weight relative to the total weight of polyol and **2**. To warrant good reaction rates, avoid thermal deactivation of the lipase and decrease the media viscosity, the temperature was kept around 65-90 °C. It is noteworthy, that at the end of the reaction, both enzyme and unreacted ethyl dihydroferulate (**2**) were recovered by filtration and flash chromatography, respectively, and recycled.

Publication Date (Web): June 18, 2015 | doi: 10.1021/bk-2015-1192.ch004

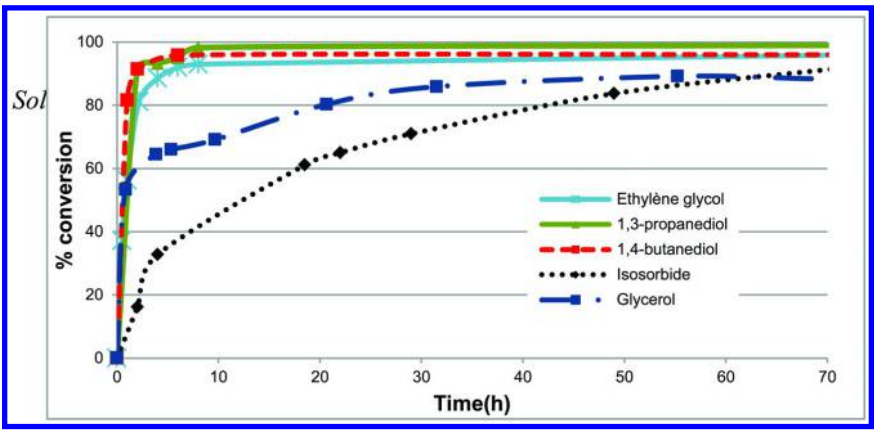

Figure 1. Kinetic studies of the lipase-mediated solvent-free transesterifications of 2 with (...) isosorbide; (---) 1,4-butanediol; (–) 1,3-propanediol; (-.-) glycerol. (Adapted with permission from reference (48). Copyright 2013 The Royal Society of Chemistry.)

Solvent-free conditions were first examined. Heating the reaction mixture (polyol, ethyl dihydroferulate (**2**) and CAL-B) at 75 °C under vacuum with continuous magnetic stirring resulted in the formation of bis- and trisphenols (**3**-**7**) in high yields. Desired products were easily separated from residual starting materials and byproducts (mainly non per-esterified compounds) by flash chromatography on silica gel or recrystallization (Yields of purified compounds are given in Table 1). In fixed conditions (ratio **2**/OH=1.5, 75 °C, 10% CAL-B by weight relative to the total weight of polyol and **2**), the key parameter controlling the yield is the reaction time. To reach optimal yields, conditions have to be optimized with respect to the polyol. Indeed, as depicted in Figure 1, 1,4-butanediol and 1,3-propanediol, which bear only primary hydroxyl groups, are very reactive and readily transesterify ethyl dihydroferulate (**2**). Kinetic studies revealed that maximal conversion is attained in 2-4 hours (Figure 1.b and 1.c). However, in the case of 1,4-butanediol, total conversation cannot be reached

In Green Polymer Chemistry: Biobased Materials and Biocatalysis; Smith, et al.;
ACS Symposium Series; American Chemical Society: Washington, DC, 2015.

even with longer reaction times (maximum yield 95%) due to the solidification of the reaction medium (**4**, m.p. = 108 °C). Isosorbide, which bears two secondary hydroxyl groups, is much less reactive and requires longer reaction time to reach maximal conversion (Figure 1.a). This decrease in reactivity, probably due to steric hindrance, was also observed for the transesterification of glycerol (Figure 1.d). To reach high yields in glycerol triesterification, longer reaction time is also required.

Enzymatic Transesterification under Azeotropic Distillation

The same transesterifications were also performed in hexanes using azeotropic distillation to push the equilibrium towards the desired products by removal of the ethanol formed. The reaction temperature was chosen to attain a steady reflux without heating the oil bath higher than 90 °C to prevent enzyme denaturation. Using this process, similar yields were obtained than in the solvent-free esterification but with slightly longer reaction times. These two processes allow the production of appreciable amounts (mainly the solvent-free process); indeed, 500 g batches can be easily run at lab-scale.

Publication Date (Web): June 18, 2015 | doi: 10.1021/bk-2015-1192.ch004

Table 1. Yields and Thermostability of the the Bis- and Trisphenols. (Adapted with permission from reference (*48*). Copyright 2013 The Royal Society of Chemistry.)

Entry	*Compound*	*Solvent-free*		*Azeotropy*		T_d*(5%)*[b] *(°C)*
		Time	*Yield*[a]	*Time*	*Yield*[a]	
1	**3** (Isosorbide)	48 h	60%	48 h	50%	285
2		72 h	85%	72 h	87%	
3		96 h	92%	144 h	98%	
4	**4** (1,4-Butanediol)	4 h	95%	6 h	95%	260
5	**5** (1,3-Propanediol)	4 h	92%	6 h	96%	303
6	**6** (Ethylene glycol)	4 h	88%	-	-	284
7		8 h	93%	-	-	
8	**7** (Glycerol)	48 h	75%	48 h	60%	298
9		72 h	92%	96 h	94%	

[a] Uncorrected yields after purification. [b] values determined by TGA under nitrogen at 10 °C.min^{-1}.

In Green Polymer Chemistry: Biobased Materials and Biocatalysis; Smith, et al.;
ACS Symposium Series; American Chemical Society: Washington, DC, 2015.

The resulting bio-based bis- and trisphenols (**3**-**7**) are all highly soluble in acetone, dichloromethane, chloroform, ethyl acetate, ethanol, tetrahydrofuran and dimethylformamide. So, all these solvents can be used for analyses or to conduct further reactions in homogenous organic media. The thermal stability of these four bis- and trisphenols (**3**-**7**) was characterized by TGA. Probably because of their aromatic nature, these new bio-based bis- and trisphenols are all stable above 250 °C (Table 1) and can therefore be used for high temperature-demanding applications.

Publication Date (Web): June 18, 2015 | doi: 10.1021/bk-2015-1192.ch004

Derivatization

Bis- and trisphenols were thereafter successfully converted into the corresponding acrylates and α,ω-dienes following single step processes in both cases by using halogenated electrophiles (Scheme 2). Bis- and trisphenols were reacted with acryloyl chloride (readily available from bio-based acrylic acid) (*104*) in presence of triethylamine and K_2CO_3 to prepare the corresponding acrylates. Etherification of bisphenols was first performed using the procedures previously reported by Meier et al. (*41*) (K_2CO_3, CH_3CN, TBAI, reflux, 16 hours). In such conditions, the corresponding α,ω-dienes were obtained in 60-85% yields. It is noteworthy that similar yields can be obtained in the absence of phase-transfer agent (i.e., TBAI) by conducting the etherification in DMF at 80 °C, for 12 hours under nitrogen, in presence of potassium carbonate.

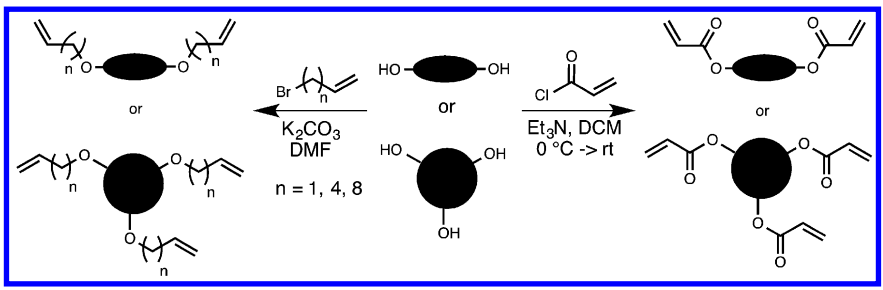

Scheme 2. One-Step Synthesis of Acrylates and Alkenyl Ethers. (Adapted with permission from reference (48). Copyright 2013 The Royal Society of Chemistry)

In Green Polymer Chemistry: Biobased Materials and Biocatalysis; Smith, et al.;
ACS Symposium Series; American Chemical Society: Washington, DC, 2015.

Publication Date (Web): June 18, 2015 | doi: 10.1021/bk-2015-1192.ch004

These efficient derivatizations considerably extend the polymerization systems in which these bio-based aliphatic/aromatic macromonomers can be used and demonstrate their potential as crosslinking agents (bi- and trifunctional) in polyvinylic systems, thus covering a wide range of applications where high thermal properties are required. In addition, through an enzymatic process involving CAL-B and H_2O_2, the terminal olefins-bearing macromonomers could be transformed into the corresponding epoxides (*105*) allowing their use for the synthesis of bio-based epoxy resins.

Synthesis of Alternating Aromatic-Aliphatic Copolyesters

The four renewable bisphenols (**6**, **5**, **4** and **3**), namely **EDF**, **PDF**, **BDF** and **IDF,** respectively, prepared from ferulic acid and, respectively, ethylene glycol, 1,3-propanediol, 1,4-butanediol or isosorbide, were reacted with four activated diacids to provide sixteen linear polymeric structures (Scheme 3). The acyl chloride pathway that consists in simply mixing bisphenol and diacyl chloride (with eventually solvent) and heating the mixture was selected to avoid toxic metal catalysts in the polymerization process. Succinyl, glutaryl, adipoyl and azelaoyl chlorides (respectively, 2, 3, 4 and 7 carbons chains, Scheme 3), that can be obtained by fermentation of sugars (*106*) (e.g., from corn stalk (*107*, *108*), straw (*109*) or cane molasses (*110*)), and from plants oils (*111*, *112*), respectively, were chosen in order to (i) prepare entirely renewable but also processable aliphatic-aromatic copolyesters, and (ii) study the impact of the structure of the diacyl chlorides on the resulting thermal properties of the copolyesters.

These polycondensations were conducted at 100-180 °C under inert atmosphere and studied in bulk as well as in solvent (anhydrous *o*-dichlorobenzene 200-1000 $g.L^{-1}$, total weight of monomers in volume of solvent). After cooling to room temperature, the resulting polymers were directly recovered by precipitation in cold methanol (in solvent polycondensations) or after dissolution in chloroform prior precipitation (bulk polycondensations).

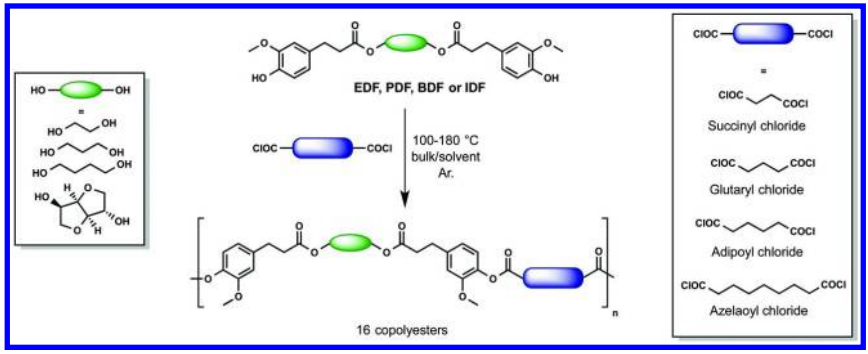

Scheme 3. Metal-Free Preparation of Sixteen Aliphatic-Aromatic Copolyesters. (Adapted with permission from reference (49). Copyright 2014 John Wiley & Sons)

In Green Polymer Chemistry: Biobased Materials and Biocatalysis; Smith, et al.;
ACS Symposium Series; American Chemical Society: Washington, DC, 2015.

Publication Date (Web): June 18, 2015 | doi: 10.1021/bk-2015-1192.ch004

Table 2. Polymerization of the Four Systems at 180 °C in Bulk[a]

Entry	*Bisphenol*	*Dichloride*	*Polymer*	M_n *(kDa)*	M_w [b] *(kDa)*	*Conv.* [c] *(%)*	$Đ_M$ [b]	DP_w [b]	T_d *(5%)* [d] *(°C)*	T_d *(50%)* [d] *(°C)*	T_g [e] *(°C)*
1	**EDF**	Succinyl	**PSEDF**	5.6	13.6	99	2.4	26	343	413	35
2		Glutaryl	**PGEDF**	6.2	12.4	99	2.0	24	353	416	24
3		Adipoyl	**PAdEDF**	9.4	20.7	99	2.2	39	355	413	23
4		Azelaoyl	**PAzEDF**	8.3	18.6	97	2.2	33	364	424	8
5	**PDF**	Succinyl	**PSPDF**	7.6	13.7	96	1.8	28	348	399	23
6		Glutaryl	**PGPDF**	16.2	44.9	99	2.8	85	365	409	20
7		Adipoyl	**PAdPDF**	4.3	11.2	98	2.6	21	335	401	8
8		Azelaoyl	**PAzPDF**	6.6	12	97	1.8	21	360	410	5
9	**BDF**	Succinyl	**PSBDF**	5.2	10.5	96	2.0	20	360	412	26
10		Glutaryl	**PGBDF**	11.1	26.3	99	2.4	49	367	409	17
11		Adipoyl	**PAdBDF**	13.2	31.2	99	2.4	56	357	406	13
12		Azelaoyl	**PAzBDF**	5.1	8.7	96	1.7	15	360	412	0
13	**IDF**	Succinyl	**PSIDF**	3.6	7.5	95	2.1	13	351	410	76
14		Glutaryl	**PGIDF**	9.5	36	99	3.8	60	354	410	59
15		Adipoyl	**PAdIDF**	6.7	15.6	99	2.3	26	358	414	49
16		Azelaoyl	**PAzIDF**	4.1	7.9	98	1.9	12	349	409	35

[a] Conditions : bisphenol:diacyl chloride ratio = 1:1 with a reaction time of 8 hours; [b] M_w, $Đ_M$ et DP_w calculated from SEC analysis with polystyrene calibration; [c] calculated with the residual monomer amounts determined from the corresponding peak area on SEC traces of crude reaction mixtures prior precipitation; [d] values determined by TGA under nitrogen at 10 °C.min^{-1}; [e] values determined by DSC under nitrogen at 10 °C.min^{-1}

Study and Optimization of Polycondensation Parameters

Polycondensation occurred even at moderate temperatures (100 and 120 °C) but required very long reaction times to reach satisfying M_n values. Such conditions should therefore be considered for the preparation of pre-polymers only. Rising the temperature to 150-180 °C considerably increased the efficiencies of the condensation and allowed the formation of polymers within few hours. These systems being very viscous even at 180 °C, the use of a solvent as viscosity reducer was necessary. In order to work at elevated temperature, *o*-dichlorobenzene - with a boiling point of 180.5 °C - was selected. At high concentration (1000 $g.L^{-1}$) the use of solvent did not affect the reactivity of the system. However, more diluted reaction mixtures (200 $g.L^{-1}$) slowed down the reaction and led to polymers with lower M_n values. In optimal polymerization conditions, copolyesters were obtained with M_w values ranging from 7.5 up to 44.9 kDa.

Publication Date (Web): June 18, 2015 | doi: 10.1021/bk-2015-1192.ch004

Thermal Analysis

Copolymers incorporating isosorbide (Table 2, entries 13-16) exhibited, as expected, higher thermal stability than the aliphatic diol-based copolymers (entries 1-12) most probably because of the rigid bicyclic structure of isosorbide. For a given bisphenol, the chain length of the diacyl chloride does not significantly impacts the thermal stability of the copolyesters (±10 °C). In all cases, degradation under inert atmosphere occurred above 340 °C (Table 2). This relatively high thermal stability is probably brought by the aromatic moieties of the bisphenols. Incorporating rigid bicyclic structures like isosorbide in the polymer strongly increases its T_g when compared to aliphatic diols (Table 2). From the diacyl chloride point of view, the shorter the aliphatic chain the higher the T_g. Therefore, by condensing 1,4-butanediol-based bisphenol **BDF** and azelaoyl diacyl chloride, **PAzBDF** was obtained with a T_g value as low as 0 °C. More interestingly, **PSIDF** - which originates from isosorbide-based **IDF** and succinyl chloride - exhibits thermal properties similar to those of PET with a T_g of 76 °C, making it a potential renewable substitute.

Whatever the nature of the internal diol and diacyl chloride, the eight polymers are stable at least up to 340 °C. Unlike the homopolycondensation of AB-type *p*-hydroxycinnamic acids derivatives (*22–27*), the copolycondensation of bisphenols and diacyl chlorides allows to expand the range of T_g values thanks to a greater structural flexibility. In fact, by playing with both the chain length of the diacyl chloride and the structure of the internal diol of the bisphenols, one can tailor the T_g of these bio-based polymers from 0 to 76 °C. The use of rigid bicyclic diol (e.g., isosorbide) and/or short chain diacyl chloride (e.g., succinyl chloride) increases the T_g. On the contrary, the use of more flexible diol (e.g., 1,4-butanediol) and/or long chain diacyl chloride (e.g., azelaoyl chloride) reduces the T_g as well as the intrinsic viscosity of the resulting polymer.

In Green Polymer Chemistry: Biobased Materials and Biocatalysis; Smith, et al.;
ACS Symposium Series; American Chemical Society: Washington, DC, 2015.

Publication Date (Web): June 18, 2015 | doi: 10.1021/bk-2015-1192.ch004

Synthesis of Alternating Aromatic-Aliphatic Poly(ester-urethane)s

Bisphenols **EDF**, **PDF**, **BDF** and **IDF** were reacted with two commercially available diisocyanates - aliphatic 1,6-hexamethylene diisocyanate (HDI), and aromatic 1,4-toluene diisocyanate (TDI) - in various conditions to form eight thermoplastic PEUs through a thermal process thus avoiding the use of metal catalysts (Scheme 4). Having chosen a thermal polymerization process for the synthesis of these PEUs, all polyadditions were conducted at relatively high temperatures under inert atmosphere (argon), in bulk as well as in solvent (ca. 100-140 °C and 60-100 °C, respectively), with a ratio NCO:OH fixed at 1:1.

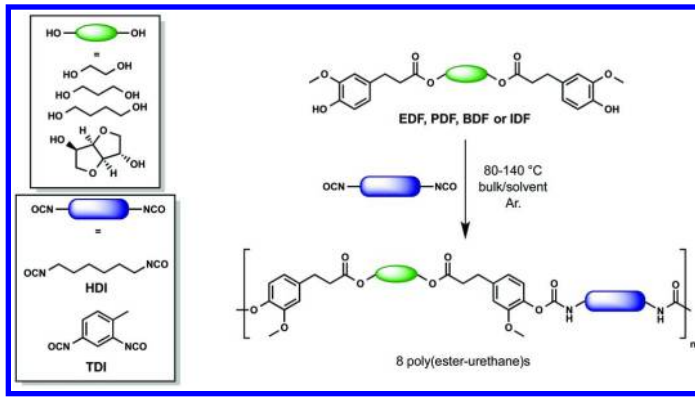

*Scheme 4. Synthesis of Eight PEUs from Two Commercially Available Isocyanates (HDI, TDI) and Four Bio-based Bisphenols (**EDF**, **PDF**, **BDF** and **IDF**). (Adapted with permission from reference (50). Copyright 2015 Elsevier)*

As expected, due to the low reactivity of phenols in polyurethane systems, raising the temperature to 140 °C was required to achieve higher M_w in reasonable reaction times. Firstly performed without solvent, polyadditions led to highly viscous systems almost gel in nature at 140 °C. Thus, low boiling point or high evaporation rate solvents, that are easier to remove from PEUs after precipitation, were selected as viscosity reducer. Chloroform, methyl ethyl ketone (MEK), 1,4-dioxane and methyl isobutyl ketone (MIBK) were therefore considered and tested in polyaddition reactions at their respective boiling temperature with a concentration of 1000 $g.L^{-1}$ (total weight of monomers). MIBK was not selected to run the polymerization reaction in homogenous media as it only dissolved monomers and short oligomers but not the polymers.

Boiling point of chloroform (62.1 °C) was proved too low to allow formation of the polymers in reasonable time. MEK and 1,4-dioxane both solubilized this system and possessed boiling points high enough (79.6 and 101.1 °C, respectively) to provide interesting kinetics. Faster kinetic being observed at lower temperature with MEK, the latter was preferred to 1,4-dioxane and selected to conduct polymerizations.

In Green Polymer Chemistry: Biobased Materials and Biocatalysis; Smith, et al.;
ACS Symposium Series; American Chemical Society: Washington, DC, 2015.

Publication Date (Web): June 18, 2015 | doi: 10.1021/bk-2015-1192.ch004

Table 3. Results of the Polymerizations of the 8 Poly(ester-urethane)s Conducted during 72 h Either in Bulk at 140 °C or in MEK (1000 g.L^{-1}) at Reflux. (Adapted with permission from reference (*50*). Copyright 2015 Elsevier.)

Entry	*Polymer*	*Media*	M_n [a] *(kDa)*	M_w [a] *(kDa)*	*Conv.* [b] *(%)*	$Đ_M$	DP_w [a]	T_d (5%) [c] *(°C)*	T_d (50%) [c] *(°C)*	T_g [d] *(°C)*
1	**PHDI-EDF**	Bulk	1.7	4.2	88	2.5	7	221	333	34
2		MEK	7.1	12.8	>99	1.8	22	220	340	41
3	**PTDI-EDF**	Bulk	1.8	3.7	85	2.0	6	200	319	80
4		MEK	8.6	19.0	>99	2.2	32	201	325	96
5	**PHDI-PDF**	Bulk	3.8	14.6	95	3.8	24	213	311	38
6		MEK	10.3	22.6	>99	2.2	37	225	338	38.1
7	**PTDI-PDF**	Bulk	2.2	7.1	84	3.1	12	197	321	73
8		MEK	4.8	9.7	98	2.0	16	203	332	75
9	**PHDI-BDF**	Bulk	2.8	5.9	91	2.0	10	225	336	29
10		MEK	5.4	10.6	93	2.0	18	224	326	28
11	**PTDI-BDF**	Bulk	2.9	7.3	93	2.5	11	184	330	62
12		MEK	6.6	12.3	99	1.8	20	214	320	79
13	**PHDI-IDF**	Bulk	2.6	6.4	93	2.4	10	223	360	67
14		MEK	11.7	25.5	>99	2.2	38	228	357	68
15	**PTDI-IDF**	Bulk	2.6	8.0	95	3.0	12	211	362	107
16		MEK	7.9	24.2	>99	3.1	36	204	348	127

[a] values determined by SEC analysis with polystyrene calibration; [b] calculated with the residual monomer amounts determined from the corresponding pic area on SEC traces of crude reaction mixtures prior precipitation; [c] values determined by TGA under nitrogen at 10 °C.min^{-1}; [d] values determined by DSC under nitrogen at 10 °C.min^{-1}

Comparing bulk and in-solvent polymerizations (Table 3, entries 1, 3, 5, 7, 9, 11, 13, 15 *vs* 2, 4, 6, 8, 10, 12, 14, 16) demonstrated the interest of using MEK as viscosity reducer in polymerization media (1000 $g.L^{-1}$). Indeed, for the same reaction time (72 h) and system (A_2/B_2), higher M_n and DP_w were obtained in MEK compared to the bulk procedure (M_n: 5-10 *vs* 1.7-4 $kg.mol^{-1}$, DP_w: 16-38 *vs* 6-24) as well as higher conversion rates, despite the lower temperature (80 *vs* 140 °C). It is noteworthy that all resulting polyurethanes are transparent or can be obtained as white powders when precipitated in cold methanol.

Thermal Characterization

All polymers were stable up to more than 180 °C (T_d 5%), an interesting feature for polyurethanes systems (*113*). These unexpected but relatively good thermal stability of our phenolic polyurethanes is probably due to the presence of the methoxy group on the aromatic rings, vicinal to the phenols involved in the urethane bonds, that probably stabilizes the system thereby preventing thermal decomposition. This feature emphasizes the interest of using ferulic derivatives to form phenyl alkyl urethanes. As expected, compared to their HDI-based counterparts, TDI-based polymers showed lower thermostability due to the lower stability of aromatic-aromatic urethane linkages compared to aromatic-aliphatic ones (*114*). Similarly to what was observed with the copolyesters described above (*49*), varying the bisphenol structure had a low impact on the thermal stability of the resulting PEUs.

As shown in Table 3, PEUs obtained from the polyaddition of aliphatic HDI and **EDF**, **PDF** and **BDF** bisphenols prepared from aliphatic diol (ethylene glycol, 1,3-propanediol and 1,4-butanediol, respectively) in MEK showed the lowest T_g (28-41 °C) demonstrating that the shorter the internal diol, the higher the T_g (**EDF** > **PDF** > **BDF**). The use of the bisphenol prepared from isosorbide (**IDF**), because of its rigid bicyclic structure, considerably increased the T_g of the resulting polymers (up to 128 °C). From the isocyanate point of view, for a given bisphenol, replacing aliphatic HDI by aromatic TDI dramatically increased the T_g due to the higher aromatic content. The changes in T_g (Table 3, 28 to 128 °C) associated with the nature of the internal diol and isocyanate structure indicate that the aromatic based PEUs have a wider glass transition region over which their mechanical properties will vary as compared to the aliphatic based PEUs.

Synthesis of Poly(ester-alkenamer)s

Thanks to the ease of handling and high functional group tolerance of the Ru-based catalysts used in acyclic diene metathesis (ADMET), this method is a very useful approach for the construction of defined polymer architectures (*115*) and allowed the synthesis of renewable polymers, such as polyesters, polyethers, polyamides and many others, very promising for commercial applications (*41*, *115–124*). Even though extensive research has been performed to develop

In Green Polymer Chemistry: Biobased Materials and Biocatalysis; Smith, et al.;
ACS Symposium Series; American Chemical Society: Washington, DC, 2015.

Publication Date (Web): June 18, 2015 | doi: 10.1021/bk-2015-1192.ch004

commercial ferulic acid derived renewable polymers (*22–35*, *49*, *59*), only one example has been reported on ADMET polymerization involving ferulic acid derivatives as diene substrates. Indeed, Meier and co-workers reported on the use of a bisallylated ferulic acid derivative (**2**) as α,ω-diene monomer for the synthesis of renewable poly(ester-alkenamer)s (*120*). In their study, homopolymerization and copolymerization of **2** with oleic and erucic-derived α,ω-dienes resulted in polymers with molecular weights of 2-3 kDa and 9 kDa, respectively. Though these polymers were obtained in relatively low molecular weights, this study demonstrated the potentialities of ferulic acid-derived monomers in ADMET chemistry.

Publication Date (Web): June 18, 2015 | doi: 10.1021/bk-2015-1192.ch004

Syntheses and ADMET Polymerization of Ferulic Acid-Derived α,ω-Diene Monomers

In order to study the impact of both the chain length of the olefin and the rigidity/flexibility of the diester core of the monomer on the polymerizations and the thermal properties of the resulting poly(ester-alkenamer)s, we studied six α,ω-diene monomers synthesized from **IDF** and **BDF** and three bromo-alkenes (3-bromoprop-1-ene, 6-bromohex-1-ene et 10-bromodec-1-ene) (Scheme 5). With the six ferulic acid-derived α,ω-diene monomers in hand, we proceeded to the study of their behaviour in ADMET polymerization conducted in presence of Hoveyda-Grubbs second generation catalyst (**HG-II**), in mass under continuous vacuum (ca. 20 mbar) to guarantee the efficient removal of ethylene and thus shift the equilibrium towards polymerization, and in presence of 1,4-benzoquinone (2 eq. relative to catalyst) to prevent olefin isomerization (2% mol) (Scheme 6) (*125*). Indeed, previous works by Abbas (*126*) and Meier (*41*) have shown **HG-II** to be the most active towards the cross metathesis of terminal olefins with acrylates and vanillin-based α,ω-dienes, respectively.

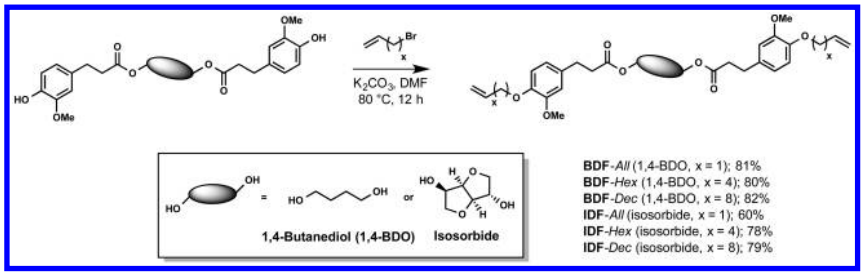

Scheme 5. Synthesis of the Six Ferulic Acid-Derived α,ω-Diene Monomers. (Reproduced with permission from reference (52). Copyright 2015 Elsevier)

Publication Date (Web): June 18, 2015 | doi: 10.1021/bk-2015-1192.ch004

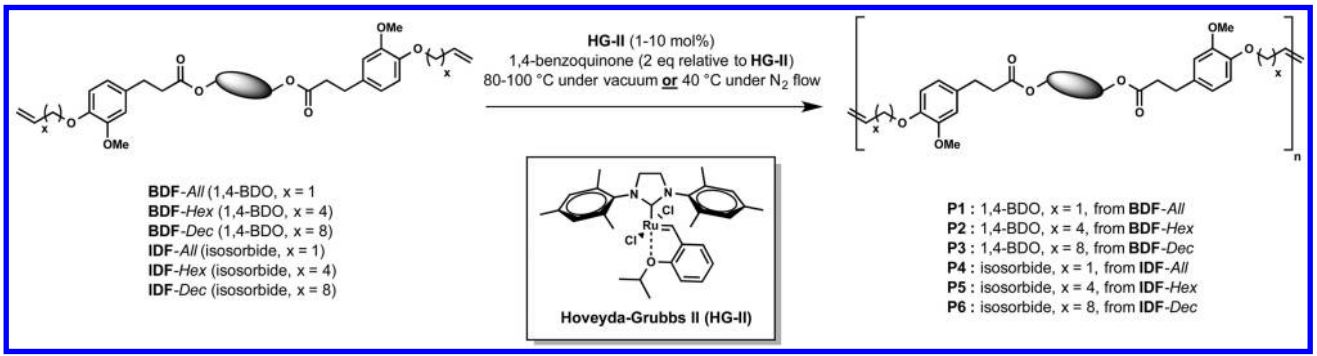

Scheme 6. ADMET Polymerization of the Six α,ω-Diene Monomers Derived from Ferulic Acid. (Reproduced with permission from reference (52). Copyright 2015 Elsevier)

Publication Date (Web): June 18, 2015 | doi: 10.1021/bk-2015-1192.ch004

Structural Analysis

It is noteworthy that ADMET polymerization of monomers bearing allyl moieties only provides low molecular weight polymers as proven by the observation in the ^{1}H NMR spectra of substantial signals corresponding to terminal double bonds at 5.2-5.5 and 6.0-6.2 ppm. Polymers with relatively high molecular weights were obtained from all other monomers (Table 4). Whatever the bromo alk-1-ene used, higher molecular weights are always obtained with **BDF**-based α,ω-dienes (**P2**). Such results could be explained by the higher flexibility of the aliphatic chain of 1,4-butanediol compared to the rigid bicyclic structure of isosorbide and the resulting lower viscosity of **BDF**-based monomers. However, interestingly, switching from hex-1-ene to dec-1-ene (Table 4, Entries 6, 8, 10 and 12) does not provide higher molecular weights. Furthermore, while molecular weights of **IDF**-derived poly(ester-alkenamer)s (**P5** vs. **P6**) remain unchanged or increase by only 14% from dec-1-ene to hex-1-ene (Table 4, Entries 3-4 and 7-8), those of **BDF**-derived polymers (**P2** vs. **P3**) significantly increase by 121-140% (Table 4, Entries 1-2 and 5-6). As shown in Table 4, heating the reaction mixture from 80 to 100 °C significantly improves the molecular weights by lowering the viscosity of the reaction medium and thus facilitating both ethylene removal and stirring. The **IDF**-based monomers are the ones that benefit most from this rise in temperature resulting in a molecular weight increase of ca. 101% (79% for **BDF**).

Table 4. GPC and TGA Analytical Data of the Synthesized Polymers via ADMET in Mass[a,b]. (Adapted with permission from reference (*52*). Copyright 2015 Elsevier.)

Entry	*Temp. (°C)*	*Monomer*	*Polymer*	*Yield (%)*	M_w[c] *(kDa)*	M_n[c] *(kDa)*	DP_n[c]	$Đ_M$[c]	$T_{d\,5\%}$[d] *(°C)*	T_g[e] *(°C)*
1	80	**BDF**-*Hex*	**P2**	93	26.5	20.5	34	1.3	283	-5.5
2	80	**BDF**-*Dec*	**P3**	92	10.4	6.3	10	2.3	370	-20.4
3	80	**IDF**-*Hex*	**P5**	94	12.5	5.4	8	1.6	287	14.7
4	80	**IDF**-*Dec*	**P6**	96	11.8	5.9	8	2.0	344	6.3
5	100	**BDF**-*Hex*	**P2**	92	42.8	25.4	42	1.7	314	-7.7
6	100	**BDF**-*Dec*	**P3**	90	20.5	12.3	19	1.7	314	-21.6
7	100	**IDF**-*Hex*	**P5**	95	27.2	10.6	16	2.6	291	18.2
8	100	**IDF**-*Dec*	**P6**	94	21.6	9.9	14	2.2	334	6.7

[a] **HG-II** 1 mol%, 1,4-benzoquinone (2 mol%), DCM (2 M), 40 °C, 4 hours; [b] **HG-II** 1 mol%, 1,4-benzoquinone (2 mol%), vacuum, 4 hours; [c] GPC data of crude polymers; [d] TGA data under nitrogen at 60 mL.min^{-1}; [e] DSC data recorded at 10 °C.min^{-1}, value determined at the 2nd heating scan

In Green Polymer Chemistry: Biobased Materials and Biocatalysis; Smith, et al.;
ACS Symposium Series; American Chemical Society: Washington, DC, 2015.

Publication Date (Web): June 18, 2015 | doi: 10.1021/bk-2015-1192.ch004

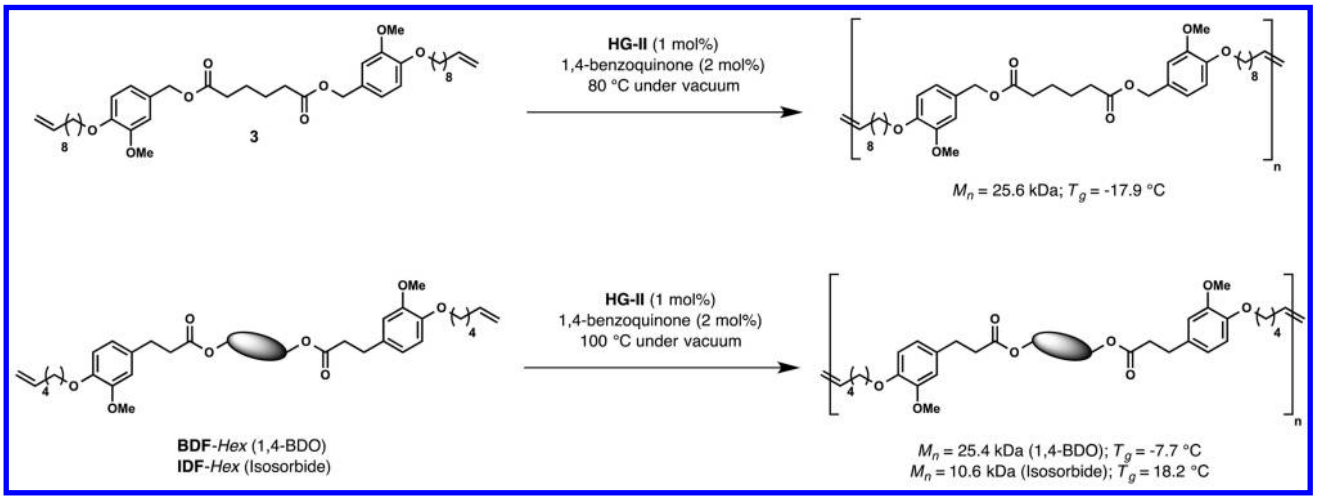

Scheme 7. Ferulic Acid- and Vanillin-Derived Poly(ester-alkenamer)s via ADMET. (Reproduced with permission from reference (52). Copyright 2015 Elsevier)

Finally and as expected, increasing the catalyst loading above 1 mol% resulted in decreasing molecular weights. Using lower catalyst loadings (e.g., 0.1-0.5 mol%) or longer reactions times (8 hours) did not lead to higher molecular weight. In summary, in mass polymerization conducted with 1 mol% **HG-II**, at 100 °C for 4 hours proved to be the optimal procedure to efficiently polymerize these monomers via ADMET. In such conditions, **BDF**- and **IDF**-based poly(ester-alkenamer)s (**P2**/**P3** and **P5**/**P6**) were obtained with number average molecular weight (M_n) in the range of 12.3-25.4 and 9.9-10.6 kDa, respectively. In terms of reactivity, **BDF**-*Hex* α,ω-diene proves more reactive than monomer **2** as previously reported by Meier and co-workers (*116*) and as efficient as their recently published vanillin-derived α,ω-diene **3** which gives similar molecular weights when submitted to ADMET polymerization with **HG-II** (Scheme 7) (*41*).

Publication Date (Web): June 18, 2015 | doi: 10.1021/bk-2015-1192.ch004

Thermal Properties

TGA analyses of the monomers revealed a thermostability in the range of 302-349 °C (Table 4), the latter being significantly impacted by the nature of the diester (1,4-butanediol vs. isosorbide) and the alkene length (C_6 vs. C_{10}). Indeed, **IDF**-based monomers prove more stable than the ones deriving from **BDF**; furthermore, replacing hex-1-ene by dec-1-ene in **BDF**- and **IDF**-based monomers strongly increases their thermostability by 24.8 and 13.2 °C, respectively.

Thermal analyses of polymers **P2-P6** showed significant differences in $T_{d\ 5\%}$ and glass transition temperature (T_g) depending on the nature of the internal diester and the alkene length. Aromatic in nature, all poly(ester-alkenamer)s exhibit a thermostability in the range of 283-370 °C, the dec-1-ene based ones being the most stable (Table 4, Entries 2, 4, 6 and 8). The nature of the internal diester, however, has a relatively low impact on the degradation temperature (Table 3, Entries 6-8). Similarly to what was observed with the previously reported copolyesters (*49*) and poly(ester-urethane)s (*50*) derived from these ferulic acid-based bisphenols, the rigid bicyclic structure of isosorbide also greatly increases the T_g of poly(ester-alkenamer)s (**P5** and **P6**) compared to their **BDF**-based counterparts (**P2** and **P3**). Varying the nature of the α,ω-diene monomers thus provides T_g in the range of -21.6 to 18.2 °C. From a strictly thermal properties perspective, **BDF**-*Dec* based poly(ester-alkenamer) (**P3**) represents a renewable alternative to polyethylene (PE) (*127*). Finally, it is noteworthy that all polymers are amorphous and do not show melting points (T_m) on DSC.

Conclusion

A novel class of bio-based bis- and trisphenols was prepared in very good yield and high purity from ferulic acid through a highly selective lipase-catalyzed enzymatic process. These new bio-based A_2- and A_3-type structures combine terminal phenol groups and aliphatic or cyclic segments. Their successful derivatizations into either acrylates or alkenyl ethers in a one-step process extend their applications as monomers, crosslinking agents in polyvinylic

systems (chemical or UV-curing), and precursors for the synthesis of bio-based epoxy resins. These successful derivatizations demonstrate that these bis- and trisphenols can be employed in a broad range of polymeric systems (*e.g.*, polyesters, polyurethanes, polyacrylates, polyolefins, epoxy resins) to prepare thermoplastic as well as thermoset materials.

The potential of such ferulic-based bisphenols in polymer synthesis, was investigated through their use as monomers for the preparation of new classes of alternating aliphatic-aromatic renewable thermoplastic copolyesters, poly(ester-urethane)s and poly(ester-alkenamer)s. Thermal analyses revealed that, regardless of the type of polymer, their T_g could be easily and finely tuned by judiciously choosing the aliphatic segments associated to ferulic acid and the chain length of the diacyl chloride/alkene or the nature of the isocyanate. In addition, these new ferulic-acid based polymers proved to exhibit a relatively high thermal stability.

Though these new biobased polymers were not obtained with relatively high DP_w and M_w values, these preliminary results nevertheless constitute a proof of concept and demonstrate the potential of such alternating ferulic acid-based renewable aliphatic-aromatic polymers. Further studies combining these different methods and varying stoichiometric ratio between bisphenol and co-monomers will follow, allowing a better control of the molar masses of our polymers. Prepared from renewable feedstocks (e.g., ferulic acid, 1,4-butanediol, isosorbide), these new polymers could therefore be envisaged as sustainable substitutes to conventional petro-based polyesters.

Publication Date (Web): June 18, 2015 | doi: 10.1021/bk-2015-1192.ch004

References

1. Gandini, A. *Green Chem.* **2011**, *13*, 1061–1083.
2. Maisonneuve, L.; Lebarbé, T.; Grau, E.; Cramail, H. *Polym. Chem.* **2013**, *4*, 5472–5517.
3. Belgacem, M. N.; Gandini, A. In *Monomers, Polymers, and Composites from Renewable Resources*; Elsevier: Amsterdam, The Netherlands, 2008.
4. Babu, R. P.; O'Connor, K.; Seeram, R. *Prog. Biomater.* **2013**, *2*, 8.
5. Kreye, O.; Mutlu, H.; Meier, M. A. R. *Green Chem.* **2013**, *15*, 1431–1455.
6. Wageningenur Home Page; https://www.wageningenur.nl/en/show/SPLASHEU-research-project-on-algaebased-polymers-kicks-off.htm (accessed Jan 12, 2015).
7. Stevens, E. S. In *Green Plastics: An Introduction to the New Science of Biodegradable Plastics*; Princeton University Press: Princeton, NJ, 2002.
8. Ishioka, R.; Kitakuni, E.; Ichikawa, Y. In *Biopolymers, Polyesters III - Applications and Commercial Products*; Doi, Y., Steinbüchel, A., Eds.; Wiley-VCH Verlag GmbH: Weinheim, Germany, 2002; Vol. 4, p 275.
9. Gruber, P.; O'Brien, M. In *Biopolymers, Polyesters III - Applications and Commercial Products*; Doi, Y., Steinbüchel, A., Eds.; Wiley-VCH Verlag GmbH: Weinheim, Germany, 2002; Vol. 4, p 235.

10. Asrar, J.; Gruys, K. J. In *Biopolymers, Polyesters III - Applications and Commercial Products*; Doi, Y., Steinbüchel, A., Eds.; Wiley-VCH Verlag GmbH: Weinheim, Germany, 2002; Vol, 4, p 53.
11. Imai, Y. *High Perform. Polym.* **1995**, *7*, 337–345.
12. Madhavamoorthi, P. *Synthetic Fibers* **2004**, *33*, 16–28.
13. Tuck, C. O.; Perez, E.; Horvath, I.; Sheldon, R. A.; Poliakoff, M. *Science* **2012**, *337*, 695–699.
14. Koike, T. *Polym. Eng. Sci.* **2012**, *52*, 701–717.
15. Aouf, C.; Nouailhas, H.; Fache, M.; Caillol, S.; Boutevin, B.; Fulcrand, H. *Eur. Polym. J.* **2013**, *49*, 1185–1195.
16. Voirin, C.; Caillol, S.; Sadavarte, N. V.; Tawade, B. V.; Boutevin, B.; Wadgaonkar, P. P. *Polym. Chem.* **2014**, *5*, 3142–3162.
17. Boerjan, W.; Ralph, J.; Baucher, M. *Annu. Rev. Plant Biol.* **2003**, *54*, 519–546.
18. Ralph, J.; Lundquist, K.; Brunow, G.; Lu, F.; Kim, H.; Schatz, P. F.; Marita, J. M.; Hatfield, R. D.; Ralph, S. A.; Christensen, J. H.; Boerjan, W. *Phytochem. Rev.* **2004**, *3*, 29–60.
19. Lange, H.; Decina, S.; Crestini, C. *Eur. Polym. J.* **2013**, *49*, 1151–1173.
20. U.S. Department of Energy Home Page; http://www.nrel.gov/docs/fy04osti/35523.pdf (accessed Jan 12, 2015).
21. Ligaas, G.; Tüzün, A.; Ronda, J. C.; Galià, M.; Cadiz, V. *Polym. Chem.* **2014**, *5*, 6636–6644.
22. Mialon, L.; Vanderhenst, R.; Pemba, A. G.; Miller, S. A. *Macromol. Rapid Commun.* **2011**, *32*, 1386–1392.
23. Mialon, L.; Pemba, A. G.; Miller, S. A. *Green Chem.* **2010**, *12*, 1704–1706.
24. Charbonneau, L. F. Thermotropic polyesters derived from ferulic acid and a process for preparing the polyesters. U.S. Patent 4,230,817, Oct. 28, 1980.
25. Li, J.-H.; Chen, M.-Q.; Hu, N.; Ni, Z.-B.; Jin, S.-Y.; Lou, Y. Review on homo- and co-polymerization of p-hydroxycinnamic acids. *Gaofenzi Tongbao* **2010**, *10*, 60–65.
26. Palacios, J.; Perez, C. *New Polym. Mater.* **1990**, *2*, 167–178.
27. Elias, H. G.; Palacios, J. A. *Makromol. Chem.* **1985**, *5*, 1027–1045.
28. Kaneko, T.; Matsusaki, M.; Hang, T. T.; Akashi, M. *Macromol. Rapid Commun.* **2004**, *25*, 673–677.
29. Tanaka, Y.; Tanabe, T.; Shimura, Y.; Okada, A. *J. Polym. Sci., Part B: Polym. Lett.* **1975**, *13*, 235–242.
30. Sapich, B.; Stumpe, J. *Macromolecules* **1998**, *31*, 1016–1023.
31. Stumpe, J.; Ziegler, A. *Macromolecules* **1995**, *28*, 5306–5311.
32. Jin, X.; Carfagna, C.; Nicolais, L.; Lanzetta, R. *Macromolecules* **1995**, *28*, 4785–4794.
33. Wang, S.; Kaneko, D.; Kan, K.; Jin, X.; Kaneko, T. *Pure Appl. Chem.* **2012**, *12*, 2559–2568.
34. Hatanaka, N.; Okawa, H. Photoreactive liquid crystal aligning agent, and liquid crystal alignment device and method for production thereof. KR Patent 102013006325, Jan. 16, 2013.
35. Zhao, Q.; Wu, W. *Polymer* **2009**, *4*, 998–1004.
36. Du, J.; Fang, Y.; Zheng, Y. *Polymer* **2007**, *19*, 5541–5547.

37. Ouimet, M. A.; Griffin, J.; Carbone-Howell, A. L.; Ashley, L.; Wu, W.-H.; Stebbins, N. D.; Di, R.; Uhrich, K. E. *Biomacromolecules* **2013**, *14* (3), 854–861.
38. Matsusaki, M.; Kishida, A.; Stainton, N.; Ansell, C. W. G.; Akashi, M. *J. Appl. Polym. Sci.* **2001**, *82*, 2357–2364.
39. Kreye, O.; Oelmann, S.; Meyer, M. A. R. *Macromol. Chem. Phys.* **2013**, *13*, 1452–1464.
40. Akashi, M.; Matsusaki, F.; Fujita, Y.; Onishi, M. Bioabsorbable material and in-vivo indwelling device made thereof. U.S. Patent 8,222,349, Mar. 3, 2009.
41. Firdaus, M.; Meier, M. A. R. *Eur. Polym. J.* **2013**, *49*, 156–166.
42. Quentin, M.; Allasia, V.; Pegard, A.; Allais, F.; Ducrot, P.-H.; Favery, B.; Levis, C.; Martinet, S.; Masur, C.; Ponchet, M.; Roby, D.; Schlaich, L.; Jouanin, L.; Keller, H. *PLoS Pathog.* **2009**, *5* (1) DOI:10.1371/journal.ppat.1000264.
43. Allais, F.; Aouhansou, M.; Majira, A.; Ducrot, P.-H. *Synthesis* **2010**, *16*, 2787–2793.
44. Allais, F.; Ducrot, P.-H. *Synthesis* **2010**, *16*, 1649–1659.
45. Mouterde, L. M. M.; Flourat, A. L.; Cannet, M. M. M.; Ducrot, P.-H.; Allais, F. *Eur. J. Org. Chem.* **2013**, *1*, 173–179.
46. Cottyn, B.; Kollman, A.; Waffo Teguo, P.; Ducrot, P.-H. *Chem.−Eur. J.* **2011**, *17*, 7282–7287.
47. Dean, J. C.; Kusaka, R.; Walsh, P. S.; Allais, F.; Zwier, T. S. *J. Am. Chem. Soc.* **2014**, *136*, 14780–14795.
48. Pion, F.; Reano, A. F.; Ducrot, P.-H.; Allais, F. *RSC Adv.* **2013**, *3*, 8988–8993.
49. Pion, F.; Ducrot, P.-H.; Allais, F. *Macromol. Chem. Phys.* **2014**, *215*, 431–439.
50. Oulame, M. Z.; Pion, F.; Ducrot, P.-H.; Allais, F. *Eur. Polym. J.* **2015**, *63*, 186–193.
51. Subrayan, R. P.; Zhang, S.; Jones, F. N.; Swarup, V.; Yezrielev, A. I. *J. Appl. Pol. Sci.* **2000**, *10*, 2212–2228and references 1-3 therein.
52. Barbara, I.; Flourat, A. L.; Allais, F. *Eur. Polym. J.* **2015**, *62*, 236–243.
53. Gross, R. A.; Kumar, A.; Kalra, B. *Chem. Rev.* **2001**, *101*, 2097–2124.
54. Kobayashi, S. *Macromol. Rapid Commun.* **2009**, *30*, 237–266.
55. Mahapatro, A.; Kalra, B.; Kumar, A.; Gross, R. A. *Biomacromolecules* **2003**, *4*, 544–551.
56. Lassalle, V. L.; Ferreira, M. L. *J. Chem. Technol. Biotechnol.* **2008**, *11*, 1493–1502.
57. Kobayashi, S. *Proc. Jpn. Acad., Ser. B* **2010**, *4*, 338–365.
58. Doaa, A. R. M.; Wafaa, A. H. *J. Appl. Sci. Res.* **2009**, *5*, 2466–2476.
59. Sangeetha, R.; Arulpandi, I.; Geetha, A. *Res. J. Microbiol.* **2011**, *6*, 1–24.
60. Guyot, B.; Bosquette, B.; Pina, M.; Graille, J. *Biotechnol. Lett.* **1997**, *6*, 529–532.
61. Bulsman, G. J. H.; Helteren, C. T. W.; Kramer, G. F. H.; Veldsink, J. W.; Derksen, J. T. P.; Cuperus, F. P. *Biotechnol. Lett.* **1998**, *2*, 131–136.
62. Stamatis, H.; Sereti, V.; Kolisis, F. N. *J. Mol. Catal. B:* **2001**, *4-6*, 323–328.
63. Giulani, S.; Piana, C.; Setti, L.; Hochkoeppler, A.; Pifferi, P. G.; Williamson, G.; Faulds, C. B. *Biotechnol. Lett.* **2001**, *4*, 325–330.

64. Lue, B. M.; Karboune, S.; Yebaoh, F. K.; Kermasha, S. *J. Chem. Technol. Biotechnol.* **2005**, *4*, 462–468.
65. Sabally, K.; Karboune, S.; St-Louis, R.; Kermasha, S. *J. Am. Oil Chem. Soc.* **2006**, *2*, 101–107.
66. Safari, M.; Karboune, S.; St-Louis, R.; Kermasha, S. *Biocatal. Biotransform.* **2006**, *4*, 272–279.
67. Vosmann, K.; Weitkamp, P.; Weber, N. *J. Agric. Food Chem.* **2006**, *54*, 2969–2976.
68. Sun, S.; Yang, G.; Bi, Y.; Xiao, F. *Biotechnol. Lett.* **2009**, *12*, 1885–1889.
69. Zoumpanioti, M.; Merianou, E.; Karandreas, T.; Stamatis, H.; Xenakis, A. *Biotechnol. Lett.* **2010**, *10*, 1457–1462.
70. Figueroa-Espinoza, M. C.; Villeneuve, P. *J. Agric. Food Chem.* **2005**, 2779–2787.
71. Sabally, K.; Karboune, S.; Yebaoh, F. K.; Kermasha, S. *Biocatal. Biotransform.* **2005**, *1*, 37–44.
72. Sabally, K.; Karboune, S.; St-Louis, R.; Kermasha, S. *Biocatal. Biotransform.* **2007**, *2-4*, 211–218.
73. Yang, Z.; Feddern, V.; Glasius, M.; Guo, Z.; Xu, X. *Biotechnol. Lett.* **2011**, *4*, 673–679.
74. Cassani, J.; Luna, H.; Navarro, A.; Castillo, E. *Electron. J. Biotechnol.* **2007**, *10*, 508–513.
75. Feddern, V.; Yang, Z.; Xu, X.; Badiale-Furlong, E.; Almeida de Souza-Soares, L. *Ind. Eng. Chem.* **2011**, *50*, 7183–7190.
76. Compton, D. L.; Laszlo, J. A.; Berhow, M. A. *J. Am. Oil Chem. Soc.* **2000**, *5*, 513–519.
77. Compton, D. L.; King, J. W. *J. Am. Oil Chem. Soc.* **2001**, *1*, 43–47.
78. Compton, D. L.; Laszlo, J. A.; Berhow, M. A. *J. Am. Oil Chem. Soc.* **2006**, *9*, 753–758.
79. Laszlo, J. A.; Compton, D. L. *J. Am. Oil Chem. Soc.* **2006**, *9*, 765–770.
80. Sun, S.; Shan, L.; Liu, Y.; Jin, Q.; Wang, X.; Wang, Z. *Biotechnol. Lett.* **2007**, *12*, 1947–1950.
81. Sun, S.; Shan, L.; Liu, Y.; Jin, Q.; Wang, X. *Biotechnol. Lett.* **2007**, *6*, 945–949.
82. Compton, D. L.; Laszlo, J. A *Biotechnol. Lett.* **2009**, *6*, 889–896.
83. Xin, J.-Y.; Zhang, L.; Chen, L.-L.; Zheng, Y.; Wu, X.-M.; Xia, C.-G. *Food Chem.* **2009**, *112*, 640–645.
84. Katsoura, M. H.; Polydera, A. C.; Tsironis, L. D.; Petraki, M. P.; Rajacic, S. K.; Tselepis, A. D.; Stamatis, H. *New Biotechnol.* **2009**, *1-2*, 83–91.
85. Chen, B.; Liu, H.; Guo, Z.; Huang, J.; Wang, M.; Xu, X.; Zheng, L. *J. Agric. Food Chem.* **2011**, *59*, 1256–1263.
86. Carde, T. DOE/GO-102001-1461; New Continuous Isosorbide Production from Sorbitol: Office of Industrial Technologies (OIT). *Agriculture Project Fact Sheet*; 2012.
87. Adelman, D. J.; Charbonneau, L. F.; Ung, S. Heating mixture of ethylene glycol and isosorbide, terephtalic acid or its alkyl ester under pressure; removal of distillate comprising water or volatile alkanol products;

continuing reaction in presence of polycondensation catalyst. U.S. Patent 6,656,577, Dec. 2, 2003.
88. Okada, M.; Okada, Y.; Tao, A.; Aoi, K. *J. Appl. Polym. Sci.* **1996**, *62*, 2257–2265.
89. Okada, M.; Tsunoda, K.; Tachikawa, K.; Aoi, K. *J. Appl. Polym. Sci.* **2000**, *77*, 338–346.
90. Malhotra, S. V.; Kumar, V.; East, A.; Jaffe, M. *Bridge* **2007**, *37*, 17–24.
91. Kricheldorf, H. R. *J. Macromol. Sci., Rev. Macromol. Chem. Phys.* **1997**, *C37*, 599–631.
92. Juais, D.; Naves, A. F.; Li, C.; Gross, R. A.; Catalani, L. H. *Macromolecules* **2010**, *43*, 10315–10319.
93. Review on isosorbide-based polyesters: Okada, M.; Aoi, K. *Curr. Trends Polym. Sci.* **2002**, *7*, 57–70.
94. Review on sugar-based polymers: Feng, X.; East, A. J.; Hammond, W. B.; Zhang, Y.; Jaffe, M. *Polym. Adv. Technol.* **2011**, *1*, 139–150.
95. Medimagh, R.; Chatti, S.; Alves, S.; Hammed, N.; Loupy, A.; Zarrouk, H. *C. R. Chim.* **2007**, *10*, 234–250.
96. Chatti, S.; Kricheldorf, H. R.; Schwartz, G. *J. Polym. Sci., A: Polym. Chem.* **2006**, *44*, 3616–3628.
97. Gorna, K.; Gogolewski, S. *J. Biomed. Mater. Res. A* **2006**, *79A*, 128–138.
98. Okada, M.; Tsunoda, K.; Tachikawa, K.; Aoi, K. *J. Appl. Polym. Sci.* **2000**, *77*, 338–346.
99. Biobased ethylene glycol: FKUR Home Page; http://www.fkur.com/produkte/globio-bio-pet.html (accessed Jan 18, 2015).
100. Biobased 1,3-propanediol: Dupont Tate and Lyle Home Page; http://www.duponttateandlyle.com (accessed Jan 18, 2015).
101. Yim, H.; Haselbeck, R.; Niu, W.; Pujol-Baxley, C.; Burgard, A.; Boldt, J.; Khandurina, J.; Trawick, J. D.; Osterhout, R. E.; Stephen, R.; Estadilla, J.; Teisan, S.; Schreyer, H. B.; Andrae, S.; Yang, T. H.; Lee, S. Y.; Burk, M. J.; Van Dien, S. Biobased 1,4-butanediol. *Nat. Chem. Biol.* **2011**, *7*, 445–452.
102. Wang, Z.-X.; Zhuge, J.; Fang, H.; Prior, B. A. *Biotechnol. Adv.* **2001**, *19*, 201–223.
103. Sun, S.; Shan, L.; Jin, Q.; Liu, Y.; Wang, X. *Biotechnol. Lett.* **2007**, *6*, 945–949.
104. Arkema, BASF/Cargill/Novozyme and Dow Chemical/OPX are investigating using fermented sugar to produce 3-hydroxypropionic acid (3-HP), an acrylic acid precursor.
105. Aouf, C.; Lecomte, J.; Villeneuve, P.; Dubreucq, E.; Fulcrand, H. *Green Chem.* **2012**, *14*, 2387–2336.
106. Song, H.; Lee, S. Y. *Enzyme Microb. Technol.* **2006**, *39*, 352–361.
107. Wang, D.; Li, Q.; Yang, M.; Zhang, Y.; Su, Z.; Xing, J. *Process Biochem.* **2011**, *46*, 365–371.
108. Zheng, P.; Fang, L.; Xu, Y.; Dong, J.-J.; Ni, Y.; Sun, Z.-H. *Bioresour. Technol.* **2010**, *101*, 7889–7894.
109. Zheng, P.; Dong, J.-J.; Sun, Z.-H.; Ni, Y.; Fang, L. *Bioresour. Technol.* **2009**, *100*, 2425–2429.

Publication Date (Web): June 18, 2015 | doi: 10.1021/bk-2015-1192.ch004

110. Liu, Y.-P.; Zheng, P.; Sun, Z.-H.; Ni, Y.; Dong, J.-J.; Zhu, L.-L. *Bioresour. Technol.* **2008**, *99*, 1736–1742.
111. Goebel, C. G.; Brown, A. C.; Oeshlschlaeger, H. F.; Rolfes, R. P. Method of making azelaic acid. U.S. Patent 2,813,113, May, 7, 1957.
112. Hill, K. *Pure Appl. Chem.* **2000**, *72*, 1255–1264.
113. Song, Y. M.; Chen, W. C.; Yu, T. L.; Linliu, K.; Tseng, Y. H. *J. Appl. Polym. Sci.* **1996**, *62*, 827–834.
114. Wei, Y.; Cheng, F.; Li, H.; Yu, J. *J. Sci. Ind. Res.* **2005**, *64*, 435–439.
115. Mutlu, H.; de Espinosa, L. M.; Meier, M. A. R. *Chem. Soc. Rev.* **2011**, *40*, 1404–1445.
116. Kreye, O.; Tóth, T.; Meier, M. A. R. *Eur. Polym. J.* **2011**, *47*, 1804–1816.
117. Mutlu, H.; Meier, M. A. R. *Macromol. Chem. Phys.* **2009**, *210*, 1019–1025.
118. de Espinosa, L. M.; Meier, M. A. R.; Ronda, J. C.; Galià, M.; Cadiz, V. *J. Polym. Sci., Part A: Polym. Chem.* **2010**, *48*, 1649–1660.
119. Baughman, T. W.; Wagener, K. B. *Adv. Polym. Sci.* **2005**, *176*, 1–42.
120. Türünç, O.; de Espinosa, L. M.; Meier, M. A. R. *Macromol. Rapid. Commun.* **2011**, *32*, 1357–1361.
121. Günther, S.; Lamprecht, P.; Luinstra, G. A. *Macromol. Symp.* **2010**, *293*, 15–19.
122. Lebarbé, T.; More, A. S.; Sane, P. S.; Grau, E.; Alfos, C.; Cramail, H. *Macromol. Rapid Commun.* **2014**, *35*, 479–483.
123. Lebarbé, T.; Negal, M; Grau, E.; Alfos, C.; Cramail, H. *Green Chem.* **2014**, *16*, 1755–1758.
124. Del Rio, E.; Lligadas, G.; Ronda, J. C.; Galià, M.; Meier, M. A. R.; Càdiz, V. *J. Polym. Sci., A: Polym. Chem.* **2011**, *49*, 518–525.
125. Hong, S. H.; Sanders, D. P.; Lee, C. W.; Grubb, R. H. *J. Am. Chem. Soc.* **2005**, *31*, 17160–17161.
126. Abbas, M.; Slugovc, C. *Tetrahedron Lett.* **2011**, *52*, 2560–2562.
127. Gaur, U.; Wunderlich, B. *Macromolecules* **1980**, *13*, 445–446.

Publication Date (Web): June 18, 2015 | doi: 10.1021/bk-2015-1192.ch004

Publication Date (Web): June 18, 2015 | doi: 10.1021/bk-2015-1192.ch005

Chapter 5

Emerging Enzyme-Based Technologies for Wastewater Treatment

Andrew J. Maloney,[1] Chenbo Dong,[1,2] Alan S. Campbell,[1,3] and Cerasela Zoica Dinu*,[1]

[1]Department of Chemical Engineering, West Virginia University, 395 Evansdale Drive, Engineering Science Building, Room 445, Morgantown, West Virginia 26506
[2]Department of Civil and Environmental Engineering, Rice University, 6100 Main Street, Houston, Texas 77005
[3]Department of Biomedical Engineering, Carnegie Mellon University, 15B S 25th Street, Pittsburgh, Pennsylvania 15203
***E-mail: Cerasela-Zoica.Dinu@mail.wvu.edu.**

In an effort to reduce the need for increased treatment and because of its high importance, interest in "green-based technologies" for wastewater management has picked up in recent years. Green methods aim to be logistically feasible, reliable, efficient, less time and energy consuming and highly cost-effective. This review provides an overview of the state-of-the-art technologies currently used for wastewater treatment and proposes developing novel solutions using enzymes and enzyme-based conjugates to remediate active chemicals and their metabolic products thereby ensuring water reusability. Addressing the global challenges of water quality with biotechnological approaches will provide the optimum conditions for prolonged green decontamination and reduced logistical burdens.

In Green Polymer Chemistry: Biobased Materials and Biocatalysis; Smith, et al.;
ACS Symposium Series; American Chemical Society: Washington, DC, 2015.

Publication Date (Web): June 18, 2015 | doi: 10.1021/bk-2015-1192.ch005

The Need for Wastewater Treatment

Water is the foremost natural resource in the world; approximately 2.5% of the available source is in surface freshwater with only about 1/3 of this being readily accessible for human use (*1*). In the United States, 40% of the freshwater is used for agriculture, 42% for thermoelectric power generation, 5% for industry purposes, and only 9% is used by domestic households (*2*). However, many surface water resources are vulnerable to pollution; for instance, water can be contaminated relatively easily from fertilizer run-off (*3*), as a side effect of the industry and its usage of harsh organic solvents (*4*), or from everyday life (*5*) and the treatment of human waste and fecal matter (*6*).

To address increasing water pollution concerns nationwide, investment policies and research strategies that increase water use efficiency and decrease water waste have been developed and implemented (*7–9*). For instance, the policies applied by the Environmental Protection Agency (EPA) and Natural Resources Defense Council (NRDC) have regulated the disposal of unused or expired drugs or of pharmaceutical discharges (*10*), and adopted strict metal ion guidelines (*11*) in order to reduce the impact of such pollutants or their metabolites if/when released accidentally. Complementary, research trends have looked at the development of industrial-grade products from reaction conditions that require milder solvent systems and reagents (*12*, *13*), while research strategies considered both the contaminant characteristics and its persistence (*14*) in the environment (*15*). For instance, for a contaminant that does not mix with the ground water but only floats on its surface, remediation treatments were employed to either guide the contaminant to an "aspiratory" reservoir (*16*) or skim the contaminant from the water using material-based sponges, i.e., polypropylene fiber fabric (*17*) and woolen felt (*18*). Other treatments and decontamination technologies rely on chemical scrubbing (*19*), adsorption (*20–22*), precipitation via electrolysis (*23*), and chemical precipitation (*24*). While effective, such methods either need frequent replacement of the active decontaminating agent or are relatively inefficient, time consuming and expensive.

Engineered Nanoparticles-Based Strategies for Wastewater Treatment

Recent studies applied nanotechnology and selected characteristics of nanomaterials to increase the efficiency, reliability and feasibility of wastewater treatment (Figure 1). When adsorbents made up of activated carbon (such as rice husks (*22*) and corn biochar (*21*)) or nanoparticles (such as modified silica or carbon nanotubes (*20*)) were used to remediate oil spills, considerably larger contaminant absorption capability was recorded (*25*). The super-hydrophobicity of carbon nanotubes for instance also prevented water adsorption, further confirming their increased potential for water clearance (*25*). While chemical adsorption tends to be successful for removal of contaminants, it can become inefficient in long term because the mechanism of removal relies on chemical or physical interaction of the absorbant with the substrate available surface area.

In Green Polymer Chemistry: Biobased Materials and Biocatalysis; Smith, et al.;
ACS Symposium Series; American Chemical Society: Washington, DC, 2015.

With the substrate becoming saturated, the efficiency of adsorption decreases overtime which will eventually lead either to replacement or active maintenance of the adsorption area to ensure sustainable wastewater treatment.

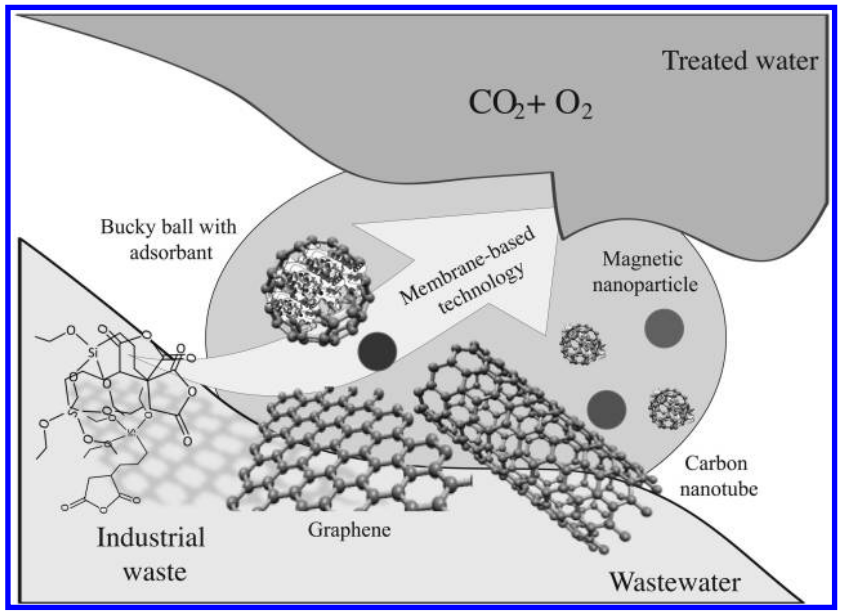

Figure 1. Diagram of a wastewater treatment platform of industrial products. The system is based on membranes containing nanotechnology products (i.e., carbon nanotubes, bucky balls, graphene or magnetic nanoparticles) capable to adsorb and degrade industrial contaminants.

Magnetic iron oxide nanoparticles were shown to adsorb organic compounds and inorganic metals from water while allowing for easy separation and recovery though an applied external magnetic field (*26–28*). Previous research strategies reported for instance that iron oxide submicron-wires could be successfully prepared by novel microwave heating method of graphite/$Fe(CO)_5$ mixture; such wires showed enhanced performance for Cr(VI) removal from polluted water (*29*). Further, nanoengineered mesoporous organosilica synthesized using wet chemistry also demonstrated great ability for the removal of a wide range of organic and inorganic pollutants (*30*), from heavy metal species (*31*), to toxic anions (*32*), and radionuclides (*30*). Similarly, synthetic metallic catalysts obtained through organic synthesis reactions (*33*) demonstrated high efficiency and reliability when used for wastewater treatment (*20–22*); the solubility of such metal catalysts reduced the requirement for organic solvents usage and therefore decreased the amount of waste.

Publication Date (Web): June 18, 2015 | doi: 10.1021/bk-2015-1192.ch005

Publication Date (Web): June 18, 2015 | doi: 10.1021/bk-2015-1192.ch005

Typically, remediation techniques based on metal catalysts rely on a chemical degradation reaction where the metal catalyst usage allows for its active recovery and thus reusability. Gil-Lorenzo et. al., for instance used pyrite nanoparticles as fenton-like reagents for the remediation of phtalocyanine (*34*), Han and Yan looked at deactivating chlorinated hydrocarbons through bimetallic nickel-iron nanoparticles for remediation (*35*), while others have looked at using BiOI-titanium dioxide (TiO_2) for nanoparticle-based water treatment (*36*).

Recently, it was also proposed that metal-oxide nanosupports immersed in water and under light irradiation generate hydrogen peroxide (H_2O_2) known to reduce biochemical oxygen demand (BOD) or chemical oxygen demand (COD) of industrial wastewater (*37*). H_2O_2 was shown to be a superior candidate for wastewater treatment because of its ability of oxidizing organic pollutants (*34*, *37*, *38*). Specifically, several research groups have looked at creating "green" fenton reagents in conjunction with a H_2O_2 source capable to oxidize the organic pollutants (*34*, *37*, *39*). TiO_2-based photocatalysis for instance involves the generation of electron-hole pairs (e^-/h^+) (*40*) and formation of superoxide radical anions (O_2^-), hydroxyl radicals (•OH), and hydroperoxyl radicals (•OOH) (*41–43*). During TiO_2-mediated Bis(2-chloroethoxy)methane photodegradation, the H_2O_2 was generated from a combination of $2(ClCH_2CH_2O)_2CHO_2$• intermediate under UV light irradiation (*44*). In addition, the TiO_2-based photocatalysis process was shown to eliminate sulforhodamine-B dye in aqueous environment (*45*) through the same mechanism of peroxide generation (*46*). The presence of H_2O_2 was confirmed during the dye degradation by measuring the amount of the generated H_2O_2 and determining both its rate of formation and the rate of dye decomposition. Other experiments have showed that both nitrogen-doped TiO_2 under visible light and/or sunlight irradiation (*47*) and sintered nanocrystalline-TiO_2 semiconductor electrode (NSE) used as anodes (*48*) at room temperature and in a photo-electrochemical reactors could generate H_2O_2 to be used for water purification (*48*). Additional studies have also shown that H_2O_2 could be generated upon irradiation of WO_3 photoanodes or platinized WO_3 nanoparticles, or TiO_2 nanosupports synthesized by hydrothermal processing (*49*), with such particles showing increased wastewater treatment efficiencies (*50*).

Despite this extensive body of research, the current production costs and recycling issues associated with the fabrication, characterization, and usages of such nano-based technologies inhibit their large-scale implementation (*51*). Further, even though the metallic nanoparticles have been promising in terms of reusability and decontamination efficiencies, they were also shown to possess environmental drawbacks. Specifically, heavier metals such as nickel have been shown to be carcinogenic if leakage occurs (*52*); further, any potential spills or leaks of the nanoparticle itself into the water supply could cause an even more detrimental effect (*52*) due to its accumulation and influence on the aquatic life (*53*). With accumulation depending on the metal concentration as well as the exposure time, water quality parameters such as pH, conductivity, and dissolved oxygen content also become affected (*54*) constituting a risk not only for the organisms that it contains but also for the predatory fishes, birds and mammals feeding on such contaminated stocks (*55*).

Publication Date (Web): June 18, 2015 | doi: 10.1021/bk-2015-1192.ch005

Are Biological Means for Water Decontamination Feasible?

The most effective means for surface water decontamination remain preventing further accidental or intentional release of contaminated sources and allowing for the natural biological, chemical, and physical life-regulated processes to break down the existing contaminant or its metabolic products over time. However, depending on the nature of the contaminant, this process is time consuming and at times, inefficient. Biologically "inclined" methods such as activated sludge (*56*), biotrickling filters (*19*), and vermicompost (*57*), or the use of biological species as the "workhorses" for synthesis (*58*) of decontamination species to replace the function of harsher chemicals (*59*), have been recently examined as a potential route for biological-based, i.e., green, decontamination. However, such methods face major drawbacks regarding their reliability, feasibility and efficiency. Specifically, a problem in conventional active sludge process for water treatment is the high sludge production (*60*); further, the conventional activated sludge process may not meet modern environmental protection requirements. Moreover, the biotrickling filter could not be successfully applied to highly concentrated volatile organic compounds (VOCs) because of its limited efficiency (*61*). It was also reported that when vermicompost for instance was used, the efficiency of the process was difficult to maintain at temperatures below 35°C (*61*). For biological means to be implemented for wastewater treatment, more complex processes that can increase methods efficiency, feasibility, reliability and shelf-life need to be implemented (*62*).

Enzymes for Wastewater Treatment

The efficiency of catalytic reactions as well as the high selectivity, make the enzyme-based water pollution monitoring and wastewater treatment system one of the preferable choices capable of reducing the logistical burdens associated with usage of harsh chemicals. Recent research has shown that the peroxidase family (EC:1.11.1.7) (*63*) is capable of degrading a wide spectra of aromatic compounds (*64*) from anilines (*65*) to phenols (*66*), and from aromatic dyes (*67*), to polyaromatic hydrocarbons (*68*), and polychlorinated biphenyls (*69*), all products of industrial contamination (*70*). For instance, Bayramoglu and peers used horseradish peroxidase (HRP) to remove phenol and p-chlorophenol from solution (*66*); phenolic compounds are known to be major pollutants of industrial wastewaters. The authors showed that HRP covalently immobilized onto magnetic beads retained a high activity and stability and performed higher phenol conversions than its free counterpart, thus indicating the potential of the immobilized HRP to be successfully used for large-scale continuous enzymatic degradation of such pollutants. Similarly, Bhunia et. al., used HRP and provided a systematic analysis of the efficiency of removal of azo dyes (i.e., Remazol blue); anaerobic transformations of such dyes could result in the formation and accumulation of highly toxic aromatic amines which are known for their carcinogenic effects (*67*). The authors showed that HRP has broad substrate specificity as well as as an optimum pH where dye degradation occurs with

In Green Polymer Chemistry: Biobased Materials and Biocatalysis; Smith, et al.;
ACS Symposium Series; American Chemical Society: Washington, DC, 2015.

high efficiency. Additionally, Koller et. al., used HRP and showed removal of about 90% of chlorinated dibenzodioxins (PCDD) and dibenzofurans (PCDF), two significant environmental pollutants (*69*). Specifically, the authors evaluated the efficiency of 2,5-Dichlorobiphenyl (PCB9) and 2,2′,5,5′-tetrachlorobiphenyl (PCB52) degradation when used at similar concentrations to what are currently found in the water contaminated sources and found that to be fast and efficient, in a reaction period of only 220 min.

For a peroxidase-based reactor to be used for wastewater treatment, the enzyme needs to: (1) be immobilized to thus increase its reusability, lifetime, and improve its stability; and (2) allow efficient interaction with its substrate (i.e., H_2O_2 for the peroxidase family) to thus be capable of pollutant degradation. Immobilization onto nanosupports such as nanotubular aluminosilicate (*71*), graphene oxide (*72*), carbon nanotubes (*73–75*), graphene oxide sheets (*74*), nanodiamonds (*76*), and metal-oxide particles (*77*), was achieved either through physical or chemical means or through encapsulation into a gel (*78*) or membrane (*79*, *80*). Optimization of the immobilization conditions at any of these nanosupport interfaces involved controlling the enzyme interactions with the nanosupport or encapsulator (with or without a linker) (*74*) to preserve its functionality and catalytic behavior. Typically, the immobilization interfaces could lead to non-specific interactions with the enzymes that could change its structure and conformation and decrease its catalytic activity (*74*). Previous studies have shown that additionally, protein-protein interactions (*74*, *81*) at such nanosupport interfaces could also lead to enzyme loss of activity (*82*).

For physical immobilization that relies primarily on nonspecific, hydrophobic interactions between enzyme and the nanosupport (*77*), it was observed that enzyme loadings (amount of enzyme/ amount of the support), activities and catalytic efficiencies (both relative to free enzyme in solution) are somewhat variable due to the inherent non-specificity of the interactions or the non-uniformity of enzyme loading (*74*). Complementary, for covalent immobilization that uses chemical reactions to form a covalent bond between the nanosupport and the enzyme (i.e., through a zero EDC/NHS chemistry between carboxylic acids and amines (*73*) or through the glutaraldehyde chemistry involving an interaction between amines and carbonyl groups) (*83*), it was shown that the chemical groups of the enzyme can be manipulated to interact with the functional groups of the nanosupport (*83*) with a variety of support functionalizations influencing the immobilization efficiency as well as its "initiator" (e.g., carboxylic acid (*73*), hydroxyl (*76*), amine (*76*), or carbonyl (*76*) respectively). Lastly, covalent immobilization though a linker molecule (e.g., polyethylene glycol, PEG) (*74*), was used to reduce direct contact between the nanosupport and the enzyme (*74*, *84*). The potential benefits of using such polymeric linkers are associated with their ability to allow for controlling the distance between the enzyme and the nanosupport, thus minimizing nonspecific interaction and sterical conformation changes of the enzyme and thus increasing its catalytic efficiency. In addition, covalent association of enzymes via peptide-modified surfaces used as linkers were shown to maintain enzyme specific activity as well stability, and controlled its orientation at the support interface (*85*). While there was no single nanosupport recommended as the optimum one for

Publication Date (Web): June 18, 2015 | doi: 10.1021/bk-2015-1192.ch005

all enzymes being tested, some general trends have been observed. For instance, research has shown that more curved nanosupports are more desirable than their flatter counterparts because they tend to limit the nonspecific interactions as well as enzyme-enzyme interactions (*73*, *86–88*). Campbell et. al., for instance have demonstrated that soybean peroxidase, glucose oxidase, and chloroperoxidase have activities ranging from 3% to nearly 30% depending on the immobilization method and the charge and morphology of the nanosupport being used (*74*, *77*).

Immobilization was shown to increase the mechanical and thermal stability of the enzymes while decreasing the probability of enzyme leaching into solution (*75*); mechanical and thermal stabilities are needed when reusability and increased lifetime of the enzyme-based conjugates are considered. Particularly, Verma et al., showed that the thermal stability of lipase was greatly improved upon its immobilization onto carbon nanotubes (*89*), while Klein and coworkers showed a similar phenomenon for β-D-Galactosidase immobilized onto chitosan (*90*). Further, affinity immobilization was shown to exploit the specificity of the enzyme to the substrate, in different physiological conditions, to increase enzyme immobilization capacity and reusability (*91*). Moreover, entrapment of enzymes in gels or fibers was shown to result in reduced enzyme leaking and increase in its mechanical stability (*80*).

However, even though analysis and improvements of efficiency, selectivity and stability of enzymes immobilized onto nanosupports have offered opportunities for enzyme implementation in wastewater treatment (*92*), the poor performance of an enzyme-based technology due to the limited reaction time or the limited available substrate required for enzyme functionality, have hindered its large scale, industrial implementation.

Proposed Means and Support Studies for the Next Generation of Self-Sustainable Wastewater Treatment Platforms

We now propose that the next generation of green and efficient wastewater treatment platforms based on enzymes can be fabricated through direct immobilization of the biocatalyst onto a nanosupport which is capable to generate enzyme's required substrate through a reaction at its interface. Such a strategy would not only allow for the immobilization and reusability of enzyme but would further permit for the substrate required by the enzyme to be generated on demand thus creating a self-sustainable wastewater treatment platform.

To demonstrate the feasibility of this proposal, our preliminary studies showed that carbon nanotubes can be used as nanosupports for dual enzyme immobilization and natural catalytic chain reactions at their nanointerfaces (*73*). Specifically, the approach involved immobilizing two enzymes namely glucose oxidase (GOX) and chloroperoxidase (CPO) onto carbon nanotubes either via physical and chemical means. The two enzymes maintained their functionality and were able to generate their products with high efficiencies as well as allow for a chain reaction to occur at the carbon nanotube interface to lead to hypochlorous acid generation—a potent microbial decontaminant (Figure 2) (*73*). However, while carbon nanotubes allowed for high loadings and efficiencies did not allow

In Green Polymer Chemistry: Biobased Materials and Biocatalysis; Smith, et al.;
ACS Symposium Series; American Chemical Society: Washington, DC, 2015.

Publication Date (Web): June 18, 2015 | doi: 10.1021/bk-2015-1192.ch005

for creation of a self-sustainable system since the two enzymes both required the substrated to be added for the reaction to occur.

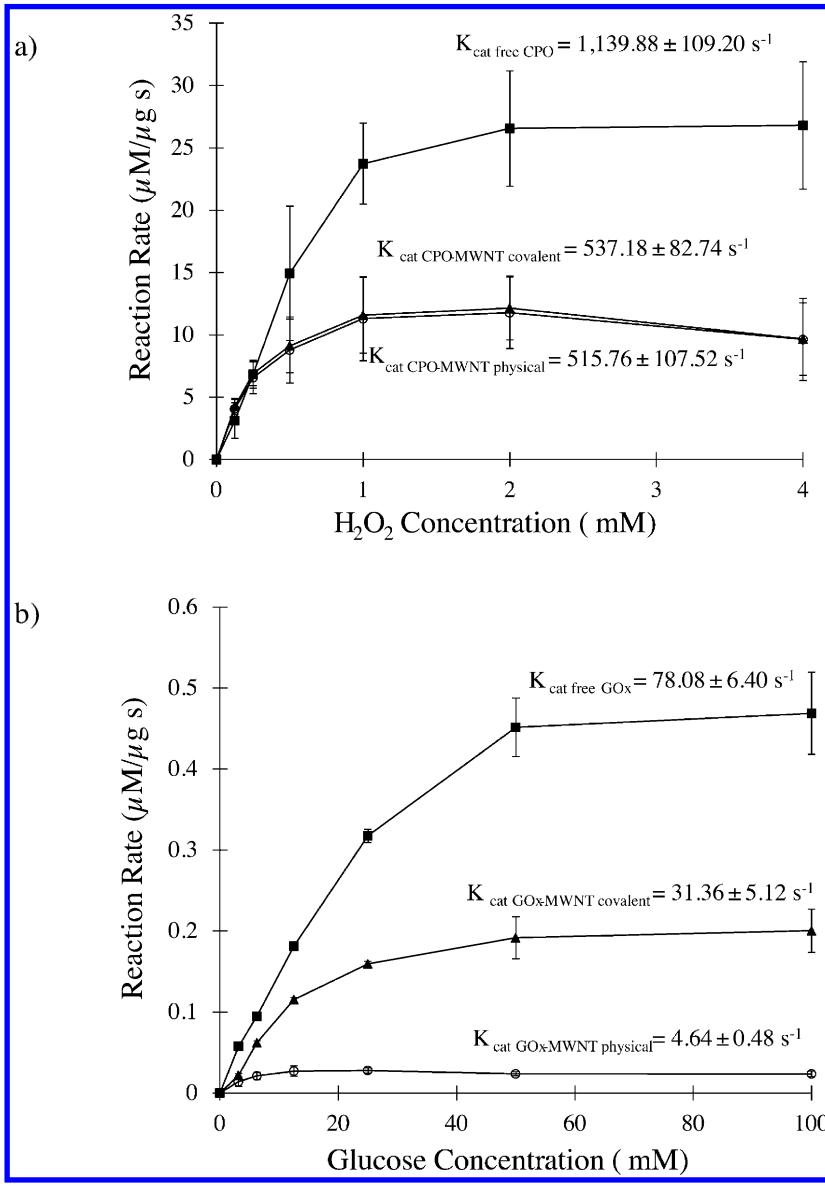

Figure 2. Michaelis-Menten kinetics of enzyme-based MWNTs conjugates. a) CPO-based conjugates (physically immobilized-open circles; covalently immobilized- filled triangles) kinetics relative to free CPO in solution (filled squares). b) GO_x-based conjugates (physically immobilized-open circles; covalently immobilized- filled triangles) kinetics relative to free GO_x in solution (filled squares). Reproduced with permission from reference 78. Copyright 2012 Elsevier.

Publication Date (Web): June 18, 2015 | doi: 10.1021/bk-2015-1192.ch005

Publication Date (Web): June 18, 2015 | doi: 10.1021/bk-2015-1192.ch005

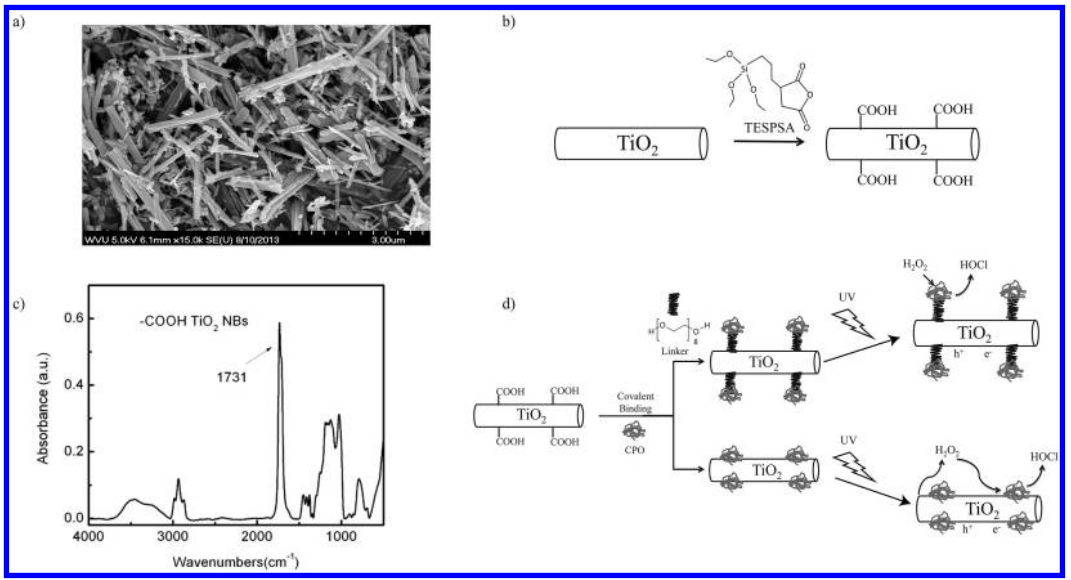

Figure 3. a) Scanning Electron Microscopy (SEM) images of pristine titanium dioxide revealing their morphology and aspect ratios; b) Functionalization of photocatalyst pristine titanium dioxide results in the formation of carboxyl functionalized nanobelts or TiO_2-NBs. c) FTIR spectrum of TiO_2-NBs reveals the presence of the carboxyl peak at 1731 cm^{-1}, confirming -COOH functionalization. d) CPO enzyme immobilization onto TiO_2-NBs with and without the use of a PEG linker. The PEG linker brings the enzyme away from the nanosupport. The concept of hypochlorus (HOCl) generation using the CPO-based conjugates. The UV irradiation of the TiO_2-NBs photocatalysts will generate hydrogen peroxide (H_2O_2) to be used by CPO for in situ HOCl-based decontamination.

Publication Date (Web): June 18, 2015 | doi: 10.1021/bk-2015-1192.ch005

Considering for instance TiO_2, a photocatalyst that produces reactive oxygen species from water when excited under UV light (*93–95*), one can envision using this support as a platform to produce the necessary H_2O_2 to be used as the substrate by immobilized peroxidases to thus ensure a viable self-sustainable platform for wastewater treatment as proposed above. Even though this photocatalyst has been extensively studied for the decontamination of a wide variety of water contaminants (*94*, *96*) as well as contaminants in the air (*97*), to our knowledge there are no previous studies that attempted using this nanointerface to generate H_2O_2 for efficient enzyme kinetics.

Our preliminary results showed that these nanosupports can be produced from pristine anatase TiO_2 via hydrothermal processing (*98*). The nanosupports were found to be 60-300 nm wide and several micrometers in length (SEM; Figure 3a). The pristine anatase TiO_2 nanosupports were further carboxyl functionalized using 3-triethoxysilylpropyl succinic anhydride to allow the formation of TiO_2 nanobelts or TiO_2-NBs (Figure 3b); no significant changes were identified in the TiO_2-NBs morphology or length distribution upon such carboxyl functionalization. Carboxyl functionalities were confirmed using Fourier Transform Infrared Spectroscopy (FTIR; Figure 3c); specifically, the large peak identified at 1731 cm^{-1} confirmed the presence of the C=O bond present onto the TiO_2-NBs (*99*).

Table 1. Characterization of CPO-TiO_2 Hybrid System for *in Situ* Generation of HOCl

Parameter	*CPO-TiO_2*	*CPO-PEG-TiO_2*
Loading (mg protein/mg nanosupport)	0.10 ± 0.03	0.04 ± 0.02
Loading function of enzyme offered (%)	20	8
Specific retained activity relative to free enzyme (%)	0.30 ± 0.13	12.00 ± 1.63
V_{max} (μM μg^{-1} s^{-1})	0.54 ± 0.11	4.64 ± 0.87
K_m (μM H_2O_2)	270 ± 80	490 ± 70
K_{cat} (s^{-1})	22.68 ± 4.62	194.88 ± 36.54
η	0.02	0.17

In order to generate enzyme-nanosupport hybrid systems, we used the TiO_2-NBs as scaffolds for the covalent immobilization of model CPO through EDC/NHS chemistry (*100*, *101*) or EDC/NHS chemistry with a PEG spacer (*75*) (Figure 3d). The PEG spacer was highly hydrophilic, with a length of 3.2 nm; previous studies have shown that such a spacer has little or no chemical effect on enzyme immobilization however it allows for its improved solubility of

In Green Polymer Chemistry: Biobased Materials and Biocatalysis; Smith, et al.;
ACS Symposium Series; American Chemical Society: Washington, DC, 2015.

the nanosupport interface (*84*). The CPO-TiO_2-NBs and CPO-PEG-TiO_2-NBs conjugates showed enzyme loadings of 0.10 ± 0.03 and 0.04 ± 0.02 mg enzyme/mg nanosupport respectively, which represented 20% and 8% of the amount of protein initially offered during the immobilization process (Table 1). The activity of the CPO immobilized at the TiO_2-NBs interface was evaluated using the colorimetric reaction showing the conversion of monochlorodimedon to dichlorodimedon in the presence of H_2O_2 (*74*).

The CPO-TiO_2-NBs conjugates retained about 0.3%, while CPO-PEG-TiO_2-NBs conjugates retained about 12% activity when compared to the activity of the same amount of free CPO in solution (Table 1). The low activity observed for CPO-TiO_2-NBs was attributed to the interface reactions between the enzyme and the TiO_2-NBs nanosupport surface. Specifically, previous studies have shown that nanosupports with lower curvature favor enzyme-enzyme interactions and their non-specific attachment which in turn could lead to enzyme denaturation (*75*, *102*, *103*). Further, at the working pH of 4.8 that is slightly above the isoelectric point of CPO (pI = 4) (*104*), the enzyme has a net negative charge while the TiO_2-NBs (isoelectric point, pI = 6.5) (*105*) has a net positive charge, thus favoring the adsorption or non-specific immobilization of the enzyme and leading to the observed reduced enzyme activity. Meanwhile, the higher activity observed for the CPO-PEG-TiO_2-NBs was presumably due to the PEG spacer that brough the enzyme away from the nanosupport thus reducing its non-specific interaction with the nanosupport as well as its denaturation at the nanointerface (*106*).

Kinetic constants were evaluated for the free CPO and compared to the kinetics of the CPO-based conjugates, i.e., CPO-TiO_2-NBs and CPO-PEG-TiO_2-NBs, by using non-linear regression plots (*107*). Namely, the K_m (substrate concentration at which the initial reaction rate is half maximal) and V_{max} (maximum initial rate of an enzyme catalyzed reaction) values of the CPO-TiO_2-NBs and CPO-PEG-TiO_2-NBs conjugates are shown in Table 1 and reflect comparison to the free CPO in solution. The K_m values were on the same order of magnitude for all analyzed samples; specifically they were found to be 480, 270 and 490 μM, respectively, for the free, CPO-TiO_2-NBs and CPO-PEG-TiO_2-NBs conjugates indicating that there was no significant conformational change of the enzyme active site upon immobilization. The apparent K_m for the directly covalently conjugated enzyme was decreased by about 40% when compared to that of the free enzyme or the PEG covalently conjugated enzyme that showed no significant change. V_{max} values were on the same order of magnitude (i.e., 27, 0.5 and 4.6 μM mg^{-1} s^{-1}, respectively for the free, CPO-TiO_2-NBs and CPO-PEG-TiO_2-NBs conjugates); the V_{max} for the covalently immobilized enzyme decreased about 98% and about 81% for the PEG immobilized samples when compared to the free enzyme in solution. The smaller V_{max} obtained for the covalently immobilized enzyme was presumably due to the enzyme coming into direct contact with the nanosupport, which lead to decreased substrate reaction and consequently slow reaction rate. Our reported K_m and V_{max} results are on the same order of magnitude with previous reports for carbon nanotubes (*103*), polymer coated magnetic nanoparticles interfaces (*108*) or mesoporous silicate (*109*). Any deviations are presumably resulted from the environmental differences in which the experiments were performed.

Publication Date (Web): June 18, 2015 | doi: 10.1021/bk-2015-1192.ch005

The efficiency factor η was also calculated from the maximum reaction rates of the immobilized CPO (both CPO-TiO_2-NBs and CPO-PEG-TiO_2-NBs) relative to the rate of the free enzyme in solution using:

$$\eta = \frac{v_{immobilized}}{v_{free}},$$

where $v_{immobilized}$ is the reaction rate of the immobilized enzyme (directly through covalent immobilization or through PEG and covalent immobilization respectively) and v_{free} is the reaction rate of the free enzyme (Table 1). The efficiency factor for the CPO-TiO_2-NBs was 0.02 while the η for the CPO-PEG-TiO_2-NBs was 0.17. The reduction in the efficiency factor of the immobilized enzyme further confirmed the non-specific interactions with the nanosupport interface and thus enzyme denaturation (*75*, *102*, *103*).

Further tests of enzyme-nanosupport hybrid systems will evaluate the efficiency of both H_2O_2 and subsequently hypochlorus acid generation, their rate of production and decomposition, all upon enzyme-based conjugates irradiation under UV (i.e. UV-A (λ = 316-400 nm) or UV-C (λ = 235-280 nm). Upon demonstration of the hypothesis for this CPO model system, the approach could be extended to soybean peroxidase (SBP) for its applicability in green treatments of products resulted from industrial contamination of water (*70*) such as anilines (*65*), phenols (*66*), or aromatic dyes (*67*), and polyaromatic hydrocarbons (*68*).

Publication Date (Web): June 18, 2015 | doi: 10.1021/bk-2015-1192.ch005

Conclusions

Because of enzyme's versatility and high catalytic efficiency which allow decontamination in mild, green conditions, there is presently a wide variety of ongoing research for designing enzyme-based platforms that allow efficient wastewater treatment. The challenges that limit such platforms large-scale, industrial implementation are however associated with the high cost of synthesizing enzymes *in situ* and/or the use of non-standardized immobilization techniques to ensure improved enzyme reusability, stability and extended shel-f-life. Future research is undergoing to permit great control over the immobilization and reusability of enzymes while ensuring that the substrate to be used can be generated on demand to thus overcome the observed limitations and form the next generation of self-sustainable wastewater treatment platforms.

Acknowledgments

National Science Foundation (CBET-1033266) supported this work. A.J. Maloney thanks the Barry Goldwater Scholarship and Excellence in Education Program.

Publication Date (Web): June 18, 2015 | doi: 10.1021/bk-2015-1192.ch005

References

1. Postel, S. L.; Daily, G. C.; Ehrlich, P. R. *Science* **1996**, *271*, 785–788.
2. Kennedy, J. F.; Barber, N. L.; Linsey, K. S.; Lovelace, J. K.; Maupin, M. A. *Geol. Surv. Circ.* **2005**, *1344*, 1–52.
3. Ielpo, P.; Cassano, D.; Lopez, A.; Pappagallo, G.; Uricchio, V. F.; De Napoli, P. A. *Chem. Cent. J.* **2012**, *6*, 1–12.
4. Plechkova, N. V.; Seddon, K. R. *Chem. Soc. Rev.* **2008**, *37*, 123–150.
5. Abdel-Raouf, N.; Al-Homaidan, A. A.; Ibraheem, I. B. *Saudi J. Biol. Sci.* **2012**, *19*, 257–275.
6. Bixler, J. N.; Cone, M. T.; Hokr, B. H.; Mason, J. D.; Figueroa, E.; Fry, E. S.; Yakovlev, V. V.; Scully, M. O. *Proc. Natl. Acad. Sci. U.S.A.* **2014**, *111*, 7208–7211.
7. *Managing an Uncertain Future: Climate Change Adaptation Strategies for California's Water*; California Department of Water Resources, Sacramento, CA, 2008; http://www.water.ca.gov/climatechange/docs/ClimateChangeWhitePaper.pdf (accessed Feb 5, 2015).
8. *Energy Efficiency in Water and Wastewater Facilities: A Guide to Developing and Implementing Greenhouse Gas Reduction Programs*; U.S. Environmental Protection Agency; Washington, DC, 2013.
9. Saouma, E. *The State of Food and Agriculture*; FAO Agriculture Series, 26; Rome, Italy, 1993; pp 1−328.
10. Ferrer, I.; Zweigenbaum, J. A.; Thurman, E. M. *J. Chromatogr. A* **2010**, *1217*, 5674–5686.
11. D. van Halem, S. A. B.; Amy, G. L.; van Dijk, J. C. *Drinking Water Eng. Sci.* **2009**, *2*, 29–34.
12. Makarov, V. V.; Love, A. J.; Sinitsyna, O. V.; Makarova, S. S.; Yaminsky, I. V.; Taliansky, M. E.; Kalinina, N. O. *Acta Nat.* **2014**, *6*, 35–44.
13. Singh, B. N.; Rawat, A. K.; Khan, W.; Naqvi, A. H.; Singh, B. R. *PLoS One* **2014**, *9*, e106937.
14. Gao, M. R.; Zhang, S. R.; Jiang, J.; Zheng, Y. R.; Tao, D. Q.; Yu, S. H. *J. Mater. Chem.* **2011**, *21*, 16888–16892.
15. Wang, S. B.; Peng, Y. L. *Chem. Eng. J.* **2010**, *156*, 11–24.
16. Wingender, J.; Flemming, H. C. *Int. J. Hyg. Environ. Health* **2011**, *214*, 417–423.
17. Pendergast, M. M.; Hoek, E. M. V. *Energy Environ. Sci.* **2011**, *4*, 1946–1971.
18. Patil, S. V.; Patil, C. D.; Salunke, B. K.; Salunkhe, R. B.; Bathe, G. A.; Patil, D. M. *Appl. Biochem. Biotechnol.* **2011**, *163*, 463–472.
19. Gabriel, D.; Cox, H. H. J.; Deshusses, M. A. *J. Environ. Eng.* **2004**, *130*, 1110–1117.
20. Esmaeili Bidhendi, M.; Nabi Bidhendi, G. R.; Mehrdadi, N.; Rashedi, H. *J. Environ. Health Sci. Eng.* **2014**, *12*, 1–6.
21. Fang, C.; Zhang, T.; Li, P.; Jiang, R. F.; Wang, Y. C. *Int. J. Environ. Res. Public Health* **2014**, *11*, 9217–9237.
22. Yakout, S. M. *Chem. Cent. J.* **2014**, *8*, 1–7.
23. Can, B. Z.; Boncukcuoglu, R.; Yilmaz, A. E.; Fil, B. A. *J. Environ. Health Sci. Eng.* **2014**, *12*, 1–10.

24. Deng, Y.; Englehardt, J. D.; Abdul-Aziz, S.; Bataille, T.; Cueto, J.; De Leon, O.; Wright, M. E.; Gardinali, P.; Narayanan, A.; Polar, J.; Tomoyuki, S. *Water Res.* **2013**, *47*, 850–858.
25. Zhu, K.; Shang, Y. Y.; Sun, P. Z.; Li, Z.; Li, X. M.; Wei, J. Q.; Wang, K. L.; Wu, D. H.; Cao, A. Y.; Zhu, H. W. *Front. Mater. Sci.* **2013**, *7*, 170–176.
26. Zeng, M.; Huang, Y.; Zhang, S.; Qin, S.; Li, J.; Xu, J. *RSC Adv.* **2014**, *4*, 5021–5029.
27. Zhao, Y.; Li, J.; Zhao, L.; Zhang, S.; Huang, Y.; Wu, X.; Wang, X. *Chem. Eng. J.* **2014**, *235*, 275–283.
28. Yang, X.; Li, J.; Wen, T.; Ren, X.; Huang, Y.; Wang, X. *Colloids Surf., A* **2013**, *422*, 118–125.
29. Liu, Z.; Chen, L.; Zhang, L.; Poyraz, S.; Guo, Z. H.; Zhang, X. Y.; Zhu, J. H. *Chem. Commun.* **2014**, *50*, 8036–8039.
30. Walcarius, A.; Mercier, L. *J. Mater. Chem.* **2010**, *20*, 4478–4511.
31. Chandra, D.; Das, S. K.; Bhaumik, A. *Microporous Mesoporous Mater.* **2010**, *128*, 34–40.
32. Hamoudi, S.; El-Nemr, A.; Bouguerra, M.; Belkacemi, K. *Can. J. Chem. Eng.* **2012**, *90*, 34–40.
33. Manea, F.; Houillon, F. B.; Pasquato, L.; Scrimin, P. *Angew. Chem., Int. Ed.* **2004**, *43*, 6165–6169.
34. Gil-Lozano, C.; Losa-Adams, E.; A, F. D.; Gago-Duport, L. *Beilstein J. Nanotechnol.* **2014**, *5*, 855–864.
35. Han, Y.; Yan, W. *Water Res.* **2014**, *66C*, 149–159.
36. Chen, Y.; Xu, X.; Fang, J.; Zhou, G.; Liu, Z.; Wu, S.; Xu, W.; Chu, J.; Zhu, X. *Sci. World J.* **2014**, *2014*, 1–8.
37. Bahmani, P.; Rezaei Kalantary, R.; Esrafili, A.; Gholami, M.; Jonidi Jafari, A. *J. Environ. Health Sci. Eng.* **2013**, *11*, 1–9.
38. Osuji, A. C.; Eze, S. O.; Osayi, E. E.; Chilaka, F. C. *Sci. World J.* **2014**, *2014*, 1–8.
39. Riano, B.; Coca, M.; Garcia-Gonzalez, M. C. *Chemosphere* **2014**, *117C*, 193–199.
40. Gu, C.; Shannon, C. *J. Mol. Catal. A: Chem.*. **2007**, *262*, 185–189.
41. Daneshvar, N.; Salari, D.; Khataee, A. R. *J. Photochem. Photobiol., A* **2003**, *157*, 111–116.
42. Dionysiou, D. D.; Suidan, M. T.; Bekou, E.; Baudin, I.; Laine, J. M. *Appl. Catal., B* **2000**, *26*, 153–171.
43. da Silva, C. G.; Faria, J. L. *J. Photochem. Photobiol., A* **2003**, *155*, 133–143.
44. Chen, C. C.; Wu, R. J.; Yao, I. C.; Lu, C. S. *J. Hazard. Mater.* **2009**, *172*, 1021–1032.
45. Chen, C. C.; Zhao, W.; Li, J. Y.; Zhao, J. C. *Environ. Sci. Technol.* **2002**, *36*, 3604–3611.
46. Chalasani, R.; Vasudevan, S. *ACS Nano* **2013**, *7*, 4093–4104.
47. Sun, J. H.; Qiao, L. P.; Sun, S. P.; Wang, G. L. *J. Hazard. Mater.* **2008**, *155*, 312–319.
48. Peralta-Hernandez, J. M.; Meas-Vong, Y.; Rodriguez, F. J.; Chapman, T. W.; Maldonado, M. I.; Godinez, L. A. *Water Res.* **2006**, *40*, 1754–1762.
49. Seabold, J. A.; Choi, K. S. *Chem. Mater.* **2011**, *23*, 1105–1112.

50. Kim, J.; Lee, C. W.; Choi, W. *Environ. Sci. Technol.* **2010**, *44*, 6849–6854.
51. Savage, N.; Diallo, M. S. *J. Nanopart. Res.* **2005**, *7*, 331–342.
52. Jose, C. C.; Xu, B.; Jagannathan, L.; Trac, C.; Mallela, R. K.; Hattori, T.; Lai, D.; Koide, S.; Schones, D. E.; Cuddapah, S. *Proc. Natl. Acad. Sci. U.S.A.* **2014**, *111*, 14631–14366.
53. Waseem, A.; Arshad, J.; Iqbal, F.; Sajjad, A.; Mehmood, Z.; Murtaza, G. *BioMed Res. Int.* **2014**, *2014* (813206), 1–36.
54. Stokes, P. M.; Bailey, R. C.; Groulx, G. R. *Environ. Health Perspect.* **1985**, *63*, 79–87.
55. Omar, W. A.; Zaghloul, K. H.; Abdel-Khalek, A. A.; Abo-Hegab, S. *Arch. Environ. Contam. Toxicol.* **2013**, *65*, 753–764.
56. Xu, G. H.; Wang, Y. K.; Sheng, G. P.; Mu, Y.; Yu, H. Q. *Sci. Rep.* **2014**, *4*, 1–7.
57. Pereira Mde, G.; Neta, L. C.; Fontes, M. P.; Souza, A. N.; Matos, T. C.; Sachdev Rde, L.; dos Santos, A. V.; da Guarda Souza, M. O.; de Andrade, M. V.; Paulo, G. M.; Ribeiro, J. N.; Ribeiro, A. V. *Sci. World J.* **2014**, *2014*, 917348.
58. Pasquato, L.; Pengo, P.; Scrimin, P. *Supramol. Chem.* **2005**, *17*, 163–171.
59. Khan, M.; Adil, S. F.; Tahir, M. N.; Tremel, W.; Alkhathlan, H. Z.; Al-Warthan, A.; Siddiqui, M. R. *Int. J. Nanomed.* **2013**, *8*, 1507–1516.
60. Ratsak, C. H.; Maarsen, K. A.; Kooijman, S. A. L. M. *Water Res.* **1996**, *30*, 1–12.
61. He, Z.; Zhou, L. C.; Li, G. Y.; Zeng, X. Y.; An, T. C.; Sheng, G. Y.; Fu, J. M.; Bai, Z. P. *J. Hazard. Mater.* **2009**, *167*, 275–281.
62. Gupta, A. K.; Gupta, M. *Biomaterials* **2005**, *26*, 3995–4021.
63. Gray, J. S. S.; Yang, B. Y.; Hull, S. R.; Venzke, D. P.; Montgomery, R. *Glycobiology* **1996**, *6*, 23–32.
64. Chen, Z. Y.; Li, H.; Peng, A. P.; Gao, Y. Z. *Environ. Sci. Pollut. Res.* **2014**, *21*, 10696–10705.
65. Nakamoto, S.; Machida, N. *Water Res.* **1992**, *26*, 49–54.
66. Bayramoglu, G.; Arica, M. Y. *J. Hazard. Mater.* **2008**, *156*, 148–155.
67. Bhunia, A.; Durani, S.; Wangikar, P. P. *Biotechnol. Bioeng.* **2001**, *72*, 562–567.
68. Baborova, P.; Moder, M.; Baldrian, P.; Cajthamlova, K.; Cajthaml, T. *Res. Microbiol.* **2006**, *157*, 248–253.
69. Koller, G.; Moder, M.; Czihal, K. *Chemosphere* **2000**, *41*, 1827–1834.
70. Cheng, J.; Yu, S. M.; Zuo, P. *Water Res.* **2006**, *40*, 283–290.
71. Zhai, R.; Zhang, B.; Wan, Y. Z.; Li, C. C.; Wang, J. T.; Liu, J. D. *Chem. Eng. J.* **2013**, *214*, 304–309.
72. Zhang, F.; Zheng, B.; Zhang, J. L.; Huang, X. L.; Liu, H.; Guo, S. W.; Zhang, J. Y. *J. Phys. Chem. C* **2010**, *114*, 8469–8473.
73. Campbell, A. S.; Dong, C.; Dordick, J. S.; Dinu, C. Z. *Process Biochem.* **2013**, *48*, 1355–1360.
74. Campbell, A. S.; Dong, C.; Meng, F.; Hardinger, J.; Perhinschi, G.; Wu, N.; Dinu, C. Z. *ACS Appl. Mater. Interfaces* **2014**, *6*, 5393–5403.

Publication Date (Web): June 18, 2015 | doi: 10.1021/bk-2015-1192.ch005

Publication Date (Web): June 18, 2015 | doi: 10.1021/bk-2015-1192.ch005

75. Dinu, C. Z.; Zhu, G.; Bale, S. S.; Anand, G.; Reeder, P. J.; Sanford, K.; Whited, G.; Kane, R. S.; Dordick, J. S. *Adv. Funct. Mater.* **2010**, *20*, 392–398.
76. Krueger, A.; Lang, D. *Adv. Funct. Mater.* **2012**, *22*, 890–906.
77. Campbell, A. S.; Dong, C.; Maloney, A.; Hardinger, J.; Hu, X.; Meng, F.; Guiseppe-Elie, A.; Wu, N.; Dinu, C. Z. *Nano LIFE* **2014**, *04*, 1450005.
78. de Lathouder, K. M.; Smeltink, M. W.; Straathof, A. J.; Paasman, M. A.; van de Sandt, E. J.; Kapteijn, F.; Moulijn, J. A. *J. Ind. Microbiol. Biotechnol.* **2008**, *35*, 815–824.
79. Zhang, Y. P.; Liu, T. H.; Wang, Q.; Zhao, J. H.; Fang, J.; Shen, W. G. *Macromol. Res.* **2012**, *20*, 484–489.
80. Shen, Q. Y.; Yang, R. J.; Hua, X.; Ye, F. Y.; Zhang, W. B.; Zhao, W. *Process Biochem.* **2011**, *46*, 1565–1571.
81. Pangule, R. C.; Brooks, S. J.; Dinu, C. Z.; Bale, S. S.; Salmon, S. L.; Zhu, G.; Metzger, D. W.; Kane, R. S.; Dordick, J. S. *ACS Nano* **2010**, *4*, 3993–4000.
82. Tang, C.; Saquing, C. D.; Sarin, P. K.; Kelly, R. M.; Khan, S. A. *J. Membr. Sci.* **2014**, *472*, 251–260.
83. Mateo, C.; Palomo, J. M.; Fernandez-Lorente, G.; Guisan, J. M.; Fernandez-Lafuente, R. *Enzyme Microb. Technol.* **2007**, *40*, 1451–1463.
84. Manta, C.; Ferraz, N.; Betancor, L.; Antunes, G.; Batista-Viera, F.; Carlsson, J.; Caldwell, K. *Enzyme Microb. Technol.* **2003**, *33*, 890–898.
85. Fu, J. L.; Reinhold, J.; Woodbury, N. W. *PloS One* **2011**, *6*, e18692.
86. Zdobinsky, T.; Maiti, P. S.; Klajn, R. *J. Am. Chem. Soc.* **2014**, *136*, 2711–2714.
87. Gokhale, A. A.; Lee, I. *Top. Catal.* **2012**, *55*, 1231–1246.
88. Pavlidis, I. V.; Patila, M.; Bornscheuer, U. T.; Gournis, D.; Stamatis, H. *Trends Biotechnol.* **2014**, *32*, 312–320.
89. Verma, M. L.; Naebe, M.; Barrow, C. J.; Puri, M. *PLoS One* **2013**, *8*, e73642.
90. Klein, M. P.; Fallavena, L. P.; Schoffer Jda, N.; Ayub, M. A.; Rodrigues, R. C.; Ninow, J. L.; Hertz, P. F. *Carbohydr. Polym.* **2013**, *95*, 465–470.
91. Haider, T.; Husain, Q. *Int. J. Pharm.* **2008**, *359*, 1–6.
92. Zhang, Z. S.; Donaldson, A. A.; Ma, X. X. *Biotechnol. Adv.* **2012**, *30*, 913–919.
93. Takahara, Y. K.; Hanada, Y.; Ohno, T.; Ushiroda, S.; Ikeda, S.; Matsumura, M. *J. Appl. Electrochem.* **2005**, *35*, 793–797.
94. Khodadoust, S.; Sheini, A.; Armand, N. *Spectrochim. Acta, Part A* **2012**, *92*, 91–95.
95. Wu, T. X.; Liu, G. M.; Zhao, J. C.; Hidaka, H.; Serpone, N. *J. Phys. Chem. B* **1999**, *103*, 4862–4867.
96. Malato, S.; Fernandez-Ibanez, P.; Maldonado, M. I.; Blanco, J.; Gernjak, W. *Catal. Today* **2009**, *147*, 1–59.
97. Besov, A. S.; Krivova, N. A.; Vorontsov, A. V.; Zaeva, O. B.; Kozlov, D. V.; Vorozhtsov, A. B.; Parmon, V. N.; Sakovich, G. V.; Komarov, V. F.; Smirniotis, P. G.; Eisenreich, N. *J. Hazard. Mater.* **2010**, *173*, 40–46.
98. Wang, J.; Li, M.; Zhi, M. J.; Manivannan, A.; Wu, N. Q. *Prog. Probab.* **2009**, *61*, 71–76.

99. Guo, H.; Wang, X.; Qian, Q.; Wang, F.; Xia, X. *ACS Nano* **2009**, *3*, 2653–2659.
100. Wang, J.; Tafen, D. N.; Lewis, J. P.; Hong, Z. L.; Manivannan, A.; Zhi, M. J.; Li, M.; Wu, N. Q. *J. Am. Chem. Soc.* **2009**, *131*, 12290–12297.
101. Tafen, D. N.; Wang, J.; Wu, N. Q.; Lewis, J. P. *Appl. Phys. Lett.* **2009**, *94*, 93101–93103.
102. Borkar, I. V.; Dinu, C. Z.; Zhu, G. Y.; Kane, R. S.; Dordick, J. S. *Biotechnol. Progr.* **2010**, *26*, 1622–1628.
103. Grover, N.; Borkar, I. V.; Dinu, C. Z.; Kane, R. S.; Dordick, J. S. *Enzyme Microb. Technol* **2012**, *50*, 271–279.
104. Aoun, S.; Chebli, C.; Baloulene, M. *Enzyme Microb. Technol* **1998**, *23*, 380–385.
105. Sharabi, D.; Paz, Y. *Appl. Catal., B* **2010**, *95*, 169–178.
106. Dinu, C. Z.; Borkar, I. V.; Bale, S. S.; Campbell, A. S.; Kane, R. S.; Dordick, J. S. *J. Mol. Catal. B: Enzym.* **2012**, *75*, 20–26.
107. Al-Haque, N.; Santacoloma, P. A.; Neto, W.; Tufvesson, P.; Gani, R.; Woodley, J. M. *Biotechnol. Progr.* **2012**, *28*, 1186–1196.
108. Wang, W.; Xu, Y.; Wang, D. I. C.; Li, Z. *J. Am. Chem. Soc.* **2009**, *131*, 12892–12893.
109. Han, Y. J.; Watson, J. T.; Stucky, G. D.; Butler, A. *J. Mol. Catal. B: Enzym.* **2002**, *17*, 1–8.

Publication Date (Web): June 18, 2015 | doi: 10.1021/bk-2015-1192.ch005

Publication Date (Web): June 18, 2015 | doi: 10.1021/bk-2015-1192.ch006

Chapter 6

Enzymatic Synthesis of Non-Natural Oligo- and Polysaccharides by Phosphorylase-Catalyzed Glycosylations Using Analogue Substrates

Jun-ichi Kadokawa*

Graduate School of Science and Engineering, Kagoshima University, 1-21-40 Korimoto, Kagoshima 890-0065, Japan
***E-mail: kadokawa@eng.kagoshima-u.ac.jp.**

In this chapter, enzymatic synthesis of non-natural oligo- and polysaccharides by phosphorylase-catalyzed glycosylations using analogue substrates as a glycosyl donor is presented. Because phosphorylase shows loose specificity for recognition of substrates, analogue substrates of a native one, α-D-glucose 1-phosphate, have been used as a glycosyl donor in the phosphorylase-catalyzed glycosylations. For example, potato phosphorylase-catalyzed xylosylation, (*N*-formyl)glucosaminylation, and mannosylation of maltooligosaccharides with α-D-xylose, (*N*-formyl)-α-D-glucosamine, and α-D-mannose 1-phosphates to give non-natural oligosaccharides having a unit of the corresponding monosaccharide residues at the non-reducing end. Because thermostable phosphorylase (from *Aquifex aeolicus* VF5) exhibited the different recognition specificity from potato one, this enzyme catalyzed glucuronylation using α-D-glucuronic acid 1-phospahte as a glycosyl donor. Successive mannosylations took place by thermostable phosphorylase catalysis to produce non-natural heterooligosaccharides composed of α-(1→4)-linked plural mannose residues at the non-reducing end. Anionic dendritic α-glucans were synthesized by thermostable phosphorylase-catalyzed glucuronylation of a highly branched cyclic dextrin (glucan dendrimer, GD) as a multifunctional glycosyl acceptor because of the presence of a number

In Green Polymer Chemistry: Biobased Materials and Biocatalysis; Smith, et al.;
ACS Symposium Series; American Chemical Society: Washington, DC, 2015.

of α-(1→4)-glucan non-reducing ends. The following thermostable phosphorylase-catalyzed glucosaminylation of the products further gave amphoteric dendritic α-glucans.

Introduction

Publication Date (Web): June 18, 2015 | doi: 10.1021/bk-2015-1192.ch006

Oligo- and polysaccharides are widely distributed in nature and the large diversity of their structures has been found so far (*1*). Naturally occurring oligosaccharides present in glycoproteins, glycolipids, and other glycoconjugates exhibit important roles and functions in various biological processes. Polysaccharides are one of three major classes of biological macromolecules in nature, in which the others are proteins and nucleic acids, and act as vital materials for *in vivo* functions such as providing an energy resource and acting as a structural material (*2*). Such oligo- and polysaccharide chains are structurally composed of monosaccharide units linked through glycosidic bonds. A glycosidic linkage is a type of covalent bond that joins a monosaccharide residue to another group, typically another saccharide moiety. Natural saccharide chains have very complicated structures owing to not only to a structurally diversity of monosaccharide residues, but also to the differences in stereo- and regio-types of glycosidic linkages. The large diversity of such saccharide chain structures contributes to serve a whole range of biological functions and a subtle change in the structure has a profound effect on the properties and functions of the saccharide chains (*3–5*). For example, both the two representative natural polysaccharides, cellulose and starch, are glucose polymers, but composed of stereoregularly opposite β-(1→4)- and α-(1→4)-glucosidic linkages, respectively. Owing to the difference in such stereofashion of the linkages among the same glucose repeating units, the roles of cellulose and starch in nature are completely different, that is, the structural material and the energy provider, respectively (*6*, *7*). On the basis of the above viewpoints, the precision synthesis of non-natural oligo- and polysaccharides has been attracted much attention in carbohydrate and materials sciences to provide new functional bio-related materials.

Figure 1 shows typical reaction scheme of the glycosylation reaction between two glucose substrates, a donor and an acceptor, for the possible formation of α-(1→4)- and β-(1→4)-linked glucose dimers, maltose and cellobiose. For design of the glycosyl donor and acceptor, an anomeric carbon of the glycosyl donor is activated by introducing a leaving group, and a hydroxy group in the glycosyl acceptor, which takes part in the glycosylation, is used as a free form, whereas the rest of hydroxy groups in both the donor and acceptor are protected. For the stereo- and regioselective formation of a glycosidic linkage, not only the leaving group (X) and protective groups (R, R'), but also a catalyst and a solvent should appropriately be selected (*8–10*). Among possible fashions of glycosidic linkages, only one kind of the linkage must be constructed in the glycosylation to produce saccharide chains with well-defined structure, which exhibit a potential for applications as high performance functional materials. However, the perfect

In Green Polymer Chemistry: Biobased Materials and Biocatalysis; Smith, et al.;
ACS Symposium Series; American Chemical Society: Washington, DC, 2015.

control in stereo- and regioselectivities of glycosidic linkages from various donor and acceptor substrates is still a challenging research topic in the general chemical glycosylations (*11*).

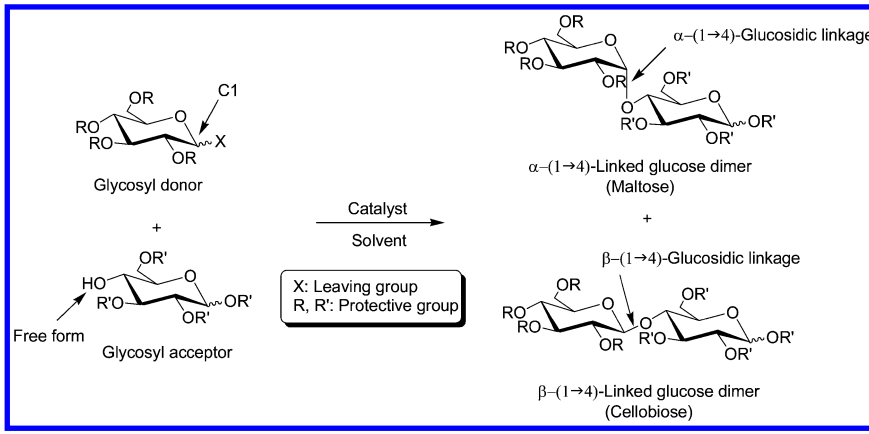

Figure 1. Typical reaction manner of glucosylation between two glucose substrates.

Alternative to the chemical glycosylations, *in vitro* approach by enzymatic catalysis has been significantly developed, so-called 'enzymatic glycosylation' because enzymatic reaction is the superior method in terms of stereo- and regioselectivities compared with that by chemical catalysis (*12*). In six main classes of enzymes, transferase and hydrolase have been practically used as catalysts in enzymatic glycosylations (*13*, *14*). In the enzymatic glycosylation, a glycosyl donor and a glycosyl acceptor can be employed in their unprotected forms, even where the reaction is progressed in stereo- and regio-controlled fashion in aqueous media under mild conditions. Similar to the chemical glycosylation, the enzymatic formation of a glycosidic linkage between an anomeric position of a monosaccharide residue and one of hydroxy groups of the other monosaccharide residue can be achieved by the reaction of an activated glycosyl donor at an anomeric position with a glycosyl acceptor (Figure 2). In the reaction, first, the glycosyl donor is recognized by enzyme and interacted at the anomeric position to form a glycosyl-enzyme intermediate. Then, it is attacked by the hydroxy group of the glycosyl acceptor in the stereo- and regioselective manner according to specificity of each enzyme, leading to the direct formation of the unprotected glycoside. As aforementioned, the enzymes, which have been employed to catalyze the practical glycosylations, are mainly glycosyl transferase and glycosyl hydrolase. Moreover, the former is subclassfied into synthetic enzyme (Leloir glycosyl transferase) and phosphorolytic enzyme (phosphorylase) (*15*, *16*). Because polysaccharides are theoretically produced by repeated glycosylations, enzymatic approaches have been employed for the efficient synthesis of polysaccharides (enzymatic polymerization) (*17–22*).

Publication Date (Web): June 18, 2015 | doi: 10.1021/bk-2015-1192.ch006

In Green Polymer Chemistry: Biobased Materials and Biocatalysis; Smith, et al.;
ACS Symposium Series; American Chemical Society: Washington, DC, 2015.

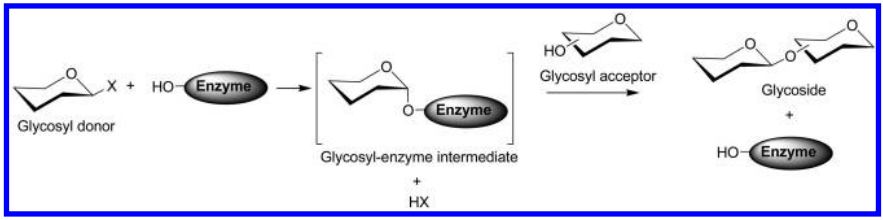

Figure 2. General scheme for enzymatic glycosylation.

Phosphorylases catalyze phsophorolytic cleavage of a glycosidic linkage at the non-reducing end of each specific saccharide chain in the presence of inorganic phosphate to produce 1-phosphate of a monosaccharide residue and the saccharide chain with one smaller degree of polymerization (DP) (*14*, *16*). Because the bond energy of the phosphate at the anomeric position of the product is comparable with that of the glycosidic linkage in the saccharide chain, the phosphorylase-catalyzed reactions are reversible. By means of the reversibility, phosphorylases have been employed as the catalyst for enzymatic glycosylations (*23*). In the reactions, the monosaccharide 1-phosphates are used as a glycosyl donor and the monosaccharide residue is transferred from the donor to the non-reducing end of an specific glycosyl acceptor to construct a stereo- and regiocontrolled glycosidic linkage accompanied with liberating inorganic phosphate. The regio- and stereospecificities of phosphorylases are known to be very strict and each phosphorylase acts on only a specific type of the glycosidic linkage and a monosaccharide 1-phosphate. Of the phosphorylases found in nature so far, α-glucan phosphorylase (glycogen phosphorylase, starch phosphorylase, hereafter, this enzyme is simply called 'phosphorylase' in this chapter) is the most extensively studied.

Characteristic Feature of Phosphorylase-Catalyzed Enzymatic Reactions

Phosphorylase is the enzyme that catalyzes the reversible phosphorolysis of α-(1→4)-glucans at the non-reducing end, such as starch and glycogen, in the presence of inorganic phosphate, to produce α-D-glucose 1-phosphate (Glc-1-P) (Figure 3) (*14*, *16*). Depending on the reaction conditions, phosphorylase catalyzes the enzymatic glucosylation using Glc-1-P as a glycosyl donor to form α-(1→4)-glucosidic linkage (*16*). As a glycosyl acceptor, oligosaccharides composed of α-(1→4)-glucan chain, that is, maltooligosaccharides, are used. In the glucosylation, a glucose residue is transferred from Glc-1-P to the non-reducing end of the acceptor to produce α-(1→4)-glucan chain with one larger DP. Phosphorylase specifically has the smallest DP value in α-(1→4)-glucan chains to recognize, and accordingly, maltooligosaccharides with DPs higher than the smallest one should be used as the glycosyl acceptor. The smallest substrates for the phosphorolysis and glucosylation recognized by potato phosphorylase are maltopentaose (Glc_5) and maltotetraose (Glc_4), respectively. Recently, it has been reported that the smallest DPs of substrates accepted by phosphorylase isolated

Publication Date (Web): June 18, 2015 | doi: 10.1021/bk-2015-1192.ch006

In Green Polymer Chemistry: Biobased Materials and Biocatalysis; Smith, et al.;
ACS Symposium Series; American Chemical Society: Washington, DC, 2015.

from thermophilic bacteria sources (thermostable phosphorylase) for the former and latter reactions are one smaller than those by potato phosphorylase, i.e., Glc_4 and maltotriose (Glc_3), respectively (*24–26*). These observations suggest that phosphorylases exhibit different recognition specificities for the substrates depending on their sources.

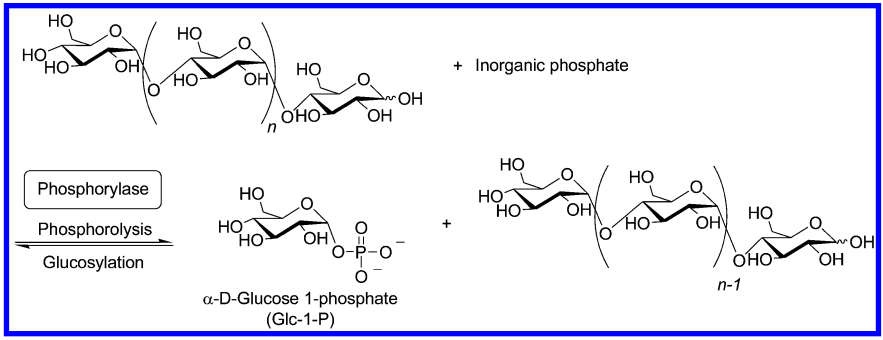

Figure 3. Phosphorylase-catalyzed reversible reactions, phosphorolysis and glucosylation.

When the excess molar ratio of Glc-1-P to the acceptor is present in the reaction system, phosphorylase catalyzes an enzymatic polymerization according to the reaction manner of successive glucosylations at the elongating non-reducing ends to produce a polysaccharide composed of α-(1→4)-glucan chain, that is, amylose (*26–29*). The enzymatic polymerization by phosphorylase catalysis is one of the efficient methods to provide a pure amylose sample because amylose samples purified from natural starch sources often contain amylopectin, the other component of starch, owing to difficulty in the perfect separation of amylose and amylopectin. Furthermore, the polymerization manner catalyzed by phosphorylase belongs to chain-growth polymerization and the glycosyl acceptor is often called a 'primer' of the polymerization because the polymerization is exactly initiated at the non-reducing end of the acceptor. Therefore, the phosphorylase-catalyzed enzymatic polymerization proceeds analogously as a living polymerization because of excluding the occurrence of termination and chain-transfer reaction. Accordingly, the molecular weights (or DPs) of the produced amyloses can be controlled by the Glc-1-P/acceptor feed ratios and their polydispercities are narrow ($M_w/M_n < 1.2$) (*30*). It should be noted further that the phosphorylase-catalyzed reactions take place using the immobilized maltooligosaccharides as the glycosyl acceptor, whose reducing ends are covalently linked to another material such as a polymeric chain because the reducing end does not participate in the reaction (*31*). The immobilized glycosyl acceptor typically serves multifunction due to the presence of the plural non-reducing α-(1→4)-linked glucan ends, implying the synthesis of amylose-containing polysaccharide materials by the phosphorylase-catalyzed enzymatic polymerization using such multifunctional immobilized glycosyl acceptors (*32–36*).

Publication Date (Web): June 18, 2015 | doi: 10.1021/bk-2015-1192.ch006

Because enzymes often show loose specificity for recognition of the substrate structure, the extension of the phosphorylase-catalyzed enzymatic glucosylation has been investigated using analogue substrates of Glc-1-P as a glycosyl donor to obtain non-natural oligosaccharides having the different monosaccharide residues at the non-reducing end (*37*, *38*). In addition, a highly branched polysaccharide having a number of α-(1→4)-glucan non-reducing ends has been used as a multifunctional glycosyl acceptor in the phosphorylase-catalyzed glycosylations using analogue substrates to produce new functional polysaccharide materials (*35*). This chapter reviews the synthesis of non-natural oligo- and polysaccharides having different monosaccharide residues at the non-reducing ends by the phosphorylase-catalyzed enzymatic glycosylations using analogues substrates of Glc-1-P.

Publication Date (Web): June 18, 2015 | doi: 10.1021/bk-2015-1192.ch006

Synthesis of Non-Natural Oligosaccharides by Phosphorylase-Catalyzed Enzymatic Glycosylations Using Analogue Substrates

Potato phosphorylase has been found to recognize several monosaccharide 1-phosphates as the analogue substrates of Glc-1-P, and accordingly catalyzed the enzymatic glycosylations using such substrates as a glycosyl donor to produce non-natural oligosaccharides having the corresponding monosaccharide residues at the non-reducing end (Figure 4) (*37*, *38*). For example, potato phosphorylase has recognized α-D-xylose 1-phosphate (Xyl-1-P) and thus a pentasaccharide having a xylose unit at the non-reducing end has been obtained by the phosphorylase-catalyzed xylosylation of Glc_4 as a glycosyl acceptor with Xyl-1-P as a glycosyl donor, where Glc_4 is a smallest substrate for the glucosylation by potato phosphorylase catalysis (*39*). Because the structural difference of Xyl-1-P from Glc-1-P is only the absence of a CH_2OH group at a position 6, a highly possibility for recognition as the analogue substrate by potato phosphorylase has been supposed. When the potato phosphorylase-catalyzed enzymatic reaction of Glc_4 with Xyl-1-P was carried out, the MALDI-TOF MS and ^1H NMR spectrum of the crude products indicated the production of mainly a pentasaccharide having a Xyl unit. However, because the analytical data did not provide sufficient evidences to position the Xyl unit at the non-reducing end of the product, the treatment of the reaction mixture with glucoamylase (GA, EC 3.2.1.3), which catalyzed an exowise hydrolysis at the non-reducing end of α-(1→4)-glucans, to reveal the position of the Xyl unit in the produced pentasaccharide. If the Xyl unit is positioned at the non-reducing end, GA does not recognize the pentasaccharide as the different non-reducing end structure, and accordingly its GA-catalyzed hydrolysis is not progressed. The ^1H NMR spectrum of the treated materials indicated no occurrence of the enzymatic hydrolysis, suggesting the Xyl unit was positioned at the non-reducing end.

In Green Polymer Chemistry: Biobased Materials and Biocatalysis; Smith, et al.;
ACS Symposium Series; American Chemical Society: Washington, DC, 2015.

Publication Date (Web): June 18, 2015 | doi: 10.1021/bk-2015-1192.ch006

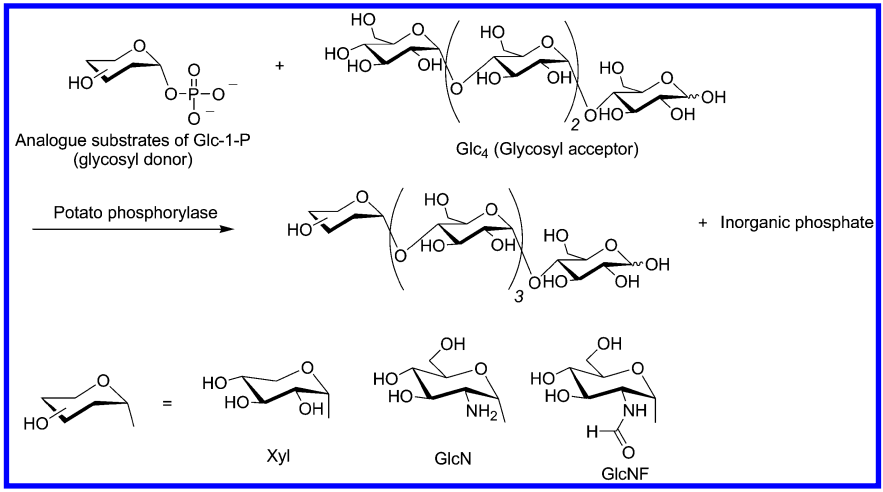

Figure 4. Enzymatic synthesis of non-natural oligosaccharides by potato phosphorylase-catalyzed glycosylations using analogue substrates of Glc-1-P.

It was also reported that α-D-glucosamine 1-phosphate (GlcN-1-P) was recognized as a glycosyl donor by potato phosphorylase (*40*). After the potato phosphorylase-catalyzed glucsaminylation of Glc_4 as a glycosyl acceptor with GlcN-1-P as a glycosyl donor was performed, *N*-acetylation of the crude products lyophilized from the reaction mixture was conducted using acetic anhydride in aqueous Na_2CO_3 solution. Because the difference in the molecular masses of Glc and GlcN units was only 1, which was able to be made larger by the *N*-acetylation of the latter unit, that is, *N*-acetyl-d-glucosamine (GlcNAc), the MS measurement was performed on the *N*-acetylated materials to clearly reveal the structures. In the MALDI-TOF MS of the *N*-acetylated crude products, a significant peak corresponding to the molecular mass of a pentasaccharide containing a GlcNAc unit (GlcNAc-Glc_4) was detected. This data supported that the potato phosphorylase catalyzed the glucosaminylation using GlcN-1-P as a glycosyl donor. To confirm the position of the GlcN unit at the non-reducing end of the pentasaccharide, the treatment of the *N*-acetylated materials with GA was performed. In the MALDI-TOF MS of the treated products, a peak corresponding to the molecular mass of GlcNAc-Glc_4 remained intact, supporting that the GlcNAc unit was positioned at the non-reducing end. The pentasaccharide produced by the present enzymatic reaction has basic nature because of the presence of an amino group in the GlcN residue.

It was further found that potato phosphorylase did not catalyze the glucosaminylation using *N*-acetyl-α-D-glucosamine 1-phsophate as a glycosyl donor because the bulky acetamido group in this substrate blocked approach to the active site of the enzyme (*41*). On the other hand, *N*-formyl-α-D-glucosamine 1-phosphate (GlcNF-1-P), which had a smaller substituent than the acetyl group, was recognized as a glycosyl donor by potato phosphorylase (*41*). This allowed the potato phosphorylase-catalyzed enzymatic glucosaminylation of Glc_4 as a

In Green Polymer Chemistry: Biobased Materials and Biocatalysis; Smith, et al.;
ACS Symposium Series; American Chemical Society: Washington, DC, 2015.

glycosyl acceptor with GlcNF-1-P to give a pentasaccharide having a GlcNF unit (GlcNF-Glc_4). The MALDI-TOF MS and ^1H NMR spectrum of the isolated product fully supported the GlcNF-Glc_4 structure.

Synthesis of acidic oligosaccharides containing a glucuronic (GlcA) residue as an acidic moiety has also been attempted by phosphorylase-catalyzed glucuronylation using α-D-glucuronic acid 1-phosphate (GlcA-1-P) as a glycosyl donor. However, potato phosphorylase did not recognize GlcA-1-P, and thus the desired anionic oligosaccharide was not produced by the catalysis of this enzyme. Interestingly, it was found that thermostable phosphorylase from *Aquifex aeolicus* VF5 (*42*) recognized GlcA-1-P and catalyzed the glucuronylation of Glc_3, which was a smallest glycosyl acceptor for this enzyme, to produce an acidic tetrasaccharide having a GlcA residue (GlcA-Glc_3) (Figure 5) (*43*). The MALDI-TOF MS of the crude products after the treatment with GA exhibited a significant peak corresponding to the molecular mass of GlcA-Glc_3. The ^1H NMR spectrum of the isolated material also supported the structure of the tetrasaccharide with a GlcA residue.

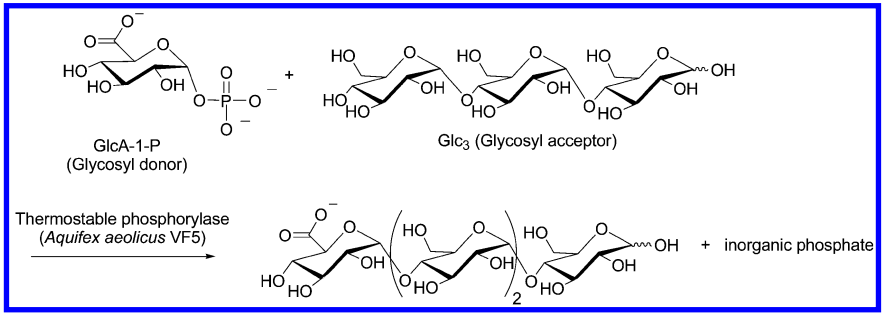

Figure 5. Enzymatic synthesis of acidic tetrasaccharide by thermostable phosphorylase-catalyzed glucuronylation using GlcA-1-P.

As aforementioned, potato phosphorylase catalyzes the successive glucosylations as the polymerization manner to produce the α-(1→4)-glucan chain when the native substrate, Glc-1-P, is used as a glycosyl donor. The above results using the analogue substrates indicate, on the other hand, that if the transfer of a monosaccharide residue from the analogue substrates to the non-reducing end of the acceptor occurs once, further glycosylation was suppressed because the different structures from Glc residue at the non-reducing end are not recognized at the acceptor cite of potato phosphorylase. Taking the different recognition behavior of thermostable phosphorylase from potato one into account, the author found that the former enzyme (from *Aquifex aeolicus* VF5) catalyzed the different reaction manner from the latter enzyme when α-D-mannose 1-phosphate (Man-1-P) was used as a glycosyl donor (*44*). When the thermostable phosphorylase-catalyzed reaction of Glc_3 with Man-1-P was carried out, successive mannosylations took place to give non-natural heterooligosaccharides composed of α-(1→4)-linked mannose chains at the

In Green Polymer Chemistry: Biobased Materials and Biocatalysis; Smith, et al.;
ACS Symposium Series; American Chemical Society: Washington, DC, 2015.

Publication Date (Web): June 18, 2015 | doi: 10.1021/bk-2015-1192.ch006

non-reducing end of Glc_3 (Figure 6). The MALDI-TOF MS of the crude products after the treatment with GA (feed ratio of Man-1-P to Glc_3 = 10:1) observed several peaks separated by m/z 162, which correspond to the molecular masses of tetra-octa-saccharides having one-five Man residues with Glc_3 ($Man_{1\sim4}$-Glc_3), supporting the occurrence of the successive mannosylations by thermostable catalysis. The hexasaccharide fraction was isolated from the crude products by preparative HPLC and its ^1H NMR spectrum fully supported the structure of Man_3-Glc_3. In contrast to this study, when potato phosphorylase-catalyzed mannosylation of Glc_4 with Man-1-P was conducted, only a Man residue was transferred to the non-reducing end of Glc_4 to give a pentasaccharide having a Man residue (Figure 6) (*45*).

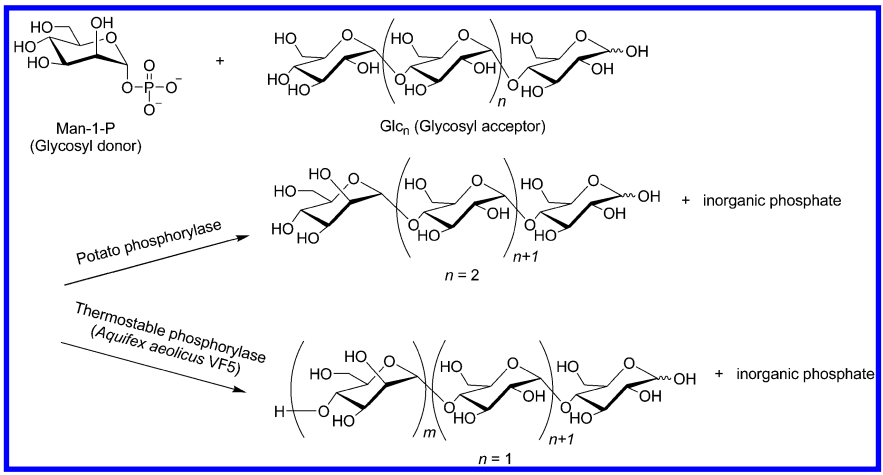

Figure 6. Difference in mannosylation manners using Man-1-P as glycosyl donor by potato and thermostable phosphorylase catalyses.

Synthesis of Dendritic α-Glucans Having Functional Groups at Non-Reducing Ends by Phosphorylase-Catalyzed Enzymatic Glycosylations Using Analogue Substrates

The aforementioned studies indicate that both the functional groups, amino and carboxylic acid groups, are introduced at the non-reducing ends of α-(1→4)-glucan chains by the phosphorylase-catalyzed glucosaminylation and glucuronylation, respectively. By means of the latter enzymatic reaction, dendritic anionic α-glucans has been synthesized (*46*). For this purpose, a highly branched cyclic dextrin (glucan dendrimer, GD) was employed as a multifunctional glycosyl acceptor. This material is a water-soluble dextrin that is produced from amylopectin by cyclization catalyzed by branching enzyme (EC 2.4.1.18) (*47–49*). Because GD has a number of the non-reducing α-(1→4)-glucan ends, this acts as a multifunctional glycosyl acceptor for the phosphorylase-catalyzed

In Green Polymer Chemistry: Biobased Materials and Biocatalysis; Smith, et al.;
ACS Symposium Series; American Chemical Society: Washington, DC, 2015.

Publication Date (Web): June 18, 2015 | doi: 10.1021/bk-2015-1192.ch006

glycosylation. The thermostable phosphorylase-catalyzed glucuronylation of GD (M_n = 1.25 x 10^5, M_w = 1.42 x 10^5, number average unit chain lengths = 15.0 glucose residues, the number of non-reducing ends = ca. 59) with GlcA-1-P was carried out in feed ratios of donor/acceptor (non-reducing end) = 0.5, 1, and 2 (Figure 7). The products were isolated using anion exchange column and the structures were confirmed by the ^{1}H NMR analysis. The glucuronylation ratios of the GlcA residues to the non-reducing ends was calculated from the integrated ratio of the two kinds of the H-4 signals in the non-reducing Glc and GlcA residues to be 34.8, 50.5, and 64.4% in the products obtained by the donor/acceptor feed ratios of 0.5, 1, and 2, respectively. These results indicated the glucuronylation ratios were controlled by the feed ratios.

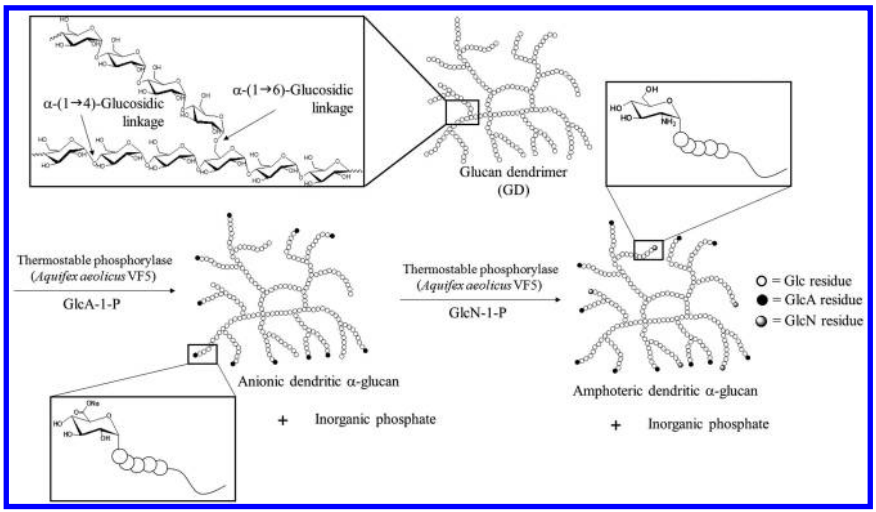

Figure 7. Enzymatic synthesis of anionic and amphoteric a-glucans by thermostable phosphorylase catalyzed glucuronylation and subsequent glucosaminylation using GD as multifunctional glycosyl acceptor.

The enzymatic synthesis of dendritic amphoteric α-glucans having both glucuronic acid and glucosamine residues at the non-reducing ends was further conducted by the subsequent thermostable phosphorylase-catalyzed glucosaminylation of the acidic products (Figure 7) (*50*). The successive reactions in various glycosyl donor feed rations gave the amphoteric materials having the different GlcA/GlcN ratios. The ζ-potential values of the products were changed from positive to negative depending on the pH change from acidic and basic. The values of their inherent isoelectric points (pIs) were calculated by the pH values, where ζ-potential was zero charge, which were reasonably dependent upon the GlcA/GlcN ratios in the products. On the basis of the dynamic light scattering measurement, all the amphoteric products formed large aggregates in water at pH = pI, whereas disassembled at pH shifted from pI. At pH = pI, the structure of the amphoteric α-glucans is more hydrophobic and less stable due to absence of

Publication Date (Web): June 18, 2015 | doi: 10.1021/bk-2015-1192.ch006

In Green Polymer Chemistry: Biobased Materials and Biocatalysis; Smith, et al.;
ACS Symposium Series; American Chemical Society: Washington, DC, 2015.

intermolecular repulsive forces, leading to the tendency of assembly. On the other hand, the electrostatic repulsion between the cationic/cationic or anionic/anionic groups in the materials at the different pH values from pI appeared, resulting in prevention of assembly. These properties of the present materials are similar as those of proteins.

Conclusion

The present chapter overviewed the enzymatic synthesis of non-natural oligo- and polysaccharides by phosphorylase-catalyzed glycosylations using analogue substrates. Potato phosphorylase-catalyzed glycosylations using several monosaccharide 1-phosphates as a glycosyl donor occurred to produce non-natural oligosaccharides having a unit of the corresponding monosaccharide residues at the non-reducing end. In addition to these substrates, thermostable phosphorylase from *Aquifex aeolicus* VF5 recognized GlcA-1-P in the glucuronylation to yield an anionic oligosaccharide having a GlcA unit at the non-reducing end. This enzyme also catalyzed successive mannosylations using Man-1-P to produce α-(1→4)-linked mannose chains. By means of the thermostable phosphorylase-catalyzed glucuronylation of GD as a multifunctional glycosyl acceptor with GlcA-1-P, the anionic dendritic α-glucans were synthesized. The glucosaminylation of the products with GlcN-1-P by thermostable phosphorylase catalysis was then conducted to give the amphoteric dendritic α-glucans. Such non-natural oligo- and polysaccharides have the highly potential to be employed as practical materials in the biological, medicinal, and pharmaceutical research fields. Because the analogue substrates have been provided by organic synthetic procedures, the approach from the viewpoint of the synthetic organic chemistry is in demand to investigate the present studies. The author, therefore, states the efficient collaboration between the research fields of synthetic organic chemistry and enzymatic technology will contribute to the further progress in the enzymatic synthesis of functional non-natural oligo- and polysaccharides in the future.

Publication Date (Web): June 18, 2015 | doi: 10.1021/bk-2015-1192.ch006

References

1. Berg, J. M.; J. Tymoczko, L.; Stryer, L. *Biochemistry*, 6th ed.; W. H. Freeman & Co.: New York, 2006; Chapter 11.
2. Schuerch, C. In *Encyclopedia of Polymer Science and Engineering*, 2nd ed.; Mark, H. F., Bilkales, N., Overberger, C. G., Eds.; John Wiley & Sons: New York, 1986; Vol. 13, pp 87−162.
3. *Carbohydrates in Chemistry and Biology*; Ernst, B., Hart, G. W., Sinaÿ, P., Eds.; Wiley-VCH: Weinheim, Germany, 2000.
4. *Glycoscience*, 2nd ed.; Fraser-Reid, B. O., Tatsuta, K., Thiem, J. Coté, G. L., Flitsch, S., Ito, Y., Kondo, H., Nishimura, S.-I., Yu, B., Eds.; Springer: Berlin, 2008.
5. Varki, A., Cummings, R. D., Esko, J. D., Freeze, H. H., Stanley, P., Bertozzi, C. R., Hart, G. W., Etzler, M. E., Eds.; *Essentials of Glycobiology*, 2nd ed.; Cold Spring Harbor Laboratory Press: New York, 2009.

6. Klemm, D.; Heublein, B.; Fink, H.–P.; Bohn, A. *Angew. Chem., Int. Ed.* **2005**, *44*, 3358–3393.
7. Lenz, R. W. *Adv. Polym. Sci.* **1993**, *107*, 1–40.
8. Paulsen, H. *Angew. Chem., Int. Ed. Engl.* **1982**, *21*, 155–173.
9. Schmidt, R. R. *Angew. Chem., Int. Ed. Engl.* **1986**, *25*, 212–235.
10. Toshima, K.; Tatsuta, K. *Chem. Rev.* **1993**, *93*, 1503–1531.
11. Mydock, L. K.; Demchenko, A. V. *Org. Biomol. Chem.* **2010**, *8*, 497–510.
12. Desmet, T.; Soetaert, W.; Bojarová, P.; Křen, V.; Dijkhuizen, L.; Eastwick-Field, V.; Schiller, A. *Chem. Eur. J.* **2012**, *18*, 10786–10801.
13. Shoda, S.; Izumi, R.; Fujita, M. *Bull. Chem. Soc. Jpn.* **2003**, *76*, 1–13.
14. Seibel, J.; Jördening, H.-J.; Buchholz, K. *Biocatal. Biotransform.* **2006**, *24*, 311–342.
15. *Handbook of Glycosyltransferases and Related Genes*; Taniguchi, N., Honke, K., Fukuda, M., Eds.; Springer: Tokyo, 2002.
16. Kitaoka, M.; Hayashi, K. *Trends Glycosci. Glycotechnol.* **2002**, *14*, 35–50.
17. Kobayashi, S.; Uyama, H.; Kimura, S. *Chem. Rev.* **2001**, *101*, 3793–3818.
18. Kobayashi, S. *J. Polym. Sci., Part A: Polym. Chem.* **2005**, *43*, 693–710.
19. Kobayashi, S. *Proc. Jpn. Acad., Ser. B* **2007**, *83*, 215–247.
20. Kobayashi, S.; Makino, A. *Chem. Rev.* **2009**, *109*, 5288–5353.
21. Kadokawa, J.; Kobayashi, S. *Curr. Opin. Chem. Biol.* **2010**, *14*, 145–153.
22. Kadokawa, J. *Chem. Rev.* **2011**, *111*, 4308–4345.
23. Kadokawa, J.; Kaneko, Y. *Engineering of Polysaccharide Materials – by Phosphorylase-Catalyzed Enzymatic Chain-Elongation*; Pan Stanford Publishing Pte. Ltd.: Singapore, 2013.
24. Boeck, B.; Schinzel, R. *Eur. J. Biochem.* **1996**, *239*, 150–155.
25. Yanase, M.; Takata, H.; Fujii, K.; Takaha, T.; Kuriki, T. *Appl. Environ. Microbiol.* **2005**, *71*, 5433–5439.
26. Yanase, M.; Takaha, T.; Kuriki, T. *J. Food Agric.* **2006**, *86*, 1631–1635.
27. Ziegast, G.; Pfannemüller, B. *Carbohydr. Res.* **1987**, *160*, 185–204.
28. Fujii, K.; Takata, H.; Yanase, M.; Terada, Y.; Ohdan, K.; Takaha, T.; Okada, S.; Kuriki, T. *Biocatal. Biotransform.* **2003**, *21*, 167–172.
29. Ohdan, K.; Fujii, K.; Yanase, M.; Takaha, T.; Kuriki, T. *Biocatal. Biotransform.* **2006**, *24*, 77–81.
30. Takata, H.; Takaha, T.; Okada, S.; Takagi, M.; Imanaka, T. *J. Ferment. Bioeng.* **1998**, *85*, 156–161.
31. Kitamura, S.; Yunokawa, H.; Mitsuie, S.; Kuge, T. *Polym. J.* **1982**, *14*, 93–99.
32. Kaneko, Y.; Kadokawa, J. In *Handbook of Carbohydrate Polymers*; Ito, R., Matsuo, Y., Eds.; Nova Science Publishers, Inc.: Hauppauge, NY, 2009; Chapter 23; pp 671−691.
33. Omagari, Y.; Kadokawa, J. *Kobunshi Ronbunshu* **2011**, *68*, 242–249.
34. Kadokawa, J. In *Biobased Monomers, Polymers, and Materials*; Smith, P. B., Gross, R. A., Eds.; ACS Symposium Series 1105; American Chemical Society: Washington DC, 2012, pp 237–255.
35. Kadokawa, J. In *Green Polymer Chemistry: Biocatalysis and Materials II*; Chen, H. N., Gross, R. A., Smith, P. B., Eds.; ACS Symposium Series 1144; American Chemical Society: Washington DC, 2013, pp 141–161.

36. Kadokawa, J. *Pure Appl. Chem.* **2014**, *86*, 701–709.
37. Kadokawa, J. In *Oligosaccharides: Sources, Properties and Applications*; Gordon, N. S., Ed.; Nova Science Publishers, Inc.: Hauppauge NY, 2011; Chapter 10; pp. 269−281.
38. Kadokawa, J. *Trends Glycosci. Glycotechnol.* **2013**, *25*, 57–69.
39. Nawaji, M.; Izawa, H.; Kaneko, Y.; Kadokawa, J. *J. Carbohydr. Chem.* **2008**, *27*, 214–222.
40. Nawaji, M.; Izawa, H.; Kaneko, Y.; Kadokawa, J. *Carbohydr. Res.* **2008**, *343*, 2692–2696.
41. Kawazoe, S.; Izawa, H.; Nawaji, M.; Kaneko, Y.; Kadokawa, J. *Carbohydr. Res.* **2010**, *345*, 631–636.
42. Bhuiyan, S. H.; Rus'd, A. A.; Kitaoka, M.; Hayashi, K. *J. Mol. Catal. B: Enzym.* **2003**, *22*, 173–180.
43. Umegatani, Y.; Izawa, H.; Nawaji, M.; Yamamoto, K.; Kubo, A.; Yanase, M.; Takaha, T.; Kadokawa, J. *Carbohydr. Res.* **2012**, *350*, 81–85.
44. Shimohigoshi, R.; Takemoto, Y.; Yamamoto, K.; Kadokawa, J. *Chem. Lett.* **2013**, *42*, 822–824.
45. Evers, B.; Thiem, J. *Bioorg. Med. Chem.* **1997**, *5*, 857–863.
46. Takemoto, Y.; Izawa, H.; Umegatani, Y.; Yamamoto, K.; Kubo, A.; Yanase, M.; Takaha, T.; Kadokawa, J. *Carbohydr. Res.* **2013**, *366*, 38–44.
47. Takata, H.; Takaha, T.; Okada, S.; Takagi, M.; Imanaka, T. *J. Bacteriol.* **1996**, *178*, 1600–1606.
48. Takata, H.; Takaha, T.; Okada, S.; Hizukuri, S.; Takagi, M.; Imanaka, T. *Carbohydr. Res.* **1996**, *295*, 91–101.
49. Takata, H.; Takaha, T.; Nakamura, H.; Fujii, K.; Okada, S.; Takagi, M.; Imanaka, T. *J. Ferment. Bioeng.* **1997**, *84*, 119–123.
50. Takata, Y.; Shimohigoshi, R.; Yamamoto, K.; Kadokawa, J. *Macromol. Biosci.* **2014**, *14*, 1437–1443.

Publication Date (Web): June 18, 2015 | doi: 10.1021/bk-2015-1192.ch006

Publication Date (Web): June 18, 2015 | doi: 10.1021/bk-2015-1192.ch007

Chapter 7

Water-Insoluble Glucans from Sucrose via Glucansucrases. Factors Influencing Structures and Yields

Gregory L. Côté* and Christopher D. Skory

Renewable Product Technology Research Unit, National Center for Agricultural Utilization Research, Agricultural Research Service, United States Department of Agriculture, 1815 North University Street, Peoria, Illinois 61604

***E-mail: Greg.Cote@ars.usda.gov.**

Dextrans and related glucans produced from sucrose by lactic acid bacteria have been studied for many years and are used in numerous commercial applications and products. Most of these glucans are water-soluble, except for a few notable exceptions from cariogenic *Streptococcus* spp. and a very small number of *Leuconostoc mesenteroides* strains. The ability to produce water-insoluble glucans *in situ* may be of value in enhanced oil recovery, encapsulation technology and in the production of biocompatible films and fibers. There are several different ways in which these enzymes can be exploited to produce water-insoluble glucans with varying properties. In previous work, we found that modifying a single amino acid from a *L. mesenteroides* glucansucrase significantly altered the proportions of linkage types, with correlating changes in the physical properties of the polysaccharide. Here we present results of our studies on factors affecting the structures and yields of these insoluble glucans. For example, addition of soluble dextran or an enzyme that produces a soluble dextran can increase the yield of insoluble glucan. However, the insoluble glucan product contains a lower proportion of α(1→3) linkages. We also show that the yield is drastically affected

In Green Polymer Chemistry: Biobased Materials and Biocatalysis; Smith, et al.;
ACS Symposium Series; American Chemical Society: Washington, DC, 2015.

by both substrate and enzyme concentrations. Studies using cloned enzymes indicate no significant differences between the insoluble-glucan producing enzymes from *L. mesenteroides* strains NRRL B-523 and B-1118.

Introduction

The type strain of *Leuconostoc mesenteroides* (NRRL B-1118; also known as ATCC 8293) has been known for many years to make an insoluble dextran (*1*, *2*). Recently, this strain and the closely related strain, NRRL B-523, have received attention for their potential in microbially enhanced oil recovery (MEOR), in which the insoluble glucans are exploited for bioplugging (*3–6*). In particular, the ability to generate polymers *in situ* renders these systems particularly interesting (*4*, *7*). We initially decided to examine the structures and biosynthesis of the extracellular glucans, since they are the components of interest in MEOR. However, applications in many other fields have also been considered.

A number of glucansucrases involved in synthesizing various glucan linkages have been characterized from both *Streptococcus* and *Leuconostoc* (*8*, *9*). Because of their importance in the etiology of dental caries, streptococcal glucansucrases have been studied in great detail (*10*, *11*). Broadly speaking, there are two types of streptococcal glucansucrases: GTF-S (glucosyltransferase, soluble), which synthesize water-soluble glucans, and GTF-I (glucosyltransferase, insoluble), which synthesize water-insoluble glucans. The former glucans are predominantly α(1→6)-linked, with various amounts of branching through 1,3,6-substituted D-glucopyranosyl units, and are called dextrans. The latter glucans are water-insoluble due to the presence of long sequences of α(1→3)-linked D-glucopyranosyl units. Because of the structural and functional differences, the insoluble streptococcal glucans are often referred to as "mutan" (*12*). Many of the GTF enzymes from various species of *Streptococcus* have been sequenced, cloned, and characterized.

Similar glucansucrases have also been identified in *L. mesenteroides*, a lactic-acid bacterium involved in fermentation of plant matter, including kimchi and sauerkraut, and a frequent contaminant of sugar mills and processing plants. *L. mesenteroides* is the source of glucansucrases for the commercial production of dextran, which is used for blood plasma extenders and related pharmaceutical applications, and cross-linked dextran gels for chromatographic supports (*13*). A few strains of *L. mesenteroides* are known to produce insoluble glucans similar to those produced by dental plaque streptococci (*1*, *2*), but aside from one strain, namely NRRL B-523 (*5*), very little research has been carried out on the glucansucrases responsible for their synthesis.

Three putative dextransucrases (*Dsr*) (GenBank accession YP_819207, YP_818338, and YP_819212) were previously identified (*14*) from the genome sequence of the *L. mesenteroides* type strain NRRL B-1118 (*15*) and found to have significant sequence identity to DsrS from strain B-512F (*16*), DsrE from strain B-1299 (*17*), and DsrP from *L. mesenteroides* IBT-PQ (*18*), respectively. DsrS from B-512F is known to catalyze the formation of predominantly

Publication Date (Web): June 18, 2015 | doi: 10.1021/bk-2015-1192.ch007

In Green Polymer Chemistry: Biobased Materials and Biocatalysis; Smith, et al.;
ACS Symposium Series; American Chemical Society: Washington, DC, 2015.

α(1→6)-linked glucans and DsrE from B-1299 synthesizes a mixture of α(1→6) and α(1→2)-linkages. It has been reported that YP_818338 codes for a 2-domain glucansucrase, which is closely related to DsrE from *L. mesenteroides* B-1299 (*19*).

Pure versus Mixed Enzyme Systems

We previously cloned and characterized the glucansucrase YP_819212 (DsrI) and demonstracted that it produced a water-insoluble glucan (*20*). However, the glucan differed somewhat in its structure from that previously described for the native strain as it occurred in nature (*2*). In particular, methylation analysis indicated small but significant differences in the percentage of α(1→3)-linked and α(1→6)-linked D-glucopyranosyl linkages. The glucan from our cloned enzyme contained a higher percentage of α(1→3)-linkages compared to that produced by the parent strain (*2*). We hypothesized that the difference may be due to the fact that the glucan produced in the native system is the product of a mixture of enzymes. Here we present evidence to support this idea, using cloned DsrI and DsrS enzymes from *L. mesenteroides* NRRL B-1118 to synthesize similar co-polymers.

Cloning and Expression of *L. mesenteroides* dsrS Gene

The *dsrS* gene was PCR amplified from *L. mesenteroides* NRRL B-1118 DNA using primers DsrS P1 5′- CGC GAA CAG ATT GGA GGT gac agt agt gta cct gat gtg agt g -3′ and DsrS P2 5′- CGA ATT CGG ATC CTC TAG cag aaa gct tat gct gac aca g -3′, which were designed to amplify the entire coding region for protein YP819207 except for a 42 amino acid signal peptide sequence predicted by the SignalP 3.0 Server (*21*). The 4,502-bp amplicon was then cloned into an *E. coli* expression vector pE-SUMOpro Kan (LifeSensors, Malvern, PA), a plasmid that utilizes an *N*-terminal small ubiquitin-like modifier (SUMO) to enhance solubility and contains an *N*-terminal polyhistidine (His_6) tag for purification. Sequence ligation independent cloning (*22*), SLIC, was utilized to assemble the *dsrS* amplicon with vector pE-SUMOpro Kan digested with BsaI. The sequence of resulting plasmid, pDsrS-SUMO, was confirmed before proceeding to protein isolation.

Expression of the DsrI (*20*) and DsrS were performed using *E. coli* BL21(DE3) grown at 37°C in LB broth to an OD600=0.5. Cells were induced with isopropyl β-D-1-thiogalactopyranoside (IPTG) to a final concentration of 1 mM and then shifted to 15°C with continued shaking at 200 rpm for 18 hrs. Cells were harvested and suspended in a minimal volume of 20 mM NaH_2PO_4 (pH 8.0). Benzonase nuclease and phenylmethanesulfonylfluoride (PMSF), a serine protease inhibitor, were then added to a final concentration of 25 units/ml and 1.25 mM, respectively, before lysing cells with a French press at an internal pressure of 16,000 psi (110,000 kPa). After centrifugation, the cell-free supernate was adjusted to 500 mM NaH_2PO_4 (pH 8.0) and 300 mM NaCl. Protein was bound to PrepEase nickel resin (Affymetrix, Santa Clara, CA) by gently mixing 1

Publication Date (Web): June 18, 2015 | doi: 10.1021/bk-2015-1192.ch007

In Green Polymer Chemistry: Biobased Materials and Biocatalysis; Smith, et al.;
ACS Symposium Series; American Chemical Society: Washington, DC, 2015.

g resin per gram of original wet cell pellet for 15 min. The suspension was poured onto a column with a 50µm filter frit, washed twice with four volumes of buffered saline (50 mM NaH_2PO_4 pH8.0, 300 mM NaCl) and eluted with three volumes of elution buffer (50 mM NaH_2PO_4 pH8.0, 300 mM NaCl, 250 mM imidazole). Fractions containing glucansucrase protein were combined and diluted with buffered saline to reduce imidazole concentration to below 150 mM. The SUMO fusion was cleaved according to manufacturer's recommendations using SUMO Protease 1, which recognizes the tertiary structure of SUMO and does not cleave within the protein of interest. Protease cleavage and removal of the SUMO fusion from the purified protein should yield DsrI and DsrS protein identical to that of the mature enzymes secreted by *L. mesenteroides* NRRL B-1118. Uncleaved glucansucrase protein and released N-terminal SUMO modifier, both of which contain the His_6, were removed by passing the digested protein back over the PrepEase resin. Enzymes thus prepared were electrophoretically pure. The buffer for the recovered protein was finally exchanged with 20 mM sodium acetate (pH 5.5) containing 2mM $CaCl_2$ with 0.01% sodium azide as a preservative.

Publication Date (Web): June 18, 2015 | doi: 10.1021/bk-2015-1192.ch007

Analytical

Enzyme assays were based on the incorporation of ^{14}C-labelled glucose from ^{14}C-(U)-labeled sucrose (PerkinElmer-NEN, Waltham, MA) into alcohol-insoluble polysaccharide, according to a modification of the method described by Germaine et al. (*23*). In a typical example, 30µL of 0.3M ^{14}C-sucrose in acetate buffer was incubated with 60µL of enzyme solution at 30°C. At timed intervals, 15 µL aliquots were withdrawn and absorbed onto 1.5cm squares of Whatman 3MM chromatography/filter paper. The squares were immediately dropped into a beaker containing approximately 150-200 mL of stirred methanol. A metal screen was used to protect the paper squares from maceration by the stir bar. After washing with three changes of methanol for ten minutes per wash, they were dried under a heat lamp and counted for ^{14}C content in Ecolume cocktails (MPBio, Solon, OH) using a Beckman-Coulter (Brea, CA) LSC-6500 liquid scintillation counter. An enzyme unit is defined here as the amount of enzyme activity that incorporates one µmole of glucose into glucan in one minute.

For water-soluble glucan analysis, 1 mL of enzyme solution (0.8 U/mL) was mixed with 15 mL of 1M sucrose in acetate buffer, and diluted to 50 mL. After standing overnight at room temperature (22°C), the dextran was collected by mixing with an equal volume of ethanol, followed by centrifugation. The dextran was redissolved and reprecipitated twice, then dissolved in water and freeze-dried. Structural analyses of the glucans were carried out by methylation, hydrolysis, and gas-liquid chromatography of the peracetylated aldononitrile derivatives as described by Seymour et al. (*24*).

How Mixed Enzyme Systems Affect Product Structure

The recombinant enzyme DsrS produced water-soluble glucan from sucrose. Methylation analysis results from the soluble glucan product from DsrS are shown in Table 1. The peracetylated aldononitrile (PAAN) derivatives of 2,3,4-tri-*O*-

methyl glucose constitute 73% of the dextran, indicating a predominantly α(1→6)-linked glucan. Branching occurs through 3,6-disubstituted residues as indicated by the presence of 11 mole percent of 2,4-di-*O*-methyl PAAN derivative.

It is likely that the insoluble glucan occurring in cultures of *L. mesenteroides* NRRL B-1118 grown on sucrose is the product of two or more glucansucrases acting together to produce a hybrid product. Such a product could arise from the action of DsrI acting via acceptor reactions on soluble dextran formed by DsrS, to produce a glucan with sequences of 3-linked α-D-glucopyranosyl units attached to a backbone of 6-linked α-D-glucopyranosyl units. The data shown in Table 1 support such a hybrid type of structure. A similar mechanism has been proposed for insoluble glucans formed by mixed-enzyme systems of GTF-I and GTF-S from *Streptococcus* spp. (*25–28*) and subsequently demonstrated by NMR spectroscopy of ^{13}C-labelled products (*29*).

Although the hybrid polymer has a structure that yields analytical results that fall between those of the soluble dextran and the insoluble glucan, it is not a precise 50/50 average of the two individual glucans, as seen in Table 1. It is likely that the proportions of linear 3-linked α-D-glucopyranosyl and 6-linked α-D-glucopyranosyl units may vary considerably, as well as the extent of branching, depending on concentrations of the two enzymes and their individual products, among other factors. Indeed, the two analyses reported in the literature for native insoluble glucan differ significantly (*2*, *30*). It known that the degree of branching in highly branched dextrans from both *Leuconostoc* and *Streptococcus* can vary considerably, depending on conditions of biosynthesis (*31*, *32*). This work demonstrates that the products of multi-enzyme glucansucrase systems are hybrid copolymers, and suggests approaches for customized glucan synthesis using multi-enzyme systems or polysaccharide acceptors.

Publication Date (Web): June 18, 2015 | doi: 10.1021/bk-2015-1192.ch007

Table 1. Methylation Analysis Results of NRRL B-1118 Glucans Produced by Various Enzyme Preparations

Methylated PAAN product	*Mole percent*				
	DsrS	DsrI[a]	Mixture[b]	Native[c]	Native[d]
2,3,4,6-tetra-*O*-Me Glc	16	15	13	4	11
2,3,4-tri-*O*-Me Glc	73	29	71	69	66
2,4,6-tri-*O*-Me Glc	ND	44	10	22	13
2,4-di-*O*-Me Glc	11	9	6	5	10
2,6-di-*O*-Me Glc	ND	4	ND	ND	ND

[a] From Côté and Skory (*20*). [b] Insoluble glucan synthesized by a mixture of equal units of DsrI and DsrS. [c] From Pearce et al. (*2*). [d] From Slodki et al. (*30*). ND = none detected.

In Green Polymer Chemistry: Biobased Materials and Biocatalysis; Smith, et al.;
ACS Symposium Series; American Chemical Society: Washington, DC, 2015.

Influence of Substrate and Enzyme Concentrations

Variable yields of insoluble glucan with DsrI in some of our early experiments led us to investigate the roles of enzyme and sucrose concentrations on the structure and yield of water-insoluble glucan.

To measure the effect of enzyme and sucrose concentration, a series of reactions were carried out containing 7.5 mL of buffer with concentrations of sucrose ranging from 67mM to 933 mM and enzyme ranging from 0.017 U/mL to 1.667 U/mL. Reactions were monitored by TLC, and when all of the sucrose had been consumed, the insoluble glucan product was isolated, dried, and weighed.

Publication Date (Web): June 18, 2015 | doi: 10.1021/bk-2015-1192.ch007

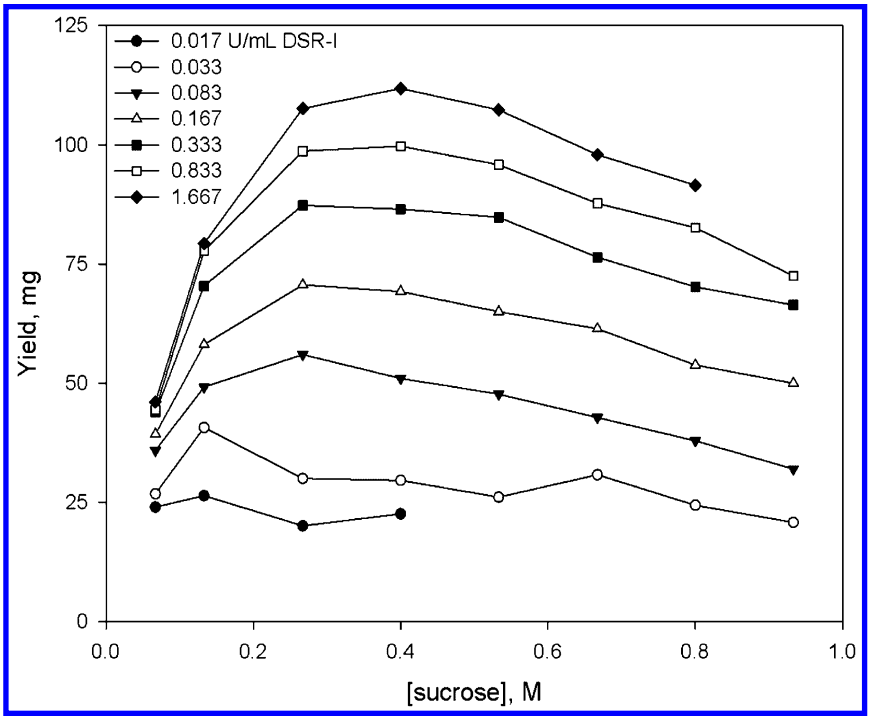

Figure 1. Absolute yields of water-insoluble glucan as a function of sucrose and enzyme (DsrI) concentration.

Figure 1 shows the effect of sucrose concentration and enzyme activity on the amount of glucan produced, expressed as weight of glucan. From these data, it is evident that the optimum sucrose concentration for maximum yield depends partially on the amount of enzyme used. At higher levels of enzyme activity, the optimum sucrose concentration is approximately 0.3 – 0.4 M. At lower enzyme levels, the optimum occurs at lower sucrose concentrations. Regardless of sucrose concentration, the yield is directly proportional to the amount of enzyme present. If

one calculates the percent of theoretical yield from sucrose rather than the absolute amount of glucan formed, Figure 2 shows that the optimum yield occurs at high enzyme levels and low sucrose concentrations. Furthermore, the maximum yields do not exceed 25% of the theoretical maximum yield from sucrose, despite the fact that all of the sucrose was consumed in the reactions.

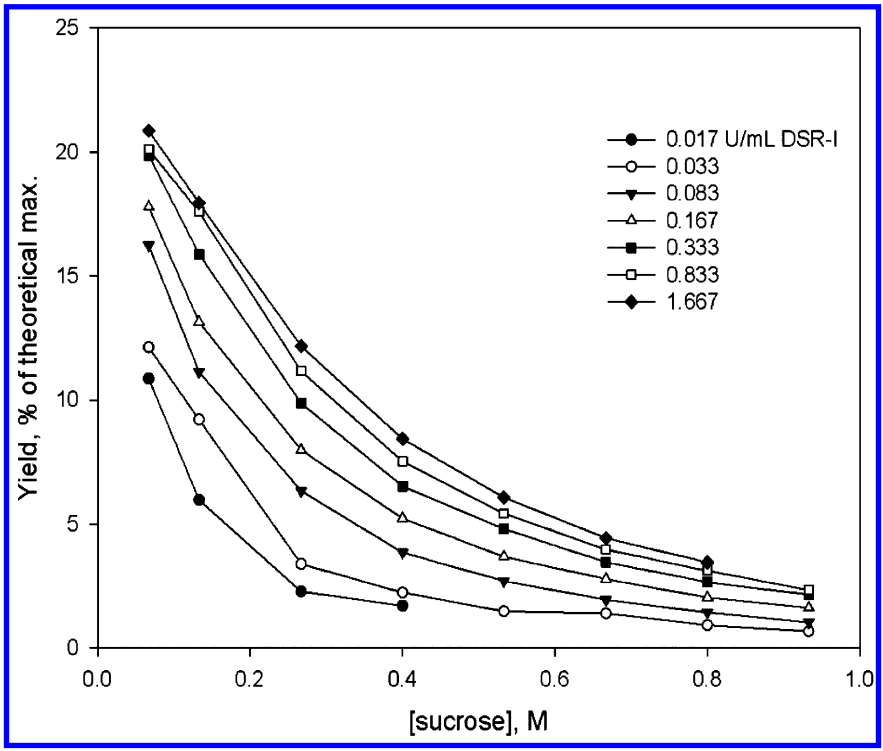

Figure 2. Relative yield of water-insoluble glucan as a function of sucrose and enzyme (DsrI) concentration.

These results can be interpreted in light of the fact that the insoluble glucan is not the sole product of the enzyme. We have examined the reaction products by TLC, and find that two phenomena occur that diminish the yield of glucan. Firstly, fructose released during the glucosyl transfer reaction participates in what are known as acceptor reactions (*33*). The major product of glucosyl transfer to fructose is leucrose (*34*), with isomaltulose being a minor product (*35*). Furthermore, as the concentration of glucan containing a high proportion of α(1→3) linkages increases, it eventually reaches a saturation point, whereupon it precipitates from the aqueous solution phase. The precipitated glucan may bring associated enzyme out of solution with it, resulting in what is essentially an immobilized enzyme surrounded by gel-like glucan. At that point, the acceptor

In Green Polymer Chemistry: Biobased Materials and Biocatalysis; Smith, et al.;
ACS Symposium Series; American Chemical Society: Washington, DC, 2015.

Publication Date (Web): June 18, 2015 | doi: 10.1021/bk-2015-1192.ch007

reactions would become more favorable, since the small oligosaccharide products can freely diffuse out of the gel matrix. Thus, the yield of water-insoluble glucan is limited by the fact that it is insoluble and closely associated with the enzyme.

We have been able to overcome this drawback to some extent by performing the reactions in dialysis tubing. An enzyme solution is placed in a length of dialysis tubing, which is immersed in a vessel of buffered sucrose solution. This prevents the fructose concentration from building up as the reaction proceeds, thus diminishing the relative extent of acceptor reactions. A similar approach has been described by O'Brien and Payne (*36*).

Another approach to increasing yields is to add a small amount of water-soluble dextran. Figure 3 shows results of an experiment in which 4 units of DsrI was incubated with 684 mg of sucrose in 6 mL of acetate buffer until all sucrose was consumed. Various amounts of water-soluble commercial dextran (Mw=2,000,000) were added, and the yields of water-insoluble glucan were determined as above. The structures of the products were analyzed by measuring their susceptibility to endodextranase hydrolysis, as previously described (*20*).

Publication Date (Web): June 18, 2015 | doi: 10.1021/bk-2015-1192.ch007

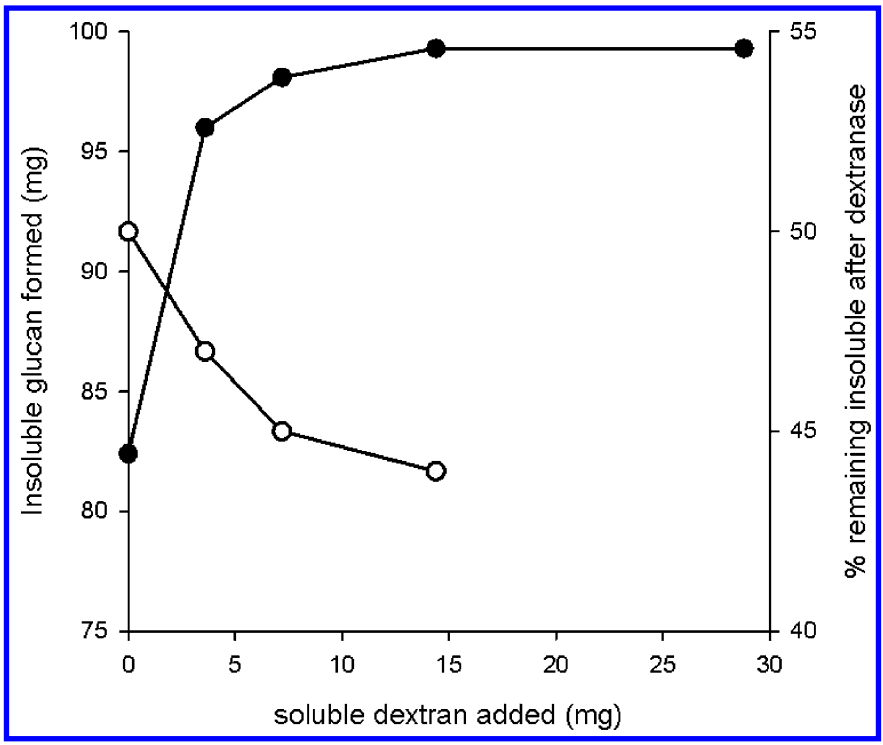

Figure 3. Increase in yield of water-insoluble glucan produced by DsrI upon addition of water-soluble dextran. Filled circles: Yield of insoluble glucan. Open circles: Percent remaining insoluble after dextranase digestion.

The yield of water-insoluble glucan was increased from 82 mg to 99 mg (17 mg, for a 20% increase) by addition of as little as 5 mg of soluble dextran. Such increases in yields have been exploited for streptococcal glucansucrases, and have been interpreted as a "priming" mechanism for the enzyme (*37*). Although the actual mechanism of so-called "primer reactions" is not well understood, it is likely that the actual mechanism is a combination of allosteric activation and graft copolymer formation, since the so-called "primers" are not essential for glucan formation (*38–40*). Evidence for this comes from the observation that the glucan formed in the presence of dextran is more susceptible to hydrolysis and solubilization by endodextranase, indicating a higher percentage of α1→6-linkages (Figure 3). This could arise from formation of a graft, or hybrid, polymer structure, as discussed in the preceding section describing dextrans formed by enzyme mixtures.

Thus, we can conclude that the presence of water-soluble dextran, either added exogenously or synthesized endogenously by dextransucrase, can influence both the yields and structures of insoluble glucans formed by DsrI. The addition of dextran may increase the yield of water-insoluble glucan, but the resulting glucan contains a lower proportion of α(1→3)-linkages.

Influence of Enzyme Source

Jeanes and her colleagues (*1*) showed that the bacterial source strain has a marked influence on the structure of the dextran produced. Pearce et al. (*2*) demonstrated that the same holds true for water-insoluble glucans. To determine if this was the case when pure, cloned enzymes were used, we compared the water-insoluble glucans produced by DsrI from strains NRRL B-523 and NRRL B-1118. These two enzymes have a 94.8% amino acid sequence homology, and are essentially identical in the region surrounding the active site.

The insoluble-glucan producing glucansucrase DsrI from *L. mesenteroides* NRRL B-523 was cloned and expressed in *E. coli* as previously described for strain NRRL B-1118 (*20*). The isolated SUMO-His_6-tagged enzymes were either used without further treatment, or were proteolyzed to remove the SUMO-His_6 tag. The tagged and the proteolyzed enzymes from both strains were used to synthesize water-insoluble glucan from sucrose under identical conditions. One unit of enzyme was incubated with 684 mg of sucrose in 6 mL of buffer, and the reactions were mixed by gentle rotation until TLC indicated all sucrose had been consumed. The insoluble glucan was isolated by centrifugation, washed and dried, then weighed. Yields were not significantly different between the strains, nor were they different between the enzymes with or without the SUMO-His_6 tag. The glucans were also analyzed by dextranase digestion, and by methylation and NMR as previously described (*20*). All three methods indicated no statistically significant differences among the four different enzyme preparations in the relative proportions of α(1→3) and α(1→6)-linked glucosyl units present in the insoluble glucan products.

In Green Polymer Chemistry: Biobased Materials and Biocatalysis; Smith, et al.;
ACS Symposium Series; American Chemical Society: Washington, DC, 2015.

Publication Date (Web): June 18, 2015 | doi: 10.1021/bk-2015-1192.ch007

In their 1990 paper, Pearce et al. (*2*) presented data showing small differences between the insoluble glucans produced by strains NRRL B-523 and B-1118. No estimates of error were given, so it is not known if the differences were significant. However, Slodki et al. (*30*) in an earlier paper presented data showing a much larger difference in the percentage of α(1→3) linkages between the same two strains. We can only provide conjecture as to the reasons for this discrepancy, but it may be due to batchwise variation in the glucans resulting from variations in the relative activities of DsrI and DsrS enzymes. It should be noted that the products they examined were from crude cultures of the wild-type bacteria, which contain multiple glucansucrases.

Based on the similarity of the product glucans, and on the high degree of sequence homology, we can conclude that the purified or cloned insoluble-glucan producing enzymes from *L. mesenteroides* NRRL B-523 and B-1118 are essentially interchangeable.

Summary and Outlook

This work represents a first step toward a better understanding of the factors influencing the enzymatic synthesis of water-insoluble glucans from sucrose. The cloning of glucansucrases and expression as secreted enzymes will contribute significantly to the eventual commercialization of these glucans, but much work needs to be done to increase the yields from sucrose, either by reaction optimization or by enzyme engineering. Co-production of prebiotic or functional oligosaccharides in addition to the insoluble glucans could represent one possible approach. We anticipate that a wide variety of products could be developed using the materials described herein, including functional food and feed ingredients, wound dressings, absorbent polymers, biocomposites, bioplastics, biodegradable films and fibers, and adhesives, to mention just a few.

Acknowledgments

We thank Suzanne Unser and Kristina Glenzinski for their many hours of technical assistance, and Dr. Karl Vermillion for his expert advice and assistance pertaining to NMR spectroscopy. We also thank Drs. Joseph Rich and Ryan Cormier for valuable advice and support. This work was supported and carried out by the U.S. Department of Agriculture. Mention of trade names or commercial products in this publication is solely for the purpose of providing specific information and does not imply recommendation or endorsement by the U.S. Department of Agriculture. USDA is an equal opportunity provider and employer.

References

1. Jeanes, A.; Haynes, W. C.; Wilham, C. A.; Rankin, J. C.; Melvin, E. H.; Austin, M. J.; Cluskey, J. E.; Fisher, B. E.; Tsuchiya, H. M.; Rist, C. E. *J. Am. Chem. Soc.* **1954**, *76*, 5041–5052.

Publication Date (Web): June 18, 2015 | doi: 10.1021/bk-2015-1192.ch007

2. Pearce, B. J.; Walker, G. J.; Slodki, M. E.; Schuerch, C. *Carbohydr. Res.* **1990**, *203*, 229–246.
3. Wu, Y.; Surasani, V. K.; Li, L.; Hubbard, S. S. *Geophysics* **2014**, *79*, E61–E73.
4. Surasani, V. K.; Li, L.; Ajo-Franklin, J. B.; Hubbard, C.; Hubbard, S. S.; Wu, Y. *Energy Fuels* **2013**, *27*, 6538–6551.
5. Padmanabhan, P. A.; Kim, D.-S. *Carbohydr. Res.* **2002**, *337*, 1529–1533.
6. Padmanabhan, P. A.; Kim, D.-S.; Pak, D.; Sim, S. J. *Carbohydr. Polym.* **2003**, *53*, 459–468.
7. Vilcaez, J.; Li, L.; Wu, D.; Hubbard, S. S. *Geomicrobiol. J.* **2013**, *30*, 813–828.
8. Monchois, V.; Willemot, R.-M.; Monsan, P. *FEMS Microbiol. Rev.* **1999**, *23*, 131–151.
9. van Hijum, S. A.; Kralj, S.; Ozimek, L. K.; Dijkhuizen, L.; van Geel-Schutten, I. G. *Microbiol. Mol. Biol. Rev.* **2006**, *70*, 157–76.
10. Montville, T. J.; Cooney, C. L.; Sinskey, A. J. *Adv. Appl. Microbiol.* **1978**, *24*, 55–84.
11. Hamada, S.; Slade, H. D. *Microbiol. Rev.* **1980**, *44*, 331–384.
12. Guggenheim, B.; Newbrun, E. *Helv. Odontol. Acta* **1969**, *13*, 84–97.
13. Leathers, T. D. In *Polysaccharides I. Polysaccharides from Prokaryotes*; Vandamme, E. J., DeBaets, S., Steinbüchel, A., Eds.; Biopolymers, Wiley-VCH: Weiheim, Germany, 2002; Vol. 5, pp 299−321.
14. Olvera, C.; Centeno-Leija, S.; Lopez-Munguía, A. *Antonie van Leeuwenhoek* **2007**, *92*, 11–20.
15. Makarova, K.; Slesarev, A.; Wolf, Y.; Sorokin, A.; Mirkin, B.; Koonin, E.; Pavlov, A.; Pavlova, N.; Karamychev, V.; Polouchine, N.; Shakhova, V.; Grigoriev, I.; Lou, Y.; Rohksar, D.; Lucas, S.; Huang, K.; Goodstein, D. M.; Hawkins, T.; Plengvidhya, V.; Welker, D.; Hughes, J.; Goh, Y.; Benson, A.; Baldwin, K.; Lee, J. H.; Diaz-Muniz, I.; Dosti, B.; Smeianov, V.; Wechter, W.; Barabote, R.; Lorca, G.; Altermann, E.; Barrangou, R.; Ganesan, B.; Xie, Y.; Rawsthorne, H.; Tamir, D.; Parker, C.; Breidt, F.; Broadbent, J.; Hutkins, R.; O'Sullivan, D.; Steele, J.; Unlu, G.; Saier, M.; Klaenhammer, T.; Richardson, P.; Kozyavkin, S.; Weimer, B.; Mills, D. *Proc. Natl. Acad. Sci. U.S.A.* **2006**, *103*, 15611–15616.
16. Monchois, V.; Remaud-Simeon, M.; Russell, R. R. B.; Monsan, P.; Willemot, R.-M. *Appl. Microbiol. Biotechnol.* **1997**, *48*, 465–472.
17. Bozonnet, S.; Dols-Laffargue, M.; Fabre, E.; Pizzut, S.; Remaud-Simeon, M.; Monsan, P.; Willemot, R. M. *J. Bacteriol.* **2002**, *184*, 5753–5761.
18. Olvera, C.; Fernandez-Vazquez, J. L.; Ledezma-Candanoza, L.; Lopez-Munguía, A. *Microbiology* **2007**, *153*, 3994–4002.
19. Kralj, S.; Grijpstra, P.; Van Leeuwen, S. S.; Kamerling, J. P.; Dijkhuizen, L. Proceedings of the Eighth Carbohydrate Bioengineering Meeting, Naples, Italy. May 10-13, 2009; Abstract number P49.
20. Côté, G. L.; Skory, C. D. *Appl. Microbiol. Biotechnol.* **2012**, *93*, 2387–2394.
21. Bendtsen, J. D.; Nielsen, H.; von Heijne, G.; Brunak, S. *J. Mol. Biol.* **2004**, *340*, 783–95.

22. Li, M. Z.; Elledge, S. J. *Nat. Methods* **2007**, *4*, 251–256.
23. Germaine, G. R.; Schachtele, C. F.; Chludzinski, A. M. *J. Dent. Res.* **1974**, *53*, 1355–1360.
24. Seymour, F. R.; Slodki, M. E.; Plattner, R. D.; Jeanes, A. *Carbohydr. Res.* **1977**, *53*, 153–166.
25. Fukui, K.; Moriyama, T.; Miyake, Y.; Mizutani, K.; Tanaka, O. *Infect. Immun.* **1982**, *37*, 1–9.
26. Hanada, N.; Takehara, T.; Itoh, M.; Saeki, E. *FEMS Microbiol. Lett.* **1986**, *36*, 173–175.
27. Walker, G. J.; Schuerch, C. *Carbohydr. Res.* **1986**, *14*, 259–270.
28. Takehara, T.; Ansai, T.; Yamashita, Y.; Itoh-Andoh, M.; Kunimori, A. *Oral Microbiol. Immunol.* **1992**, *7*, 155–158.
29. Mukasa, H.; Tsumori, H.; Shimamura, A. *Carbohydr. Res.* **2001**, *333*, 19–26.
30. Slodki, M. E.; England, R. E.; Plattner, R. D.; Dick, W. E. *Carbohydr. Res.* **1986**, *156*, 199–206.
31. Côté, G. L.; Robyt, J. F. *Carbohydr. Res.* **1983**, *119*, 141–156.
32. Côté, G. L.; Robyt, J. F. *Carbohydr. Res.* **1984**, *127*, 95–107.
33. Koepsell, H. J.; Tsuchiya, H. M.; Hellman, N. N.; Kazenko, A.; Hoffman, C. A.; Sharpe, E. S.; Jackson, R. W. *J. Biol. Chem.* **1953**, *200*, 793–801.
34. Stodola, F. H.; Koepsell, H. J.; Sharpe, E. S. *J. Am. Chem. Soc.* **1952**, *74*, 3202–3203.
35. Sharpe, E. S.; Stodola, F. H.; Koepsell, H. J. *J. Org. Chem.* **1960**, *25*, 1062–1063.
36. O'Brien, J. P.; Payne, M. S. U.S. Patent Appl. 2013/0244288A1, 2013.
37. Payne, M. S.; Brun, Y.; He, H.; Scholz, T. U.S. Patent Appl. 2014/0087431A1, 2014.
38. Robyt, J. F.; Corrigan, A. J. *Arch. Biochem. Biophys.* **1977**, *183*, 726–731.
39. Robyt, J. F.; Martin, P. J. *Carbohydr. Res.* **1983**, *113*, 301–315.
40. Robyt, J. F.; Yoon, S.-H.; Mukerjea, R. *Carbohydr. Res.* **2008**, *343*, 3039–3048.

Publication Date (Web): June 18, 2015 | doi: 10.1021/bk-2015-1192.ch007

Publication Date (Web): June 18, 2015 | doi: 10.1021/bk-2015-1192.ch008

Chapter 8

Biosynthesis, Properties, and Biodegradation of Lactate-Based Polymers

John Masani Nduko,[1] Jian Sun,[1] and Seiichi Taguchi*[,1,2]

[1]Division of Biotechnology and Macromolecular Chemistry, Graduate School of Engineering, Hokkaido University, N13W8, Kita-ku, Sapporo 060-8628, Japan
[2]CREST, JST, 4-1-8 Honcho, Kawaguchi, Saitama, 332-0012, Japan
***E-mail: staguchi@eng.hokudai.ac.jp. Tel/Fax: +81-11-706-6610.**

The tight crude oil supply and its negative impacts on the environment have accelerated efforts towards the search for alternatives to the conventional petrochemical-derived plastics. Polylactic acid (PLA), a polymer produced from renewable resources has emerged as a potential substitute to the conventional synthetic petrochemical-derived plastics owing to their biodegradable and bioresorbable nature. Despite these advantages, PLA has had little success as a substitute to the conventional petrochemical-derived plastics because the PLA synthesis; a two-step bio-chemo process where fermentative lactic acid is polymerized using heavy metal catalysts is expensive. Furthermore, the heavy metal catalyst remnants in the polymer hinder the use of PLA for medical devices and food handling packages. To overcome these obstacles, bacteria have been genetically manipulated to synthesize lactate (LA)-based polymers in a single-step metal-free system. This chapter reviews the production of LA-based polymers using a lactate-polymerizing enzyme (LPE). Production of LA-enriched and PLA-like polymers in bacteria from glucose and xylose, metabolic/ genetic engineering for polymer yield enhancement, polymer properties, and the biodegradability of the LA-based polymers will be discussed. Moreover, future perspectives on the synthesis and applications of the LA-based polymers will be mentioned.

In Green Polymer Chemistry: Biobased Materials and Biocatalysis; Smith, et al.;
ACS Symposium Series; American Chemical Society: Washington, DC, 2015.

Publication Date (Web): June 18, 2015 | doi: 10.1021/bk-2015-1192.ch008

Introduction

In recent decades, there has been significant research focusing on the reduction of fossil-fuel dependence and building a sustainable future, specifically through the use of polymers derived from renewable resources (*1*). Polylactic acid (PLA) belongs to a family of aliphatic polyesters and is considered biodegradable and compostable. PLA is a thermoplastic, high-strength, high-modulus polymer made from renewable resources as alternative to the conventional synthetic petrochemical-derived polymers such as polypropylene (*2*). PLA has good mechanical properties, light weight, and it is easily processed on standard plastics equipment to yield molded parts, film, or fibers. Due to its biodegradability and biocompatibility, PLA is attractive for applications in the medical and agricultural fields (*3*–*5*). PLA research has concentrated not only on their synthesis, but also on their modification through blending, stereocomplexation, and copolymerization among others so as to enhance their properties and biodegradability (*6*, *7*). PLAs are therefore potential substitutes to the petrochemical-derived plastics.

Currently, PLA is synthesized via a two-step process whereby fermentative lactic acid is oligomerized into lactides, which are subsequently polymerized by the ring-opening process using heavy metal catalysts into high molecular weight polymers (*8*, *9*). The stereochemical structure of the polymer can easily be modified by polymerizing a controlled mixture of the L- or D-isomers to vary the polymer properties (*10*). The two-step process for PLA synthesis is costly making the polymer expensive compared to its petrochemical-derived counterparts (*11*). Moreover, the remnants of the heavy metal catalysts limit PLA application in the medical and food handling fields because of potential toxicity (*12*).

To overcome these challenges, there have been concerted efforts to establish a metal-free single-step microbial system; the microbial plastic factory (MPF) for the production of PLA. Establishment of such a system could have been possible if microorganisms that synthesize PLA could be discovered. The natural process for the microbial synthesis of PLA has not been recorded thus; the establishment of an MPF for PLA synthesis is a daunting task (*8*). However, some bacteria that synthesize polyhydroxyalkanoates (PHAs) have been characterized (*13*). PHAs are biodegradable materials and have properties similar to the petrochemical-derived plastics such as polypropylene. The best characterized PHA is polyhydroxybutyrate [P(3HB)], whose synthesis involves two steps; monomer supply and polymerization. The polymerization step is very crucial and is mediated by PHA synthases (polymerizing enzymes), which play a critical role in polymerizing various monomers depending on the substrate specificity of the PHA synthase (*14*).

Lactic acid is structurally similar to PHA monomers hence; it could be polymerized by PHA synthases similarly to the other PHA monomers. Nevertheless, the efforts by Valentin et al. (*15*) and Yuan et al. (*16*), which attempted to obtain a PHA synthase that could polymerize lactic acid, were unsuccessful. However, on the premise that PHA synthases could be engineered to expand their substrate specificity, Taguchi et al. (2008) exploited the PHA biosynthetic system for the establishment of an MPF for the synthesis of LA-based polymers. In this study, representative PHA synthases and some mutant PHA

In Green Polymer Chemistry: Biobased Materials and Biocatalysis; Smith, et al.;
ACS Symposium Series; American Chemical Society: Washington, DC, 2015.

synthases were examined using an *in vitro* chemo-enzymatic system (*17*). Luckily, a PHA synthase mutant designated as lactate-polymerizing enzyme (LPE) that incorporated lactic acid to form P(LA-*co*-3HB) copolymer was discovered. Using LPE, an MPF for the synthesis of LA-based polymers was reported for the first time in 2008 (Figure 1) (*8*). The MPF was possible by expressing the requisite LA and 3HB monomer supplying enzymes along with LPE in *Escherichia coli* (*E. coli*). The first LA-based polymer was P(LA-*co*-3HB) having 6 mol% of LA. These pioneering studies laid the foundation on which subsequent studies related to enhancement of the LA fraction in the copolymer, improvement of polymer yield, variation of polymer property and copolymerization of different monomers were conducted.

This chapter will give a brief synopsis into the discovery of LPE and its application for the production of LA-based polymers with varying LA fractions. The transfer of the P(LA-*co*-3HB) production system into *Corynebacterium glutamicum* (*C. glutamicum*) for the synthesis of PLA-like polymers, metabolic/genetic engineering of bacteria for improvement of LA fractions and polymer yields from glucose and xylose will be discussed. Polymer properties resulting thereof, the biodegradability of P(LA-*co*-3HB) copolymers and the future perspectives regarding the MPF for the synthesis of advanced polymers will be highlighted in detail.

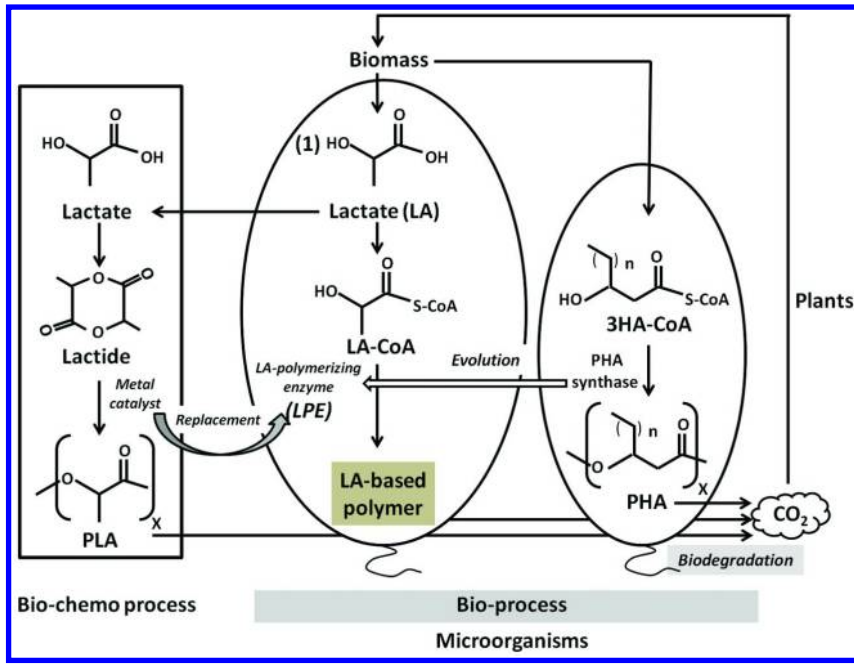

Figure 1. Conversion process for producing lactate (LA)-based polymers. Conventional two-step bio-chemo process involves fermentation (1) and chemical polymerization (2) converted into a novel single-step bio-process using microorganisms. The lactate-polymerizing enzyme (LPE) works as the key to the conversion process. Figure adapted from Nduko et al. (18).

In Green Polymer Chemistry: Biobased Materials and Biocatalysis; Smith, et al.;
ACS Symposium Series; American Chemical Society: Washington, DC, 2015.

Publication Date (Web): June 18, 2015 | doi: 10.1021/bk-2015-1192.ch008

Publication Date (Web): June 18, 2015 | doi: 10.1021/bk-2015-1192.ch008

Biosynthesis of Lactate (LA)-Based Polymers

Production of LA-Based Polymers

As already mentioned, PLA is synthesized in a multi-step process, which is different from that of the PHAs. PLA is basically synthesized via 3 processes; (i) production of lactic acid through microbial fermentation, (ii) purification of lactic acid and preparation of its cyclic dimer (lactide), and (iii) ring-opening polymerization of the lactides or polymerization by polycondensation (*9*). However, such bio-chemo process of PLA synthesis involving multiple preparation and purification steps although well established, is energy-consuming and requires harmful chemical catalysts for the polymerization process. This hampers the economic and environmental impacts of the material (*10*).

Unlike PLA, PHAs are wholly synthesized *in vivo* via a two-step process; monomer supply and polymerization, and are stored as intracellular inclusions (*19*). Their biosynthetic pathways have been characterized in previous studies (*14*). A typical PHA is polyhydroxybutyrate [P(3HB)], whose biosynthetic pathway is shown in Figure 2, and is extensively investigated in *Ralstonia eutropha*. In *R. eutropha*, two molecules of acetyl-CoA are condensed by to generate acetoacetyl-CoA in a reaction catalyzed by a 3-ketothiolase (PhaA). Acetoacetyl-CoA is then reduced to 3-hydroxybutyryl-CoA by NADPH-dependent acetoacetyl-CoA reductase (PhaB), which can be polymerized by a PHA synthase (PhaC) to form P(3HB) (*14*).

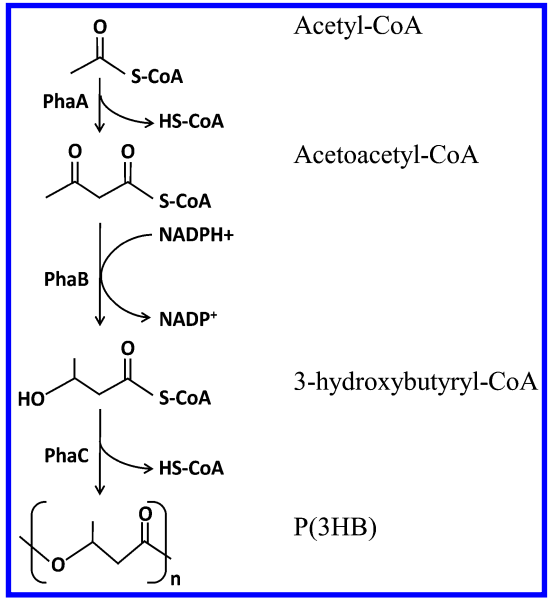

Figure 2. Biosynthetic pathway for the synthesis of P(3HB)in Ralstonia eutropha. PhaA, β-ketothiolase; PhaB, NADPH-dependent acetoacetyl-CoA reductase; PhaC, polyhydroxyalkanoate (PHA) syynthase.

In Green Polymer Chemistry: Biobased Materials and Biocatalysis; Smith, et al.;
ACS Symposium Series; American Chemical Society: Washington, DC, 2015.

The establishment of a single-pot bioprocess for PLA synthesis analogous to PHAs will overcome the need for the use of metal catalysts and purification of lactic acid; hence the cost of production will possibly be reduced. An 'LA-polymerizing enzyme (LPE)', which can function as an alternative to a metal catalyst would be desirable to establish such a bioprocess (*8*). The simplest strategy would have been the discovery of PLA producing microorganisms, but this has not succeeded so far (*20*). Recently, a whole cell biosynthesis system for LA-based polymer production without the heavy metal catalysts was constructed in engineered bacteria (*8*, *21*). The LPE was an engineered PhaC [Pha*C*1$_{Ps}$(ST/QK)], which incorporated LA unit together with 3HB to form P(LA-*co*-3HB). Using this engineered LPE, copolymers and terpolymers have been produced of varying LA fraction up to over 90 mol% and have been extensively reviewed (*18*, *21–24*).

Publication Date (Web): June 18, 2015 | doi: 10.1021/bk-2015-1192.ch008

Production of LA-Enriched Copolymers

The monomeric constituents and their ratio affect polymer properties due to the altered crystallinity and melting temperatures (T_m) (*25*). Previously, it had been demonstrated that incorporation of 6 mol% of LA into P(LA-*co*-3HB) reduces the T_m of the copolymer compared to that of P(3HB) (*8*). This result suggested that new polymer materials could be obtained by variation of the LA fraction in the copolymers. As a result, strategies intended to regulate monomer composition of the copolymers were applied to enhance incorporation of LA into the P(LA-*co*-3HB) copolymers (*22*, *26*).

Firstly, in an earlier *in vitro* chemo-enzymatic system for the production of P(LA-*co*-3HB), the LA fraction in the copolymer was 36 mol% when LA-CoA and 3HB-CoA were equimolar (*17*). This fraction was significantly higher than the 6 mol% of LA fraction in P(LA-*co*-3HB) synthesized by recombinant *E. coli* *in vivo* (*8*). This discrepancy between the *in vivo* and the *in vitro* LA fractions in the P(LA-*co*-3HB) indicated inadequate lactic acid supply in the *E .coli* cells. Effectively, a metabolically engineered *E.coli* JW0885 (*ΔpflA*) was employed to improve the lactic acid concentrations, consequently enhancing the LA fraction in the copolymer (*22*). As a result, using *E. coli* JW0885 (*ΔpflA*) expressing the same set of enzymes for P(LA-*co*-3HB) production under the same culture conditions as the parent strain led to the synthesis of P(LA-*co*-3HB) with 26 mol% of LA; confirming that the metabolic engineering strategy for lactic acid overproduction was effective for the enrichment of LA units in the P(LA-*co*-3HB).

Under aerobic conditions, pyruvate in *E. coli* is converted into acetylCoA whereas it is converted into lactic acid under anaerobic conditions. Therefore, for improved LA fractions in P(LA-*co*-3HB), recombinant *E. coli* JW0885 cells were cultivated under anaerobic conditions for the production of P(LA-*co*-3HB). This resulted into improved the LA fraction in P(LA-*co*-3HB) to 47 mol% (*22*). This result suggested that high lactic acid production under anaerobic culture conditions was effective in improving LA fractions in the copolymers. Although, high LA fractions were obtained under anaerobic conditions, polymer content

of the polymer was less than 2% of the dry cells of bacteria; indicating that P(LA-*co*-3HB) production systems achieving LA fractions and high polymer productivity were necessary.

Therefore, the new strategy for improved LA fraction/ polymer productivity was by enzyme engineering of LPE. Thus, *E. coli* JW0885 expressing an evolved LPE was used for P(LA-*co*-3HB) production. The analysis of cells expressing evolved LPE (eLPE) cultivated for polymer production indicated under aerobic conditions, P(LA-*co*-3HB) with 47 mol% LA and polymer contents of 62% was obtained (*22*). Furthermore, using this system under anaerobic conditions, copolymers having 62 mol% LA were obtained however with less than 1% polymer content. The strategy of enzyme evolutionary engineering was crucial in finding a suitable mutant with enhanced LA-polymerization capability and high polymer productivity.

Publication Date (Web): June 18, 2015 | doi: 10.1021/bk-2015-1192.ch008

The Synthesis of PLA-like Polymers

When P(6 mol% LA-*co*-3HB) was produced, it was observed that in the absence of 3HB-CoA supply, LA-based polymer is not synthesized (*8*). This result demonstrated the essentiality of 3HB for the polymerization of LA. However, through NMR analysis the presence of the LALALA triad sequence in the polymers was demonstrated; suggesting the potential of synthesizing highly LA-enriched polymers (*26*). To effect this, Shozui et al. eliminated the 3HB-CoA supplying pathway from the P(LA-*co*-3HB) production system and replaced with PhaJ4 for 3-hydroxyvalerate (3HV) supply from extraneously added valerate (*23*). The cells, when supplied with 0.5 g/L valerate, P(LA-*co*-3HB-*co*-3HV) with 96 mol% of LA was produced. For improved LA fractions, one strategy is to reduce the 3HB supply. In this study, the 3HB supply pathway was replaced with 3HV supply. This strategy was effective as nearly PLA was synthesized. Nevertheless, 3HB was detected in the polymer; possibly supplied from the β-oxidation pathway. These results however demonstrated that PLA-like polymers could be produced in bacteria in a single-step process.

Production of P(LA-*co*-3HB) in *Corynebacterium glutamicum*

The synthesis of P(LA-*co*-3HB) had only been achieved in *E. coli* (*8*, *22*, *23*). However, the use of *E .coli* has limitations due to the production of endotoxins (*27*). Therefore, to upgrade this prototype system to the practical scale, the Gram positive *C. glutamicum* which has Generally Recognized As Safe (GRAS) status, is endotoxin free and a widely used chassis for industrial production of amino acids is suitable for the production of LA-based polymers (*28*). *C. glutamicum* had already been demonstrated for the production of PHAs; thus suggesting its potential as a host for the production of LA-based polymers (*29–31*). The necessary pathways for the synthesis of P(LA-*co*-3HB) were assembled in *C. glutamicum* and the cells cultivated for polymer production (*21*). The recombinant *C. glutamicum* cells cultivated on glucose were analyzed and the *C. glutamicum* synthesized copolymers with 97 mol% LA which was a stark contrast of those obtained in *E. coli* (47 mol% of LA) expressing the same set of

In Green Polymer Chemistry: Biobased Materials and Biocatalysis; Smith, et al.;
ACS Symposium Series; American Chemical Society: Washington, DC, 2015.

genes (*21*, *26*). The high LA fractions of P(LA-*co*-3HB) polymers synthesized by *C. glutamicum* was possibly due to a weak 3HB supply in *C. glutamicum*. This was supported by the fact that the P(3HB) yield was lower compared to that of P(LA-*co*-3HB) when the D-LA-CoA supplying enzyme PCT was eliminated. This led to an investigation of the necessity of the 3HB-CoA supplying enzymes. The investigation indicated that unlike *E. coli*, *C. glutamicum* could still produce P(LA-*co*-3HB)s with almost 100% LA fraction [P(99.3 mol% LA-*co*-3HB)] despite the elimination of PhaA and PhaB from the system (*21*). Since 3HB units appeared in the PLA-like polymer, there possibly is an endogenous 3HB-CoA supplying pathway in *C. glutamicum*. The polymer yield of the PLA-like polymer was lower compared to the polymers synthesized with the presence of PhaA and PhaB. The PLA-like polymer produced in *C. glutamicum* had strong resonances of LA in the ^{1}H-NMR analysis which is similar to the characteristic of chemically synthesized PLA. This study demonstrated the ability of *C. glutamicum* to produce PLA-like polymers, which suggested that the bacterium milieu and/ or genetic diversity plays a critical role in controlling the monomer composition of P(LA-*co*-3HB).

Publication Date (Web): June 18, 2015 | doi: 10.1021/bk-2015-1192.ch008

Xylose Use for the Production of P(LA-*co*-3HB)

Although PLA and PHAs have the potential to replace petrochemical-based plastics, they have had little success due to their high cost of production (*11*, *13*). This is because; the refined sugars from sugarcane, sugar beet, and starch feedstocks that are normally used for the production of PLA and PHAs are expensive and they are also used as food hence their use is not sustainable (*11*, *14*). Alternatively, lignocellulosic biomass, which is inedible, carbon rich, renewable, abundant, and inexpensive could be used as a carbon source for P(LA-*co*-3HB) production. Lignocellulosic biomass averagely consists of 30 – 55% cellulose, 25 – 50% hemicellulose and 10 – 40% lignin (*32*). Cellulose has been hydrolyzed into glucose for the production of bioethanol and a number of bioproducts (*33*). In contrary, the hemicellulose portions, which are rich in xylose, are underutilized. For instance, in Kraft pulping processes, hemicellulose is dissolved in black liquor along with lignin and combusted for power generation (*34*). Since hemicellulose has a lower heating value compared to lignin, its utilization for the production of polymers and fuels could be more efficient (*34*).

In a 2013 study, the application of xylose for the production of P(LA-*co*-3HB) was reported for the first time (*35*). The advantage of using of xylose for the production of P(LA-*co*-3HB) was justified by the higher cellular polymer content and LA fraction of the copolymer compared to the utilization of glucose. In earlier studies using glucose, copolymers with LA fraction greater than 50 mol% were characterized with low polymer yields (less than 1 g/L) from 20 g/L glucose, limiting exploration of polymer properties (*25*). However, when using xylose, 7.3 g/L of P(60 mol% LA-*co*-3HB) was obtained, demonstrating the dual advantage of using xylose (*35*). To exploit the advantage of xylose, two distinct strategies were explored to improve LA fractions and polymer yields (*36*). First, in the earlier study, a Δ*pflA* mutant of *E. coli* was demonstrated to strengthen the supply

of lactic acid, which could eventually be incorporated into P(LA-*co*-3HB) (*22*, *37*). However, other gene disruptants, which are known to increase lactic acid production had not been evaluated for P(LA-*co*-3HB) synthesis from xylose. Thus, the parent strain, *E. coli* BW25113 and four mutants (Δ*pta*, Δ*ackA*, Δ*poxB,* and Δ*dld*), which redirects the carbon flux at the pyruvate node into lactic acid (*38*) were recruited for P(LA-*co*-3HB). It was found that the knockout mutants; *Δpta*, *ΔackA*, and *Δdld* had higher polymer productivities (6.5–7.4 g/L) than BW25113 (6.3 g/L) (*36*). Regarding the LA fractions in P(LA-*co*-3HB)s, the *Δpta* and *Δdld* mutants had higher LA fractions (58 and 66 mol%, respectively) compared to BW25113 (56 mol%), which demonstrated that the mutations were effective for improving both or either of the polymer productivity or the LA fractions in the polymers. Since the *ΔpflA* and *Δdld* single-gene knockout mutants were found to increase both the P(LA-*co*-3HB) productivity and LA fraction, the two mutations were combined to create a dual mutant, *E. coli* JWMB1. The strain exhibited an additive effect on the increase of the LA fraction (73 mol% LA) in P(LA-*co*-3HB), which was the highest value among the conditions having P(LA-*co*-3HB) productivity greater than 1 g/L (*36*).

Another strategy focused on the enhancement of xylose uptake by *E. coli.* In *E. coli*, there are two different D-xylose-specific transport systems; the XylE, a member of the major facilitator superfamily of transporters and the ATP-binding cassette (ABC) transporter encoded by the *xylFGH* operon (*39*). The ATP-dependent transporter is the major xylose transporter, and could reduce the amount of ATP available to the cells. Therefore, to eliminate the possibility of ATP limitation, a non-ATP consuming galactitol permease, GatC that has been demonstrated to transport xylose efficiently for lactic acid production (*40*) was overexpressed in *E. coli*. The GatC overexpression in *E. coli* parent strain, BW25113 increased the polymer productivity (7.7 g/L) without significant change in the LA/3HB ratio. The GatC overexpression was found to increase the LA fraction in some mutants. To analyze the full potential of GatC overexpression, xylose concentration was increased up to 40 g/L. It was then found that polymer yields improved, dependent on the xylose concentration (*36*). Indeed, P(66 mol% LA-*co*-3HB) yields of 14.4 g/L were obtained in BW25113 overexpressing GatC from 40 g/L, which was the highest PHA yield obtained from sugars under the same culture conditions. Carbon flux analysis indicated that strains with higher LA fractions in the copolymers had higher lactic acid. However, it should be noted that higher lactic acid in the medium could not result into higher polymer yields since LPE requires 3HB-CoA for the incorporation of LA-CoA; thus, the inverse relationship between LA fraction and polymer. The essentiality of 3HB-CoA for the synthesis of LA-based polymers has been interpreted as a role of 3HB-CoA as a priming unit of polymerization (*12*). Evaluation of the carbon number also revealed that polymerizing LA was more carbon efficient than polymerizing 3HB which had a carbon loss in terms of CO_2. This is because one LA unit (C_3) is generated from one pyruvate molecule (C_3), while one 3HB unit (C_4) is generated using two pyruvate molecules ($C_3 \times 2$). This stoichiometry contributes to the high-yield production of LA-enriched P(LA-*co*-3HB), namely, the copolymer with higher LA fraction like the case of xylose utilization should have higher polymer yields than one with lower LA fractions like the case of

Publication Date (Web): June 18, 2015 | doi: 10.1021/bk-2015-1192.ch008

glucose (*36*). In these studies, it was found that mutants reported to increase lactic acid could increase the LA fraction in P(LA-*co*-3HB), suggesting that the mutations causes redistribution of the carbon flux. Although some of the mutants had increased LA fraction in the copolymers, they had residual xylose in the fermentation media, indicating that the polymerization step was the bottleneck, possibly due to the LA-incorporation capacity of LPE.

The overexpression of GatC had a beneficial effect of improving polymer productivity. The metabolic engineering strategies demonstrated that xylose could be utilized efficiently to produce LA-enriched P(LA-*co*-3HB), which were further enhanced by the overexpression of the GatC transporter than the use of glucose. Since xylose forms a major proportion of lignocellulosic biomass, its use for the production of P(LA-*co*-3HB) could improve the economics of lignocellulose biomass use; whereby currently only glucose is used efficiently.

Publication Date (Web): June 18, 2015 | doi: 10.1021/bk-2015-1192.ch008

Properties of LA-Based Polymers

Enantiomeric Purity of LA-Based Polymers

Enantiopurity is a key factor that affect PLA regarding its thermal properties (*41*). The homopolymers of LA enantiomers, P[(*R*)-LA] (PDLA) and P[(*S*)-LA] (PLLA), are crystalline polymers with the melting point (T_m) of about 180 °C. The stereocomplex of PDLA and PLLA has been achieved and its T_m has reached to 220 to 230 °C (*42*). Therefore, controlling the enantiopurity is crucial in regulating polymer properties. The LA enantiomer that was incorporated into the polymer was analyzed by chiral HPLC. All the P(LA-*co*-3HB) samples synthesized by bacteria exhibited that peaks characteristic of (*R*)-LA and (*R*)-3HB (*26*). It has been well studied that wild type PHA synthases are specific toward *R*-form of the monomers, such as *R*-3HB (*43*). As the envolved PHA synthase, LPE was found to inherit the enantiospecificity and polymerize the (*R*)-LA with (*R*)-3HB *in vivo*. In an *in vitro* research, (*S*)-LA-CoA was supplied together with (*R*)-3HB for the synthesis of polymer, however, only P(*R*-3HB) was synthesized (*44*). On ther other hand, the enatioselectivity towards LA in the in vivo system should be also considered on the side of the monomer supplying enzymes; lactate dehydrogenase (LdhA) and PCT. *E. coli* intrinsically produces (*R*)-LA by native LdhA (*45*). Then, (*R*)-LA is converted into (*R*)-LA-CoA by PCT. It has been known that PCT has no strict enantiospecificity (*20*), therefore, LdhA and LPE are the main determinants that contribute to the enantiomeric configuration of LA in the LA-based polymers. Currenty, chemical synthesis of P(LA-*co*-3HB) with 100% e.e. has not been achieved, therefore, the enantioselectivity of the biosynthesis is an advantage to produce optically pure P(LA-*co*-3HB)s with variety of properties.

Sequential Structure and Molecular Weight of LA-Based Polymers

The sequential structure of copolymer i.e. random or block affects polymer properties (*46*). NMR is one of the most useful tools to analyze the monomer distribution in the copolymer (*47*). Th investigation of monomer sequence of

In Green Polymer Chemistry: Biobased Materials and Biocatalysis; Smith, et al.;
ACS Symposium Series; American Chemical Society: Washington, DC, 2015.

P(LA-*co*-3HB) bases on the NMR signals of LA unit that affected by both the neighboring monomer units. In particular, the methane group of LA unit can be a good 'fingerprint' to characterize the monomer sequence of the polymer (*8*). In the case of P(LA-*co*-3HB)s, the triplet sequences, LA-LA-LA, LA-LA-3HB, 3HB-LA-LA and 3HB-LA-3HB were observed. The ^{1}H–^{13}C COSY-NMR profile revealed sufficient amount of LA-LA and LA-LA-LA, indicating the LPE can polymerize LA unit next to another LA unit sequentially. In addition, all the triplet sequences were detected in the P(LA-*co*-3HB), revealing that the LA and 3HB unit were distributed randomly in the copolymers (*26*).

It is well known that the moleculer weight can affect the tensile strength of polymer (*48*). It was found that the molecular weight of biosynthesized LA-based polymer has an inverse relationship with LA fraction (Table 1) (*23*, *25*). This may be due to the fact that although LPE has acquired the ability to polymerize LA unit, the LA-CoA was still not preferencially used as the substrate to synthsize high-molecular weight polymers by LPE. However, more works are necessary to clearify this important issue.

Publication Date (Web): June 18, 2015 | doi: 10.1021/bk-2015-1192.ch008

Thermal and Mechanical Properties of LA-Based Polymers

The thermal properties play an important role as they have an effect on the quality of polymers in aspects such as heat resistance and crystallization. As examples, PLA and P(3HB) exhibit transparent and opaque properties that are consistent with their glass transition temperatures (T_g) (61°C and −7°C, respectively) (*25*). P(LA-*co*-3HB)s exhibited increased T_g values at a range of −6 to 34°C, dependent on the LA fractions (*25*). On the other hand, P(LA-*co*-3HB)s with 29–47 mol% LA displayed lower melting temperature (T_m) and melting enthalpy (ΔH_m) compared to those of the P(3HB) and PLA homopolymers. The lowered T_m may due to the copolymerization of different monomers that inhibited crystal packing of the polymer compared to the individual homopolymers (*25*). The lowered ΔH_m indicates a reduction of amount of the crystal (Table 1)[a].

The PLA-like polymer, which synthesized by *C. glutamicum*, exhibited comparable T_g and T_m with chemically synthesized PLA in the same molecular weight (*21*). PLA-like polymer was nearly PDLA and it was used to form stereocomplex with chemically synthesized PLLA. The T_m of this formed stereocomplex was 202 °C which was higher than that of each polymer (*23*). These results indicated that the biosynthesized PLA-like polymer had comparable thermal and functional properties with the chemically-synthesized counterpart.

Transparency of films of P(LA-*co*-3HB) were influenced by the LA fraction in copolymers. Using solvent-casting method, P(3HB) formed an opaque film while PLA formed a completely clear film. On the other hand, P(LA-*co*-3HB)s can be processed into semi-transparent films depending on the LA-fraction (*25*). Copolymers exhibited increased transparency along with the increased LA fractions. Additionally, copolymer film with significant transparency was obtained when LA units is higher than 15 mol%, indicating crystallinity of the copolymer was effectively reduced accompanied with lowered T_m and ΔH_m (*25*, *26*).

In Green Polymer Chemistry: Biobased Materials and Biocatalysis; Smith, et al.;
ACS Symposium Series; American Chemical Society: Washington, DC, 2015.

Publication Date (Web): June 18, 2015 | doi: 10.1021/bk-2015-1192.ch008

Table 1. LA Fraction-Dependent Thermal and Mechanical Properties of LA-Based Polymers[a]

Polymer composition (mol%)		*Molecular weight*		*Mechanical properties*			*Thermal properties*		
3HB	*LA*	*Weight everage molecular weight (×10⁴)*	*Weight everage molecular weight /number everage molecular weight*	*Tensile strength (MPa)*	*Young's modulus (MPa)*	*Elongation at break (%)*	*Glass transition temperature (°C)*	*Melting temperature(°C)*	*ΔH_m (cal g^{-1})*
4	96	1.3	1.7	N.D.	N.D.	N.D.	49.3	153.3	9.5
53	47	7	2.3	7±2	153±15	84±20	-8, 34	140, 157	0.4, 1.9
60	40	7	3.5	6±0	148±10	64±7	-8, 30	140, 156	0.3, 1.4
71	29	9	2.2	7±7	154±5	156±34	-8, 25	141, 158	0.2, 0.9
85	15	82	2.4	10±0	194±5	75±2	-9, 19	149, 167	0.6, 3.2
96	4	74	4.6	30±4	905±136	7±1	-6	160, 174	1.8, 5.4
100	0	70	2.3	19±1	1079±215	9±1	-7	159, 176	1.6, 9.9
0	100	2.0		52±2	1020	2	60	153	2.2

[a] Data adapted from Yamada et al. (*25*).

The LA fractions of P(LA-*co*-3HB) also affect the mechanical properties of these copolymers significantly. Young's modulus of P(LA-*co*-3HB)s were in a range of 148–905 MPa, which were lower than those of PLA (1020 MPa) and P(3HB) (1079 MPa). The young's modulus of P(LA-*co*-3HB)s decreased along with the increase of the LA fraction. P(LA-*co*-3HB)s exhibited advanced flexibility compared to PLA and P(3HB) homopolymers (*25*). In particular, the elongation at break of the P(LA-*co*-3HB) with 29 mol% LA had reached to 156% (*25*). These results proved that P(LA-*co*-3HB)s are a more elastic material than the respective homopolymers.

Biodegradation of P(LA-*co*-3HB)

Microbial Degradation of P(LA-*co*-3HB)

P(LA-*co*-3HB) is thought to be a potent biobased plastic material because of its semi-transparency and flexibility as described above. To explore the application of this novel polymer, it is important to understand its biodegradability. P(LA-*co*-3HB) is biosynthesized as a hybrid of PDLA and P(3HB) and the biodegradation of P(LA-*co*-3HB) would depend on the degradability of both homopolymers. To date, P(3HB) has been proved to be degradable by a variety of microorganisms possessing P(3HB) depolymerases, while PDLA is hardly biodegraded (*49*). Therefore, biodegradability of the copolymer incorporating LA and 3HB was an interesting subject. The distinguish biodegradability of P(3HB) and PDLA suggests that the biodegradation of P(LA-*co*-3HB) may be limited by the LA fraction in P(LA-*co*-3HB).

The screening of P(LA-*co*-3HB)-degrading microorganisms was performed using soil samples collected from different locations in Hokkaido University, Sapporo, Japan. The degradation activity was judged by the decrease of turbidity of liquid medium which contained LA-enriched copolymer P(67 mol% LA-*co*-3HB) emulsion that is readily biosynthesized. During the screening, from 500 soil samples, 216 samples degraded both P(67 mol% LA-*co*-3HB) and P(3HB) while 93 samples only degraded P(3HB) but not P(67 mol% LA-*co*-3HB), suggesting that the microorganisms isolated can be grouped into two groups; those that degrade P(3HB) only, and those that degrade P(67 mol% LA-*co*-3HB) as well as P(3HB) (*50*). The result that about half of the samples exhibited degradation ability toward P(67 mol% LA-*co*-3HB) indicated that P(LA-*co*-3HB)-degrading microorganisms widely exist in the soil of these sampling sites.

Out of 216 samples that had P(LA-*co*-3HB) degradation ability, one sample with *Variovorax* sp. C34 generating the largest halo on the P(LA-*co*-3HB) emulsion containing agar plate, which suggested a higher degradation activity compared to other 215 samples. (*50*). *Variovorax* sp. C34, was found to generate a halo on P(67 mol% LA-*co*-3HB) plate and P(3HB) plate, but not on PDLA-containing plate (Figure 3). For comparison, recombinant *E. coli* BL21 (DE3) expressing the gene encoding the P(3HB) depolymerase ($PhaZ_{Af}$) from *Alcaligenes faecalis* T1 was grown on the same plates. The $PhaZ_{Af}$ was presumably extracellularly exported and exhibited degradation activity toward

In Green Polymer Chemistry: Biobased Materials and Biocatalysis; Smith, et al.;
ACS Symposium Series; American Chemical Society: Washington, DC, 2015.

Publication Date (Web): June 18, 2015 | doi: 10.1021/bk-2015-1192.ch008

P(3HB), but not P(67 mol% LA-*co*-3HB) (*50*). The results suggest the isolated C34 bacterium secretes degrading enzyme(s) with different substrate specificity than $PhaZ_{Af}$ (Figure 3).

Phylogenic tree constructed based on the 16S rDNA sequence, *Variovorax* sp. C34 was found close to extracellular P(3HB) depolymerase-secreting bacteria, such as *Acidovorax sp*. TP4 (*51*), *Comamonas sp*. (*52*) *Comamonas testosteroni* (*53*) and *Delftia acidovorans* (*54*), which are the members of *Comamonadaceae* family.

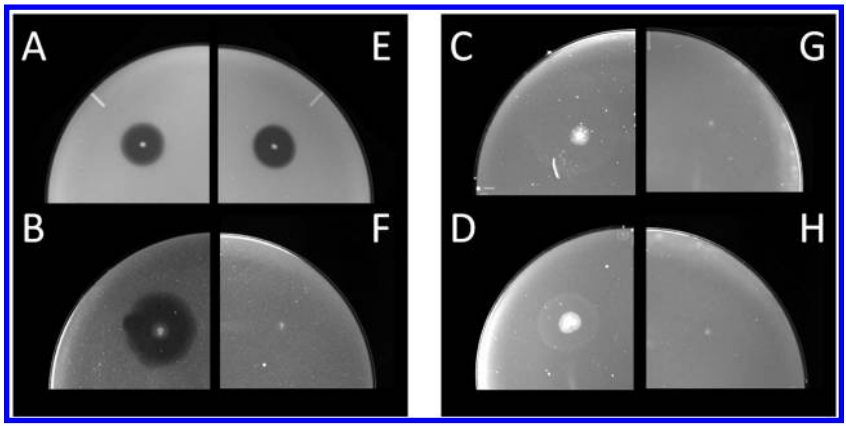

Figure 3. Clear zone obtained by Variovorax sp. C34 on YE argar plates containing emulsion of P(3HB) (A), P(67 mol% LA-co-3HB) (B), PDLA (C) and PLLA (D), respectively; recombinant E. coli expressing the $phaZ_{Af}$ gene from A. faecalis T1 on M9 argar medium plates containing emulsion of P(3HB) (E), P(67 mol% LA-co-3HB) (F), PDLA (G) and PLLA (H), respectively.

Publication Date (Web): June 18, 2015 | doi: 10.1021/bk-2015-1192.ch008

Characterization of P(LA-*co*-3HB) Depolymerase

Enzymatic activity toward P(67 mol% LA-*co*-3HB) degradation was detected from the culture supernatant of *Variovorax* sp. C34, indicating that the enzyme which contributed to the degradation of P(67 mol% LA-*co*-3HB) was an extracellular depolymerase. For further investigation of the enzymatic degradation mechanism, the P(LA-*co*-3HB) depolymerase was purified by the sucrose density isoelectric-focusing electrophoresis.

The polymer emulsions, containing P(67 mol% LA-*co*-3HB), P(3HB), PLLA and PDLA respectively, were treated with purified P(LA-*co*-3HB) depolymerase. The purified depolymerase exhibited degradation activity toward both P(67 mol% LA-*co*-3HB) and P(3HB), but not PLLA or PDLA (Figure 4) which concurred with the halo formation result obtained in the cell level. This result suggested that the biodegradability of LA homopolymer was greatly changed by incorporation of 3HB unit.

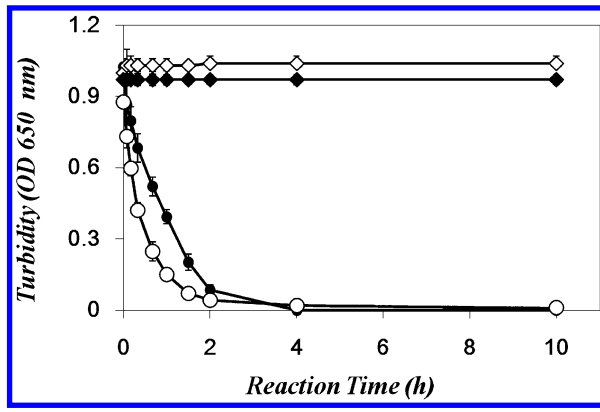

Figure 4. Enzymatic reaction of emulsified polymers treated with P(LA-co-3HB) depolymerase. P(3HB) (black ball), P(67 mol% LA-co-3HB) (white ball), PDLA (white diamond) and PLLA (black diamond). Data from reference (50).

Publication Date (Web): June 18, 2015 | doi: 10.1021/bk-2015-1192.ch008

During the degradation of the polymers that were treated by P(LA-*co*-3HB) depolymerase, the degradation speed of P(67 mol% LA-*co*-3HB) was faster than that of P(3HB) (*50*), suggesting the crystallinity of P(67 mol% LA-*co*-3HB) is lower than P(3HB) (*55*, *56*).

$PhaZ_{Af}$ and P(LA-*co*-3HB) depolymerase exhibited different substrate specificity toward P(3HB) and P(67 mol% LA-*co*-3HB). $PhaZ_{Af}$ only degraded P(3HB) while P(LA-*co*-3HB) depolymerase degraded both polymers, suggesting that the hydrolysis of the P(67 mol% LA-*co*-3HB) by $PhaZ_{Af}$ was inhibited by the presence of the LA units in the polymer chain, but not that of P(LA-*co*-3HB) depolymerase. The results indicated that the newly isolated depolymerase degraded P(67 mol% LA-*co*-3HB) that not only by decomposition of the 3HB contained fragment. Therefore, further investigation on the degrading mechanism of P(LA-*co*-3HB) depolymerase will be necessary for understanding the biodegradation of P(LA-*co*-3HB). For this purpose the degradation products of P(3HB) and P(LA-*co*-3HB) will be analyzed qualitatively and quantitatively. How much 3HB is necessary for biodegradation of P(LA-*co*-3HB) will be another intereting research subject.

Conclusion and Future Perspectives

As discussed here, the success of the establishment of an MPF for the production of LA-based polymers was hinged on the discovery of an engineered enzyme (LPE) that was integrated into a synthetic pathway. The first MPF synthesized copolymers had low LA fractions (6 mol% LA) (*8*). However, this

pioneering study laid the foundation for subsequent studies whereby through the interaction of enzyme evolutionary engineering, metabolic engineering, and fermentation techniques, the LA fractions in P(LA-*co*-3HB) were significantly improved (*25*, *26*, *37*). The evolved LPE (eLPE) in particular gave LA fractions of about 50 mol% in metabolically engineered *E. coli* with relatively high yields from glucose (*25*). The replacement of the 3HB-CoA supply pathway with extraneous valerate as a 3HV monomer precursor resulted into the synthesis of a PLA-like terpolymer (96 mol% of LA), which was similar to chemically synthesized PLA in terms of properties (*23*). When the P(LA-*co*-3HB) synthesis system was transferred into *C. glutamicum*, PLA-like polymers were synthesized (*21*), suggesting that further exploration of production hosts might be useful in enhancing polymer yields and LA fractions concurrently.

For industrial scale-up, the production of P(LA-*co*-3HB) copolymers faces the challenge of high production cost, mainly due to the high cost of glucose derived from foodstocks such as sugarcane, corn starch and sugar beet. Towards the reduction of the production cost, the efficient use of the lignocellulosic biomass sugars is inevitable. The use of glucose for the production of PHAs has been demonstrated to be efficient whereas, the use of xylose is known to be inefficient. In this report, methods for the efficient utilization of xylose were developed and enhanced to obtain high productivities of P(LA-*co*-3HB) with high LA fractions, which is critical in reducing the cost of producing LA-based polymers (*35*). Xylose utilization presented a new platform for the production of P(LA-*co*-3HB)s with LA fractions >50 mol% at high productivities, which will facilitate future exploration of material properties of LA-enriched P(LA-*co*-3HB)s, which was impossible with the use of glucose. Metabolic engineering strategies to maximize the lactic acid flux from xylose were carried out and were found to be effective in improving LA fractions/ yields in P(LA-*co*-3HB) (*36*). Exploration for depolymerases identified enzymes that could degrade P(LA-*co*-3HB); demonstrating that P(LA-*co*-3HB) is biodegradable hence it is ecofriendly as a petrochemical-based plastics substitute (*50*).

The aforementioned approaches for high yield production of P(LA-*co*-3HB) in combination with the utilization of lignocellulosic biomass have a potential for the establishment of a biorefinery for the production of the biodegradable P(LA-*co*-3HB). Therefore, the studies discussed here are worthwhile and contributes to the establishment of a system that can be scaled up with low operating costs hence improving the competitiveness of P(LA-*co*-3HB)s against the petrochemical-derived plastics.

In the production of P(LA-*co*-3HB) copolymers with enhanced LA fractions, it has been found that the molecular weights of the polymers decreases with the increase in LA fractions in P(LA-*co*-3HB) (*12*). To further advance this platform to the industrial level, further studies for the improvement of the molecular weights of P(LA-*co*-3HB) are required. In addition, further studies are necessary to determine the applications of P(LA-*co*-3HB)s and commercialize them. Moreover, although pure glucose and xylose attained high P(LA-*co*-3HB) productivities, substitution with lignocellulosic biomass hydrolysates is essential towards establishment of a robust system that can be scaled up for the creation of a biorefinery for the production of P(LA-*co*-3HB)s.

Publication Date (Web): June 18, 2015 | doi: 10.1021/bk-2015-1192.ch008

Publication Date (Web): June 18, 2015 | doi: 10.1021/bk-2015-1192.ch008

Abbreviations

LA: Lactic acid/lactate
PLA: polylatic acid/polylactate
LPE: Lactate-polymerizing enzyme
MPF: Microbial plastic factory
HAs: hydroxyalkanoates
PHAs: polyhydroxyalkanoates
3HB: 3-hydroxybutyrate
P(3HB): Poly(3-hydroxybutyrate)
P(LA-*co*-3HB): Poly(lactate-*co*-3-hydroxybutyrate)
3HB-CoA: 3-hydroxybutyl-CoA
PhaB: Acetoacetyl-CoA reductase
PflA: Pyruvate formate-lyase activating enzyme
$PhaC_{Re}$: Polyhydroxyalkanoates synthase from Ralstonia eutropha
$PhaC1_{Ps}$: Polyhydroxyalknaoates synthase from Pseudomonase sp.61-3
3HV: 3-hydroxyvalerate
3HV-CoA: 3-hydroxyvaleryl-CoA
P(LA-*co*-3HB-*co*-3HV): Poly(lactic acid-*co*-3-hydroxybutyrate-*co*-3-hydroxyvalerate)
LA96: P(LA-*co*-3HB-*co*-3HV) with 96 mol% LA
SCL: Short-chain-length
MCL: Medium-chain-length
$PhaC1_{Ps}$(STQK): $PhaC1_{Ps}$ with two mutations; Ser325Thr and Gln481Lys
$PhaC1_{Ps}$(STFSQK): $PhaC1_{Ps}$ with three mutations; Ser325Thr , Phe392Ser and Gln481Lys
PhaJ4: R-specific enoyl-CoA hydratase
FadA: 3ketoacyl-CoA thiolase
FadB: 3-hydroxyacyl-CoA/(*S*)-specific enol-CoA hydratase
LdhA: Lactate dehydrogenase
PTA: Phosphate acetyltransferase
ackA: Acetate kinase
PoxB: Pyruvate oxidase
iLDHs: NAD^+-independent lactate dehydrogenase
XylE: D-xylose transporter
ATP: Adenosine triphosphate
GatC: Galacticol- permease IIC component
$PhaZ_{Af}$: PHAs depolymerase from *Alcaligenes faecalise* T1
PhaZ: PHAs depolymerase

Acknowledgments

The works described here were partially supported by the Research Foundation of Institute for Fermentation, Osaka (IFO) (to S. T.), Japans Society for the Promotion of Science (JSPS) Kakenhi (Nos. 23310059 and 26660080 to S.T.), JST, CREST (to S. T.), and JSPS (to J. S.).

Publication Date (Web): June 18, 2015 | doi: 10.1021/bk-2015-1192.ch008

References

1. Mecking, S. *Angew. Chem., Int. Ed.* **2004**, *43*, 1078–1085.
2. Carrasco, F.; Pages, P.; Gamez-Perez, J.; Santana, O. O.; Maspoch, M. L. *Polym. Degrad. Stab.* **2010**, *95*, 116–125.
3. Auras, R.; Harte, B.; Selke, S. *Macromol. Biosci.* **2004**, *4*, 835–864.
4. Lasprilla, A. J. R.; Martinez, G. A. R.; Lunelli, B. H.; Jardini, A. L.; Filho, R. M. *Biotech. Adv.* **2012**, *30*, 321–328.
5. Rasal, R. M.; Janorkar, A. V.; Hirt, D. E. *Prog. Polym. Sci.* **2010**, *35*, 338–356.
6. Garlotta, D. *J. Polym. Environ.* **2001**, *9*, 63–84.
7. Zhang, M.; Thomas, N. L. *Adv. Polym. Technol.* **2011**, *30*, 67–79.
8. Taguchi, S.; Yamada, M.; Matsumoto, K.; Tajima, K.; Satoh, Y.; Munekata, M.; Ohno, K.; Kohda, K.; Shimamura, T.; Kambe, H.; Obata, S. *Proc. Natl. Acad. Sci. U.S.A.* **2008**, *105*, 17323–17327.
9. Chisholm, M. H. *Pure Appl. Chem.* **2010**, *82*, 1647–1662.
10. Corma, A.; Iborra, S.; Velty, A. *Chem. Rev.* **2007**, *107*, 2411–2502.
11. Nampoothiri, K. M.; Nair, N. R.; John, R. P. *Bioresour. Technol.* **2010**, *101*, 8493–8501.
12. Matsumoto, K.; Taguchi, S. *Appl. Microbiol. Biotechnol.* **2010**, *85*, 921–932.
13. Chen, G. Q. *Chem. Soc. Rev.* **2009**, *38*, 2434–2446.
14. Verlinden, R. A. J.; Hill, D. J.; Kenward, M. A.; Williams, C. D.; Radecka, I. *J. Appl. Microbiol.* **2007**, *102*, 1437–1449.
15. Valentin, H.; Steinbüchel, A. *Appl. Microbiol. Biotechnol.* **1994**, *40*, 699–709.
16. Yuan, W.; Jia, Y.; Tian, J.; Snell, K. D.; Müh, U.; Sinskey, A. J.; Lambalot, R. H.; Walsh, C. T.; Stubbe, J. *J. Arch. Biochem. Biophys.* **2001**, *394*, 87–98.
17. Tajima, K.; Han, X.; Satoh, Y.; Ishii, A.; Araki, Y.; Munekata, M.; Taguchi, S. *Appl. Microbiol. Biotechnol.* **2009**, *94*, 365–376.
18. Nduko, J. M.; Matsumoto, K.; Taguchi, S. In *Biobased Monomers, Polymers, and Materials*; Smith, P. B., Gross, R. A., Eds.; ACS Symposium Series 1105; American Chemical Society: Washington, DC, 2012; pp 213−235.
19. Anderson, A. J.; Dawes, E. A. *Microbiol. Rev.* **1990**, *54*, 450–472.
20. Taguchi, S. *Polym. Degrad. Stab.* **2010**, *95*, 1421–1428.
21. Song, Y.; Matsumoto, K. i.; Yamada, M.; Gohda, A.; Brigham, C.; Sinskey, A.; Taguchi, S. *Appl. Microbiol. Biotechnol.* **2012**, *93*, 1917–1925.
22. Yamada, M.; Matsumoto, K.; Shimizu, K.; Uramoto, S.; Nakai, T.; Shozui, F.; Taguchi, S. *Biomacromolecules* **2010**, *11*, 815–819.
23. Shozui, F.; Matsumoto, K.; Motohashi, R.; Sun, J. A.; Satoh, T.; Kakuchi, T.; Taguchi, S. *Polym. Degrad. Stab.* **2011**, *96*, 499–504.
24. Nduko, J. M.; Matsumoto, K.; Taguchi, S. In *Green Polymer Chemistry: Biocatalysis and Materials II*; Cheng, H. N., Gross, R. A., Smith, P. B., Eds.; ACS Symposium Series 1144; American Chemical Society: Washington, DC, 2013; pp 175−197.
25. Yamada, M.; Matsumoto, K. i.; Uramoto, S.; Motohashi, R.; Abe, H.; Taguchi, S. *J. Biotechnol.* **2011**, *154*, 255–260.

26. Yamada, M.; Matsumoto, K.; Nakai, T.; Taguchi, S. *Biomacromolecules* **2009**, *10*, 677–681.
27. Valappil, S. P.; Boccaccini, A. R.; Bucke, C.; Roy, I. *Antonie Van Leeuwenhoek* **2007**, *91*, 1–17.
28. Takors, R.; Bathe, B.; Rieping, M.; Hans, S.; Kelle, R.; Huthmacher, K. *J. Biotechnol.* **2007**, *129*, 181–190.
29. Jo, S. J.; Maeda, M.; Ooi, T.; Taguchi, S. *J. Biosci. Bioeng.* **2006**, *102*, 233–236.
30. Jo, S. J.; Matsumoto, K. I.; Leong, C. R.; Ooi, T.; Taguchi, S. *J. Biosci. Bioeng.* **2007**, *104*, 457–463.
31. Tateno, T.; Hatada, K.; Tanaka, T.; Fukuda, H.; Kondo, A. *Appl. Microbiol. Biotechnol.* **2009**, *84*, 733–739.
32. Alonso, D. M.; Bond, J. Q.; Dumesic, J. A. *Green Chem.* **2010**, *12*, 1493–1513.
33. Kumar, R.; Singh, S.; Singh, O. V. *J. Ind. Microbiol. Biotechnol.* **2008**, *35*, 377–391.
34. FitzPatrick, M.; Champagne, P.; Cunningham, M. F.; Whitney, R. A. *Bioresour. Technol.* **2010**, *101*, 8915–8922.
35. Nduko, J. M.; Matsumoto, K.; Ooi, T.; Taguchi, S. *Metab. Eng.* **2013**, *15*, 159–166.
36. Nduko, J. M.; Matsumoto, K.; Ooi, T.; Taguchi, S. *Appl. Microbiol. Biotechnol.* **2014**, *98*, 2453–2460.
37. Shozui, F.; Matsumoto, K.; Nakai, T.; Yamada, M.; Taguchi, S. *Appl. Microbiol. Biotechnol.* **2010**, *85*, 949–954.
38. Zhou, L.; Zuo, Z. R.; Chen, X. Z.; Niu, D. D.; Tian, K. M.; Prior, B. A.; Shen, W.; Shi, G. Y.; Singh, S.; Wang, Z. X. *Curr. Microbiol.* **2011**, *62*, 981–989.
39. Hasona, A.; Kim, Y.; Healy, F. G.; Ingram, L. O.; Shanmugam, K. T. *J. Bacteriol.* **2004**, *186*, 7593–7600.
40. Utrilla, J.; Licona-Cassani, C.; Marcellin, E.; Gosset, G.; Nielsen, L. K.; Martinez, A. *Metab. Eng.* **2012**, *14*, 469–476.
41. Sodergarda, A.; Stolt, M. *Prog. Polym. Sci.* **2002**, *27*, 1123–1163.
42. Ikada, Y.; Jamshidi, K.; Tsuji, H.; Hyon, S. H. *Macromolecules* **1987**, *20*, 904–906.
43. Rehm, B. H. *Biochem. J.* **2003**, *376*, 15–33.
44. Tajima, K.; Satoh, Y.; Satoh, T.; Itoh, R.; Han, X.; Taguchi, S.; Kakuchi, T.; Munekata, M. *Macromolecules* **2009**, *42*, 1985–1989.
45. Zhou, S. D.; Shanmugam, K. T.; Ingram, L. O. *Appl. Environ. Microbiol.* **2003**, *69*, 2237–2244.
46. Wolf, F. F.; Friedemann, N.; Frey, H. *Macromolecules* **2009**, *42*, 5622–5628.
47. Kricheldorf, H. R. *Chemosphere* **2001**, *43*, 49–54.
48. Sudesh, K.; Abe, H.; Doi, Y. *Prog. Polym. Sci.* **2000**, *25*, 1503–1555.
49. Kawai, F.; Nakadai, K.; Nishioka, E.; Nakajima, H.; Ohara, H.; Masaki, K.; Iefuji, H. *Polym. Degrad. Stab.* **2011**, *96*, 1342–1348.
50. Sun, J.; Matsumoto, K. i.; Nduko, J. M.; Ooi, T.; Taguchi, S. *Polym. Degrad. Stab.* **2014**, *110*, 44–49.

51. Kobayashi, T.; Sugiyama, A.; Kawase, Y.; Saito, T.; Mergaert, J.; Swings, J. *J. Environ. Polym. Degr.* **1999**, *7*, 9–18.
52. Jendrossek, D.; Knoke, I.; Habibian, R. B.; Steinbüchel, A.; Schlegel, H. G. *J. Environ. Polym. Degr.* **1993**, *1*, 53–63.
53. Kasuya, K.; Doi, Y.; Yao, T. *Polym. Degrad. Stab.* **1994**, *45*, 379–386.
54. Kasuya, K.; Inoue, Y.; Tanaka, T.; Akehata, T.; Iwata, T.; Fukui, T.; Doi, Y. *Appl. Environ. Microbiol.* **1997**, *63*, 4844–4852.
55. Abe, H.; Doi, Y. *Int. J. Biol. Macromol.* **1999**, *25*, 185–192.
56. Iwata, T.; Shiromo, M.; Doi, Y. *Macromol. Chem. Phys.* **2002**, *203*, 1309–1316.

Publication Date (Web): June 18, 2015 | doi: 10.1021/bk-2015-1192.ch008

Publication Date (Web): June 18, 2015 | doi: 10.1021/bk-2015-1192.ch009

Chapter 9

Combining Sustainable Polymerization Routes for the Preparation of Polyesters, Polycarbonates, and Copolymers

Charles Romain and Charlotte K. Williams*

317 RCS1, Department of Chemistry, Imperial College London, South Kensington Campus, London SW7 2AZ, United Kingdom
***E-mail: c.k.williams@imperial.ac.uk.**

Ring-Opening Polymerizations (ROP) and Ring-Opening Copolymerizations (ROCOP) of 'oxygenated' cyclic monomers (lactones, cyclic carbonates, epoxides, anhydrides) are promising routes to afford well-defined polymers. It is notable that both ROP and ROCOP require monomers that could be bio-derived, in line with the aspirations of sustainable polymerization processes. In addition, these two different methodologies can be combined to extend the scope of 'oxygenated' synthetic polymers.

We have recently reported that a single catalyst may be applied for both ROCOP and ROP, so as to readily produce via a 'one-pot' procedure various copolymers. We have also uncovered a novel chemoselective catalyst control pathway, whereby the nature of the metal chain end group controls the polymerization cycle, and thereby the composition of the copolymer.

Introduction

Routes for Polyesters and Polycarbonates

Polyesters (PE) and polycarbonates (PC) are important classes of polymers which may contain different repeat unit chemistry (including combinations of aromatic, semi-aromatic, saturated backbones) and therefore have various different applications (including areas such as packaging, fibres and specialist

In Green Polymer Chemistry: Biobased Materials and Biocatalysis; Smith, et al.;
ACS Symposium Series; American Chemical Society: Washington, DC, 2015.

medical applications). PE and PC are industrially produced on large scale (> 5Mt/year), mainly by polycondensation methods: the condensation of diols and diacids affords polyesters whereas the condensation of diols and phosgene yields polycarbonates (*1*). Despite their commercial success, from the point of view of new materials synthesis, such routes are generally poorly controlled, require harsh conditions, only allow access to limited types of polymer architectures and produce side-products.

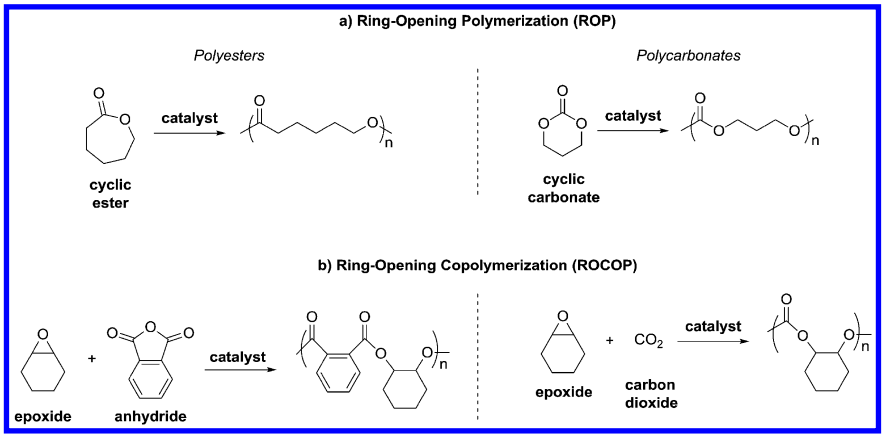

Figure 1. Ring-opening polymerization routes for the preparation of polyesters and polycarbonates.

Alternatively, aliphatic PE and PC can be obtained by the ring opening polymerization (ROP) of cyclic esters (*2–4*) or cyclic carbonates (*5*, *6*), respectively (Figure 1). Thus, for example, the ROP of ε-caprolactone (ε-CL) yields the corresponding polycaprolactone (PCL), whereas the ROP of trimethylene carbonate (TMC) yields the corresponding linear polytrimethylene carbonate PTMC. These routes are well-controlled and yield, under mild conditions, well-defined polymers (with predicatable values for M_n, PDI, end-groups, etc). A plethora of catalysts (*2–6*) have been reported for ROP, some of which are highly stereocontrolled, enabling control over the resulting polymer tacticity (*7*). However, ROP is limited in terms of the substrate scope, in particular there remain only a narrow range of commercially available lactones/cyclic carbonates. Most studies are carried out using lactide (LA), ε-caprolactone (ε-CL) or β-butyrolactone (β-BL) or with trimethylene carbonate (TMC). It is notable that β-malolactatonates, monomers which are difficult to homopolymerize using ROP, have recently been copolymerized with other cyclic esters and carbonates as a route to polyhydroxyalkanoates (PHA) (*8*, *9*). Indeed, the synthesis of new cyclic esters (*10*, *11*) and cyclic carbonates for use in ROP is an important field (*12–14*).

In Green Polymer Chemistry: Biobased Materials and Biocatalysis; Smith, et al.;
ACS Symposium Series; American Chemical Society: Washington, DC, 2015.

Publication Date (Web): June 18, 2015 | doi: 10.1021/bk-2015-1192.ch009

Publication Date (Web): June 18, 2015 | doi: 10.1021/bk-2015-1192.ch009

As described in Figure 1, PE and PC can also be obtained by the ring-opening copolymerizartion (ROCOP) of epoxides and anhydrides/carbon dioxide (*15*, *16*). Thus, the perfectly alternating copolymerization of epoxides with cyclic anhydrides affords polyesters (*17–19*), whereas the perfectly alternating copolymerization of epoxides with carbon dioxide affords polycarbonates (*20–26*). These ROCOP reactions are controlled polymerizations, enabling predictable polymer chain lengths (M*n*, PDI), end group functionalities and, in some cases, tacticities. The ROCOP route is also advantageous in that it combines two different monomers, thereby enabling the differentiation of polymer composition/structure, and therefore polymer thermal and mechanical properties, by changing either or both of the co-monomers (*17*, *27*). Control over the ROCOP stereochemistry has very recently been exemplified by Coates and co-workers, in the first report of stereocomplex polyester prepared via ROCOP of propylene oxide and succinic anhydride (*27*).

Renewable Monomers for Polyesters and Polycarbonates

It is notable that both ROP and ROCOP routes require monomers, namely cyclic esters, cyclic carbonates, epoxides and anhydrides (Figure 2), that can be bio-derived (*4*, *28*), in line with the goals of sustainable polymerization processes (*29*).

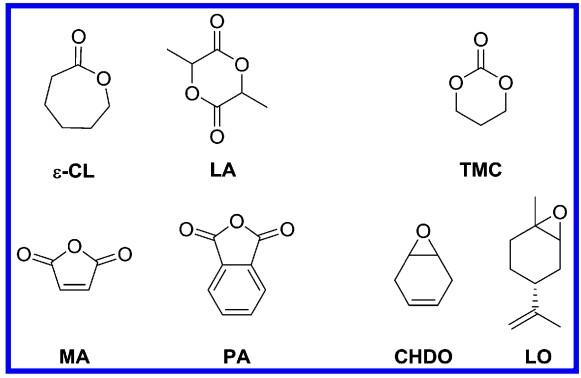

Figure 2. Selected examples of commonly investigated monomers that could be derived from renewable resources.

The use of CO_2 as a carbon feedstock for PC synthesis is also of high interest from a sustainable chemistry perspective as CO_2 is abundant, cheap and non-toxic (*24*). A recent life cycle analysis study on CO_2-derived polycarbonates shows that the incorporation of 20% wt. of CO_2 reduces the greenhouse gas emissions by 11-19% and reduces fossil resource depletion by 13-16%, as compared to an equivalent petrochemical polymer (such as polyethers) (*30*).

In Green Polymer Chemistry: Biobased Materials and Biocatalysis; Smith, et al.;
ACS Symposium Series; American Chemical Society: Washington, DC, 2015.

Considering the syntheses of cyclic monomers from biomass, the fermentation of carbohydrates enables the facile production of (di)acids such as lactic acid and succinic acid. These diacids can subsequently be converted to lactide and succinic anhydride, respectively (*31*). In addition, from a hydroxymethylfurfural (HMF) platform, it is possible to obtain monomers such as ε-CL or phthalic anhydride (Figure 3) (*32*, *33*). For example, Lobo *et al*, recently reported the synthesis of phthalic anhydride resulting from the Diels-Alder reaction between furan and maleic anhydride, followed by the subsequent elimination of water (*33*). Naturally derived terpenes are a viable source for various different epoxides, including limonene oxide and pinene oxide (*31*, *34*). In addition, in collaboration with Meier and co-workers we have reported the synthesis of unsatured cyclohexene oxide, starting from fatty acid derived 1,4-cyclohexanediene (Figure 3) (*35*).

Thus, there is a considerable potential for both the ROP and ROCOP methodologies to apply bio-derived monomers in line with the tenets of new green polymerization processes (*29*).

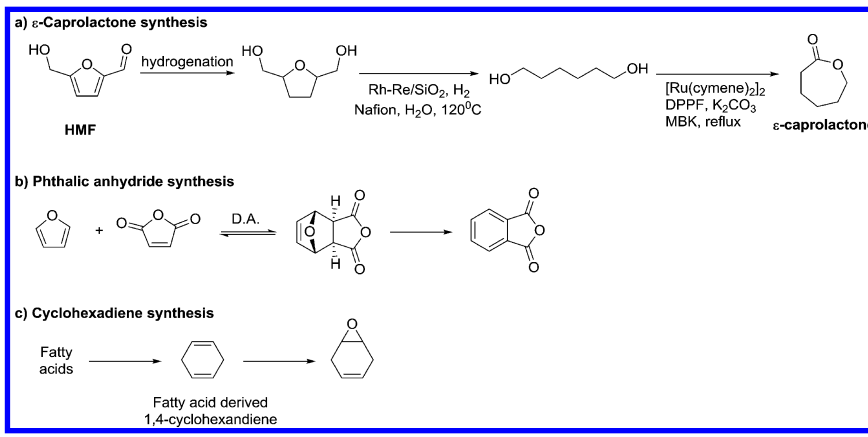

Figure 3. Selected examples of the synthesis of cyclic esters, cyclic anhydrides and epoxides obtained from renewable resources.

Tandem Catalyses for Poly(ester-*co*-carbonates)

Given the success of the ROCOP and ROP routes to polyesters and polycarbonates, research has focussed on combining these two different methodologies to extend the scope of synthetic polymers and enable the synthesis of block copolymers such as poly(ester-*co*-carbonates) (*16*, *36–41*). Thus, by combing two ROP processes, Romain et al. reported a sequential 'one-pot' synthesis, using a single catalyst, to prepare poly(trimethylene carbonate-*co*-lactides) featuring a heterotactic PLA block (*36*). Similarly, Guillaume and Carpentier and co-workers have described various syntheses, characterizations and properties of poly(ester-*co*-carbonates) obtained via sequential ROP of cyclic carbonates and cyclic esters (including lactones and

Publication Date (Web): June 18, 2015 | doi: 10.1021/bk-2015-1192.ch009

β-malolactonates) (*37*, *38*, *42*). Furthermore, Darensbourg et al. reported a tandem catalysis approach which combines ROCOP and ROP (*39*). The use of a cobalt salen catalyst for the ROCOP of styrene oxide/CO_2 enables the efficient production of polystyrene carbonate, then after the addition of water to quench the ROCOP reaction, the DBU catalysed ROP of lactide can occur yielding block copolymers (*39*). Our research group have also applied tandem catalyses to combine ROCOP and ROP. Using a dizinc catalyst for ROCOP enabled the selective production of polycarbonate polyols. These polycarbonates were subsequently applied as macro-initiators for the yttrium catalysed ROP of lactide, enabling the preparation of ABA type poly(lactide-*co*-cyclohexenecarbonate-lactides) (*43*).

As part of on-going studies into the preparation of block copoly(ester-carbonates), we have recently discovered that a single catalyst may be applied for both ROCOP and ROP, so as to produce various copolymers (*40*). We have also uncovered a novel chemoselective catalyst control, whereby the nature of the metal chain end group controls the polymerization cycle, and thereby the composition of the copolymer.

Publication Date (Web): June 18, 2015 | doi: 10.1021/bk-2015-1192.ch009

Di-Zinc and Magnesium Catalysts for ROCOP

Epoxide/CO_2 Copolymerizations

Our group have previously reported a series of bimetallic homogeneous catalysts for epoxide/CO_2 copolymerizations (*44–49*). In particular, the di-zinc (*44–47*) and di-magnesium (*48*) catalysts were of significant potential due to their ability to operate under mild conditions with high activities and selectivities. The catalysts are homogeneous bimetallic complexes, whereby the metals are coordinated by a macrocyclic ancillary ligand and carboxylate co-ligands. The molecular structures of the carboxylate derivatives show that the complexes are 'bowl shaped', with one κ^2-acetate group bridging the two metal centres on the concave face and one κ^1-acetate co-ligand coordinating on the convex face of the molecule (*46*, *47*).

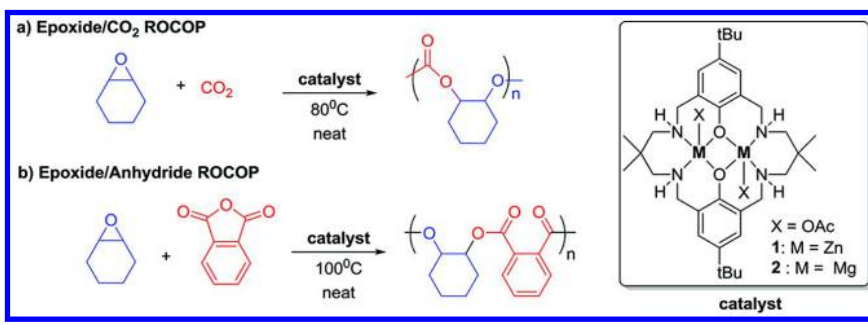

Figure 4. The ROCOP processes for the synthesis of polycarbonates (a) and polyesters (b).

In Green Polymer Chemistry: Biobased Materials and Biocatalysis; Smith, et al.;
ACS Symposium Series; American Chemical Society: Washington, DC, 2015.

Both the di-zinc and magnesium catalysts are active at only 1 atmosphere pressure of CO_2 affording perfectly alternating polycarbonates (> 99% carbonate linkages) (*46*, *48*). The catalysts are also highly selective for polymer formation (>96%), with little or no formation of cyclic carbonate by-products (using cyclohexene oxide as the epoxide). Kinetic investigations, using the di-zinc catalyst, showed that the rate law is first order with respect to epoxide concentration and first order with respect to catalyst concentration (*46*). There is no dependence of the polymerization rate on CO_2 pressure, between 1 and 40 bar, suggesting a zero order dependence with respect to CO_2. This rate law suggests that the CO_2 insertion reaction is not the rate determining step. The study of the catalytic cycle using DFT suggests a polymer chain shuttling mechanism (Figure 5) (*47*). According to such a mechanism, during propagation, the zinc alkoxide bond attacks CO_2 leading to the formation of a new zinc carbonate bond. Subsequently, this zinc carbonate species attacks a coordinated CHO molecule to regenerate a zinc alkoxide bond. The DFT calculations suggest that the rate limiting step is carbonate attack on bound epoxide, in line with the experimental kinetic investigation (Figure 5).

Publication Date (Web): June 18, 2015 | doi: 10.1021/bk-2015-1192.ch009

Epoxide/Anhydride Copolymerizations

The promising results obtained using bimetallic catalysts for epoxide/CO_2 copolymerizations prompted the investigation of the same catalysts for epoxide/anhydride copolymerizations (Figure 4). Both the di-zinc and magnesium catalysts were investigated for the ROCOP of cyclohexene oxide and phthalic anhydride. Both catalysts showed good activity, at 100 °C in neat epoxide or in toluene, forming alternating polyesters without significant formation of ether linkages (*50*). The catalysts show moderate to good activities, with turn-over-frequencies up to 100 h^{-1} for the di-magnesium catalyst (which was four times more active than the di-zinc catalyst). Kinetic studies showed that the rate was zero order (independent) of anhydride concentration (*50*), in line with the related zero order dependence on CO_2 for the related ROCOP of CO_2/epoxides. It is proposed that during propagation, there is a fast insertion of the anhydride into the zinc-alkoxide bond, followed by the slow insertion of the epoxide into the zinc carboxylate bond (Figure 5).

ROP of Cyclic Esters

Polyester versus Polycarbonate Formation

The success of the bimetallic catalysts for ROCOP prompted the investigation of the same catalysts for the ROP of cyclic esters. Interstingly, the di-zinc catalyst, **1** (Figure 4), was unable to polymerize ε-CL, either in neat monomer or under a range of solvent conditions. The ROP reactions were unsuccessful even in the presence of excess alcohol, which may function as a chain transfer agent, or under a range of different temperatures. It was discovered, however, that the addition of a catalytic quantity of epoxide (10 mol. % cyclohexene oxide vs. ε- CL) yielded an active ROP catalyst system (Figure 6 and Table 1). The catalyst was

In Green Polymer Chemistry: Biobased Materials and Biocatalysis; Smith, et al.;
ACS Symposium Series; American Chemical Society: Washington, DC, 2015.

able to polymerize up to 200 equivalents of ε-caprolactone in less than 1 hour. Alternatively, the cyclohexene oxide can be used as the reaction solvent (where it is present in approximately nine times higher concentration than ε-caprolactone) resulting in the exclusive formation of polycaprolactone (*i.e.* there is no evidence at all for any formation of poly(cyclohexene oxide).

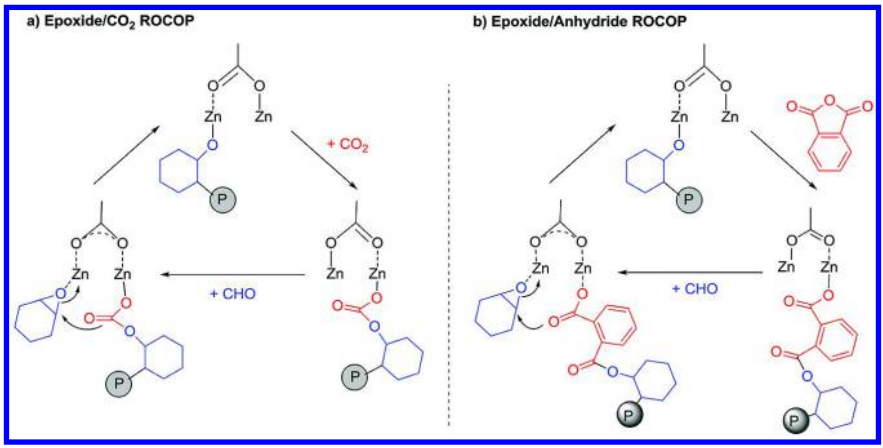

Figure 5. Chain-shuttling mechanisms proposed for the ROCOP processes.

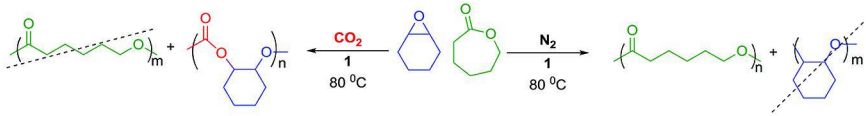

Figure 6. Polyester or polycarbonate formation, under N_2 (left) and CO_2 gas (right) atmospheres.

Interestingly, using the same monomer mixture (ε-CL/CHO = 200/800) but adding CO_2 led to exclusive formation of polycarbonate (polycyclohexene carbonate), resulting from ROCOP without any formation of polycaprolactone (Figure 6). Comparing the activity of the di-zinc catalyst for both polymerizations, under the same reaction conditions, shows that the ROCOP is significantly slower (TOF = 20 h^{-1}) compared to the ROP of ε-CL (TOF ~ 100 h^{-1}). Thus, the observed selectivity appears not to relate to the overall activity of the catalysts, but rather to particular selectivity occurring during the catalytic cycles.

In Green Polymer Chemistry: Biobased Materials and Biocatalysis; Smith, et al.;
ACS Symposium Series; American Chemical Society: Washington, DC, 2015.

Publication Date (Web): June 18, 2015 | doi: 10.1021/bk-2015-1192.ch009

Table 1. Different Reaction Conditions for ROP and ROCOP Using 1

CHO (eq.)	*ε-CL (eq.)*	*CO_2 (bar)*	*Solvent*	*Time*	*Polymer*	*M_n[a] (g/mol)*	*PDI[a]*
-	200	-	Neat	16h	-	-	-
20	200	-	Toluene	2h[b]	PCL	21040	1.4
900	100	-	Neat	2h[b]	PCL	6020	1.2
900	100	1	Neat	15h	PCHC	1040	1.1

Reaction conditions: ***1*** *=* ***1*** *eq., 80 °C.* [a] *Determined by SEC vs. polystyrene standards,* [b] *Not optimized time.*

Publication Date (Web): June 18, 2015 | doi: 10.1021/bk-2015-1192.ch009

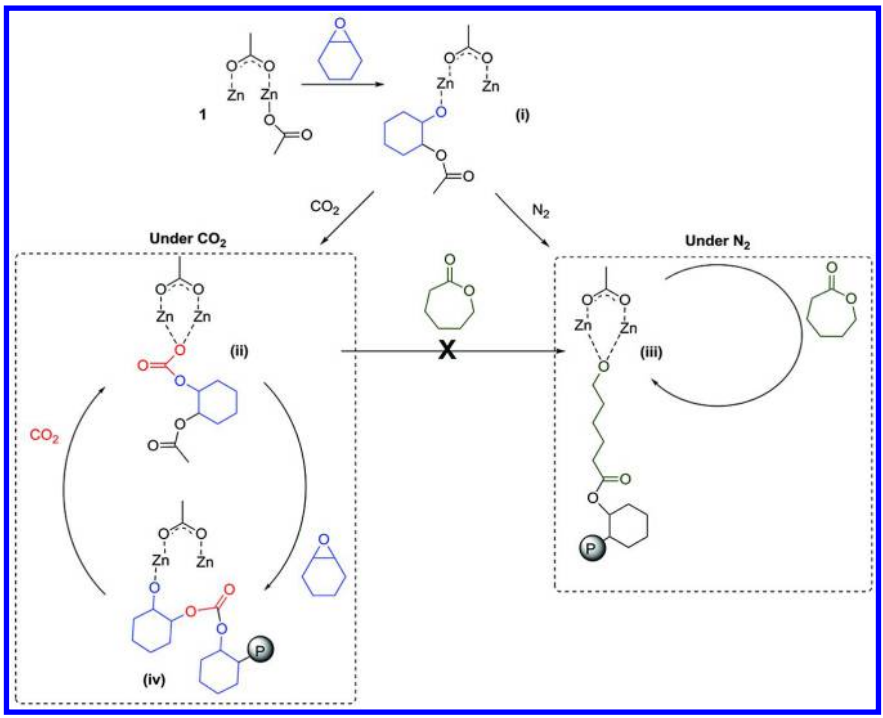

Figure 7. The two polymerization cycles, enabling the production of polycarbonates (left) or polyesters (right).

Chemoselectivity

Such a reactivity can be rationalized by gaining insight into the mechanism. Thus, whereas catalyst **1** is unable to ring-open ε-CL in the absence of any additive, the catalyst reacts, and ring-opens, an equivalent of epoxide (CHO) to generate, *in-situ*, an alkoxide group as described in Figure 7. Under a N_2 atmosphere, this latter alkoxide intermediate (**i**) is a viable initiator for the ROP

of ε-CL affording production of PCL. Under the same conditions, but where CO_2 is present, it is proposed that rapid CO_2 insertion into the *in-situ* generated Zn-alkoxide bond [intermediate (**i**)] occurs immediately leading to the formation of a zinc carbonate species (**ii**). The latter zinc carbonate intermediate (**ii**) is unable to initiate the ROP of ε-CL but is a viable intermediate and initiator for the ROCOP of cyclohexene oxide/carbon dioxide to afford polycarbonate production. Thus, it is proposed that the catalytic selectivity arises from the nature of the Zn-O bond. The zinc carbonate or carboxylate species can only initiate/propagate ROCOP, whereas the zinc alkoxide species can initiate/propagate both ROCOP and ROP. Thus, by controlling the nature of the Zn-O bond, a particular catalytic cycle can be selected.

Publication Date (Web): June 18, 2015 | doi: 10.1021/bk-2015-1192.ch009

Combining ROP and ROCOP Routes

With this mechanistic hypothesis and observed chemo-selectivity, it was possible to combine and control the ROP and ROCOP processes using a single catalyst as described in Figure 8 (*40*).

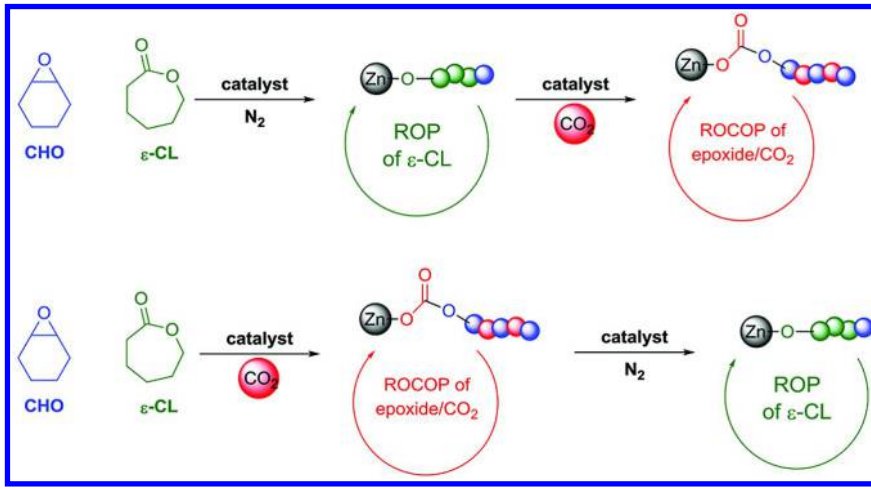

Figure 8. Combination of ROP and ROCOP processes, in one-pot with a single catalyst.

The di-zinc catalyst afforded PCL quantatively, using a mixture of ε-CL/CHO (200/800). The subsequent addition of CO_2 led to the *in-situ* formation of the zinc-carbonate intermediate (**i**) which initiated the ROCOP process and led to the subsequent formation of the polycarbonate block (Figure 9). The reverse order of monomer additions was also viable: when the dizinc catalyst was mixed with epoxide/CO_2/lactone, the polycarbonate block was selectively formed. Then, after the removal of the CO_2, using cycles of vacuum/nitrogen, the carbonate species (**i**) was transformed to the zinc alkoxide species (**iii**), by reaction with epoxide, and this species led to quantitative formation of a PCL block.

In Green Polymer Chemistry: Biobased Materials and Biocatalysis; Smith, et al.;
ACS Symposium Series; American Chemical Society: Washington, DC, 2015.

Publication Date (Web): June 18, 2015 | doi: 10.1021/bk-2015-1192.ch009

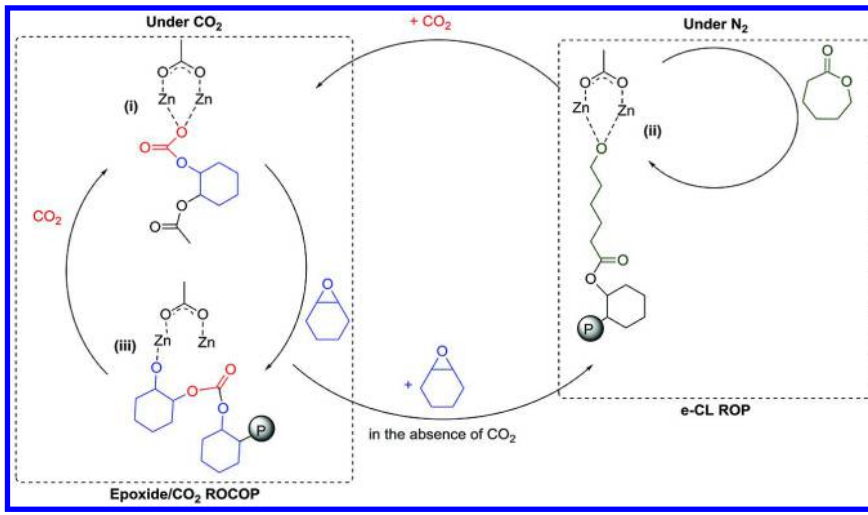

Figure 9. Illustrates the 'switch' between ROP and ROCOP processes.

Conclusions

Di-zinc and magnesium catalysts were good initiators for various ring-opening copolymerizations, using either epoxides/CO_2 or epoxides/anhydrides and affording the corresponding polycarbonates or polyesters. The di-zinc catalyst, in the presence of epoxide, was also an active initiator (catalyst) for the ring-opening polymerization of ε-caprolactone. In addition, the di-zinc catalyst was able to selectively form block copoly(ester-carbonates) using mixtures of up to three different monomers and by combining the ROCOP and ROP processes. Finally, in the presence of an exogenous switch reagent, it is possible to 'switch' from ROCOP to ROP, or vice versa, to selectively afford various block copolymers. The scope of this methodology will be extended to include other cyclic monomers and it is envisaged it could lead to the production of new copolymers of controllable composition and properties.

References

1. Okada, M. *Prog. Polym. Sci.* **2002**, *27*, 87–133.
2. Dechy-Cabaret, O.; Martin-Vaca, B.; Bourissou, D. *Chem. Rev.* **2004**, *104*, 6147–6176.
3. Platel, R. H.; Hodgson, L. M.; Williams, C. K. *Polym. Rev.* **2008**, *48*, 11–63.
4. Williams, C. K.; Hillmyer, M. A. *Polym. Rev.* **2008**, *48*, 1–10.
5. Darensbourg, D. J.; Moncada, A. I.; Wilson, S. J. In *Green Polymerization Methods : Renewable Starting Materials, Catalysis and Waste Reduction*; Mathers, R. T, Meier, M. A. R., Eds.; Wiley-VCH Verlag GmbH & Co, KGaA: Weinheim, Germany, 2011; pp 163−200.

Publication Date (Web): June 18, 2015 | doi: 10.1021/bk-2015-1192.ch009

6. Ajellal, N.; Carpentier, J.-F.; Guillaume, C.; Guillaume, S. M.; Helou, M.; Poirier, V.; Sarazin, Y.; Trifonov, A. *Dalton Trans.* **2010**, *39*, 8363–8376.
7. Thomas, C. M. *Chem. Soc. Rev.* **2010**, *39*, 165–173.
8. Jaffredo, C. G.; Guillaume, S. M. *Polym. Chem.* **2014**, *5*, 4168–4194.
9. Jaffredo, C. G.; Chapurina, Y.; Guillaume, S. M.; Carpentier, J.-F. *Angew. Chem., Int. Ed.* **2014**, *53*, 2687–2691.
10. Winkler, M.; Raupp, Y. S.; Köhl, L. A. M.; Wagner, H. E.; Meier, M. A. R. *Macromolecules* **2014**, *47*, 2842–2846.
11. Blake, T. R.; Waymouth, R. M. *J. Am. Chem. Soc.* **2014**, *136*, 9252–9255.
12. Brignou, P.; Priebe Gil, M.; Casagrande, O.; Carpentier, J.-F.; Guillaume, S. M. *Macromolecules* **2010**, *43*, 8007–8017.
13. Suriano, F.; Coulembier, O.; Hedrick, J. L.; Dubois, P. *Polym. Chem.* **2011**, *2*, 528–533.
14. Helou, M.; Brusson, J.-M.; Carpentier, J.-F.; Guillaume, S. M. *Polym. Chem.* **2011**, *2*, 2789–2795.
15. Brulé, E.; Guo, J.; Coates, G. W.; Thomas, C. M. *Macromol. Rapid Commun.* **2011**, *32*, 169–185.
16. Jeske, R. C.; Rowley, J. M.; Coates, G. W. *Angew. Chem. Int. Ed.* **2008**, *47*, 6041–6044.
17. Jeske, R. C.; DiCiccio, A. M.; Coates, G. W. *J. Am. Chem. Soc.* **2007**, *129*, 11330–11331.
18. Nejad, E. H.; van Melis, C. G. W.; Vermeer, T. J.; Koning, C. E.; Duchateau, R. *Macromolecules* **2012**, *45*, 1770–1776.
19. Nejad, E. H.; Paoniasari, A.; Koning, C. E.; Duchateau, R. *Polym. Chem.* **2012**, *3*, 1308–1313.
20. Coates, G. W.; Moore, D. R. *Angew. Chem., Int. Ed.* **2004**, *43*, 6618–6639.
21. Darensbourg, D. J.; Mackiewicz, R. M.; Phelps, A. L.; Billodeaux, D. R. *Acc. Chem. Res.* **2004**, *37*, 836–844.
22. Darensbourg, D. J. *Chem. Rev.* **2007**, *107*, 2388–2410.
23. Klaus, S.; Lehenmeier, M. W.; Anderson, C. E.; Rieger, B. *Coord. Chem. Rev.* **2011**, *255*, 1460–1479.
24. Kember, M. R.; Buchard, A.; Williams, C. K. *Chem. Commun.* **2011**, *47*, 141–163.
25. Lu, X.-B.; Darensbourg, D. J. *Chem. Soc. Rev.* **2012**, *41*, 1462–1484.
26. Lu, X.-B.; Ren, W.-M.; Wu, G.-P. *Acc. Chem. Res.* **2012**, *45*, 1721–1735.
27. Longo, J. M.; DiCiccio, A. M.; Coates, G. W. *J. Am. Chem. Soc.* **2014**, 15897–15900.
28. Tschan, M. J. L.; Brule, E.; Haquette, P.; Thomas, C. M. *Polym. Chem.* **2012**, *3*, 836–851.
29. Schroder, K.; Matyjaszewski, K.; Noonan, K. J. T.; Mathers, R. T. *Green Chem.* **2014**, *16*, 1673–1686.
30. von der Assen, N.; Bardow, A. *Green Chem.* **2014**, *16*, 3272–3280.
31. Corma, A.; Iborra, S.; Velty, A. *Chem. Rev.* **2007**, *107*, 2411–2502.
32. van Putten, R.-J.; van der Waal, J. C.; de Jong, E.; Rasrendra, C. B.; Heeres, H. J.; de Vries, J. G. *Chem. Rev.* **2013**, *113*, 1499–1597.
33. Mahmoud, E.; Watson, D. A.; Lobo, R. F. *Green Chem.* **2014**, *16*, 167–175.

34. Ciriminna, R.; Lomeli-Rodriguez, M.; Demma Cara, P.; Lopez-Sanchez, J. A.; Pagliaro, M. *Chem. Commun.* **2014**, *50*, 15288–15296.
35. Winkler, M.; Romain, C.; Meier, M. A. R.; Williams, C. K. *Green Chem.* **2015** DOI:10.1039/C4GC01353K.
36. Romain, C.; Heinrich, B.; Laponnaz, S. B.; Dagorne, S. *Chem. Commun.* **2012**, *48*, 2213–2215.
37. Guerin, W.; Helou, M.; Carpentier, J.-F.; Slawinski, M.; Brusson, J.-M.; Guillaume, S. M. *Polym. Chem.* **2013**, *4*, 1095–1106.
38. Guerin, W.; Helou, M.; Slawinski, M.; Brusson, J.-M.; Guillaume, S. M.; Carpentier, J.-F. *Polym. Chem.* **2013**, *4*, 3686–3693.
39. Wu, G.-P.; Darensbourg, D. J.; Lu, X.-B. *J. Am. Chem. Soc.* **2012**, *134*, 17739–17745.
40. Romain, C.; Williams, C. K. *Angew. Chem., Int. Ed.* **2014**, *53*, 1607–1610.
41. Darensbourg, D. J.; Wu, G.-P. *Angew. Chem., Int. Ed.* **2013**, *52*, 10602–10606.
42. Helou, M.; Moriceau, G.; Huang, Z. W.; Cammas-Marion, S.; Guillaume, S. M. *Polym. Chem.* **2011**, *2*, 840–850.
43. Kember, M. R.; Copley, J.; Buchard, A.; Williams, C. K. *Polym. Chem.* **2012**, *3*, 1196–1201.
44. Kember, M. R.; Knight, P. D.; Reung, P. T. R.; Williams, C. K. *Angew. Chem., Int. Ed.* **2009**, 931–933.
45. Kember, M. R.; White, A. J. P.; Williams, C. K. *Inorg. Chem.* **2009**, *48*, 9535–9542.
46. Jutz, F.; Buchard, A.; Kember, M. R.; Fredrickson, S. B.; Williams, C. K. *J. Am. Chem. Soc.* **2011**, *133*, 17395–17405.
47. Buchard, A.; Jutz, F.; Kember, M. R.; White, A. J. P.; Rzepa, H. S.; Williams, C. K. *Macromolecules* **2012**, *45*, 6781–6795.
48. Kember, M. R.; Williams, C. K. *J. Am. Chem. Soc.* **2012**, *134*, 15676–15679.
49. Saini, P. K.; Romain, C.; Williams, C. K. *Chem. Commun.* **2014**, *50*, 4164–4167.
50. Saini, P. K.; Romain, C.; Zhu, Y.; Williams, C. K. *Polym. Chem.* **2014**, *5*, 6068–6075.

Publication Date (Web): June 18, 2015 | doi: 10.1021/bk-2015-1192.ch009

Publication Date (Web): June 18, 2015 | doi: 10.1021/bk-2015-1192.ch010

Chapter 10

Aluminum Salen and Salan Polymerization Catalysts: From Monomer Scope to Macrostructure Control

J. P. MacDonald and M. P. Shaver*

Department of Chemistry, The University of Edinburgh, Joseph Black Building, David Brewster Road, Edinburgh, UK EH9 3FJ, United Kingdom
***E-mail: michael.shaver@ed.ac.uk. Tel +44 (0) 131 650 4726.**

Aluminum salen and salan complexes have been extensively employed as catalysts for the ring-opening polymerization of cyclic esters. The high tunability of the ligand framework has encouraged the systematic study of substituent effects on optimizing polymer and copolymer synthesis. Building on early work, designed catalysts are able to produce highly isotactic or heterotactic poly(lactic acid). The monomer scope has grown to include β-lactones, δ-valerolactone, lactide, (substituted) ε-caprolactones and macrolactones, with a significant level of control over molecular weight and dispersity (Đ). Polymer macrostructures have also been explored, often resulting in well-defined and predictable products. Macrostructures synthesized include random copolymers, AB diblock and ABA triblock copolymers and polymer stars. Polymer macrostructure control can tune properties not accessible through homopolymerization.

In Green Polymer Chemistry: Biobased Materials and Biocatalysis; Smith, et al.;
ACS Symposium Series; American Chemical Society: Washington, DC, 2015.

Introduction

Salan and Salen Ligands

The term "salen" originally referred solely to the unsubstituted ligand with an ethylene diimine bridge (N,N′-bis(salicylidene)-1,2-ethanediamine) but is now used for the entire class of tetradentate ligands with various alterations to the phenoxy rings and diimine bridges. Complexes with many transition metals have been synthesized and used for a variety of catalytic applications, particularly in heterocycle transformations, including manganese complexes for enantioselective olefin epoxidation (*1*, *2*), cobalt complexes for enantioselective ring opening of epoxides (*3*, *4*) and aluminum and chromium complexes for carbonylation of heterocycles (*5–7*).

Salan ligands are similar to salen ligands, combining two amine donors instead of imine donors in the backbone. The term was first introduced by Atwood to describe saturated salen compounds (*8*, *9*). Although there are fewer metal salan complexes exploited in polymerizations, many have been synthesized (*10–13*).

Ring-Opening Polymerization

The ring-opening polymerization (ROP) of cyclic esters is of continued interest as it allows for the synthesis of well-defined polymers that are inherently biodegradable and often sourced from renewable monomers. Early ROP systems were based on unsupported metal compounds such as $AlEt_3/H_2O$, $Al(O^iPr)_3$, ethylaluminoxane or $ZnEt_2/H_2O$ and β-butyrolactone (β-BL, Figure 1) (*14–16*).

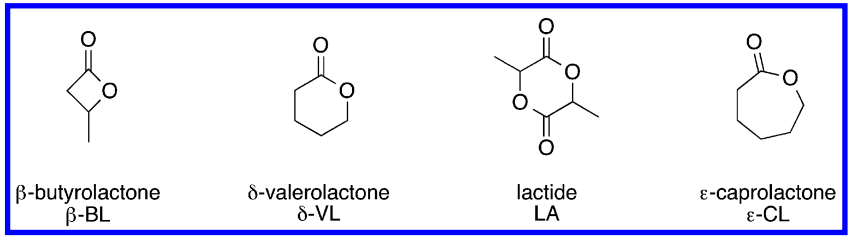

Figure 1. Monomers for ring-opening polymerization.

Novel catalysts were developed based on tin. Tin(II) 2-ethylhexanoate ($Sn(oct)_2$) was shown to be an extremely efficient catalyst for ROP of lactide, and remains the most common catalyst used today (*17*). $Sn(oct)_2$ allowed for the formation of high molecular weight (10^5 – 10^6 Daltons) poly(lactic acid). Reaction times were also short, reaching high conversion within minutes to a few hours. Unfortunately, high temperatures are often required (~ 140˚C) and the system results in either intra or intermolecular transesterification. In an effort to produce more controlled polymers by crowding the coordination sphere, metal complexes supported by chelating ligands have been studied extensively. Many different metals have been studied including tin, zinc (*18*, *19*), calcium (*20*), magnesium (*21*), lanthanides (*22*), group IV metals (*23*, *24*), indium (*25*) and aluminum.

In Green Polymer Chemistry: Biobased Materials and Biocatalysis; Smith, et al.;
ACS Symposium Series; American Chemical Society: Washington, DC, 2015.

Publication Date (Web): June 18, 2015 | doi: 10.1021/bk-2015-1192.ch010

Aluminum complexes have received particularly robust attention. Spassky reported an aluminum complex with a simple (*R*)-3,3-dimethyl-1,2-butanediol ligand in 1989 for the polymerization of *rac*-β-BL (**1**, Figure 2) (*26*). This complex was found to be quite slow under the investigated conditions (neat, 20˚C) reaching < 20% conversion after 18 days. N. Nomura reported an aluminum complex (**2**) with a salicylaldimine ligand, which was also found to be slow for β-BL polymerization with conversion reaching only 60% after 3 days at 70˚C (*27*). Efforts were made by K. Nomura to improve **2** by removing the *para*-methyl substituent and replacing the *ortho*-methyl subtituent with a bulkier *tert*-butyl group, while varying the aryl imino group. Unfortunately, this resulted in a decrease in activity, with low molecular weight oligomeric poly(3-hydroxybutyrate) being formed (*28*). Complex **3** was found to be the most active of the three, reaching high coversion with 0.5 mol% catalyst loading. The polymerization was found to be moderately controlled, with Đ = 1.25 and 1.22 for polymerizations conducted at 85 and 100˚C, respectively (*29*).

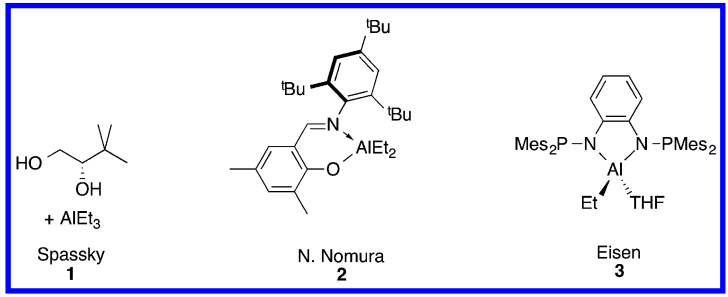

Figure 2. Early aluminum catalysts for the ring-opening polymerization of cyclic esters.

Aluminum Salen and Salan Catalysts in ROP

Catalyst Synthesis

Salan and salen ligands are both easily prepared from commercially available reagents. Salen ligands are prepared via imine condensation between two equivalents of 2-hydroxybenzaldehyde, or its substituted derivatives, and one equivalent of diamine (Scheme 1).

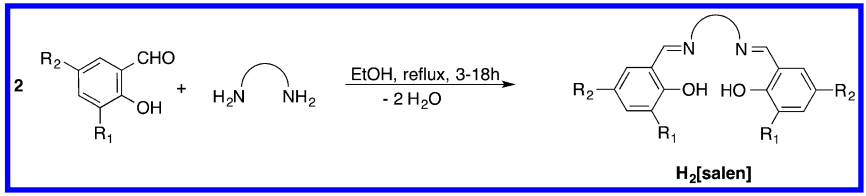

Scheme 1. General Synthesis of H_2[salen] Ligands

In Green Polymer Chemistry: Biobased Materials and Biocatalysis; Smith, et al.;
ACS Symposium Series; American Chemical Society: Washington, DC, 2015.

Publication Date (Web): June 18, 2015 | doi: 10.1021/bk-2015-1192.ch010

Similarly, salan ligands are typically prepared via reflux of two equivalents of a substituted phenol and one equivalent of diamine with an excess of paraformaldehyde (Scheme 2).

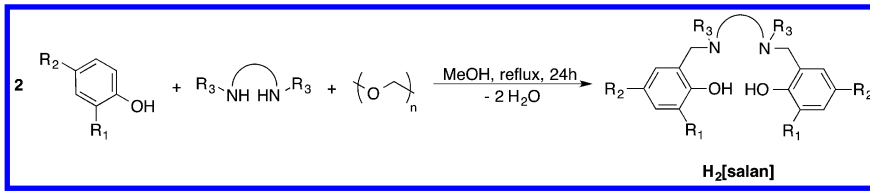

Scheme 2. General Synthesis of H_2[salan] Ligands

Publication Date (Web): June 18, 2015 | doi: 10.1021/bk-2015-1192.ch010

Catalyst precursors are then prepared by treating a solution of ligand in toluene with a slight excess of trialkylaluminum and heating, usually to 110˚C, for 18 hours (Scheme 3). Filtration and washing with cold hexane afford the desired complexes in good yields.

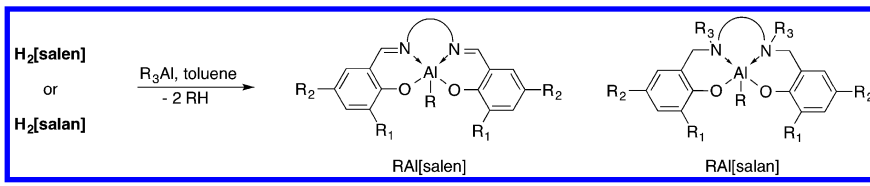

Scheme 3. General Synthesis of Aluminum Salen and Salen Complexes

Catalyst Tuning

The efficacy of the ligand and complex synthesis has permitted extensive catalyst tuning. Both the phenol substituents and the amine/imine bridge of the catalyst greatly affect the rate and level of control of a polymerization. The first ring-opening polymerization of a cyclic ester using an aluminum salen complex was reported by Spassky in 1991 (*30*). Complex **4** (Figure 3) was capable of polymerizing functional oxiranes and β-butyrolactone (β-BL). For the ROP of β-BL, only low molecular weight poly(3-hydroxybutyrate) (P(3HB)) was obtained. When **4** was later used as in the ROP of *rac*-lactide, it gave moderate control over the polymerization and gave slightly isotactic PLA ($P_m = 0.68$) (*31*). A subsequent report investigated a similar species with a methyl group on each of the imine carbons (**5**) (*32*). This resulted in a significant increase in polymerization rate, nearly three times faster than $Al(O^iPr)_3$ ($k_{app} = 374$ h^{-1} *vs.* 138 h^{-1}) (*33*).

Spassky followed up this early work with a chiral aluminum salen complex, *(R)*-**6**, with a *(R)*-1,1′-binapthyl diimine bridge (*34*). A chiral backbone was chosen to determine if this would lead to preferential insertion of one lactide

In Green Polymer Chemistry: Biobased Materials and Biocatalysis; Smith, et al.;
ACS Symposium Series; American Chemical Society: Washington, DC, 2015.

enantiomer over the other, an observed phenomenon in epoxide polymerization. The chiral catalyst, *(R)*-**6**, led to the preferential insertion of one lactide enantiomer over the other, promoting a stereoselective polymerization. Interestingly, the chiral complex, *(R)*-**6**, is more active than **4**, despite preferentially inserting d-lactide. The resulting polymer was characterized by differential scanning calorimetry (DSC) and showed a now characteristic increase in the melting temperature *vs.* P(l-LA) or P(d-LA)), a result of sterocomplex PLA formation. Coates produced syndiotactically enriched PLA from *meso*-lactide and *(R)*-**6** (*35*), the first such PLA tacticity, as confirmed by ^{1}H NMR experiments (*36*). Coates also explored the racemic derivative, *rac*-**6**, which produced stereoblock PLA chains forming with an average of 11 lactide monomer insertions per stereoblock (*37*). This was proposed to occur via living polymer chain exchange between metal centers (*38*).

Gibson and coworkers synthesized a 5-chloro salen derivative, **7**, in an attempt to increase catalyst activity (*39*). **7** was found to polymerize *rac*-lactide and l-lactide at room temperature. While the complex showed slight improvement over **4**, conversion only reached 25% after 24 hours in dichloromethane. Even though polymerization occurred relatively slowly, the reaction was living with predictable molecular weights and low dispersities. Polymerization reached 70 and 83% conversion for *rac*-lactide and l-lactide, respectively.

In 2002, Feijen developed an aluminum salen complex with bulky *tert*-butyl groups in the 3 and 5 positions of the phenoxy ring and a cyclohexyl bridge (Jacobsen ligand) in both racemic (*rac*-***v***) and enantiopure forms (*(R)*-**8**) (*40*). This work correlated well with previous results and demonstrated that the bulky *tert*-butyl groups gave polymers with significantly higher isospecificity than previously observed (P_m = 0.92 for *(R)*-**8**, 0.93 for *rac*-**8**). However, contrasting to what was observed with previous catalysts, *(R)*-**8** demonstrated preference for L-lactide over D-lactide ($k_l/k_d \approx 14$) (*41*).

Isoselectivity using achiral aluminum salen complexes was further demonstrated by Nomura (*42*) and Chen (*43*, *44*). Isoselectivity was improved by either using a more flexible diimine bridge or addition of steric bulk in the *ortho*-phenoxy positions. The Gibson group published a detailed study on tuning aluminum salen catalysts featuring many new complexes as well as a reinvestigation of previous catalysts (Table 1) (*45*).

Aluminum salan complexes have not received the same level of attention as their aluminum salen analogues. The first reported ROP of a cyclic ester with an aluminum salan complex was by Gibson in 2004 (*46*). Eight salan-type initiators were investigated with varying substitution (**37** – **44**, Figure 4). It was found that all of the complexes yielded PLA with predictable molecular weight and low dispersites (< 1.1). Polymerization rates trended H > Cl > Me > *tert*-butyl for phenoxy substitution with methylamino complexes more active than benzyl derivatives. Complexes **37**, **39** and **40** favored isotactic enriched PLA while the remaining complexes gave heterotactic enriched PLA. The two chloro-substituted complexes, **43** and **44**, gave the highest level of heterotacticity with P_r = 0.96 and 0.88, respectively.

Publication Date (Web): June 18, 2015 | doi: 10.1021/bk-2015-1192.ch010

Publication Date (Web): June 18, 2015 | doi: 10.1021/bk-2015-1192.ch010

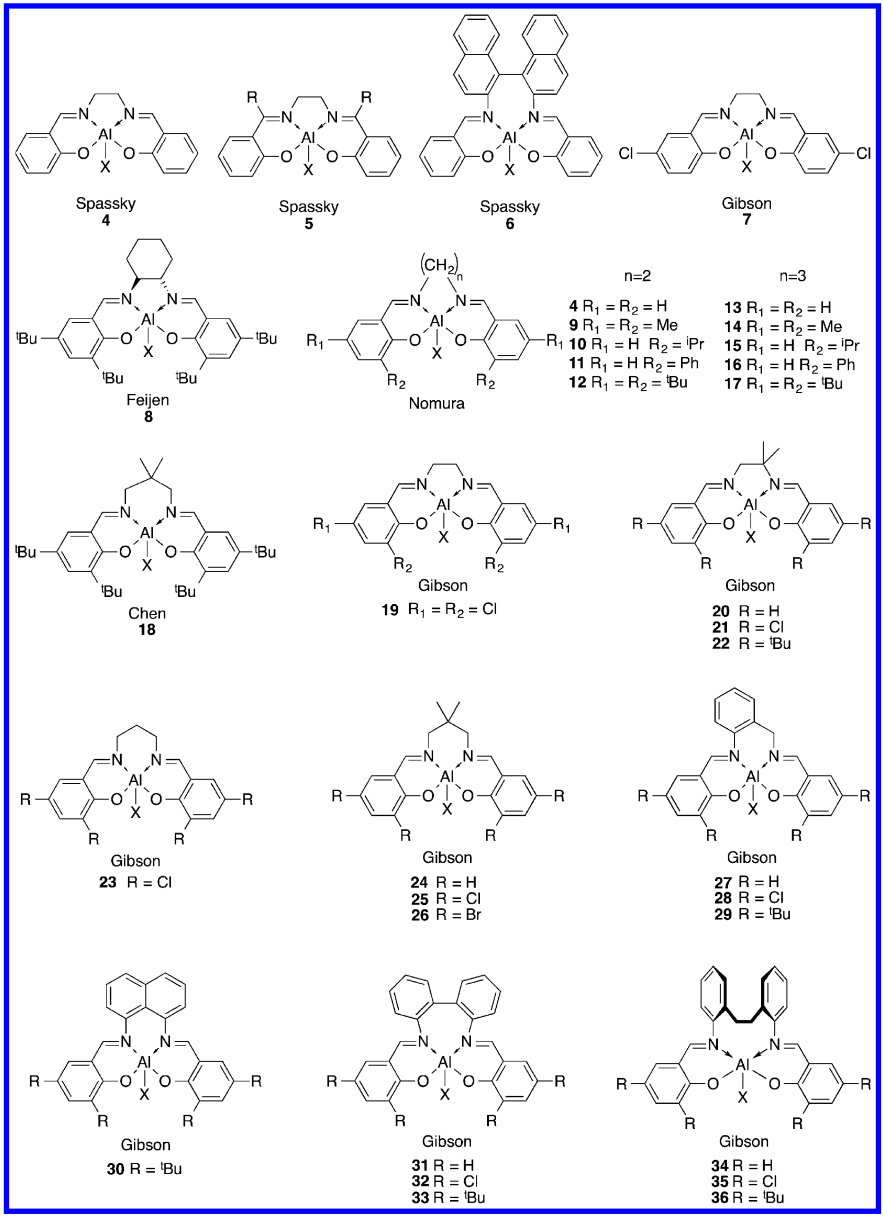

Figure 3. Aluminum salen complexes for ring-opening polymerization.

In Green Polymer Chemistry: Biobased Materials and Biocatalysis; Smith, et al.;
ACS Symposium Series; American Chemical Society: Washington, DC, 2015.

Table 1. – *Rac*-Lactide Polymerization with Aluminum Salen Complexes[a]

[Al]	M_n	*Đ*	P_m	k_{app}[b]	*[Al]*	M_n	*Đ*	P_m	k_{app}
4	4390	1.76	0.68	59	**18**	7430	1.20	0.85	159
7	4290	1.43	0.70	103	**26**	8140	1.19	0.64	3609
19	7130	1.58	0.56	181	**27**	7570	1.40	0.68	928
12	5900	1.27	0.83	1	**28**	9320	1.13	0.63	4380
20	8220	1.34	0.68	49	**29**	7920	1.08	0.86	84
21	7540	1.38	0.60	292	**30**	10780	1.14	0.72	784
22	7250	1.31	0.77	1	**31**	7350	1.23	0.50	1.23
13	6560	1.40	0.75	661	**32**	3500	1.33	0.37	8
23	9700	1.08	0.60	1009	**33**	6560	1.26	0.63	1
17	9590	1.07	0.88	133	**34**	7350	1.23	0.50	86
24	6190	1.35	0.63	1073	**35**	8950	1.24	0.60	85
25	7470	1.37	0.59	6420	**36**	8100	1.20	0.55	3

[a] *Rac*-lactide polymerization in toluene at 50°C with $[Al]_0:[M]_0 = 50:1$. $M_{n,th} = 7200$. [b] $k_{app} \times 10^{-6}$ s^{-1}. Note: Different concentrations used in different studies make it difficult to directly compare with these findings.

Feijen developed a series of aluminum salan complexes with a cyclohexyl diamine bridge, with both racemic and (*R,R*) analogues (*47*). Racemic and enantiopure complexes with either no phenoxy substitution or methyl phenoxy substitution gave isotactic enriched PLA but with only moderate isoselectivity (P_m up to 0.66), while chloro phenoxy substitution yielded heterotactic biased PLA (P_r up to 0.73). These selectivites were lower than previously reported salan and salen complexes. They were also the first salan complexes tested in *meso*-lactide polymerization, giving syndiotactically enriched PLA ($P_r = 0.70$).

Fulton reported the synthesis of a piperazine bridged salan complex (**48**) (*48*). The study focussed on the nature of the metal complex as well as the initiating X group. It was found that the nature of X had minimal impact on polymer conversion (ε-caprolactone: 0 - 47%; lactide: 0%). Fulton also found that bimetallic species of the type $[salan]Al_2X_4$ were more active than the corresponding monometallic species. This was explored in more detail by Wang and coworkers (*49*) Using the aluminum-alkyl complexes, ε-caprolactone was polymerized to high conversion with broad dispersities, from 1.8 – 2.1. Using benzyl alcohol as an initiator with the bimetallic complexes gave increased control. Polymerizations still reached high conversions, even at high monomer loading, with dispersities as low as 1.19. Yao and coworkers continued with complex **48**, with 5-methyl phenoxy substitution replacing 5-*tert*-butyl substitution (**49**), which yielded similar results (*50*). Jones and coworkers modified the diamine bridge to a homopiperazine (**50** – **54**) resulting in higher activity, facilitating polymerization of ε-caprolactone, δ-valerolactone and *rac*-lactide (*51*).

In Green Polymer Chemistry: Biobased Materials and Biocatalysis; Smith, et al.;
ACS Symposium Series; American Chemical Society: Washington, DC, 2015.

Publication Date (Web): June 18, 2015 | doi: 10.1021/bk-2015-1192.ch010

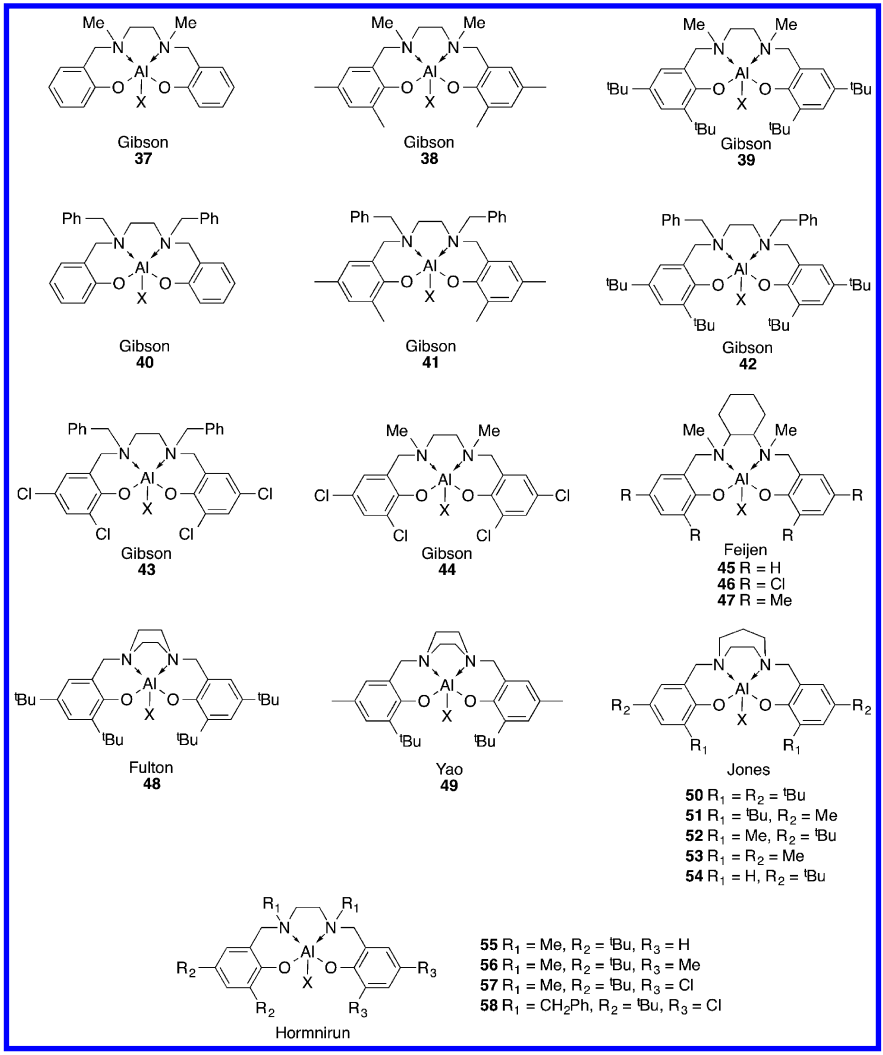

Figure 4. Aluminum salan complexes for ring-opening polymerization.

Hormnirun reported a series of asymmetrically substituted aluminum salan complexes for ROP of *rac*-lactide (**55** - **58**) (*52*). Polymerizations showed excellent control over molecular weight and dispersity, giving heterotactically enriched PLA with P_r = 0.64 – 0.74. As expected, chloro-phenoxy substitution gave PLA with higher P_r values and methylamino diamine bridged complexes decreased heterotacticity. Our group has also contributed to the development of novel aluminum salen and salan complexes that show increased activity and/or increased levels of microstructure control. Our first report involved the synthesis of aluminum salan and salen complexes with a bulky *ortho*-adamantyl phenoxy ligand framework (**59**, **60**, Figure 5). We hypothesized that the increased bulk would improve isoselectivity.

Publication Date (Web): June 18, 2015 | doi: 10.1021/bk-2015-1192.ch010

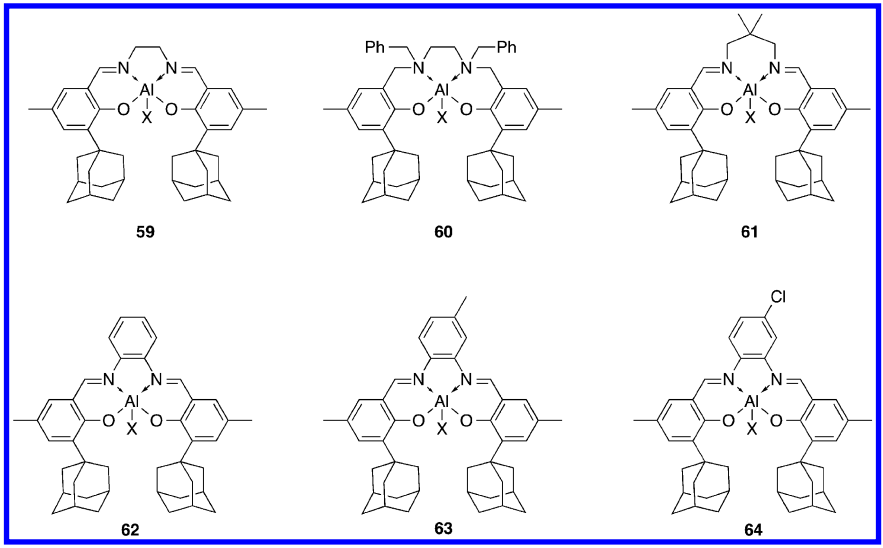

Figure 5. Adamantyl-substituted aluminum salen and salan complexes.

Aluminum salen compound **59** produced highly isotactic PLA from *rac*-lactide, with P_m = 0.89 (Table 2). The catalyst was found to be robust, as no decrease in isoselectivity as monomer concentration was increased (up to 1000 eq.) or under immortal polymerization conditions (10 eq. chain exchange alcohol).

Table 2. – Living vs Immortal Polymerization of Rac-Lactide

Catalyst	$[LA]_0:[Al]_0:[ROH]_0$	*Type*	M_n	$Đ$	P_m
17	50:1:1	living	9590	1.07	0.88
	1000:1:10	immortal	17900	1.06	0.86
59	100:1:1	living	6100	1.07	0.88
	1000:1:10	immortal	4800	1.07	0.88

The bulky aluminum salan derivative did not yield significant PLA (≤ 5% conversion) under similar conditions – living or immortal, nor did the rigid phenyl bridged compounds. Under immortal conditions, **43** was found to still produce heterotactic enriched PLA.

In Green Polymer Chemistry: Biobased Materials and Biocatalysis; Smith, et al.;
ACS Symposium Series; American Chemical Society: Washington, DC, 2015.

Publication Date (Web): June 18, 2015 | doi: 10.1021/bk-2015-1192.ch010

Monomer Scope

While the coordination chemistry efforts in developing aluminum salan and aluminum salen complexes for ring-opening polymerization is extensive, there has been less effort on expanding the monomer scope and applicability of these catalysts. Most complexes have been tested only in the ROP of lactide and ε-caprolactone.

Poly(3-hydoxyalkanoate)s (PHAs) are an important class of aliphatic polyesters that can be produced either by microorganisms or designer catalysts. Producing PHAs from Lewis acidic catalysts has been of interest for several decades as it allows for the formation of (co)polymers and different tactic microstructures not easily accessible by microorganisms (*53*, *54*). As discussed previously, the first aluminum salen ROP catalyst, **4**, had shown poor activity in *rac*-β-BL polymerization (*55*). However, β-BL polymerization was not explored for many of the subsequent salen complexes.

Our group has demonstrated that **17**, previously reported by Nomura, and **43**, previously reported by Gibson, are amongst the most efficient catalysts for the ROP of *rac*-β-BL (*56*). The polymerization was robust, running under a variety of temperatures and reaction conditions without significant loss of control. Aluminum salen complex **17** was able to polymerize up to 500 equivalents of *rac*-β-BL reaching high conversion. Molecular weights were in good agreement with theoretical values and Đs were quite low (1.06 - 1.14). Using the bulkier aluminum salen complex, **59,** P(3-HB) was produced with better control (Đ ≤1.05) but rates were significantly slower. The aluminum salan complex **43** was found to be more controlled than **17** and **59** (Đ = 1.03 – 1.05). P(3-HB) could be produced in bulk or in solution (toluene or THF) with temperatures ranging from 25 – 120˚C, while little change polymer properties is observed. It should be noted that the bulky aluminum salan complex **60** showed no activity for *rac*-β-BL polymerization under similar conditions. *Rac*-β-BL polymerziation also operated under immortal conditions with catalysts **17** or **43** , even with extremely high amounts of chain transfer agent: $[\beta\text{-BL}]_0:[\text{Al}]_0:[\text{ROH}]_0 = 1000:1:50$. Our subsequent report on *ortho*-adamantyl substituted complexes also investigated *rac*-β-BL polymerization with a particular focus on polymerization kinetics (*57*). Polymerization of *rac*-β-BL with phenylene bridged complexes **62** – **64** as well as isopentyl bridged complex **61** were not good catalysts for β-BL polymerization (Đ = 1.37 – 2.21). The more rigid phenylene-bridged complexes were significantly slower (k_{app} = 1.5, 2.1 and 1.0 $\times 10^{-6}$ s^{-1} for **62**, **63** and **64**, respectively) than the alkyl substituted complexes (k_{app} = 33.5 and 28.7 $\times 10^{-6}$ s^{-1} for **59** and **61**, respectively).

Beyond β-BL, many other β-lactones are accessible, and of significant interest in homo and copolymerizations, including β-valerolactone (β-VL), β-heptanolactone (β-HL) and β-tridecalactone (β-TDL), as shown in Figure 6. Salen complex **17** and salan complex **43** are very good catalysts for these monomers, the second report of homopolymerization of β-VL and the first for β-HL and β-TDL for any catalyst, not just aluminum (*58*).

In Green Polymer Chemistry: Biobased Materials and Biocatalysis; Smith, et al.;
ACS Symposium Series; American Chemical Society: Washington, DC, 2015.

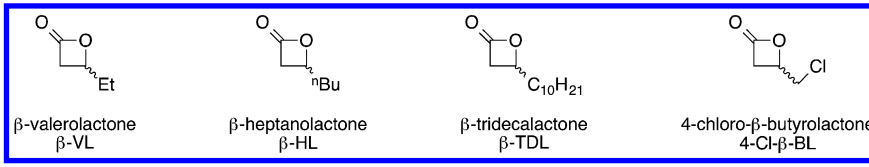

Figure 6. Structure of substituted β-lactones.

Homopolymerizations of these alkyl substituted β-lactones was living and molecular weights were also in good agreement with theoretical values. As expected, as the length of the alkyl chain increases, the rate of polymerization decreases (k_{app} = 0.0065 min^{-1} (β-VL), 0.0040 min^{-1} (β-HL) and 0.0017 min^{-1} (β-TDL), Figure 7). The polymers were found to be amorphous , as expected for an atactic PHA, with decreasing T_g as alkyl chain increased. The T_g of β-BL, β-VL and β-HL are 5 (*59*), -19.8 and -30.8˚C, respectively; decreasing long alkyl chains cause disruption in the ordering of polymer chains. Changing the catalyst to **43** yielded polymerizations with similar molecular weight, dispersity and rate. Contrary to β-BL polymerization with **43**, no activity was observed at room temperature.

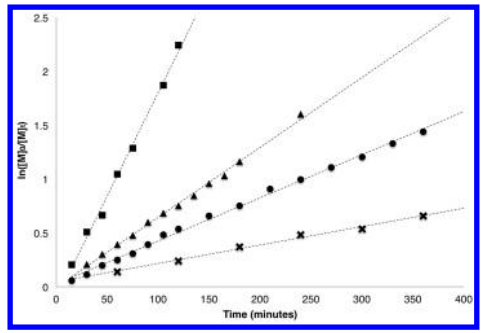

Figure 7. Kinetic plot of β-lactone homopolymerization (▪ = β-BL (0.0194 min^{-1}), •=β-VL (0.0065 min^{-1}), ▲=β-HL (0.0040 min^{-1}), ×=β-TDL (0.0017 min^{-1})).

In an unpublished contribution, we have shown that **17** and **43** are able to polymerize 4-chloro-β-butyrolactone (*60*). Polymerizations conducted at 120˚C were uncontrolled for **17** (85% conversion, M_n = 4340, $M_{n,th}$ = 10350, Đ = 1.73) and controlled for **43** (>99% conversion, M_n = 10030, $M_{n,th}$ = 12150, Đ = 1.17) while polymerizaions at 85˚C were extremely well controlled for both catalysts, albeit with 7 h reaction times (69% conversion, M_n = 6890, $M_{n,th}$ = 8220, Đ = 1.03 for **17**, >99% conversion, M_n = 11900, $M_{n,th}$ = 12150, Đ = 1.03 for **43**). Propagation even occurred at 25˚C with **43**, requiring 14 days to reach complete conversion (Đ = 1.02; k_{app} = 0.012 h^{-1}).

δ-Valerolactone (δ-VL) polymerization is a more challenging monomer than β-BL, lactide or ε-caprolactone due to the reduced level of ring strain. Despite this, there have been many catalysts capable of forming poly(δ-valerolactone) through ROP. Although there have been reports of species similar to aluminum

In Green Polymer Chemistry: Biobased Materials and Biocatalysis; Smith, et al.;
ACS Symposium Series; American Chemical Society: Washington, DC, 2015.

Publication Date (Web): June 18, 2015 | doi: 10.1021/bk-2015-1192.ch010

salen complexes facilitating polymerization (aluminum half-salen complexes), only a few of the previously mentioned reports include δ-VL polymerization (*61*). Jones and coworkers have investigated the ROP of δ-VL using complexes **51** – **54**. Polymerizations were found to be relatively uncontrolled (Đ = 1.77, 1.12, 1.54, 1.50 and 1.25 using **50**, **51**, **52**, **53** and **54**, respectively) (*51*). While control was observed when using **51**, only low conversion (*ca*. 30%) was obtained. Cao demonstrated that aluminum salen complex **65** could also polymerize δ-VL reaching moderate conversion with relatively high dispersities (1.6 - 2.1) (*62*).

Cao published one of the first ε-CL polymerizations with salen complex **65** (and its dimer) showing high activity, although Dispersities were relatively high (1.21 – 1.65) (*62*). The homopiperazine-bridged salan complexes also polymerize ε-CL with only **51** offering any control (Đ = 1.15), albeit at low conversion.

Our group has found **17** and **43** are both able to efficiently polymerize ε-CL (*60*). Polymerization at 120˚C was uncontrolled for both catalysts (Đ = 1.33 – 1.58). Polymerizations at 85˚C showed better control, paying close attention to reaction time. Polymerization reached complete conversion after 5 minutes (M_n = 10630, $M_{n,th}$ =11520, Đ = 1.33 for **17**, M_n = 8940, $M_{n,th}$ = 11520, Đ = 1.14 for **43**). Increasing the reaction time with **43** showed an increase in Đ to 1.34, indicating transesterification was likely occurring. Polymerizations were also conducted at 25˚C, yielded even more controlled poly(ε-caprolactone) (M_n = 9780, $M_{n,th}$ =11520, Đ = 1.15, k_{app} = 0.3605 min^{-1} for **17**, M_n = 8870, $M_{n,th}$ = 11520, Đ = 1.05, k_{app} = 0.0901 min^{-1} for **43**).

Feijen further demonstrated the flexibility of (*R,R*)-**8**, reporting the polymerization of ε-CL as well as two methyl-substituted derivatives (Figure 8), 4-methyl-ε-caprolactone (4-Me-ε-CL) and 6-methyl-ε-caprolactone (6-Me-ε-CL) (*63*). Polymerization of ε-CL with (*R,R*)-**8** reached 96% conversion after 2.5 hours at 90˚C with moderate dispersity control (1.21), however molecular weights were two times higher than predicted. 4-Me-ε-CL polymerization required longer reaction times of 6 and 27 hours at 90 and 70˚C, respectively, to reach high conversion. Similarly, P(4-Me-ε-CL) molecular weights were twice as high as predicted and Đs broadened to 1.25 – 1.28. Interestingly, 6-Me-ε-CL resulted in a much more controlled polymerization with Đ= 1.04 at 90˚C. With a methyl group in closer proximity to the site of ring-opening, reaction time was increased significantly to 336 hours to reach 96% conversion. Polymerization of 6-Me-ε-CL was also performed in bulk, reaching 91% conversion after 530 hours. While the dispersity increased to 1.39, molecular weights were well controlled.

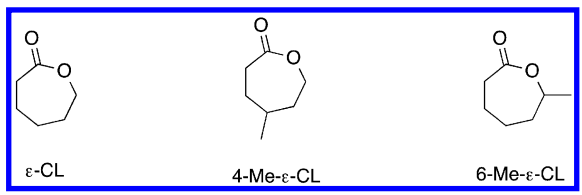

Figure 8. Structure of ε-caprolactone (ε-CL), 4-methyl-ε-caprolactone (4-Me-ε-CL) and 6-methyl-ε-caprolactone (6-Me-ε-CL).

In Green Polymer Chemistry: Biobased Materials and Biocatalysis; Smith, et al.;
ACS Symposium Series; American Chemical Society: Washington, DC, 2015.

Publication Date (Web): June 18, 2015 | doi: 10.1021/bk-2015-1192.ch010

Macrolactones are of interest in ROP as the longer uninterrupted ethylene chains with regular ester linkages could potentially serve as biodegradable alternatives to polyethylene. While there is very limited work on ROP of macrolactones with aluminum complexes, Duchateau has demonstrated its promise (*64*), using **4** and **13** to polymerize macrolactones decalactone (DL), undecalactone (UDL), pentadecalactone (PDL) and hexadecalactone (HDL), as shown in Figure 9.

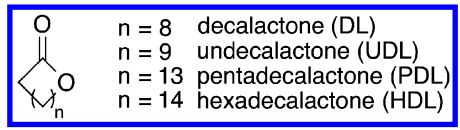

Figure 9. Macrolactones used in ring-opening polmerization.

Polymerizations proceeded to high conversion (84 - 98%) with relatively broad dispersities (1.6 – 1.8) and molecular weights slightly higher than theoretical values. As expected, polymerizations were slower for macrolactones (k_{app} = 0.01 – 0.04 min^{-1}) than for smaller lactones such as ε-CL (k_{app} = 0.25 min^{-1}). The bulkier complex **13** was slower with lower conversion (87%) than when using **4** (99%) under similar conditions. A subsequent report investigated several other salen complexes as well as copolymers of PDL with ε-CL (*65*). All aluminum salen complexes tested (Figure 10) were capable of PDL polymerization to high conversion after 24 hours at 100˚C (83 – 99%).

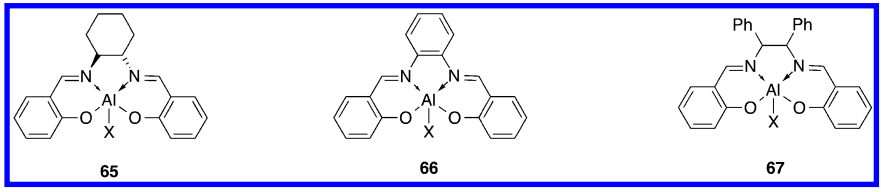

Figure 10. Aluminum salen complexes for macrolactone polymerization.

Macrostructure Control

We have to this point focused on polymerization of a single monomer to form a linear homopolymer. Different polymer macrostructures, however, have also been explored to achieve properties not accessible with these simple homopolymers. Aluminum salen and salan complexes have been shown to be powerful catalysts for both microstructure and macrostructure control.

In Green Polymer Chemistry: Biobased Materials and Biocatalysis; Smith, et al.;
ACS Symposium Series; American Chemical Society: Washington, DC, 2015.

Publication Date (Web): June 18, 2015 | doi: 10.1021/bk-2015-1192.ch010

Publication Date (Web): June 18, 2015 | doi: 10.1021/bk-2015-1192.ch010

Block copolymers have been of interest to polymer chemists for decades. In ring-opening polymerization, early block copolymers were synthesized from lactide and β-BL using tin complexes (*66*). More recently, the aluminum salen and salan complexes at the focus of this chapter have proven to be particularly good catalysts for controlled copolymerization.

Our group reported the synthesis of AB block copolymers of poly(ethylene glycol) (PEG) and PLA with a particular focus on the impact of PLA tacticity (*67*). A monomethoxy-PEG (mPEG) macroinitiator with aluminum salen **17** or **59** and aluminum salan **43** were used to make PEG-*b*-PLA with isotactic or heterotactic enriched PLA blocks, respectively. The copolymers were found to form micelles and their micellar stability was studied. Polymer molecular weights were in excellent agreement with the theoretical values and dispersities were low (1.1 – 1.2). Copolymers containing atactic (prepared using tin(II) 2-ethylhexanoate) or heterotactic enriched PLA blocks had lower micellar stability than the ones with isotactic enriched PLA. Atactic and heterotactic block copolymers also showed a faster degradation and shorter erosion times. This is consistent with PLA homopolymers, with the more crystalline isotactic PLA having longer degradation times than heterotactic or atactic PLA. Thus, PEG-*b*-PLA properties can be tuned using aluminum salen and aluminum salan complexes to yield polymers with targeted thermal and self-assembly properties.

Cui, Chen and coworkers have also reported block copolymers of PEG/PLA (*68*). They exploited the cataylsts ability to undergo chain exchange between metal centers while using **18** and **43** as catalysts to generate heterotacic-isotactic stereoblock PLA segment(s). AB and ABA block copolymers were generated from PEG and mPEG macroinitiators, respectively, yielding well-defined polymers.

Duchateau has synthesized AB block copolymers, using two different approaches (*65*). The first was a one-pot reaction, relying on the relative rates of polymerization to generate an AB block-like copolymer. Although not true AB diblock, it was hypothesized that it could have similar properties. Copolymers of PDL and ε-CL were synthesized in this manner but it was found that as the polymerization proceeded, the block-like nature of the polymer decreased as a result of transesterification. To avoid this, a sequential addition of monomer was used to generate AB block copolymer PPDL-*b*-PCL. Polymerization was continued until full conversion of PDL was achieved. At this point, ε-CL was introduced and the reaction continued. A systematic approach to varying ε-CL polymerization times confirmed that longer reaction times correlated with increased transesterification, until a fully random polymer is formed after 1 hour. This could be controlled by quenching the polymerization as soon as ε-CL has reached full conversion. Characterization of the block copolymer showed two distinct melting temperatures, one for each monomer, while the random copolymer resulted in a single averaged melting temperature.

In Green Polymer Chemistry: Biobased Materials and Biocatalysis; Smith, et al.;
ACS Symposium Series; American Chemical Society: Washington, DC, 2015.

Jones has synthesized triblock copolymers using ε-CL, δ-VL and *rac*-lactide using salan complexes **50**-**52** by sequential addition of monomers (*51*). Polymer dispersites were relatively broad (1.63 – 1.77) but monomer conversion high, although no further study on randomization was reported.

We recently synthesized ABA triblock copolymers of an isotactic P(L-LA) A block and poly(3-hydroxyalkanoate) B block using **17** as a catalyst. β-Butyrolactone, β-valerolactone and β-heptanolactone were used to prepare the PHA middle block. Copolymers were prepared by sequential addition of monomers to create a series of P(L-LA$_n$-*b*-HA$_m$-*b*-L-LA$_n$), where the ratio of n to m and nature of PHA block were investigated. This was the first report of using an aluminum salen complex to generate block copolymers containing PLA and PHA. It was found that polymers could be generated with careful attention to polymerization temperature, with low Đ (< 1.2) and predictable molecular weights. The thermal properties were also investigated by differential scanning calorimetry (DSC). DSC analysis revealed that ABA copolymers prepared using β-BL or β-VL resulted in tunable thermal properties based on the P(L-LA):P(3-HA) ratio. However, when copolymers were prepared from β-HL, samples were found to either show a single glass transition temperature (independent of polymer ratios) or two distinct glass transition temperatures. This is characteristic of a phase separated material, which was further supported by small angle X-ray scattering data.

Publication Date (Web): June 18, 2015 | doi: 10.1021/bk-2015-1192.ch010

End Group Control

Aluminum salen complexes are tolerant to a variety of initiating groups, as discussed previously (*48*). Fulton demonstrated that changing the nature of the initiating group between methoxide, ethoxide, isopropoxide, *tert*-butoxide and triflate had relatively little effect on the polymerization. This has been shown to be beneficial when using more functionally diverse end groups for post polymerization reactions. Dove has further demonstrated the diverse nature of initiating groups, as well as terminating groups, that can be used with aluminum salen and salan complexes to prepare dual-functionalized polymer chains (*69*). Four initiating groups (isopropanol, 1,3-propanediol, 1,1,1-tris(hydroxymethyl)ethane and dipentaerythritol) and 12 terminating agents (methanol, acetyl chloride, hexanoyl chloride, benzoyl chloride, isonicotinyl chloride, anthranocyl chloride, isobutyroyl chloride, pivaloyl chloride, hexynoyl chloride, maleimide acid chloride and Me-PEG-COCl) were found to be successful. Terminating agents had no discernable effect on the polymer molecular weight and dispersity. All initiating groups yielded well controlled polymers with predictable molecular weights. Dove has also shown that by using an alcohol functionalized maleimide would still allow for a very controlled polymerization of *rac*-lactide with **17**, **23** or **43** (*70*). Post-polymerization end group functionalization was also performed to yield α-ω-maleimido functionalized stereoregular PLA. This allowed for formation of well-defined cyclic PLA polymers through thiol Michael-additions (Scheme 4). Our group has also

exploited the functional group tolerance in initiating groups with aluminum salen and salan complexes (*71*). Building from a hexyne functionalized initiator (5-hexyn-1-ol), well-defined polymers from *rac*-lactide, L-lactide and β-BL were synthesized using **17** and later used in click chemistry.

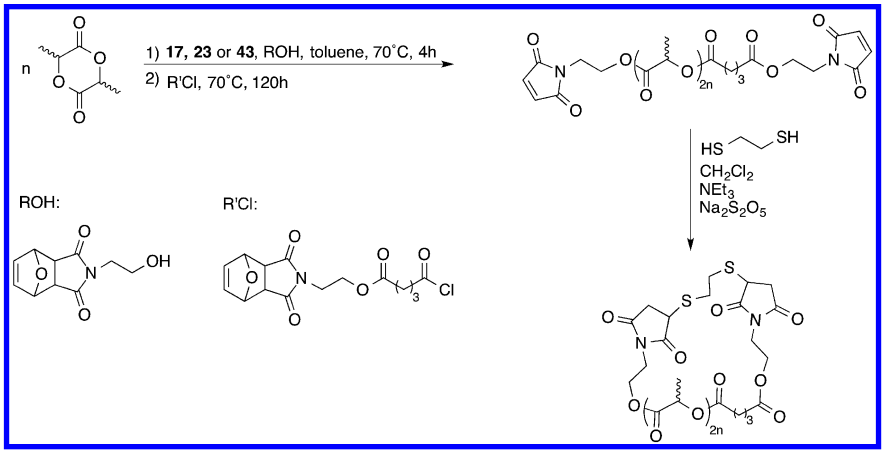

Scheme 4. Synthesis of Cyclic PLA Using "Thiol-ene" Click Chemistry

Cui, Chen and coworkers have employed a fluorescent initiator for *rac*-lactide polymerization. Using **18** under living and immortal conditions gave isotactically enriched PLA with a fluorescent endgroup (*72*). They have also used a mixed aluminium salen (**18**) and salan (**43**) to target the level of selevtivity, resulting in either crystalline or amorphous PLA (*68*).

Polymer Stars

Polymer stars of aliphatic polyesters offer many properties not accessible in linear polymers, particularly due to their higher concentration of end-groups, tuning rheological, biomedical and mechanical properties (*73*).

Early work in using aluminum salen and aluminum salan complexes was carried out by Dove (*69*). This involved the synthesis of well-defined PLA using aluminum salen complexes **17** and **23** as well as aluminum salan complex **43** to introduce α,ω-functionality by a modification of procedures developed by Jérôme (*74*). While different different alcohols were used as initiators to generate linear polymers, dipentaerythritol (DPE) was used to generate a six-arm polymer star. These polymer stars were characterized by NMR and GPC, revealing the polymerizations were very well controlled with various end group functionality possible. Molecular weight was in good agreement with theoretical molecular weights, with correspondingly low dispersites of 1.04 – 1.12.

In Green Polymer Chemistry: Biobased Materials and Biocatalysis; Smith, et al.;
ACS Symposium Series; American Chemical Society: Washington, DC, 2015.

Publication Date (Web): June 18, 2015 | doi: 10.1021/bk-2015-1192.ch010

Subsequent reports by our group investigated the affect of tacticity on the thermal properties and hydrolytic degradation of polymer stars with a DPE core (Figure 11) (*75*, *76*). It was found that there was a significant increase in T_g and T_m as the amount of isotacticity bias increases. Polymer stars synthesized from *rac*-lactide showed higher T_m and T_ds than when purely isotactic samples were prepared from L-lactide indicating the potential for stereocomplexation. The impact of tacticity was also observed in hydrolytic degradation, with isotactic polymer stars having increased degradation times. The number of errors, and thus the isotacticity bias, gave control over degradation times, correlating with the semicrystallinity of the samples as measured by p-XRD. Samples with a heterotactic bias were found to be more thermally stable, but only marginally more hydrolytically stable, compared to atactic samples.

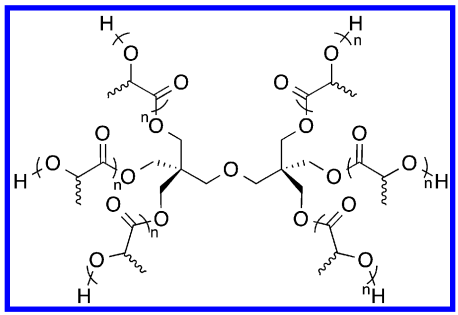

Figure 11. Poly(lactic acid) star polymer with a dipentaerythritol core.

Our group have also generated polymer stars with a modified β-cyclodextrin (β-CD) cores with *rac*-β-BL, *rac*-lactide, L-lactide and *rac*-lactide/glycolide arms (*71*). Synthesis of the polymer stars using the hydroxyl groups of the heptakis(2,6-di-O-methyl)-β-CD as the initiator (core first) led to polymerizations with poor yields, inconsistent initiation and molecular weights that were not in good correlation with theoretical values. However, by employing an arms first strategy, where alkyne terminated homopolymer was first synthesized, well-defined polymer stars with a β-CD core could be prepared. The alkyne-terminated polymers, built using the aforementioned 5-hexyn-1-ol initiator, were attached to an azide functionalized β-CD core via click chemistry. Homopolymers were synthesized with both tin(II) 2-ethylhexanoate and **17**, with only the aluminum catalyst offering good control. Polymer stars from *rac*-lactide with a ratio of 10 – 50 monomer units per arm were synthesized, yielding polymers with Đ = 1.03 – 1.15. Similarly, arms derived from β-BL or L-lactide were prepared, with similarly good control (β-BL: 10 – 50 monomers per arm, Đ = 1.01 – 1.14; L-Lactide: 10 – 50 monomers per arm, Đ = 1.01 – 1.05). The polymer stars with PLA arms were investigated for the controlled release of 7-methoxycoumarin (7-MC), monitored by fluorescence spectroscopy. Uncatalyzed hydrolytic degradation was very slow and 7-MC release diffusion controlled. However, enzymatic degradation occurred much quicker, suggesting potential future application of these stars in drug delivery.

In Green Polymer Chemistry: Biobased Materials and Biocatalysis; Smith, et al.;
ACS Symposium Series; American Chemical Society: Washington, DC, 2015.

Publication Date (Web): June 18, 2015 | doi: 10.1021/bk-2015-1192.ch010

Cui, Chen and coworkers have also used their mixed aluminium salen and salan system with triol initiator tri(2-hydroxyethyl)amine to generate three arm polymer stars (*68*). By varying the ratio of **18** and **43**, targeted tuning of the polymer properties was achieved. Using a higher ratio of **43** yielded PLA with a higher amount of heterotactic bias, resulting in an amorphous sample. Alternatively, using a higher ratio of **18** yielded a more crystalline sample.

Conclusion

Aluminum salen and aluminum salan complexes are excellent catalysts for the ring-opening polymerization of many different cyclic esters. Systematically changing the nature of the salen ligand framework offers control over the tacticity of polymers built from racemic monomers such as *rac*-lactide. Tuning of the ligand framework of aluminum salan catalysts also offers tacticity control, particularly in accessing highly heterotactic aliphatic polyesters. The aluminum salen and salan complexes open many different monomers, ranging from substituted β-propiolactones to macrolactones. The robust nature also allows for the synthesis of well-defined polymer structures under mild conditions including AB diblock and ABA triblock copolymers. Biodegradable polymers with tunable thermal properties, microphase separation and degradation can be targeted. Polymer stars have also been synthesized with a variety of cores, yielding polymer macrostuctures that are well controlled and have predictable molecular weights.

References

1. Zhang, W.; Loebach, J. L.; Wilson, S. R.; Jacobsen, E. N. *J. Am. Chem. Soc.* **1990**, *112*, 2801–2803.
2. Jacobsen, E. N.; Zhang, W.; Muci, A. R.; Ecker, J. R.; Deng, L. *J. Am. Chem. Soc.* **1991**, *113*, 7063–7064.
3. Martinez, L. E.; Leighton, J. L.; Carsten, D. H.; Jacobsen, E. N. *J. Am. Chem. Soc.* **1995**, *117*, 5897–5898.
4. Larrow, J. F.; Schaus, S. E.; Jacobsen, E. N. *J. Am. Chem. Soc.* **1996**, *118*, 7420–7421.
5. Church, T. L.; Getzler, Y. D. Y. L.; Byrne, C. M.; Coates, G. W. *Chem. Commun.* **2007**, 657–674.
6. Getzler, Y. D. Y. L.; Mahadevan, V.; Lobkovsky, E. B.; Coates, G. W. *J. Am. Chem. Soc.* **2002**, *124*, 1174–1175.
7. Kramer, J. W.; Lobkovsky, E. B.; Coates, G. W. *Org. Lett.* **2006**, *8*, 3709–3712.
8. Atwood, D. A.; Benson, J.; Jegier, J. A.; Lindholm, N. F.; Martin, K. J.; Pitura, R. J.; Rutherford, D. *Main Group Chem.* **1995**, *1*, 99–113.
9. Atwood, D. A. *Coord. Chem. Rev.* **1997**, *165*, 267–296.
10. Gu, X.; Zhang, Y.; Xu, Z.-J.; Che, C.-M. *Chem. Commun.* **2014**, *50*, 7870–7873.
11. Sergeeva, E.; Kopilov, J.; Goldberg, I.; Kol, M. *Chem. Commun.* **2009**, 3053–3055.

Publication Date (Web): June 18, 2015 | doi: 10.1021/bk-2015-1192.ch010

Publication Date (Web): June 18, 2015 | doi: 10.1021/bk-2015-1192.ch010

12. Rao, D.-Y.; Li, B.; Zhang, R.; Wang, H.; Lu, X.-B. *Inorg. Chem.* **2009**, *48*, 2830–2836.
13. Egami, H.; Katsuki, T. *Angew. Chem. Int. Ed.* **2008**, *47*, 5171–5174.
14. Gross, R. A.; Zhang, Y.; Konrad, G.; Lenz, R. W. *Macromolecules* **1988**, *21*, 2657–2668.
15. Teranishi, K.; Iida, M.; Araki, T.; Yamashita, S.; Tani, H. *Macromolecules* **1974**, *7*, 421–427.
16. Iida, M.; Araki, T.; Teranishi, K.; Tani, H. *Macromolecules* **1977**, *10*, 275–284.
17. Dechy-Cabaret, O.; Martin-Vaca, B.; Bourissou, D. *Chem. Rev.* **2004**, *104*, 6147–6176.
18. Rieth, L. R.; Moore, D. R.; Lobkovsky, E. B.; Coates, G. W. *J. Am. Chem. Soc.* **2002**, *124*, 15239–15248.
19. Guillaume, C.; Carpentier, J.-F.; Guillaume, S. M. *Polymer* **2009**, *50*, 5909–5917.
20. Poirier, V.; Roisnel, T.; Carpentier, J.-F.; Sarazin, Y. *Dalton Trans.* **2009**, 9820–9827.
21. Liu, Y.-C.; Lin, C.-H.; Ko, B.-T.; Ho, R.-M. *J. Polym. Sci. A Polym. Chem.* **2010**, *48*, 5339–5347.
22. Amgoune, A.; Thomas, C. M.; Ilinca, S.; Roisnel, T.; Carpentier, J.-F. *Angew. Chem. Int. Ed.* **2006**, *45*, 2782–2784.
23. Saha, T. K.; Rajashekhar, B.; Gowda, R. R.; Ramkumar, V.; Chakraborty, D. *Dalton Trans.* **2010**, *39*, 5091–5093.
24. Jeffery, B. J.; Whitelaw, E. L.; Garcia-Vivo, D.; Stewart, J. A.; Mahon, M. F.; Davidson, M. G.; Jones, M. D. *Chem. Commun.* **2011**, *47*, 12328–12330.
25. Xu, C.; Yu, I.; Mehrkhodavandi, P. *Chem. Commun.* **2012**, *48*, 6806–6808.
26. Le Borgne, A.; Spassky, N. *Polymer* **1989**, *30*, 2312–2319.
27. Nomura, N.; Aoyama, T.; Ishii, R.; Kondo, T. *Macromolecules* **2005**, *38*, 5363–5366.
28. Iwasa, N.; Fujiki, M.; Nomura, K. *J. Mol. Catal. A: Chem.* **2008**, *292*, 67–75.
29. Majoumo-Mbe, F.; Smolensky, E.; Lönnecke, P.; Shpasser, D.; Eisen, M. S.; Hey-Hawkins, E. *J. Mol. Catal. A: Chem.* **2005**, *240*, 91–98.
30. Vincens, V.; Le Borgne, A.; Spassky, N. *Makromol. Chem. Macromol. Symp.* **1991**, *47*, 285–291.
31. Wisniewski, M.; Borgne, A. L.; Spassky, N. *Macromol. Chem. Phys.* **1997**, *198*, 1227–1238.
32. Bhaw-Luximon, A.; Jhurry, D.; Spassky, N. *Polym. Bull. (Berlin)* **2000**, *44*, 31–38.
33. Dubois, P.; Jacobs, C.; Jerome, R.; Teyssie, P. *Macromolecules* **1991**, *24*, 2266–2270.
34. Spassky, N.; Wisniewski, M.; Pluta, C.; Le Borgne, A. *Macromol. Chem. Phys.* **1996**, *197*, 2627–2637.
35. Ovitt, T. M.; Coates, G. W. *J. Am. Chem. Soc.* **1999**, *121*, 4072–4073.
36. A. M. Thakur, K.; T. Kean, R.; A. M. Thakur, K.; T. Zell, M.; E. Padden, B.; J. Munson, E. *Chem. Commun.* **1998**, 1913–1914.
37. Ovitt, T. M.; Coates, G. W. *J. Polym. Sci. A Polym. Chem.* **2000**, *38*, 4686–4692.

38. Ovitt, T. M.; Coates, G. W. *J. Am. Chem. Soc.* **2002**, *124*, 1316–1326.
39. Cameron, P. A.; Jhurry, D.; Gibson, V. C.; White, A. J. P.; Williams, D. J.; Williams, S. *Macromol. Rapid Commun.* **1999**, *20*, 616–618.
40. Zhong, Z.; Dijkstra, P. J.; Feijen, J. *Angew. Chem. Int. Ed.* **2002**, *41*, 4510–4513.
41. Zhong, Z.; Dijkstra, P. J.; Feijen, J. *J. Am. Chem. Soc.* **2003**, *125*, 11291–11298.
42. Nomura, N.; Ishii, R.; Akakura, M.; Aoi, K. *J. Am. Chem. Soc.* **2002**, *124*, 5938–5939.
43. Tang, Z.; Chen, X.; Pang, X.; Yang, Y.; Zhang, X.; Jing, X. *Biomacromolecules* **2004**, *5*, 965–970.
44. Tang, Z.; Chen, X.; Yang, Y.; Pang, X.; Sun, J.; Zhang, X.; Jing, X. *J. Polym. Sci. A Polym. Chem.* **2004**, *42*, 5974–5982.
45. Hormnirun, P.; Marshall, E. L.; Gibson, V. C.; Pugh, R. I.; White, A. J. P. *Proc. Natl. Acad. Sci. U.S.A.* **2006**, *103*, 15343–15348.
46. Hormnirun, P.; Marshall, E. L.; Gibson, V. C.; White, A. J. P.; Williams, D. J. *J. Am. Chem. Soc.* **2004**, *126*, 2688–2689.
47. Du, H.; Velders, A. H.; Dijkstra, P. J.; Sun, J.; Zhong, Z.; Chen, X.; Feijen, J. *Chem. Eur. J.* **2009**, *15*, 9836–9845.
48. Johnstone, N. C.; Aazam, E. S.; Hitchcock, P. B.; Fulton, J. R. *J. Organomet. Chem.* **2010**, *695*, 170–176.
49. Li, W.; Wu, W.; Wang, Y.; Yao, Y.; Zhang, Y.; Shen, Q. *Dalton Trans.* **2011**, *40*, 11378–11381.
50. Li, W.; Yao, Y.; Zhang, Y.; Shen, Q. *Chin. J. Chem.* **2012**, *30*, 609–615.
51. Hancock, S. L.; Jones, M. D.; Langridge, C. J.; Mahon, M. F. *New J. Chem.* **2012**, *36*, 1891–1896.
52. Sumrit, P.; Hormnirun, P. *Macromol. Chem. Phys.* **2013**, *214*, 1845–1851.
53. Shelton, J. R.; Agostini, D. E.; Lando, J. B. *J. Polym. Sci. A Polym. Chem.* **1971**, *9*, 2789–2799.
54. Zhang, Y.; Gross, R. A.; Lenz, R. W. *Macromolecules* **1990**, *23*, 3206–3212.
55. Le Borgne, A.; Vincens, V.; Jouglard, M.; Spassky, N. *Makromol. Chem. Macromol. Symp.* **1993**, *73*, 37–46.
56. Cross, E. D.; Allan, L. E. N.; Decken, A.; Shaver, M. P. *J. Polym. Sci. A Polym. Chem.* **2013**, *51*, 1137–1146.
57. Agatemor, C.; Arnold, A. E.; Cross, E. D.; Decken, A.; Shaver, M. P. *J. Organomet. Chem.* **2013**, *745–746*, 335–340.
58. MacDonald, J. P.; Parker, M. P.; Greenland, B. W.; Hermida-Merino, D.; Hamley, I. W.; Shaver, M. P. *Polym. Chem.* **2015**in press.
59. Qu, X.-H.; Wu, Q.; Liang, J.; Zou, B.; Chen, G.-Q. *Biomaterials* **2006**, *27*, 2944–2950.
60. MacDonald, J. P.; Shaver, M. P. *The University of Edinburgh, Edinburgh, UK. Personal communication* **2014**.
61. Darensbourg, D. J.; Karroonnirun, O.; Wilson, S. J. *Inorg. Chem.* **2011**, *50*, 6775–6787.
62. Yang, J.; Yu, Y.; Li, Q.; Li, Y.; Cao, A. *J. Polym. Sci. A Polym. Chem.* **2005**, *43*, 373–384.

Publication Date (Web): June 18, 2015 | doi: 10.1021/bk-2015-1192.ch010

63. Breteler, M. R. T.; Zhong, Z.; Dijkstra, P. J.; Palmans, A. R. A.; Peeters, J.; Feijen, J. *J. Polym. Sci. A Polym. Chem.* **2007**, *45*, 429–436.
64. van der Meulen, I.; Gubbels, E.; Huijser, S.; Sablong, R. l.; Koning, C. E.; Heise, A.; Duchateau, R. *Macromolecules* **2011**, *44*, 4301–4305.
65. Pepels, M. P. F.; Bouyahyi, M.; Heise, A.; Duchateau, R. *Macromolecules* **2013**, *46*, 4324–4334.
66. Hiki, S.; Miyamoto, M.; Kimura, Y. *Polymer* **2000**, *41*, 7369–7379.
67. Agatemor, C.; Shaver, M. P. *Biomacromolecules* **2013**, *14*, 699–708.
68. Zhao, W.; Wang, Y.; Liu, X.; Chen, X.; Cui, D.; Chen, E. Y. X. *Chem. Commun.* **2012**, *48*, 6375–6377.
69. Stanford, M. J.; Dove, A. P. *Macromolecules* **2008**, *42*, 141–147.
70. Stanford, M. J.; Pflughaupt, R. L.; Dove, A. P. *Macromolecules* **2010**, *43*, 6538–6541.
71. Tennekone, G. K.; Wagner, B. D.; Shaver, M. P. *Green Materials* **2013**, *2*, 31–42.
72. Zhao, W.; Wang, Y.; Liu, X.; Cui, D. *Chem. Commun.* **2012**, *48*, 4483–4485.
73. Cameron, D. J. A.; Shaver, M. P. *Chem. Soc. Rev.* **2011**, *40*, 1761–1776.
74. Dubois, P.; Jerome, R.; Teyssie, P. *Macromolecules* **1991**, *24*, 977–981.
75. Cameron, D. J. A.; Shaver, M. P. *J. Polym. Sci. A Polym. Chem.* **2012**, *50*, 1477–1484.
76. Shaver, M. P.; Cameron, D. J. A. *Biomacromolecules* **2010**, *11*, 3673–3679.

Publication Date (Web): June 18, 2015 | doi: 10.1021/bk-2015-1192.ch010

Publication Date (Web): June 18, 2015 | doi: 10.1021/bk-2015-1192.ch011

Chapter 11

Creation of Functional Peptides by Evolutionary Engineering with Bioorthogonal Incorporation of Artificial Components

Seiichi Tada,[1] Takanori Uzawa,[1,2] and Yoshihiro Ito[*,1,2]

[1]Nano Medical Engineering Laboratory, RIKEN, 2-1 Hirosawa, Wako, Saitama 351-0198, Japan
[2]Emergent Bioengineering Materials Research Team, RIKEN Center for Emergent Matter Science, 2-1 Hirosawa, Wako, Saitama 351-0198, Japan
[*]E-mail: y-ito@riken.jp.

Molecular evolutionary engineering is a method used to harness the power of natural selection to evolve proteins or RNA with desirable properties not found in nature. The possibility of evolving a commonly existing biomolecule into a variety of functional biomolecules has now been realized in the form of aptamers through the development of *in vitro* selection. In addition to their high affinity and high specificity for desired targets, aptamers are easily synthesized chemically and can be modified for downstream applications. Although aptamers were originally selected from a library containing only natural components, the past decade has seen a wealth of new aptamers selected from libraries containing unnatural components to provide new aptamer functions artificially. Here we highlight this transition (the shift between selection from natural components and selection from unnatural components) and the applications of the selected aptamers. For the selection, functional molecule was attached to tRNA through amino acid and the misacylated tRNA was incorporated into *in vitro* selection process.

In Green Polymer Chemistry: Biobased Materials and Biocatalysis; Smith, et al.;
ACS Symposium Series; American Chemical Society: Washington, DC, 2015.

Publication Date (Web): June 18, 2015 | doi: 10.1021/bk-2015-1192.ch011

Introduction

Biomacromolecules, including peptides and proteins, are among the most effective Green Polymers because of their variety of functions provided by different pattern of sequences and biodegradability. Thus far, a large number of peptides and proteins have been utilized for chemical engineering, clinical treatment and other applications.

For further improvement of their function, such as binding affinity and catalytic activity, *in vitro* selection method is a quite promising methodology (*1*). Phage display, one of the most famous methods, was developed as the first example of *in vitro* selection method (*2*), and other methods including ribosome display (*3*), mRNA display (*4*, *5*) and *in vitro* compartment method (*6*) were reported. These methods have provided a number of peptides and proteins with various functions through the selection of better sequences from a library of random-sequence peptides or mutant proteins. This methodology of selection is also called as "evolutionary molecular engineering", because of the similarity to Darwinian evolution in the natural world.

Recently evolutionary molecular engineering has evolved onto the next generation of artificial peptide aptamers selected from a library including unnatural amino acids (Figure 1). Although the original *in vitro* selection method has a limitation on usage of only the 20 natural amino acids as the components of random peptide library, incorporation of unnatural, or artificial, amino acid into the random library was achieved by using misacylated tRNA (*7*, *8*) and nonliving translation system (*3*–*5*). The resulting peptide aptamer with artificial component should be expected to have special functions which are not seen in natural peptides consisting of canonical amino acids.

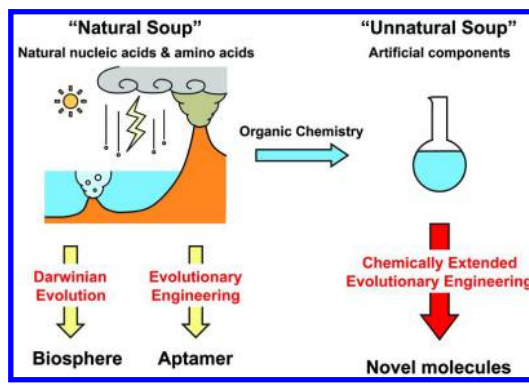

Figure 1. Schematic image of in vitro selection of functional peptides modified with unnatural amino acid. Reproduced with permission from reference (1). Copyright 2013 The Royal Society of Chemistry.

In Green Polymer Chemistry: Biobased Materials and Biocatalysis; Smith, et al.;
ACS Symposium Series; American Chemical Society: Washington, DC, 2015.

In this review, first we discuss the method of peptide aptamer selection from unnatural amino acid-containing random sequence library. Subsequently, we introduce our recent studies of functional peptides, such as fluorogenicity (*9*), photoresponsivity (*10*, *11*) and better inhibition effect against an enzyme (*12*), with artificially modified amino acids.

In Vitro Selection of Peptide Aptamer Incorporating Unnatural Amino Acid

The introduction of a novel, unnatural amino acid into the desired position of a peptide sequence was accomplished by using unnatural amino acid-conjugated tRNA. Noren *et al.* synthesized misacylated suppressor tRNA, which recognized amber stop codon, by modifying unnatural amino acid and applied that tRNA to cell-free translation system (*7*). The obtained protein had the unnatural residue at amber codon position (Figure 2).

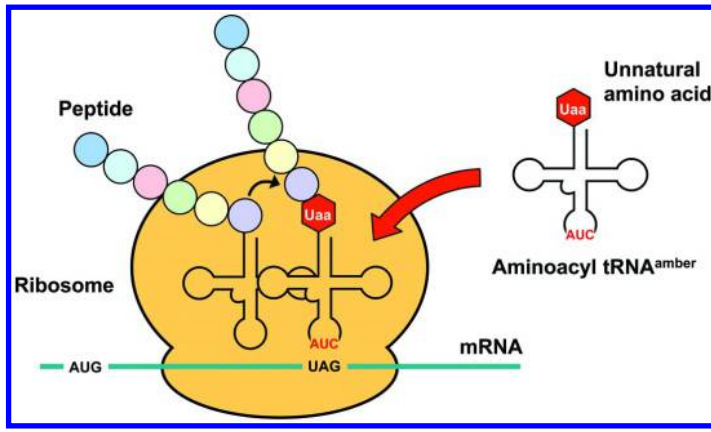

Figure 2. Incorporation of an unnatural amino acid (Uaa) with misacylated tRNA^{amber}. Reproduced with permission from reference (1). Copyright 2013 The Royal Society of Chemistry.

This technique can be utilized for peptide aptamer selection with ribosome display and mRNA display methods. In these *in vitro* selection methods, cell-free translation system is used for association of mRNA and translated product of peptide, therefore unnatural amino acids can be incorporated into a peptide sequence of mRNA/peptide complex by just adding unnatural amino acid-conjugating tRNA to translation system solution (*3*, *13*).

Based on this selection method, we selected various functional peptide aptamers containing unnatural residues including fluorophore, photoresponsive molecule and enzyme inhibitor, respectively (*9–12*). These peptide aptamers were selected by ribosome display method with each artificial component-conjugated tRNA (Figure 3). Briefly, we prepared DNA templates encoding random peptide sequences including a stop-codon (UAG) at fixed position for incorporation of

In Green Polymer Chemistry: Biobased Materials and Biocatalysis; Smith, et al.;
ACS Symposium Series; American Chemical Society: Washington, DC, 2015.

Publication Date (Web): June 18, 2015 | doi: 10.1021/bk-2015-1192.ch011

unnatural amino acid, but any other stop codons were removed from peptide sequence. These DNA templates were transcribed into an mRNA pool (library) and subsequently translated with cell-free translation system containing tRNA with unnatural amino acid. This translation process provided the complex of mRNA, translated peptide and ribosome because of lack of any stop codons, except UAG codon for incorporation of unnatural amino acid. We incubated this complex solution with target molecule-immobilized magnetic beads and collected high-affinity peptide complexes to the target molecule. After purification of mRNA and subsequent RT-PCR, DNA templates of high-affinity peptide sequences were amplified and used for the next selection round. We repeated this selection process several times and obtained DNA templates were analyzed their sequences. We synthesized some of selected peptide sequences and finally decided the sequence of a functional peptide aptamer by estimating the function of selected peptide candidates.

Publication Date (Web): June 18, 2015 | doi: 10.1021/bk-2015-1192.ch011

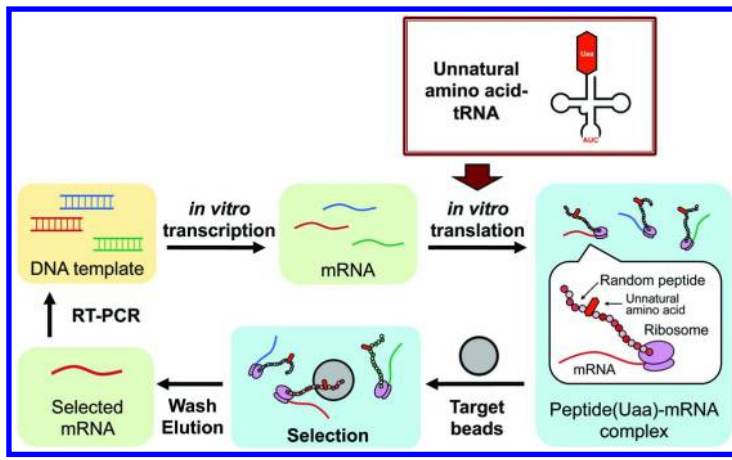

Figure 3. Selection process of ribosome display from random peptide library with unnatural amino acids.

We have reported three kinds of functional peptide aptamers with unnatural amino acids by using ribosome display and misacylated tRNA. First example is a fluorogenic peptide aptamer containing NBD fluorophore, which bound to Ca^{2+}-containing form of calmodulin molecule and increase its fluorescence intensity (*9*). The second example is a photoresponsive peptide aptamer containing azobenzene molecule (*10*, *11*). This peptide changes its binding affinity to target molecules by irradiation of UV light. The third example is a "superinhibitor" peptide containing a small inhibitor molecule, which provide higher inhibiting effect than that of normal inhibitor molecule (*12*). We discuss these functional peptides in following parts.

Fluorogenic Peptide Aptamer

Molecular probes that can both bind to a target and indicate a signal of the presence of the target protein have been developed for the easier detection of specific proteins. For this purpose, enzymatic degradation of a signaling substrate was used to detect specific enzymes (*14–16*). However, these strategies cannot be applied to any arbitrarily selected target proteins, in contrast to the strategies for creating antibodies and aptamers. Therefore we endeavored to generate a signaling peptide with the characteristics of both aptamers and signaling molecular probes. We planned to select a functional peptide aptamer, which emits fluorescence upon specific binding to an arbitrarily selected protein, from a pool of random sequence peptides containing a fluorogenic amino acid (*9*). We chose 7-nitro-2,1,3-benzoxadiazole (NBD; Figure 4) as the fluorogenic probe, because its fluorescence intensity increases drastically only in a hydrophobic environment. We expected that the NBD would directly contribute to the interaction between the peptide and the target protein by forming part of the molecular recognition site, and upon binding, emit fluorescence.

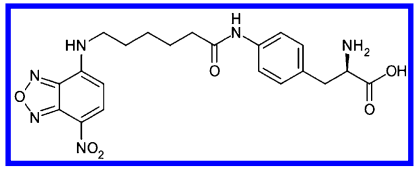

Figure 4. 7-nitro-2,1,3-benzoxadiazole (NBD) conjugated aminophenylalanine.

We prepared misacylated tRNA of NBD-conjugated aminophenylalanine and performed ribosome display selection of fluorogenic peptide aptamers using that tRNA. In this peptide selection, a calcium-signal transducer protein calmodulin (CaM) was used as a target molecule because its mechanism of binding to various peptides and proteins has been extensively studied (*17*, *18*). Upon Ca^{2+} binding, its N- and C-terminal lobe-domains, which are connected by a central helical linker region, undergo a conformational change that exposes a hydrophobic patch for interaction with other peptides and proteins.

After six rounds of selection and subsequent functional analysis, we finally obtained a fluorogenic peptide aptamer sequence C5 (YWDKIKDXIGG, where X is NBD-aminophenylalanine). C5 peptide synthesized with solid phase method showed specific binding to Ca^{2+}-bound CaM and significant increase of fluorescence signal from NBD, whereas in the absence of Ca^{2+} the fluorescence intensity increased only minimally (Figure 5). Based on the fluorescence titration, the dissociation constant (K_d) was determined to be 1.03 ± 0.16 μM, which is supported by an observation using surface plasmon resonance (850 nM).

Publication Date (Web): June 18, 2015 | doi: 10.1021/bk-2015-1192.ch011

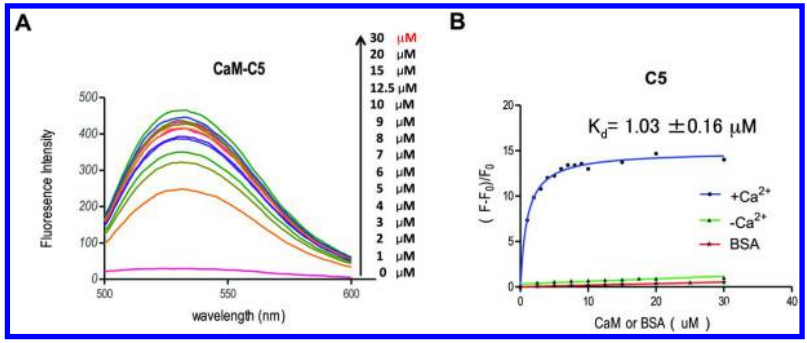

Figure 5. Fluorescence change of C5 peptide upon specific binding to Ca^{2+}-bound CaM. (A) The fluorescence intensity of the C5 peptide increased upon addition of increasing concentrations of CaM while in the presence of Ca^{2+}. (B) The relative fluorescence intensity change at 535 nm clearly shows that the C5 peptide only emits fluorescence in the presence of Ca^{2+}-bound CaM. Reproduced with permission from reference (9). Copyright 2014 The Royal Society of Chemistry.

Publication Date (Web): June 18, 2015 | doi: 10.1021/bk-2015-1192.ch011

We succeeded selection of a fluorogenic peptide against Ca^{2+}-bound CaM using a peptide pool incorporating an artificial fluorogenic probe. To the best of our knowledge, this peptide is the first example of the successful selection of a fluorogenic peptide from a random sequence pool. This technology could prove to be useful for the development of separation-free immunoassays and bio-imaging analyses.

Photoresponsive Peptide Aptamer

Artificial control of dynamic molecular recognition is one of the important and promising research fields (*19–21*). Control by light irradiation has been utilized as a dominant external stimulus against dynamic molecular recognition (*22*, *23*), Although many photoresponsive molecules have been reported, such as photoresponsive crown ethers (*24*, *25*), a photo-chemically driven molecular machine (*26*), a light-powered molecular pedal (*27*) and so on, these examples were based on a rigorous molecular design (commonly termed "rational design"). Therefore the design of the photo-responsive host molecule for arbitrary targets, which is structurally complicated or unknown, would be difficult and was not achieved.

We proposed an approach to achieve the photocontrol of dynamic molecular recognition with an arbitrary target by using an *in vitro* selection method. We isolated a photo-responsive peptide aptamer which recognizes a target by using ribosome display (*10*).

An azobenzene molecule was chosen for application of photoresponsive property to peptide aptamer and coupled with aminoacyl tRNA. This azobenzene-conjugated tRNA was used for ribosome display selection of a photoresponsive peptide aptamer binding to a target material, streptavidin-conjugated magnetic beads. We first incubated mRNA-peptide complex library containing azobenzene with streptavidin beads for 30 min under dark conditions, in which almost azobenzene took trans-form. Subsequently, the beads were irradiated with ultraviolet light for 10 min. In this step, peptides with cis-form azobenzenes can be released from the beads, since conformational changes of the peptides by the trans–cis isomerization of azobenzenes are accompanied by the changes in affinity to streptavidin.

After five rounds of these selection processes, finally a high binding affinity sequence LA81 (GVTXRRFIXYV, where X is azobenzene-aminophenylalanine) was obtained. This peptide sequence showed better binding affinity to streptavidin beads than other selected peptide sequences (Figure 6A). The dissociation constant of the LA81 peptide bound to the microbead was calculated to be 6.31 μM by curve-fitting to a Langmuir isotherm. In addition, LA81 adsorbed onto the microbead under visible light irradiation but this adsorption was significantly reduced by UV irradiation (Figure 6B). In contrast, a scrambled sequence peptide (control) did not bind and showed no photo-responsiveness.

In order to confirm the wide utility of this selection strategy to various target molecules, we selected another photoresponsive peptide aptamer, which bound to different target material, glutathione-immobilized microbeads (*11*). After eight rounds of ribosome display selection process using azobenzene-carrying aminoacyl tRNA and glutathione beads, two peptide sequences B09 and B69 (RNGXSSGRHGD and KDGXGGEEGET, respectively, where X is azobenzene-aminophenylalanine) were chosen as photoresponsive peptide aptamers. Both of these peptides bound to the target beads, but B09 showed higher affinity compared to B69 peptide (Figure 7A). The dissociation constants of the B09 and B69 peptides bound to the microbeads were calculated as 5.21 and 1.19 μM, respectively, by curve fitting to a Langmuir isotherm. One of the peptides, B09, adsorbed onto the microbeads under visible light irradiation but this adsorption was significantly reduced by UV irradiation, although the B69 peptide did not show significant photoresponsive differences in adsorption behavior (Figure 7B). This less photoresponsiveness of the B69 peptide is likely caused by a lack of some components in the ribosome display. Additionally, streptavidin beads-binding peptide LA81 showed larger affinity change than glutathione beads-binding peptide B09. This difference seemed to be due to the number of azobenzene molecule incorporated to peptide sequence. LA81 carried two azobenzene molecules in its sequence, resulting in larger comformational change after UV irradiation.

Publication Date (Web): June 18, 2015 | doi: 10.1021/bk-2015-1192.ch011

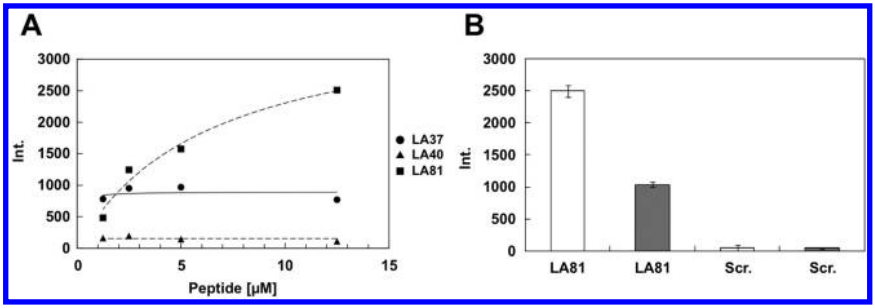

Figure 6. Binding analysis on selected photoresponsive peptides binding to streptavidin beads. (A) Binding of peptides containing LA37, LA40 and LA81 sequences (VLIMVAVXASS, HSCXVTIDVFF and GVTXRRFIXYV, respectively, where X represents azobenzene-aminophenylalanine). The bound microbead was stained with an FITC-labeled anti-FLAG-antibody and its fluorescent intensity was quantified by a microplate reader. (B) Photo-responsive binding of peptides containing LA81 or a scrambled sequence. White bar: under the visible light irradiation conditions; grey bar: under the UV irradiation conditions. Reproduced with permission from reference (10). Copyright 2012 The Royal Society of Chemistry.

We succeeded the selection of photo-responsive peptide aptamers against two kinds of target materials using *in vitro* selection combined with photo-manipulation. The photo-responsive peptide sequence will be available as a protein-tag for the purification of biologically significant protein. Moreover, the photo-responsive peptide that binding nanomaterials, such as carbon nanotube, could also be applicable in particular photo-switching nanodevices.

Superinhibitor Consisting of Small Molecule and Peptide Aptamer

The discovery and development of selective inhibitors against protein kinase is highly demanded for the treatment of cancer and a number of neurological, immunological, metabolic, and infectious diseases (*28*, *29*). Threfore, direct *in vitro* selection of peptides with inhibitory activity has been reported (*30–32*). Especially, Li and Roberts introduced penicillin molecule into a mRNA-display peptide library by post-translational modification and isolated peptide-drug conjugates with at least 100-fold higher activity against *Staphylococcus aureus* penicillin-binding protein 2a (*32*). This strategy, however, requires chemical reactions after *in vitro* translation and may produce unwanted by-products.

We chose the small molecule purvalanol B (PVB), which inhibits cyclin-dependent kinase 2 (CDK2) with nanomolar IC_{50} values, as a component of peptide-based inhibitor because the interaction between PVB and CDK2 has been well studied, and the carboxylic acid of the 6-anilino substituent of PVB can be modified without affecting the inhibitor-kinase interaction (*12*).

In Green Polymer Chemistry: Biobased Materials and Biocatalysis; Smith, et al.;
ACS Symposium Series; American Chemical Society: Washington, DC, 2015.

Publication Date (Web): June 18, 2015 | doi: 10.1021/bk-2015-1192.ch011

Therefore, we coupled the carboxylic acid of PVB with aminophenylalanine and charged the product to suppressor tRNA for incorporation of PVB into a random-sequence peptide library during ribosome display selection. We aimed to isolate a peptide–drug conjugation with higher inhibitory activity due to increase of the interaction sites (Figure 8).

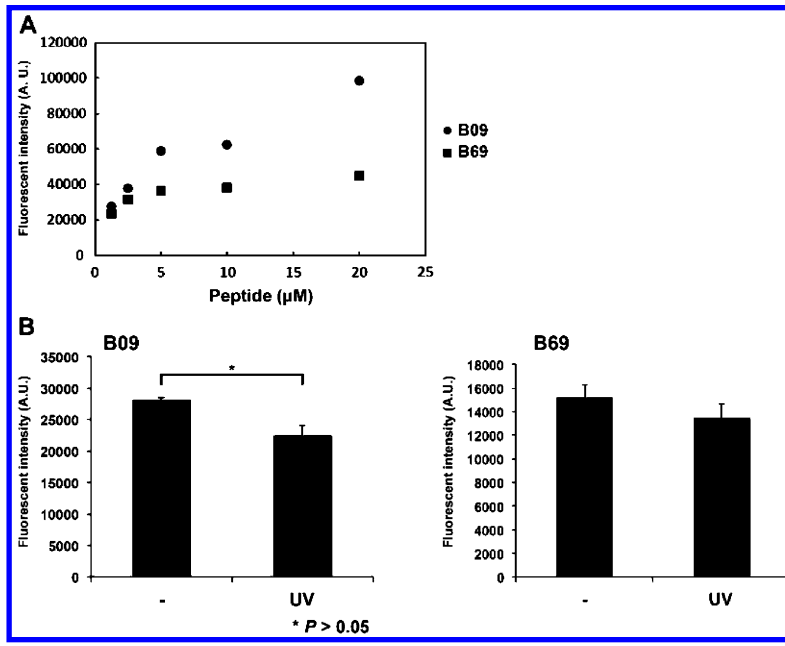

Figure 7. Binding experiments on selected photoresponsive peptides binding to glutathione beads. (A) Binding of peptides containing B09 and B69 sequences and fluorescein at N-terminus. The amount of bound peptide to the microbeads was estimated by measuring the fluorescent intensity with a microplate reader. (B) Photoresponsive binding of peptides containing either the B09 or B69 sequence. Reproduced with permission from reference (11). Copyright 2014 Elsevier.

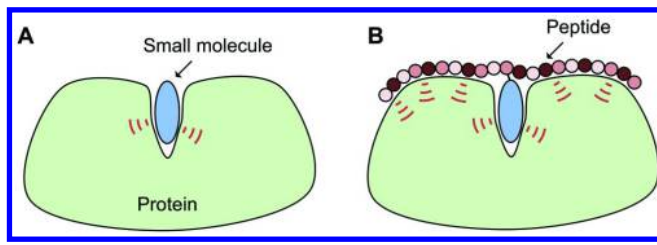

Figure 8. Principle of enhancement of the inhibitory activity of a small molecule by a peptide. (A) Small molecule interacts with a protein. (B) Peptide–small molecule conjugate interacts with the protein.

Publication Date (Web): June 18, 2015 | doi: 10.1021/bk-2015-1192.ch011

After six iterative rounds of selection process, a peptide sequence A5 (SKLXRFTGCSC, where X is PVB-aminophenylalanine) was found as an effective inhibitor peptide. We examined the inhibitory activity of A5 and PVB as 15 well as control peptide, whose PVB residue was replaced to phenylalanine, using a fluorescence resonance energy transfer-based Z0-LYTE assay kit. A5 inhibited CDK2/cyclin A with an IC_{50} of 34 nM, while single PVB molecule was a less potent inhibitor of CDK2/cyclin A, with an IC_{50} value of 263 nM. As we expected, control peptide did not exhibit inhibitory activity (Figure 9). Because PVB-aminophenylalanine exhibited nearly the same inhibitory activity as PVB, the higher inhibitory activity of A5 compared with PVB arises from the peptide. Thus, we also succeeded in developing novel inhibitor peptide with higher inhibitory effect by using unnatural amino acid-modified ribosome display system.

Publication Date (Web): June 18, 2015 | doi: 10.1021/bk-2015-1192.ch011

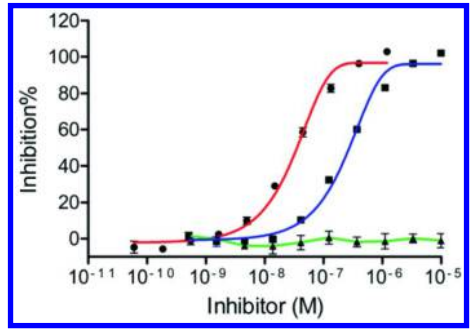

Figure 9. Inhibitory activities of A5 peptide (circles), PVB (squares), and control peptide (triangles) against CDK2/cyclin A. The results indicate that the peptide enhances the inhibitory effect of PVB against CDK2/cyclin A. Reproduced with permission from reference (12). Copyright 2014 The Royal Society of Chemistry.

Concluding Remarks and Future Outlook

In this article, we described our recent studies involving the selection of functional peptide aptamers carrying unnatural residues. These results indicated that the function of peptide aptamers could be expanded by introducing artificial, small molecules, such as fluorophores, photoresponsive module, and inhibitors into the random peptide library during *in vitro* selection. Our functional peptides were selected without any negative selection process; therefore their functions, especially binding affinity, would be improved even more by additional negative selection. Thus, the dual use of bioorthogonal incorporation of unnatural amino acids and evolutionary molecular engineering is a highly promising technology to produce various functional peptides and green polymers.

References

1. Uzawa, T.; Tada, S.; Wang, W.; Ito, Y. *Chem. Commun.* **2013**, *49*, 1786–1795.
2. Smith, G. P. *Science* **1985**, *228*, 1315–1317.
3. Mattheakis, L. C.; Bhatt, R. R.; Dower, W. J. *Proc. Natl. Acad. Sci. U.S.A.* **1994**, *91*, 9022–9026.
4. Nemoto, N.; Miyamoto-Sato, E.; Husimi, Y.; Yanagawa, H. *FEBS Lett.* **1997**, *414*, 405–408.
5. Roberts, R. W.; Szostak, J. W. *Proc. Natl. Acad. Sci. U.S.A.* **1997**, *94*, 12297–12302.
6. Tawfik, D. S.; Griffiths, A. D. *Nat. Biotechnol.* **1998**, *16*, 652–656.
7. Noren, C. J.; Anthony-Cahill, S. J.; Griffith, M. C.; Schultz, P. G. *Science* **1989**, *244*, 182–188.
8. Bain, J. D.; Glabe, C. G.; Dix, T. A.; Chamberlin, A. R.; Diala, E. S. *J. Am. Chem. Soc.* **1989**, *111*, 8013–8014.
9. Wang, W.; Uzawa, T.; Tochio, N.; Hamatsu, J.; Hirano, Y.; Tada, S.; Saneyoshi, H.; Kigawa, T.; Hayashi, N.; Ito, Y.; Taiji, M.; Aigaki, T.; Ito, Y. *Chem. Commun.* **2014**, *50*, 2962–2964.
10. Liu, M.; Tada, S.; Ito, M.; Abe, H.; Ito, Y. *Chem. Commun.* **2012**, *48*, 11871–11873.
11. Tada, S.; Zang, Q.; Wang, W.; Kawamoto, M.; Liu, M.; Iwashita, M.; Uzawa, T.; Kiga, D.; Yamamura, M.; Ito, Y. *J. Biosci. Bioeng.* **2015** in press.
12. Wang, W.; Hirano, Y.; Uzawa, T.; Liu, M.; Taiji, M.; Ito, Y. *Med. Chem. Commun.* **2014**, *5*, 1400–1403.
13. Li, S.; Millward, S.; Roberts, R. *J. Am. Chem. Soc.* **2002**, *124*, 9972–9973.
14. Perez, J. M.; Josephson, L.; O'Loughlin, T.; Hogemann, D.; Weissleder, R. *Nat. Biotechnol.* **1999**, *17*, 375–378.
15. Wosnick, J. H.; Mello, C. M.; Swager, T. M. *J. Am. Chem. Soc.* **2005**, *127*, 3400–3405.
16. Zhang, J.; Shibata, A.; Ito, M.; Shuto, S.; Ito, Y.; Mannervik, B.; Abe, H.; Morgenstern, R. *J. Am. Chem. Soc.* **2011**, *133*, 14109–14119.
17. Meador, W. E.; Means, A. R.; Quiocho, F. A. *Science* **1992**, *257*, 1251–1255.
18. Ikura, M.; Clore, G. M.; Gronenborn, A. M.; Zhu, G; Klee, C. B.; Bax, A. *Science* **1992**, *256*, 632–638.
19. Lehn, J. M. *Chem. Soc. Rev.* **2007**, *36*, 151–160.
20. Bellotto, S.; Chen, S.; Rebollo, I. R.; Wegner, H. A.; Heinis, C. *J. Am. Chem. Soc.* **2014**, *136*, 5880–5883.
21. Jafari, M. R.; Deng, L.; Kitov, P. I.; Ng, S.; Matochko, W. L.; Tjhung, K. F.; Zeberoff, A.; Elias, A.; Klassen, J. S.; Derda, R. *ACS Chem. Biol.* **2014**, *9*, 443–450.
22. Willner, I. *Acc. Chem. Res.* **1997**, *30*, 347–356.
23. Champin, B.; Mobian, P.; Sauvage, J. P. *Chem. Soc. Rev.* **2007**, *36*, 358–366.
24. Shinkai, S.; Ogawa, T.; Nakaji, T.; Kusano, Y.; Nanabe, O. *Tetrahedron Lett.* **1979**, *20*, 4569–4572.
25. Shinkai, S.; Nakaji, T.; Ogawa, T.; Shigematsu, K.; Manabe, O. *J. Am. Chem. Soc.* **1981**, *103*, 111–115.

26. Ballardini, R.; Balzani, V.; Gandolfi, M. T.; Prodi, L.; Venturi, M.; Phillip, D.; Ricketts, H. G.; Stoddart, J. F. *Angew. Chem., Int. Ed.* **1993**, *32*, 1301–1303.
27. Muraoka, T.; Kinbara, K.; Aida, T. *Nature* **2006**, *440*, 512–515.
28. Noble, M. E. M.; Endicott, J. A.; Johnson, L. N. *Science* **2004**, *303*, 1800–1805.
29. Zhang, J. M.; Yang, P. L.; Gray, N. S. *Nat. Rev. Cancer* **2009**, *9*, 28–39.
30. Colas, P.; Cohen, B.; Jessen, T.; Grishina, I.; McCoy, J.; Brent, R. *Nature* **1996**, *380*, 548–550.
31. Ueno, S.; Yoshida, S.; Mondal, A.; Nishina, K.; Koyama, M.; Sakata, I.; Miura, K.; Hayashi, Y.; Nemoto, N.; Nishigaki, K.; Sakai, T. *Proc. Natl. Acad. Sci. U.S.A.* **2012**, *109*, 11121–11126.
32. Li, S.; Roberts, R. W. *Chem. Biol.* **2003**, *10*, 233–239.

Publication Date (Web): June 18, 2015 | doi: 10.1021/bk-2015-1192.ch011

Publication Date (Web): June 18, 2015 | doi: 10.1021/bk-2015-1192.ch012

Chapter 12

Thermoplastic Elastomers from Vegetable Oils via Reversible Addition-Fragmentation Chain Transfer Polymerization

Nacú Hernández,[1] Mengguo Yan,[1] R. Christopher Williams,[2] and Eric Cochran[*,1,3]

[1]Department of Chemical and Biological Engineering, 3127 Sweeney Hall, Iowa State University, Ames, Iowa 50011, U.S.A.
[2]Department of Civil, Construction, and Environmental Engineering, 490 Town Engineering Building, Iowa State University, Ames, Iowa 50011, U.S.A.
[3]Present address: 1035 Sweeney Hall, Ames, Iowa 50011, U.S.A.
[*]E-mail: ecochran@iastate.edu.

We present the controlled radical polymerization of vegetable oils, *e.g.* soybean oil, with styrene into thermoplastic elastomers. We have discovered that under certain reaction conditions controlled radical polymerization, such as RAFT, limits the number of initiation sites and drastically reduces the rate of chain transfers and termination reactions. This discovery introduces the capability of producing customized chain architectures such as block copolymers (BCPs) from vegetable oils. Here we report the synthesis of poly(styrene-*b*-AESO-*b*-styrene) (PS-PAESO-PS) triblock copolymers with properties similar to petroleum based thermoplastic elastomers.

Introduction

Over the past several decades, vegetable oils have been considered a cost competitive and environmentally friendly alternative to petroleum-based chemicals, especially in the polymer industry. They are composed of triglycerides (triglycerides are composed of a glycerol molecule and three fatty acids (FA); a

In Green Polymer Chemistry: Biobased Materials and Biocatalysis; Smith, et al.;
ACS Symposium Series; American Chemical Society: Washington, DC, 2015.

list of common FA can be found in Table 1), as shown below in Figure 1, and possess an average of 3.6 double bonds. These double bonds provide multiple opportunities for monomer modification and polymerization.

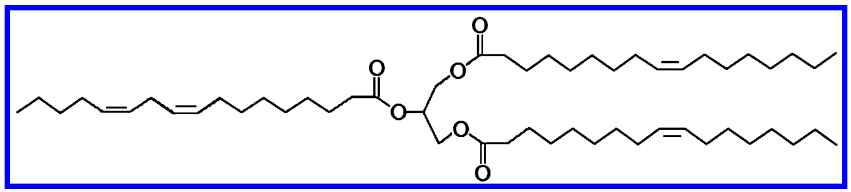

Figure 1. Structure of a triglyceride molecule present in vegetable oils.

Publication Date (Web): June 18, 2015 | doi: 10.1021/bk-2015-1192.ch012

Unmodified vegetable oils (*e.g.* soybean oil, peanut oil, sunflower oil and canola oil) contain mostly isolated double bonds with low reactivities making them unsuitable for polymerization. However, higher reactivities can be found in vegetable oils such as tung oil or bitter gourd seed oil which contain naturally occurring conjugated double bonds, where thermal or cationic polymerization can be used (*1*, *2*).

In order to more efficiently utilize vegetable oils' active sites, double bond modification has been used as a way of creating monomers capable of producing polymers through different polymerization techniques. For example: Larock *et al.* made use of a rhodium-catalyzed isomerization process to increase the reaction activity of vegetable oils. They were able to produce a vegetable oil with conjugated double bonds that subsequently was synthesized into thermosetting polymers via cationic polymerization (*3*, *4*). Moreover, in the early 1990s, J. V. Crivello *et al.* reported the polymerization of epoxidized soybean oil via cationic polymerization (*5*). Epoxidized vegetable oils have been utilized, more recently, in the production of epoxy resins by curing them with diamine hardeners (*6*) or by using a thermal catalyst (*7*). Once epoxidized, vegetable oils can also be used in the production of polyols using ring opening agents, such as methanol or other mono-alcohols, with fluoroboric acid (HBF_4) as a catalyst (*8*). $LiAlH_4$ was also reported as a catalyst capable of converting epoxidized triglycerides into polyols (*9*). Additionally, Zhang *et al.* developed a solvent and catalyst-free route to synthesize polyols from castor oil and polyurethanes therefrom (*10*).

A number of interesting modifications on vegetable oils have also been used: a combination of ozonolysis and hydrogenation (*11*), hydroformylation and hydrogenation using a rhodium catalyst (*12*), oxidation and reduction, epoxidation and acrylation, Friedel-Craft acylation (*13*), amongst others (*14*).

The acrylation of vegetable oils was first used in the late 1960s (*15*), making them quite susceptible to chain growth polymerization. Wool *et al.* employed acrylated epoxidized soybean oil as monomers in the polymerization of a variety of thermoset materials, including sheet molding composites (*16*), adhesives, elastomeric materials, coatings, foams, etc. (*17–23*)

Table 1. Common Fatty Acids Found in Common Vegetable Oils

Fatty Acid	Formula	Structure	Occurrence
Oleic	$C_{18}H_{34}O_2$	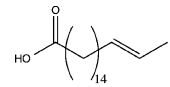	olive oil, pecan oil, canola oil, peanut oil, macadamia nut oil, sesame oil
Linoleic	$C_{18}H_{32}O_2$	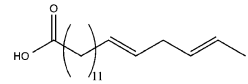	safflower oil, sunflower oil, soybean oil, cottonseed oil
α-Linolenic	$C_{18}H_{30}O_2$	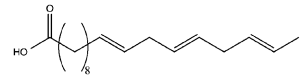	linseed oil and in lower levels in many other seed oils
α-Eleostearic	$C_{18}H_{34}O_3$	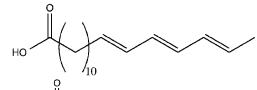	tung oil, bitter gourd seed oil
Ricinoleic	$C_{18}H_{34}O_3$	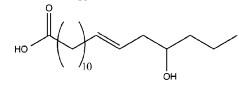	castor oil
Stearic	$C_{18}H_{36}O_2$	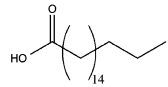	plant fats

Publication Date (Web): June 18, 2015 | doi: 10.1021/bk-2015-1192.ch012

Currently there are numerous examples of vegetable oil modification combined with thermal, cationic or free radical polymerization routes that have yielded thermoset plastics. Uncontrolled chain branching and crosslinking is inevitable using these conventional polymerization routes due to the multifunctional nature of triglycerides. These shortcomings have been circumvented by the use of single fatty acids instead of the triglycerides. Wang *et al.* used lauryl acrylate derived from vegetable oils as soft block in the production of TPEs (*24*). Maiti *et al.* reported the incorporation of homopolymers with fatty acid pendants to block copolymers via Reversible Addition Fragmentation Chain Transfer polymerization (RAFT). These monomers displayed crystalline behavior dependent on the size of the fatty acids (*25*).

Nonetheless, there is an absence in the literature regarding controlled radical polymerization strategies, such as RAFT, applied to triglycerides or to any other bulk multifunctional monomer.

Thermoplastic Elastomers

Thermoplastic elastomers (TPEs) are a class of polymer with elastic properties that are also able to be processed and recycled as thermoplastics. High strain, weak intermolecular forces, as well as reversible and immediate responses, are known properties of elastomers (*26*). They are composed of an amorphous domain enclosed by crystalline domains, see Figure 2. Crystalline domains are the commonly referred as the "hard" phase and the amorphous domains as the "soft" phase.

In Green Polymer Chemistry: Biobased Materials and Biocatalysis; Smith, et al.;
ACS Symposium Series; American Chemical Society: Washington, DC, 2015.

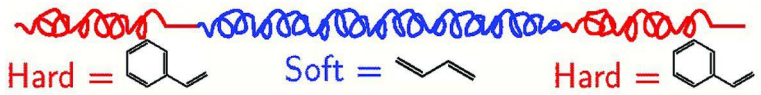

Figure 2. Representation of a typical styrenic block copolymer thermoplastic elastomer. The crystalline domains are colored in red while the amorphous domain is colored in blue.

There are six main TPE classes found commercially:

- styrenic block copolymers,
- polyolefin blends,
- elastomeric alloys,
- thermoplastic polyurethanes,
- thermoplastic copolyesters, and
- thermoplastic polyamides.

This contribution presents the use of acrylated epoxidized soybean oil (AESO) (with different degrees of acrylation) as a renewable substitute of the "soft" phase in the production of tunable branched, see Figure 3, styrenic based TPEs, *e.g.* styrene-butadiene-styrene (SBS), via RAFT.

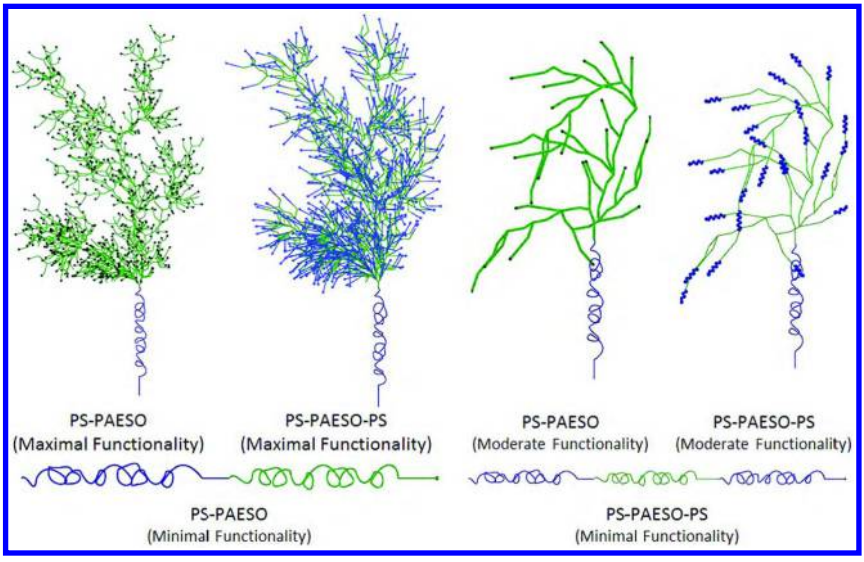

Figure 3. Representation of the different AESO derived styrenic block copolymers according to their degree of acrylation (functionality).

In Green Polymer Chemistry: Biobased Materials and Biocatalysis; Smith, et al.;
ACS Symposium Series; American Chemical Society: Washington, DC, 2015.

Publication Date (Web): June 18, 2015 | doi: 10.1021/bk-2015-1192.ch012

Publication Date (Web): June 18, 2015 | doi: 10.1021/bk-2015-1192.ch012

RAFT Polymerization

Due to controllled/living free radical polymerization (CFRP), high molecular weight hyperbranched polymers can be obtained without gelation (*27*). CFRP techniques such as atom transfer radical polymerization (ATRP) (*21*) and RAFT (*24*) have been recently used in the creation of styrene-based thermoplastic elastomers from vegetable oils. Glass transition temperatures (T_g) have been shown to range from as low as -40°C to as high as 25°C. Compared to ATRP, which requires the use of metal catalyst [Cu(I)/Cu(II)] and initiators, RAFT can be more environmental friendly as it only requires the use of an organic chain transfer agents to control polymerization.

RAFT polymerization follows the same initiation and radical-radical termination mechanism as conventional free radical polymerization (FRP). Unlike the extremely short propagation process in FRP (usually lasting only from 5 to 10 seconds before individual chains get terminated) RAFT process can effectively suppress living radicals from being terminated. Living radicals can be captured by the chain transfer agent and turned into dormant species. Subsequently, the rapid equilibrium between living radicals and dormant species enables polymer chains to have an equal chance to grow and survive the entire polymerization, see Figure 4.

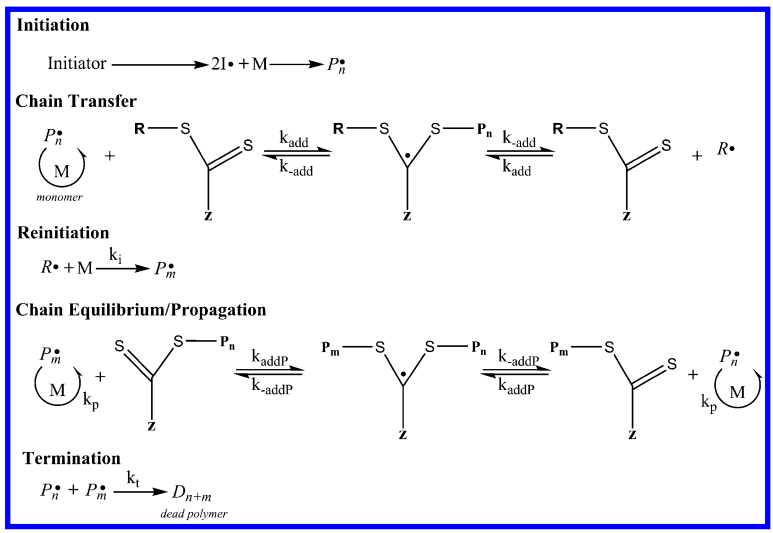

Figure 4. Main mechanism of RAFT polymerization (28, 29).

In 1998, RAFT was developed in Australia by G. Moad, E. Rizzardo and S. H. Tang from the Commonwealth Scientific and Industrial Research Organisation (*28*, *29*). Numbers of different architectural polymers have since been synthesized, including block copolymers, star polymers, dendritic polymers, hyperbranched polymers, etc. (*30*)

In Green Polymer Chemistry: Biobased Materials and Biocatalysis; Smith, et al.;
ACS Symposium Series; American Chemical Society: Washington, DC, 2015.

Experimental Section

Materials

Epoxidized soybean oil (ESO) (Archer Daniels Midland) was received and used without further purification. Soybean oil, epoxidized acrylate (Sigma-Aldrich) was purified by passing through a column packed with inhibitor remover and silica gel. 2,2′-azobis(isobutyronitrile) (AIBN, 98% Sigma-Aldrich) was recrystallized in ethanol prior to use. Ethyl 2-(ethoxycarbonothioylthio)-2-methylpropanoate (ETMP) was synthesized following method from Bergman *et al.* (*31*) 1,4-Dioxane (Reagent grade, Fisher), diethyl ether, acrylic acid, hydroquinone, toluene, and pyridine (99%) were used without further purification.

Publication Date (Web): June 18, 2015 | doi: 10.1021/bk-2015-1192.ch012

Synthesis

Acrylated Epoxidized Soybean Oil

20 grams of ESO, 9.94 grams of acrylic acid, and 3.8 grams of toluene were added into a 200 mL flask. 0.38 grams of pyridine and 1.40 grams of hydroquinone were added as catalyst and inhibitor, respectively. The reaction was carried out for 14 hours at 95 °C. Once the reaction reached room temperature, excess sodium bicarbonate was added to neutralize the system. Ethyl ether was added at a volume ratio of 1:1 ESO to ethyl ether. The product was then passed through a silica gel column, followed by rotary evaporation to remove excess solvent and dried on vacuum oven over night.

Chain Transfer Agent Synthesis

The procedure below is analogous to the method described by Bergman *et al.* (*31*) Potassium hydroxide (0.05 mol) was stirred in ethanol (20 mL) at room temperature until completely dissolved. Carbon disulfide (10 mL) was then added over 90 minutes, and the solution was allowed to stir for five hours. Ethyl α-bromoisobutyrate (14.8 mL) was added dropwise and the solution was stirred for 12 hours before the mixture was filtered and the solvent was removed by evaporation. The resulting yellow liquid was diluted with diethyl ether and passed through a chromatography column packed with basic alumina several times. Diethyl ether was removed by rotary evaporation and further dried using a vacuum oven overnight. ^{1}H-NMR (600 MHz): δ1.27 (t, 3H, **CH_3**CH_2), 1.39 (t, 3H, **CH_3**CH_2), δ1.61 (s, 6H, **CH_3**C), δ4.17 (m, 2H, **CH_2**CH_3), δ4.59 (m, 2H, **CH_2**CH_3).

In Green Polymer Chemistry: Biobased Materials and Biocatalysis; Smith, et al.;
ACS Symposium Series; American Chemical Society: Washington, DC, 2015.

RAFT Polymerization of Polystyrene Macro-CTA

Styrene, chain transfer agent (ETMP), AIBN and 1,4-dioxane were added into a round bottom flask. After the mixture was fully dissolved, argon was used to purge the solution for 20 min. The reaction was carried out at 90°C for 4 hours.

RAFT Polymerization of Poly(styrene-b-AESO)

For the synthesis of poly(styrene-b-AESO), AESO was dissolved in dioxane and transferred to the reaction vessel containing the styrene homopolymer and was allowed to react for 6 hours at 70°C before the reaction was cooled down and precipitated three times in excess methanol and water. The product was stirred in a 2:1 ratio by volume of methanol to ethanol solution to remove unreacted AESO monomer. The product was vacuum dried for 24 hours, at room temperature, see Figure 5.

Publication Date (Web): June 18, 2015 | doi: 10.1021/bk-2015-1192.ch012

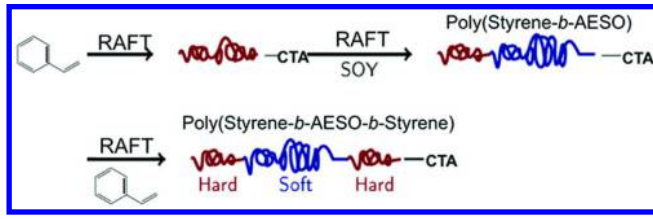

Figure 5. Representation of the RAFT polymerization process to synthesize styrene-soybean oil based thermoplastic diblock and triblock copolymers.

RAFT Polymerization of Poly(styrene-b-AESO-b-styrene)

For the synthesis of poly(styrene-b-AESO-b-styrene), the diblock was redissolved in dioxane, styrene and AIBN was added. The reaction vessel was bubbled with Argon for 1 hour and the reaction proceeded for 2 hours at 70°C. The final product was precipitated three times in excess methanol and water. The product was filtered and vacuum dried at room temperature for 24 hours, see Figure 6.

Publication Date (Web): June 18, 2015 | doi: 10.1021/bk-2015-1192.ch012

Figure 6. Image of a poly(styrene-b-AESO-styrene) triblock copolymer. Reproduced with permission from reference (32).

Results and Discussion

The use of RAFT polymerization has successfully produced vegetable oil based block copolymers with thermoplastic and elastic properties. This result is surprising since each polytriglyceride repeat unit has the potential to crosslink with at least one other polytriglyceride. When approximately a fraction of 1/N of such units have crosslinked (N denotes the average degree of polymerization), the polymers are said to be at their "gel point" at which an infinite polymer network has formed (*27*). Moreover, due to the multiple reaction sites of AESO, polymerizations tend to have larger polydispersity due to the different polymer chains growing at same time, see Figure 7.

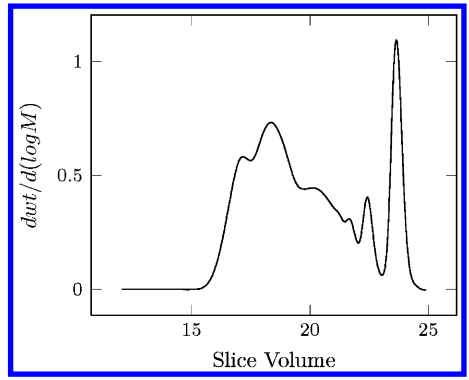

Figure 7. Typical size exclusion chromatography (SEC) trace of PAESO showing the multimodal nature of triglycerides growing at different rates.

In Green Polymer Chemistry: Biobased Materials and Biocatalysis; Smith, et al.;
ACS Symposium Series; American Chemical Society: Washington, DC, 2015.

Publication Date (Web): June 18, 2015 | doi: 10.1021/bk-2015-1192.ch012

We have discovered, however, that under the appropriate polymerization conditions (temperatures, solvent/monomer concentration, chain transfer agent (CTA)/Initiator) RAFT can sufficiently limit the polymerization of triglycerides so that they terminate at a desired molecular weight and block composition. Table 2 provides examples of four different poly(AESO) reaction conditions, with their corresponding monomer, initiator (AIBN) and CTA concentration, along with their reaction rate constant (k_a) and gelation time.

Table 2. Gelation Time, Rate Constant and Reaction Conditions

Reaction	*[Monomer] ×10⁴/ (mol/L)*	*[AIBN] ×10⁷/ (mol/L)*	*[CTA] ×10⁷/ (mol/L)*	*k_a / min⁻¹*	*Gelation time*
2	1.51	3.62	7.25	0.0116	58min
4	1.26	3.02	6.05	0.0095	--
1	1.51	1.45	7.25	0.0066	85min
3	1.26	1.21	6.05	0.0058	--

The reaction rate constant was calculated by taking aliquots and tracking the double bonds conversion of the product (using ^{1}H-NMR) over the reaction time, see Figure 8, where the ($[C=C]_0/[C=C]$) represents the double bond conversion.

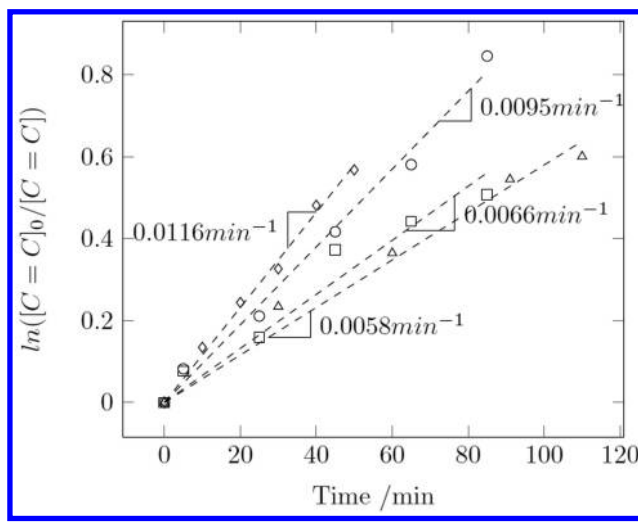

Figure 8. Graph showing conversion vs time of four different RAFT polymerizations of AESO.

To produce diblock and triblock copolymers, styrene was first polymerized to create the polystyrene macro-CTA to be used in the subsequent block copolymer synthesis. Its change in molecular weight (M_n) was tracked over time, see Figure 9(A).

Publication Date (Web): June 18, 2015 | doi: 10.1021/bk-2015-1192.ch012

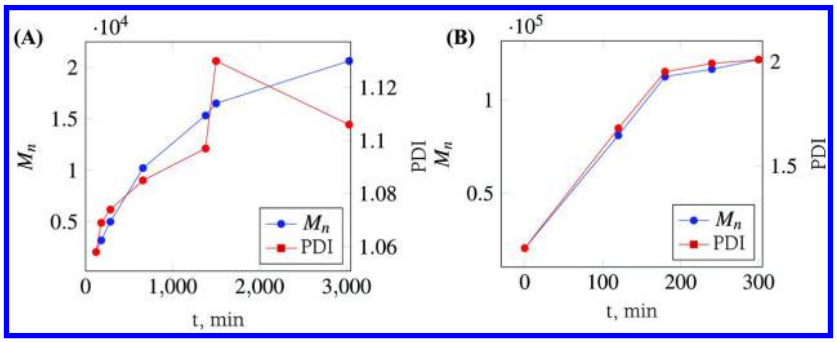

Figure 9. (A) Graph showing the molecular weight (number average) increase of the styrene homopolymer as a function of time. (B) Graph showing the molecular weight increase of the diblock as a function of time. Reproduced with permission from reference (27). Copyright 2014 The Royal Society of Chemistry.

Poly(styrene-*b*-AESO) was then synthesized and its M_n was monitored as a function of time, see Figure 9(B). Molecular weights and molecular weight distributions were determined via Size Exclusion Chromatograph (SEC) with respect to polystyrene standards using HPLC chloroform as the solvent and a Waters 2414 refractive index detector. After the addition of the final styrene block, the final product poly(styrene-*b*-AESO-*b*-styrene) (Figure 6) was subject to different characterization techniques. NMR was used to calculate the percentage of polystyrene in the product, see Figure 10, indicating a 22.4% styrene content. ^{1}H-NMR spectra were determined on a Varian VXR-300 spectrometer using deuterated chloroform ($CDCl_3$) as the solvent.

Publication Date (Web): June 18, 2015 | doi: 10.1021/bk-2015-1192.ch012

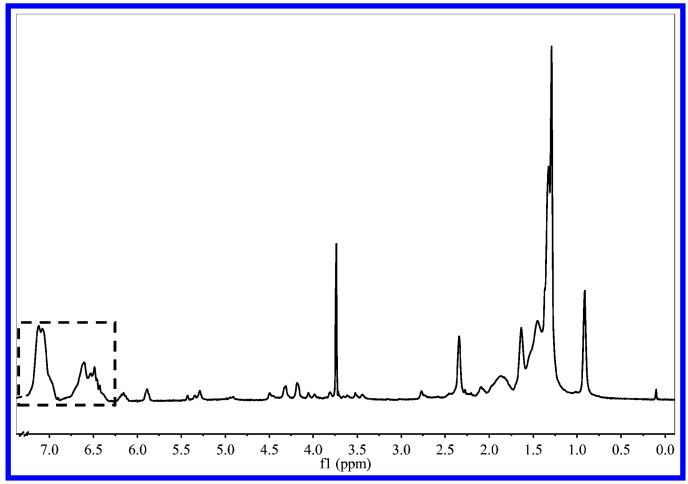

Figure 10. Graph showing the [1]H-NMR spectra of the poly(styrene-b-AESO-styrene) triblock, where the dashed rectangle shows the polystyrene location.

Differential scanning calorimetry (DSC), see Figure 11, showed the glass transition (Tg) for the PAESO at -10°C, however no visible Tg can be seen for the styrene. DSC experiments were conducted on a TA-Instruments Q2000 Differential Scanning Calorimeter equipped with liquid nitrogen cooling system (LNCS). Three consecutive heating and cooling cycles where done for each sample (-100°C to 150°C) using standard aluminum pans and a heating/cooling rate of 10°C/min. Dynamic shear rheology measurements were performed in a ARES Strain Control Dynamic Shear Rheometer equipped with a convection oven. The sample was tested in a parallel plate geometry using a frequency/ temperature dynamic sweep test (80 – -40°C and 1–100 rad/s) at a temperature decrement of 10°C and a strain of 2.5% (within the linear viscoelastic regime). Figure 12 shows the master curve of the poly(styrene-*b*-AESO-*b*-styrene) triblock copolymer at a reference temperature of T_{ref} = 80°C, showing liquid like behavior at high temperature/low frequency ($G' \propto \omega^2$), a rubbery plateau with modulus of $G_N^0 \approx$ 6.4 GPa, typical of a rubbery entangled thermoplastic, no glassy regime was observed at lower temperatures. As is evident from the master curve, the material follows the time temperature superposition principle, and the linear regression of the shift factors to the Williams-Landel-Ferry (WLF) model yields C_1=4.4 and C_2=95.2°C with a correlation coefficient of R^2 =0.998.

Publication Date (Web): June 18, 2015 | doi: 10.1021/bk-2015-1192.ch012

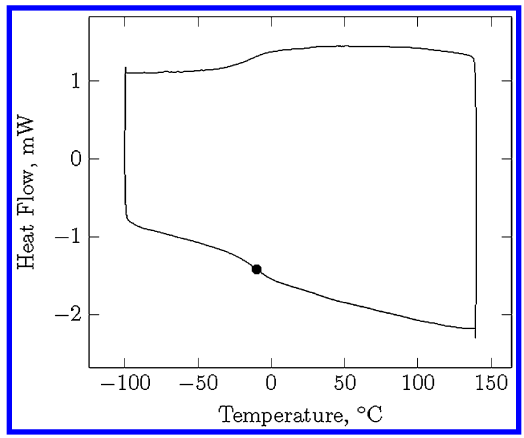

Figure 11. DSC plot of the poly(styrene-b-AESO-b-styrene) sample. The graph shows a Tg at -10°C for the PAESO, no Tg was detected for the PS.

Real-space images of BCPs were collected with a Tecnai G² F20 scanning/transmission electron microscope at a high tension voltage of 200 kV sections were stained with Osmium tetraoxide (OsO_4) before imaging. Real-space images of the poly(styrene-*b*-AESO-*b*-styrene) triblock copolymer reveal a semi-periodic microstructure having black colored styrene islands surrounded by the lighter AESO regions, see Figure 13. The ability of these polymers to microphase separate demonstrates that there is a strong incompatibility between the two blocks, hence the formation of a rich AESO and styrene microdomains (*27*).

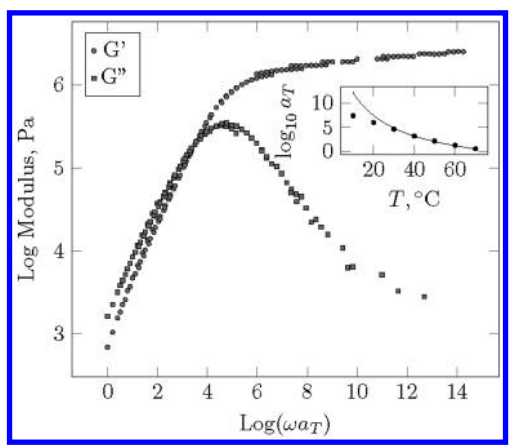

Figure 12. Master curve of poly(styrene-b-AESO-b-styrene) with Tref =80°C, with shift factors provided in the inset. The shift factors fit the WLF model well (r^2 = 0.998), with C_1 = 4.4 and C_2 = 95.2°C.

In Green Polymer Chemistry: Biobased Materials and Biocatalysis; Smith, et al.;
ACS Symposium Series; American Chemical Society: Washington, DC, 2015.

Publication Date (Web): June 18, 2015 | doi: 10.1021/bk-2015-1192.ch012

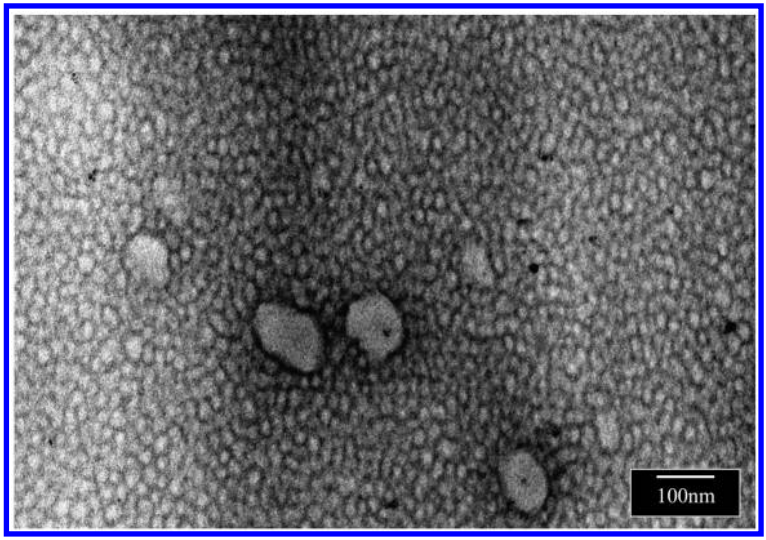

Figure 13. TEM image of the poly(styrene-b-AESO-b-styrene) triblock copolymer, image shows a percolation morphology of black islands (polystyrene) surrounded by lighter regions (poly(AESO)). Reproduced with permission from reference (27). Copyright 2014 The Royal Society of Chemistry.

Applications

Block copolymers containing styrene and butadiene, particularly the Kraton® SBS family of polymers have been used in a wide range of applications: from pressure sensitive adhesives, to tires, packaging materials, footwear, and as an asphalt modifier. Asphalt modification with SBS type TPEs is known to substantially improve the physical and mechanical properties of asphalt paving mixtures. TPEs increase asphalt elasticity at high temperatures, as a result of an increased storage modulus and a decreased phase angle, improving rutting resistance. In addition, they increase the complex modulus but lower the creep stiffness at low temperatures, improving cracking resistance (*21*).

For the past few years the price of butadiene, the principal component of SBS polymers, has increased dramaticallyand experienced a fair amount of variability. Moreover, with the accelerated growth in the developing markets and their need to construct roadway infrastructure, asphalt will face an increasing demand in the next decade. Thus the need for new types of cost effective, environment-friendly, polymers that can be used as replacements of the SBS type polymers in asphalt modification (*21*). This scenario creates an excellent opportunity to use poly(AESO) based polymers as asphalt modifiers in a market very forgiving in terms of material properties.

In Green Polymer Chemistry: Biobased Materials and Biocatalysis; Smith, et al.;
ACS Symposium Series; American Chemical Society: Washington, DC, 2015.

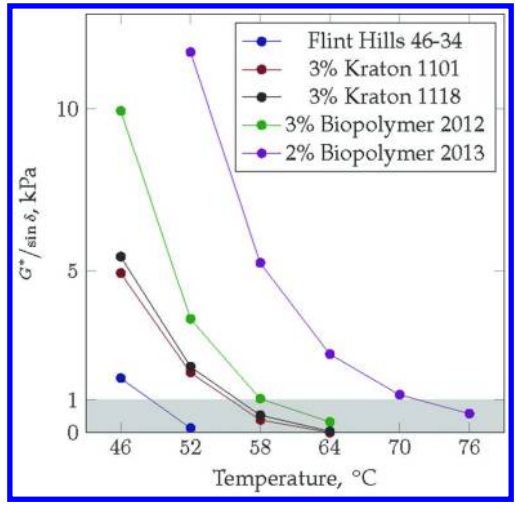

Figure 14. Graph shows the complex modulus (G) versus temperature of four polymer modified asphalts and the neat asphalt. The gray section represents industry's failure temperature. The higher the failing temperature the better the grade of the asphalt. Reproduced with permission from reference (27). Copyright 2014 The Royal Society of Chemistry.*

Asphalt modification tests were performed by the Civil Engineering Department at Iowa State University, led by Dr. Chris Williams. Initial tests were conducted on asphalt modified with two distinct poly(styrene-*b*-AESO-*b*-styrene) (refered to as Biopolymer 2012 and 2013) triblock copolymers and compared to unmodified asphalt (Flint Hills 46-34) and to asphalt modified with two commercially available SBS polymers: Kraton® D1101 and Kraton® D1118. Polymers were blended at a 3% weight with asphalt (with exception with biopolymer 2013 that was mixed at at 2% weight) in a shear mixer at 180°C for 2 hours and subsequently isochronally tested at 10 rad/s in a dynamic shear rheometer. This test is used to measure the elastic properties of the asphalt at different temperatures and to find the upper working temperatures, that can be found when the complex shear modulus crosses 1.1 kPa. Rheological testing results of the asphalt-polymer blends show the poly(styrene-*b*-AESO-*b*-styrene) triblock copolymers improves the complex shear modulus of the asphalt to a greater extent (failing temperature: 58°C and 72°C vs 55°C) than the commercially available SBS polymers, see Figure 14.

Conclusion

Advances in polymerization technology and in the understanding of renewable resources, *i.e.* vegetable oils, has led to the synthesis of soybean oil derived thermoplastic elastomers. SBS-like triblock copolymers were synthesized with styrene and acrylated epoxidized soybean oil, replacing the petroleum based butadiene. We found that RAFT polymerization allows the construction of

macromolecules with precisely defined degrees of polymerization and gives the ability to form complex molecular architectures such as block copolymers. This findings contrast the past two decades of research that yielded highly crosslinked materials through free radical polymerization and cationic polymerization of vegetable oils.

New applications for the biopolymers, see Figure 15, and improvements to the current polymerization techniques are now being investigated and will be reported in future communications.

Figure 15. Possible applications for the use of vegetable oil based TPEs. Reproduced with permission from reference (32).

Acknowledgments

The authors gratefully acknowledge financial support from NSF-DMR-0847515 and from the MRSEC Program of the National Science Foundation under Award Number DMR-0819885. The authors also acknowledge support from NSF ARI-R2 for funding the renovation of the research laboratories used for these studies.

In Green Polymer Chemistry: Biobased Materials and Biocatalysis; Smith, et al.;
ACS Symposium Series; American Chemical Society: Washington, DC, 2015.

Publication Date (Web): June 18, 2015 | doi: 10.1021/bk-2015-1192.ch012

References

1. Li, F.; Larock, R. C. Synthesis, Structure and Properties of New Tung Oil−Styrene−Divinylbenzene Copolymers Prepared by Thermal Polymerization. *Biomacromolecules* **2003**, *4*, 1018–1025.
2. Galià, M.; de Espinosa, L. M.; Ronda, J. C.; Lligadas, G.; Cádiz, V. Vegetable oil-based thermosetting polymers. *Eur. J. Lipid Sci. Technol.* **2010**, *112*, 87–96.
3. Larock, R.; Dong, X.; Chung, S.; Reddy, C. K.; Ehlers, L. Preparation of conjugated soybean oil and other natural oils and fatty acids by homogeneous transition metal catalysis. *J. Am. Oil Chem. Soc.* **2001**, *78*, 447–453.
4. Andjelkovic, D. D.; Larock, R. C. Novel Rubbers from Cationic Copolymerization of Soybean Oils and Dicyclopentadiene. 1. Synthesis and Characterization. *Biomacromolecules* **2006**, *7*, 927–936.
5. Crivello, J. V.; Narayan, R. Epoxidized Triglycerides as Renewable Monomers in Photoinitiated Cationic Polymerization. *Chem. Mater.* **1992**, *4*, 692–699.
6. White, J. E.; Earls, J. D.; Sherman, J. W.; López, L. C.; Dettloff, M. L. Step-growth polymerization of 10,11-epoxyundecanoic acid. Synthesis and properties of a new hydroxy-functionalized thermoplastic polyester. *Polymer* **2007**, *48*, 3990–3998.
7. Park, S. J.; Jin, F. L.; Lee, J. R. Synthesis and Thermal Properties of Epoxidized Vegetable Oil. *Macromol. Rapid Commun.* **2004**, *25*, 724–727.
8. Zlatanić, A.; Petrović, Z. S.; Dušek, K. Structure and Properties of Triolein-Based Polyurethane Networks. *Biomacromolecules* **2002**, *3*, 1048–1056.
9. Zhang, C.; Ding, R.; Kessler, M. R. Reduction of Epoxidized Vegetable Oils: A Novel Method to Prepare Bio-Based Polyols for Polyurethanes. *Macromol. Rapid Commun.* **2014**, *35*, 1068–1074.
10. Zhang, C.; Xia, Y.; Chen, R.; Huh, S.; Johnston, P. A.; Kessler, M. R. Soy-castor oil based polyols prepared using a solvent-free and catalyst-free method and polyurethanes therefrom. *Green Chem.* **2013**, *15*, 1477–1484.
11. Jose, J.; Pourfallah, G.; Merkley, D.; Li, S.; Bouzidi, L.; Leao, A. L.; Narine, S. S. Thermoplastic polyesters and co-polyesters derived from vegetable oil: synthesis and optimization of melt polycondensation for medium and long chain poly([small omega]-hydroxyfatty acid)s and their ester derivatives. *Polym. Chem.* **2014**, *5*, 3203–3213.
12. Guo, A.; Demydov, D.; Zhang, W.; Petrovic, Z. Polyols and Polyurethanes from Hydroformylation of Soybean Oil. *J. Polym. Environ.* **2002**, *10*, 49–52.
13. Wagner, H.; Luther, R.; Mang, T. Lubricant base fluids based on renewable raw materials: Their catalytic manufacture and modification. *Appl. Catal., A* **2001**, *221*, 429–442.
14. Desroches, M.; Escouvois, M.; Auvergne, R.; Caillol, S.; Boutevin, B. From Vegetable Oils to Polyurethanes: Synthetic Routes to Polyols and Main Industrial Products. *Polym. Rev.* **2012**, *52*, 38–79.
15. Nevin, C. S. Vicinal acryloxy hydroxy long chain fatty compounds andpolymers thereof. U.S. Patent 3,225,989, Dec. 21, 1965.

16. Wool, R.; Kusefoglu, S.; Palmese, G.; Khot, S.; Zhao, R. High modulus polymers and composites from plant oils. U.S. Patent 6,121,398 A, September 19, 2000.
17. Lu, J.; Khot, S.; Wool, R. P. New sheet molding compound resins from soybean oil. I. Synthesis and characterization. *Polymer* **2005**, *46*, 71–80.
18. Stockmayer, W. H. Theory of Molecular Size Distribution and Gel Formation in Branched-Chain Polymers. *J. Chem. Phys.* **1943**, *11*, 45–55.
19. Korolyov, G. V., Mogilevich, M. *Three-Dimensional Free-Radical Polymerization*; Springer-Verlag: Berlin Heidelberg, 2009.
20. Yang, L.; Dai, C.; Ma, L.; Lin, S. Conjugation of Soybean Oil and it's Free-Radical Copolymerization with Acrylonitrile. *J. Polym. Environ.* **2011**, *19*, 189–195.
21. Cochran, E. W.; Williams, R. C.; Hernandez, N. B.; Cascione, A. Thermoplastic elastomers via atom transfer radical polymerization of plant oil. U.S. Patent Application 2013/0184383 A1, July 18, 2013.
22. Matyjaszewski, K.; Patten, T. E.; Xia, J. Controlled/"Living" Radical Polymerization. Kinetics of the Homogeneous Atom Transfer Radical Polymerization of Styrene. *J. Am. Chem. Soc.* **1997**, *119*, 674–680.
23. Lodge, T. P.; Hiemenz, P. *Polymer Chemistry*; CRC Press Taylor & Francis Group: Boca Raton, FL, 2007.
24. Wang, S.; Vajjala Kesava, S.; Gomez, E. D.; Robertson, M. L. Sustainable Thermoplastic Elastomers Derived from Fatty Acids. *Macromolecules* **2013**, *46*, 7202–7212.
25. Maiti, B.; De, P. RAFT polymerization of fatty acid containing monomers: controlled synthesis of polymers from renewable resources. *RSC Adv.* **2013**, *3*, 24983–24990.
26. Shanks, R.; Kong, I., Thermoplastic Elastomers. In *Thermoplastic Elastomers*; El-Sonbati, A., Ed.; InTech: Rijeka, Croatia, 2012; pp 137−154.
27. Hernandez, N. B.; Williams, R. C.; Cochran, E. W. The battle for the "green" polymer. Different approaches for biopolymer synthesis: bioadvantaged vs. bioreplacement. *Org. Biomol. Chem.* **2014**, *12*, 2834–2849.
28. Moad, G.; Rizzardo, E.; Thang, S. H. Living Radical Polymerization by the RAFT Process. *Aust. J. Chem.* **2005**, *58*, 379–410.
29. D'Agosto, F. Handbook of RAFT Polymerization. *Macromol. Rapid Commun.* **2008**, *29*, 934–935.
30. Moad, G.; Rizzardo, E.; Thang, S. H. Living Radical Polymerization by the RAFT Process – A Second Update. *Aust. J. Chem.* **2009**, *62*, 1402–1472.
31. Bergman, J. A.; Hernandez, N. B.; Cochran, E. W.; Heinen, J. M. Thermodynamics of Chain Architecture in Acrylic Block Terpolymers. *Macromolecules* **2014**, *47*, 5960–5970.
32. Cochran, E. W.; Williams, R. C.; Hernandez, N. B.; Cascione, A. Thermoplastic elastomers via Reversible Addition-Fragmentation Chain Transfer polymerization of triglycerides. U.S. Patent Application 2014/0343192, November 11, 2014.

Publication Date (Web): June 18, 2015 | doi: 10.1021/bk-2015-1192.ch013

Chapter 13

From Biorefinery to Performance Technology: Transforming Renewable Olefinic Building Blocks into Lubricants and Other High-Value Products

Kathleen O'Leary Havelka* **and Gregory E. Gerhardt**

Elevance Renewable Sciences, Inc., 2501 Davey Road, Woodridge, Illinois 60517, U.S.A.
***E-mail: Kathleen.Havelka@elevance.com.**

Increasing performance requirements in a variety of markets and regulations toward more sustainable products and processes globally has led to high interest and investment in the chemical industry to research the properties of bio-based feedstocks as a sustainable and economical alternative to petroleum. This paper will review Elevance's biorefinery process that prepares building blocks from renewable feedstocks using a cross metathesis with olefins. The biorefinery outputs include olefins and esters that can be tailored to obtain desired properties for a broad range of applications. Data will be presented comparing Elevance's polymer and monomer technology to conventional technology. Examples of the benefits of this new polymer and monomer technology include Elevance's functionalized poly-α-olefins show improved formulation compatibility and cleanliness in operation versus conventional PAOs in synthetic lubricants. Elevance's newly commercialized monomer, octadecanedioic acid shows improved water and chemical resistance versus shorter chain alternatives. These are some examples of the advantages that building blocks from a cross metathesis of bio-based oils and olefins can provide across multiple market segments and application areas versus conventional building blocks.

In Green Polymer Chemistry: Biobased Materials and Biocatalysis; Smith, et al.;
ACS Symposium Series; American Chemical Society: Washington, DC, 2015.

Publication Date (Web): June 18, 2015 | doi: 10.1021/bk-2015-1192.ch013

Introduction

The transformation towards a bio-based economy is critical to sustainable chemical enterprise and offers significant opportunities for research and development. Bio-based technology development research and capacity accelerated in the mid-2000s and remains high today. Due to the availability of low cost renewable feedstocks, a number have shown improved performance from a variety of chemical, biological and catalytic transformations at industrial scale, including:

- Transesterification of vegetable oils (*1*): Recognized as a way to improve lubricant performance by replacing glycerol with monohydric alcohols and other polyols, such as 2-ethylhexanol and trimethylolpropane, respectively.
- Advanced genetic engineering: Can decrease the polyunsaturation that has led to the development and availability of high oleic oils (*2–4*).
- Synthetic biology: Can be used to design living yeasts, to convert plant-based sugars into renewable hydrocarbon molecules (*5*, *6*).
- Novel catalyst development: Takes advantage of the unsaturation found in natural oils through a metathesis process to produce high-performing specialty products and materials (*7*, *8*).

As a result, bio-based technology today is more advanced than in the past with new materials developed from new technology that are bio-based and offer very high performance. Additionally, these materials can be produced at scale cost competitively through manufacturing improvements and economies of scale (*9*). Lubricant researchers can use these new tools to meet and exceed properties obtained from current synthetic lubricants to enable optimal equipment performance while reducing impact on the environment. In particular, metathesis-processed renewable oils have the ability to generate building blocks that are derived from combining the best of two diverse chemistries, petroleum and bio-based at the molecular level, to obtain the benefits of each in a single, new product.

Metathesis Technology

Metathesis is a reversible reaction between two olefins, in which the double bonds are broken and then reformed into new olefin products as shown in Equation 1. Phillips Petroleum developed the first commercial process of olefin metathesis in the 1960s (*10*). The focus at that time, was to convert propylene into ethylene and 2-butene. Since metathesis is a reversible reaction and the demand for polymer grade propylene grew from the 1970s on, this led to the use of the Phillips Triolefin process in a reverse way.

In Green Polymer Chemistry: Biobased Materials and Biocatalysis; Smith, et al.;
ACS Symposium Series; American Chemical Society: Washington, DC, 2015.

Equation 1:

Publication Date (Web): June 18, 2015 | doi: 10.1021/bk-2015-1192.ch013

Until recent breakthroughs by Yves Chauvin (*11*), Robert H. Grubbs (*12*), and Richard R. Schrock (*13*), metathesis technology was limited to non-polar olefins. Chauvin and his student, Jean-Louis Herrison, characterized the reaction mechanism as representing a great step forward in understanding how the catalyst functions (*11*). This understanding enabled the fundamental research of Schrock and Grubbs to develop catalyst technologies that are significantly more efficient than traditional metathesis catalysts as well as being air stable and tolerant to polar groups. Grubbs and Schrock's contributions have transformed the development and production of a wide range of materials from fuels and lubricants to life-saving pharmaceuticals. Chauvin, Grubbs and Schrock were recognized for the importance of their work with a Nobel Prize in Chemistry in 2005 (*14*).

Elevance Technology - Metathesis

Elevance Renewable Sciences, Inc. (Elevance), which creates novel specialty chemicals from natural oils, uses proprietary metathesis catalyst technology to transform renewable oils into novel, high-performing ester, olefin and triglyceride molecules and multi-functional polymers (*15*). Compounds can be metathesized alone (self-metathesis) or in combination with another compound (cross-metathesis). Elevance's biorefinery design is based on the cross-metathesis of a natural oil with an α-olefin (*15*, *16*). These natural oils can come from a variety of plant and animal sources, including palm, mustard, soybean, canola, and when they become commercially available, jatropha or algal oils, enabling options that allow local sourcing to each refinery.

Elevance's metathesis reaction combines a natural oil with other co-reactants in the presence of a proprietary catalyst, producing olefins, oleochemicals and specialty chemicals. The olefins are removed by distillation and may be used mixed or further processed by fractionation. The remaining material is transesterified with alcohols to methyl esters. The reaction products are distilled to separate the oleochemicals from the specialty chemicals as shown in Figure 1.

The specialty chemical molecule contains unsaturation and ester functionality, creating a molecule with olefin and mid-chain length oleochemical attributes previously unavailable at commercial scale. The difunctional specialty chemicals are derivatized into a variety of materials for lubricant, polymer and consumer ingredient markets.

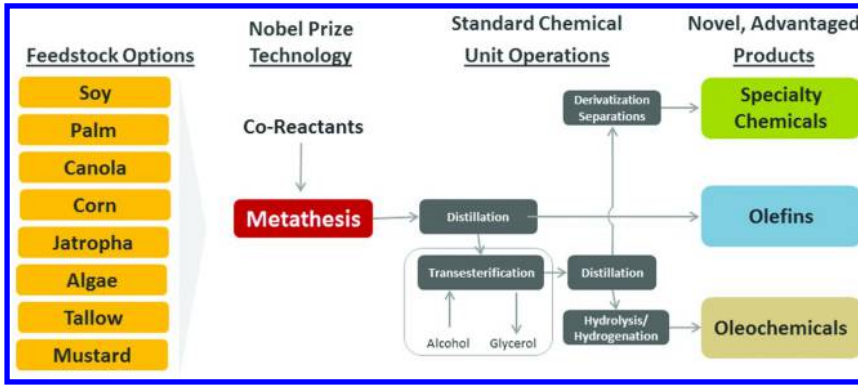

Figure 1. Metathesis Biorefinery Process (15, 16).

Publication Date (Web): June 18, 2015 | doi: 10.1021/bk-2015-1192.ch013

Structure-Property Relationships

The di-functional reaction products of metathesis-processed natural oils provide versatile chemical building blocks to synthesize new structures with improved properties, e.g., compatibility and water resistance. These transformations cannot be done easily with petroleum starting materials. The di-functional materials provide the ability to create novel molecular architectures, by controlling polarity, molecular weight, geometry and degree of branching. This versatility has been applied to design and syntheses of new structures that provide improved properties across a broad range of applications (*17*). This paper will review and discuss the rationale behind the design of selected chemistries, platform chemicals and novel structures that have been synthesized from these building blocks.

Derivitization 9-Decenoic Acid Methyl Ester (9-DAME)

9-decenoic acid methyl ester (9-DAME) is an exciting new platform chemical with olefin and carboxylate. This difunctionality provides a variety of derivatization and innovation possibilities as shown in Figure 2. All the transformations shown have been successfully accomplished (*17*), enabling completely different structures, branching and geometries. Like acrylic acid (a product with a similar di-functional structure), 9-DAME is potentially a platform chemical that can be used as a building block for a wide variety of applications and industries (*18*).

In Green Polymer Chemistry: Biobased Materials and Biocatalysis; Smith, et al.;
ACS Symposium Series; American Chemical Society: Washington, DC, 2015.

Publication Date (Web): June 18, 2015 | doi: 10.1021/bk-2015-1192.ch013

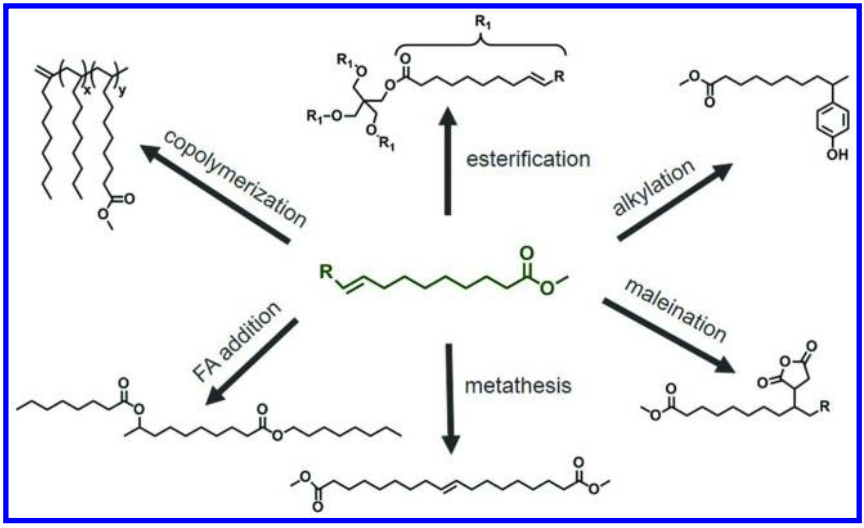

Figure 2. Applications of 9-Decenoic Acid Methyl Ester as a Building Block.

This paper will present examples and discuss the broad range of properties that are obtainable, and the increased performance possible across the spectrum of commercial markets, including: consumer ingredients, engineering polymers, coatings, lubricants and additives.

Diacids

Another example of a specialty building block that can come from metathesis of renewable oils are diacids. The diacids can be made from metathesis of vegetable oils and 9-DAME. An example is Elevance Inherent™ C18 Diacid, as shown below in figure 3, was commercialized on Sept. 17, 2013 (*19*).

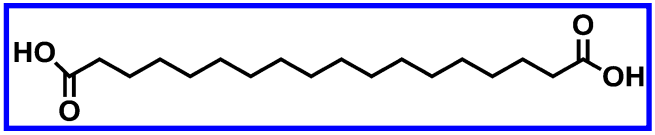

Figure 3. Elevance Inherent™ C18 Diacid.

Elevance Inherent™ C18 Diacid is a mid-chain length, bio-based diacid that enables producers of polyamides and polyurethanes, lubricants and adhesives to significantly expand their portfolios. It allows for cost-competitive products that demonstrate performance not possible from products made with more common, shorter-chain diacids.

Using Elevance Inherent™ C18 Diacid in polyester polyols enables the creation of new, previously unattainable pre-polymers. It helps polyurethane manufacturers create polymers with exceptional solvent resistance, hydrolytic

stability, optical clarity and toughness that will benefit automotive, food service, medical and other markets (*20*). It also has shown excellent performance in greases as a reactive intermediate.

Functionalized Poly-α-Olefins (PAOs)

In addition to specialty building blocks being made from metathesis of renewable oils, olefins are made. α-Olefins, such as 1-decene, from the Biorefinery have been converted into Green PAO, as shown in Figure 4A, using conventional PAO oligomerization processes (*21*), and it performs like conventional PAO. The main drawback to PAO is that it is very non-polar and as a result, additive solvency aids are frequently added to compatibilize PAO with polar lubricant additives. These compatibilizers are often esters. Polymer esters can also be synthesized by oligomerizing 9-decene methyl ester (9-DAME) (*22*), which are interesting and highly polar new structures as shown in Figure 4B. The structure with the most potential in being PAO-like with improved solvency is one where an olefin and 9-DAME are copolymerized into a functionalized PAO as shown in Figure 4C.

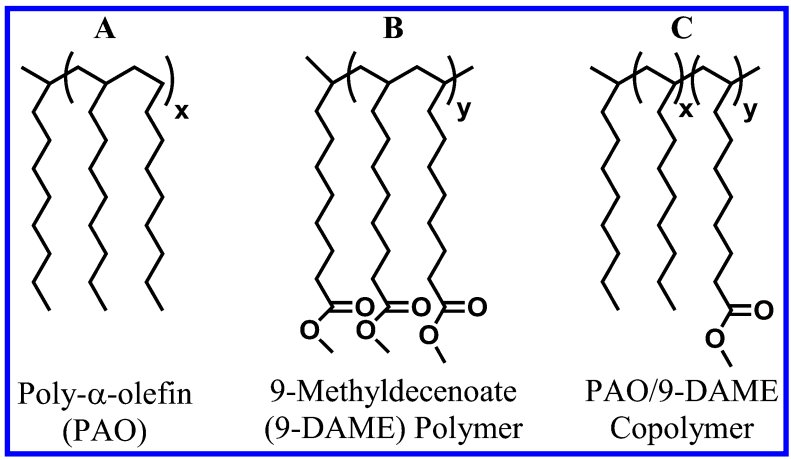

Figure 4. Poly-α-olefin and Poly-9-DAME homo and copolymers.

The PAO/9-DAME copolymer takes advantage of the PAO structure while slightly increasing its polarity to increase its formulation compatibility and its affinity to associate with surfaces to provide reduced friction and wear. In fact a copolymer was recently launched under the name Elevance Aria™ WTP 40 (mentioned above) at the 18th annual ICIS World Base Oils & Lubricants Conference on Feb. 19, 2014.

Homo- and co-polymers have been made of varying molecular weight that provide low- to high-viscosity PAO and functionalized PAOs (*23*). PAO is commercially manufactured by varying catalysts and process conditions to produce a range of oligomers of various molecular weights (*24*). There are no

Publication Date (Web): June 18, 2015 | doi: 10.1021/bk-2015-1192.ch013

synthesis tools in conventional PAO manufacturing to control polarity. The polarity of the co-polymer shown in Figure 4C has been adjusted by varying the ratio of the olefin to the olefin esters, and the copolymers molecular weight. Additionally the ester in 4B and 4C can undergo further reactions to modify its polarity and viscosity. Elevance Aria™ WTP 40 is a new and novel synthetic base stock that shows differentiated and improved performance as compared to PAO 40, and mixtures of PAO 40 and ester, such as improved formulation compatibility, cleanliness and friction and wear reduction to help improve fuel economy and extend equipment life.

Applications of Biorefinery Streams to High-Value Products

Metathesis-processed renewable oils have broad application in several large and growing markets that are grouped into three platforms: Consumer & Industrial Ingredients; Engineered Polymers & Coatings; and Lubricants & Additives.

Consumer and Industrial Ingredients

Elevance's Consumer & Industrial Ingredients platform provides category-changing performance through novel materials that are available today. In the personal care and cleaning markets, the metathesis technology offers a range of renewable olefins that can be converted to drop-in renewable alternatives to existing petroleum-based materials in the market today, such as alkanes and PAO. It also offers novel ingredients and di-functional building blocks that provide unique physical and performance characteristics as routes to high-performing products that meet market needs, examples include: natural emollients with silicone feel, cold water detergent boosters and low VOC, high-performing cleaners (*18*).

Some recent product development include Elevance Smooth, a line of plant-based multi-functional polymers, and Elevance Soft, a line of plant-based emollients, are the first personal care product lines for use in a wide range of personal care applications (*25*). As well as being derived from renewables, they have excellent spreading power while providing a non-greasy after feel in personal care formulations. In the surfactant market, Stepan Company recently announced a powerful new cleaning solution, STEPOSOL® MET-10U that is the first commercial product launched by Stepan as part of its joint development agreement with Elevance (*26*). The novel surfactant is derived from natural oils, delivering superior performance with a smaller environmental footprint as compared to solvents.

Engineered Polymers and Coatings

Elevance's Engineered Polymers & Coatings platform provides proprietary technology and unique feedstock products that enable new and expanded engineering polymer product lines (*27*). This enables one to efficiently address industry challenges, including moisture uptake or chemical resistance, enhanced

Publication Date (Web): June 18, 2015 | doi: 10.1021/bk-2015-1192.ch013

product clarity and electrical properties, and the adhesion of dissimilar materials (*28*). The initial target markets for Engineered Polymers & Coatings are high-performance polymers that can be made from Elevance's di-functional building block molecules. The three sub-segments where di-functional building blocks show high potential for innovation include:

- specialty polyamides, polyesters and polyols
- epoxies and polyurethanes
- coatings and adhesives

Key end-use applications include automotive (under-the-hood applications, cables and hoses) (*29*) electrical and electronics (electronic components, wire and cable, and cell phones) (*30*); fibers and textiles (carpet, high-performance canvas, bristles and filters) (*31*).

Epoxies and polyurethanes are commonly used as high-performance coatings to provide resistance to chemicals, heat and corrosion (*32*). The commercial availability of Elevance Inherent™ C18 Diacid (octadecanedioic acid) enables producers of polyamides and polyurethanes, lubricants and adhesives to significantly expand their portfolios with cost-competitive products that demonstrate performance not possible from products made with more common, shorter-chain diacids.

Publication Date (Web): June 18, 2015 | doi: 10.1021/bk-2015-1192.ch013

Lubricants and Additives

There are several key market drivers of the lubricant industry that currently and in the future will significantly influence product designs (*33*).

1. Emission and fuel economy regulations continue to tighten in developed and emerging economies (*34*). Consumers and governments demand higher fuel economy and lower emissions from an economic and health perspective.
2. OEMs are responding to regulations in part by redesigning powertrains. Changes include: lighter-weight materials (*35*); redesigned equipment; increased use of coating technologies on moving parts (*36*); and more power from smaller displacement engines. OEM response to regulations is increasing performance demands on lubricants.
3. Globalization and sustainability are megatrends that are influencing society, politicians, consumers, industry executives and the lubricant industry. Consumers want more sustainable products (*37*), and this is driving more environmentally sustainable and high-performing solutions globally.

The net result is that lubricants are shifting in technology toward higher quality and higher performance (*38*), and the lubricant industry is becoming more complex with an increasingly diverse range of equipment designs (*39*), performance targets and geographic customized solutions. Therefore, these solutions must meet the

ever-changing landscape of performance and environmental needs without any performance detriment. Synthetic and bio-based synthetic base stocks are potential solution (*40*).

Lubricants and Additives Market Drivers

Globally, high-performance synthetic base oils represent the fastest growing segment of the lubricant base oils market (*41*). This growth is largely driven by increased demand from consumers and OEMs for higher fuel efficiency and increased equipment performance. Renewable building blocks have the ability to replace critical feedstocks for PAOs, POEs and other high-value base stocks. Base stocks and fuels are typically enhanced with additives that allow a given product to meet performance requirements that the fuel or lubricant alone is not able to achieve. Several additives that are bio-based have the potential to improve cold flow properties, increase lubricity and detergency in fuels and lubricants, improving fuel economy and increasing equipment life.

Higher-performing lubricants are needed to meet future lubricant performance and sustainability needs. Elevance's bio-based base stocks are enabling its partners and customers the uniformity, consistency and performance previously only available from petroleum and synthetic ester base oils. Elevance recently expanded commercial availability of Elevance Aria™ WTP 40, a high-viscosity lubricant base stock that combines the composition and properties of two key synthetic base stock technologies into a single, high-performance molecule designed to provide differentiated performance in broad markets such as engine and gear lubricants, industrial and hydraulic fluids, and greases. It is discussed in more detail below.

Bio-Based Lubricants

Bio-based lubricants have long been part of the lubricants market. Evidence of animal fat used as a lubricant has been found in ancient remains dating to 1400 B.C. (*42*) Animal fat and vegetable oils were the main lubricant materials until the birth of the petroleum industry in 1859. While the definition of bio-based lubricants varies, in this paper, bio-based lubricants are defined as lubricants derived from renewable materials.

Historically, bio-based lubricants range from vegetable oils to simple and complex esters derived from renewable oils (*43*), such as the fatty acids from fats and oils reacted with alcohols or polyols to produce esters such as trimethylolpropane (TMP) trioleate. Vegetable oil lubricants offer biodegradability, renewability and high viscosity index making them an excellent choice for environmentally sensitive applications (*44*). Overcoming vegetable oils inherent drawbacks of oxidative instability, poor low temperature properties and emulsibility is required to better compete commercially with products based on mineral oils (*45*).

Publication Date (Web): June 18, 2015 | doi: 10.1021/bk-2015-1192.ch013

In Green Polymer Chemistry: Biobased Materials and Biocatalysis; Smith, et al.;
ACS Symposium Series; American Chemical Society: Washington, DC, 2015.

Base Stock and Additive Market

The lubricant base stock market comprises two main categories: mineral and synthetic (*43*).

- Mineral base stocks are complex mixtures of hydrocarbons and paraffins obtained from refined crude oil. This includes American Petroleum Institute (API) Groups I, II and III (*43*).
- Synthetic base stocks are produced from chemical synthesis (*43*), tailored to have a controlled molecular structure with predictable properties and contain low or no sulphur or aromatic impurities. This includes API Groups IV and V (*43*). Mineral oil Group III base oil has a unique acceptance of being classified as "synthetic" in many parts of the world including the United States despite being obtained from refined crude oil due to Group III's high quality and performance profile (*46*).

Table 1 details the composition and physical properties of base stock groups. API base stock definitions are composition and physical properties with the exception of Group IV poly-α-olefins (PAO), which is feedstock and chemical structurebased (*47*).

Table 1. API Base Stock Groups

Base Stock Group	*Weight, % Sulphur*	*Weight, % Saturates*	*Viscosity Index (VI)*
I	>0.03	and/or <90	80 - 119
II	<0.03	>90	80 - 119
III	<0.03	>90	120 +
IV	All poly-α-olefins (PAO)		
V	All other base stocks not included in Groups I, II, III, IV. Example Group V base stocks are esters, phosphate esters, polyalkyleneglycols, silicones.		

Synthetic base stocks are the base oil of choice for high-performance lubricant applications because of the physical properties that are obtained through molecular control of the structures. Group IV is poly-α-olefin (PAO) that is made by the catalytic oligomerization of alpha olefins. PAO is recognized as a top-tier base stock in engine applications because of its high viscosity index (VI) that indicates a wide operating temperature range, low volatility and excellent low-temperature properties. Group V is defined as all other chemically synthesized base stocks.

In Green Polymer Chemistry: Biobased Materials and Biocatalysis; Smith, et al.;
ACS Symposium Series; American Chemical Society: Washington, DC, 2015.

Within Group V, the key materials of commercial importance are alkyl esters, such as polyolester (POE), polyalkylene glycol (PAG) and phosphate esters. Group V base stocks are the preferred lubricant base oil for some severe applications. Esters have been used exclusively in aviation lubricants for more than 40 years worldwide due to their high viscosity index, flowability at low temperatures, clean operation at high temperatures and low volatility. Frequently, esters are mixed with other base stocks to enhance and balance lubricant properties. Synthetic and bio-based synthetic lubricants are the fastest growing segment of the lubricants base stock market because they offer the possibility of addressing sustainability through performance and renewability (*48*).

Synthetic and Bio-based Base Stocks and Additive Characteristics

Synthetic base stocks are made by controlling the molecular architecture of the base oil. PAOs are produced by catalytically oligomerizing α-olefins (*49*). Di-functional specialty chemicals offer synthetic flexibility including oligomerization, condensation and transesterification to produce functionalized base oils that provide the wide temperature performance and stability of PAOs combined with the functional attributes of esters. This versatility provides access to base stocks that are inherently more compatible with the additive packages (*50*), with increased lubricity and solvency, helping to improve fuel economy and increase wear and sludge resistance (*51*). The base stocks produced with metathesized natural oil biorefinery outputs can be made to a wide range of viscosities, from very low to high (*52*).

The most important property of a lubricant is the viscosity; viscosity is the fluid's resistance to flow. High viscosity means that a fluid is thicker and does not flow as easily. For example, honey has a much higher viscosity than water. The viscosity of oil is usually between that of water and honey. A higher viscosity fluid will typically make a thicker film between moving surfaces and support greater loads. Multi-grade oils are essential for the longevity of modern engines as the oil needs to be capable of providing protection at both high and low temperatures (*53*). Most modern engine oils are multi-grade to suite the climate where it is used and are identifiable through the label such as 5W-30. The 5W-30 label means that the oil falls into two viscosity grades. In this case, 5W for winter grade indicates that it flows at very low temperature and the 30 indicates that its viscosity is 30 cSt at 100C (*53*). Multi-grades are made possible by viscosity modifiers (a polymer) (*54*), which slows down the rate of thinning as the oil warms up and slows down the rate of thickening as the oil cools down.

The thickness of the fluid film and operating conditions determine the lubrication condition requirements. The viscosity of the lubricant must be correct to protect parts from very high shock loads (*55*), and the chemical structure must protect the surfaces during contact. The base stocks made with biorefinery outputs have high viscosity index (*56*), predicting good performance across a wide operating temperature range that will be seen in automotive and in industrial lubricants. Other applications suited to biorefinery outputs include metalworking fluids, hydraulic fluids and greases (*57*).

In Green Polymer Chemistry: Biobased Materials and Biocatalysis; Smith, et al.;
ACS Symposium Series; American Chemical Society: Washington, DC, 2015.

Publication Date (Web): June 18, 2015 | doi: 10.1021/bk-2015-1192.ch013

In lubricant additives, applications for metathesized natural oils are quite diverse and can include processing aids (*58*) as well as performance components that reduce friction and increase cleanliness. Metathesized natural oils have shown promise as additives for greases by reducing the time and temperature needed to form a complex grease (*59*). Metathesized natural oils can also act as friction modifiers (*60*). Friction modifiers are added to lubricants to reduce the surface friction of the moving parts. Typically friction modifiers are polar compounds that have a high affinity for metal surfaces and possess long alkyl chains to provide lubricity (*61*). Metathesized natural oils have these inherent properties and can be further derivatized with polar groups and alkyl chains to produce lower coefficients of friction to help improve fuel economy and reduce wear.

Publication Date (Web): June 18, 2015 | doi: 10.1021/bk-2015-1192.ch013

Lubricant Applications

Lubricants are divided into different categories based on their application and classified by viscosity. Viscosity is considered to be the most important indicator of suitability for lubricant applications (*62*) in automotive, industrial, hydraulic fluids and metalworking. Viscosity is major contributor to lubricating efficiency. Viscosity, chemistry of the base oil and additives are critically important in to lubricant performance, including: friction loss, heat generation, mechanical efficiency, load carrying capacity, film thickness, lubricant flow and wear.

Engine Oils

Engine oils represent the largest volume segment (*63*) in the lubricant market. Mineral oil-based lubricants are the largest in volume in the market. Synthetic lubricants are the fastest growing part of the market because of their cost-performance characteristics. Synthetic motor oil offers significantly longer drain intervals (period between oil changes) and can improve fuel economy (*64*). An important strategy to improve fuel economy (*65*) is low viscosity lubricant formulations that have low volatility and have good low temperature properties.

These properties are typically investigated by looking at the NOACK volatility (ASTM D5800) versus kinematic viscosity (KV) (ASTM D445) at 100°C and NOACK Volatility versus Cold Crank Simulator (CCS) (ASTM D5293-08) at -30C of base stocks as shown in Figure 5 and 5B, respectively. Predicted fuel economy performance improves as NOACK and CCS results move toward the lower left hand corner on both charts (*66*). Figure 5A simulates viscosity under operating conditions. Typically, the lower the viscosity, the higher the volatility. If an oil is too volatile, it will experience viscosity increase during operation from evaporative losses of low molecular weight fractions and higher viscosity fractions increase. Viscosity increase may be detrimental to performance in terms of reducing fuel economy and potentially resulting in bulk viscosities becoming "out of grade," that is bulk lubricant viscosity rising above the recommended viscosity grades for the equipment.

The order of improved performance shown in Figure 5A is Group III < Group IV (PAO) < Elevance bio-based oil. The low volatility of the very low viscosity base stocks is due to the intermolecular association occurring in the Elevance base stock but cannot occur in the non-polar systems. Figure 5B represents viscosity under cold start conditions; the order of improved performance again is Group III < Group IV (PAO) < Elevance bio-based oil. The improved low temperature properties of Elevance bio-based oil is attributed to the unique chemical structure that interferes with molecular packing and consequently prevents gelling at low temperatures.

Publication Date (Web): June 18, 2015 | doi: 10.1021/bk-2015-1192.ch013

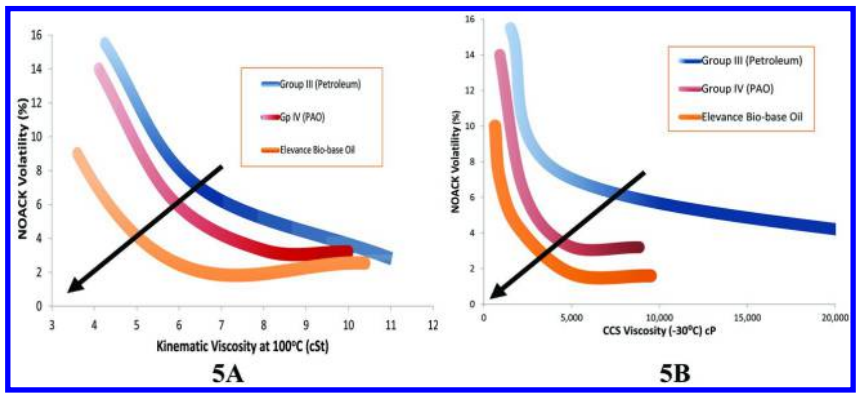

Figure 5. NOACK Volatility vs. KV @ 100°C (A) vs CCS @ - 30°C (B).

Reducing lubricant viscosity reduces the energy needed to pump lubricants in an engine and resistance (friction) of moving two lubricated metal parts across each other. Reducing viscosity, however, will also reduce the thickness of the lubricating film that can negatively impact engine metal protection and cause a detrimental effect on wear at operating temperatures. The mini-traction-machine (MTM) is a rolling and sliding test that mimics friction and wear conditions of equipment by independently varying load, speed and temperature (*67*). It directly measures friction and indirectly measures wear as shown in the MTM data in Figure 6. The MTM test was ran at 115°C under tribological conditions that mimic the engine in operation. The data indicates the coefficient of friction is reduced in the following order - Group III > Group IV (PAO) > Elevance bio-based oil. The micrographs showed lowest scratching on the surface, which infers improved wear protection for Elevance bio-base oil (*68*).

In Green Polymer Chemistry: Biobased Materials and Biocatalysis; Smith, et al.;
ACS Symposium Series; American Chemical Society: Washington, DC, 2015.

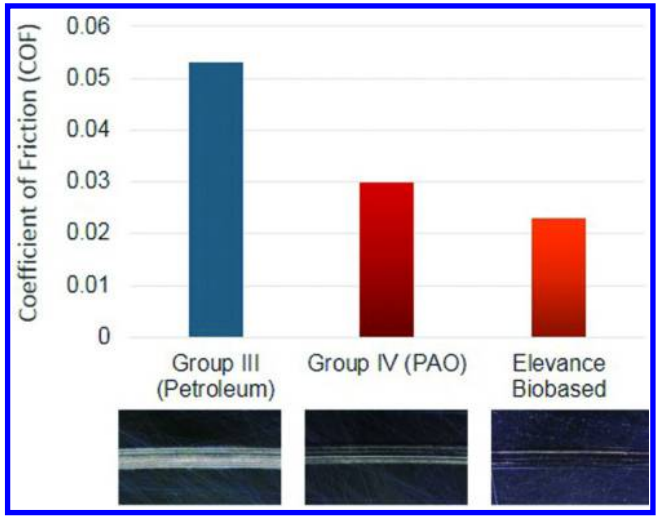

Figure 6. Coefficient of Friction Data and Wear Micrographs at 115°C.

Publication Date (Web): June 18, 2015 | doi: 10.1021/bk-2015-1192.ch013

These data indicate that Elevance bio-based oils provide good lubricity to improve fuel economy and may lower wear to increase protection of the engine.

Industrial and Automotive Gear Oils

Synthetic industrial and automotive gear oils operate under severe service conditions that require lubricants that are highly stable under extreme operating conditions (*69*). Higher viscosity synthetic base stocks, ranging from a kinematic viscosity (KV) at 100°C from 40 to 100 cSt, are often used in lubricant formulations to provide increased film thickness at high temperatures and protection during shock loading. PAO 40 is often used, because it has high viscosity, low volatility, high thermal oxidation resistance and high viscosity index that translate to broad operating temperature range (*49*). The main drawback for high viscosity PAO base stock is its nonpolar characteristics, limiting its compatibility with additive systems that contain polar groups.

To improve additive solubility and formulation stability of PAO base stock containing lubricants, lubricant formulators typically add a compatibilizer such as adipate esters or polyol esters (*70*). The esters can also provide additional cleanliness benefits in operation. The drawback to use of esters is the potential

for elastomer or seal swelling (*71*) due to their high polarity and relatively small molecular weight. It would be desirable to have the PAO performance and ester functionality in one molecule with polarity matched to the needs of modern additive packages. This concept has the potential of giving the best of both worlds in terms of lubricant performance, formulation stability and seal compatibility. Elevance's bio-based Aria WTP 40 (*56*) compares favorably to PAO 40 (*72*). It has higher viscosity index indicating a broad operating temperature range, and it has additional solvency as demonstrated by the reduction in aniline point as shown in Table 2.

Publication Date (Web): June 18, 2015 | doi: 10.1021/bk-2015-1192.ch013

Table 2. Comparison of PAO 40 and Elevance Aria™ WTP 40

Base Stock Characteristic	*Test*	*Elevance Aria™ WTP 40*	*Commercial PAO 40*
KV 100°C*	ASTM D445	40	39
KV 40°C*	ASTM D445	304	396
Viscosity Index*	ASTM D2270	165	143
Pour Point, °C*	ASTM D97	-34	-33
Aniline Point, °C	ASTM D611	99	160

* *Data from producer PAO 40 product data sheet* (*72*).

To determine if the increase in solvency translates to a benefit in the application, an API GL-5 (80W-90) gear oil formulation was blended. API GL-5 lubricant was also blended with 100 percent PAO 40 base stock which did not solubilize all the commercial additive package as demonstrated by the hazy appearance of the PAO 40 and additive formulation. Due to the hazy appearance, 10 percent ester was added to compatibilize the additive package with PAO 40 as recommended by the additive package producer. Since the ester reduced the viscosity of PAO 40 formulation, Elevance Aria™ WTP 40 lubricant formulation contains 10 percent PAO 4 to equalize the viscosity of the two formulations. Equal viscosity is important to ensure viscosity is not a variable contributing to differences in performance. The formulations were then used in bench tests designed to simulate gear oil operating conditions, i.e., 4-ball wear (ASTM D4172) and MTM (*73*). The data is summarized in Figure 7. The 4-ball wear tests showed lower wear scar diameter, and the MTM showed lower friction for the bio-based Elevance Aria™ WTP 40 formulation from 0 to 50% slide to roll ratio (*74*). This implies that Elevance Aria™ WTP 40 adsorbed on the friction surfaces and formed a tribofilm that protects the components.

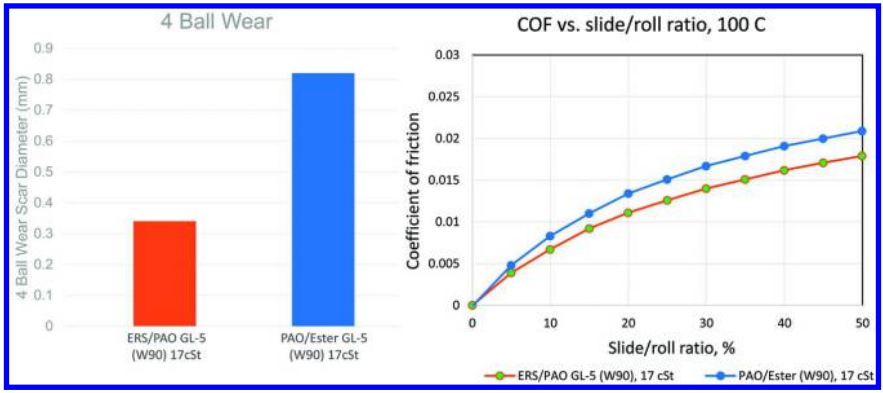

Figure 7. 4-Ball Wear and MTM Friction Comparison of PAO 40 and Aria WTP 40.

The friction and wear data are very encouraging for the bio-based base stock.

Additional tests of the same formulations was conducted to determine the ability to improve cleanliness. An automotive gear bench test, L-60-1 (ASTM D 5704) thermal and oxidative stability performance test, was used. L-60-1 performance test was chosen because it is a gear lubricant test that determines the cleanliness of the large and small gear and deterioration of finished lubricants under severe conditions. The gear lubricants were tested for 50 hours at elevated temperatures in the presence of air and copper. At the end of test, the large and small gears and the used oil were analyzed. Both formulations passed the test as shown in Table 3 and Figure 8. However, the formulation containing bio-based Elevance Aria™ WTP 40 demonstrated improved cleanliness versus PAO 40/ester-based API GL-5 lubricant. Elevance Aria™ WTP 40 performance is particularly impressive in the gear visual rating (Fig. 8) which indicate reduced varnish and sludge, making it potentially well suited for protecting equipment in severe service applications.

Table 3. L-60-1 Data for PAO 40 vs Elevance Aria™ WTP 40 in API GL-5 Lubricant Formulation

Base oils in API GL-5 finished lubricant formulation	*KV @ 100°C (cSt)*	*Varnish[1] (Rating)*	*Sludge[1] (Rating)*
API GL-5 Spec		>7.5	>9.4
PAO 40 / ester	28	8	9.5
Elevance Aria™ WTP 40	28	10	9.7

[1] *Higher value ratings indicate improved performance.*

Publication Date (Web): June 18, 2015 | doi: 10.1021/bk-2015-1192.ch013

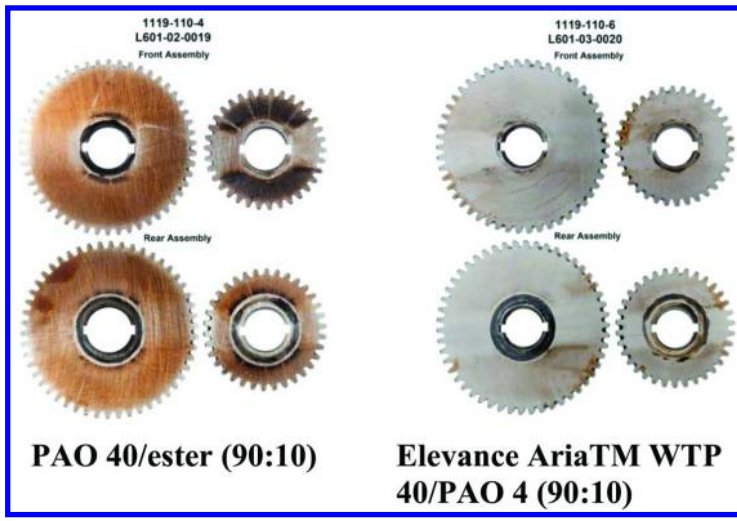

Figure 8. L-60-1 (ASTM D5704) Results Comparison of PAO40 and Aria WTP 40-based Formulations.

Publication Date (Web): June 18, 2015 | doi: 10.1021/bk-2015-1192.ch013

Grease Applications

The most viscous lubricant is a grease. Like other lubricants, it contains a base oil and additives. In addition, grease contains thickeners that form a matrix holding the lubricant (base oil and additives) in place (*75*). The function of grease is to remain in contact with and lubricate moving surfaces without leaking out. Its main requirement is to retain its properties under shear forces and pressure at all temperatures it experiences during use.

The base stock and additives used in greases are similar to that used in other lubricants. The key difference between fluid lubricants and greases is the thickener component which creates a polymer-like matrix, holding the grease together. Thickener component technology ranges from salts of fatty acids to clays and polymers. Bio-based derivatives are showing performance not only as a potential base stocks and additives but also as the thickeners. The bio-based thickeners are showing advantages in forming the matrix by reducing time and temperature required to make the grease. Also the increased flexibility in the choice of thickener and the polarity of the bio-based base stock provides the opportunity to tailor the grease performance and compatibility as has been done with engine and industrial lubricants.

Conclusions and Future

The lubricants industry is facing increasing performance requirements to meet enacted legislation. In the large and global lubricants market totaling approximately $39 billion, metathesized vegetable oil technology offers higher levels of performance from bio-based technology than was previously possible. Renewable chemical building blocks offer the lubricants industry new versatile materials enabling the synthesis of high-performance, bio-based base stocks and additives for engine lubricants, industrial lubricants, greases and metalworking fluids.

The future of the lubricants industry requires next generation technology that is sustainable and capable of delivering improved fuel economy, lower emissions and improved metal protection in modern, high-power density engines. Renewable building blocks and derivatives made from metathesized vegetable oils represent a key enabler for the formulation of next-generation, high-performing lubricants and additives.

Publication Date (Web): June 18, 2015 | doi: 10.1021/bk-2015-1192.ch013

References

1. Arbain, N. H.; Salimon, J. Synthesis and Characterization of Ester Trimethylolpropane Based Jatropha Curcas Oil as Biolubricant Base Stocks. *J. Sci. Technol.* **2011**, 47–58.
2. Clemente, T. E.; Cahoon, E. B. Soybean Oil: Genetic Approaches for Modification of Functionality and Total Content. *Plant Physiol.* **2009**Nov, *151* (3), 1030–1040.
3. Auld, D. L; Heikkinen, M. K; Erickson, D. A; Sernyk, J. L.; Romero, J. E Rapeseed mutants with reduced levels of polyunsaturated fatty acids and increased levels of oleic acid. *Crop Sci.* **1992**, *32*, 657–662.
4. Kinney, A. J. Development of genetically engineered oilseeds: from molecular biology to agronomics. In *Physiology, Biochemistry and Molecular Biology of Plant Lipids*; Williams, J. P., Khan, M. U., Lem, N. W., Eds.; Kluwer Academic Press: Dordrecht, The Netherlands, 1997; pp 298−301, ISBN 0-7923-4379-4.
5. Atsumi, S.; Hanai1, T.; Liao, J. C. *Nature* **2008**, *451*, 86–89.
6. Milbrant A.; Kitchin, C.; McCormick, R. The Feasibility of Producing and Using Bio-Massed Based Diesel and Jet Fuel in the United States; National Renewable Energy Laboratory: Golden, Colorado, 2013; p 6.
7. Kaufman, A. J.; Ruebusch, R. J. In Proceedings World Conference on Oleochemicals, Kuala Lumpur, Malaysia, 1990; Applewhite, T. H., Ed.; American Oil Chemists' Society: Champaign, IL, 1991; p 10.
8. Schwab, P.; France, M. B.; Ziller, J. W.; Grubbs, R. H. A Series of Well-Defined Metathesis Catalysts—Synthesis of [RuCl2(= CHR′)(PR3)2] and Its Reactions. *Angew. Chem., Int. Ed. Engl.* **1995**, *34*, 2039–2041.
9. Banks, R. L.; Banaslack, D. S.; Hudson, P. S.; Norell, J. R. *J. Mol. Catal.* **1982**January, *15*, 21–33.
10. Banks, R. L.; Bailey, G. C. *Ind. Eng. Chem. Prod. Res. Dev.* **1964**, *3* (3), 170–173.

11. Hérisson, J. L.; Chauvin, Y. Catalyse de transformation des oléfines par les complexes du tungstène. II. Télomérisation des oléfines cycliques en présence d'oléfines acycliques. *Makromol. Chem.* **1971**, *141* (1), 161–176.
12. Grubbs, R. H.; Carr, D. D.; Hoppin, C.; Burk, P. L. Consideration of the Mechanism of the Metal Catalyzed Olefin Metathesis Reaction. *J. Am. Chem. Soc.* **1976**, *98* (12), 3478–3483.
13. Schrock, R. R. High-oxidation-state molybdenum and tungsten alkylidene complexes. *Acc. Chem. Res.* **1986**, *19* (11), 342.
14. The official website of the Nobel Prize; http://www.nobelprize.org/nobel_prizes/chemistry/laureates/2005/ (accessed Feb. 4, 2015).
15. Elevance Renewable Sciences Technology; http://www.elevance.com/technology/metathesis (accessed Feb. 4, 2015).
16. Cohen, S.; Luetkens, M. L.; Balakrishnan, C.; Snyder, R. Methods of Refining and Producing Fuel from Natural Oil Feedstocks. U.S. Patent Application 2011/0113679, May 19, 2011.
17. Abraham, T. W.; Hiroki, K.; Lee, C. W.; Pederson, R. L.; Shrodi, Y.; Tupi, M. J. Methods of Making Organic Compounds by Metathesis. U.S. Patent Application 2009/0264672, Oct. 22, 2009.
18. *Elevance Renewable Sciences Products*; http://www.elevance.com/products (accessed Feb. 4, 2015).
19. Abraham, T.; Kaido, H.; Lee, C. W.; Pederson, R. L.; Schrodi, Y.; Tupy, J. U.S. Patent Application 2009/0264672.
20. Elevance Renewable Sciences News Release; [online] http://www.elevance.com/media/news-releases/elevance-expands-commercial-availability-of-elevance-aria-wtp-40 (accessed Feb. 4, 2015).
21. Shubkin, R. L. Polyalphaolefins. In *CRC Handbook of Lubrication: Theory and Practice in Tribology: Vol. III, Monitoring, Materials, Synthetic Lubricants, and Applications*; Booser, R. E., Ed.; CRC Press: Boca Raton, FL, 1993; pp 219–235.
22. Loveless, F. C. Catalytic Poly alpha-olefin Processes. U.S. Patent 4,642,410, Feb. 10, 1987.
23. DiBiase, S. A.; Rizvi, S. Q. A; Hategan, G. Functionalized Monomers and Polymers. U.S. Patent 8,846,587, Sept. 30, 2014.
24. Lahtele, M.; Pakkanen, T. A. Molecular Modeling of Polyalphaolefin Synthetic Oils. *J. Phys. Chem.* **1995**, *99*, 10267–10271.
25. Littich, R.; Ilseman, A.; Hategan, G.; Liang, Y.; Koers, K.; Morie-Bebel, M. Bio-based alternatives for silicone and petrochemical emollients from natural oil metathesis. *Household Pers. Care Today* **2014**May/June, *9* (3).
26. *Elevance Renewable Sciences Technology*; http://www.stepan.com/products/Surfactants/STEPOSOL-MET-10U (accessed Feb. 4, 2015).
27. *Elevance Renewable Sciences News Release*; http://www.elevance.com/media/news-releases/elevance-announces-commercial-availability-of-bio-based-inherent-C18-diacid (accessed Feb. 4, 2015).
28. Mekonnen, T.; Mussone, P.; Khalil, H.; Bressler, D. *J. Mater. Chem. A* **2013**, *1*, 13379–13398.
29. Harper, C. A. *Handbook of Plastics, Elastomers, and Composites*; McGraw Hill: New York, 1996.

Publication Date (Web): June 18, 2015 | doi: 10.1021/bk-2015-1192.ch013

30. Okpala, C. C. *Int. J. Eng. Res. Dev.* **2013**October, *8* (11), 17–23.
31. Rosato, D. V.; Matthew V. *Plastic Product Material and Process Selection Handbook*; Elsevier: New York, 2004; p 85.
32. Hollaway, L. *Handbook of Polymer Composites for Engineers*; Woodhead Publishing: Cambridge, England, 1994.
33. McKinsey website; http://www.mckinsey.com/~/media/mckinsey/dotcom/client_service/Automotive%20and%20Assembly/PDFs/McK_The_road_to_2020_and_beyond.ashx (accessed Feb. 4, 2015).
34. Directive 1999/94/EC of the European Parliament and of the Council of 13 December 1999, relating to the availability of consumer information on fuel economy and CO_2 emissions in respect of the marketing of new passenger cars; http://ec.europa.eu/environment/co2/9994/en.pdf (accessed Feb. 16, 2015).
35. Forbes, A. *Fiberglass & Composite Materials: An Enthusiast's Guide to High Performance Non-Metallic Materials for Automotive Racing and Marine Use*; HP Books: London, 1996; p 86.
36. *Piston Ring Handbook*; Federal-Mogul: Burscheid GmbH, August 2008.
37. Belz, F-M.; Peattie, K. *Sustainability Marketing: A Global Perspective*; John Wiley & Sons: New York, 2012.
38. Bergstra, R. J.; Baillargeon, D. J.; Deckman, D. E.; Goes, J. A. Advanced Low Viscosity Synthetic Passenger Vehicle Engine Oils. *Lubr. Sci.* **2006**Feb28, *16* (1).
39. Combustion in IC (Internal Combustion) Engines; p 37, http://me.queensu.ca/Courses/MECH435/6.CombustioninICEngines.pdf (accessed Feb. 14, 2015).
40. Cummins Solutions; [online] http://cumminsemissionsolutions.com/ces/navigationAction.do?url=SiteContent+en+HTML+EmissionsTechnology+-Worldwide_Emissions_Regualtions (accessed Feb. 14, 2015).
41. Frost and Sullivan.*The U.S. Synthetic Base Stock Markets*; 2008; pp 3-3
42. ASTM Digital Library; [online] http://www.astm.org/DIGITAL_LIBRARY/MNL/PAGES/MNL11464M.htm (accessed Feb. 14, 2015).
43. Bartels, T. Lubricants and Lubrication. In *Ullmann's Encyclopedia of Industrial Chemistry*; Wiley: Weinheim, 2005.
44. USDA Website "Biodegradable Hydraulic Fluid Nears Market"; http://www.ars.usda.gov/is/pr/2000/000419 (accessed Feb. 16, 2015).
45. Erhan, S. V.; Asadauskas, S. Lubricant Base Stocks from Vegetable Oils. *Ind. Crops Prod.* **2000**, *11*, 281.
46. *Fuels & Lubricants Handbook, Hydrocarbon Chemistry*; ASTM: West Conshohocken, PA, 2003; pp 169−184, Section 7.
47. *Base Stock Group Names & Characteristics*; American Petroleum Institute: Washington, DC, 2011; API 1509, Appendix E.
48. Kline & Company. *Global Lubricant Base stocks 2009 – 2011 Webinar: Market Analysis and Assessment*; 2011, slide 24 (accessed Dec. 19, 2014)
49. White, J. L.; Choi, D. D. *Polyolefins: Processing, Structure Development, And Properties*; Hanser Verlag: Munich, 2005.
50. *Chemistry and Technology of Lubricants*, 3rd ed.; Mortier, R. M., Fox, M. F., Orszulik, S. T., Ed.; Springer: Netherlands, 2010.

Publication Date (Web): June 18, 2015 | doi: 10.1021/bk-2015-1192.ch013

51. Rudnick, L. R. *Synthetics, Mineral Oils, and Bio-Based Lubricants: Chemistry and Technology*, 2nd ed.; CRC Press: London, U.K., 2013; p 904.
52. DiBiase, S. A.; Rizvi, S. Q. A.; Hategan, G. Maleinated Derivatives. U.S. Patent Application 2012/0264664.
53. Ponticel, P. *SAE codifies new oil viscosity grade (SAE 16)*; http://www.sae.org/, SAE International (accessed Sept. 10, 2014).
54. Tanver, S.; Chandra, S; Prasad, R. *Rheology of multigrade engine oils*. *Indian J. Chem. Eng.* **2006**March, *13*, 180–184.
55. Johnson, M. Selecting the correct lubricants. *Tribol. Lubr. Technol.* **2008**September, 24–29.
56. Elevance Aria™ WTP 40 Technical Data Sheet; [online] http://www.elevance.com/resources/products/#ariajump (accessed Feb. 16, 2015).
57. Machinery Lubrication website, Elevance Expands Availability of Lubricant Base Stock, Feb 25, 2014; http://www.machinerylubrication.com/Read/29659/elevance-lubricant-availability (accessed Feb. 16, 2015).
58. Elevance-Concert™ GC-350 Grease Processing Aid Marketing Sheetl; [online] http://www.elevance.com/resources/products/#ariajump (accessed Feb. 16, 2015).
59. Elevance press release, Elevance Concert™ GC-350 Grease Processing Aid Launched to Meet Demand for Improved Performance and Sustainability, June 12, 2014; http://www.elevance.com/media/news-releases/elevance-concert-gc-350-grease-processing-aid (accessed Feb. 16, 2015).
60. Van Rensselar, J. Metathesis Power Marketability of Biobased Lubricants. *J. Soc. Tribol. Lubr. Eng.*, October 31, 2013; http://www.stle.org/resources/articledetails.aspx?did=1856 (accessed Feb. 16, 2015).
61. Liston, T. V. Engine Lubricant Additives: What they are and how they function. *J. Soc. Tribol. Lubr. Eng.* **1992**May, 389–397.
62. *Basics of Lubrication*; http://www.stle.org/resources/lubelearn/lubrication/#fluids (accessed Feb. 16, 2015).
63. *Global Automotive Engine Oil Market Size, Share, Segment Analysis and Forecast to 2020*, January 16, 2015; [online] http://www.mynewsdesk.com/us/persistence-market-research-2/pressreleases/global-automotive-engine-oil-market-size-share-segment-analysis-and-forecast-to-2020-1106452 (accessed Feb. 16, 2015).
64. Rudnick L. R.; Shubkin, R. L. *Synthetic Lubricants And High- Performance Functional Fluids*; CRC Press: London, U.K., 1999; Vol. 1, 30−39.
65. Okuyama, Y.; Shimokoji, D.; Sakurai, T.; Maruyama, M. *Study of Low-Viscosity Engine Oil on Fuel Economy and Engine Reliability*; SAE Technical Paper 2011-01-1247, 2011; doi:10.4271/2011-01-1247.
66. *Chevron Global Lubricants, Performance of Base Oils and Future Trends - The Evolution of Base Oil Technology - Part 3*, Sept 2003; [online] http://www.machinerylubrication.com/Read/533/base-oil-trends (accessed Feb. 10, 2015.)
67. Booth, J. E.; Nelson, K. D.; Harvey, T J.; Wood, R. J. K. Martinez, J. G.; Powrie, H. E. G. Mini-Traction-Machine Tests to Assess the Effect of Base Oil and Additive Interactions on Surface Charge and Friction. Presented at

Publication Date (Web): June 18, 2015 | doi: 10.1021/bk-2015-1192.ch013

the ASME/STLE 2007 International Joint Tribology Conference, San Diego, California, October 22–24, 2007.
68. Liang, Y; Counter, K.; Havelka, K.; Rizvi, S,; Christensen, A.; Erhan, S. Development of A High Performance Synthetic Base Stock From Natural Oil Metathesis, Presented at the 2014 STLE Tribology Frontiers Conference, Rosemont, IL, Oct. 26−28, 2014.
69. Bartz, W. Synthetic Hydraulic Fluids for High Performance Applications. *Lubr. Eng*. **2000**October, 42–53.
70. Is Synthetic Oil Better? *Machinery Lubrication*; [online] http://www.machinerylubrication.com/Read/2021/synthetic-oil (accessed Feb. 16, 2015).
71. Roslaili, A. A.; Amirah, S. M.; Nazry, K.; Nihla, A. Determination of Structural and Dimensional Changes of O-Ring Polymer/Rubber Seals Immersed in Oils. *Int. J. Civ. Environ. Eng.* **1996**, *10* (05).
72. SpectraSyn™ 40 Polyalphaolefin (PAO) Fluid Product Datasheet; [online] http://www.exxonmobilchemical.com/Chem-English/brands/spectrasyn-hi-vis-pao-grades-and-datasheets.aspx?ln=productsservices (accessed Feb. 16, 2015).
73. Kothavale, B. S. Evaluation of Extreme Pressure Properties Lubricating Oils Using Four Ball Friction Testing Machine. *Int. J. Adv. Eng. Technol.* **2010**, 0976–3945.
74. Kennedy, D. M.; Hashmi, M. S. Methods of wear testing for advanced surface coatings and bulk materials. *J. Mater. Process. Technol.* **1998**, *77*, 246–253.
75. *NLGI Lubricating Grease Guide*, 4th ed.; National Lubricating Grease Institute: Kansas City, MO, 1996.

Publication Date (Web): June 18, 2015 | doi: 10.1021/bk-2015-1192.ch013

Publication Date (Web): June 18, 2015 | doi: 10.1021/bk-2015-1192.ch014

Chapter 14

Polyacids from Corn Oil as Curing Agents for Epoxy Resins

Jian Hong,[1] Djavan Hairabedian,[1,2] Zoran S Petrović,[1] and Andrew Myers*,[1]

[1]Kansas Polymer Research Center, Pittsburg State University, 1701 South Broadway Street, Pittsburg, Kansas, 66762 U.S.A.
[2]Department of Chemistry, Pittsburg State University, 1701 South Broadway Street, Pittsburg, Kansas, 66762 U.S.A.
***E-mail: amyers@pittstate.edu.**

Vegetable oils are sustainable and environmentally benign sources for new monomers and polymers. Here we report the preparation and use of polyacids derived from corn oil as curing agents for commercial epoxy resins (DER332). First, epoxidized corn oil (ECO) was polymerized by ring-opening polymerization in the presence of boron trifluoride diethyl etherate as catalyst. The effect of catalyst concentration from 1 to 4 mol% was studied. Soluble fraction and thermal analysis showed that the product with highest crosslink density was with 2 mol %. Second, by hydrolysis, polymerized ECO was converted to a polyacid with acid value of 158 mgKOH/g and used for curing epoxy resins. DSC, TGA, DMA and tensile properties of cured epoxy resins were studied.

Introduction

With increasing energy crises and environmental concerns, more and more researchers turn their interest from petroleum to sustainable sources, such as vegetable oils and animal fats (*1–4*). Vegetable oils are triglycerides consisting of five major fatty acids: palmitic (C16:0), stearic (C18:0), oleic (C18:1), linoleic (C18:2), and linolenic (C18:3) (*5*). The first two are saturated, while the other three contain some unsaturation. Typical corn oil composition is as follows: 13 % of palmitic and 3 % of stearic acids, 31 % of oleic, 52 % of linoleic, and 1

In Green Polymer Chemistry: Biobased Materials and Biocatalysis; Smith, et al.;
ACS Symposium Series; American Chemical Society: Washington, DC, 2015.

% linolenic acids (*5*). According to a report from the National Corn Growers Association released in 2013, the U.S. is the largest producer of corn in the world with 10,780 million bushels produced annually, which accounts for 32 % of the world's corn supply (*6*). Corn contains around 3.8 % of corn oil which is an abundant resource for valuable chemicals. Additionally, wate materials from the corn oil to ethanol process, specifically distillers dried grains with soluble (DDGS), contains up to 15 % corn oil and is widely available for inexpensive markets like animal feed.

As we know, triglycerides contain two kinds of functional groups: carbon-carbon double bonds in the fatty acid chain and the ester group in the triglyceride linkage. With different chemical modifications, various useful chemicals can be obtained from vegetable oils. However, aside from methanolysis of triglycerides at the ester group to produce biodiesel (*7*, *8*), most chemicals derived from vegetable oils are through one or multi step reactions of double bonds. Epoxidized vegetable oils are prepared by epoxidation of double bonds, and polyols or polyacids can be obtained by ring-opening of epoxy rings with proper nucleophiles (*9–12*). Alternatively, polyols can also be produced by ozonolysis and reduction of double bonds (*13*), while ozonolysis and oxidation of double bonds produces polyacids (*14*). Erhan et al. (*15*, *16*) reported one method to obtain polyacids involving the reaction of two functional groups: epoxidation of double bonds, epoxy ring-opening polymerization, and hydrolysis of ester groups (Scheme 1).

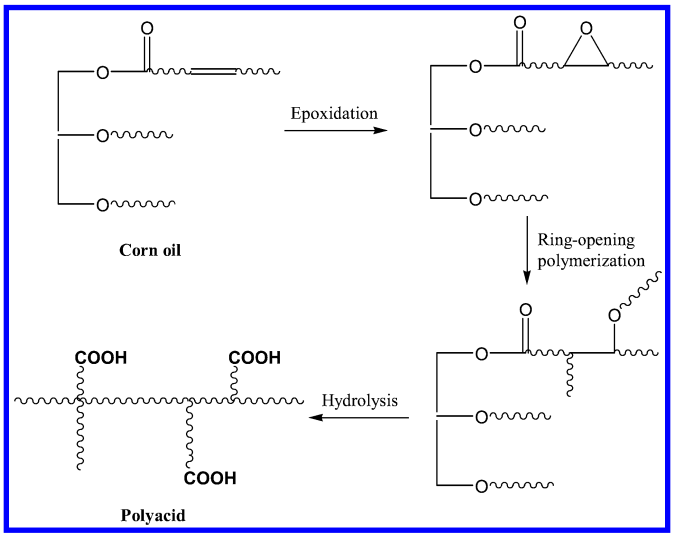

Scheme 1. Synthesis of polyacids from corn oil

Polyacids can be converted to polysoaps by neutralizing the polyacid with an appropriate base and using it as a surfactant. Furthermore, in the epoxy resins industry, carboxylic acids are one of most popular hardening reagents. Epoxy

In Green Polymer Chemistry: Biobased Materials and Biocatalysis; Smith, et al.;
ACS Symposium Series; American Chemical Society: Washington, DC, 2015.

Publication Date (Web): June 18, 2015 | doi: 10.1021/bk-2015-1192.ch014

resins cured by polyacids have good flexibility and weatherability. Here we report polyacids prepared from corn oil and use them to cure commercial epoxy resin, DER 332 which is a bisphenol A diglycidylether based epoxy resin.

Experimental Part

Materials

Commercial-grade refined, bleached and deodorized (RBD) corn oil was purchased from Wal-Mart (Pittsburg, KS, USA) with the "best used by" date of 1/25/2013. Fluoroboric acid (HBF_4, 48 wt % in water), Amberlite IR 120H ion exchange resin, benzimidazole, and boron trifluoride diethyl etherate ($BF3{\cdot}OEt2$) were purchased from Sigma-Aldrich. DER 332 epoxy resin was obtained from the Dow Chemical Company. Hydrogen peroxide (H_2O_2, 30 wt% in water), acetic acid (CH_3COOH), and other reagents were purchased from Fisher Scientific. All reagents were used as received.

Publication Date (Web): June 18, 2015 | doi: 10.1021/bk-2015-1192.ch014

Methods

Iodine value (IV) and acid value (AV) were determined by the Hanus method according to IUPAC 2.205 and the indicator method following IUPAC 2.201, respectively. The epoxy-group oxygen content (EOC) was determined by direct titration of epoxy groups with HBr according to the standard method for oils and fats.

FT-IR spectra were obtained from Shimadzu IR Affinity-1. A liquid film spread on one KBr plate technique was used. Gel permeation chromatography (GPC) was performed with a Waters gel permeation chromatograph (Milford, MA, USA), consisting of a 515 pump, a 410 differential refractometer, four phenogel 5μ columns (50, 10^2, 10^3 and 10^4 Å) and Millennium software. The flow rate of tetrahydrofuran (THF) eluent was 1 mL/min at 30 °C.

Differential scanning calorimetry (DSC) was performed on TA DSC Q100 at a heating and cooling rate of 10 °C/min under nitrogen. Glass transition temperature (T_g) was determined from the second scanning curves. Thermogravimetric analysis (TGA) was performed on a TA TGA Q500. Samples were heated under nitrogen using a heating ramp of 10 °C/min from 25 to 600 °C. Dynamic mechanical analysis (DMA) was carried out on TA 2980 from TA Instruments. The testing was performed in the tension mode under nitrogen at a heating rate of 3 °C/min and a mechanical vibration frequency of 1 Hz.

Synthesis of Polyacids

Epoxidation of Corn Oil

Epoxidation was performed via the *in situ* peroxyacetic acid method to epoxidize corn oil (*9*). Corn oil, acetic acid, Amberlite IR-120 H ion exchange resin (25 wt% of oil) and toluene (50 wt% of oil) were added into a 3-neck round bottom flask equipped with a condenser, thermometer, magnetic stir bar and an

addition funnel (apparatus shown in Figure 1a). The molar ratio of double bonds to acetic acid is 1:0.5. Hydrogen peroxide (molar ratio to double bond 1.5:1) was added drop-wise into the reaction mixture via addition funnel when the reaction temperature reached 60 °C. After all hydrogen peroxide was added, the reaction temperature was increased to 70 °C and maintained for 7 hours. The mixture was cooled to room temperature and ion exchange resin was separated by vacuum filtration. The water phase was separated via a separatory funnel. The organic phase was washed with hot water and hot 5 wt% sodium chloride solution until the pH reached approximately 7. Toluene in the organic phase was removed by rotary evaporation under low pressure (50-70 mmHg) followed by high vacuum (6-10 mmHg) at 70 °C. Quantitative pale yellowish epoxidized corn oil (>98 %) was obtained with EOC of 6.8 % (theoretical EOC was 7.0 % calculated from corn oil IV of 120 g I_2/100g).

Publication Date (Web): June 18, 2015 | doi: 10.1021/bk-2015-1192.ch014

Ring-Opening Polymerization of Epoxidized Corn Oil (PECO)

Epoxidized corn oil was polymerized via ring-opening polymerization according to the literature (*15*, *16*). 40 g epoxidized oil and 400 mL CH_2Cl_2 were added to a 500-mL round bottom flask fitted with a magnetic stirrer, condenser and dropping funnel. Then appropriate weight of $BF_3{\cdot}OEt_2$ was added drop-wise over 2 min under N_2 condition. The solution was stirred at room temperature under N_2 condition for 3 hours and 3 mL ethanol was added to the mixture to deactivate the catalyst. The solvent was removed using a rotary evaporator at low pressure (50-70 mmHg) and the polymer was washed twice with hexane. The pale yellowish solid polymer was obtained after drying under high vacuum (6-10 mmHg) at 70 °C.

Hydrolysis of Polymerized Epoxidized Corn Oil

Hydrolysis was conducted by following a literature method (*16*). 10 g PECO was cut into pieces and put into 200 mL of 0.4M NaOH solution. The solution was refluxed for 24 hours. Then the solid was filtered and the solution was cooled to room temperature. The solution was poured into 320 mL of 1.0M HCl and the gel was precipitated. The gel was washed with water three times and 10 % (v/v) aqueous acetic acid two times. 8.0 g (80 % yield) yellowish polyacid with AV of 158 mg KOH/g was obtained after drying under high vacuum (6-10 mmHg) at 70 °C.

Polyacid Curing Epoxy Resin (DER 332)

Polyacids and DER 332 were mixed with different molar ratio of [Acid] to [Epoxy]. 2 wt% of benzimidazole was used as catalyst. The mixture was poured into a steel mold (100ï¿½100ï¿½1 mm^3) and heated at 100 °C for 24 hours. The cured films were characterized with DSC, TGA, DMA, and tested mechanical properties.

Results and Discussion

Synthesis of Polyacids

Polyacids were prepared from corn oil using a three-step procedure. The first step was epoxidation of corn oil. The second step was ring-opening polymerization of epoxidized corn oil with a cationic initiator. The last step was hydrolysis of polymerized epoxidized corn oil.

As for second step, the effect of catalyst concentration on crosslink density was studied. Four catalyst concentrations were used: 1, 2, 3, and 4 mol%. It was found that with 2 mol % of catalyst, the product had the lowest hexane soluble fraction (4.3 %) and the highest T_g (-18.8 °C), indicating 2 mol % of catalyt gave product the highest crosslink density. Then, polymerized epoxidized corn oil with 2 mol% catalyst was hydrolyzed to produce polyacid.

Publication Date (Web): June 18, 2015 | doi: 10.1021/bk-2015-1192.ch014

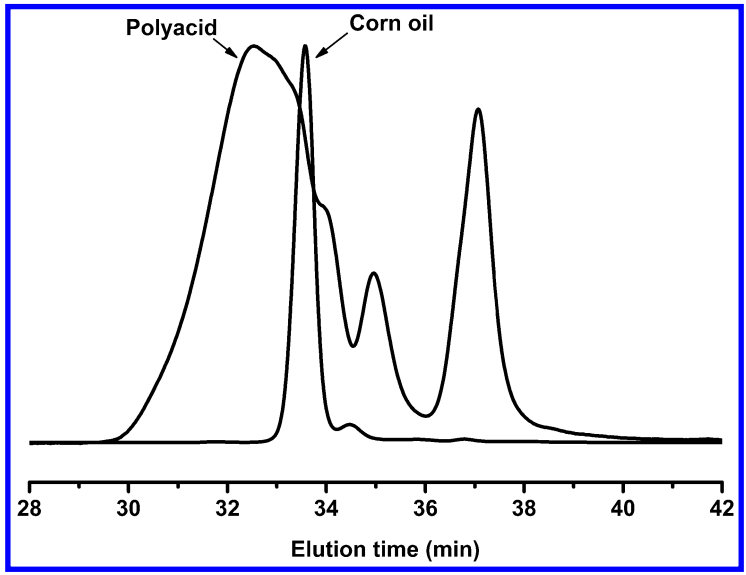

Figure 1. GPC curves of corn oil and polyacid.

From GPC profile (Figure 1) it can be seen that the polyacid consists of oligomers. The peak at 37.2 min represents mono-acid. From the peaks' area, the content of mono-acid can be roughly calculated, which was 20 %. It is higher than common saturated fatty acid content of corn oil (~16 %), which means besides saturated fatty acids, some epoxidized fatty acids did not undergo ring-opening polymerization. TGA curve of polyacid showed an initinal thermal

In Green Polymer Chemistry: Biobased Materials and Biocatalysis; Smith, et al.;
ACS Symposium Series; American Chemical Society: Washington, DC, 2015.

decomposition stage under 300 °C, which can be attributed to the mono-acid. The IR spectrum of polyacid (Figure 2) showed the characteristic acid C=O stretch peak at 1711 cm^{-1} and O-H stretch peak in the range of 3000-3500 cm^{-1}, in addition of strong peak of ether at 1075 cm^{-1} and weak peak of epoxy at 811 cm^{-1}. At the same time, corn oil's double bond (3010 cm^{-1}) disappeared, indicating double bonds were converted to epoxy or ether groups. However, IR spectrum of polyacid showed a side peak of ester C=O stretching (1745 cm^{-1}), indicating that part of the triglycerides were not hydrolyzed. This was confirmed by AV of polyacid (158 mg KOH/g), which is lower than theoretical (198 mg KOH/g).

Publication Date (Web): June 18, 2015 | doi: 10.1021/bk-2015-1192.ch014

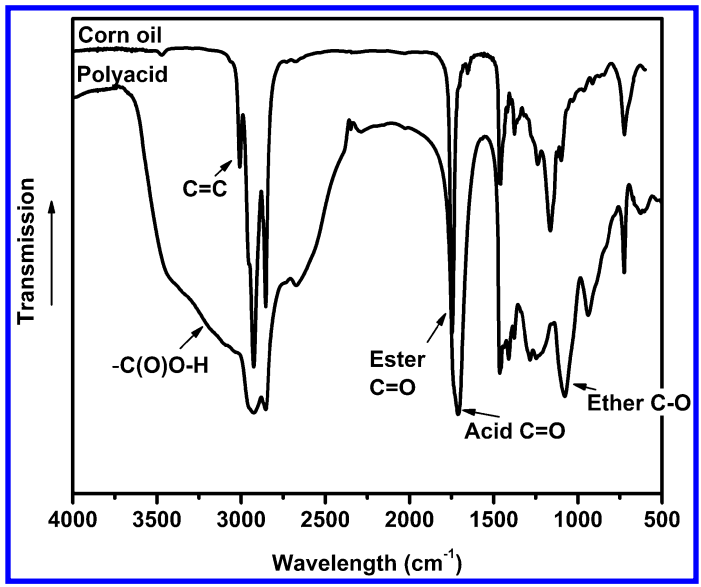

Figure 2. FT-IR spectra of corn oil and polyacid.

Epoxy Resins Cured by Polyacid

In order to investigate the effect of polyacid content on properties of final cured resin, three different ratios of [acid] to [epoxy] were used: 1:0.8, 1:1, and 1:1.2. Due to polyacid as kind of weak acid and to accelerate the reaction of acid and epoxy, benzimidazole was used as catalyst. Mixtures of polyacid, DER 332, and catalyst were placed in the mold and kept at 100 °C for 24 hours. The cured resins are yellowish and transparent. Polymers thermal and mechanical properties are listed in Table 1.

Table 1. Thermal and Mechanical Properties of Polyacids Cured Epoxy Resins

Resin	T_g (°C)		TGA (°C)		Tensile strength (MPa)	Elongation (%)
	DSC	DMA[a]	$T_{5\%}$[b]	T_{max}[c]		
Polymer-0.8	11.9	35	334	417	1.25±0.09	61.7±1.8
Polymer-1.0	17.0	39	344	417	1.65±0.04	74.8±3.4
Polymer-1.2	19.3	44	364	416	3.26±0.20	74.9±4.6

[a] T_g was read from the peak of Tanδ curve. [b] Temperature at 5 % weight loss. [c] Temperature at maximum degradation rate (read from the peak of Deriv. weight curve).

Publication Date (Web): June 18, 2015 | doi: 10.1021/bk-2015-1192.ch014

The T_g of polymers were determined by DSC (Figure 3) and DMA (Figure 4), and found to range from 11.9 to 19.3 °C and 35 to 44 °C (Table 1), respectively. Regardless of the method used, polymer-1.2 exhibited the highest T_g, while polymer-0.8 exhibited the lowest, which can be explained by polymer-1.2 having the highest cross-linking density. As shown in Scheme 2, acid attacks the epoxy ring and forms a hydroxyl group (Step 1 in Scheme 2). The hydroxyl group can also attack another epoxy ring to get polyether (Step 2 in Scheme 2). Due to Step 2, the cured system with higher content of polyacid will result in some pendant acid groups, and further decrease cross-link density.

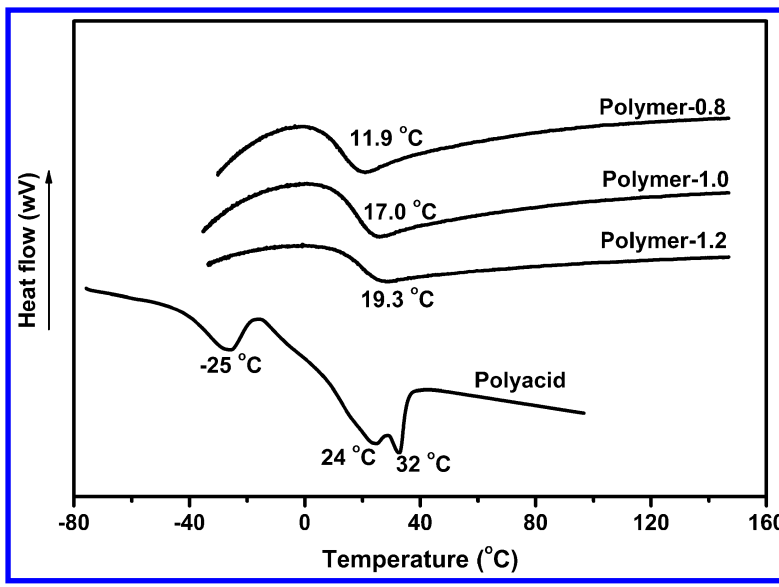

Figure 3. DSC curves of polyacid and cured epoxy resins.

In Green Polymer Chemistry: Biobased Materials and Biocatalysis; Smith, et al.;
ACS Symposium Series; American Chemical Society: Washington, DC, 2015.

Publication Date (Web): June 18, 2015 | doi: 10.1021/bk-2015-1192.ch014

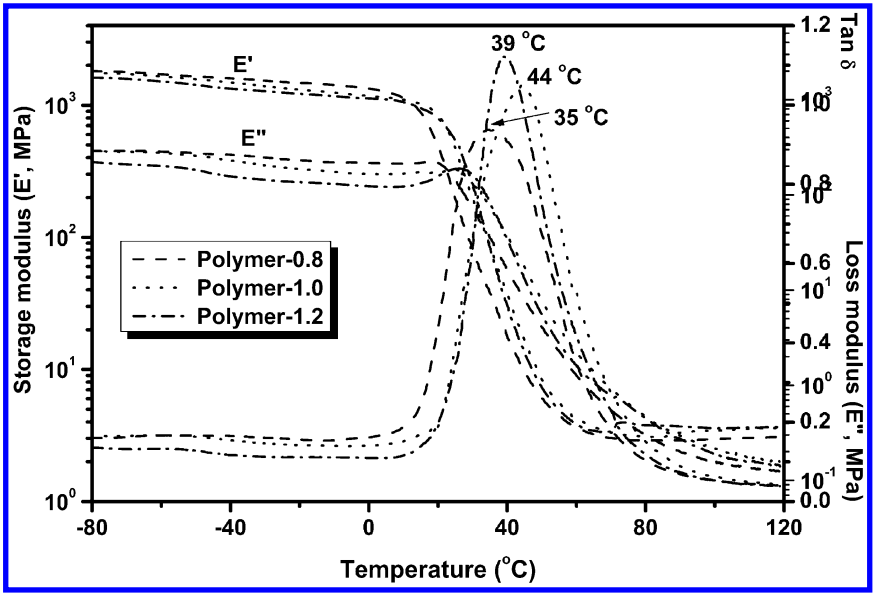

Figure 4. DMA curves of polyacid and cured epoxy resins.

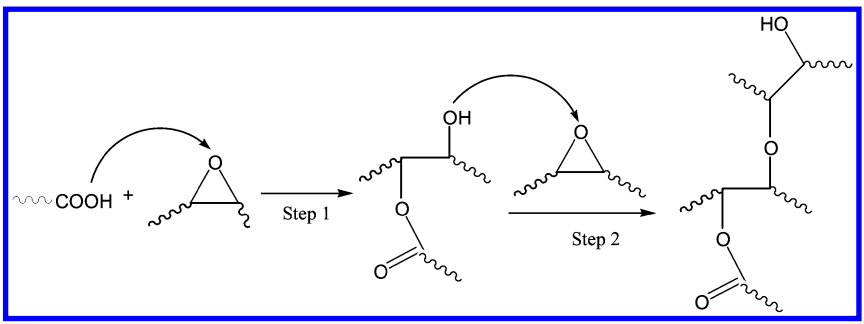

Scheme 2. Reaction of acid with epoxy

Unlike polyacid, three polymers did not have significant decomposition under 300 °C and all three exhibited similar decomposition behavior (Figure 5). The TGA curves of polymers indicated similar maximum weight loss temperature (~417 °C). It can be explained that most of the mono-acid reacted with epoxy. The decomposition process resulted in the formation of a small char at ~500 °C in all cases. However, polymer-0.8 which has the highest content of polyacid showed the lowest initial decomposition temperature (334 °C at 5 % weight loss), and 30 °C lower than that of polymer-1.2 (364 °C) which has the lowest content of polyacid, This is because polymer-1.2 has the highest cross-linking density.

In Green Polymer Chemistry: Biobased Materials and Biocatalysis; Smith, et al.;
ACS Symposium Series; American Chemical Society: Washington, DC, 2015.

Publication Date (Web): June 18, 2015 | doi: 10.1021/bk-2015-1192.ch014

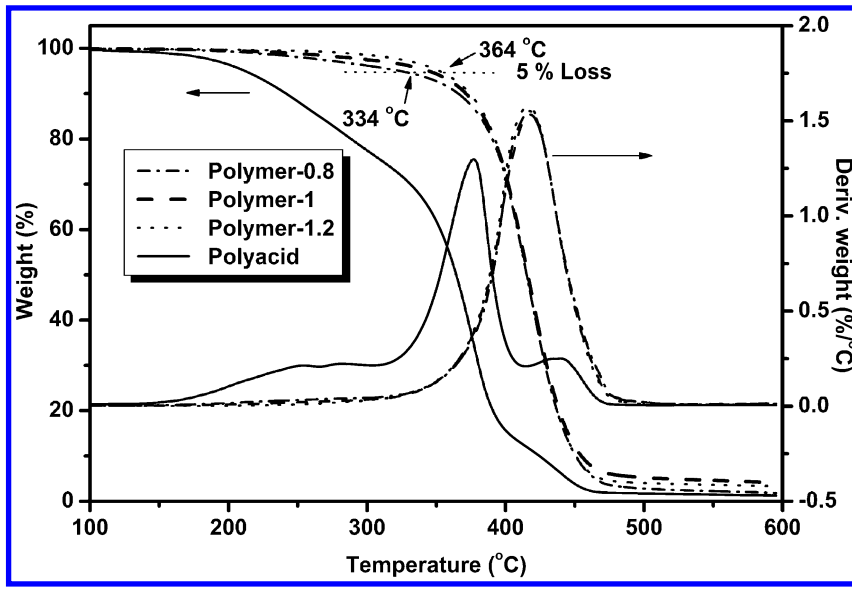

Figure 5. TGA curves of polyacid and cured epoxy resins.

Typical stress-strain relationships of polymers are provided in Figure 6 and mechanical data are listed in Table 1. Polymers behaved as elastomers. Their tensile strengths at break increased as polyacid content decreased. Polymer-1.2 has the highest tensile strength (3.26 MPa) and the highest elongation at break (74.9 %) because of the highest cross-linking density.

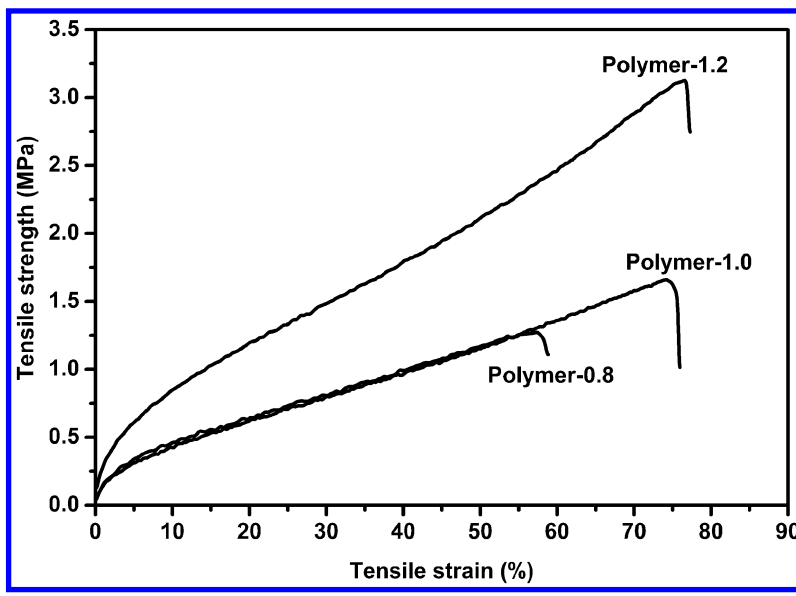

Figure 6. Typical stress-strain relationships of polyacid cured epoxy resins.

In Green Polymer Chemistry: Biobased Materials and Biocatalysis; Smith, et al.;
ACS Symposium Series; American Chemical Society: Washington, DC, 2015.

Conclusions

Polyacid with AV of 158 mg KOH/g was successfully obtained from corn oil by epoxidation, ring-opening polymerization, and hydrolysis. The epoxy resins cured with this polyacid were transparent, had T_g in the range of 12-19 °C, and exhibited good thermal stability with 5 % weight loss up to 334 °C. With increasing ratio of epoxy from 0.8 to 1.2, the cured epoxy resin's tensile strength at breaking point increased from 1.25 to 3.26 MPa, while breaking elongation from 58.7 to 74.9 %. The cured epoxy resins are potential packaging materials.

Acknowledgments

Financial support by the United States Department of Agriculture (USDA) is gratefully acknowledged (Award No. 2008-38924-19200).

Publication Date (Web): June 18, 2015 | doi: 10.1021/bk-2015-1192.ch014

References

1. Lu, Y.; Larock, R. C. Novel polymeric materials from vegetable oils and vinyl monomers: preparation, properties, and applications. *ChemSusChem* **2009**, *2*, 136–147.
2. Galia, M.; Montero, d. E. L.; Ronda, J. C.; Lligadas, G.; Cadiz, V. Vegetable oil-based thermosetting polymers. *Eur. J. Lipid Sci. Technol.* **2009**, *112*, 87–96.
3. Petrović, Z. S. Polyurethanes from Vegetable Oils. *Polym. Rev.* **2008**, *48*, 109–155.
4. Meier, M. A. R.; Metzger, J. O.; Schubert, U. S. Plant oil renewable resources as green alternatives in polymer science. *Chem. Soc. Rev.* **2007**, *36*, 1788–1802.
5. Gunstone, F. D. *Fatty acid and lipid chemistry*, 1st ed.; Springer: New York, 1996; p 69.
6. National Corn Growers Association. *The World of Corn* [Online]; NCGS: Chesterfield, MO, 2013; 20 pp, http://www.ncga.com/upload/files/documents/pdf/WOC%202013.pdf (accessed Jan 26, 2015).
7. Dizge, N.; Aydiner, C.; Imer, D. Y.; Bayramoglu, M.; Tanriseven, A.; Keskinler, B. Biodiesel production from sunflower, soybean, and waste cooking oils by transesterification using lipase immobilized onto a novel microporous polymer. *Bioresour. Technol.* **2009**, *100*, 1983–1991.
8. Lee, A. F.; Bennett, J. A.; Manayil, J. C.; Wilson, K. Heterogeneous catalysis for sustainable biodiesel production via esterification and transesterfication. *Chem. Soc. Rev.* **2014**, *43*, 7887–7916.
9. Zlatanic, A.; Lava, C.; Zhang, W.; Petrovic, Z. S. Effect of structure on properties of polyols and polyurethanes based on different vegetable oils. *J. Polym. Sci., Part B: Polym. Phys.* **2004**, *42*, 809–819.
10. Desroches, M.; Escouvois, M.; Auvergne, R.; Caillol, S.; Boutevin, B. From Vegetable Oils to Polyurethanes: Synthetic Routes to Polyols and Main Industrial Products. *Polym. Rev.* **2012**, *52*, 38–79.

11. Petrović, Z. S. Polyurethanes from Vegetable Oils. *Polym. Rev.* **2008**, *48*, 109–155.
12. Zeimaran, E.; Kadir, M. R. A.; Nor, H. M; Kamarul, T.; Djordjevic, I. Synthesis and characterization of polyacids from palm acid oil and sunflower oil via addition reaction. *Bioorg. Med. Chem. Lett.* **2013**, *23*, 6616–6619.
13. Ccetković, I.; Milić, J.; Ionescu, M.; Petrović, Z. S. Preparation of 9-hydroxynonanoic acid methyl ester by ozonolysis of vegetable oils and its polycondensation. *Hem. Ind.* **2008**, *62*, 319–328.
14. Ackman, R. G.; Retson, M. E.; Gallay, L. R.; Vandenheuvel, F. A. Ozonolysis of unsaturated fatty acid. *Can. J. Chem.* **1961**, *39*, 1956–1963.
15. Biresaw, G.; Liu, Z. S.; Erhan, S. Z. Investigation of the surface properties of polymeric soaps obtained by ring-opening polymerization of epoxidized soybean oil. *J. Appl. Polym. Sci.* **2008**, *108*, 1976–1985.
16. Liu, Z.; Erhan, S. Ring-Opening Polymerization of Epoxidized Soybean Oil. *J. Am. Oil. Chem. Soc.* **2010**, *87*, 437–444.

Publication Date (Web): June 18, 2015 | doi: 10.1021/bk-2015-1192.ch014

Publication Date (Web): June 18, 2015 | doi: 10.1021/bk-2015-1192.ch015

Chapter 15

Modifications of Plant Oils for Value-Added Uses

H. N. Cheng*,[1] and Atanu Biswas[2]

[1]Southern Regional Research Center, USDA Agricultural Research Service, 1100 Robert E. Lee Boulevard, New Orleans, Louisiana 71024, U.S.A.
[2]National Center for Agricultural Utilization Research, USDA Agricultural Research Service, Peoria, Illinois 61604, U.S.A.
***E-mail: hn.cheng@ars.usda.gov.**

Plant oils are valuable agricultural commodities and useful raw materials for the preparation of value-added products. In this article, a review is made of the various structural modifications made on plant oils in the authors' laboratories. The reactions include Diels-Alder, ene reaction, transesterification, acid or enzymatic hydrolysis, heat-bodying reaction, hydrogenation, epoxidation, formation of acetonide, aminohydrin, and azidohydrin, click reaction, and polymerization. A wide range of products have been made from plant oils and their epoxidized derivatives. Many of these reaction pathways produce new triglyceride structures not previously reported. The properties of selected products have been tested, particularly in lubricant applications to enhance viscosity, thermal stability, or mechanical wear.

Introduction

In addition to being important items for food and agriculture, plant oils are also useful renewable raw material for the development of novel substances (*1*, *2*). Current interest in this field of research is high. Some examples of modified vegetable oils are epoxidized oil (*3*, *4*), soybean oil methyl ester (methyl soyate) (*5*, *6*), maleated products (*7*, *8*), and soybean oil polymers (*9–11*). Applications

In Green Polymer Chemistry: Biobased Materials and Biocatalysis; Smith, et al.;
ACS Symposium Series; American Chemical Society: Washington, DC, 2015.

include lubricants (*12*), paints, coatings, and adhesives (*13*, *14*), plastics (*15*, *16*), and biomedical materials (*13*). Several recent review articles are available (*12–18*).

For many years the present authors and their collaborators at USDA have been active in this area. In this article, a review is being conducted of some of the work done in their laboratories. A schematic summary of the reaction pathways is provided in Figure 1.

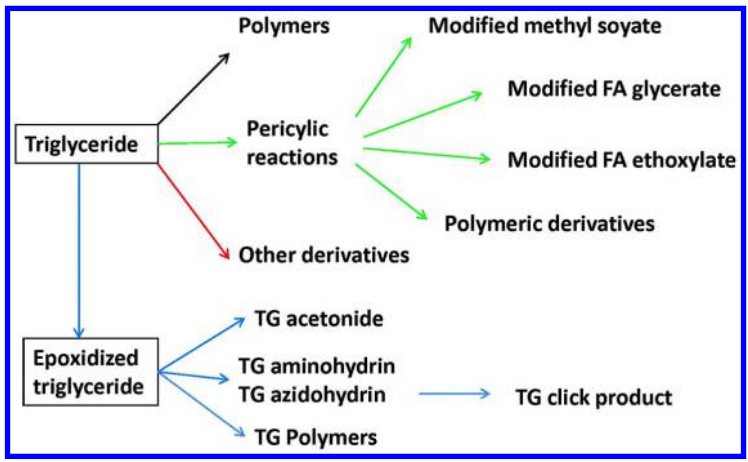

Figure 1. Scheme of the modification and polymerization reactions conducted on triglycerides (TG) by the authors and their collaborators in the past 8 years.

Reactions Directly with Triglycerides

The reality of the current market for chemical products is that they are price-competitive. In product development, it would be desirable (wherever possible) to decrease the number of reaction steps in order to save on processing cost. One way to achieve the cost reduction is to make products directly from plant oils. Several examples of these reactions are given below.

Pericyclic Reactions - Polymer Formation

Pericyclic reactions include Diels-Alder and ene reactions (*19*, *20*). The present authors have found these reactions to be particularly useful in generating new triglyceride derivatives and new polymers from plant oils. Thus, in a recent paper (*21*), they studied the reaction of soybean oil (SBO) with 4-phenyl-1,2-4-triazoline-3,5-dione (PTAD). The reaction schemes are shown in Figure 2.

In Green Polymer Chemistry: Biobased Materials and Biocatalysis; Smith, et al.;
ACS Symposium Series; American Chemical Society: Washington, DC, 2015.

Publication Date (Web): June 18, 2015 | doi: 10.1021/bk-2015-1192.ch015

Publication Date (Web): June 18, 2015 | doi: 10.1021/bk-2015-1192.ch015

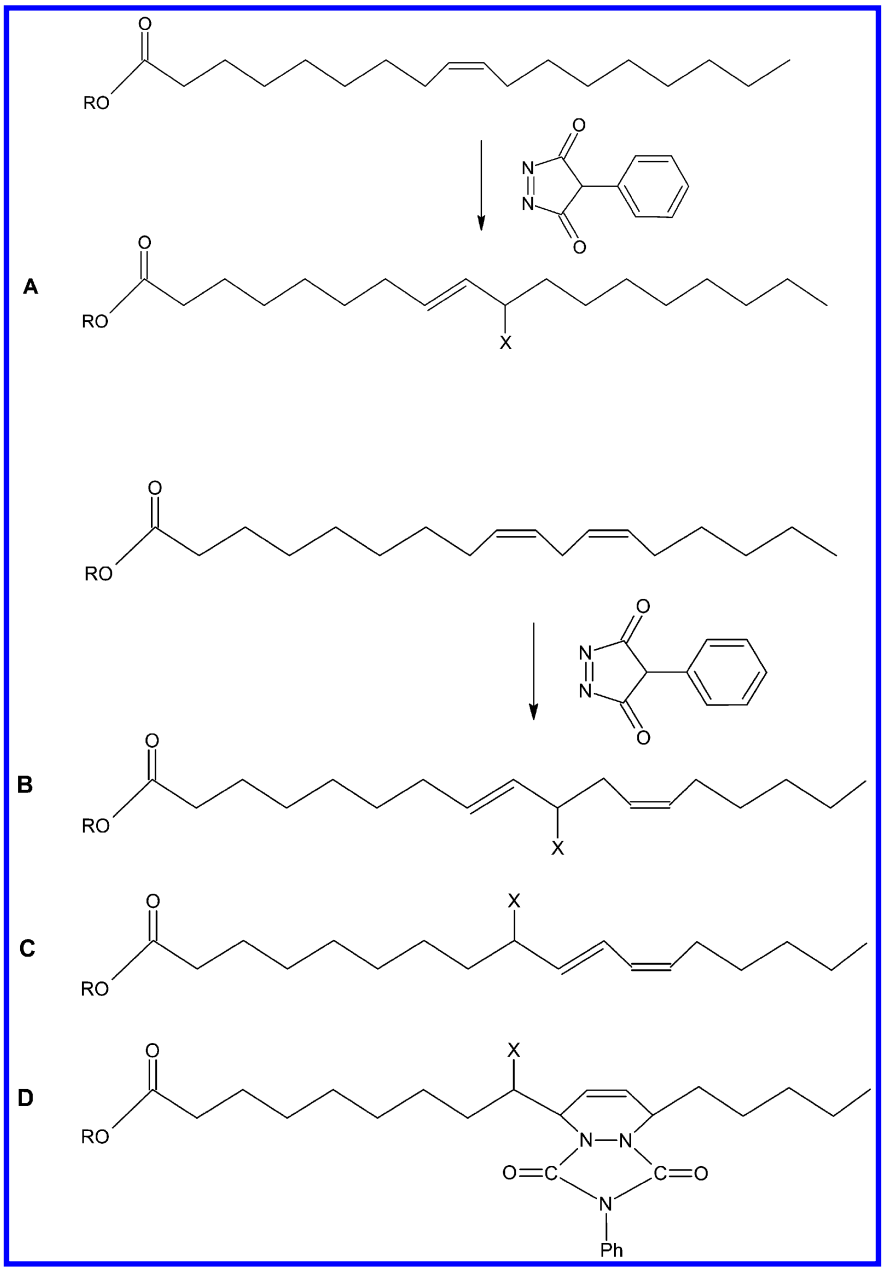

Figure 2. Reaction schemes for oleate and linoleate with the reaction of PTAD.

The process required no solvent or catalyst and entailed only the mixing of triglyceride and PTAD. ^{1}H NMR was used to determine the chemical structures generated from oleate and linoleate and to monitor the reactions. In the PTAD reaction, both ene (structures **A, B, C**) and Diels-Alder (structure **D**) products were

In Green Polymer Chemistry: Biobased Materials and Biocatalysis; Smith, et al.;
ACS Symposium Series; American Chemical Society: Washington, DC, 2015.

found. Higher PTAD used in the reaction produced higher yields of all products. With increasing temperature, the yield of **B** increased slightly, that of **C** decreased slightly, and that of **D** increased more noticeably. Owing to polymer formation, the reaction product mixture exhibited a self-curing behavior as a function of time. Thus, the viscosity of a mixture containing PTAD and soybean oil in a 3:10 weight ratio increased 40-fold in about 2 h at room temperature, suggesting its possible use as an additive in lubricants, caulking, cement and thickener applications.

A related reaction entailed diethyl azodicarboxylate (DEAD) (*22*). DEAD and SBO were mixed together in the absence of catalyst and solvent. In a microwave oven the reaction was achieved in 5–15 minutes at 90-110ºC. (The reaction could also be conducted using conventional heat.) Interestingly, in this case only ene reaction products (e.g., structure **E**) were found (Figure 3). This reaction product mixture also exhibited a self-curing behavior as a function of time (*23*), although not as fast as the reaction involving PTAD.

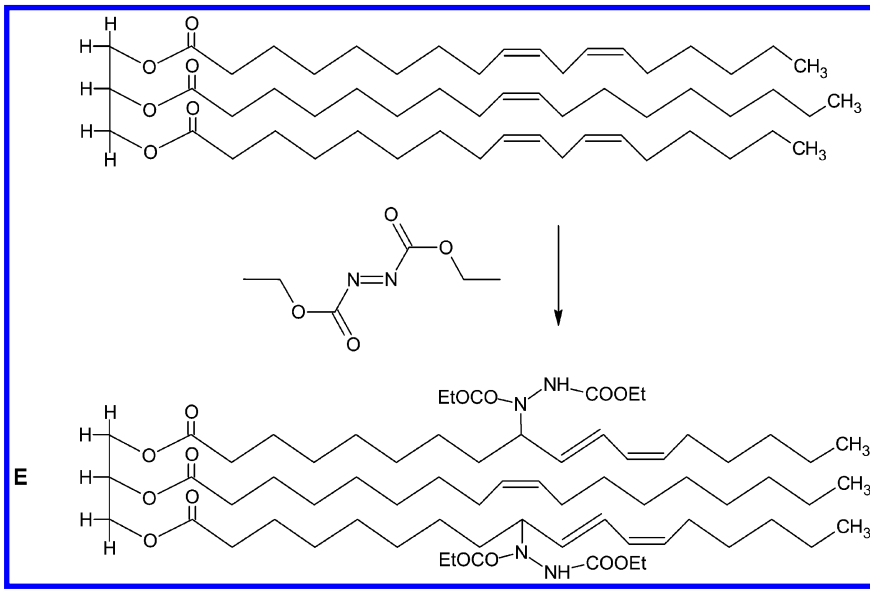

Figure 3. Schematic diagram for the reaction of soybean oil with DEAD. Structure E is a generic representation, where the DEAD moiety can be attached to different carbons at α positions to the double bonds in the product.

It may be noted that most of the current lubricants originate from petroleum stock, which may make them environmentally less friendly and more difficult to dispose of. Plant oils are good platforms for new products that can substitute for conventional mineral oil-based lubricating oils and synthetic esters.

Pericyclic Reactions - Other Derivatives

In the previous section, it was shown that the pericyclic reaction of SBO and DEAD produced SBO-aza-dicarboxylate ester (structure **E**). In another paper

In Green Polymer Chemistry: Biobased Materials and Biocatalysis; Smith, et al.;
ACS Symposium Series; American Chemical Society: Washington, DC, 2015.

Publication Date (Web): June 18, 2015 | doi: 10.1021/bk-2015-1192.ch015

(*24*), it was also shown that the alkaline and the enzymatic hydrolysis of this product produced different products (Figure 4). Thus, lipase hydrolysis cleaved the glycerol from the triglyceride to generate the fatty acid-aza-dicarboxylate (**G**). Hydrolysis with NaOH, however, produced the hydrazine derivative of the fatty acids (**H**).

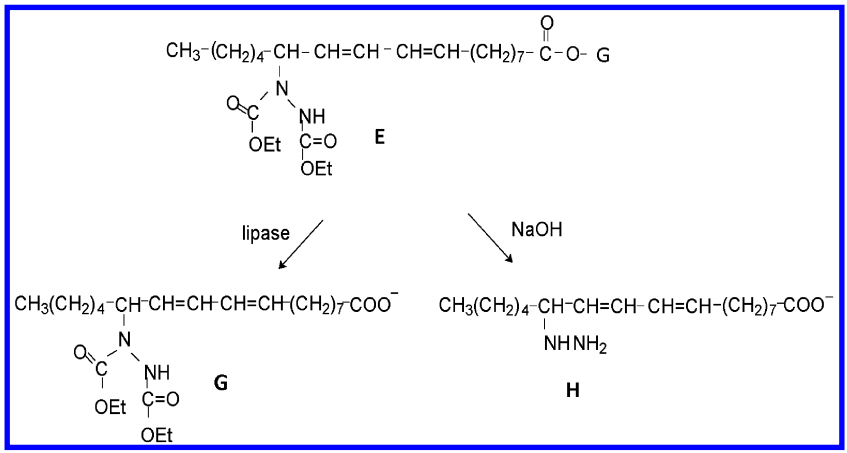

Figure 4. Enzymatic and alkaline hydrolysis of soybean oil-DEAD adduct.

Other derivatives of SBO-aza-dicarboxylate ester (**E**) may also be of interest. This compound can be subjected to transesterification with methanol, similar to the formation of methyl soyate (*25*). Thus, the addition of a lipase to a mixture of SBO, methanol, and water enabled this reaction to occur, as shown in Figure 5.

The reaction shown in Figure 5 can decrease the molecular weight of the SBO-DEAD reaction product, and thereby its viscosity. As noted in the previous section, the SBO-DEAD product can undergo self-curing reaction with substantial increase in viscosity. Thus, the combination of self-curing reaction and transesterification with methanol can permit a range of viscosities to be achieved, depending on the specific need of the end-use application.

Other compounds can be synthesized through transesterification with polyols. Two examples of enzyme-catalyzed reactions are shown in Figure 6 for glycerol and poly(ethylene glycol) (PEG) (*25*). In both cases, surfactant-like structures were produced, each with a fatty acid derivative coupled to a water-soluble moiety.

Other Triglyceride Derivatives

Plant oils typically contain olefins and esters, both of which can be modified to form different derivatives. In fact, the number of possibilities to derivatize triglycerides is very large and limited only by the researcher's creativity and availability of time and manpower. Two examples from the authors' work can be cited here. In the first example, SBO was subjected to microwave-irradiation (MI) and heat bodying (HB) at 200–250ºC for 20–60 min (*26*). Both procedures produced increased viscosity compared with untreated SBO. Pour point decreased

In Green Polymer Chemistry: Biobased Materials and Biocatalysis; Smith, et al.;
ACS Symposium Series; American Chemical Society: Washington, DC, 2015.

Publication Date (Web): June 18, 2015 | doi: 10.1021/bk-2015-1192.ch015

from −9ºC for the untreated SBO, −15ºC for the HB oil, and −18ºC for the MI oil despite viscosity increases. Pressurized DSC analysis showed higher oxidative stability for HB oil with even higher stability for MI oil. MI treatment improved the cold-flow behavior of SBO but reduced its potential as a lubricant.

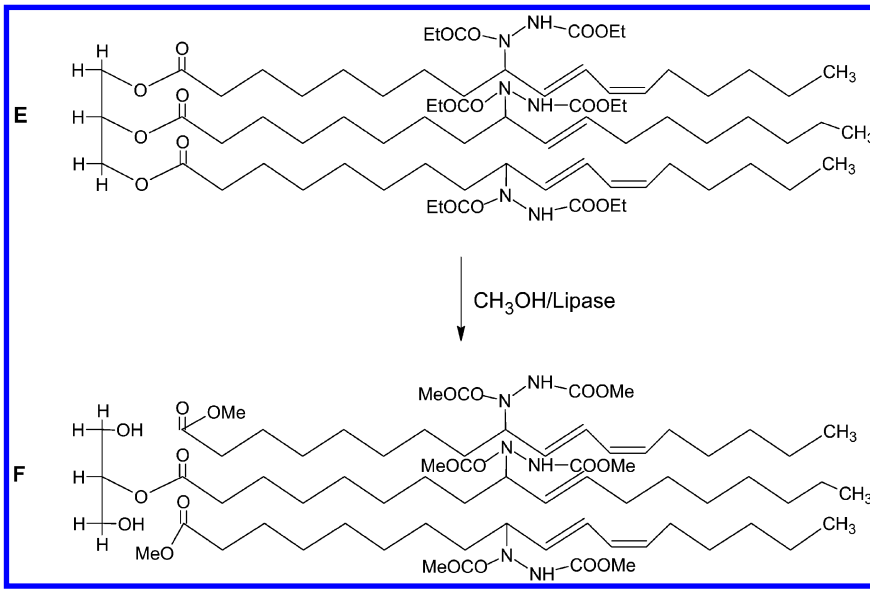

Figure 5. Enzyme-catalyzed transesterification of SBO-DEAD adduct with methanol.

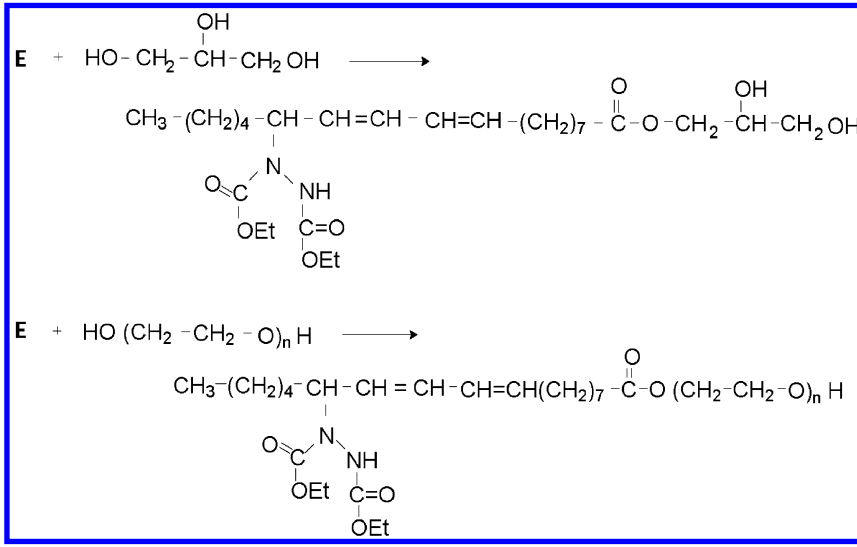

Figure 6. Two examples of enzymatic transesterification with polyols.

In Green Polymer Chemistry: Biobased Materials and Biocatalysis; Smith, et al.;
ACS Symposium Series; American Chemical Society: Washington, DC, 2015.

Publication Date (Web): June 18, 2015 | doi: 10.1021/bk-2015-1192.ch015

In the second example, hydrogenation was applied to cottonseed oil. Eleven catalysts based on Ni, Pd, and Pt from two manufacturers were used for hydrogenating cottonseed oil, with the goal of minimizing trans fatty acid (TFA) content (*27*). Despite different temperatures, catalyst levels, and reaction times being used, the data from each catalyst type fell on the same curve when the TFA level was plotted against the iodine value (IV). Under low-pressure, high-mixing hydrogenation conditions, Ni, Pd, and Pt catalysts all produced 5% TFA and 5% stearic acid at 95 IV; however, at 70 IV, only Pt catalysts produced 9% TFA and about 17% stearic acid. Kinetic modeling provided a better understanding of the relative reaction rates involved in hydrogenation. Pt catalysts converted linoleic and oleic acids more slowly to TFA and quickly hydrogenated TFA, thereby leading to low TFA levels. Furthermore, in a direct comparison of hydrogenated soybean oil and cottonseed oil, lower TFA and stearic levels were found with hydrogenated cottonseed oil (*28*).

Publication Date (Web): June 18, 2015 | doi: 10.1021/bk-2015-1192.ch015

Polymers Directly from Triglycerides

In the last section it was mentioned that soybean oil and cottonseed oil were hydrogenated at different levels using commercial Ni, Pt and Pd catalysts under different hydrogenation conditions. Since the reactivity of plant oils often depends on the amount and the type of olefins present, the ability to vary the olefin type and amount is useful in generating targeted triglyceride derivatives. This possibility was pointed out in a recent report (*29*). A preliminary study of the thermal polymerization of soybean oil, cottonseed oil, and hydrogenated cottonseed oil (carried out at 330 °C for 6 hours in nitrogen) produced polymers with viscosities in decreasing order: soybean oil polymer > cottonseed oil polymer > polymer derived from cottonseed oil that had been hydrogenated to IV 97. These viscosity results for the polymers are consistent with the amounts of unsaturation present in the starting oils. Appropriate blending of hydrogenated and/or unhydrogenated triglyceride oils may also be used for polymerization to optimize the properties of the resulting products.

Reactions with Epoxidized Triglycerides

It is well known that plant oils can be epoxidized; in fact, epoxidized soybean oil is a commercial product and employed as a poly(vinyl chloride) plasticizer, among other applications. Because the epoxidized soybean oil is commercially available, it is a useful synthon for the development of additional products, as shown in the examples below.

Triglyceride Acetonide

In the first example, a new type of branched soybean oil and its methyl ester was made that involved the formation of acetonides from epoxide (*30*) (Figure 7).

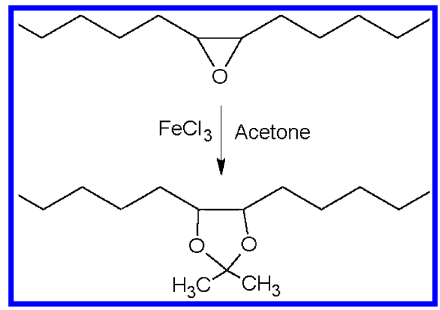

Figure 7. Formation of acetonide from epoxidized triglyceride.

Publication Date (Web): June 18, 2015 | doi: 10.1021/bk-2015-1192.ch015

The procedure entailed the room-temperature reaction in the presence of ferric chloride catalyst and was found to be facile and environmentally friendly. The products were fully characterized with the help of model compounds, including elemental analysis, IR, NMR, and GC-MS. From the analytical results, it appeared that the reaction could readily be used to make acetonides out of soybean oil, methyl soyate, methyl linoleate, and methyl oleate. There are many advantages of this reaction. First, the acetonide reaction produces a branched fatty acid moiety, which can provide improved properties for methyl soyate and soybean oil. Secondly, the reaction is catalyzed by ferric chloride, which is less likely to cause hydrolysis of the ester or the glyceride. Thirdly, the use of room temperature results in reduced energy usage. Finally, acetone is inexpensive and has a good environmental profile.

Triglyceride Aminohydrin

One of the interesting reactions is to convert the epoxide functionality into aminohydrin. Thus, a facile (and environmentally friendly) reaction was discovered between epoxidized methyl oleate and aniline to produce an oleate-aniline adduct, without the formation of fatty amide (*31*) (Figure 8).

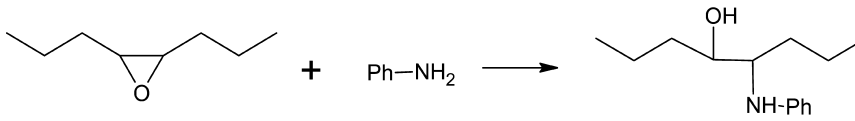

Figure 8. Conversion of epoxide to aminohydrin with the aid of ionic liquids (IL).

The reaction shown in Figure 8 was carried out neat, with a catalytic amount of an ionic liquid. No solvent was used, no byproducts were produced, and the ionic liquid could be recovered and recycled. The reaction products were fully characterized by NMR and GC-MS. Subsequent work indicated that a triglyceride

modified with aniline improved its thermal stability and mechanical wear for the lubricant application (*32*). The advantages of this reaction are that it is easily performed, gives good yield, and requires only a small amount of ionic liquid as a catalyst. The reaction is a good method to introduce an aromatic amine onto the fatty acid structure.

A variation of this study is the addition of diethylamine onto epoxidized oil, using $ZnCl_2$ as a catalyst (Figure 9) (*33*). In this case, an aliphatic aminohydrin is obtained.

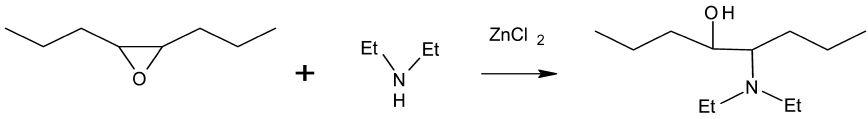

Figure 9. Reaction of epoxide with diethylamine in the presence of $ZnCl_2$.

Publication Date (Web): June 18, 2015 | doi: 10.1021/bk-2015-1192.ch015

Triglyceride Azidohydrin and Its Click Derivatives

Another interesting reaction is to convert the epoxide functionality into azidohydrin, also with the help of an ionic liquid (*34*) (Figure 10).

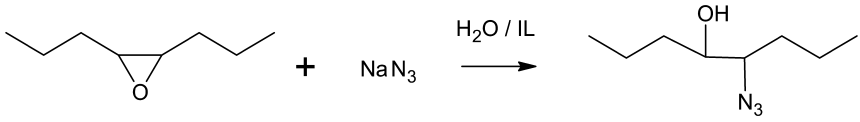

Figure 10. Conversion of epoxide to azidohydrin with the aid of ionic liquids (IL).

The azidization reaction was carried out in water with only a small amount of an ionic liquid as a catalyst. The distribution of azide and alcohol functionalities on the fatty acid moiety was approximately random. This reaction was applied to methyl oleate, methyl linoleate, soybean oil, and methyl soyate, and high yields were observed. The resulting chemical structures were confirmed by ^{13}C NMR.

In addition, the azide product was subjected to the click reaction with phenylacetylene (Figure 11) (*35*). The reaction was relatively easy to do and gave high yields. The click reaction turned out to be a convenient method to attach an acetylene-containing moiety (phenylacetylene, in this case) onto a fatty ester or a triglyceride.

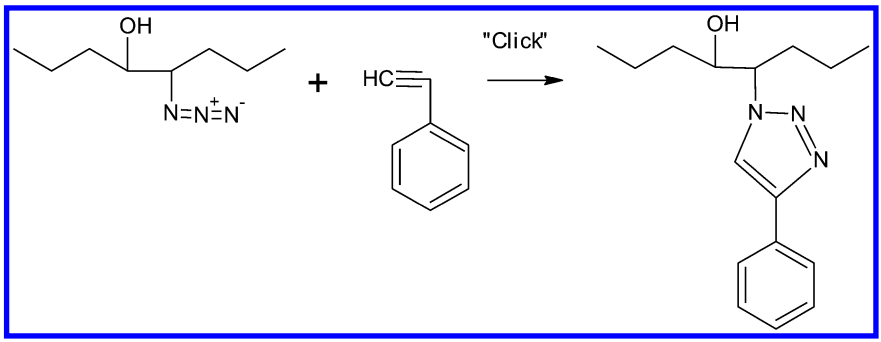

Figure 11. Click reaction between azidohydrin and phenylacetylene.

Publication Date (Web): June 18, 2015 | doi: 10.1021/bk-2015-1192.ch015

Polymers from Epoxidized Triglyceride

Liu and Erhan showed earlier that the use of BF_3-etherate could polymerize epoxidized soybean oil into an insoluble material (*36*). It was noted that the product could be converted into hydrogels by saponification for possible use in personal care. Subsequently Liu and Biswas (*37*) showed that fluoroantimonic acid hexahydrate could be employed as a catalyst in ethyl acetate. More recent work suggested that fluorosulfonic acid was also a potent catalyst for the polymerization of vernonia oil (*38*) and soybean oil (*39*). In addition, furan-like structure can be produced, which can undergo Diels-Alder reaction to produce further derivatives (*40*).

Conclusions and Perspectives

Plant oils are valuable agricultural commodities and useful raw materials for the preparation of value-added products. In this article, a review is made of the various structural modifications made on plant oils in the authors' laboratories. A wide range of products have been made from plant oils and their epoxidized derivatives. The reactions include Diels-Alder, ene reaction, transesterification, acid or enzymatic hydrolysis, heat-bodying reaction, hydrogenation, epoxidation, formation of acetonide, aminohydrin, azidohydrin, click reaction, and polymerization. Some of these products are useful in lubricants to enhance viscosity, thermal stability, or mechanical wear. Yet, these products serve only as harbingers for what can potentially be done. With proper incentives and further efforts, many more new reaction pathways and new structures can surely be produced in the future. Further products may also be possible but require appropriate applications development and customer input.

A key determinant in the future growth of plant oils as raw materials for industrial products is the price and the availability of plant oils relative to petroleum crude. Currently petroleum-based products still dominate the market. Because of their extended time of use, the manufacturing facilities are already in place to produce the petroleum-based products, and the companies have qualified

those products for various applications. Nonetheless, with increasing awareness of the need for sustainability, environmental stewardship, and green chemistry in the future, the use of agri-based, renewable raw materials is expected to increase in the future, but it will take time to slowly replace the well-entrenched petroleum-based products. Whereas the public support of sustainability can encourage increased R&D in this area, ultimately the long-term commercial prospect of triglyceride-based products will depend on the ease of use and the cost effectiveness of the new products, the success of marketing, the response from manufacturers of petroleum-based products, and other business-related considerations.

Publication Date (Web): June 18, 2015 | doi: 10.1021/bk-2015-1192.ch015

Acknowledgments

Thanks are due to many collaborators over the years whose names appear in the publications cited. Mention of trade names or commercial products in this publication is solely for the purpose of providing specific information and does not imply recommendation or endorsement by the U.S. Department of Agriculture. USDA is an equal opportunity provider and employer.

References

1. Karak, N. *Vegetable Oil-Based Polymers*; Woodhead Publishing: Cambridge, U.K., 2012.
2. Erhan, S. Z. *Industrial Uses of Vegetable Oils*; AOCS Press: Champaign, Illinois, U.S.A., 2005.
3. Petrovic, Z. S.; Zlatanic, A.; Lava, C. C.; Sinadinovic-Fiser, S. Epoxidation of soybean oil in toluene with peroxoacetic and peroxoformic acids: kinetics and side reactions. *Eur. J. Lipid Sci.Technol.* **2002**, *104*, 293–299.
4. Kuo, M. C.; Chou, T. C. Kinetics and mechanism of the catalyzed epoxidation of oleic acid with oxygen in the presence of benzaldehyde. *Ind. Eng. Chem. Res.* **1987**, *26*, 277–284.
5. Knothe, G. Dependence of biodiesel fuel properties on the structure of fatty acid alkyl esters. *Fuel Process. Technol.* **2005**, *86*, 1059–1070.
6. Srivastava, A.; Prasad, R. Triglycerides-based diesel fuels. *Renewable Sustainable Energy Rev.* **2000**, *4*, 111–133.
7. Warth, H.; Mulhaupt, R.; Hoffmann, B.; Lawson, S. Polyester networks based upon epoxidized and maleinated natural oils. *Angew. Makromol. Chem.* **1997**, *249*, 79–92.
8. Tran, P.; Seybold, K.; Graiver, D.; Narayan, R. Free radical maleation of soybean oil via a single-step process. *J. Am. Oil Chem. Soc.* **2005**, *82*, 189–194.
9. Li, F.; Hanson, M. V.; Larock, R. C. Soybean oil-divinylbenzene thermosetting polymers: R. C. Soybean oil-divinylbenzene thermosetting polymers: synthesis, structure, properties and their relationships. *Polymer* **2001**, *42*, 1567–1579.

10. Sharma, V.; Kundu, P. P. Addition polymers from natural oils: a review. *Prog. Polym. Sci. (Oxford)* **2006**, *31*, 983–1008.
11. Khot, S. N.; Lascala, J. J.; Can, E.; Morye, S. S.; Williams, G. I.; Palmese, G. R.; Kusefoglu, S. H.; Wool, R. P. Development and application of triglyceride-based polymers and composites. *J. Appl. Polym. Sci.* **2001**, *82*, 703–723.
12. Soni, S.; Agarwal, M. Lubricants from renewable energy sources – a review. *Green Chem. Lett. Rev.* **2014**, *7*, 359–382.
13. Lligadas, G.; Ronda, J. C.; Galià, M.; Cádiz, V. Renewable polymeric materials from vegetable oils: a perspective. *Mater. Today* **2013**, *16*, 337–343.
14. United Soybean Board. *Soy-based paints and coatings*; http://soynewuses.org/wp-content/uploads/44422_TDR_PaintsCoatings.pdf (accessed on January 20, 2015).
15. Xia Y., ; Larock, R. C. Vegetable oil-based polymeric materials: synthesis, properties, and applications. *Green Chem.* **2010**, *12*, 1893–1909.
16. Guner, S. F.; Yagci, Y.; Erciyes, A. T. Polymers from triglyceride oils. *Prog. Polym. Sci.* **2006**, *31*, 633–670.
17. Biswas, A.; Sharma, B. K.; Willett, J. L.; Erhan, S. Z.; Cheng, H. N. Soybean oil as a renewable feedstock for nitrogen-containing derivatives. *Energy Environ. Sci.* **2008**, *1*, 639–644.
18. Meier, A. R. M.; Metzger, J. O.; Schubert, U. S. Plant oil renewable resources as green alternatives in polymer science. *Chem. Soc. Rev.* **2007**, *36*, 1788–1902.
19. Fleming, I. *Pericyclic Reactions*; Oxford University Press: Oxford, 1998.
20. Sankararaman, S. *Pericyclic Reactions - A Textbook*, 1st ed; Wiley-VCH: Weinheim, 2005.
21. Biswas, A.; Cheng, H. N.; Kim, S.; Liu, Z. Modified triglyceride oil through reactions with phenyltriazolinedione. *J. Am. Oil Chem. Soc.* **2014**, *91*, 125–131.
22. Biswas, A.; Sharma, B. K.; Willett, J. L.; Vermillion, K.; Erhan, S. Z.; Cheng, H. N. Novel modified soybean oil containing hydrazino-ester: synthesis and characterization. *Green Chem.* **2007**, *9*, 85–89.
23. Biswas, A.; Sharma, B. K.; Willett, J. L.; Erhan, S. Z.; Cheng, H. N. Room-temperature self-curing ene reactions involving soybean oil. *Green Chem.* **2008**, *10*, 298–303.
24. Biswas, A.; Shogren, R. L.; Woods, K. K.; Erhan, S. Z.; Cheng, H. N. New bio-based materials from soybean oil: hydrazine and related derivatives. *ACS Polym. Prepr.* **2006**, *47*, 259–260.
25. Biswas, A.; Shogren, R. L.; Willett, J. L.; Erhan, S. Z.; Cheng, H. N. Enzymatic Products from Modified Soybean Oil Containing Hydrazinoester. *ACS Symp. Series* **2008**, *999*, 76–85.
26. Biswas, A.; Adhvaryu, A.; Stevenson, D. G.; Sharma, B. K.; Willett, J. L.; Erhan, S. Z. Microwave irradiation effects on the structure, viscosity, thermal properties and lubricity of soybean oil. *Ind. Crops Prod.* **2007**, *25*, 1–7.
27. Cheng, H. N.; Dowd, M. K.; Easson, M. W.; Condon, B. D. Hydrogenation of Cottonseed Oil wi B.D. Hydrogenation of Cottonseed Oil with Nickel,

Palladium and Platinum Catalysts. *J. Am. Oil Chem. Soc.* **2012**, *89*, 1557–1566.
28. Cheng, H. N.; Rau, M. W.; Dowd, M. K.; Easson, M. W.; Condon, B. D. Comparison of Soybean and Cottonseed Oils upon Hydrogenation with Nickel, Palladium and Platinum Catalysts. *J. Am. Oil Chem. Soc.* **2014**, *91*, 1461–1469.
29. Cheng, H. N.; Rau, M.; Dowd, M. K.; Easson, M. W.; Condon, B. D. Hydrogenated cottonseed oil as raw material for biobased materials. *ACS Symp. Ser.* **2013**, *1144*, 359–371.
30. Biswas, A.; Sharma, B. K.; Vermillion, K.; Willett, J. L.; Cheng, H. N. Synthesis of Cyclic Ketal from Soybean Oil and Fatty Esters. *J. Agric. Food Chem.* **2011**, *59*, 3066–3070.
31. Biswas, A.; Sharma, B. K.; Doll, K.; Willett, J. L.; Erhan, S. Z.; Vermillion, K.; Cheng, H. N. Synthesis of an Amine-Oleate Derivative Using an Ionic Catalyst. *J. Agric. Food Chem.* **2009**, *57*, 8136–8141.
32. Biswas, A., Doll, K.; Cheng, H. N.; Sharma, B. K.. Process for preparation of nitrogen-containing vegetable oil-based lubricant additive. U.S. Patent 8,841,470, September 23, 2014.
33. Biswas, A.; Adhvaryu, A.; Gordon, S. H.; Erhan, S. Z.; Willett, J. L. Synthesis of diethylamine functionalized soybean oils. *J. Agric. Food Chem.* **2005**, *53*, 9485–9490.
34. Biswas, A.; Sharma, B. K.; Willett, J. L.; Adhvaryu, A.; Erhan, S. Z.; Cheng, H. N. Azide Derivatives of Soybean Oil and Fatty Esters. *J. Agric. Food Chem.* **2008**, *56*, 5611–5616.
35. Biswas, A.; Sharma, B. K.; Klasson, K. T.; Cheng, H. N. New Bio-Based Materials From Vegetable Oil: Amination and Click Reactions. *ACS Polym. Prepr.* **2011**, *52*, 78–79.
36. Liu, Z.; Erhan, S. Z. Ring-opening Polymerization of Epoxidized Soybean Oil. *J. Am. Oil Chem. Soc.* **2010**, *87*, 437–444.
37. Liu, Z.; Biswas, A. Fluoroantimonic acid hexahydrate (HSbF6-6H2O) catalysis: The ring-opening polymerization of epoxidized soybean oil. *Appl. Catal., A* **2013**, *453*, 370–375.
38. Biswas, A.; Cheng, H. N.; Klasson, K. T.; Liu, Z.; Berfield, J.; Ayorinde, F. O. Direct polymerization of vernonia oil through cationic means. *J. Am. Oil Chem. Soc.* **2014**, *91*, 2111–2116.
39. Biswas, A.; Liu, Z.; Cheng, H. N. Polymerization of Epoxidized Triglyceride with Fluorosulfonic Acid. *Int. J. Polym. Anal. Charact.* Submitted for publication.
40. Biswas, A.; Liu, Z.; Berfield, J. L.; Cheng, H. N. Synthesis of Novel Plant Oil Derivatives: Furan and Diels-Alder Reaction Products. *Int. J. Agric. Sci. Technol.* Accepted for publication.

Publication Date (Web): June 18, 2015 | doi: 10.1021/bk-2015-1192.ch015

Publication Date (Web): June 18, 2015 | doi: 10.1021/bk-2015-1192.ch016

Chapter 16

Soy-Based Building Blocks for Advanced Photocure Coating Systems

Vijay Mannari,* Chintankumar Patel, Wenyin Li, and Ali Kiamanesh

Coatings Research Institute, 118 Sill Hall, Eastern Michigan University, Ypsilanti, Michigan 48197
***E-mail: vmannari@emich.edu. Phone: +1 734-487-1235.**

Photocuring technology is among the fastest-growing advanced coating technologies primarily due to their sustainability features, potential for enabling new products, and economy. Despite these benefits, the materials used in the current photocure systems are predominantly derived from petrochemical sources, making them unsustainable over the long term. Development of renewable resource-based alternate materials tailored for photocure applications is, therefore, critical to future sustainable development of photocure coating technology.

This presentation highlights our research efforts in developing a platform of soybean oil-based value-added building blocks and demonstration of their suitability as alternative raw materials in advanced UV-curing coating compositions. A hyper-branched soy urethane acrylate (HSPU) has been developed and used as the primary component of UV-curable composition. Coatings based on HSPU with varying acrylate content (using reactive diluent) and high bio-based content have been characterized and compared. Due to hyperbranched structure and large free volume in their inherent structure, they exhibited interesting properties for many potential industrial applications. Another group of soy-based derivatives—low viscosity and high-functionality acrylate monomers—have been designed and used as reactive diluent in UV-cure formulation. The study demonstrates potential of these low odor and bio-based reactive diluents as partial or full replacement of conventional reactive diluents.

In Green Polymer Chemistry: Biobased Materials and Biocatalysis; Smith, et al.;
ACS Symposium Series; American Chemical Society: Washington, DC, 2015.

Publication Date (Web): June 18, 2015 | doi: 10.1021/bk-2015-1192.ch016

Introduction

Over the past few decades, many advanced technologies in the field of printing inks and coatings have been commercialized, primarily to address environmental concerns and related regulations. Among these technologies are water-borne, high-solids, powder coatings, and radiation curable coatings and inks. All these technologies have their own merits and challenges and hence, depending upon end-use requirements of the products, have grown in different market segments.

Radiation curable coatings, and more specifically the UV-cure coatings, very clearly stand apart from other systems in terms of their low environmental impact, efficiency, low energy consumption, and ability to enable new products. These benefits are primary drivers for the growth of UV-curable systems, in both the traditional and emerging new areas of applications. Despite these benefits, if we take a closer look at the supply chain of the materials used for UV-cure systems, it is evident that almost all of the materials used have fossil petroleum origin. This makes the current UV-cure systems unsustainable. For future sustainable development and environmental leadership, we must reduce our dependence on petroleum-based resources and reduce the carbon footprint of UV-cure systems.

Bio-based materials, such as plant oils, are excellent renewable resources, and using their chemical functionality, they can be transformed into many different types of polymers and intermediates (*1–6*). Our research group has focused on developing a platform of polymer building blocks derived from soybean oil for coatings and related applications (*7–19*). Polymeric and oligomeric materials used for UV-cure systems must meet stringent requirements of functionality, reactivity, viscosity, thermo-mechanical properties of their films, and cost for their successful deployment as film formers (*20*). In the present study we have designed, developed, and demonstrated application of some novel soy-based oligomers and reactive diluents as alternative sustainable materials for UV-cure systems.

Experimental

Materials

Epoxy methyl soyate (EMS) (Vikoflex 7010), Epoxy methyl linseedate (EML) (Vikoflex 9010), and Dipropylene glycol diacrylate (DPGDA) (SARTOMER SR-508) were procured from Arkema, U.S.A.. Epoxy acrylate oligomer (Rahn 10-620/TM20) was supplied by Rahn U.S.A. Corp., USA. Aliphatic urethane diacrylate (Ebecryl 4833) used in this study was supplied by Cytec, U.S.A.. Toluene diisocyanate (TDI) was received from Bayer Material Science, U.S.A.. 2-hydroxyethyl acrylate (HEA) was procured from San Ester Corp. All the above materials were used as received. All other chemicals such as ethyltriphenylphosphonium bromide (ETPPB), triethylamine (TEA), acrylic acid

(AA), methyl ether of hydroquinone (MEHQ), calcium oxide (ReagentPlus), 48% aqueous solution of tetrafluoroboric acid (TFBA), dibutyltin dilaurate (DBTDL), toluene, and methyl isobutyl ketone (MIBK) were purchased from Sigma Aldrich, U.S.A.. Toluene and MIBK were dried overnight over molecular sieve before use. Irgacure 184 and Irgacure 819, used as photoinitiators, were supplied by BASF, U.S.A.. Low carbon cold-rolled steel panels (type R) were purchased from Q-panel Lab products, U.S.A..

Characterization Methods

FTIR Spectroscopy

The reactive diluents and oligomer synthesized in this study were characterized for their functional groups by FTIR spectroscopy in the mid-operating range of 4000–400 cm^{-1} using Bruker Tensor 27 FTIR analyzer. The representative spectra of %T (transmission) versus wave number are recorded. FT-IR spectroscopy has also been used to determine percent extent of conversion of acrylate groups during UV-curing process using peak-area method.

Size Exclusion Chromatography

The reactive diluents and oligomer were also characterized for molecular weight using gel-permeation chromatography (GPC). A GPC system consisting of three Phenogel columns from Phenomenex (U.S.A.)—PhenogelTM 5µ 50A, PhenogelTM 5µ 100A, and PhenogelTM 5µ 500A, covering molecular weight range from 100 – 15000 g/mol—Viscotek VE 3580 RI detector, and Malvern 270 Dual detector was used. The sample was dissolved in HPLC grade tetrahydrofuran (THF) (4 – 6 mg/ml). Sample injection volume was 100 µL, flow rate of carrier solvent (THF) was 1.00 ml min-1, and operating temperature was 45°C. Retention time of standard samples of mono-dispersed polystyrene of different molecular weight ranging from 162 through 232763 (12 standards), dissolved in THF, were used for generating molecular weight scale (caliberation curve). The average molecular masses, Mn, Mw, and polydispersity index, were determined by software OmniSEC 4.7.

Thermal Analysis

The differential scanning calorimetry (DSC) analysis of cured films was performed using DSC Q 2000 from TA instruments, U.S.A.. 6 to 7 mg samples were accurately weighed in a standard aluminium pan, and scanning was done by ramping the temperature from –30 °C to 175 °C at a heating rate of 10 °C/min.

Publication Date (Web): June 18, 2015 | doi: 10.1021/bk-2015-1192.ch016

Gel Content of the Cured Films

To evaluate crosslinking in the film, the gel content of the cured coatings was evaluated by immersing the accurately weighed free films (25mm×12.5mm) in methyl ethyl ketone (MEK). After 24 h of immersion, the films were dried in oven at 80 °C for 1 h and accurately weighed. The gel content (% by mass) was calculated as follows:

$$\% \text{ Gel content} = (Wg/ Wf) \times 100$$

Where, Wf is the mass of the original dry film and Wg is the mass of the film after extraction with MEK.

Publication Date (Web): June 18, 2015 | doi: 10.1021/bk-2015-1192.ch016

Coating Properties

The cured coating films were evaluated for different mechanical properties such as adhesion (ASTM D 3359-02), impact resistance (ASTM D 2794 - 93), pencil hardness (ASTM D -3363 - 05), and Konig pendulum hardness (ASTM 4366-95). The dry film thickness of the coatings was measured by a "micro-tri-gloss µ" instrument from BYK-Gardner, Germany. The solvent resistance was determined by a double rub test using methyl ethyl ketone (MEK) as solvent (ASTM D 5402 - 06). It should to be noted that the pencil hardness reported refers to the hardest pencil that produced gouge in the film.

Tensile Properties of Cured Films

The tensile properties of the cured free films (0.5 inch x 3 inch) were evaluated as per standard method (ASTM D 2370) at a cross head speed of 0.2 inch per min and 2 inch of gauge length. Tensile properties of films are reported in Table 7.

Synthesis

Synthesis of Acrylated EMS (EMSHEAT) by Trans-Esterification of EMS with HEA

In a three-neck flask equipped with mechanical stirrer, thermo couple, and heating mantle connected with temperature controller, 3 mole of HEA, 1 mole of EMS, and MEHQ (0.5% by mass of HEA) were charged and heated to 120 °C. Calcium oxide, 1% by mass of EMS, which was calcined at 700 °C for 2 h prior to use was added to the reaction mass, and reaction was carried out at 90 – 95 °C for 3 h. After completion of reaction, calcium oxide was allowed to settle, and the supernatant liquid mass was washed with distilled water and diethyl ether to remove excess HEA. 10% (W/W) solution of NaCl was used to assist better separation during washing. Diethyl ether was then evaporated in a rotary vacuum evaporator to obtain the final product (EMSHEAT).

Publication Date (Web): June 18, 2015 | doi: 10.1021/bk-2015-1192.ch016

Table 1. Typical Characteristics of RDs

Reactive Diluent Identity	*Average Functionality (Calculated)*	*Wt. per Acrylate (WPA), g. (Calculated)*	*Saponification Value (ASTM D 464)*	*Viscosity* @25°c, (Cp)*	*% Bio-Based Content (Calculated)*
Soy-RD1	1.14	349	301	206.3	84.7
Soy-RD2	2.12	206	360	103.3	74.9
Lin-RD1	1.47	290	320	464.1	81.1
DPGDA	2.00	121	463	10.0	0

* *spindle#1, 750 rpm.*

Reactive diluents Soy-RD1, Soy-RD2, and Lin-RD1 were prepared by acrylation of EMS, EMSHEAT, and EML, respectively, using identical processes. In a typical process for all the RDs prepared, molar excess of acrylic acid was used with one equivalent of oxirane compound. Acrylic acid was placed in a three-neck flask equipped with mechanical stirrer, water condenser, thermocouple, and heating mantle connected with temperature controller to which 1% by mass of TEA was added. The reaction mixture was then heated to 100 °C and EMS/EMSHEAT/EML (as applicable) was added drop wise over a period of 1 h at 100 °C. The reaction was further continued until weight percent of oxirane oxygen (%OOC, ASTM D 1652 – 04) was reduced below 0.2%. After completion of reaction, the excess acrylic acid was removed by washing its diethyl ether solution with distilled water, followed by washing with 5% (W/W) solution of sodium bicarbonate and finally by distilled water. Diethyl ether was then removed in a rotary vacuum evaporator to obtained Soy-RD1, Soy-RD2, and Lin-RD-3 reactive diluents. The representative chemical structures of RDs are shown in Figure 1.

Publication Date (Web): June 18, 2015 | doi: 10.1021/bk-2015-1192.ch016

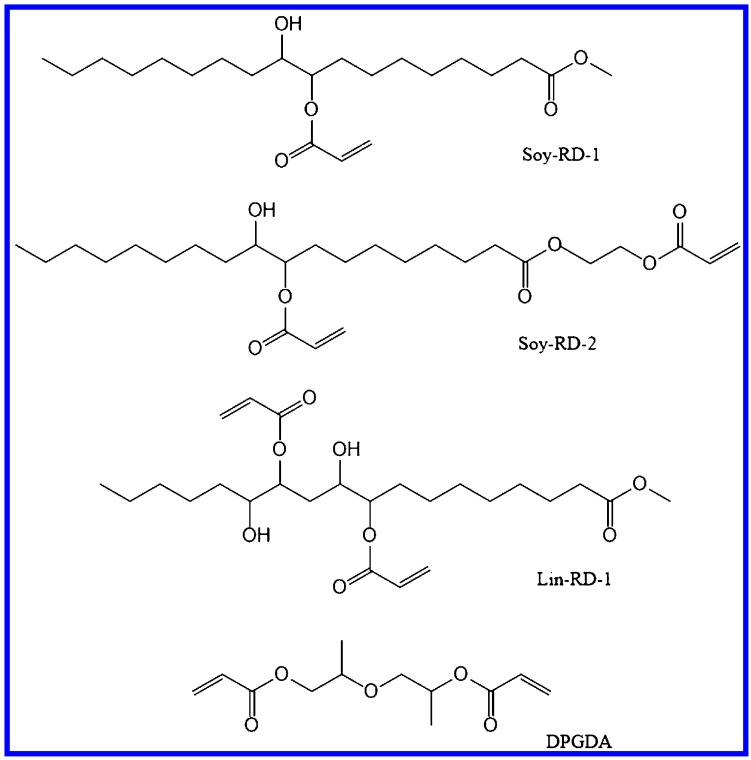

Figure 1. Representative structures of reactive diluents used in the study.

The reactive diluents were characterized for saponification value (ASTM D 464 – 05), acid value (ASTM D 465 – 05), and viscosity (ASTM D 4287-00) by using cone and plate viscometer (Brookfield CAP 2000+). Their properties are presented in Table 1.

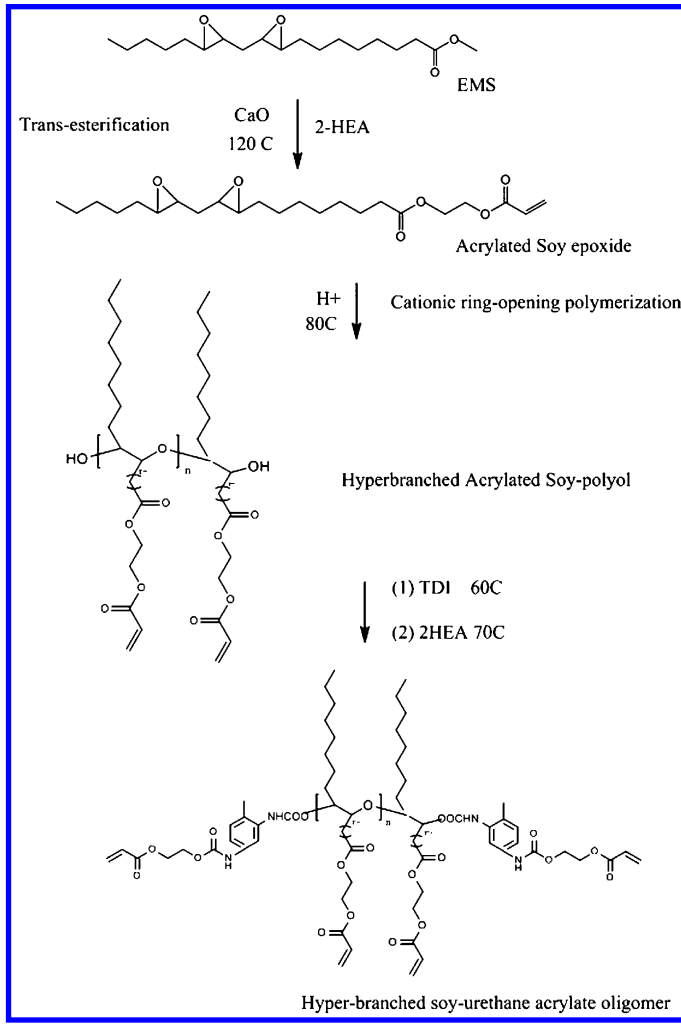

Figure 2. Schematic representation of preparation of HSUA.

Synthesis of Hyper-Branched Soy-Urethane Acrylate Oligomer (Soy-UA)

Hyper-branched soy-urethane acrylate was synthesized by a series of steps shown below. All the intermediates were characterized to conform their structure before using them for the next step. A simplified reaction scheme is shown in

In Green Polymer Chemistry: Biobased Materials and Biocatalysis; Smith, et al.;
ACS Symposium Series; American Chemical Society: Washington, DC, 2015.

Publication Date (Web): June 18, 2015 | doi: 10.1021/bk-2015-1192.ch016

Figure 2. In the first step, EMSHEAT was synthesized from EMS as per the procedure shown above for reactive diluents. A hyper-branched soy-polyol (EMSHEATP) was then synthesized from EMSHEAT by cationic ring opening polymerization through oxirane groups to yield a soy-polyol with pendent acrylate groups (EMSHEAT polyol). For the reason of simplicity, hyper-branched structure is not shown in Figure 2. EMSHEAT (100.0 g) and 50 mg MEHQ were placed in a three-neck flask equipped with a mechanical stirrer and a thermometer. The reaction mass was cooled to 7 -10°C using an ice bath, and 1g TFBA was added while stirring at 600 rpm. The ice bath was then removed and the reaction was continued for 2 h at room temperature.

Publication Date (Web): June 18, 2015 | doi: 10.1021/bk-2015-1192.ch016

Synthesis of Soy-Urethane Acrylate Oligomer from EMSHEATP (Soy-UA)

In a 100 ml Erlenmeyer flask with a standard taper outer joint, 38.11 g (0.05 eq of hydroxyl) of EMSHEATP was accurately weighed and dissolved in 1:1 (w/w) mixture of toluene and MIBK to give 67% solid content in final composition. 200 ppm DBTDL was added as catalyst. The solution was cooled at 5 °C using an ice-bath. To the cooled solution, 8.7 g (0.1 eq of isocyanates) TDI was added in 2 min under efficient stirring using a magnetic stirrer. The reaction was continued for 2 h in an ice-cold water bath with a gradual increase in temperature up to 20 °C. The reaction continued at 35-40 °C until the desired percent isocyanate content (% NCO) (ASTM D 2572-97) was reached to ensure complete reaction of hydroxyl groups of EMSHEATP. Subsequently, 5.8 g (0.05 eq hydroxyl) of HEA was added to the flask and reacted further at 35 – 40 °C until % NCO content was reached to 0%. Throughout the reaction, care was taken to avoid moisture coming in contact with reaction mixture.

Preparation of Coating Composition

Two types of conventional coating systems, aliphatic urethane acrylate and epoxy acrylate, were studied using different bio-based reactive diluents (Soy-RD1, Soy-RD2 and Lin-RD1) as well as with conventional petrochemical-based reactive diluent (DPGDA). The type and relative proportions of oligomer and reactive diluent used in various coating compositions are shown in Tables 2 and 3. They are mixed with photoinitiator (4 phr, mixture of Irgacure 184: Irgacure 819, 80:20 by wt, used as 50% solution in acetone) under magnetic stirring for 10 min before application. Low-carbon cold-rolled steel panels (Q-panel, type R, 3”x 6”x 0.032”) were cleaned with acetone, and coatings were applied to it with a wire bar applicator to give it a dry film thickness of 50-60 μ. Coatings were given flash off at ambient condition for 30 min and then cured with UV at energy density of 2500 mJ/cm^2. Coatings were conditioned at ambient conditions for minimum 12 h before analysis.

Table 2. Film Properties of UV-Cured Coatings*, **: EA/Reactive Diluent System

Reactive Diluent Type	*Oligomer-/RD Ratio (By Wt.)*	*Konig Hardness (s)*	*Pencil Hardness*	*MEK Double-Rub*	*Impact Resistance(lb·in) Direct*	*Reverse*
Soy-RD-1	100:00	215.6	>5H	>200	20	<20
	80:20	177.8	H	>200	<20	<20
	70:30	147	H	>200	20	<20
	60:40	120.4	H	>200	20	<20
	50:50	86.8	F	>200	40	<20
	40:60	54.6	B	90	40	<20
Soy-RD-2	100:00	215.6	>5H	>200	20	<20
	80:20	184.8	4H	>200	20	<20
	70:30	161	4H	>200	20	<20
	60:40	133	4H	>200	20	<20
	50:50	93.8	2H	>200	20	<20
	40:60	63	4B	106	20	<20
Lin-RD-1	100:00	215.6	>5H	>200	20	<20
	80:20	233.8	4H	>200	<20	<20
	70:30	215.6	4H	>200	20	<20
	60:40	184.8	4H	>200	20	<20
	50:50	154	4H	>200	20	<20
	40:60	109.2	4H	>200	40	<20
DPGDA	100:00	215.6	>5H	>200	20	<20
	80:20	246.4	>5H	>200	20	<20
	70:30	239.4	>5H	>200	<20	<20
	60:40	236.6	>5H	>200	<20	<20
	50:50	232.4	>5H	>200	<20	<20
	40:60	229.6	>5H	>200	<20	<20

** UV energy density = 2500 mJ/cm2.* *** Dry-film thickness = 50-55 microns.*

Publication Date (Web): June 18, 2015 | doi: 10.1021/bk-2015-1192.ch016

Table 3. Film Properties UV-cured Coatings*, **: UA/Reactive Diluent System

Reative Diluent	*Oligomer/RD Ratio (By Wt.)*	*Konig Hardness (s)*	*Pencil Hardness*	*MEK Double-Rub*	*Impact Resistance(lb·in) Direct*	*Reverse*
Soy-RD-1	100:00	53.2	4B	54	160	160
	80:20	37.8	4B	45	160	160
	70:30	22.4	4B	40	160	160
	60:40	14	3B	30	160	160
Soy-RD-2	100:00	53.2	4B	54	160	160
	80:20	25.2	4B	48	160	160
	70:30	19.6	4B	45	160	160
	60:40	16.8	B	40	160	160
Lin-RD-1	100:00	53.2	4B	54	160	160
	80:20	61.6	2B	120	160	160
	70:30	47.6	2B	70	160	160
	60:40	25.2	B	60	160	160
DPGDA	100:00	53.2	4B	54	160	160
	80:20	166.6	H	>200	40	120
	70:30	161	H	>200	40	60
	60:40	152.6	B	>200	20	<20

* *UV energy density = 2500 mJ/cm2.* ** *Dryfilm thickness = 50-55 micron.*

Publication Date (Web): June 18, 2015 | doi: 10.1021/bk-2015-1192.ch016

Results and Discussion

Design of Soy-Based Reactive Diluents

Reactive diluents (RDs) are important components of UV-cure coating formulations. Besides their main roles of lowering viscosity of the compositions, they also significantly influence cure speed, cross-link density, and film shrinkage, among other factors (*21*). One of the major concerns of conventional RDs is their unpleasant odor, skin irritancy, and sensitization (*22*). Soy and linseed oil-based reactive diluents prepared in the present study have been designed to overcome these challenges while maintaining good viscosity reduction characteristics. A series of reactive diluents have been prepared with different chemistry, varying chemical structure, and functionality. Figure 1 shows simplified chemical structures of RDs prepared for this study. The typical characteristics and their bio-based contents, as calculated by a following formula, are shown in Table 1.

In Green Polymer Chemistry: Biobased Materials and Biocatalysis; Smith, et al.;
ACS Symposium Series; American Chemical Society: Washington, DC, 2015.

$$\%\ Biobased\ Content = \frac{amount\ of\ biobased\ carbon}{amount\ of\ total\ carbon} X\ 100$$

Table 1 also shows the average acrylate functionality of reactive diluents studied. To calculate average functionality, we have used the difference in saponification number of starting compounds (methyl esters) and the final products (acrylated products) as the basis. Molecular weights of the starting compounds (methyl esters), determined both by GPC analysis and calculated from their saponification values, were very close and were also used in calculations of average functionality of reactive diluents.

FT-IR spectra for all the reactive diluents studied have been recorded for their functional group characterization. All of the oil-derived reactive diluents RD1, RD2, and RD3 essentially showed fairly identical absorption peaks, indicating similarity of their functional group types. A representative FT-IR spectrum for RD1 is shown as Figure 3. A strong absorption at 1728 cm^{-1} typical of alpha-beta unsaturated carbonyl stretching, and absence of a peak at 1741 cm^{-1} for corresponding methyl ester, indicates complete trans-esterification of methyl ester and formation of acrylate functions. Peaks at 1407 cm^{-1} (CH=CH2 scissoring band of terminal alkene), 810 cm^{-1} (C-H out-of-plane bending vibration), and medium intensity peaks at 1619 cm^{-1} and 1636 cm^{-1} (corresponding to C=C stretch) clearly show presence of acrylate functional groups in reactive diluents. Among other important absorption peaks that support the proposed structure of reactive diluents are strong peaks at ~2850-2930 cm^{-1} c(C-H stretching of methylene groups in fatty acid chains), 1190 (C-O stretching of ester), and a broad peak at 3433 cm^{-1} (H-bonded O-H stretch) of hydroxy groups formed by epoxide ring opening. Further, disappearance of peaks at 844 cm^{-1} characteristic of internal epoxides of EMS and EML indicates conversion of epoxides to beta-hydroxyl acrylates. These FT-IR results combined with the saponification values obtained for reactive diluents (Table 1) provide reasonable evidence for chemical structures of reactive diluents shown in Figure 1.

Publication Date (Web): June 18, 2015 | doi: 10.1021/bk-2015-1192.ch016

Study of Viscosity Profile

Viscosity reduction profile of RDs is very important, among many other factors, for their successful applications in UV-cure coatings and inks. In order to study viscosity reduction profile of bio-based RDs, two conventional oligomers, an epoxy acrylate oligomer (10-620/TM20 (Rahn, U.S.A.)) and an aliphatic urethane acrylate (EBECRYL 4833(CYTEC), have been selected. Epoxy acrylate oligomer and aliphatic urethane acrylate oligomers are referred to as EA and UA, respectively, in the subsequent discussion. Viscosity of all the samples were measured using Brookfield CAP 2000+ cone and plate viscometer. Depending on the viscosity of the samples, appropriate spindle type and rpm and temperatures were used to measure their viscosity. These details are shown in Figure 4. Their viscosity profiles are shown in Figure 4. DPGDA, a conventional petro-based RD, has also been used as reference RD.

Publication Date (Web): June 18, 2015 | doi: 10.1021/bk-2015-1192.ch016

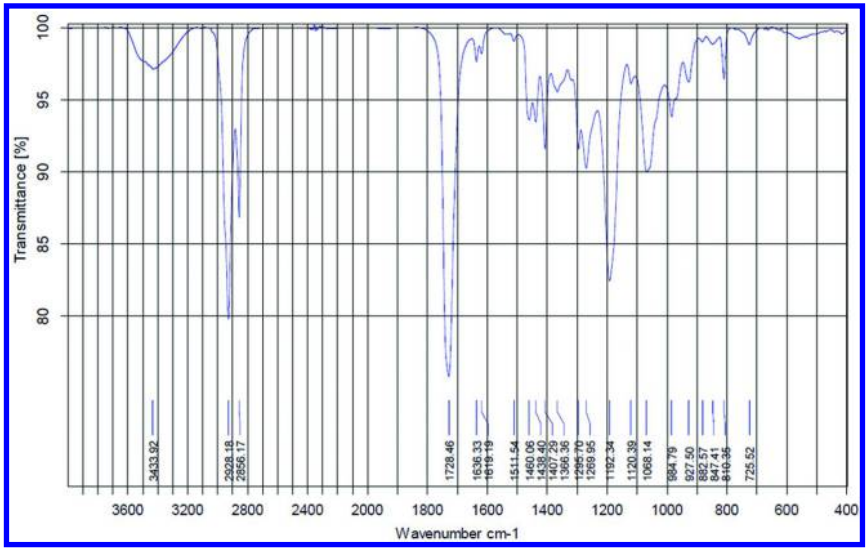

Figure 3. Represntative FT-IR spectrum for reactive diluent RD1.

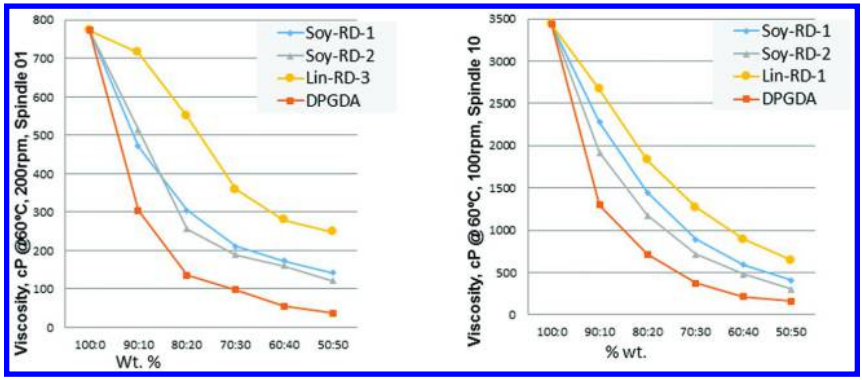

Figure 4. Viscosity profile of different reactive diluents with epoxy acrylate (left) and urethane acrylate oligomer (right).

As is evident from the results, all the bio-based RDs can dissolve acrylate oligomers and their solutions were clear and free-flowing, indicating their good compatibility. It is observed that the order of relative viscosity reducing potential of RDs is DPGDA > Soy-RD-2 > Soy-RD1 > Lin-RD-1. This trend is observed with both EA and UA oligomers. In general, the viscosity-reducing power of

an RD is primarily dependent on the polarity of reactive diluents or solvents, among other factors. In the case of RDs used in this study, the polar ester group would help solvate oligomer through polar-polar interaction and/or H-bonding interaction. The ester group contents are expressed as saponification numbers in Table 1; the higher the saponification number, the higher their ester group content. However, the results show an interesting trend. As expected, DPGDA (sap. value = 463) shows much greater viscosity-reduction power than all other bio-based RDs. Among the bio-based RDs, Soy-RD-2 (Sap.value=360) shows the highest viscosity-reducing power. Surprisingly, Lin-RD-1 (Sap. value = 320) shows much lower solvency than Soy-RD-1 (sap. Value = 301) despite its higher ester content. We attribute this behavior to the internal H-bonding (*21*) resulting due to the proximity of the ester and hydroxyl group Lin-RD-1, as shown in Figure 5. While such H-bonding is possible in all three bio-based RDs, it would be much more pronounced in Lin-RD-1 since it contains a substantial fraction of linolenic ester, giving rise to a product with three esters and three hydroxyl groups in proximity. Please note that Figure 1 shows only representative structures of the RDs and that they will be mixtures of compounds based on fatty acid compositions of the oil used. The greater internal H-bond formation potential of Lin-RD-1 is also supported by its higher viscosity (Table 1) than the other soy-based RDs. Soy-RD-2, that shows the best performance, has lower –OH content (responsible for H-bonding) than Lin-RD-1 and greater ester content than Soy-RD-1.

Publication Date (Web): June 18, 2015 | doi: 10.1021/bk-2015-1192.ch016

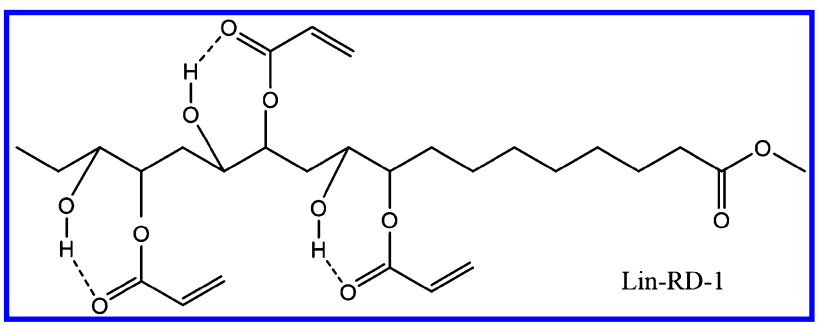

Figure 5. A simplified structure of Lin-RD-1 showing probable H-bonding.

It can be, therefore, inferred that in addition to the ester group content, the chemical structure and viscosity of reactive diluents can significantly influence their viscosity reduction power for different oligomer types. Among the RDs studied, the Soy-RD-2 appears to have the best balance of chemical structure, polarity, and viscosity and hence shows the best viscosity-reducing power.

UV-Cured Film Properties

UV-cure coatings were prepared from EA and UA oligomers and different RDs, in varying oligomer/RD ratio, to study the effect of RD type and amount on the film properties. Compositions using DPGDA, a conventional reactive diluent, were also prepared as reference. The results are presented in Tables 2 and 3. In the case of coatings based on EA oligomer (Table 2), all the films were clear and uniform with good adhesion. Epoxy acrylate is a "hard" oligomer, and incorporation of bio-based RDs resulted in lowering of film hardness, as expected. The drop in hardness is much more pronounced with Soy-RD-1 due to its lower acrylate (WPA = 349) than other RDs. Lower acrylate content of Soy-RD-1 is expected to produce films with lower cross-link density and lower hardness. It is important, however, to note that Soy-RD-1, despite its lower acrylate content, can still provide high solvent resistance (MEK-double rubs) when used at the level up to 50% by wt.

Design of Hyperbranched Soy-Based Urethane Acrylate Oligomer (HSUA)

Oligomers used for UV-cure coatings must be carefully tailored to meet such diverse requirements as low viscosity, adequate functionality, faster cure response, compatibility with other components, ease of pigment dispersion, and low cost. Further, the cured film must have balanced thermo-mechanical properties, low shrinkage, adequate cross-link density for chemical and solvent resistance, and good adhesion on a variety of substrates. These oligomer characteristics and the film properties can be achieved, for the most part, by using innovative design strategies for oligomers. The hyper-branched soy-urethane acrylate oligomer (HSUA) in this study has been prepared from epoxidized methyl ester of soy fatty acids (EMS) as starting material, which is a commercially available soy derivative. A simplified reaction scheme is shown in Figure 2. While it is a common practice to esterify oxirane groups of EMS with acrylic acid to introduce UV-curable acrylate groups, we have used a different strategy involving trans-esterification of methyl ester groups with 2-hydroxtethyl acrylate (2-HEA). We have then utilized oxirane groups to build up higher molecular weight (oligomerization) by cationic ring-opening polymerization using an acid catalyst, to obtain hyper-branched oligomeric polyol. This polyol was then reacted with excess of di-isocyanate compound to prepare –NCO-terminated product that was then end-capped with 2-HEA to introduce additional acrylate groups. Using this unique strategy, we have been able to prepare soy-urethane acrylate oligomer with hyper-branched structure. The hyper-branching, though not shown in Figure 2, will arise due to oxirane functionality of > 1 (~ 1.4) of EMS. We hypothesized that this HSUA with unique hyper-branched structure, uniform distribution of acrylate groups along the oligomer, and some dangling chain ends would provide balance of such desirable properties as low viscosity, good cure response, uniform cross-link density, reduced shrinkage, and, of course, high bio-based content. The characteristics of oligomer are shown in Table 4.

In Green Polymer Chemistry: Biobased Materials and Biocatalysis; Smith, et al.;
ACS Symposium Series; American Chemical Society: Washington, DC, 2015.

Publication Date (Web): June 18, 2015 | doi: 10.1021/bk-2015-1192.ch016

Table 4. Characteristics of HSUA

Properties	*Value*
Molecular Wt. (GPC) (Mn)	1576
Molecular Wt. (GPC) (Mw)	9759
Polydispersity index (PDI)	6.19
No. Avg. Functionality (Calculated)	5.24
Viscosity (cPs) @ 25 °C	162.8 *
Wt. per acrylate (WPA) (Calculated)	301
% Bio-based content (calculated)	59.20%

* *Spindle No. 1, 750 rpm.*

Publication Date (Web): June 18, 2015 | doi: 10.1021/bk-2015-1192.ch016

UV-Cure Coating Compositions Based on HSUA

In order to validate our design strategy and to study the potential applications, HSUA oligomer was evaluated in UV-cure compositions, with and without the use of reactive diluents. The compositions used for the study are shown in Table 5. UV-cured network of HSUA is expected to be "soft" and flexible by virtue of its hyper-branched structure, low acrylate density, and aliphatic dangling segments which will provide low cross-link density and high free-volume. Therefore, in order to study the effect of increasing cross-linking, a tri-functional TMPTA monomer has been used in varying proportion in the compositions studied.

Table 5. Film Properties UV-cured Coatings*, **: HSUA/Reactive Diluent System

Coating Code	*HSUA/TMPTA Ratio (by wt.)*	*Pendulum Hardness Konig (s)*	*Pencil Hardness*	*Cross-Cut Adhesion*	*Impact Resistance (lb·in)*	
					Direct	*Reverse*
HSUA 100	100:00	36.4	< 5B	0B	160	160
HSUA90	90:10	64.4	4B	1B	40	20
HSUA80	80:20	88.2	B	3B	40	<20
HSPU70	70:30	113.4	H	3B	20	<20

* *UV energy density = 2500 mJ/cm2.* ** *Dry-film thickness = 50-55µ.*

UV-Cured Film Properties for HSUA-Based Coatings

The properties of UV-cured coatings are reported in Tables 5 and 6.

In Green Polymer Chemistry: Biobased Materials and Biocatalysis; Smith, et al.;
ACS Symposium Series; American Chemical Society: Washington, DC, 2015.

Table 6. Film Properties UV-cured Coatings*, **: HSUA / Reactive Diluent System

Coating Code	*HSUA/TMPTA Ratio (by wt.)*	*MEK Double-Rubs*	*Gel Content (%)*	*Acrylate Conversion (FTIR) %*
HSUA100	100:00	65	83.79	100.0
HSUA90	90:10	>200	83.84	97.3
HSUA80	80:20	>200	88.93	80.1
HSPU70	70:30	>200	90.36	77.1

* *UV energy density = 2500 mJ/cm2.* ** *Dry-film thickness = 50-55 microns.*

Publication Date (Web): June 18, 2015 | doi: 10.1021/bk-2015-1192.ch016

All the coatings were characterized for extent of curing by following acrylate group conversion as well as by determination of their gel contents (Table 6). Liquid coating samples were deposited on KBr plates, and their FT-IR spectra were recorded before and after UV exposure. Acrylate group conversion was calculated by peak area ratio method by measurement of characteristic FT-IR absorption peak area at around 810cm-1, before and after curing of the films. The FT-IR peak at ~1730 cm^{-1}corresponding to carbonyl group was taken as reference, and % acrylate conversion was calculated by the following formula (*23*).

$$\% \text{ Acrylate Conversion} = \frac{(A_{810} / A_{1730})_0 - (A_{810} / A_{1730})_t}{(A_{810} / A_{1730})_0} \times 100$$

Where $(A_{810} / A_{1730})_0$ and $(A_{810} / A_{1730})_t$ are relative absorbance of C=C bonds before and after curing, respectively. Gel contents were measured using the method described earlier in the Materials and Methods section.

Coating HSUA100 shows very high acrylate conversion. In general, acrylate conversion in UV-cure coating significantly depends, among many factors, on free volume (Tg) of coatings (*24*, *25*). The greater the free volume, the more the relative mobility of the reacting species and the greater the extent of reaction (% conversion). HSUA100 with low acrylate density has high free volume and hence high conversion. As can be seen in Table 6, with increasing TMPTA contents, the acrylate conversion drops since TMPA has high acrylate density and would result in film with high cross-link density and reduced mobility of reactive species. Figure 6 shows DSC thermograms of UV-cured coatings. Interestingly, HSUA100 shows two glass transition temperatures at -9.3 °C and at 46.5°C. We believe the one at -9.3 °C might be due to the presence of volatile solvent used in the work-up of the sample. We rule out the presence of any plasticizing non-volatile contaminant based on its gel content which is comparable to other compositions studied. With increasing high acrylate content TMPTA, Tg of the films increased to > 47 °C, indicating "glassy" and highly cross-linked films.

Gel content of coatings provides information about the components that are not connected with the network structure (gel) and their relative tendency to leach out during the test (*26–28*). The increase in gel contents of coatings in Table 6 with increase in TMPTA content is clearly due to the increased acrylate density of the compositions. It is interesting to note that even though the acrylate conversion decreases with increasing TMPTA content, the networks formed become more complex and integrated, showing decrease in gel contents.

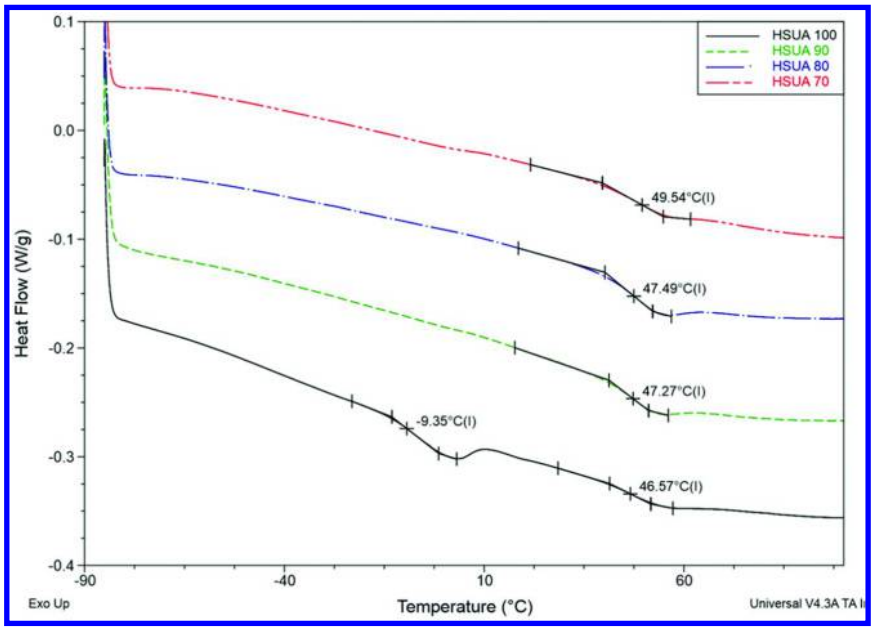

Figure 6. DSC thermograms of HSUA-based UV-cured films.

Tables 5 and 6 show the properties of UV-cured coatings based on HSUA. As expected, the HSUA produced soft film and, with increasing amounts of TMPTA, the film hardness increased progressively as evident from the Konig hardness and pencil hardness. This may be attributed to high free volume in the oligomer, resulting from low cross-link density and the dandling fatty chain structure. The lower MEK resistance for HSUA100 and its significant improvement upon addition of TMPTA can also be explained based on free volume and cross-link density of their film, as stated above. It is also observed that incorporation of TMPTA increases film brittleness (lower impact resistance) and lowers adhesion. This can be due to the increase in cross-link density and volume shrinkage arising from tri-functional TMPTA monomer.

The tensile properties of UV-cured films of HSUA-based coatings are shown in Table 7. HSUA100 showed much lower modulus, tensile strength, and % elongation, typical of moderate functionality oligomers. With increasing

In Green Polymer Chemistry: Biobased Materials and Biocatalysis; Smith, et al.;
ACS Symposium Series; American Chemical Society: Washington, DC, 2015.

Publication Date (Web): June 18, 2015 | doi: 10.1021/bk-2015-1192.ch016

TMPTA, a significant increase in modulus and drop in % elongation was observed due to the formation of constrained network. Tensile strength results indicate formation of brittle network structure with increasing TMPTA contents. Overall, the HSUA oligomer designed in the present study can successfully be used in UV-cure coatings. By suitable choice of other co-oligomers and reactive diluents, it is possible to customize properties of coatings for a target application, while maintaining high bio-based content of the final product.

Table 7. Tensile Properties* of Cured Films of HSUA Based Coatings

Coating Code	*Modulus (ksi)*	*Tensile Strength (psi)*	*% Elongation at Break*
HSUA100	32.7	1515.1	14.3
HSUA90	67.7	1031.4	2.3
HSUA80	129.4	1214.6	1.2
HSPU70	179.9	1199.0	0.8

* *Error range +/- 5%.*

Publication Date (Web): June 18, 2015 | doi: 10.1021/bk-2015-1192.ch016

Conclusion

In the present study, soy-based building blocks suitable as components for advanced UV-cure coatings have been designed and developed. Two types of soy-derived materials—urethane acrylate oligomer and a series of reactive diluents—have been synthesized and studied as primary component and their blends with conventional petro-derived materials, in UV-cure coating formulations. The study of their film properties shows that these soy-based materials with high bio-based contents have significant potential for commercial applications and present an alternate sustainable raw material platform.

Acknowledgments

Authors sincerely thank USDA for funding this research under USDA-NIFA-MICW-2012-04009. We also would like to thank Arkema for providing commercial samples of soybean oil derivatives and for consistently helping our research program.

References

1. Petrovic, Z. S.; Milic, J.; Xu, Y.; Cvetkovic, I. *Macromolecules* **2010**, *43*, 4120–4125.
2. Mutlu, H.; Meier, M. A. R. *Eur. J. Lipid Sci. Technol.* **2010**, *112*, 10–30.
3. Johannes, T. X.; Derksen, E.; Cuperus, P.; Kolster, P. *Ind. Crops Prod.* **1995**, *3*, 225–236.

4. Meier, M. A. R.; Metzgerb, J. O.; Schubert, U. S. *Chem. Soc. Rev.* **2007**, *36*, 1788–1802.
5. Lligadas, G.; Ronda, J. C.; Galia, M.; Cadiz, V. *Biomacromolecules* **2010**, *11*, 2825–2835.
6. Ronda, J. C.; Lligadas, G.; Galia, M.; Cadiz, V. *Eur. J. Lipid Sci. Technol.* **2011**, *113*, 46–58.
7. Guo, Y.; Hardesty, J. H.; Mannari, V. M. *J. Am. Oil Chem. Soc.* **2007**, *84*, 929–935.
8. Rengasamy, S.; Mannari, V. *Prog. Org. Coat.* **2013**, *76*, 78–85.
9. Rengasamy, S.; Mannari, V. *Prog. Org. Coat.* **2013**, *77*, 557–567.
10. Rengasamy, S.; Mannari, V. *J. Appl. Polym. Sci.* **2013**, *130*, 3874–3884.
11. Mannari, V.; Patel, J. Photo-curable advanced Nano-composite Coatings from Soybean Oil: sustainable Hybrids; 101st AOCS Annual Meeting & Expo, Phoenix, AZ, May 16−19, 2010.
12. Mannari, V.; Rengasamy, S. Novel Polyurethane Dispersions with High Bio-based Content; American Coatings Conference, Charlotte, NC, April 12−14, 2010.
13. Mannari, V.; Rengasamy, S. *Eur. Coat. J.* **2013**, 80–85.
14. Mannari, V. *Int. J. Polym. Mater.* **2006**, *55*, 293–305.
15. Guo, Y.; Mannari, V.; Patel, P.; Massingill, J. L. *J. Coat. Technol. Res.* **2006**, *3*, 327–331.
16. Mannari, V.; Massingill, J. *J. Coat. Technol. Res.* **2006**, *3*, 151–157.
17. Mannari, V.; Guo, Y.; Massingill, J. L., Jr. *Polym. Prepr.* **2003**, *44*, 97.
18. Mannari, V.; Rengasamy, S.; Patel, C. *Paint Coat. Ind.* **2012**, *11*, 28–31.
19. Mannari, V.; Rengasamy, S. Sustainable High Bio-based Content Polyurethane Dispersions for Advanced Water-borne and UV-cure Coatings; American Coating Conference and Show, Indianapolis, IN, May 2012**.**
20. Schwalm, R. *UV Coatings Basics, Recent Developments and New Applications*; Elsevier Science: Amsterdam, 2006**.**
21. Wypych, G. *Handbook of Solvents*; William Andrew Publishing: Norwich, New York, 2001.
22. Glockner, P.; Jung, T.; Struck, S.; Studer, K.; *Radiation Curing – Coating and Printing Inks, Technical Basics, Applications and Trouble Shooting*; Vincentz Network: Hannover, Germany, 2008.
23. Tasic, S.; Bozic, B.; Dunjic, B. *Prog. Org. Coat* **2004**, *51*, 320–327.
24. Decker, C.; Lorinczova, I. *J. Coat. Technol. Res.* **2004**, *1*, 247–256.
25. Tauber, A.; Scherzer, T.; Mehnert, R. *Coat. Technol.* **2000**, *72*, 51–60.
26. Kim, B. S.; Hrkach, J. S.; Langer, R. *Biomaterials* **2000**, *21*, 259–265.
27. Kim, H. M.; Kim, H. R.; Kim, B. S. *J. Polym. Environ.* **2010**, *18*, 291–297.
28. Subramani, S.; Lee, J. Y.; Kim, J. H.; Cheong, I. W. *Compos. Sci. Technol.* **2007**, *67*, 1561–1573.

Publication Date (Web): June 18, 2015 | doi: 10.1021/bk-2015-1192.ch016

Publication Date (Web): June 18, 2015 | doi: 10.1021/bk-2015-1192.ch017

Chapter 17

Solid Lipid Nanoparticle - Functional Template of Meso-Macrostructured Silica Materials

Sanghoon Kim, Jonathan Jacoby, Marie-José Stébé, Nadia Canilho, and Andreea Pasc*

Université de Lorraine/CNRS, SRSMC, UMR 7565, F-54506, Vandeouvre-lès-Nancy, Cedex, France
***E-mail: andreea.pasc@univ-lorraine.fr.**

Solid lipid nanoparticles (SLN) are biocolloidal dispersions able to be loaded with hydrophilic or hydrophobic ingredients, either of low molecular weight drugs or high molecular weight proteins. Their interest is not limited to colloidal science but can be extended to material design, for templating inorganic materials or to afford functional hybrid organic-inorganic materials. Indeed, dispersions of SLN can be used to prepare meso-macroporous materials through a dual templating mechanism combining self-assembling of micelles and imprinting of soft nanoparticles. Moreover, by loading SLN with curcumin, one can obtain responsive carriers, which are of interest in nanomedecine. Finally, supported biocatalysts were obtained by mineralizing green double dispersions W/SLN/W containing a lipase into the aqueous core.

Introduction

Hierarchical porous materials combine unique properties of mesostructures, such as high surface area and controllable sized pores, with those of macropores providing high diffusion and throughput rates (*1*). Typical applications of these materials are separation (*2*), catalysis (*3*), sensing (*4*) or tissue engineering (*5*). They have also potential applications as reservoirs in drug delivery systems or as inclusion cavities for macromolecules. There are a number of ways to fabricate

In Green Polymer Chemistry: Biobased Materials and Biocatalysis; Smith, et al.;
ACS Symposium Series; American Chemical Society: Washington, DC, 2015.

hierarchical macro–mesostructured silica (*6–8*), most of them combine soft and hard-templating techniques, for example by using small molecules, surfactants or polymers with hard colloidal spheres (*9*, *10*) such as polystyrene (PS), poly-(methyl methacrylate) (PMMA) latexes or silica spheres (*9*), but also starch gels (*11*), polyacrylamide-based hydrogels (*12*), aerogels (*13*), polyurethane foams (*14*) or wood tissue (*15*). Hierarchical porous materials have also been prepared without the use of hard templates, either based on *in situ* formed polymeric particles (*16*, *17*), bigels (*18*, *19*) or emulsion droplets (*20–24*), to cite some of them.

Our approach to design hierarchical porous silica is inspired by these previously reported examples, but here the originality consists in using a novel soft template, solid lipid nanoparticles (SLN). In recent years, these nanoparticles emerged in the soft matter field as promising drug carriers with target applications in pharmaceutical and biomedical domains (*25*, *26*). Silica is also known to be safe, not only for the environment, but also for the human body within a certain range of administrated dose, approved by US Food and Drug Administration (FDA). Therefore, its application field may be extended to biocompatible materials, such as bone substitutes, cements for bone repair and reconstruction, enzyme and cell immobilization (*27*), biocatalysts or biosensors (*28–33*) or for oral drug delivery (*34–38*).

Therefore, combining inorganic silica matter with solid lipid nanoparticles, SLN, appears to be a straightforward approach for the development of novel hybrid organic–inorganic biocompatible materials with high potential applications in drug delivery and food chemistry.

SLN not only have a limited toxicity, but also they can be produced in a cost-effective way by different formulation techniques: high-pressure homogenization (industrial method), emulsification–sonication, microemulsion, double emulsion, solvent emulsification–evaporation, solvent diffusion and solvent injection. SLN possess a solid lipid core matrix stabilized by a surfactant shell and are dispersed in an aqueous micellar solution of the same surfactant in excess. Therefore, they could allow the preparation of hierarchical porous materials combining both a cooperative templating mechanism (CTM) and a transcription templating mechanism (*39*).

This paper describes the synthesis of hybrid solid lipid nanoparticle SLN@meso-macroporous silica materials and their uses as novel system for nanomedicine or biocatalysis.

Porous Silica Material Templated by Solid Lipid Nanoparticles

SLN-templated porous material was prepared by adding at neutral pH a silica source (tetramethoxylsilane, TMOS) onto SLN dispersions. SLN were prepared form cetyl palmitate (NHP) and Tween 20 by the solvent injection method (*40*). The mixture was kept in an autoclave at 70 °C to allow the hydrolysis/polycondensation of the silica. The inorganic silica material was obtained after the removal of the organic particles by ethanol/dichloromethane extraction. The designed synthesis strategy is illustrated in Figure 1.

In Green Polymer Chemistry: Biobased Materials and Biocatalysis; Smith, et al.;
ACS Symposium Series; American Chemical Society: Washington, DC, 2015.

Publication Date (Web): June 18, 2015 | doi: 10.1021/bk-2015-1192.ch017

Publication Date (Web): June 18, 2015 | doi: 10.1021/bk-2015-1192.ch017

The macroporous network can be observed by scanning electron microscopy (SEM) analysis. As a matter of fact, silica beads containing spherical macropores of 0.5–1.5 μm in diameter are clearly shown in Figure 1B. The macropore diameters are of the same order of magnitude as the starting SLN. Deeper insights on the morphology of the material were reached by transmission electron microscopy (TEM) (Figure 1C) that clearly showed individual hollow silica spheres.

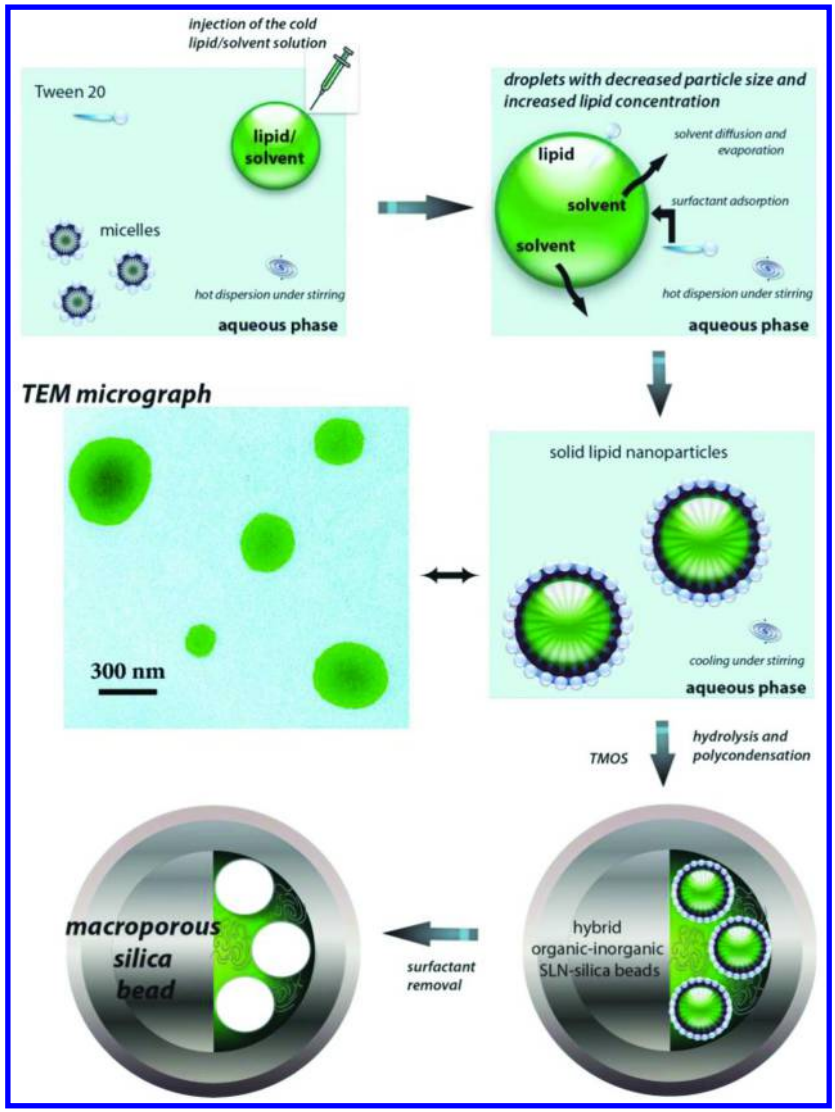

Figure 1. Schematic illustration of SLN formation and templating of macroporous silica beads. Reproduced with permission from reference (40). Copyright 2011 The Royal Society of Chemistry.

Publication Date (Web): June 18, 2015 | doi: 10.1021/bk-2015-1192.ch017

The morphology and the structure of SLN templated hierarchical meso–macroporous silica could also be tuned (*41*). By optimizing the reaction conditions such as hydrothermal temperature, TMOS amount or surfactant concentration, silica capsules could be obtained with polyoxyethylene sorbitan (Tween 20 and 40) imprinting of lipid nanoparticles, whereas block silica was obtained with Pluronic P123. Mesopore diameters of about 3 nm were obtained with Tween 20, 5 nm with Tween 40 and 9 nm with Pluronic P123. The size of the mesopores increases with the size of the starting micelles, from Tween 20 to P123. The ordering at the mesoscale also increases with the mesopore size: only wormlike silica was obtained with Tween 20; wormlike silica embedding hexagonally ordered microdomains with Tween 40 and hexagonally ordered silica with circularly ordered mesoporosity were obtained by using P123 as a porogen (Figure 2).

Hierarchical meso-macroporous silica material possessing circularly ordered mesoporosity around macropore could offer a highly confined environment for SLN encapsulated drugs (Figure 2C). Indeed, curcumin release from circularly ordered "silicalized" drug- loaded SLN shows a significant decrease of the drug released up to 20 %, as compared to wormlike "silicalized" SLN (data not published). Further details on the curcumin loading and release from various SLN@silica systems will be given in the next section.

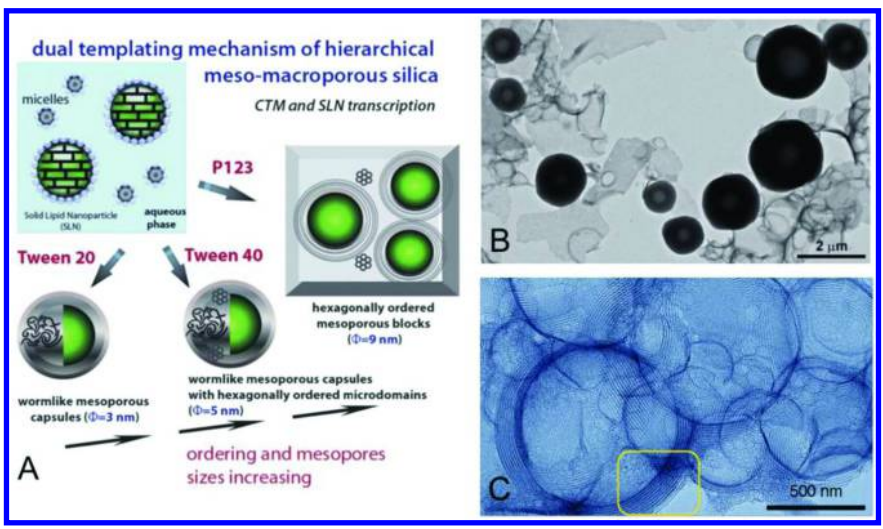

Figure 2. (A) Schematic representation of hierarchical porous silica obtained through a dual templating mechanism combining micelles (CTM) and SLN transcription; (B) TEM image of silica capsule obtained using Tween 40 based SLN; (C) TEM image of hexagonally ordered meso-macroporous silica matrix (selected zone shows circularly ordered mesoporosity around macropore). Reproduced with permission from reference (41). Copyright 2012 The Royal Society of Chemistry.

Publication Date (Web): June 18, 2015 | doi: 10.1021/bk-2015-1192.ch017

pH-Controlled Delivery of Curcumin from a Compartmentalized Solid Lipid Nanoparticle@Mesostructured Silica Matrix

In recent years, the design of nanocarriers for controlled and sustained delivery of drugs has been extensively studied in order to overcome several problems in conventional drug delivery systems, such as poor solubility, limited stability and lack of selectivity of drugs (*42–44*). Indeed, CU, a hydrophobic natural polyphenol isolated from *Curcuma longa*, has been used for centuries in indigenous medicine in the treatment of a variety of inflammatory conditions. It exhibits a wide range of pharmacological capacities, including antitumor, antioxidant, anti-inflammatory, and antimicrobial activities (*45–48*). However, the main drawback for clinical applications of curcumin are its low water solubility at acidic and physiological pH and its rapid hydrolysis under alkaline conditions to yield ferulic acid, its methyl ester and vanillin (*49*). These hurdles can be avoided by incorporating CU into nanoparticles, liposomes, micelles, complexing it with cyclodextrins (CD) in aqueous solutions (*50*) or mesoporous silica (*51*). Solid lipid nanoparticles (SLNs) loaded with CU for topical administration were also developed and characterized (*52*). SLNs with a mean size of 450 nm were found to be stable for 6 months and incorporation into SLN strongly reduced the light and oxygen sensitivity of curcuminoids. However, the organic matter based drug carriers could be instable, thus unexpected drug leaking can occur during storage (*53*). To overcome the disadvantages mentioned above, we recently designed a novel drug delivery system aimed to increase the stability, bioavailability and sustainability of the release of curcumin, through a double encapsulation of the drug into a core–shell nanomatrix combining SLNs and mesostructured silica (*54*). SLNs act as reservoirs of CU, while mesopores act as pathways to control drug release.

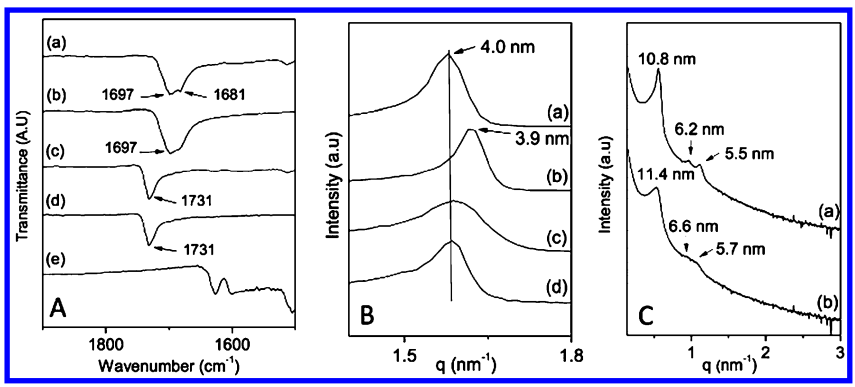

Figure 3. IR spectra (A) and SAXS pattern (B) of CU-SA-SLNs (a), blank-SA-SLNs (b), blank-NHP-SLNs (c), CU-NHP-SLNs (d), curcumin (e); SAXS pattern (C) of NHP-Mat (a) and SA-Mat (b) after removal of organic matter. Values in SAXS patterns represent Bragg distances d=2π/q, where q is the scattering vector. Reproduced with permission from reference (54). Copyright 2014 The Royal Society of Chemistry.

In Green Polymer Chemistry: Biobased Materials and Biocatalysis; Smith, et al.;
ACS Symposium Series; American Chemical Society: Washington, DC, 2015.

Publication Date (Web): June 18, 2015 | doi: 10.1021/bk-2015-1192.ch017

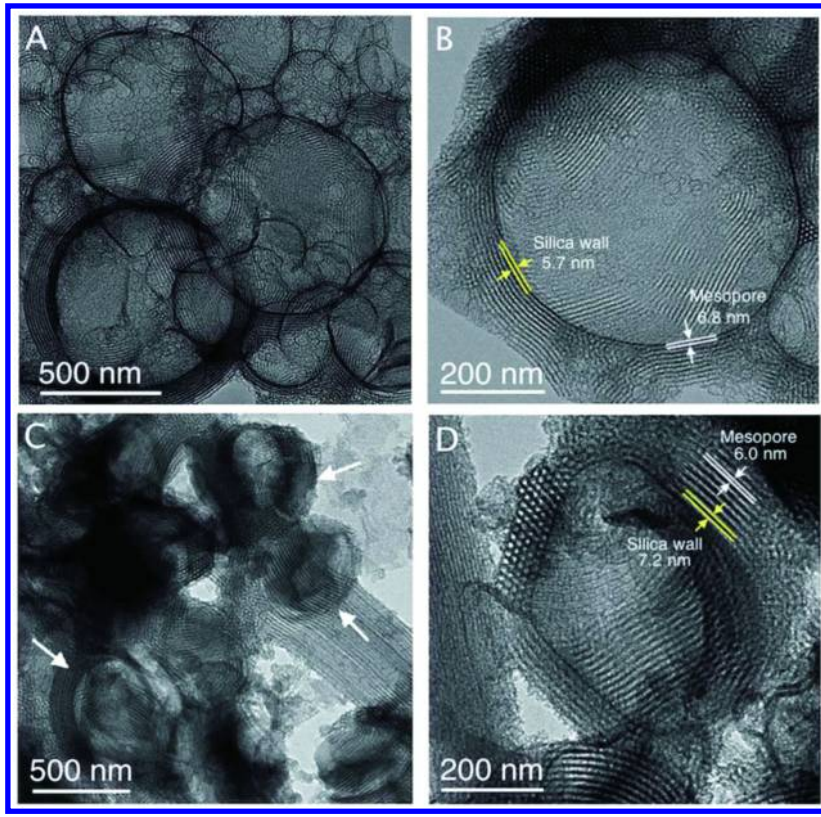

Figure 4. TEM image of meso–macroporous silica NHP-Mat (A and B) and SA-Mat (C and D) after removal of organic matter (arrows indicate macropores). Reproduced with permission from reference (54). Copyright 2014 The Royal Society of Chemistry.

The main strategy consists in silicalizing curcumin loaded SLN/micelles dispersion through a dual templating mechanism combining self-assembling of micelles into mesostructured domains (*55*) and transcription of lipid nanoparticles into macro-structured domains. Indeed, during SLN preparation, one can control the curcumin-partitioning ratio (PR) between SLN core and micelles because curcumin encapsulation amount into SLN core particularly depends on the nature of the solid lipid (cetyl palmitate (NHP) vs. stearic acid (SA)). The interaction between CU and lipid could be the main factor for different partitioning ratio. The interaction can be confirmed using SAXS and FT-IR experiments (Figure 3A and 3B). For instance, cetyl palmitate based curcumin loaded SLN (CU-NHP-SLN), which PR is only 20%, showed no significant peak shift on SAXS and FT-IR spectra, while stearic acid based SLN (CU-SA-SLN) (65% of PR) exhibits strong

interaction, confirmed by peak shift on SAXS pattern and FT-IR spectra (*56*). Besides, the size of SLN was also affected by lipid source. According to the size distribution measurement obtained from dynamic DLS, NHP based SLN showed mean particle size as 300 nm in diameter, while 400 nm in diameter was found for SA based SLN.

SLN@meso-macroporous silica matrix was obtained by adding silica precursor (tetramethoxysilane, TMOS) into curcumin-loaded solid lipid nanoparticle (SLN)/micelle dispersions, followed by hydrothermal treatment. Silica material shows hexagonally ordered mesopore network (Figure 3C and 4) as well as macropores, resulting from the imprinting of SLN. However, the size of macropores observed by TEM seems to be bigger than the size of SLN obtained by DLS. This might be due to coalescence of lipid nanoparticles, melted at 70°C during hydrothermal treatment.

The release experiments of CU-loaded hybrid SLN silica materials were carried out in 3 different receiving media (pH 1.2, 4.5 and 7.4). Figure 5 shows the cumulative release of curcumin from hybrid materials at 25°C at various pH release media. At first, the drug released from NHP-based silica matrix (Figure 5A) quickly reached the plateau within 6 h at any pH. However, the maximum cumulative release percentage was varied with respect to the pH, 100%, 88%, and 16% for pH 1.2, 4.5 and 7.4, respectively. CU release curves from SA-based silica matrix (Figure 5B) show also pH dependence (CU cumulative release: 86, 68 and 18% for pH 1.2, 4.5 and 7.4, respectively). However, the release rate is slower than that of NHP-based silica (12 h vs. 6 h for saturation).

Publication Date (Web): June 18, 2015 | doi: 10.1021/bk-2015-1192.ch017

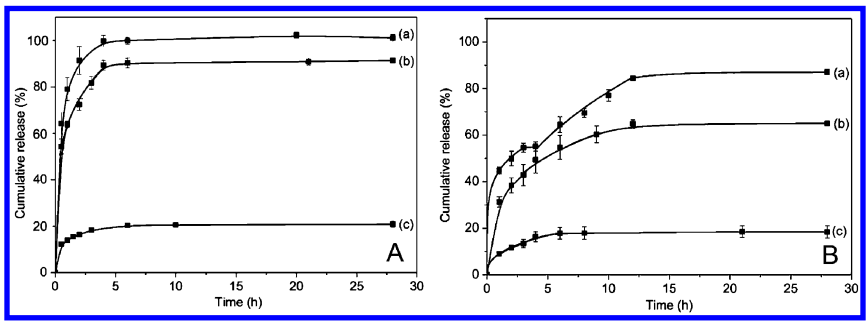

Figure 5. Curcumin cumulative release from (A) NHP-Mat (a) at pH 1.2, (b) at pH 4.5 and (c) at pH 7.4; (B) SA-Mat (a) at pH 1.2, (b) at pH 4.5 and (c) at pH 7.4. Reproduced with permission from reference (54). Copyright 2014 The Royal Society of Chemistry.

Publication Date (Web): June 18, 2015 | doi: 10.1021/bk-2015-1192.ch017

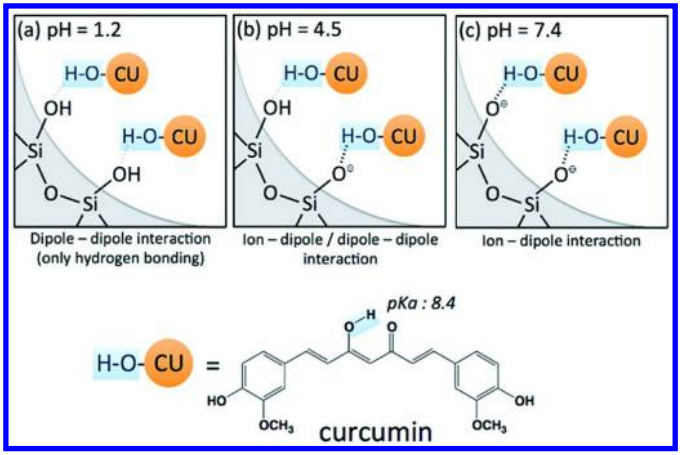

Figure 6. Possible interactions between curcumin and silanol on a silica surface (a) at pH 1.2, (b) at pH 4.5 and (c) at pH 7.4. Reproduced with permission from reference (54). Copyright 2014 The Royal Society of Chemistry.

The differences in the curcumin release behaviour might be due to the interaction between curcumin and silanol groups at the surface of silica as described in Figure 6. Moreover, after the release of CU that is encapsulated in mesopores, CU is fed only from the SLN that acts as a drug reservoir. Hence, the release rate becomes mainly dependent on the nature of SLN, which is again, influenced by pH (*57*). A plausible mechanism of the core–shell nanohybrid vectors described herein is schematized in Figure 7.

Finally, cytotoxicity studies showed that the CU-loaded materials have similar IC50 values to free curcumin making the newly designed matrices of potential interest in nanomedicine.

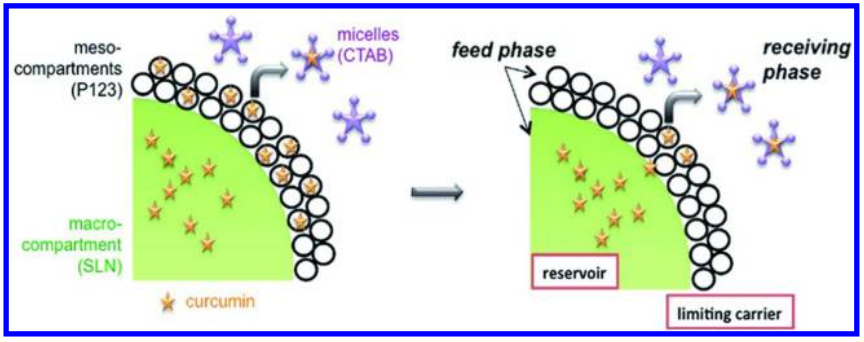

Figure 7. Graphical representation of the release mechanism of curcumin from core–shell SLN@meso-macrostructured silica. Reproduced with permission from reference (54). Copyright 2014 The Royal Society of Chemistry.

Publication Date (Web): June 18, 2015 | doi: 10.1021/bk-2015-1192.ch017

A Meso-Macro Compartmentalized Bioreactor Obtained through Silicalization of "Green" Double Emulsions: W/O/W and W/SLNs/W

Though SLN shows various advantages over traditional methods for encapsulation of a guest molecule, loading hydrophilic molecule such as enzymes into SLN has been limited because of hydrophobicity of lipid core of SLN. Several approaches have been attempted in order to increase the loading amount of the hydrophilic molecule. Functionalization (*58*) or ion pairing (*59*) of a guest molecule has showed a significant improvement of the guest molecule loading capacity. However, these methods could alter physical-chemical properties of such guest molecules. Our approach consists in using double emulsions in which the inner aqueous droplets contain the enzyme, here *Mucor miehei* lipase (MmL). This enzyme is known to be a good biocatalyst for the transesterification reaction of vegetable oils in the biodiesel production. Mineralizing this colloidal template pre-loaded with the lipase could afford an one-pot synthesis resulting in a meso-macroporous silica, which supports the enzyme (*60*). Interestingly, the macroporosity could be tailored herein by templating the silica with double emulsions that have the particularity of being converted into solid lipid nanoparticles (SLNs) by simple removal of the organic solvent (Figure 8).

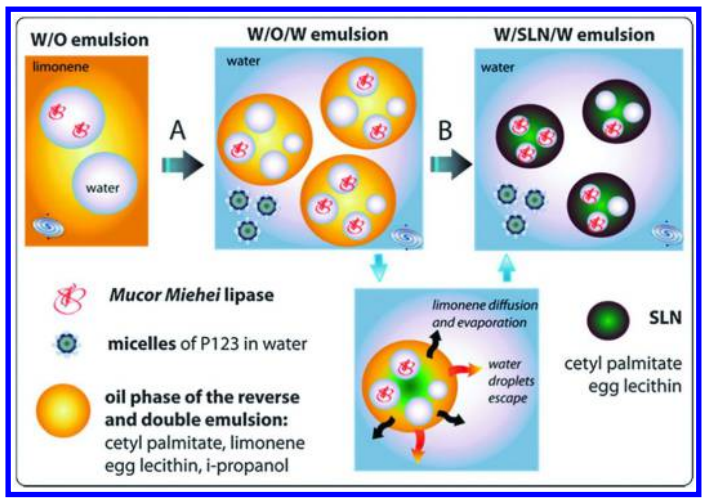

Figure 8. Illustration of the transformation of a double emulsion containing a solid lipid dissolved in an organic solvent (W/O/W) into solid lipid nanoparticles (W/SLNs/W). (A) Addition of micelles of P123; (B) evaporation of limonene. Reproduced with permission from reference (60). Copyright 2014 The Royal Society of Chemistry.

Publication Date (Web): June 18, 2015 | doi: 10.1021/bk-2015-1192.ch017

Briefly, the double emulsion (W/O/W) was prepared by adding a reverse (W/O) emulsion into an aqueous micellar solution of P123 under stirring. Dynamic light scattering measurements show that the size of aqueous droplets of the W/O emulsion is about 200–300 nm, whereas the size of the double emulsions is centered on 2 μm (Figure 9). The compartmentation of the W/O/W emulsion was also confirmed by optical microscopy (Figure 9). W/SLN/W emulsions were prepared by first evaporating 80 wt% of the double emulsion and then, by diluting the resulting highly concentrated emulsion with an aqueous solution of micelles. As determined by DLS, SLNs show a bimodal distribution centered at 130 and 550 nm (Figure 9). By introducing the enzyme (50 mg mL^{-1}), no significant changes in the droplet size were observed. Silica materials were obtained by mineralizing the colloidal template, with or without enzyme, through sol–gel synthesis. Hence, meso-macrostructured silica materials result by a dual templating mechanism that combines the self-assembly of micelles of Pluronic P123 and templating of colloidal lipid spheres of either reverse emulsion (W(MmL)/O/W) or solid nanoparticles (W(MmL)/SLN/W).

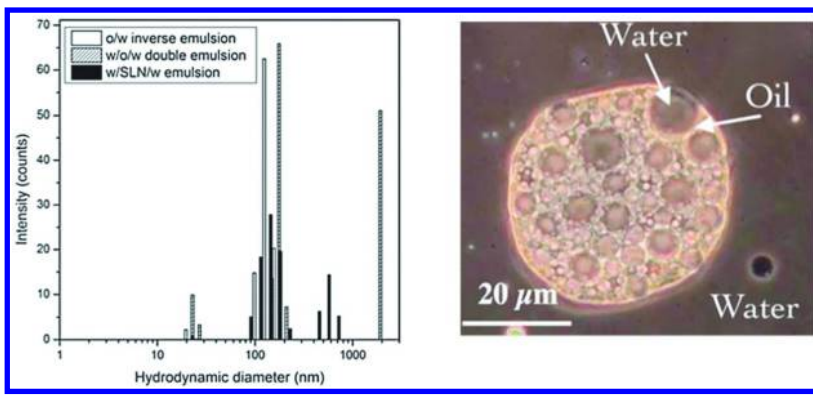

Figure 9. Hydrodynamic diameter of O/W emulsion, W/O/W and W/SLNs/W emulsion as determined by DLS and the POM micrograph showing the compartmentalization of the W/O/W emulsion. Reproduced with permission from reference (60). Copyright 2014 The Royal Society of Chemistry.

TEM image of silica materials obtained from W/O/W (Figure 10) and W/SLNs/W (Figure 11) emulsion showed the presence of ordered mesoporosity as well as macropores, which are interconnected through mesopores. Indeed, MSLN sample (Material from SLN) shows macropores with 150 - 600 nm in diameter while MDE (Material from Double Emulsion) have macropores with more than 1μm in diameter. The above results indicate that the transition from MDE to MSLN is accompanied by a decrease of macropore size. These results clearly indicate the hierarchical structure of the silica matrix. The structuring is maintained while adding the lipase into the colloidal template (Figure 11C)

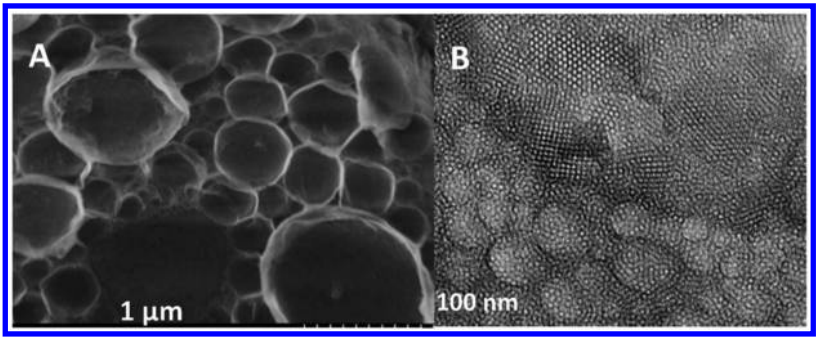

Figure 10. SEM (A) and TEM (B) micrographs of bare silica MDE. Reproduced with permission from reference (60). Copyright 2014 The Royal Society of Chemistry.

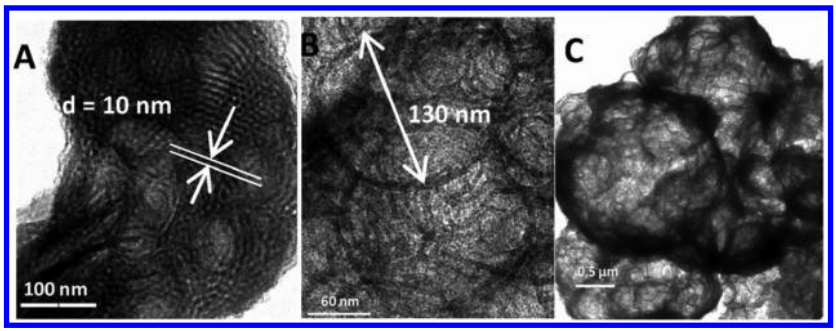

Figure 11. TEM micrographs of the bare silica material, MSLN (A and B) and of the enzyme loaded silica material, MmL-MSLN (C). Reproduced with permission from reference (60). Copyright 2014 The Royal Society of Chemistry.

Finally, the resulting materials, MmL-MDE and MmL-MSLN, were used as biocatalysts in the methanolysis of colza oil. The entrapped lipase (0.054 mg MmL per mg of silica) retains its catalytic activity and complete conversion is reached within 50 h (Figure 12, left). For comparison, the reaction was also performed using MmL that was physisorbed onto pre-synthesized mesoporous SBA-15 (0.43 mg MmL per mg of silica) having similar mesopore size, but no macropores. Complete conversion is reached within only 6 h. The difference in behaviour between SBA-15 and MDE or MSLN can be due to higher enzyme loading, almost a factor of 8. The main advantage of the method reported here is that a lower quantity of enzyme is needed. When the Mucor miehei lipase is physisorbed into SBA-15 a higher quantity of enzyme is required. It should be also noted that the encapsulation efficiency is of 100% in the case of entrapment of the enzyme into double dispersions, while of only 25% when the enzyme is physisorbed.

In Green Polymer Chemistry: Biobased Materials and Biocatalysis; Smith, et al.;
ACS Symposium Series; American Chemical Society: Washington, DC, 2015.

Publication Date (Web): June 18, 2015 | doi: 10.1021/bk-2015-1192.ch017

Figure 12 shows that even the catalytic activity of the supported enzyme decreases rapidly, the colloidal-entrapped biocatalysts showed better efficiency than the corresponding physisorbed enzyme, with up to 5 consecutive runs in the case of MmL-MSLN and 4 consecutive runs in the case of MmL-MDE, *vs.* only 2 consecutive runs for MmL-SBA-15, as reported elsewhere (*61*).

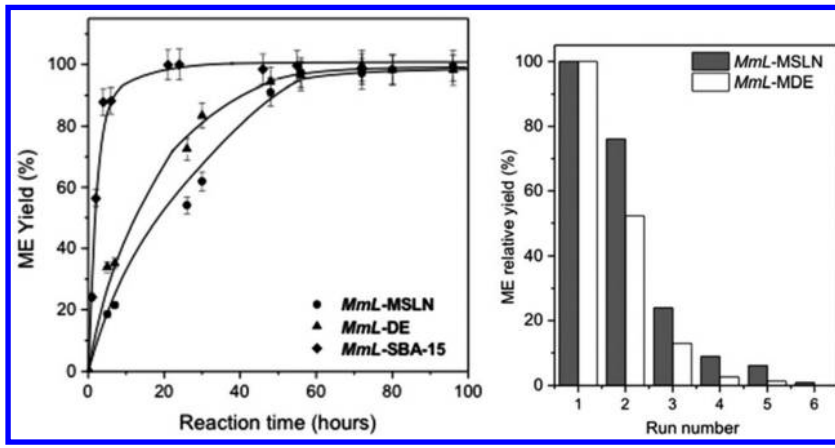

Figure 12. Variation of the methyl ester (ME) yield as a function of time (left) and variation of methyl ester (ME) yield over the recycling runs obtained using MmL-MDE and MmL-MSLN supported biocatalysts, respectively (right). Reproduced with permission from reference (60). Copyright 2014 The Royal Society of Chemistry.

The templating of silica with double emulsions containing an enzyme in the aqueous core of the hydrophobic droplets provides a viable pathway for the synthesis of supported biocatalysts. By using an oily mixture of a green solvent (*i.e.* limonene) and a solid lipid (*i.e.* cetylpalmitate), one can easily tune the size of the macrocavities from 5 μm in the case of the emulsion to 600 nm in the case of the solid lipid nanoparticles, by simply reducing the size of the colloidal template by evaporation of the organic solvent. The resulting supported biocatalyst was able to catalyse the methanolysis of colza oil, which is a reaction of interest for the biodiesel production.

Conclusion

The present paper highlights the interest of solid lipid nanoparticles to design hierarchical porous materials or compartmentalized and functionalized hybrid materials. Straightforward applications of these novel systems are addressed in nanomedicine and biocatalysis.

The morphology and the structure of hierarchical meso–macroporous silica can be easily tuned using a dual templating mechanism with micelles and solid lipid nanoparticles through systematic variations of the reaction parameters and the surfactant nature.

In Green Polymer Chemistry: Biobased Materials and Biocatalysis; Smith, et al.;
ACS Symposium Series; American Chemical Society: Washington, DC, 2015.

Publication Date (Web): June 18, 2015 | doi: 10.1021/bk-2015-1192.ch017

Curcumin-loaded meso–macrostructured silica materials were also obtained by mineralizing dispersions of solid lipid nanoparticles in micellar solutions. The release pattern of curcumin highly depends on the pH of the receiving medium and the nature of lipid source. Moreover, a two-step release pattern was observed for stearic acid based hybrid silica matrix, which suggests that SLNs may act as reservoirs of CU, while mesopores act as pathways to control drug release.

Lipase loaded-SLN@meso-macroporous silica has been synthesized via silicalization of double emulsion colloidal template. Hydrophobic droplets in of double emulsion can provide a viable pathway to tune the size of the macrocavities from micrometer, in the case of the emulsion, to submicrometer, in the case of the solid lipid nanoparticles, by simply reducing the size of the colloidal template by evaporation of the organic solvent. The resulting supported biocatalyst was able to catalyse the methanolysis of colza oil, a reaction of interest in the biodiesel production.

In conclusion, solid lipid nanoparticle(SLN)/micellar dispersion appears as a straightforward way to design novel hybrid-silica system with improved stability and sustainability of guest molecules such as drugs or enzymes.

Publication Date (Web): June 18, 2015 | doi: 10.1021/bk-2015-1192.ch017

References

1. Parlett, C. M. A.; Winson, K.; Lee, A. F. *Chem. Soc. Rev.* **2013**, *42*, 3876–3893.
2. Hu, J.-S.; Zhong, L.-S.; Song, W.-G.; Wan, L.-J. *Adv. Mater.* **2008**, *20*, 2977–2982.
3. Yuan, Z. -Y.; Su, B. -L. *J. Mater. Chem.* **2006**, *16*, 663–677.
4. Zhang, J.; Wang, S.; Xu, M.; Wang, Y.; Zhu, B.; Zhang, S.; Huang, W.; Wu, S. *Cryst. Growth Des.* **2009**, *9*, 3532–3537.
5. Zhu, Y.; Wu, C.; Ramaswamy, Y.; Kockrick, E.; Simon, P.; Kaskel, S.; Zreiqat, H. *Microporous Mesoporous Mater.* **2008**, *112*, 494–503.
6. Sun, Z.; Deng, Y.; Wei, J.; Gu, D.; Tu, B.; Zhao, D. *Chem. Mater.* **2011**, *23*, 2176–2184.
7. Liu, J.; Cai, Y.; Deng, Y.; Sun, Z.; Gu, D.; Tu, B.; Zhao, D. *Microporous Mesoporous Mater.* **2010**, *130*, 26–31.
8. Deng, Y.; Liu, C.; Yu, T.; Liu, F.; Zhang, F.; Wan, Y.; Zhang, L.; Wang, C.; Tu, B.; Webley, P. A.; Wang, H.; Zhao, D. *Chem. Mater.* **2007**, *19*, 3271–3277.
9. Khramov, A. N.; Collinson, M. M. *Chem. Commun.* **2001**, 767–768.
10. Jones, B. H.; Lodge, T. P. *Chem. Mater.* **2011**, *23*, 4824–4831.
11. Zhang, B.; Davis, S. A.; Mann, S. *Chem. Mater.* **2002**, *14*, 1369–1375.
12. Liang, C.; Dai, S.; Guiochon, G. *Chem. Commun.* **2002**, 2680–2681.
13. Drisko, G. L.; Luca, V.; Sizgek, E.; Scales, N.; Caruso, R. A. *Langmuir* **2009**, *25*, 5286–5293.
14. Li, L.-L.; Duan, W.-T.; Yuan, Q.; Li, Z.-X.; Duan, H.-H.; Yan, C.-H. *Chem. Commun.* **2009**, 6174–6176.
15. Shin, Y.; Liu, J.; Chang, J. H.; Nie, Z.; Exarhos, G. J. *Adv. Mater.* **2001**, *13*, 728–732.

16. Huang, Y.; Cai, H.; Feng, D.; Gu, D.; Deng, Y.; Tu, B.; Wang, H.; Webley, P. A.; Zhao, D. *Chem. Commun.* **2008**, 2641–2643.
17. Drisko, G. L.; Zelcer, A.; Luca, V.; Caruso, R. A.; Soler-Illia, G. J. A. A. *Chem. Mater.* **2010**, *22*, 4379–4385.
18. Lee, M. N.; Mohraz, A. *Adv. Mater.* **2010**, *22*, 4836–4841.
19. Lee, M. N.; Mohraz, A. *J. Am. Chem. Soc.* **2011**, *133*, 6945–6947.
20. Imhof, A.; Pine, D. J. *Nature* **1997**, *389*, 948–951.
21. Sen, T.; Tiddy, G. J. T.; Casci, J. L.; Anderson, M. W. *Microporous Mesoporous Mater.* **2005**, *78*, 255–263.
22. Blin, J. L.; Bleta, R.; Ghanbaja, J.; Stébé, M. J. *Microporous Mesoporous Mater.* **2006**, *94*, 74–80.
23. Schmidt-Winkel, P.; Lukens, W. W.; Yang, P. D.; Margolese, D. I.; Lettow, J. S.; Stucky, G. D. *Chem. Mater.* **2000**, *12*, 686–696.
24. Schmidt-Winkel, P.; Stucky, G. D. *Langmuir* **2000**, *16*, 356–361.
25. Das, S.; Chaudhury, A. *AAPS PharmSciTech* **2011**, *12*, 62–76.
26. Müller, R. H.; Mäder, K.; Gohla, S. *Eur. J. Pharm. Biopharm.* **2000**, *50*, 161–177.
27. Reátegui, E.; Kasinkas, L.; Kniesz, K.; Lefebvre, M. A.; Aksan, A. *J. Mater. Chem. B.* **2014**, *2*, 7440–7448.
28. Reiner, T.; Kababya, S.; Gotman, I. *J. Mater. Sci.: Mater. Med.* **2008**, *19*, 583–539.
29. Jones, J. R.; Lin, S.; Yue, S.; Lee, P. D.; Hanna, J. V.; Smith, M. E; Newport, R. J. *Proc. Inst. Mech. Eng., Part H* **2010**, *224*, 1373–1387.
30. Hertz, A.; Bruce, I. J. *Nanomedicine* **2007**, *2*, 899–918.
31. Moura, J.; Teixeira, L. N.; Ravagnani, C.; Peitl, O.; Zanotto, E. D.; Beloti, M. M.; Panzeri, H.; Rosa, A. L.; De Oliveira, P. T. *J. Biomed. Mater. Res., Part A* **2007**, *82*, 545–551.
32. Yuan, G. L.; Yin, M. Y.; Jiang, T. T.; Huang, M. Y.; Jiang, Y. Y. *J. Mol. Catal. A: Chem.* **2000**, *159*, 45–50.
33. Liu, D. M.; Chen, I. W. *Acta Mater.* **1999**, *47*, 4535–4544.
34. Cheng, S.-H.; Liao, W.-N.; Chen, L.-M.; Lee, C.-H. *J. Mater. Chem.* **2011**, *21*, 7130–7137.
35. Tan, A.; Simovic, S.; Davey, A. K.; Rades, T.; Prestidge, C. A. *J. Controlled Release* **2009**, *134*, 62–70.
36. Manzano, M.; Colilla, M.; Vallet-Regi, M. *Expert Opin. Drug Delivery* **2009**, *6*, 1383–1400.
37. Wan, Y.; Zhao, D. *Chem. Rev.* **2007**, *107*, 2821–2860.
38. Tan, A.; Simovic, S.; Davey, A. K.; Rades, T.; Boyd, B. J.; Prestidge, C. A. *Mol. Pharmaceutics* **2010**, *7*, 522–532.
39. Schubert, M. A.; Müller-Goymann, C. C. *Eur. J. Pharm. Biopharm.* **2003**, *55*, 125–131.
40. Pasc, A.; Blin, J. L.; Stébé, M. J.; Ghanbaja, J. *RSC Adv.* **2011**, *1*, 1204–1206.
41. Ravetti-Duran, R.; Blin, J. L.; Stébé, M. J.; Castel, C.; Pasc, A. *J. Mater. Chem* **2012**, *22*, 21540–21548.
42. Raemdonck, K.; Braeckmans, K.; Demeestera, J.; De Smedt, S. C. *Chem. Soc. Rev.* **2014**, *43*, 444–472.
43. Elsabahy, M.; Wooley, K. L. *Chem. Soc. Rev.* **2012**, *41*, 2545–2561.

44. Biju, V. *Chem. Soc. Rev.* **2014**, *43*, 744–764..
45. Aggarwal, B. B.; Harikumar, K. B. *Int. J. Biochem. Cell Biol.* **2009**, *41*, 40.
46. Jurenka, J. S. *Altern. Med. Rev.* **2009**, *14*, 141–153.
47. Maheshwari, R. K.; Singh, A. K.; Gaddipati, J.; Srimal, R. C. *Life Sci.* **2006**, *78*, 2081–2087.
48. Yallapu, M. M.; Jaggi, M.; Chauhan, S. C. *Drug Discovery Today* **2012**, *17*, 71–80.
49. Lin, J. K.; Pan, M. H.; Lin-Shiau, S. Y. *Biofactors* **2000**, *13*, 153–158.
50. Chirio, D.; Gallarate, M.; Trotta, M.; Carlotti, M. E.; Calcio Gaudino, E.; Cravotto, G. *J. Inclusion Phenom. Macrocycl. Chem.* **2009**, *65*, 391–402.
51. Jambhrukar, S.; Karmakar, S.; Popat, A.; Yu, M.; Yu, C. *RSC Adv.* **2014**, *4*, 709–712.
52. Tiyaboonchai, W.; Tungpradit, W.; Plianbangchang, P. *Int. J. Pharm.* **2007**, *337*, 299–306.
53. Heurtault, B.; Saulnier, P.; Pech, B.; Proust, J. E.; Benoit, J. P. *Biomaterials* **2003**, *24*, 4283–4300.
54. Kim, S.; Stébé, M. J.; Blin, J. L.; Pasc, A. *J. Mater. Chem. B* **2014**, *2*, 7910–7917.
55. Huo, Q.; Margolese, D. I.; Stucky, G. D. *Chem. Mater.* **1996**, *8*, 1147–1160.
56. Martins, S. M.; Sarmento, B.; Nunes, C.; Lucio, M.; Reis, S.; Ferreira, D. C. *Eur. J. Pharm. Biopharm.* **2013**, *85*, 488–502.
57. Zimmermann, E.; Muller, R. H. *Eur. J. Pharm. Biopharm.* **2001**, *52*, 203.
58. Sou, K. *Recent Pat. Nanomed.* **2012**, *2*, 133–145.
59. Castro, G. A.; Coelho, A. L. L. R.; Oliveira, C. A.; Mahecha, G. A. B.; Oréfice, R. L.; Ferreira, L. A. M. *Int. J. Pharm.* **2009**, *381*, 77–83.
60. Blin, J. L.; Jacoby, J.; Kim, S.; Stébé, M. J.; Canilho, N.; Pasc, A. *Chem. Commun.* **2014**, *50*, 11871–11874.
61. Jacoby, J.; Pasc, A.; Carteret, C.; Dupire, F.; Stébé, M. J.; Coupard, V.; Blin, J. L. *Process Biochem.* **2013**, *48*, 831–837.

Publication Date (Web): June 18, 2015 | doi: 10.1021/bk-2015-1192.ch017

Publication Date (Web): June 18, 2015 | doi: 10.1021/bk-2015-1192.ch018

Chapter 18

In Situ Metal-Free Synthesis of Polylactide Enantiomers Grafted from Nanoclays of High Thermostability

Giada Lo Re,* Philippe Dubois, and Jean-Marie Raquez

Center of Innovation and Research in Materials and Polymers (CIRMAP), University of Mons - UMONS, Place du Parc 23, 7000 Mons, Belgium
***E-mail: giada.lore@umons.ac.be.**

Renewable origin, controlled synthesis, good mechanical properties, and inherent biocompatibility make Polylactide (PLA) the most interesting renewable polymers for broad applications. For this reason, several strategies are carried out to span the range of applications for PLA and overcome its intrinsic drawbacks such as a low crystallization rate, thermal resistance and the use of metal-based catalysis for its synthesis. Adding nanosized fillers are among them the most studied and applied approach to enhance the performance of PLA-based materials. In order to achieve an enhanced interfacial adhesion and fine filler dispersion with the surrounding matrix, *in situ* polymerization constitutes the most viable and promising way to overcome this issue. In addition, stereocomplexation as well as organocatalysis make part of the emerging challenges to further improve the performance and extend the range of applications of the PLA-based materials such as in biomedical realm.

In this chapter, the metal-free synthesis of enantiomeric PLA/clay nanohybrids through ring-opening polymerization (ROP) of lactide is investigated, with the aim to produce stereocomplexed bionanocomposites with enhanced thermal properties. Different techniques to quench the polymerization reaction were thereby studied in order to overcome the main drawback related to the organocatalysis used for ROP of

In Green Polymer Chemistry: Biobased Materials and Biocatalysis; Smith, et al.;
ACS Symposium Series; American Chemical Society: Washington, DC, 2015.

lactide, *i.e.*, by causing intensive degradation on further melt-processing. Stereocomplexed polylactide/nanoclays bionanocomposites were prepared and their related thermal properties were investigated.

Introduction

Polylactide (PLA) is one of the most interesting and useful renewable and biodegradable polymers because of its renewable origin, biodegradability, controlled synthesis, good mechanical properties, and inherent biocompatibility (*1–5*) . However, PLA suffers from some drawbacks such as a low rigidity, slow crystallization rate and poor thermal-resistance. Moreover, the residual traces of metal-catalyst, mostly employed for its synthesis, limit its use in special applications such as the microelectronics or biomedical applications (*6*).

The literature reports several strategies in order to span the range of applications for PLA, more particularly by adding nanosized fillers, and the stereocomplexation. Nowadays, the metal-free synthesis of polylactide represents a new challenge to extend the use of PLA in the added-value market of microelectronic and biomedical applications (*7*).

Stereocomplexation is used to enhance the mechanical properties, the thermal-resistance, and the hydrolysis-resistance of PLA-based materials. Upon favorable thermodynamical parameters, in fact, an equivalent mixture of PLA of L-configuration (PLLA) and PLA of D-configuration (PDLA) forms a stereocomplex. Due to the strong Van der Waals interactions within the stereocomplex crystalline structure (*8–10*), melting temperature (T_m) of stereocomplexes can achieve a value above 220°C, which is approximately 50°C higher than T_m of either isotactic PLLA or PDLA (*11*).

Thermal, mechanical, rheological, barrier and other specific properties of the biopolymers can be improved by the incorporation of nanofillers. Blending renewable polymers with nanoparticles can yield a new class of hybrid materials, commonly known as bionanocomposites where the dispersed constituent has at least one dimension in the nanoscale size range. The nanosized dimensions of nanofillers enable their use in small quantities (weight percentage of 5-6%) into the polymer matrix. Improved thermal, mechanical and transport properties of PLA are often obtained via melt-blending layered silicate with the polylactide matrix in order to obtain bio-nanocomposites with enhanced performance (*12–18*). These improved properties are generally reached at low silicate content (less than 5 wt. %), due to the nanosized dimensions of the layered silicate. Using adequately organomodified nanoclay, specifically Cloisite 30B (Cl30B), intercalation of PLA chains into silicate galleries and even clay exfoliation throughout the polyester matrix are achieved (*19–21*). In the present work, the stereocomplexation and the addition of layered silicate nanofillers were investigated to cooperatively enhance the thermal properties and the crystallinity of PLA-based nanocomposites. Moreover, the "grafting from" approach was selected as a powerful tool for the enhancement of affinity between nanofillers and the matrix (*12*, *22*, *23*).

Publication Date (Web): June 18, 2015 | doi: 10.1021/bk-2015-1192.ch018

In Green Polymer Chemistry: Biobased Materials and Biocatalysis; Smith, et al.;
ACS Symposium Series; American Chemical Society: Washington, DC, 2015.

Nevertheless, the surface chemistry, specific surface area and volume effect of the nanofillers govern their common interactions, as well as the affinity towards the polymer matrix. These parameters, together with the size, the shape and the concentration, affect the extent of the nanofiller dispersion into the matrix. The large surface areas and low percolation thresholds as well as the availability and low cost make nanoclays the most used nanoparticles for polylactide, which attracted both industrial and academic interests. Indeed, several fields of applications such as medicine, textiles, cosmetics, agriculture, food-packaging, aerospace, construction, catalysis, and so on are expected from these bionanocomposites to substitute their petroleum-based counterparts.

Among the several methods adopted to improve the affinity between the polymeric matrix and the nanoclay, the *in-situ* polymerization of lactide, is a successful approach because of its flexibility in the synthetic parameters to tune the chain length and density on the filler surface, the improved dispersion of the filler in the matrix and related enhanced compatibility between the inorganic-organic phases. In particular, when the interactions between the filler and the polymer are of covalent bonding nature, the grafting achieved is generally combined to high performances for the resulting nanocomposites. In this respect "grafting from" methods, carrying out ring-opening polymerization of lactide through hydroxyl moieties from the quaternary ammoniums used for surface-treatment of nanoclays is preferred (*23*). As an example, PLA chains can be grafted at the surface of Cloisite®30B (CL30B), nanoclay organomodified in the presence of bis-2 hydroxyethyl, quaternary ammonium. CL30B was selected as model system among the most used, low cost and available commercial clays, due to the presence of "OH" end-group which can be used as initiator site for the ROP of lactide. In order to "graft" PLA chain from a clay surface, ROP of lactide (LA) is generally carried out in the presence of transition metal-based catalysts such as tin (II) octoate (*24*).

To avoid the current use of organometallic catalysts, we have recently reported the synthesis of PLLA and PDLA stereoisomers as directly grafted at the surface of CL30B via metal-free ROP of lactide carried out in chloroform at room temperature. To promote these reaction pathways in this work, 1,8-Diazabicyclo [5,4,0] undec-7-ene (DBU) was used as metal-free catalysts due to its excellent ability to control the polymerization of lactide at high yield (*25–27*). Although they exhibit several features such as low toxicity and compatibility, these metal-free catalysts have a high propensity to promote intensive side-reactions such as transesterification reactions at relatively high temperature and in the absence of solvent (*28*). An effective removal of the catalyst is therefore mandatory in order to obtain melt-processable PLA-based nanocomposites with improved performance. Some of us have reported that when DBU is used, a simple quenching reaction by using an excess of acid (forming the corresponding salt) followed by the precipitation of the polymer, can afford an effective way to obtain thermostable PLA (*28*). However, when stereocomplexed PLA are concerned, processing temperatures are so high, i.e., above 220°C, making these methods unsuccessful. In this chapter, current knowledge about *in situ* polymerization of polylactide from nanoclay by ROP achievements are used to prepare new bionanohybrids of clay-PLA metal free, pointing out different catalytic removal

Publication Date (Web): June 18, 2015 | doi: 10.1021/bk-2015-1192.ch018

In Green Polymer Chemistry: Biobased Materials and Biocatalysis; Smith, et al.;
ACS Symposium Series; American Chemical Society: Washington, DC, 2015.

methods. In addition to the quenching method using an excess of acid, a new route to quench the catalyst activity was investigated using the ion-exchange resin, to prepare the nanohybrids CL30B-graft-PLLA and CL30B-graft-PDLA (CL30B-*g*-PL(D)LA). The effectiveness of catalyst removal methods was assessed by the FTIR and DSC analysis on resulting nanohybrids. From the best quenching method, these nanohybrids were subsequently melt-processed together and with commercial PLA in order to elaborate stereocomplexed bionanocomposites with significantly improved thermal properties.

Experimental

Synthetic Approach

Publication Date (Web): June 18, 2015 | doi: 10.1021/bk-2015-1192.ch018

Commercial clay (CL30B, supplied by Southern Clay Products, USA), was introduced into a conditioned two-neck flask and dried under vacuum overnight. Meanwhile, L-lactide was hot-recrystallized. Briefly, L-lactide (supplied by Futerro) was dissolved in dry toluene, under stirring for 1 hour at 80 °C. Solution was put in a freezer to selectively precipitate the L-lactide monomer. The toluene was then removed from the flask by using a capillary and following by a drying step under vacuum at room temperature overnight. All products were stored in a glove box, in order to carry out the polymerization reaction under nitrogen atmosphere. Thereby, L-lactide and dried CL30B were solubilized in dry $CHCl_3$ (Sigma-Aldrich) in a flask , stirred at room temperature for 30 minutes, then DBU (Fluka), dried over BaO, was added for each mole of the hydroxyl functions. After 1 hour of polymerization reaction, the viscous solution was divided in three different flasks to carry out three different quenching methods. In a flask (a), acetic acid was added to the reaction medium, in an amount equal to that of DBU, to quench the polymerization. Liquid-liquid extraction was carried out on the second flask (b), using slightly acid water solution (0.1M) as aqueous phase to quench the polymerization. Equivalent amount of dried ion-exchange resin Amberlyst® 15, in hydrogen form (Fluka), was added into the third flask (c) and stirred for 2 hours, in order to quench the polymerization. Then, the ion-exchange resin was removed by filtering the solution. The final products (CL30B-g-PLLA-a, b and c) were recovered after drop-by-drop precipitation in 8 volumes of n-heptane, filtered and dried in vacuum overnight at 55°C.

Finally, in order to produce the enantiomeric nanohybrids designed with the 10 wt % in inorganic content (CL30B-g-PLLA and CL30B-g-PDLA), for the further melt-processing, ROP synthesis of the two enantiomeric forms of lactide were carried out using the same synthetic procedure (D-lactide supplied by Purac), quenched by the ion-exchange resin (the reasons will be discussed in the following section).

The properties of the nanohybrids, the effectiveness of the grafting and the DBU removal were assessed by thermal characterization (Differential Scanning Calorimetry, DSC, and Thermogravimetric Analyses, TGA) and Attenuated Total Reflectance Fourier transform infrared (ATR-FTIR) of the dried synthetic products or their fractions recovered after Soxlet extraction from dichloromethane (Sigma-Aldrich). Gel Permeation Chromatography (GPC) was performed in

CHCl3 at 35°C using a Polymer Laboratories liquid chromatograph equipped with a PL-DG802 degasser, an isocratic HPLC pump LC 1120 (flow rate = 1 ml/min) refractive index (ERMA 7517), an automatic injector (Polymer Laboratories GPC-RI/UV) and three columns: a PL gel 10 μm guard column and two PL gel Mixed-B 10μm columns. PS standards were used for calibration. It is worth noting that Gel Permeation Chromatography (GPC) characterization was performed on the soluble fraction recovered after Soxhlet extraction from diclorometh ane of both nanohybrids, in order to assess the molecular weight of the nanohybrids synthetized.

Melt Processing

PLA layered silicate composites and references, were prepared by melt-blending using a DSM microcompounder operating at 190°C for 10 min with a rotation speed of 60 rpm. The nanocomposites were elaborated using a commercial PLA (PLA 4032, 4% D-isomer, Naturework) at an inorganic content of 5 wt %, to further improve the inorganic content in the composition compared to the similar systems previously reported (*23*, *29*, *30*). For the sake of comparison, the stereocomplex CL30B-g-PLLA/CL30B-g-PDLA was prepared together with the corresponding reference PLA/CL30B (10 wt % of inorganic content) (see Table 1). To blend stereocomplexes (PLA/CL30B-g-PDLA and CL30B-g-PLLA/CL30B-g-PDLA blends), the temperature was increased to 220 °C for the last 2 min residence time. Inorganic content, thermal properties and thermal stability of blends were assessed using TGA and DSC techniques.

Table 1. Compositions of Composites Produced, by DSM Micro-Compounder

SAMPLE	***PLA [g]***	***CL30B [g]***	***Cl30B-g-PDLA [g]***	***Cl30B-g-PLLA [g]***	***Inorg. content [%]***
PLA 4032 (4% D-isomer)	15	-	-	-	-
PLA/Cl30B 5% inorg.	14	1	-	-	4.8*
PLA/Cl30B 10% inorg.	13	2	-	-	10.4*
PLA/Cl30B-g-PLLA 5% inorg.	7.5	-	-	7.5	5.6*
PLA/Cl30B-g-PDLA 5% inorg.	7.5	-	7.5	-	4.7*
Cl30B-g-PLLA/Cl30B-g-PDLA 10% inorg.	-	-	7.5	7.5	10.5*

* Percentages estimated referring to inorganic content detected by TGA.

Publication Date (Web): June 18, 2015 | doi: 10.1021/bk-2015-1192.ch018

Publication Date (Web): June 18, 2015 | doi: 10.1021/bk-2015-1192.ch018

In Situ Intercalative Ring-Opening Polymerization of L(D)-lactide

In order to enhance the affinity between nanofillers and the matrix, the CL30B nanofillers were employed to carry out a "grafting from" approach as reported in our previous work (*23*). This consisted to promote ring-opening polymerization (ROP) of L and D-lactide from hydroxyl moieties of quaternary ammonium available at the surface of the organomodified clay in order to synthesize CL30B-grafted bio-nanohybrids, as shown in Figure 1. To promote ROP of L(D)-lactide monomers, 1,8-Diazabicyclo [5,4,0] undec-7-ene (DBU) was employed as metal-free catalysts in chloroform at room temperature. In this respect, two enantiomeric CL30B-g-PLLA and CL30B-g-PDLA nanohybrids were prepared by respective DBU–catalyzed ring opening polymerization (ROP) of L-lactide or D-lactide initiated from the hydroxyl moieties of quaternary ammonium tallow intercalated in the galleries of CL30B (Figure 1).

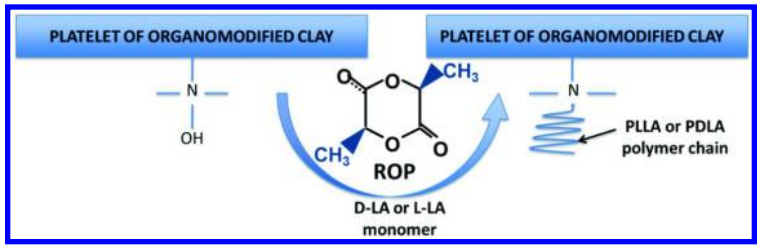

Figure 1. Illustration of the in situ polymerization of polylactic acid chains on Cloisite30B surface.

These nanohybrids were designed at an inorganic content of 10 wt % and confirmed by TGA.

In order to optimize the reaction parameters, especially concerning the selection of the quenching technique, a synthesis just of the L-form of lactide grafted on the clay surface was previously carried out. From the unique reaction solution, three different quenching techniques were performed and the thermal properties of the three different products (CL30B-g-PLLA-a, b and c) were assessed by DSC as well as the effectiveness of the catalyst by FTIR. In particular, the polymerization was quenched by three following approaches, i.e., (a) by adding acetic acid into reaction medium, (b) by liquid-liquid extraction and (c) in the presence of ion-exchange resin. These methods were followed by the selective precipitation of reaction medium into an excess of heptane.

In order to detect the presence of residual catalyst, which can cause degradation during further melt-processing, as previously reported in literature (*28*), Figures 2 and 3 show the respective ATR-FTIR spectra of the DBU, acetic acid and the corresponding salt and those of CL30B-g-PLLA nanohybrids. In Figure 2, the results obtained from spectroscopic analysis indicate that the bands of the DBU salt form, derived from reaction of DBU with acetic acid, are the C-H stretching vibration bands at 2925 and 2854 cm^{-1}, and stretching vibration bands

In Green Polymer Chemistry: Biobased Materials and Biocatalysis; Smith, et al.;
ACS Symposium Series; American Chemical Society: Washington, DC, 2015.

ν(C=N) at 1643 and 1554 cm^{-1}. As it is possible to observe, comparing Figures 2 and 3, any significant evidence of DBU traces is observed in the case of the nanohybrids, suggesting that all the precipitation techniques adopted are suitable to obtain DBU-free PLLA.

In Figure 3 the spectroscopic results of the products indeed show typical peaks of PLLA. In particular, C=O stretching band at ~1760 cm^{-1}, C-O stretching band at ~1189, 1134 and 1091 cm^{-1}, CH_3 bending vibration at ~1457 cm^{-1} and C-H bending vibrations at 1382-1370 cm^{-1}, confirming that the polymerization of PLLA was successful. The spectra of CL30B-g-PLLA-c show the slight shifted peaks compared to the CL30B-g-PLLA-a and b suggest that the treatment with the ion-exchange resin has modified both C=O and C-O stretching vibration bands.

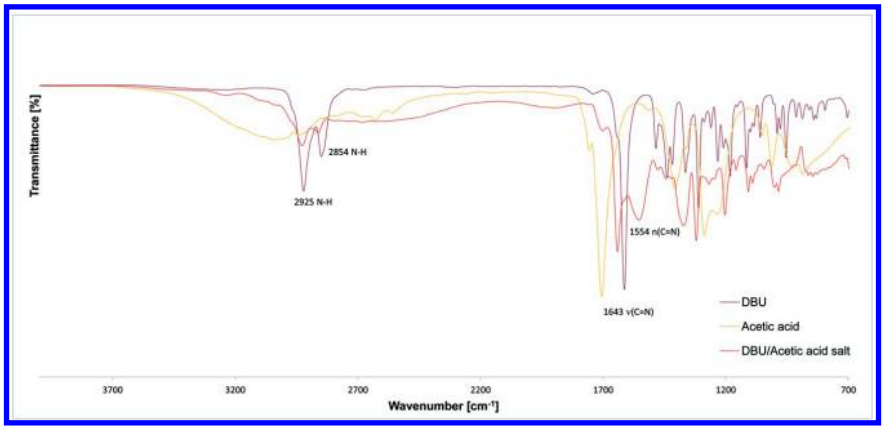

Figure 2. ATR-FTIR spectra of DBU, acetic acid and DBU/acetic acid solution.

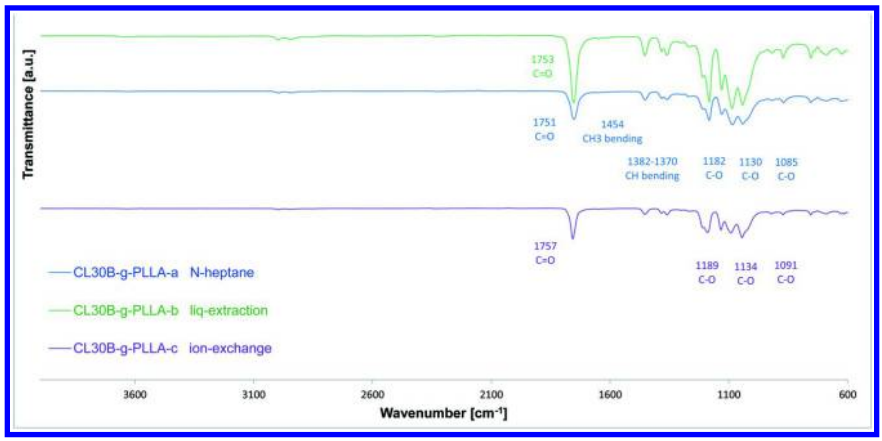

Figure 3. ATR-FTIR spectra of the insoluble fractions recovered after Soxhlet extraction from dichloromethane of different synthetic products (normalized using the peak at 1760 cm^{-1}).

In Green Polymer Chemistry: Biobased Materials and Biocatalysis; Smith, et al.;
ACS Symposium Series; American Chemical Society: Washington, DC, 2015.

Publication Date (Web): June 18, 2015 | doi: 10.1021/bk-2015-1192.ch018

Publication Date (Web): June 18, 2015 | doi: 10.1021/bk-2015-1192.ch018

To further confirm the thermostability of the nanohybrids, DSC measurements of the different CL30B-g-PLLAs were carried out. DSC measurements have shown to be an efficient way to evidence side-reactions, namely racemization of PLA-based materials on heating (*23*). In Figure 4, DSC thermograms corresponding to the second heating of different extracted products (CL30B-g-PLLA-a, b and c) are reported. In Table 2, the main results of DSC analysis were summarized.

Table 2. Values of the Glass Transition (T_g), Melting (T_m) Temperatures and Heat of Crystallization (ΔH_m) under Nitrogen Flow (Temperature Range: -80-200 °C, Heating and Cooling Rate 10°C /min, Second Heating)

DSC	*T_g [°C]*	*T_m [°C]*	*ΔH_m[J/g]*
CL30B-g-PLLA-a	50.6	160.9	36.2
CL30B-g-PLLA-b	47.5	159.2	37.0
CL30B-g-PLLA-c	54.9	162.0	34.1

Distinguishable T_g temperatures can be identified in the DSC traces. All results can be likely ascribed to PLA of low molecular length (as expected for the designed polymerization).

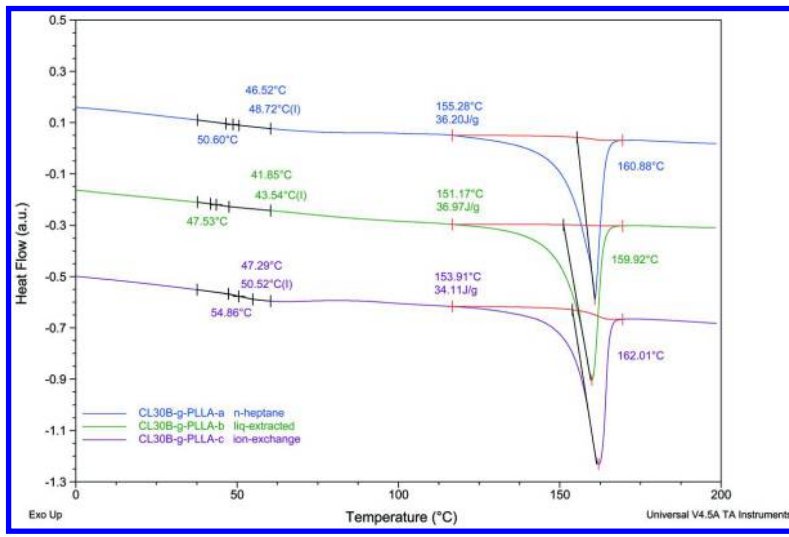

Figure 4. DSC of CL30B-g-PLLA products recovered upon these three quenching techniques.

In Green Polymer Chemistry: Biobased Materials and Biocatalysis; Smith, et al.;
ACS Symposium Series; American Chemical Society: Washington, DC, 2015.

All the thermal properties recorded for the nanohybrids are typical for a PLLA of low molecular weight, as reported in previous works (*23*, *28*). The CL30B-g-PLLA-a thermogram shows a T_g of around 50.6 °C, a T_m of around 160.9 °C and 36.2 J/g for the crystallization enthalpy. The CL30B-g-PLLA-b shows the slightly lower values of T_g and T_m, and not significant increase in the ΔH_m, compared to the CL30B-g-PLLA-a. The higher values of T_g and T_m were shown by the CL30B-g-PLLA-c product, suggesting the good effectiveness of the third quenching technique. This was further supported after carrying out 10-scan DSC measurements on those nanohybrids. After the second scan, the nanohybrids extracted from the methods (a) and (b) did not exhibit any melting and crystallization features. This indicates that DBU residues could further promote the undesirable transesterification reactions (not shown here). In contrast when ion-exchange resin is employed, the resulting nanohybrids are thermally stable. Taking in account these results, a new series of nanohybrids, two enantiomeric nanohybrids were synthetized using the same procedure and quenching the ROP by the ion-exchange resin approach.

Gel Permeation Chromatography (GPC) characterization (performed in $CHCl_3$ at 35°C) was performed on the soluble fraction recovered after Soxhlet extraction from dicloromethane of both nanohybrids, in order to assess the molecular weight of the nanohybrids synthetized. In Table 3 number-average molecular weight (M_n), the molecular weight at the maximum peak (M_p) and dispersity (DPI) are reported upon a PS calibration.

Table 3. M_n, M_p and DPI of Different Soluble Fractions PDLA and PLLA, Recovered after Soxhlet Extraction from CH_2Cl_2 of the Corresponding Nanohybrids Cl30B-*g*-PDLA and Cl30B-*g*-PLLA

SAMPLE	M_n *[g/mol]*	M_P *[g/mol]*	*DPI*
PDLA from Cl30B-*g*-PDLA	2.40 x 10^4	4.68 x 10^4	2.1
PLLA from Cl30B-*g*-PLLA	2.50 x 10^4	4.86 x 10^4	2.1

Although we may not exclude any fractionation of these samples from CH_2Cl_2, these results show that the soluble fraction issued from both nanohybrids have the same range of molecular weights. These results are further confirmed on the basis of thermal properties recorded for both nanohybrids.

To further confirm the previous results, 10-cycles DSC analysis was carried out also on the Cl30B-g-PLLA and CL30B-g-PDLA nanohybrids. As shown in Figure 5, both nanohybrids show a very significant thermostability because the main thermal properties do not change even after 10-cycles heating-cooling scans. This result confirms the effectiveness of the catalyst removal because no evidence of degradations is visible in the thermograms. The enantiomers, at 10% inorganic content, have comparable thermal properties, as shown by their respective glass transition (T_g), melting (T_m) and cold crystallization temperatures (T_c) in Figure 5. The slightly shifted values in the melting temperatures recorded, compared to

In Green Polymer Chemistry: Biobased Materials and Biocatalysis; Smith, et al.;
ACS Symposium Series; American Chemical Society: Washington, DC, 2015.

Publication Date (Web): June 18, 2015 | doi: 10.1021/bk-2015-1192.ch018

the previous results of the CL30B-g-PLLA-a b and c nanohybrids, are expected because the higher inorganic content designed for the two enantiomers CL30B-g-PLLA and CL30B-g-PDLA. In addition, they have two T_m, *that is*, ascribed to the melting and recrystallization events on heating, fairly common in low M_n polylactides or which can be attributed to a polymorphism of the two different crystal forms of polymorphic PL(D)LA (α- and α′-form crystals) (*23*).

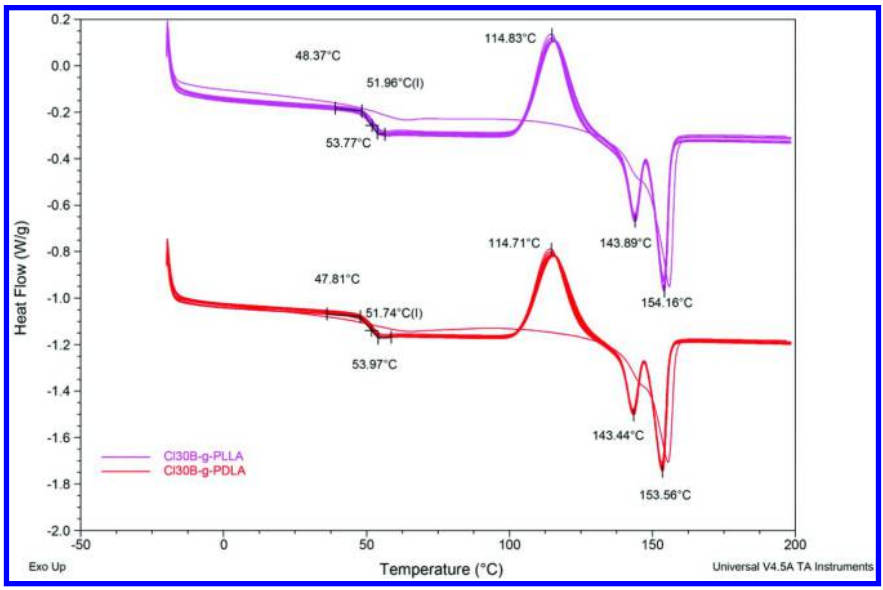

Figure 5. 10-cycles DSC scans of CL30B-g-PDLA and CL30B-g-PLLA (10 wt% of inorganic content).

In this respect, among the different quenching techniques, the ion-exchange resin approach was selected to prepare CL30B-graft-PLLA and CL30B-graft-PDLA nanohybrids thermally stable.

PLA Nanocomposites by Melt Intercalation

To further attest for the efficiency of the quenching ion-exchange resin method, those nanohydrids were subsequently melt-blended with commercial PLA using a DSM microcompounder in order to produce PLA/clay-based bio-nanocomposites. It is worth noting that well-dispersion of nanohybrids into resulting bionanocomposites could be readily achieved and demonstrated by both WAXS and TEM analyses as reported by us (*23*).

A series of DSC experiments was conducted to investigate the thermal properties of the nanocomposites. These DSC results are also compared with those of nanocomposites directly prepared from C30B nanofiller and commercial PLA. Figure 6 shows the first heating scans of nanocomposites and the main results are summarized in Table 4.

Publication Date (Web): June 18, 2015 | doi: 10.1021/bk-2015-1192.ch018

Publication Date (Web): June 18, 2015 | doi: 10.1021/bk-2015-1192.ch018

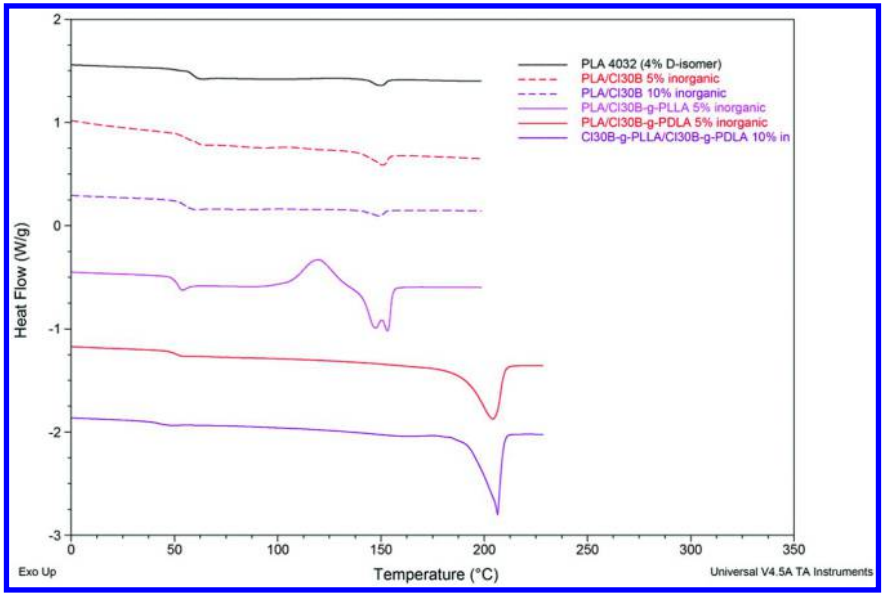

Figure 6. DSC thermograms of the first heating scan of the neat PLA and all the nanocomposites prepared.

The pure PLA matrix contains a low quantity of D-isomer (4%) and exhibits a T_g of around 59°C and an endothermic melting with a melting temperature (T_m) at 150°C. No significant differences were observed in the thermograms of both PLA/CL30B composites, suggesting that the low content of clay in the blend does not affect the thermal properties of the neat PLA. A slight decrease in the T_g suggests the plasticizer effect of the nanohybrids in the blends, likewise due to the low molecular weight of the PL(D)LA chains grafted on the nanoclay surface. The DSC results for the stereocomplex obtained by melt-blending CL30B-*g*-PLLA and CL30B-g-PDLA confirm that the as-grafted polymers are characterized by a lower glass transition temperature, compared to the commercial PLA. The thermograms of both stereocomplexes PLA/CL30B-g-PDLA and CL30B-*g*-PLLA/CL30B-*g*-PDLA interestingly exhibit a comparable melting temperature peak at 205°C, which is above 50°C, compared to the starting nanohybrids (T_m=154°C, see Figure 5) as well as the neat PLA (T_m=150°C, see Figure 6 and Table 4).

The thermal stability of the stereocomplex is also studied by the 10 heating/ cooling/heating cycles DSC, reported for both stereocomplex in Figure 7. Their main results are shown in Figs. 8 and 9.

Table 4. Values of the Glass Transition (T_g), Cold Crystallization (T_{cc}), Melting (T_m) Temperatures and Cold Crystallization and Melting Enthalpies (ΔH_{cc} and ΔH_m) Recorded from the First Heating Scan, under Nitrogen Flow (Temperature Range: -20 - 230°C, Heating Rate 10°C /min)

DSC	T_g *[°C]*	T_{cc} *[°C]*	ΔH_{cc} *[°C]*	T_m *[°C]*	ΔH_m *[J/g]*
PLA 4032 (4% D-isomer)	59.1	-	-	150.1	3
PLA/Cl30B 5% inorganic	60.6	-	-	150.7	5
PLA/Cl30B 10% inorganic	58.9	-	-	149.4	3
PLA/Cl30B-g-PLLA 5% inorganic	52.1	120.0	26	147.5-153.1	30
PLA/Cl30B-g-PDLA 5% inorganic	51.4	-	-	204.9	46
Cl30B-g-PLLA/Cl30B-g-PDLA 10% inorganic	42.5	-	-	205.4	45

Publication Date (Web): June 18, 2015 | doi: 10.1021/bk-2015-1192.ch018

These results confirm the high thermal stability of the stereocomplexes prepared by melt-blending. The melting enthalpies (Figure 9), as well as the melting temperatures (Figure 8), show the stable values (of ~40 J/g and ~200°C, respectively) for both stereocomplexes. For the PLA/Cl30B-g-PDLA stereocomplex, the cold crystallization temperature (T_{cc}) slightly decreases from 106 to 102°C by increasing the heating cycle number. In the case of the direct blend between the synthetic nanohybrids Cl30B-g-PLLA/Cl30B-g-PDLA, the cold crystallization appears after the fifth cycle, characterized by a T_{cc} of 84-85 °C and an enthalpy from 3 to 12 J/g, which increases with the heating cycle number and suggesting that the Cl30B-g-PLLA/Cl30B-g-PDLA is slightly less thermostable than the commercial PLA-based stereocomplex. It is worth noting that no evidence of further melting peaks is observed on the 10 cycle scans, Figure 7, also in the case of the stereocomplex PLA/Cl30B-g-PDLA. It is worth noting that no peaks in the temperature range of the PLA homocrystals (~150°C, see Figure 7) appears, suggesting that the full stereocomplexation of the enantiomers is achieved. This result confirms the possibility by direct melt blending to get full stereocomplexation, being considered as a significant challenge in the melt-preparation of PLA stereocomplexes (*31*, *32*).

The stereocomplexation approach, therefore, enables to improve the thermal properties of the nanocomposites. Moreover, for both stereocomplexed nanocomposites, there is no "cold" crystallization, suggesting a significant improvement in the crystallinity rate, as shown in Figures 7 and 9.

Publication Date (Web): June 18, 2015 | doi: 10.1021/bk-2015-1192.ch018

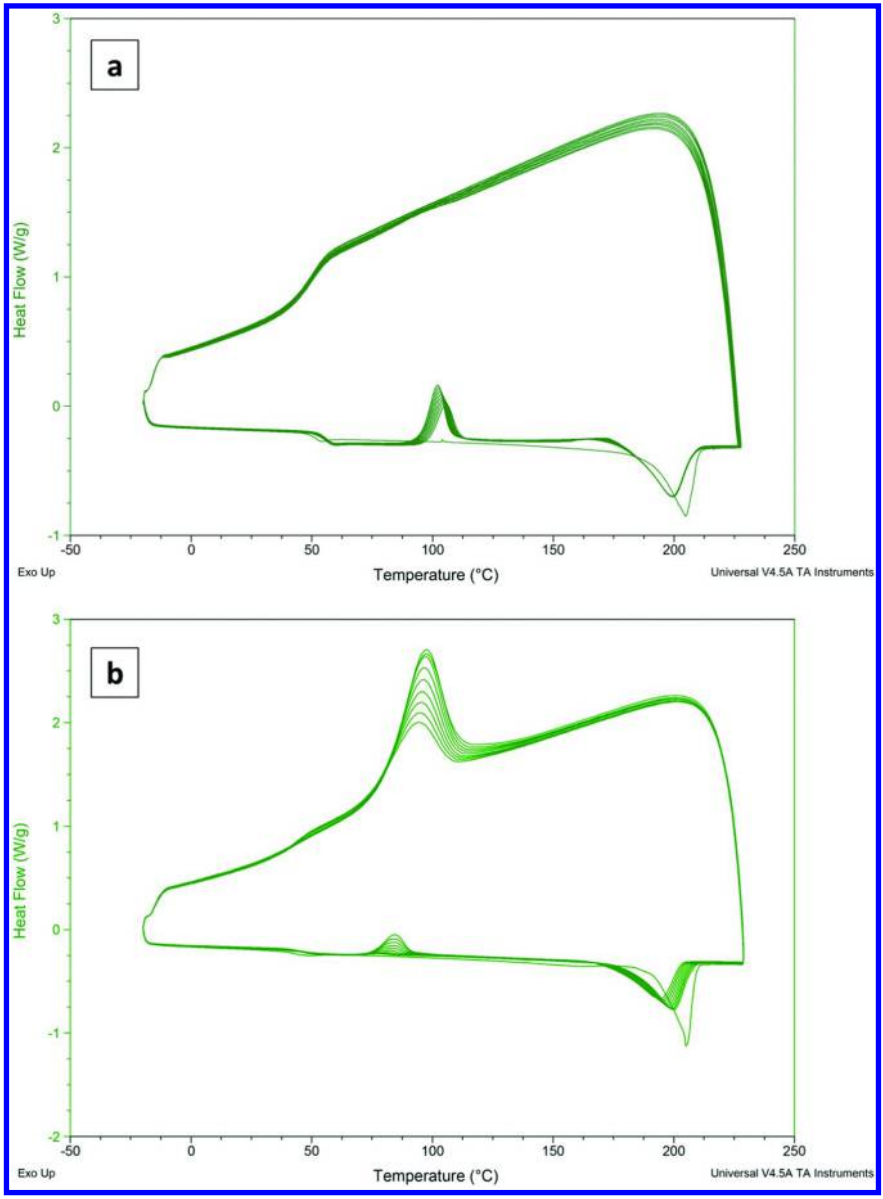

Figure 7. 10-cycles DSC heating/cooling scans under nitrogen flow (temperature range: -20-230 °C, heating rate 10°C /min), for the stereocomplex PLA/Cl30B-g-PDLA (5% inorganic), (a), and Cl30B-g-PLLA/Cl30B-g-PDLA (10% inorganic), (b).

Publication Date (Web): June 18, 2015 | doi: 10.1021/bk-2015-1192.ch018

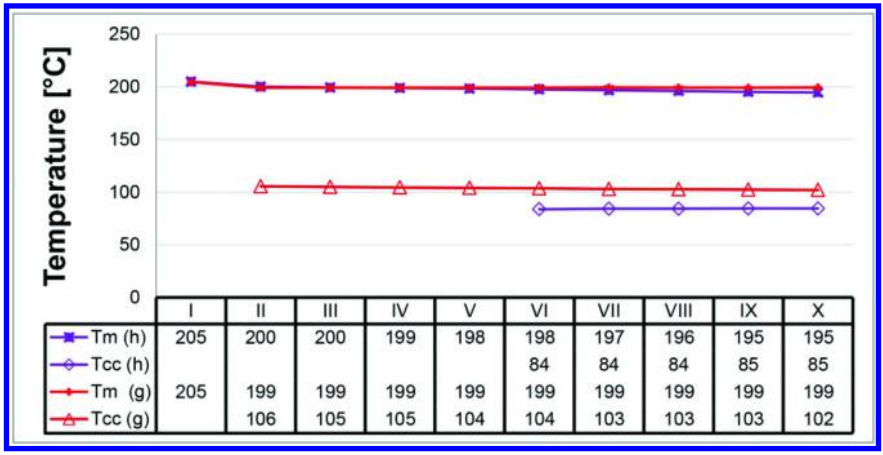

	I	II	III	IV	V	VI	VII	VIII	IX	X
Tm (h)	205	200	200	199	198	198	197	196	195	195
Tcc (h)						84	84	84	85	85
Tm (g)	205	199	199	199	199	199	199	199	199	199
Tcc (g)		106	105	105	104	104	103	103	103	102

Figure 8. Values of cold crystallization (T_{cc}) and melting (T_m) temperatures as a function of the heating cycle number (indicated with roman numerals on the top line of the summarizing table under the curve), recorded from the ten cycles DSC thermograms, under nitrogen flow (temperature range: -20-230 °C, heating rate 10°C /min), for the stereocomplex PLA/Cl30B-g-PDLA (5% inorganic, red curves) and Cl30B-g-PLLA/Cl30B-g-PDLA (10%inorganic, violet curves).

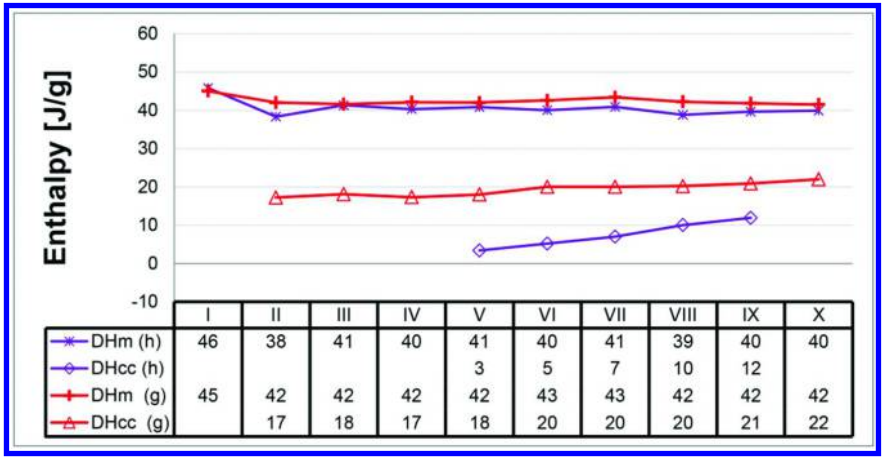

	I	II	III	IV	V	VI	VII	VIII	IX	X
DHm (h)	46	38	41	40	41	40	41	39	40	40
DHcc (h)					3	5	7	10	12	
DHm (g)	45	42	42	42	42	43	43	42	42	42
DHcc (g)		17	18	17	18	20	20	20	21	22

Figure 9. Values of cold crystallization and melting enthalpies (ΔH_{cc} and ΔH_m) as a function of the heating cycle number (indicated with roman numerals on the top line of the summarizing table under the curve), recorded from the ten cycles DSC thermograms, under nitrogen flow (temperature range: -20-230 °C, heating rate 10°C /min), for the stereocomplex PLA/Cl30B-g-PDLA (5% inorganic) and Cl30B-g-PLLA/Cl30B-g-PDLA (10 %-wt inorganic).

Publication Date (Web): June 18, 2015 | doi: 10.1021/bk-2015-1192.ch018

Conclusions

Well-defined and thermally stable Cl30B-g-PLLA (B150-L) and Cl30B-g-PDLA (B150-D) nanohybrids were prepared by DBU–catalyzed ring opening polymerization (ROP) of L-lactide and D-lactide respectively initiated from the hydroxyl moieties of quaternary ammonium cations intercalated in the galleries of Cl30B. Quenching method based on ion-exchange resins led to the preparation of thermally stable nanohybrids. As a result, the bionanocomposites obtained after melt-blending of nanohybrids with PLA were thermally stable, confirming by the full deactivation of metal-free DBU catalyst before melt-processing, overcoming the intrinsic limits related to the use of the DBU as organic catalyst in the ROP. Stereocomplexes obtained by direct melt-blending PLA and the D-isomer based nanohybrid, as well as melt-blending L and D-isomer based nanohybrids, present a higher melting temperature above 50°C than that of commercial PLA. Moreover, no evidence for the homocrystals was detected in the ten-cycle scans for both sterocomplex Cl30B-g-PLLA/Cl30B-g-PDLA and PLA/Cl30B-g-PDLA. The nanocomposites as well the starting nanohybrids show a very significant thermostability proved by their unchanged main thermal properties even after 10- heating/cooling cycles. Furthermore, it was easy to quench the catalyst activity using the ion-exchange resin, enabling to implement these materials into industrial applications.

Acknowledgments

Financial supports from Région Wallonne and European Commission in the frame of OPTI²MAT program of excellence and the 7th Framework research project ECLIPSE are gratefully acknowledged. Authors thank also the “Belgian Federal Government Office Policy of Science (BELSPO)” for its support in the frame of the PAI-6/27. J.-M. Raquez is a research associate of the F.R.S.-FNRS.

References

1. Kummerer, K. *Green Chem.* **2007**, *9*, 899–907.
2. Jenck, J. F.; Agterberg, F.; Droescher, M. *J. Green Chem.* **2004**, *6*, 544–556.
3. Gross, R. A.; Kalra, B. *Science* **2002**, *297*, 803–807.
4. Kaplan, D. L. *Biopolymer Renewable Resources;* Springer: Heidelberg, 1998; pp 1−29.
5. Lunt, J. *Polym. Degrad. Stab.* **1998**, *59*, 145–152.
6. Raquez, J.-M.; Habibi, Y.; Murariu, M.; Dubois, P. *Progr. Polym. Sci.* **2013**, *38*, 1504–1542.
7. Thomas, C.; Gladysz, J. A. *ACS Catal.* **2014**, *4*, 1134–1138.
8. He, Y.; Xu, Y.; Wei, J.; Fan, Z.; Li, S. *Polymer* **2008**, *49*, 5670–5675.
9. Zhang, J.; Sato, H.; Tsuji, H.; Noda, I.; Ozaki, Y. *Macromolecules* **2005**, *38*, 1822–1828.
10. Anderson, K. S.; Hillmyer, M. A. *Polymer* **2006**, *47*, 2030–2035.
11. Fan, Y.; Nishida, H.; Shirai, Y.; Tokiwa, Y.; Endo, T. *Polym. Degrad. Stab.* **2004**, *86*, 197–208.

12. Alexandre, M.; Dubois, P. *Mater. Sci. Eng.* **2000**, *28*, 1–63.
13. Bordes, P.; Pollet, E.; Avérous, L. Nano-biocomposites: Biodegradable polyester/nanoclay systems. *Progr. Polym. Sci.* **2009**, *34*, 125–155.
14. Chang, J. H.; An, Y. U.; Sur, G. S. Poly (lactic acid) nanocomposites with various organoclays. I. Thermomechanical properties, morphology, and gas permeability. *J. Polym. Sci., Part B: Polym. Phys.* **2002**, *41*, 94–103.
15. Ray, S. S.; Yamada, K.; Okamoto, M.; Ogami, A.; Ueda, K. New polylactide/layered silicate nanocomposites. 3. High-performance biodegradable materials. *Chem. Mater.* **2003**, *15*, 1456–1465.
16. Zenkiewicz, M.; Richert, J. Permeability of polylactide nanocomposite films for water vapour, oxygen and carbon dioxide. *Polym. Test.* **2008**, *27*, 835–840.
17. Zenkiewicz, M.; Richert, J. Effects of nanofillers and sample dimensions on the mechanical properties of injection-molded polylactide nanocomposites. *Polimery (Warsaw, Pol.)* **2008**, *53*, 591–594.
18. Zenkiewicz, M.; Richert, J.; Różański, A. Effect of blow moulding ratio on barrier properties of polylactide nanocomposite films. *Polym. Test.* **2010**, *29*, 251–257.
19. Paul, M.-A.; Alexandre, M.; Degée, P.; Calberg, C.; Jérôme, R.; Dubois, P. Exfoliated Polylactide/Clay Nanocomposites by In-Situ Coordination–Insertion Polymerization. *Macromol. Rapid Commun.* **2003**, *24*, 561–566.
20. Molinaro, S.; Cruz Romero, M.; Boaro, M.; Sensidoni, A.; Lagazio, C.; Morris, M.; Kerry, J. Effect of nanoclay-type and PLA optical purity on the characteristics of PLA-based nanocomposite films. *J. Food Eng.* **2013**, *117*, 113–123.
21. Pluta, M.; Paul, M.-A.; Alexandre, M.; Dubois, P. Plasticized polylactide/clay nanocomposites. I. The role of filler content and its surface organo-modification on the physico-chemical properties. *J. Polym. Sci., Part B: Polym. Phys.* **2006**, *44*, 299–311.
22. Lepoittevin, B.; Pantoustier, N.; Devalckenaere, M.; Alexandre, M.; Kubies, D.; Calberg, C.; Jérôme, R.; Dubois, P. Poly (ε-caprolactone)/clay nanocomposites by in-situ intercalative polymerization catalyzed by dibutyltin dimethoxide. *Macromolecules* **2002**, *35*, 8385–8390.
23. Lo Re, G.; Benali, S.; Habibi, Y.; Raquez, J.-M.; Dubois, P. *Eur. Polym. J.* **2014**, *54*, 138–150.
24. Thomas, C. M. *Chem. Soc. Rev.* **2010**, *39*, 165–173.
25. Kamber, N. E.; Jeong, W.; Waymouth, R. M.; Pratt, R. C.; Lohmeijer, B. G. G.; Hedrick, J. L. *Chem. Rev.* **2007**, *107*, 5813–5840.
26. Lohmeijer, B. G. G.; Pratt, R. C.; Leibfarth, F.; Logan, J. W.; Long, D. A.; Dove, A. P.; Hedrick, J. L. *Macromolecules* **2006**, *39*, 8574–8583.
27. Dove, A. P. *ACS Macro Lett.* **2012**, *1*, 1409–1412.
28. Coulembier, O.; Moins, S.; Raquez, J. M.; Meyer, F.; Mespouille, L.; Duquesne, E.; Dubois, P. *Polym. Degrad. Stab.* **2011**, *96*, 739–744.
29. Paul, M.-A.; Alexandre, M.; Degée, P.; Calberg, C.; Jérôme, R.; Dubois, P. *Macromol. Rapid Commun.* **2003**, *24*, 561–566.

Publication Date (Web): June 18, 2015 | doi: 10.1021/bk-2015-1192.ch018

30. Paul, M-A.; Delcourt, C.; Alexandre, M.; Degée, P.; Monteverde, F.; Rulmont, A.; Dubois, P. *Macromol. Chem. Phys.* **2005**, *206*, 484–498.
31. Tsuji, M. *Macromol. Biosci.* **2005**, *5*, 569–597.
32. Ikada, Y.; Jamshidi, K.; Tsuji, H.; Hyon, S.-H. *Macromolecules* **1987**, *20*, 904–906.

Publication Date (Web): June 18, 2015 | doi: 10.1021/bk-2015-1192.ch018

Publication Date (Web): June 18, 2015 | doi: 10.1021/bk-2015-1192.ch019

Chapter 19

A Novel Renewable Thermoplastic Polyacetal by Polymerization of Glycolaldehyde Dimer, a Major Product of the Fast Pyrolysis of Cellulosic Feedstock

Silvia D. Luebben* and James W. Raebiger

TDA Research, Inc., 12345 W 52nd Avenue, Wheat Ridge, Colorado, 80033
***E-mail: silvia@tda.com.**

In this paper, we present the first reported synthesis of poly(2,5-dihydroxy-1,4-dioxane) (PDHDO), a novel renewable thermoplastic polyacetal prepared by polymerization of glycolaldehyde dimer, namely 2,5-dihydroxy-1,4-dioxane (DHDO) via a catalytic process. The monomer can be obtained in high purity and large quantities from the fast pyrolysis of lignocellulosic feedstock at a cost that has been estimated to be competitive with that of petrochemical monomers such as ethylene or ethylene glycol. This novel polyacetal is expected to hydrolyze back to the monomer in the environment. Glycolaldehyde is present in soy and browning sauces, is a natural metabolite, and is found in the environment where it is easily oxidized. Thus, this new renewable thermoplastic could potentially be cost competitive with petrochemical polyolefins and is expected not to present issues of persistency or bio-accumulation.

Introduction

Plastics are ubiquitous materials in our modern society, used in everything from structural supports to packaging to medical devices. The overwhelming majority of plastics are made from petroleum-based feedstocks, the availability of which makes plastics inexpensive and diverse. However, there is an

In Green Polymer Chemistry: Biobased Materials and Biocatalysis; Smith, et al.;
ACS Symposium Series; American Chemical Society: Washington, DC, 2015.

Publication Date (Web): June 18, 2015 | doi: 10.1021/bk-2015-1192.ch019

ever-increasing need to change from petroleum-based feedstocks to renewable feedstocks due to the finite supply of oil reserves. The increasing global demand for a more sustainable future is leading the plastic industry to invest in the research and development of greener plastic products. While the market for bio-based resins and polymers is growing at a rate of 19% per year and is expected to approach 950,000 metric tons in 2017, the sales of bio-based plastics are still only a small fraction of those of petrochemical-based products. In fact it has been estimated that even if this growth rate continues bio-based plastics will constitute only 1% of the global plastic market in 2020 (*1*). This is due, in part, to the higher cost and the limited selection of monomers that can be obtained from bio-derived feedstocks, which in turn limits the available options when engineering polymer structures with specific functional properties and performance.

Commercial renewable thermoplastics are mainly polyolefins and polyesters, and include bio-polyethylene (PE made from ethylene that is produced by the dehydration of bio-ethanol), polylactic acid (PLA), polycaprolactone (PCL), poly(hydroxybutyrate) (PHB), polyhydroxyalkanoates (PHA), and polyesters made by condensation of bio-adipic acid or bio-succinic acid and a bio-diol such as 1,4-butanediol (BDO). Biobased polyethylene terephthalate (PET) and polypropylene (PP) are expected to become available in commercial quantities in the next five years. The aliphatic polyesters PLA, PCL, and others are both renewable and biodegradable, and their degradation products are environmentally friendly. However they cannot be used in many large-volume applications because of their limited mechanical or barrier properties and/or high cost. Furthermore their monomers are made from crops such as corn, sugar cane, or vegetable oils and therefore their production competes with that of food, although alternative non-food feedstocks are being explored. In contrast, bio-based PE, PP and PET are not biodegradable, which means they cannot be composted and therefore accumulate in landfills and the environment as much as their petrochemical analogues do.

In this work we present the synthesis of a novel renewable thermoplastic by catalytic polymerization of glycolaldehyde dimer, 2,5-dihydroxy-1,4-dioxane (DHDO). Because of ease of production and purification, benign environmental profile, and cost competitiveness (see below), we believe that glycolaldehyde is a remarkably interesting renewable raw material for the polymer industry. Specifically we wanted to make a polymer by condensation of DHDO with formation of an ether linkage between the hydroxyl groups in position 2 and 5 of the ring. The resulting polymer is the polyacetal poly(2,5-dihydroxy-1,4-dioxane) or PDHDO (Figure 1, right). To the best of our knowledge, polymers made by polymerization of either glycolaldehyde or DHDO have not been reported.

PDHDO promises to have several advantages over current renewable thermoplastics, including the fact that the monomer can be obtained in high purity and large quantities from the fast pyrolysis of cellulosic feedstock at a competitive cost and its production does not use comestible crops and therefore does not compete with the food supply chain. Furthermore, this novel polyacetal is not only renewable, but also potentially biodegradable. The monomer, which is also expected to be the ultimate product of degradation, is a non-persistent chemical and a natural metabolite.

In Green Polymer Chemistry: Biobased Materials and Biocatalysis; Smith, et al.;
ACS Symposium Series; American Chemical Society: Washington, DC, 2015.

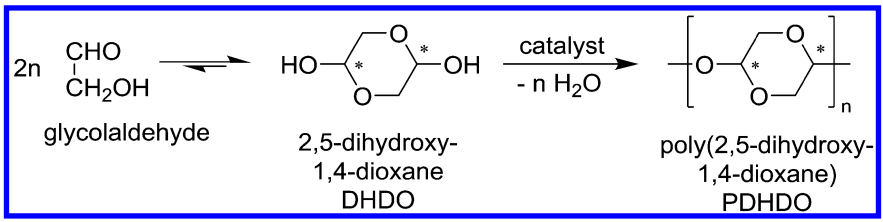

Figure 1. Spontaneous dimerization of glycolaldehyde in solution to form the crystalline cyclic compound DHDO and its polymerization to poly(2,5-dihydroxy-1,4-dioxane). The asterisks show the positions of the chiral centers.

Publication Date (Web): June 18, 2015 | doi: 10.1021/bk-2015-1192.ch019

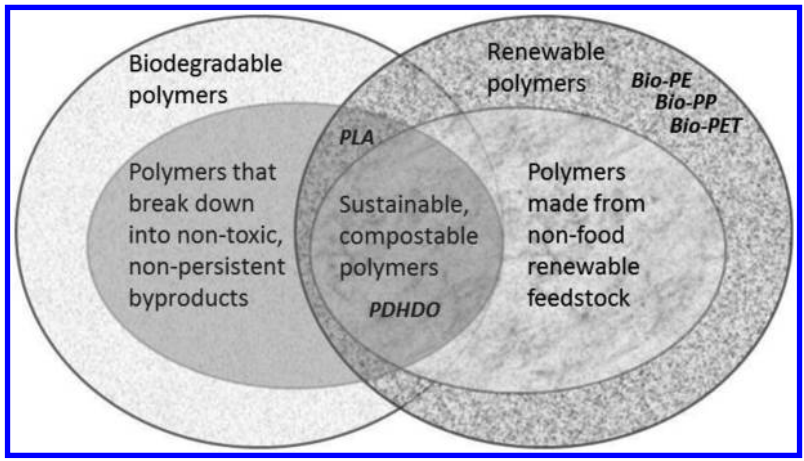

Figure 2. Diagram of the current state of green thermoplastics.

Thus, this novel polyacetal PDHDO may expand the gamut of renewable thermoplastics outside that of current polyesters and polyolefins and will fill the need for renewable and biodegradable plastics offering a combination of desirable properties within the space of green polymer chemistry, as shown in Figure 2.

DHDO has two chiral centers shown in Figure 1. Therefore, in principle, PDHDO may exist in various forms, including an atactic form in which the stereochemistry at the two chiral carbon atoms is random, and several tactic forms in which the stereochemistry at those carbons is constant; some of which are shown in Figure 3. The tacticity of a polymer is important because it greatly affects its physical and mechanical properties.

Publication Date (Web): June 18, 2015 | doi: 10.1021/bk-2015-1192.ch019

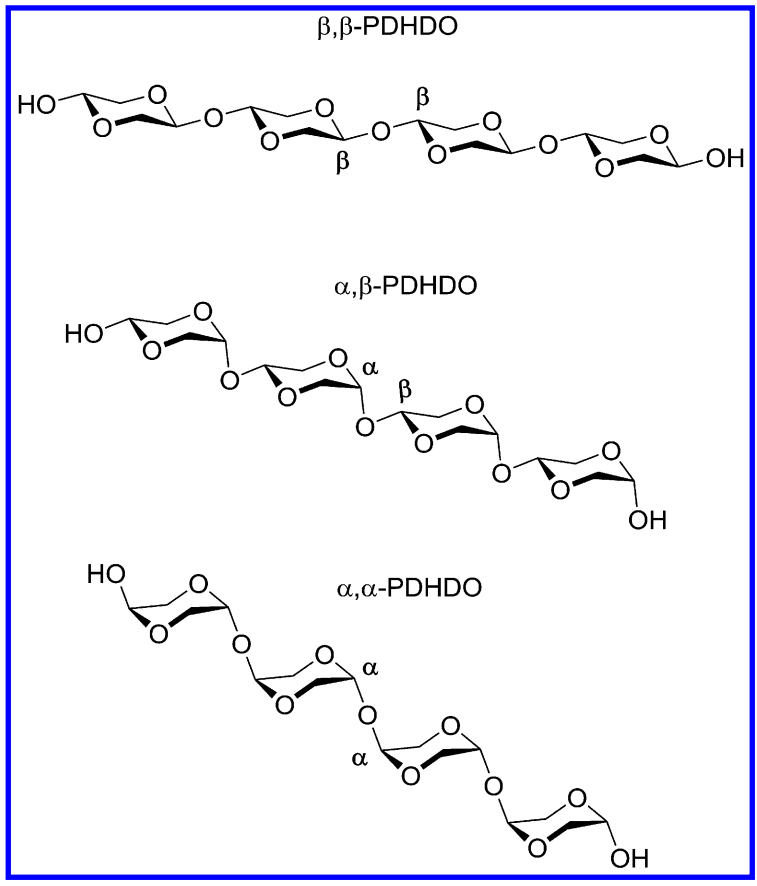

Figure 3. Structure of expected tactic forms of poly(2,5-dihydroxy-1,4-dioxane).

The Monomer: Glycolaldehyde

Glycolaldehyde (2-hydroxyacetaldehyde) is the smallest possible carbohydrate by virtue of having just two carbon atoms. It is a natural metabolite that is formed in the body from many sources, including by the metabolism of sorbitol (a common low-calorie sweetener), fructose (corn syrup), and the amino acid glycine, from purone catabolism and by the oxidative degradation

of ascorbate and xylitol (*2*, *3*). This compound is transferred by thiamin pyrophosphate during the pentose phosphate shunt (*3*). It is present in small amounts in certain foods such as soy sauce and barbeque sauce, and it is formed in the caramelization of sugars. Glycolaldehyde has an intraperitoneal-rat LD50 of 280 mg/kg (*4*). Glycolaldehyde is not a persistent chemical because it easily oxidizes in the environment to glycolic acid and then oxalic acid. It is a commonly present in forest soil since it is a cleavage product of the oxidation of the β-O-4 lignin linkage by peroxidase, and it is the substrate for certain microbial enzymes such as glyoxal oxidase (*5*). In the atmosphere it undergoes photolysis to formaldehyde and glyoxal (*6*). Glycolaldehyde does not bio-accumulate in humans because it is readily converted to acetyl coenzyme A. However, studies are ongoing to determine whether glycolaldehyde is one of the advanced glycation end-products (AGEs) involved in certain inflammatory processes and the development or worsening of certain degenerative diseases (*7*, *8*).

Publication Date (Web): June 18, 2015 | doi: 10.1021/bk-2015-1192.ch019

Glycolaldehyde cannot be isolated in pure form, since it spontaneously dimerizes in concentrated water solutions (Figure 1, left) to form the cyclic compound 2,5-dihydroxy-1,4-dioxane (DHDO, Figure 1, center), which crystallizes out of solution. We have developed a catalytic process to polymerize DHDO to PDHDO (Figure 1, right). DHDO is not a dangerous substance according to GHS (The *Globally Harmonized System* of Classification and Labelling of Chemicals), and it not is not classified as dangerous according to Directive 67/548/EEC. DHDO hydrolyzes back to glycolaldehyde in dilute water solutions and hydrolysis is expected to occur in the environment as well.

DHDO contains two chiral centers marked by the asterisks in Figure 1, thus three stereoisomers of DHDO are possible. In analogy with the accepted nomenclature for pyranose sugars, we refer to these stereoisomers as: α,α when both hydroxyl groups are in axial position (Figure 4 top); α,β when one hydroxyl group is axial and one is equatorial (Figure 4 center); and β,β when both hydroxyl groups are equatorial (Figure 4, bottom). The α,α stereoisomer can interconvert into the β,β isomer by a conformational change ("inversion of the chair"), however conversion of either forms to the α,β form requires ring opening. In the solid-state glycolaldehyde exists in its dimeric form, which is a white crystalline solid. Kobayashi reported that at room temperature two crystalline allotropes are predominant: the α allotrope has two equatorial hydroxyl groups and the β allotrope has two axial hydroxyl groups (*9*). An additional crystalline form is formed at low temperature (70 K (*10*),). Note that the Kobayashi's nomenclature is opposite of the pyranose-sugar nomenclature. Thus, the Kobayashi α crystalline allotrope is presumably composed of the β,β stereoisomer.

When dissolved in water or other polar protic solvents, the dimer partially ring-opens and dissociates into the monomer. Both the ring-open dimer and the monomer may hydrate to form a gem-diol. The dimer then may form a five member ring species. Thus, it is believed that nine to thirteen different molecular species are present in a water solution of DHDO, some of which are shown in Figure 5 (*11*, *12*). The equilibrium of species in organic solvents and in the molten state was studied by Yaylayan and coworkers, who showed partial ring opening of DHDO and cyclization into the five-member cyclic compound 2-hydroxymethyl-4-hydroxyl,1,3-dioxolane (*13*).

Publication Date (Web): June 18, 2015 | doi: 10.1021/bk-2015-1192.ch019

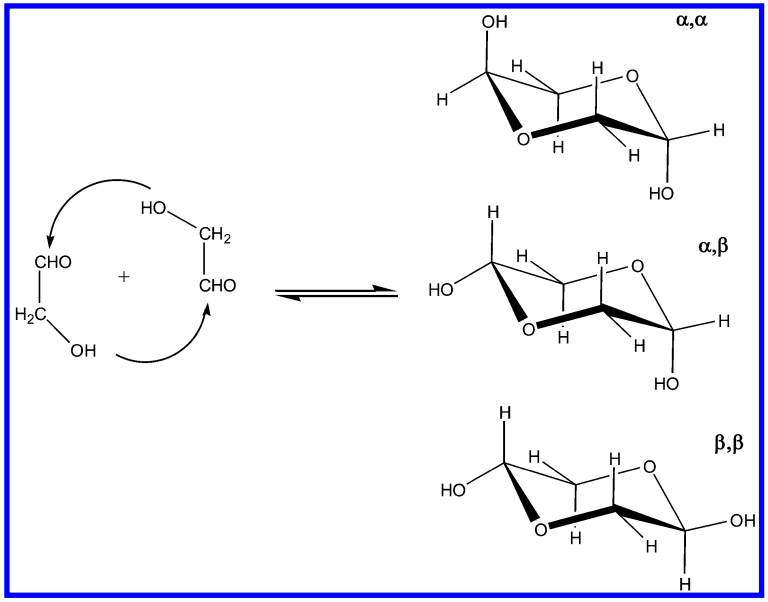

Figure 4. Stereoisomers of DHDO.

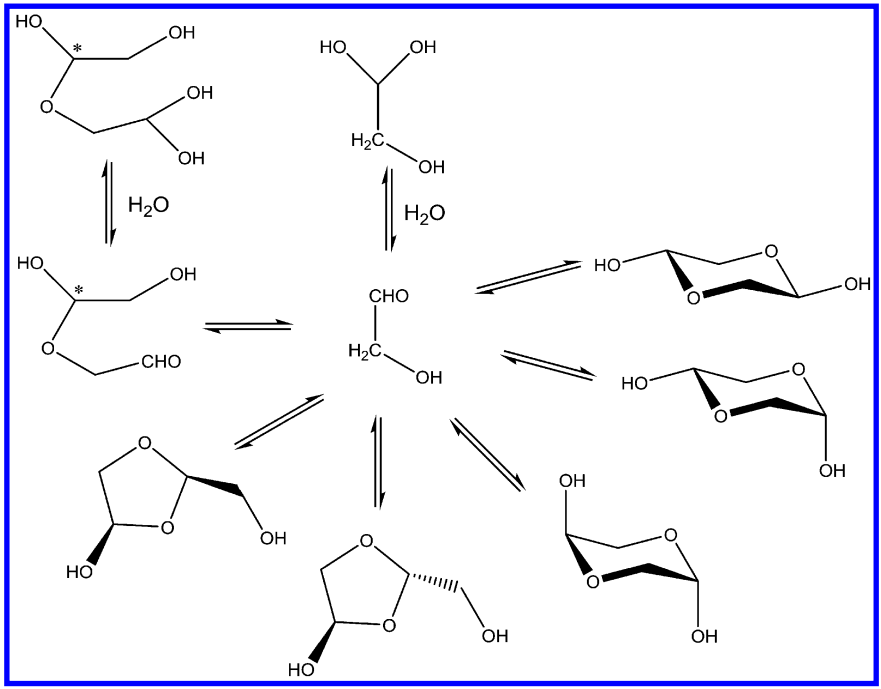

Figure 5. Species present in an aqueous solution of DHDO.

In Green Polymer Chemistry: Biobased Materials and Biocatalysis; Smith, et al.;
ACS Symposium Series; American Chemical Society: Washington, DC, 2015.

Publication Date (Web): June 18, 2015 | doi: 10.1021/bk-2015-1192.ch019

Glycolaldehyde and DHDO are renewable monomers because they can be produced in large quantities and high purity by controlled thermolysis of biomass. Several processes have been patented and/or published that describe the production of glycolaldehyde by fast pyrolysis. In some cases glycolaldehyde is a component of the aqueous phase waste stream that is obtained as a by-product during the production of bio-diesel (*14*, *15*). In other cases, the fast pyrolysis process is optimized to increase the yield in glycolaldehyde, which is the main target product (*16*, *17*).

Fast pyrolysis is one of the three main thermal processes, along with gasification and combustion, which can convert biomass into usable energy and products, including bio-oil, which can be then refined to bio-diesel. Forty-six pyrolysis reactors are currently operational worldwide to make bio-oil or bio-diesel (*18*).

Fast pyrolysis is carried out by heating small particles (less than 3 mm in size) of solid ligno-cellulosic biomass to high temperatures (350-550 °C) for a short period of time (a few seconds) in an inert atmosphere or under vacuum (*19*, *20*). This process produces a mixture of more than 300 compounds as volatile gas, liquid vapors, and aerosols. The mixture is then rapidly condensed to produce a brown, dense liquid (pyrolysis oil or bio-oil) which is about 50-75% of the original mass and typically contains 15-35% water and a variety of oxygenated organic compounds including acids, phenols, and hydroxyaldehydes. The nature and amount of each component varies upon the pyrolysis conditions and the feedstock, however glycolaldehyde is often one of the most abundant species. For example, a number of North American grass species have been subjected to fast pyrolysis and subsequent analysis of the product stream; in all cases glycolaldehyde and acetic acid are the two most abundant carbon-containing molecules present, confirming the utility of this process (*20*). A higher yield of glycolaldehyde can be obtained when using a feedstock with high cellulose or hemicellulose content and less lignin (*21*).

Several different processes have been evaluated and used to upgrade this first condensate oil, and many of them include, as a first step, the addition of water to separate a polar aqueous phase (which is often considered waste) and an apolar oil phase (the product) that is then upgraded to bio-fuel (Figure 6) by de-oxygenation (*18*). The aqueous stream contains mainly acetic acid (3-12%), glycolaldehyde (3-13%), and acetol (*20*, *22*). The glycolaldehyde yield can be increased to 17% by adding sodium chloride to the biomass during pyrolysis (*23*, *24*).

De Haan and coworkers (*14*) carried out a process analysis of the recovery of acetic acid and glycolaldehyde (as a raw material for making ethylene glycol) from the aqueous phase. They examined three different processes (solvent extraction, distillation or fractionation) and concluded that the production of either of the chemicals at €500/ton (~$0.3/lb) is profitable, but the co-production of both chemicals by extraction with 2-ethylhexanol is the most profitable route due to a combination of high recoveries and energy integration (which reduced specific energy consumption by 60%, Figure 6). De Haan's economic calculations were based on feeding 200,000 ton/yr of pyrolysis oil to the water extractor and

In Green Polymer Chemistry: Biobased Materials and Biocatalysis; Smith, et al.;
ACS Symposium Series; American Chemical Society: Washington, DC, 2015.

assuming an operating time of 8000 hr/yr; De Haan's analysis assumes that the aqueous feed is a waste stream and therefore assigns no feedstock cost the acetic acid/glycolaldehyde process. This assigns all the feedstock cost of fast pyrolysis to the biofuel, an assumption that lowers the cost of glycolaldehyde and acetic acid but raises the cost of bio-fuel. However, if the cost of the water stream is set to be equal to that of biodiesel product at $195/ton (for a biomass cost of $40/ton, *18*), this would increase the estimated cost of glycolaldehyde to $0.40/lb which is still competitive with (and in fact less than) the price of other petrochemical and renewable monomers. For example, bio-ethylene from corn costs $0.90-1.20/lb and petrochemical ethylene costs $0.30-0.60/lb (*25*). The conclusion from this work is that glycolaldehyde from fast pyrolysis is a very competitive raw material and its use as a monomer to make a bioplastic to replace polyethylene is estimated to be profitable, even if the feedstock is priced as a product and not as a free waste stream.

Publication Date (Web): June 18, 2015 | doi: 10.1021/bk-2015-1192.ch019

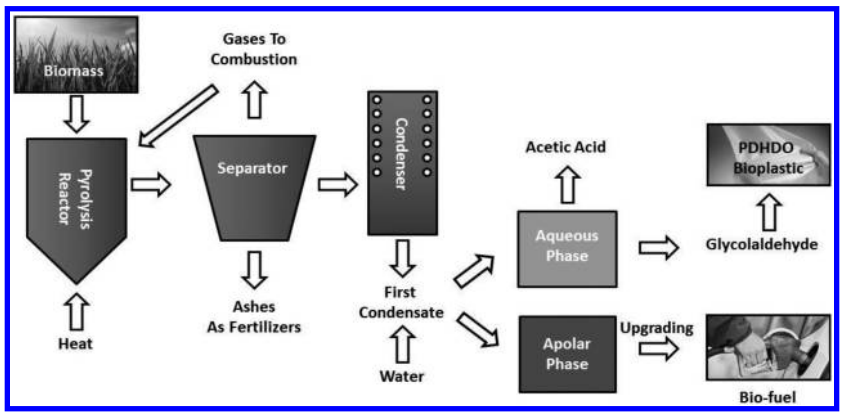

Figure 6. Schematic representation of integrated production of bio-fuel, PDHDO bio-plastic, and acetic acid in a fast pyrolysis plant.

Other authors have recognized that glycolaldehyde is a very low cost feedstock and are investigating potential uses. For example Dusselier (*26*) is developing a catalytic process to convert glycolaldehyde into novel hydroxyacids to be used for making renewable polyesters, and Vitasari (*15*) is developing a process to separate glycolaldehyde from pyrolysis oil to produce a feedstock for enzymatic conversions.

Glycolaldehyde can also be produced by hydro-thermolysis of a mixed sugar feedstock with a yield up to 70% on total biomass carbon (*17*). This approach is interesting because it produces the desired monomer in much higher yields, and it is compatible with biomass conversion by enzymatic hydrolysis (*27*) rather than fast pyrolysis. Thus, glycolaldehyde can be produced in good yield from two separate processes that are currently in use.

Natural and Synthetic Polyacetals

PDHDO is a cyclic polyacetal, a class of polymers characterized by repeating units that contain a carbon atom bonded to two oxygen atoms [-OCR′R″O-] and, typically, are the product of condensation of two alcohol molecules with a carbonyl group (Figure 7). The intermediate condensation product (a hemi-acetal) is hydrolytically less stable than the acetal. Polyacetals tend to degrade by acid-catalyzed hydrolysis at low pH by losing one monomer at a time from the polymer end, i.e. from the hemiacetalic terminal OH group. End-capped polyacetals are more resistant to hydrolysis and thermolysis, until the polymer backbone fragments and creates additional terminal hydroxyl groups.

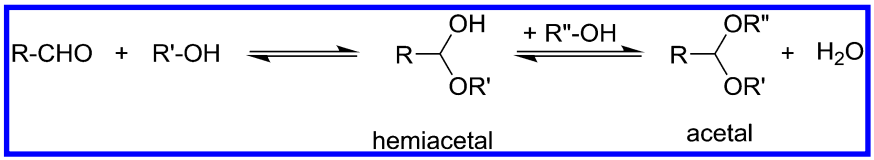

Figure 7. Structure of hemiacetal and acetal groups.

Polyoxymethylene [POM, $–(CH_2O)_n–$] is currently the only synthetic polyacetal of commercial importance, with a global capacity of 945 kTon in 2006 (*28*). It is made by polymerization of formaldehyde, and the production process requires specialized technology. To stabilize POM against hydrolytic and thermal depolymerization, the polymerization is carried to high molecular weights, and then the polymer is end-capped with acetic anhydride or ethylene glycol. Uncapped POM decomposes at 119 °C, while the ester capped version is stable to 252 °C (*29*). POM is highly crystalline and one of the strongest and stiffest thermoplastics. It also has exceptional resistance to solvents and bases. Because of its good wear resistance and a low coefficient of friction, it is used in mechanical gears and bearings (*30*).

While acetals are uncommon functional groups in synthetic polymers, they are among the most abundant linking groups in natural macromolecules. In fact all poly- and oligosaccharides, including cellulose and amylose (starch), are polyacetals. Most natural polyacetals contain cyclic repeat units, as with PDHDO. For example, cellulose's repeat units are molecules of glucose in its cyclic pyranosic form bonded to each other with an acetal β bond (Figure 8 top). Amylose is formed by repeat units of glucose in its cyclic pyranosic form bonded to each other with an acetal α bond (Figure 8 bottom).

In addition to being an economically sustainable renewable polymer PDHDO is interesting because the structures of its tactic forms have a striking analogy with the structures of these polysaccharides. In fact, the structure of the α,β form is similar to the structure of amylose (Figure 8 bottom), the β,β form resembles the structure of cellulose (Figure 8 top), and the α,α form resembles one of the forms of poly(galactose) (not shown). Compared to these natural polysaccharides PDHDO is missing the side hydroxyl groups and the CH_2OH branch, and has an additional oxygen atom in the rings. Another significant difference is that the ether linkages that bridge neighboring rings are made by condensation of two

hemiacetal hydroxyl groups in PDHDO, while they are made by condensation of one hemiacetal hydroxyl group and one alcoholic group in natural polysaccharides. In carbohydrate chemistry the hydroxyl group from a hemiacetal is often called the reducing end. Thus, natural polysaccharides have one reducing end and one non-reducing end, while PDHDO should have in principle two reducing ends.

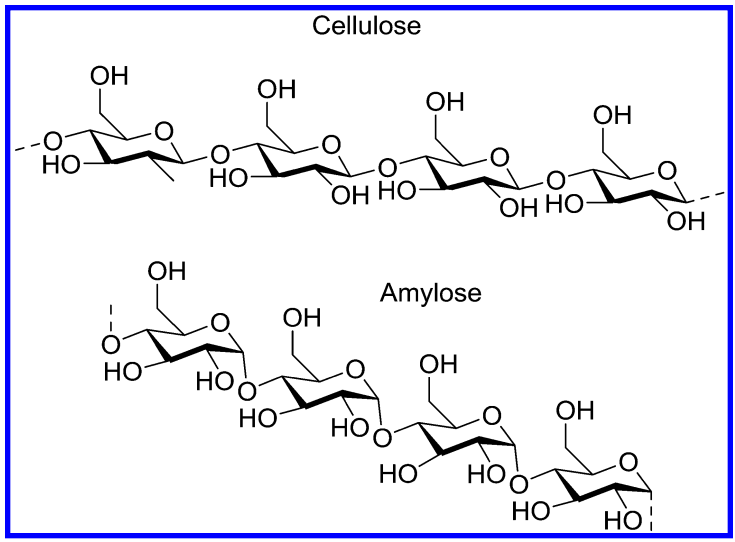

Figure 8. The stereochemical structures of cellulose (top) with β(1→4) linkages and that amylose (bottom) with α(1→4) linkages (bottom).

Results and Discussion

Synthesis

We investigated two different strategies to polymerize DHDO. The first strategy consisted of using glycosylation agents to activate the hydroxyl group of half of the monomer molecules so that they could readily form the ether linkages desired in the polymer structure. This strategy is generalized in Figure 9 (*31*). Most glycosylating agents that we evaluated produced a complex mixture of undesired products; however trimethylsilyl trifluoromethanesulfonate (TMSOTf) gave positive results.

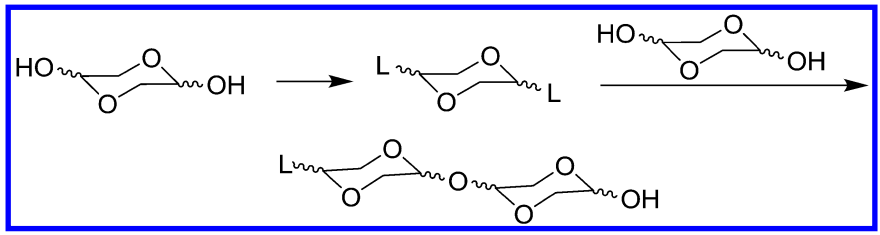

Figure 9. General strategy to form PDHDO using a glycosylating agent (L).

In Green Polymer Chemistry: Biobased Materials and Biocatalysis; Smith, et al.;
ACS Symposium Series; American Chemical Society: Washington, DC, 2015.

Publication Date (Web): June 18, 2015 | doi: 10.1021/bk-2015-1192.ch019

In a typical reaction, DHDO was added to a rigorously dried round bottom flask, dissolved in anhydrous acetonitrile, and then cooled in a bath of ice and brine (–15 ºC). Neat TMSOTf (2.2 equiv) was added to this cold suspension of the glycolaldehyde dimer dropwise over a period of around 5 minutes. After the addition of the TMSOTf was complete, the solution was homogenous and began to turn yellow. The solution was stirred overnight and allowed to warm to room temperature. The solution was evaporated under vacuum to provide a brown viscous material. This material was found to be oligomeric (see characterization below), proving that DHDO could in fact be polymerized.

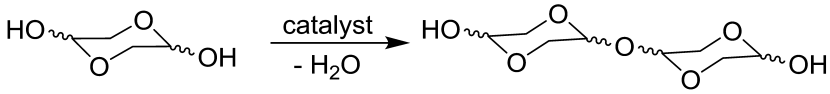

Figure 10. General strategy to catalytically polymerize DHDO.

Unfortunately, TMSOTf is an expensive reagent and the overall process was far too costly to scale-up. Thus, we changed our strategy to polymerize DHDO, by examining Lewis acid catalysts to promote dehydration under mild conditions (Figure 10). We successfully identified a catalytic method to carry out the polymerization of DHDO by dehydration of the hydroxyl groups. Among the conditions tested, the best results were obtained by using scandium triflate as the catalyst (0.05 equiv) (*32*, *33*) with a Soxhlet extraction apparatus containing 3Å molecular sieves to remove the water formed as byproduct of the reaction and by running the reaction at reduced pressure to facilitate removal of water without the risk of overheating the DHDO. We found the best solvents for this were acetonitrile (MeCN) and propionitrile (EtCN) at 150 Torr of pressure. Alternatively, the ionic liquid 1-butyl-3-methylimidazolium (BMIM) triflate could be used under a dynamic vacuum of less than 100 mTorr to directly remove water (*34–37*). These reactions produced fluffy, white solids that could be easily dissolved in dichloromethane and cast into thin films.

Spectroscopy

All oligomeric and polymeric species were carefully analyzed using NMR spectroscopy. For reference, the DHDO monomer was analyzed by ^{1}H NMR to determine the stereochemistry of the dioxane ring structure and the stability in solution. As seen in Figure 11, the monomer does not undergo ring-opening in deuterated dimethylsulfoxide (DMSO-d_6) but retains its six-member cyclic structure. The three ring protons (H_a, H_b, and H_c in Figure 11) give a clear indication of the stereochemistry of the dioxane ring, and we tentatively conclude that a single stereoisomer is present (the β,β form) with both OH groups in equatorial positions. This preliminary conclusion is based on the comparison of the H_c chemical shift at 4.61 ppm in Figure 11 with the reported chemical shifts for the anomeric protons of α- and β-D-glucose, which are at 5.1 and 4.5 ppm respectively (*38*). The anomeric proton of α-D-glucose is equatorial while the anomeric proton of β-D-glucose is axial.

In Green Polymer Chemistry: Biobased Materials and Biocatalysis; Smith, et al.;
ACS Symposium Series; American Chemical Society: Washington, DC, 2015.

Publication Date (Web): June 18, 2015 | doi: 10.1021/bk-2015-1192.ch019

Publication Date (Web): June 18, 2015 | doi: 10.1021/bk-2015-1192.ch019

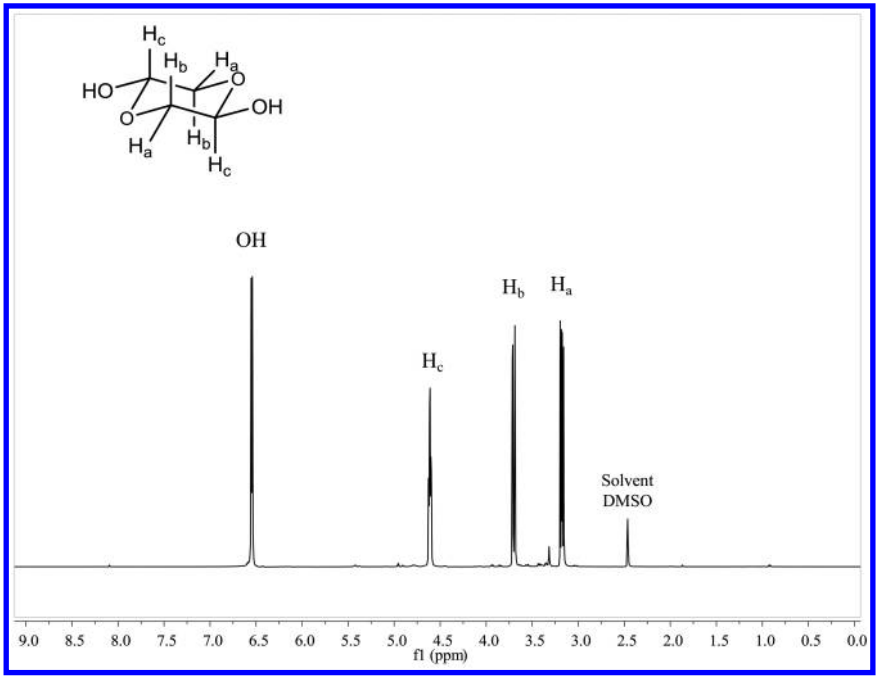

Figure 11. [1]H NMR spectrum of DHDO in DMSO-d_6.

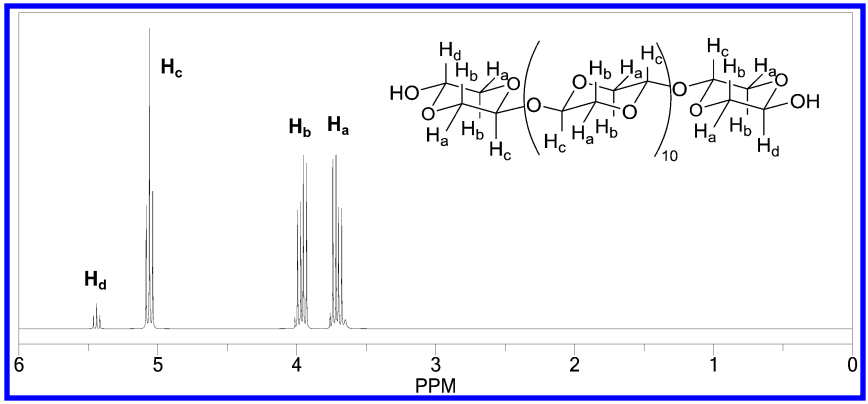

Figure 12. Predicted [1]H NMR spectrum of a tactic oligomer of PDHDO comprised of 12 units joined by equatorial-equatorial ether bridges.

In Green Polymer Chemistry: Biobased Materials and Biocatalysis; Smith, et al.;
ACS Symposium Series; American Chemical Society: Washington, DC, 2015.

A calculated spectrum of a PDHDO oligomer 12 units long is shown in Figure 12 (*39*). We should point out that this simulated oligomer is a highly tactic β,β stereoisomer and all its anomeric protons (H_c) are axial. The ring protons CH_2-CHOR are predicted to form an ABX pattern, where the AB protons (the axial and equatorial CH_2, H_a and H_b in Figure 12) form 8 separate signals and the X proton (the CH_cOR) forms four lines, two of which are overlapping. The equatorial CH (H_a) protons of the CH_2 groups are predicted to have a lower chemical shift than the axial (H_b) (3.65 ppm vs. 3.95 ppm). The signal for the proton at the terminating anomeric center (H_d) is calculated to be upfield from internal CHOH (5.45 vs. 5.10 ppm), and this signal integrates as a smaller number as the length of the polymer chain increases.

The chemical structures of PDHDO made by various methods were characterized by ^{1}H-NMR and ^{13}C-NMR spectroscopy. Figure 13 shows the actual ^{1}H-NMR spectrum of the product made with the TMSOTf method (non-catalytic). The resonances at 5.84, 4.83, and 4.57 ppm clearly indicate a 2,5-substituted-1,4-dioxane (as expected for a polymer of DHDO), though they are at higher chemical shifts than the predicted values in Figure 12. This spectrum shows that this product does not contain residual DHDO monomer. The peak at 2.0 ppm is a trace of the acetonitrile solvent and the peak at 2.5 ppm is due to the residual protons in the NMR solvent (d_6-DMSO). Very little elimination is present since there are no peaks in the region between 5.9 and 7.9 ppm. We know from prior work that the signal from the terminal CHOH should be at 5.69 ppm, but terminal groups are not visible in this spectrum. The simplicity of the ^{1}H-NMR spectrum of the product made with TMSOTf with very limited splitting indicates that it may have high tacticity, possibly derived from DHDO oligomers having a cyclic structure similarly to that of cyclodextrins. A cyclic structure seems likely due to the lack of terminal group proton signals along with the presence of just three clearly defined ring protons. This differs sharply from the spectrum of the product obtained by the catalytic process (see below) which shows a complex splitting pattern. We are conducting additional experiments to confirm this hypothesis.

Figure 14 shows the ^{13}C-NMR spectrum (proton decoupled) of the product made with the TMSOTf method. The resonances at 79.9 and 81.6 ppm are from the CH_2 and CHOR, respectively, of the 2,5-substituted 1,4-dioxane rings as expected for a polymer of DHDO. The peak at 2.4 ppm is from tetramethylsilane (in the NMR solvent), and the quartet centered at 120 ppm is from triflic acid; it is a quartet because of the coupling of three fluorine atoms (spin ½) with carbon. The latter compound is the product of the hydrolysis of the reagent TMSOTf. The peaks at 178 ppm and 14 ppm appear not to be related to the polymer. We are tentatively attributing these peaks to a side product formed by reaction of acetonitrile and TMSOTf in a Pinner-type reaction (*40*). Further investigation is ongoing.

Publication Date (Web): June 18, 2015 | doi: 10.1021/bk-2015-1192.ch019

Publication Date (Web): June 18, 2015 | doi: 10.1021/bk-2015-1192.ch019

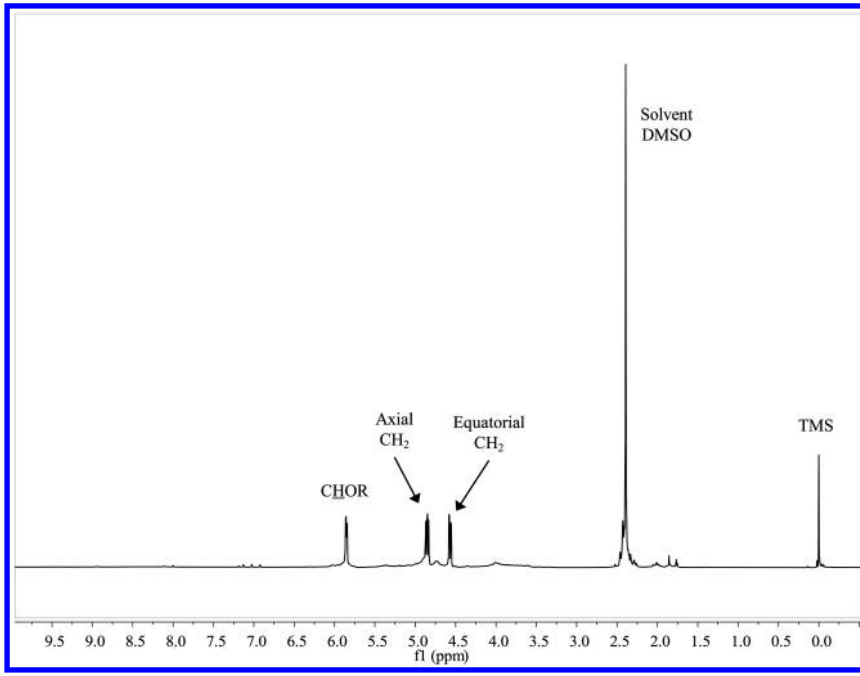

Figure 13. [1]H NMR spectrum of PDHDO synthesized using TMSOTf.

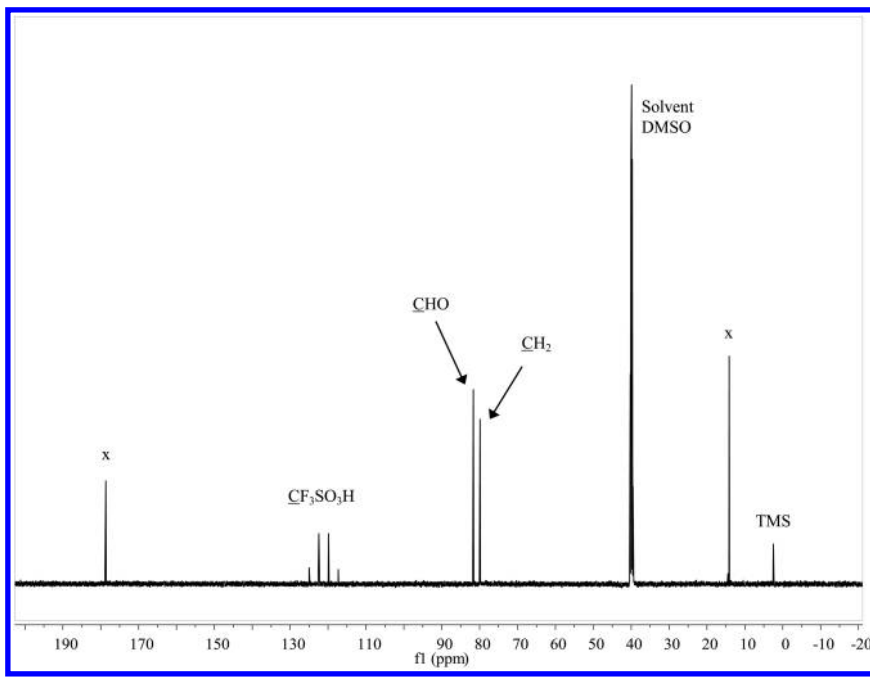

Figure 14. [13]C NMR spectrum of PDHDO synthesized using TMSOTf (x = impurity).

In Green Polymer Chemistry: Biobased Materials and Biocatalysis; Smith, et al.;
ACS Symposium Series; American Chemical Society: Washington, DC, 2015.

Publication Date (Web): June 18, 2015 | doi: 10.1021/bk-2015-1192.ch019

Figure 15 shows the ^{1}H-NMR spectrum of the product made with 5% $Sc(OTf)_3$ in acetonitrile with molecular sieves. This spectrum is significantly more complex than that of the product made with TMSOTf (Figure 13). We believe this is because the catalytic process produces an atactic polymer, while the TMSOTf process produces a tactic polymer. We tentatively conclude that the product of the catalytic process is predominantly an atactic polymer because the ring protons CH_2-CHO (see Figure 16) appear to form two sets of partially overlapping ABX patterns in the ^{1}H-NMR spectrum. In an ABX pattern the AB protons originate a set of resonances with up to 8 lines and the X proton a set of resonances with up to 4 lines.

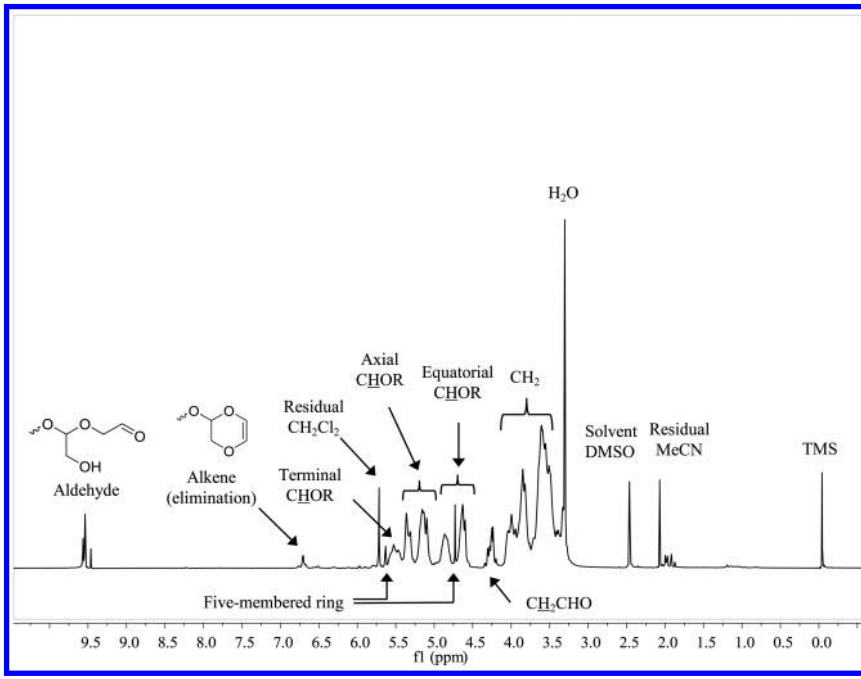

Figure 15. ^{1}H NMR specrum of PDHDO prepared using $Sc(OTf)_3$ catalyst in MeCN.

In our case the CH_2 protons AB (H_a and H_b in Figure 16) produce a set of resonances between 3.6 and 4.1 ppm which match well in chemical shift and shape to the predicted spectrum in Figure 12. The CHOR protons (H_c in Figure 16) form two separate sets of 4 lines each, the first set is centered at 5.26 ppm and is assigned to axial anomeric protons (left in Figure 16). The second set is centered at 4.74 ppm and is assigned to equatorial anomeric protons (right in Figure 16). Both chemical shifts match well the prediction and also the reported chemical shifts that were mentioned above for the anomeric protons of α- and β-D-glucose, which are at 5.1 and 4.5 ppm respectively (*38*). This assignment is also confirmed by the fact that

integration of all CHOR signals and all CH_2 signals is exactly 2:1, as expected. The spectrum contains a small signal at 5.52 ppm that we tentatively assign to terminal CHOH. Small signals due to side products are also present such as the small, sharp peaks at 5.63 and 4.73 ppm because of a small amount of five-membered ring present due to rearrangement (*12*), the peak at 6.70 ppm which is due to protons on a carbon-carbon double bond, and the peaks at 9.54 ppm which are due to aldehyde protons. Aldehyde may form if the terminal unit of the polymer ring opens, as shown in Figure 17, top. Elimination of water may also occur (Figure 17, bottom). Both side-reactions are undesired since they stop polymer growth.

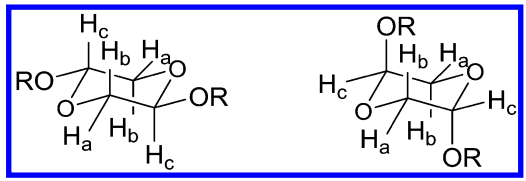

Figure 16. PDHDO repeat unit with different stereochemistry.

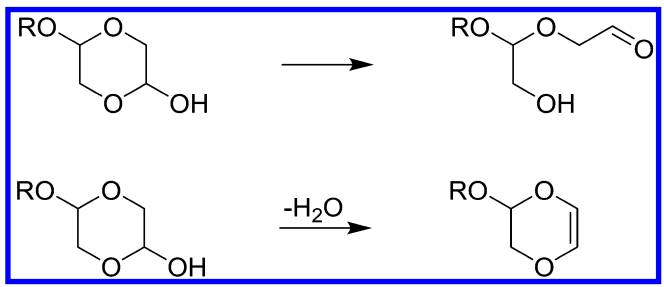

Figure 17. Undesired side reactions at terminal monomer that stop polymer growth.

The ^{1}H NMR spectrum of PDHDO made with $Sc(OTf)_3$ catalyst in the ionic liquid BMIM(OTf) (see Figure 18) was generally similar to that made in acetonitrile with some differences. The peaks were slightly broader indicative of higher MW chains, an encouraging result. Notably, there were no elimination peaks present and the aldehyde peaks were much smaller than what we observed for the polymer made in acetonitrile at only 1.5% of the ring protons. This is also very promising since it indicates that we are reducing undesired side reactions. Once again a 2:1 ratio of ring CH_2 to ring CHOR signals are observed as expected when the dioxane ring system is maintained. There also appear to be fewer peaks due to decomposition and/or rearrangement of the DHDO starting material compared to the material made in MeCN. However, peaks due to the ionic liquid are still present as it is difficult to remove entirely due to its inherently non-volatile nature.

In Green Polymer Chemistry: Biobased Materials and Biocatalysis; Smith, et al.;
ACS Symposium Series; American Chemical Society: Washington, DC, 2015.

Publication Date (Web): June 18, 2015 | doi: 10.1021/bk-2015-1192.ch019

Publication Date (Web): June 18, 2015 | doi: 10.1021/bk-2015-1192.ch019

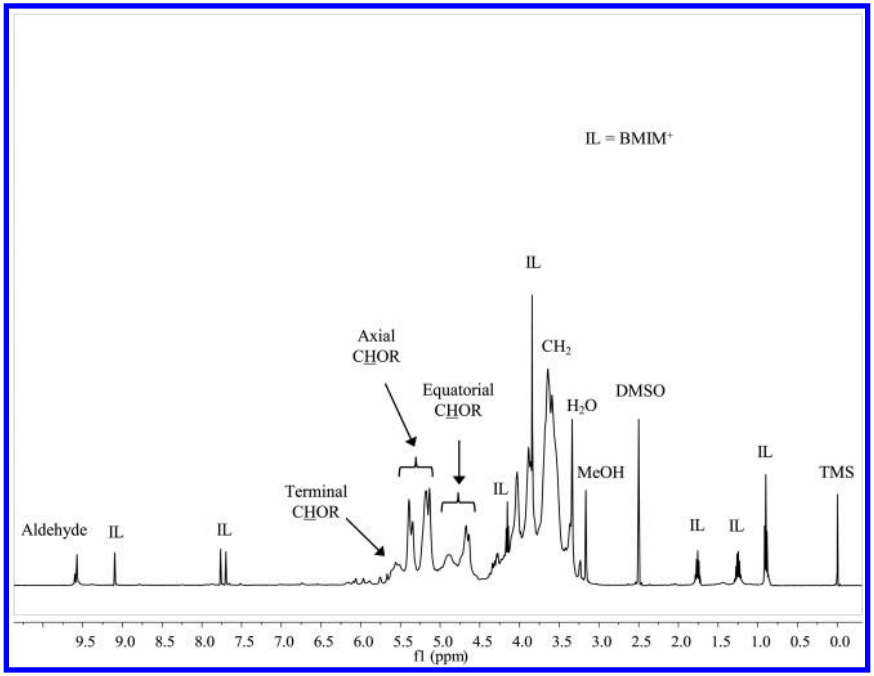

Figure 18. [1]H NMR spectrum of PDHDO prepared using Sc(OTf)$_3$ catalyst in the ionic liquid BMIM(OTf).

Gel Permeation Chromatography

GPC analysis was carried out using a Waters GPC with a UV detector and a mixed bed column. The results of the analysis are summarized in Table 1. The molecular weight of the product from the TMSOTf process was low (Mw =2311). The polymer made by the catalytic process in MeCN also had a low molecular weight (Mw = 2836). However, the molecular weight of the product could be increased by using either a higher boiling point solvent such as propionitrile or an ionic liquid. The reaction in BMIM(OTf) ionic liquid gave a product with average molecular weight by weight (Mw) of 14,600 Dalton and contained a fraction of product of significantly higher molecular weights (Mz = 33,000 Dalton). This was a promising result, indicating that a high MW polymer can in fact be prepared.

Table 1. GPC Results for PDHDO

Sample	*Mn*	*Mw*	*Mz*	*PDI*
TMSOTf Process	1007	2311	3604	2.29
Catalytic Process: $Sc(OTf)_3$ in MeCN	1617	2836	4924	1.75
Catalytic Process: $Sc(OTf)_3$ in EtCN	1585	6965	24,156	4.39
Catalytic Process: $Sc(OTf)_3$ in BMIM(OTf)	5967	14,611	33,270	2.45

Publication Date (Web): June 18, 2015 | doi: 10.1021/bk-2015-1192.ch019

Melting Point

Melting points were measured with a standard melting point apparatus. The catalytic PDHDO made with $Sc(OTf)_3$ in MeCN turned transparent at 70 °C and then flowed at about 115 °C, while the material made in BMIM(OTf) had a melting point of 110 °C. These values are expected for low MW thermoplastics. We expect to be able to significantly increase the melting point of PDHDO once we optimize the process so that the polymerization is driven to high molecular weight and the chain-ends are end capped with groups as is done commercially with POM.

Mechanical Analysis

Thin-film specimens of PDHDO made with $Sc(OTf)_3$ in MeCN or in BMIM(OTf) (12 mm x 4 mm x 0.04 mm) were tested in tension with an Instron Mechanical Tester at room temperature. PDHDO films made in MeCN or BMIM(OTf) had similar mechanical properties in spite of the different molecular weights. The specimens elongated between 400% and 800% before failing or slipping off the grips. The Young's Modulus was 40-50 kPa and tensile strength at break was 185 kPa. These values are very low for a thermoplastic and are more typical of a soft elastomer in its amorphous state. However, more characterizations are needed to confirm this conclusion.

Differential Scanning Calorimetry

DSC was measured on a piece of film of PDHDO made with $Sc(OTf)_3$ in MeCN. The specimen was first cooled to liquid nitrogen temperature, then heated at 10 °C/min to 100 °C and held there for 2 min, then cooled back to liquid nitrogen temperature and held there for 2 minutes, and finally heated at 10 °C/min to 160 °C. A plot of the heat flow vs. temperature is shown in Figure 19. The first heating scan shows a glass transition with an onset at -3 °C and a melting peak at 78-82 °C. Because of the fast cooling cycle the sample does not have time to recrystallize,

so in the second heating scan only the glass transition is visible. The shift in Tg to a higher temperature (23 °C) is larger than usual and suggests a change in the polymer structure as it was heated to 100 °C on the first heating cycle.

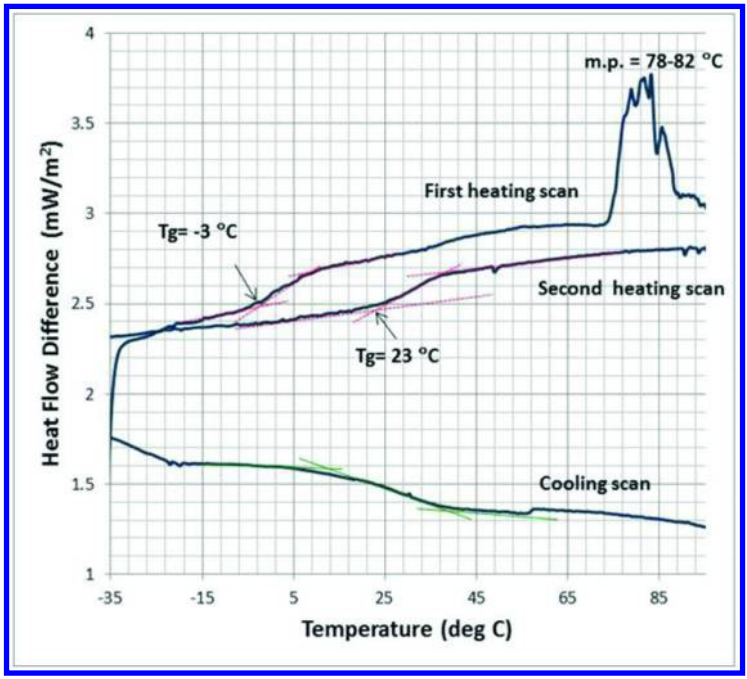

Figure 19. DSC plot of PDHDO prepared using $Sc(OTf)_3$ catalyst in MeCN.

Publication Date (Web): June 18, 2015 | doi: 10.1021/bk-2015-1192.ch019

Hydrolysis

Pellets of PDHDO synthesized in the ionic liquid were made by pressing the powdered polymer in a 13 mm diameter die to 7500 psi. The pellets were then subjected to hydrolysis in buffer solutions at pH = 4.0 and 7.0 in a shaker bath at 37 °C. The mass loss at various time intervals was measured. The average mass loss of the two pellets as a function of hydrolysis time is shown in Figure 20; after 21 days at 37 °C mass loss was 3% at pH 7 and 4% at pH 4. The higher mass loss at lower pH is expected for polyacetals. This result is typical for a specimen that has low molecular weight and where the chains are not end-capped.

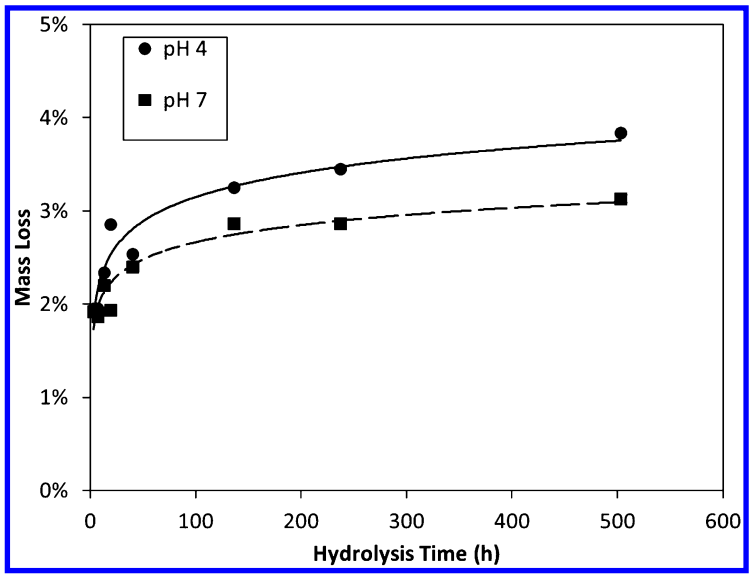

Figure 20. Hydrolysis plot of PDHDO at pH 4 and pH 7 with logarithmic fits of the data (solid line = pH 4; dashed line = pH 7).

Conclusions

Glycolaldehyde is a promising monomer for the synthesis of green polymers. It is produced in abundance from the fast pyrolysis of cellulosic feedstocks, and a process has been developed to obtain the material in pure form and high yield. Because it is made from a renewable resource that does not compete with food crops, glycolaldehyde is one of the few materials that would produce a polymer with a completely benign environmental profile. While the molecule can exist in various forms and is prone to easy degradation reactions, the isolation of pure, crystalline DHDO (2,5-dihydroxy-1,4-dioxane) containing a stable dioxane ring makes the preparation of polymeric species possible.

We have developed catalytic processes for the preparation of PDHDO, the polymer derived from glycolaldehyde. To date the catalytic process produces a polymer of relatively low molecular weight, but we have shown that changing the reaction conditions from a low boiling solvent such as acetonitrile to an ionic liquid with negligible vapor pressure results in an increase in the chain length. Investigations are ongoing in our laboratory to increase the molecular weight of PDHDO.

If the chain length of PDHDO can be increased so that it has properties similar to high-density polyethylene (HDPE), then the market possibilities for the polymer are endless. With finite petroleum feedstocks, PDHDO would fill the increasing need for a truly renewable polymer: one that is prepared from renewable, non-food

Publication Date (Web): June 18, 2015 | doi: 10.1021/bk-2015-1192.ch019

resources and that once its usable life is over, simply biodegrades back to simple organic molecules. This material would be a polymer with desirable properties; one that is both renewable and biodegradable as is necessary for a sustainable future.

The important results of this work can be summarized as follows:

1) The monomer can be easily and economically purified to a high degree because it spontaneously crystallizes out of solution.
2) The production of the monomer does not compete with food sources.
3) The cost of the monomer has been estimated to be comparable to or lower than petrochemical ethylene.
4) The production of the monomer can be integrated with the production of bio-fuel, which further reduces costs.
5) The polymer can be produced via a catalytic process that is economical and scalable.
6) The polymer is expected to hydrolyze in the environment back to the monomer, which is a natural metabolite and a non-persistent chemical.

Publication Date (Web): June 18, 2015 | doi: 10.1021/bk-2015-1192.ch019

Acknowledgments

The authors are grateful to the Editors of this book for the kind invitation to contribute to it. We also want to thank you the Environmental Protection Agency and the US Department of Agriculture for supporting this work (grants # EP-D-11-057 and. 2013-33610-20834) and Dr. Aaron Skaggs for contributing to the development of some of the polymerization methods.

References

1. World Bioplastics Market; November, 2013, Freedonia Press; http://www.prnewswire.com/news-releases/world-bioplastics-market-234217691.html (accessed October 12, 2014).
2. O'Brien, P. J.; Siraki, A. G.; Shangari, N. Aldehyde sources, metabolism, molecular toxicity mechanisms, and possible effects on human health. *Crit. Rev. Toxicol.* **2005**, *35*, 609–662.
3. Yang, K.; Feng, C.; Lip, H. Y.; Bruce, W. R.; O'Brien, P. J. Cytotoxic molecular mechanisms and cytoprotection by enzymic metabolism or autoxidation for glyceraldehyde, hydroxypyruvate and glycolaldehyde. *Chem. Biol. Interact.* **2011**, *191*, 315–321.
4. Murphy, M. J.; Dunbar, D. A.; Kaminsky, L. S. Acute toxicity of fluorinated ether anesthetics: Role of 2,2,2-trifluoroethanol and other metabolites. *Toxicol. Appl. Pharm.* **1983**, *71*, 84–92.
5. Gallo, M.; Amonette, R.; Lauber, C.; Sinsabaugh, R. L.; Zak, D. R. Microbial Community Structure and Oxidative Enzyme Activity in Nitrogen-Amended North Temperate Forest Soils. *Microb. Ecol.* **2004**, *48*, 218–229.

6. Magneron, I.; Mellouki, A.; Le Bras, G.; Moortgat, G. K.; Horowitz, A.; Wirtz, K. Photolysis and OH-Initiated Oxidation of Glycolaldehyde under Atmospheric Conditions. *J. Phys. Chem. A* **2005**, *109*, 4552–4561.
7. Lorenzi, R.; Andrades, M. E.; Bortolin, R. C.; Nagai, R.; Dal-Pizzol, F.; Fonseca Moreira, J. C. Circulating glycolaldehyde induces oxidative damage in the kidney of rats. *Diabetes Res. Clin. Pract.* **2010**, *89*, 262–267.
8. Lorenzi, R.; Andrades, M. E.; Bortolin, R. C.; Nagai, R.; Dal-Pizzol, F.; Fonseca Moreira, J. C. Glycolaldehyde induces oxidative stress in the heart: a clue to diabetic cardiomyopathy? *Cardiovasc Toxicol.* **2010**, *10*, 244–249.
9. Kobayashi, Y.; Takahara, H.; Takahashi, H.; Higasi, K. Infrared and raman studies of the structure of crystalline glygolaldehyde. *J. Mol. Struct.* **1976**, *32*, 235–246.
10. Mohaček-Grošev, V. Spectroscopic arguments for a new crystal phase of glycolaldehyde. *J. Raman Spectrosc.* **2005**, *36*, 453–461.
11. Glushonok, G. K.; Glushonok, T. G.; Shadyro, O. I. Kinetics of equilibrium attainment between molecular glycolaldehyde structures in an aqueous solution. *Kinet. Catal.* **2000**, *41*, 620–624.
12. Kua, J.; Galloway, M. M.; Millage, K. D.; Avila, J. E.; De Haan, D. O. Glycolaldehyde Monomer and Oligomer Equilibria in Aqueous Solution: Comparing Computational Chemistry and NMR Data. *J. Phys. Chem. A* **2013**, *117*, 2997–3008.
13. Yaylayan, V. A.; Harty-Majors, S.; Ismail, A. A. Investigation of the mechanism of dissociation of glycolaldehyde dimer (2,5-dihydroxy-1,4-dioxane) by FT-IR spectroscopy. *Carbohydrate Res.* **1998**, *309*, 31–38.
14. de Haan, A. B.; Meindersma, G. W.; Nijenstein, J.; Vitasari, C. A Techno-Economic Evaluation on the Feasibility of Chemicals from Pyrolysis Oil; NWBC 2011, March 22−24, 2011, Stockholm; http://www.biocoup.com/fileadmin-/user/december/Update_December_2011/93_TUE_February11.pdf (accessed October 12, 2014).
15. Vitasari, C. R.; Meindersma, G. W.; de Haan, A. B. Laboratory scale conceptual process development for the isolation of renewable glycolaldehyde from pyrolysis oil to produce fermentation feedstock. *Green Chem.* **2012**, *14*, 321–325.
16. Stradal, J. A.; Underwood, G. L. Pyrolysis of carbohydrate containing feedstock. U.S. Patent 5,393,542, 1993.
17. Majerski, P.; Piskorz, J.; Radlein, D. Production of Glycolaldehyde by Hydrous Thermolysis of Sugars. U.S. Patent 7,094,932, 2006.
18. Bridgwater, A. V. Review of fast pyrolysis of biomass and product upgrading. *Biomass Bioenergy* **2012**, *38*, 68–94.
19. Ruddy, D. A.; Schaidle, J. A.; Ferrell, J. R., III; Wang, J.; Moens, L.; Hensley, J. E. Recent advances in heterogeneous catalysts for bio-oil upgrading via ‘ex situ catalytic fast pyrolysis’: catalyst development through the study of model compounds. *Green Chem.* **2014**, *16*, 454–490.
20. Kelkar, S.; Li, Z.; Bovee, J.; Thelen, K. D.; Kriegel, R. M.; Saffron, C. M. Pyrolysis of North-American grass species: Effect of feedstock composition and taxonomy on pyrolysis products. *Biomass Bioenergy* **2014**, *64*, 152–161.
21. Bridgwater, A. V. Biomass Fast Pyrolysis. *Therm. Sci.* **2004**, *8*, 21–49.

Publication Date (Web): June 18, 2015 | doi: 10.1021/bk-2015-1192.ch019

22. Oasmaa, A.; Leppämäki, E.; Koponen, P.; Levander, J.; Tapola, E. *Physical characterization of biomass-based pyrolysis liquids: Application of standard fuel oil analyses*; Technical Research Centre of Finland: Espoo, Finland, 1997; Report No. 306.
23. Richards, G. N. Glycolaldehyde from pyrolysis of cellulose. *J. Anal. Appl. Pyrolysis* **1987**, *10*, 251–255.
24. Richards, G. N.; Zheng, G. Influence of metal ions and of salts on products from pyrolysis of wood: Applications to thermochemical processing of newsprint and biomass. *J. Anal. Appl. Pyrolysis* **1991**, *21*, 133–146.
25. Broeren, M. *Production of Bio-ethylene − Technology Brief*; IEA-ETSAP and IRENA Technology Brief I13: January 2013.
26. Dusselier, M.; Van Wouwe, P.; De Smet, S.; De Clercq, R.; Verbelen, L.; Van Puyvelde, P.; Du Prez, F. E.; Sels, B. F. Toward Functional Polyester Building Blocks from Renewable Glycolaldehyde with Sn Cascade Catalysis. *ACS Catal.* **2013**, *3*, 1786–1800.
27. Yang, B.; Daib, Z.; Ding, S.-Y.; Wyman, C. E. Enzymatic hydrolysis of cellulosic biomass. *Biofuels* **2011**, *2*, 421–449.
28. Worldwide Polyacetals 2006-2011-2025: Markets, Technologies, and Trends; Chemical Market Resources, Inc.: Houston, TX; http://cmrhoutex.com/media/mcs/PR945POM%20Prospectus.pdf (accessed May 15, 2014).
29. Beyler, C.; Hirschler, M. M. Thermal Decomposition of Polymers. In *SFPE Handbook of Fire Protection Engineering*, 3rd ed.; Powell, P., Ed.; NFPA: Quincy, MA, 2002; Chapter 7, pp 1−127.
30. Eschbach, L. Nonresorbable polymers in bone surgery. *Injury* **2000**, *31*, D22–D27.
31. *Handbook of Chemical Glycosylation: Advances in Stereoselectivity and Therapeutic Relevance*; Demchenko, A. V., Ed.; Wiley-VCH: Weinheim, Germany, 2008.
32. Inanaga, J.; Yokoyama, Y.; Hanamoto, T. Lanthanoid(III) Triflates as New Glycosylation Catalysts. Selective and Efficient Activation of 1-O-Methoxyacetyl Sugars. *Tetrahedron Lett.* **1993**, *34*, 2791–2794.
33. Yamada, H.; Hayashi, T. A substrate-unspecified glycosylation reaction promoted by copper(II) trifluoromethanesulfonate in benzotrifluoride. *Carbohydrate Res.* **2002**, *337*, 581–585.
34. Park, T.-J.; Weïwer, M.; Yuan, X.; Baytas, S. N.; Munoz, E. M.; Murugesan, S.; Linhardt, R. J. Glycosylation in room temperature ionic liquid using unprotected and unactivated donors. *Carbohydrate Res.* **2007**, *342*, 614–620.
35. Augé, J.; Sizun, G. Ionic liquid promoted atom economic glycosylation under Lewis acid catalysis. *Green Chem.* **2009**, *11*, 1179–1183.
36. Kuroiwa, Y.; Sekine, M.; Tomono, S.; Takahashi, D.; Toshima, K. A novel glycosylation of inactive glycosyl donors using an ionic liquid containing a protic acid under reduced pressure conditions. *Tetrahedron Lett.* **2010**, *51*, 6294–6297.

Publication Date (Web): June 18, 2015 | doi: 10.1021/bk-2015-1192.ch019

37. Monasson, O.; Sizun-Thomé, G.; Lubin-Germain, N.; Uziel, J.; Augé, J. Straightforward glycosylation of alcohols and amino acids mediated by ionic liquid. *Carbohydrate Res.* **2012**, *352*, 202–205.
38. Drake, E. N.; Brown, C. E. Application of NMR to biochemical kinetics. A laboratory experiment in physical biochemistry. *J. Chem. Educ.* **1977**, *54*, 124–127.
39. NMR spectra calculated using *ChemBioDraw Ultra*, version 13; CambridgeSoft Corporation: Cambridge, MA.
40. Pfaff, D.; Nemecek, G.; Podlech, J. A Lewis acid-promoted Pinner reaction. *Beilstein J. Org. Chem.* **2013**, *9*, 1572–1577.

Publication Date (Web): June 18, 2015 | doi: 10.1021/bk-2015-1192.ch019

Publication Date (Web): June 18, 2015 | doi: 10.1021/bk-2015-1192.ch020

Chapter 20

Development of Cardanol-Bonded Cellulose Resin with Nonfood Plant Resources: Low Energy Heterogeneous Synthesis Process

Kiyohiko Toyama,* Makoto Soyama, Shukichi Tanaka, and Masatoshi Iji

Smart Energy Research Laboratories, NEC Corporation, 34, Miyukigaoka, Tsukuba, Ibaraki 305-8501, Japan
***E-mail: k-toyama@bq.jp.nec.com.**

To synthesize a high-strength and heat-resistant novel cellulose-based bioplastic having a long side chain with low energy consumption, we developed a novel two-step heterogeneous process. The bioplastic is a cellulose ester synthesized by bonding a short side chain (acetic acid) and a long one (3-pentadecylphenoxy acetic acid, a derivative of cardanol, extracted from cashew nut shells). In conventional homogeneous processes, cellulose esters are recovered by precipitation with large quantities of poor solvents, which requires much energy consumption for their distillation. In the novel process, first, limited amounts of these chains are bonded in a heterogeneous system to achieve efficient product recovery by filtration without precipitation. Second, the short-chain acid is additionally bonded to attain good thermoplasticity of the final product, the cellulose resin, which is recovered by distilling the reaction solvent and the remaining short-chain component. The solvent usage was reduced by approximately 90% compared with a homogeneous process. The thermoplasticity of the resulting resin was comparable to that of a homogeneous one. Furthermore, the mechanical and thermal characteristics of the resin were greatly improved by adding a specific linear polyester, poly(butylene succinate adipate), and a glass fiber, achieving high target levels for durable products.

In Green Polymer Chemistry: Biobased Materials and Biocatalysis; Smith, et al.;
ACS Symposium Series; American Chemical Society: Washington, DC, 2015.

Introduction

Bioplastics, which are made of plant resources, have been attracting increased attention because they help to reduce petroleum resource usage and CO_2 emission. Mass-produced bioplastics such as polylactic acid (PLA) (*1*, *2*) use starch, which is generally extracted from edible plant resources. Because of concerns over future food shortages, bioplastics derived from non-edible plant resources are desired. Cellulose is a prospective candidate for such bioplastics since it is the largest non-food plant resource.

Cellulose is a polysaccharide consisting of D-glucose units linked together by β1-4 glycosidic bonds into linear chains, and it is non-melt processable and insoluble in water and most organic solvents due to intra and intermolecular hydrogen bonding. Cellulose esters of short organic acids such as cellulose acetate have been manufactured for cellulose-based bioplastics by adding external plasticizers (*3*). However, because they have narrow process windows between melting and degradation temperatures, large amounts of external plasticizers were required (*4*), which results in insufficeient durability such as in strength, heat resistance, and exudation of plasticizers. To overcome this problem, many attempts have been made to synthesize long-chain cellulose esters (*5*, *6*) or cellulose graft copolymers (*7*). In these cellulose derivatives, long chains bonded to cellulose, e.g. fatty acids, work as internal plasticizers. However, these cellulose derivatives still did not have sufficient mechanical strength, heat resistance, and water resistance for practical use in various durable products.

We recently developed a novel cellulose-based bioplastic by using a cardanol derivative as a long side chain (*8*, *9*). Cardanol is a non-edible plant resource extracted from cashew nut shells, generated in large amounts as a byproduct, and has a unique structure: a flexible and hydrophobic long side chain (carbon number: 15) with unsaturated bonds, a rigid and hydrophobic benzene ring, and a reactive phenolic hydroxyl group (*10*, *11*). The novel bioplastic was made by esterifying cellulose diacetate (CDA) with a cardanol-derived acid, 3-pentadecylphenoxy acetic acid (PAA), which was obtained by hydrogenating unsaturated bonds in the long chain and changing the phenolic hydroxyl group to the acetyl group. The resulting cardanol-bonded cellulose resin (Figure 1) has higher heat resistance and water resistance than other cellulose derivatives, such as conventional short-chain cellulose esters and long-chain cellulose esters, because the rigid and hydrophobic benzene ring of cardanol prevents heat distortion and water absorption (*5*, *9*). Furthermore, it has higher heat resistance and flexural strength than those of acrylonitrile-butadiene-styrene (ABS), which is petroleum-based and used in electronic products (*8*, *9*).

However, the process to produce the cardanol-bonded cellulose resin needed a lot of energy because it was a homogeneous process, in which a product dissolved in a solvent is isolated by adding large amounts of a poor solvent. The remaining reactant of PAA needed to be separated from the resin by precipitation with a poor solvent because it cannot be separated by distillation with low energy use due to its high boiling point. To cut back on poor solvents, which require large amounts of energy for distillation, another process to utilize isocyanate-modified cardanol

Publication Date (Web): June 18, 2015 | doi: 10.1021/bk-2015-1192.ch020

In Green Polymer Chemistry: Biobased Materials and Biocatalysis; Smith, et al.;
ACS Symposium Series; American Chemical Society: Washington, DC, 2015.

was studied (*12*). Although products could be isolated readily only by evaporating a reaction solvent, the starting material was also CDA, which had been produced by a conventional homogeneous process.

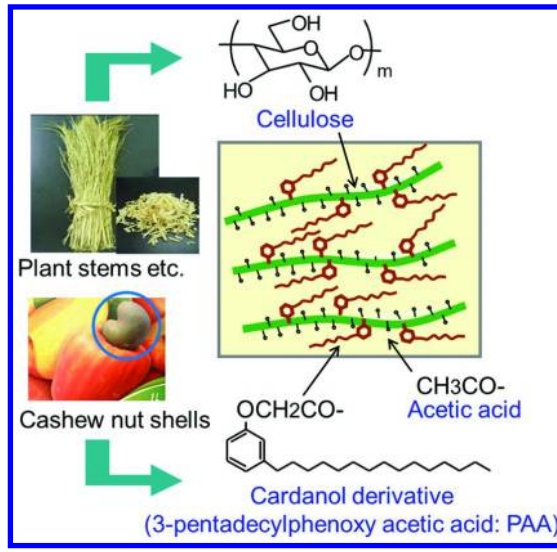

Figure 1. Molecular structure and schematic representation of cardanol-bonded cellulose resin.

Heterogeneous processes, in which cellulose derivatives are not dissolved in solvents, are promising in terms of energy reduction because they can cut back on poor solvents to recover the products as long as the swelling of the products in the solvents are limited. While there have been a lot of studies on bonding long chains to cellulose in heterogeneous systems (*5*, *6*), studies have not been sufficiently made on productivity in recovery steps, which is incompatible with the thermoplasticity of the product. This incompatibility in usual heterogeneous processes is shown in Figure 2. Although a cellulose ester can be recovered easily without poor solvent in a heterogeneous process if its swelling in a solvent is limited, its thermoplasticity is low because cellulose is not modified sufficiently. Here, thermoplasticity is an index of the extent of modification, namely, the homogneity of the product.

In this study, we developed a novel heterogeneous process, the "two-step heterogeneous process," for cardanol-bonded cellulose resin to solve the above incompatibility. In the first step, cellulose is esterified with limited amounts of PAA and acetic acid in a heterogeneous system, and the resultant product is recoverd easily by filtration without poor solvent. Swelling of the product is controlled to achieve both efficient recovery of the product and sufficient amount of PAA bonded to cellulose. In the second step, the intermediate product is further acetylated to improve its thermoplasticity, i.e., homogeneity (Figure 2). The

Publication Date (Web): June 18, 2015 | doi: 10.1021/bk-2015-1192.ch020

resultant final product (cardanol-bonded cellulose resin) is also recovered readily without poor solvent by distilling the reaction solvent and reactant agent as these agents have relatively low boiling points. The solvent usage of the process was compared with that of a homogeneous process. We also investigated the main characteristics of the resultant cellulose resin to be used in durable products and specific additives for them to improve their characteristics.

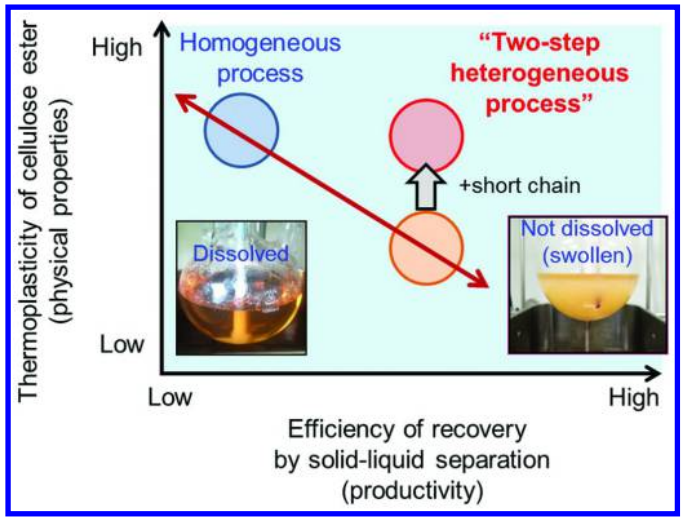

Figure 2. Relationship between efficiency of recovery step and thermoplasticity of cellulose ester.

Results and Discussion

A flow diagram of the two-step heterogeneous process is shown in Figure 3. In the first step, cellulose was esterified in a heterogeneous system by using anhydrides of PAA and acetic acid. Since the resultant intermediate product was not dissolved but moderately swollen in a solvent, it could be easily recovered by suction filtration. To control the swelling, we limited the amount of PAA and acetic acid bonded to cellulose. The degree of substitution (DS) of PAA (DS_{PAA}) was less than or equal to 0.3, and that of acetic acid was less than 1.1. At the same time, a sufficient amount of the long chain could be bonded to cellulose. DS_{PAA} was more than 0.2, which was found to be sufficient for the final product to attain enough thermoplasticity for injection molding. Both efficient solid-liquid separation and sufficient bonding of the long chain could be achieved by controlling the swelling of the cellulose ester. The solution obtained by the filtration was reused easily only by adding deficient comoponents, which lead to a reduction of the reaction solvent.

Publication Date (Web): June 18, 2015 | doi: 10.1021/bk-2015-1192.ch020

In the second step, the intermediate product was acetylated with acetic anhydride. Because this reactant and a reaction solvent are liquid components and could be distilled, the final product could also be recovered easily without poor solvent in this step. The distilled liquids could also be reused by adding defficeinet components. While thermoplasticity of the intermediate product was low, it was improved by over 10 times, as measured by melt flow rate, after the second step, reaching sufficient level for injection molding.

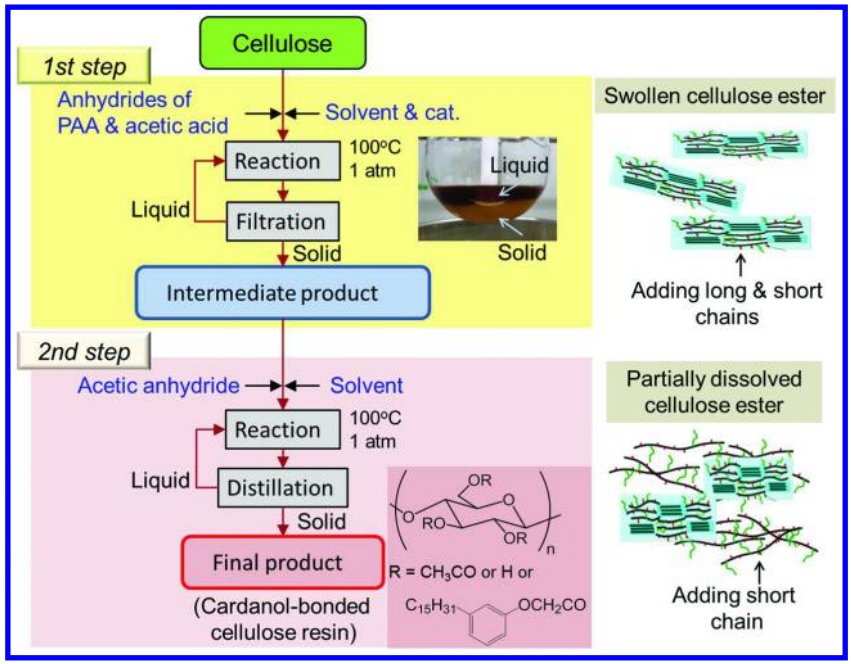

Figure 3. Flow diagram of two-step heterogeneous process.

The solvent usage of the two-step heterogeneous process was compared with that of a homogeneous process (*12*, *13*) (Figure 4). Solvent usage could be reduced by about 90% mainly because of the elimination of poor solvent. The amount of solvent is important in terms of energy for production as the energy to distill solvents constitutes a major component of the total energy of a process. We believe the accomplished reduction in solvent usage will lead to a significantly lowered energy of about 1/10 compared with the homogeneous process.

In Green Polymer Chemistry: Biobased Materials and Biocatalysis; Smith, et al.;
ACS Symposium Series; American Chemical Society: Washington, DC, 2015.

Publication Date (Web): June 18, 2015 | doi: 10.1021/bk-2015-1192.ch020

Publication Date (Web): June 18, 2015 | doi: 10.1021/bk-2015-1192.ch020

Table 1. Characteristics of Cardanol-Bonded Cellulose Resin Synthesized by Two-Step Heterogeneous Process and Its Composite

	*Cellulose acetate + plasticizer (29 wt%)**	*Cardanol-bonded cellulose resin*			
		Homo-geneous process	*Two-step heterogeneous process*		
			1st Intermediate product	*2nd Final product*	*+Additives (Polyester: 27%, Glass fiber: 10%)*
Amounts of side chains (DS: degree of substitution)	Short chain 2.1 Long chain -	2.1 0.33	0.90 0.23	2.4 0.24	2.4 0.27
Thermoplasticity: MFR (g/10min) 200°C, 500kgf/cm^2	960	150	20	275	1330
Izod impact strength (kJ/m^2)	8.8	3.5	Molding difficult	2.5	6.6
Flexural strength (MPa)	68	84		46	50
Elastic modulus (GPa)	2.6	2.3		2.8	1.6
Breaking strain (%)	>10	>10		2	>10
Glass transition temp. (°C)	109	154		140	133
Water absorption ratio (%) [Room temp. 24 hr.]	5.9	2.1		1.8	1.2

* Weight ratio of long chain component of cardanol-bonded cellulose resin: 24-31 wt%.

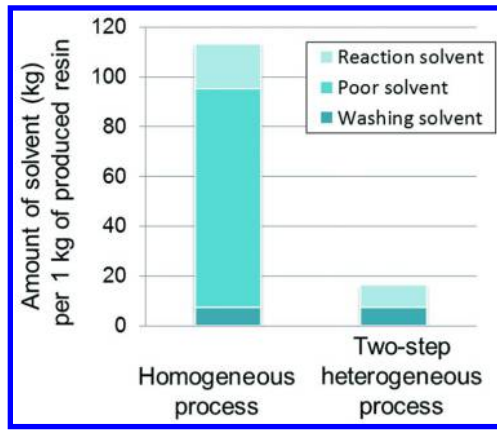

Figure 4. Solvent usage of homogeneous and two-step heterogeneous processes.

The physical properties of the cardanol-bonded cellulose resin synthesized by the two-step heterogeneous process is shown in Table 1 as well as a conventional CDA composite with an external plasticizer and the cardanol-bonded cellulose resin synthesized by a homogeneous process. While the thermoplasticity of the intermediate product of the heterogeneous process was low for injection molding, that of the final product was high enough for injection molding. Compared with the cardanol-bonded cellulose resin of the homogeneous process, the thermoplasticity, elastic modulus and water resistance of the final product of the heterogeneous process were higher, and the heat resistance (glass transition temperature) was relatively close.

However, the impact strength, flexural strength, and breaking strain were lower, which is considered to be caused by inhomogeneity of the cardanol-bonded cellulose resin synthesized by the two-step heterogeneous process. On the basis of a systematic search for additives to improve the impact strength of a cardanol-bonded cellulose resin synthesized by a homogeneous process (*14*), we found that a specific polyester, polybutylene succinate adipate (PBSA), shows the best compatibility among various polyesters with the cellulose resin of the two-step heterogeneous process, and it is a suitable additive to improve the brittleness of the latter resin. PBSA forms an amorphous state in the cellulose resin and thus gives flexibility to the resin because of the flexible structure of its main chain. Although flexural strength was decreased by adding PBSA, it could be increased by adding a glass fiber while keeping impact strength. Finally, after adding PBSA and the glass fiber, high target levels for durable products, such as electronic products, could be reached.

Compared with the CDA composite with an external plasticizer, the final product of the heterogeneous process showed higher elastic modulus, heat resistance and water resistance. Although its thermoplasticity, impact strength, flexural strength and breaking strain were lower, these properties were improved while keeping heat and water resistance by adding PBSA and the glass fiber. The resultant composite achieved high level properties for durable products as mentioned above.

Publication Date (Web): June 18, 2015 | doi: 10.1021/bk-2015-1192.ch020

Conclusion

A novel cellulose-based bioplastic bonded with cardanol as a long side chain achieved high mechanical strength and high heat resistance, and therefore, we developed a novel two-step heterogeneous process for its practical production with low energy consumption. In the first step, a modified cardanol (PAA) and acetic acid were bonded in a heterogeneous system followed by easy recovery of the intermediate product by filtration. By controlling the swelling of the product, we could achieve both an efficient recovery step and sufficient amount of PAA bonded to cellulose. In the second step, acetic acid was additionally bonded to the intermediate product, and the final product, cardanol-bonded cellulose resin, was readily recovered only by distilling liquid components. The solvent usage was reduced by about 90% compared with a homogeneous process by elimination of poor solvent, which leads to a large reduction in energy. The thermoplasticity of the resin, which was improved by the second step, was comparable with that of a homogeneous one. The characteristics of the resin were improved by adding polybutylene succinate adipate and a glass fiber, and high target levels for durable products were reached. We therefore conclude that the novel heterogeneous process is promising for mass production of the cellulose resin, and its composites are prospective for various durable products such as electronic devices.

Publication Date (Web): June 18, 2015 | doi: 10.1021/bk-2015-1192.ch020

Acknowledgments

The authors are grateful to Ms. Toshie Miyamoto and Dr. Fumi Tanabe for their support in the experiments. The work was supported by the Japan Science and Technology Agency's Advanced Low Carbon Technology Research and Development Program (ALCA).

References

1. Li, S.; Ernst, W.; Martin, P. *Biofuels, Bioprod. Biorefin.* **2010**, *4*, 25–40.
2. Serizawa, S.; Inoue, K.; Iji, M. *J. Appl. Polym. Sci.* **2006**, *100*, 618–624.
3. Zepnik, S.; Kesselring, A.; Kopitzky, R.; Michels, C. *Bioplast. Mag.* **2010**, *5*, 44–47.
4. Hwan-Man, P.; Manjusri, M.; Lawrence, T. D.; Mohanty, A. K. *Biomacromolecules* **2004**, *5*, 2281–2288.
5. Edgar, K. J.; Buchanan, C. M.; Debenham, J. S.; Rundquist, P. A.; Seiler, B. D.; Shelton, M. C.; Tindall, D. *Prog. Polym. Sci.* **2001**, *26*, 1605–1688.
6. Freire, C. S. R.; Gandini, A. *Cell. Chem. Technol.* **2006**, *40*, 691–698.
7. Roy, D.; Semsarilar, M.; Guthrie, J. T.; Perrier, S. *Chem. Soc. Rev.* **2009**, *38*, 2046–2064.
8. Iji, M.; Moon, S.; Tanaka, S. *Polym. J.* **2011**, *43*, 738–741.
9. Iji, M.; Toyama, K.; Tanaka, S. *Cellulose* **2013**, *20*, 559–569.
10. Kumar, P. P.; Parmashivappa, R.; Vithayathil, P. J.; Rao, P. V. S.; Rao, A. S. *J. Agric. Food Chem.* **2002**, *50*, 4705–4708.
11. Lubi, M. C.; Thachil, E. T. *Des. Monomers Polym.* **2000**, *3*, 123–153.
12. Tanaka, S.; Honzawa, H.; Iji, M. *J. Appl. Polym. Sci.* **2013**, *130*, 1578–1587.

13. Bogan, R. T.; Brewer, R. J. In *Encyclopedia of Polymer Science and Engineering*; Mark, H. F., Bikales, N., Overberger, C. G., Menges, G., Kroschwitz, J. I., Eds.; John Wiley & Sons: New York, 1985, Vol. 3, pp 158−181.
14. Soyama, M.; Iji, M.; Tanaka, S.; Toyama, K. *Polym. Prepr. Jpn.* **2014**, *63*, 3683–3684.

Publication Date (Web): June 18, 2015 | doi: 10.1021/bk-2015-1192.ch020

Publication Date (Web): June 18, 2015 | doi: 10.1021/bk-2015-1192.ch021

Chapter 21

Phosphorus Flame Retardants from Esters of Isosorbide and 10-Undecenoic Acid

B. A. Howell* and Y. G. Daniel

Science of Advanced Materials, Center for Applications in Polymer Science, Department of Chemistry, Central Michigan University, Mt. Pleasant, Michigan 48859-0001
***E-mail: bob.a.howell@cmich.edu.**

Polymeric materials significantly enhance the daily lives of all citizens of the developed world. For most applications these materials must be flame retardant. Organohalogen compounds, particularly brominated aryl ethers, are readily available at moderate cost, may be readily incorporated as additives into polymeric matrices, and are very effective gas-phase flame retardants. However, these are stable compounds which do not readily degrade in the natural environment. Further, they tend to bioaccumulate and may pose health hazards to the human population. For these reasons, effective alternatives are being sought. Organophosphorus compounds can serve as replacements for popular organohalogen flame retardants. Ideally, these compounds should be derived from non-toxic renewable biosources and should be degradable to innocuous products in the environment. A series of such compounds derived from esters of isosorbide (from starch) and 10-undecenoic acid (from castor oil) is being developed. Several of these display good flame-retarding behavior when incorporated into a cured DGEBA epoxy resin at levels sufficient to introduce one to two percent phosphorus.

In Green Polymer Chemistry: Biobased Materials and Biocatalysis; Smith, et al.;
ACS Symposium Series; American Chemical Society: Washington, DC, 2015.

Publication Date (Web): June 18, 2015 | doi: 10.1021/bk-2015-1192.ch021

Introduction

Concerns about environmental degradation, sustainability, and dwindling supplies of moderately-priced petroleum have led to an increasing interest in polymers and polymer additives derived from renewable biosources (*1–7*). In particular, flame retardants derived from biosources have several advantages over petrochemical materials. Starting materials are generally nontoxic (sometimes edible) and are available from plant sources on an annual basis. Products obtained from these materials are not persistent in the environment and often degrade to innocuous compounds. This is particularly the case for many organophosphorus compounds. These compounds are usually less toxic than the organohalogen compounds which they are replacing (*8–13*). Organohalogen compounds, particularly, brominated aryl ethers, are highly-effective gas-phase flame retardants readily available at modest cost. However, these compounds are persistent in the environment, tend to bioaccumulate, and may pose risks to human health (*14–17*). To some extent these may be replaced by brominated oligomeric materials that cannot migrate from a polymeric matrix in which they are placed (*18*). However, it is likely that organophosphorus compounds will be the most common replacements. In this case, a series of phosphorus esters ultimately derived from the biomaterials, starch (*19–22*) and castor oil (*23–27*), have been synthesized, fully characterized using spectroscopic and thermal methods, evaluated for thermal stability and incorporated into DGEBA epoxy resin for assessment of flame retarding properties.

Materials

Common solvents and reagents were obtained from ThermoFisher Scientific or the Aldrich Chemical Company. Diphenylphosphinic chloride, diethyl phosphite, isosorbide and 10-undecenoic acid were obtained from the Aldrich Chemical Company. 9,10-Dihydro-9-oxa-10-phosphaphenanthrene-10-oxide was from TCI. Diphenyl chlorophosphate was generously supplied by ICL-IP America, Inc. DGEBA (diglycidyl ether of bisphenol A) was supplied by the Dow Chemical Company.

Instrumentation and Characterization

Infrared spectra were obtained by attenuated total reflectance (ATR) using a Thermo Scientific Nicolet 380 FT-IR spectrophotometer. Absorptions were recorded in wavenumbers (cm^{-1}) and absorption intensities were classified in the usual fashion as very weak (vw), weak (w), medium (m), strong (s), and very strong (vs) relative to the strongest band in the spectrum. Nuclear magnetic resonance (NMR) spectra were obtained using a 5-15% solution in deuterochloroform and a Varian Mercury 300 MHz or an INOVA 500 MHz spectrometer. Proton and carbon chemical shifts are reported in parts-per-million (δ) with respect to tetramethylsilane (TMS) as an internal reference (δ = 0.00).

In Green Polymer Chemistry: Biobased Materials and Biocatalysis; Smith, et al.;
ACS Symposium Series; American Chemical Society: Washington, DC, 2015.

Phosphrus-31 chemical shifts are reported in parts-per-million (δ) with respect to triphenylphosphate as an internal reference (δ = -18.00). Electron impact mass spectra were obtained using a Hewlett-Packard 5995A Gas Chromatograph/Mass Spectrometer with an ionizing potential of 70 electron volts and temperature programmed elution into the spectrometer inlet (90°-200° C). Electrospray ionization mass spectra (ESI) were obtained using a Waters Micromass LCT Premier XE orthogonal acceleration time-of-flight mass spectrometer. The desolvation gas was nitrogen heated to 250° C at a flow rate of 200 L/hr. The sample solvent was 50:50 water/acetonitrile containing 0.1% formic acid. Sample introduction (10 μL of solution) was accomplished in flow injection mode at flow rate of 0.05 ml/min. Thermal transitions were determined by differential scanning calorimetry (DSC) using a TA instruments Q2000 instrument. Samples, contained in standard aluminum pans, were analyzed at heating rate of 5 or 10 °C min^{-1}. Thermogravimetry was performed using a TA instruments Q500 instrument. Typically, a heating rate of 5 °C min^{-1} was used. Samples (4-10 mg) were contained in a platinum pan. The sample compartment was purged with dry nitrogen at 50 cm^3 min^{-1} during analysis. Limiting oxygen index (LOI) measurements were carried out using 2-ethyl-2-methylimidazole cured DGEBA epoxy specimen of dimensions 3 x 12.7 x 127 mm containing the appropriate level of phosphorus ester according to ASTM D2863-13 and a Fire Testing Technology (FTT) LOI apparatus. Pyrolysis combustion flow calorimetry (PCFC) was conducted using a FTT microcalorimeter (FAA microcalorimeter) and optimum sample size (1-2.5 mg) according to the manufacturer's operating procedure.

Publication Date (Web): June 18, 2015 | doi: 10.1021/bk-2015-1192.ch021

Results and Discussion

There is increasing interest in generating polymer additives from renewable biomaterials. In particular, flame retardants produced from biomaterials offer several attractive advantages over more traditional materials. A strongly positive feature of this approach is that the necessary starting materials are sustainably available from plant sources. In addition, they are generally nontoxic and biodegradable.

Compounds suitable for conversion to nontoxic, biodegradable flame retardants may be generated from carbohydrates (*19–22*), plant oils (*23–27*), or food waste (*13*, *28*), Phosphorus compounds with flame-retarding potential have been developed with starch and castor oil as ultimate biosources. Starch may be readily converted to isosorbide and castor oil is a source of 10-undecenoic acid (Scheme 1).

Hydrolysis of starch, followed by aldehyde reduction and double dehydration affords isosorbide (Scheme 2). Isosorbide is now commercially available in good purity. While the current source of glucose is starch it will ultimately come from cellulose (crop residue, wood waste, switch grass, etc.). Cellulose is an attractive source of glucose. It is abundantly available and is not a food source. 10-Undecenoic (undecylenic) acid may be generated either by pyrolysis of castor oil directly or pyrolysis of ricinoleic acid, a castor oil constituent (Scheme 3).

Publication Date (Web): June 18, 2015 | doi: 10.1021/bk-2015-1192.ch021

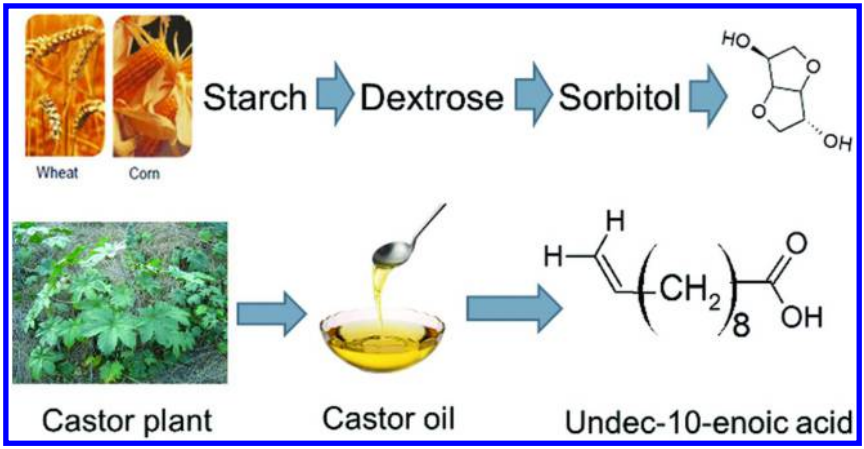

Scheme 1. Generation of Isosorbide and 10-Undecenoic Acid from Biosources

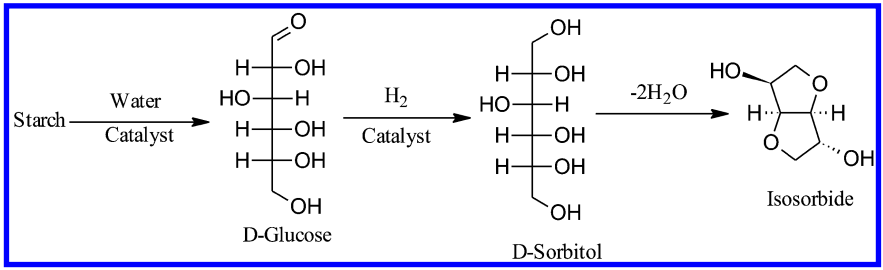

Scheme 2. Conversion of Glucose to Isosorbide

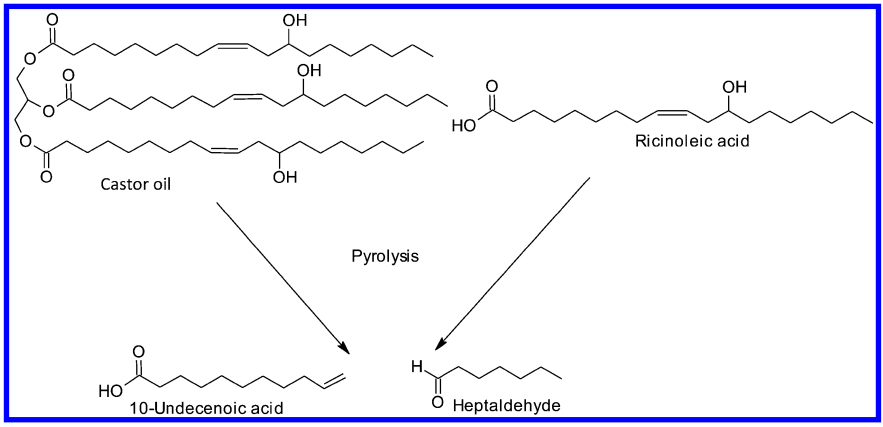

Scheme 3. Generation of 10-Undecenoic Acid

In Green Polymer Chemistry: Biobased Materials and Biocatalysis; Smith, et al.;
ACS Symposium Series; American Chemical Society: Washington, DC, 2015.

Esterification of isosorbide with 10-undecenoic acid provides a difunctional ester (Scheme 4) which can be modified to generate phosphorus compounds with flame-retarding properties. This compound can be produced in good yield and purified by chromatography. The infrared spectrum of this material (Figure 1) contains strong ester carbonyl absorption at 1739 cm^{-1} and carbon oxygen single bond absorption at 1162 cm^{-1} and 1096 cm^{-1}. The terminal carbon-carbon double bond and the associated carbon hydrogen single bond stretches are located at 1640 cm^{-1} and 3076 cm^{-1} respectively. The proton NMR spectrum of the diester (Figure 2) contains absorption for the aliphatic portion of the compound, δ 1.2-2.4, the isosorbide unit, δ 3.8-5.1 as well as the olefinic group, δ 5.2 and 5.8. The carbon-13 NMR spectrum of the diester is displayed in Figure 3. It contains absorptions for aliphatic carbon atoms, δ 24-34, the isosorbide carbon atoms, δ 70-86, olefinic carbon atoms, δ 114 and 135, and an ester carbonyl carbon atom, δ 173. The unsaturated end-groups of the diester provide suitable functionality for further conversion. Thiol-ene reaction with 2-hydroxyethanethiol generates a diol from which a variety of phosphorus esters may be prepared (Scheme 5). This reaction may be satisfactorily carried out in the presence of a radical initiator (*29*) or in the presence of ultraviolet irradiation (*30*, *31*). Ultraviolet radiation is perhaps most convenient.

Publication Date (Web): June 18, 2015 | doi: 10.1021/bk-2015-1192.ch021

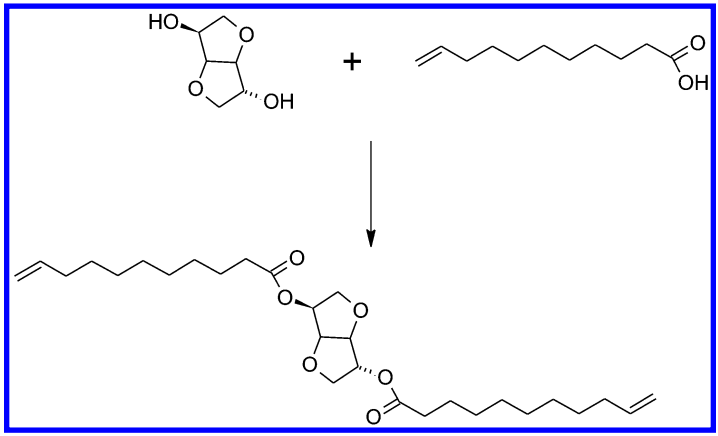

Scheme 4. Preparation of Isosorbide Di(undec-10-enoate)

In Green Polymer Chemistry: Biobased Materials and Biocatalysis; Smith, et al.;
ACS Symposium Series; American Chemical Society: Washington, DC, 2015.

Publication Date (Web): June 18, 2015 | doi: 10.1021/bk-2015-1192.ch021

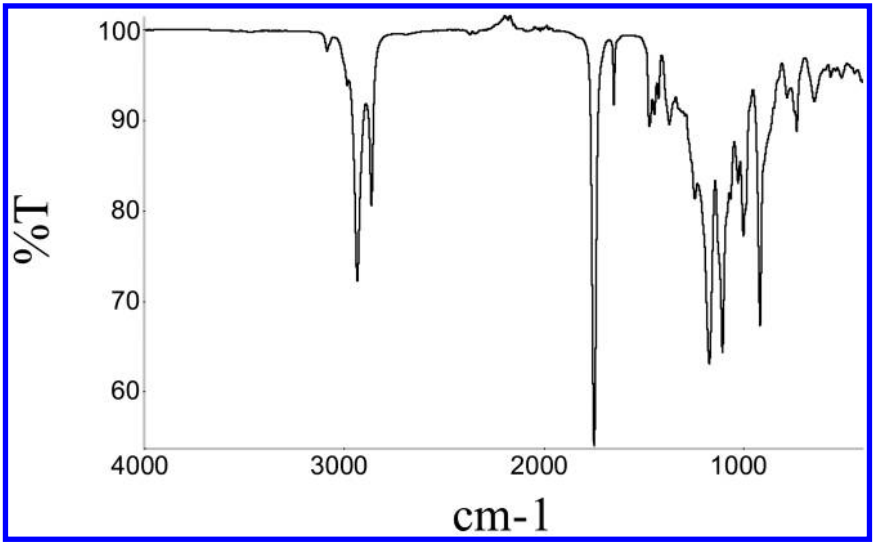

Figure 1. Infrared Spectrum of Isosorbide Di(undec-10-enoate).

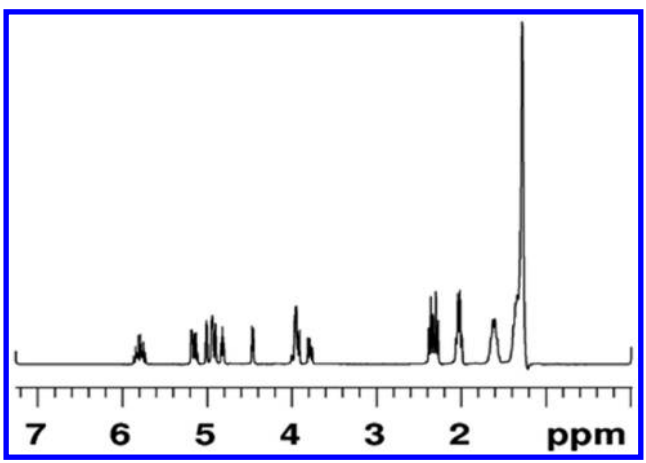

Figure 2. Proton NMR Spectrum of Isosorbide Di(undec-10-enoate).

Publication Date (Web): June 18, 2015 | doi: 10.1021/bk-2015-1192.ch021

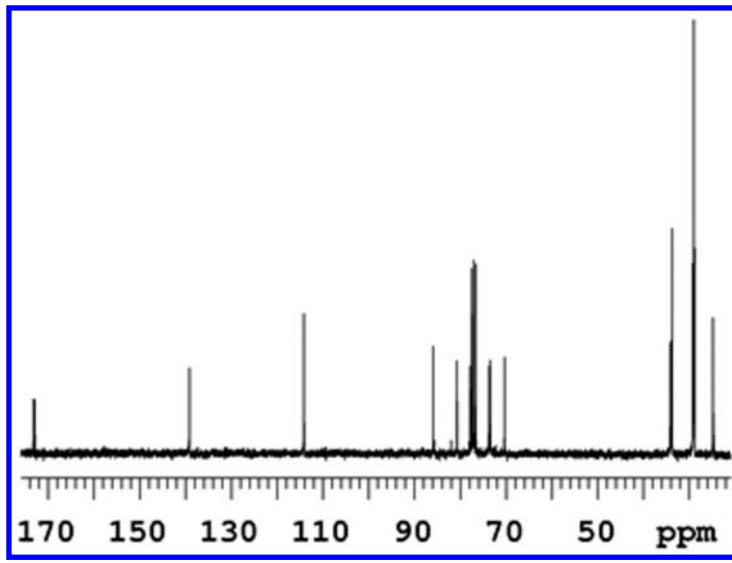

Figure 3. Carbon-13 NMR Spectrum of Isosorbide Di(undec-10-enoate).

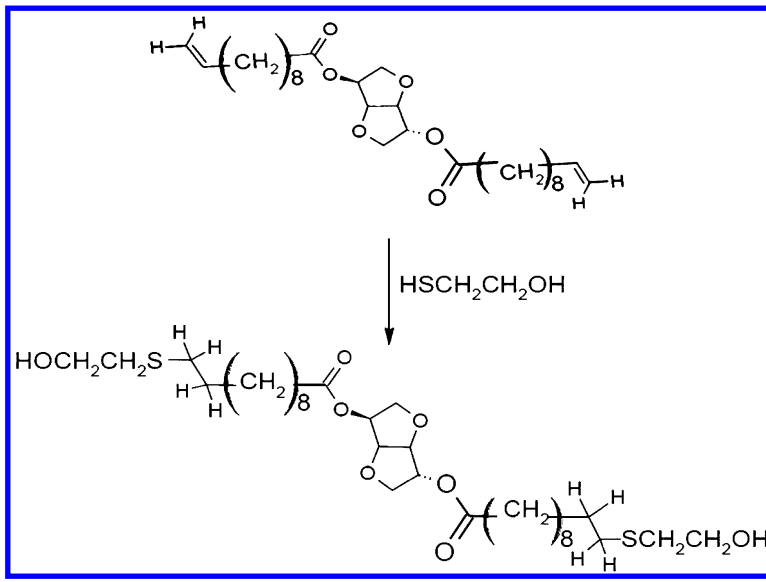

Scheme 5. Preparation of Isosorbide Di(14-hydroxy-12-thiatetradecanoate)

In Green Polymer Chemistry: Biobased Materials and Biocatalysis; Smith, et al.;
ACS Symposium Series; American Chemical Society: Washington, DC, 2015.

The infrared spectrum of the resulting diol is contained in Figure 4. The spectrum contains alcohol absorption at 3440 cm^{-1} and ester carbonyl absorption at 1741 cm^{-1}.

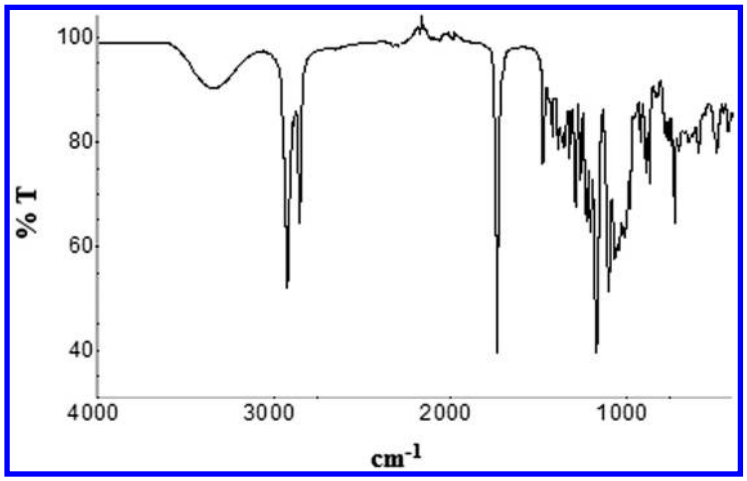

Figure 4. Infrared Spectrum of Isosorbide Di(14-hydroxy-12-thiatetradecanoate).

The proton NMR spectrum of the diol (Figure 5) contains absorption due to aliphatic protons, δ 1.2-2.9, isosorbide protons, δ 3.7-5.2, new absorption due to protons adjacent to oxygen, δ 3.67 and adjacent to sulfur, δ 2.35, as well as a hydroxyl proton, δ 1.98. The carbon-13 NMR spectrum of the diol (Figure 6) contains absorptions due to aliphatic carbon atoms, δ 24-34, the isosorbide carbon atoms δ 70-86, carbon atoms adjacent to sulfur, δ 29.2 and oxygen, δ 62.1 and carbonyl carbon atoms, δ 172.9 and 173.2 (*31*).

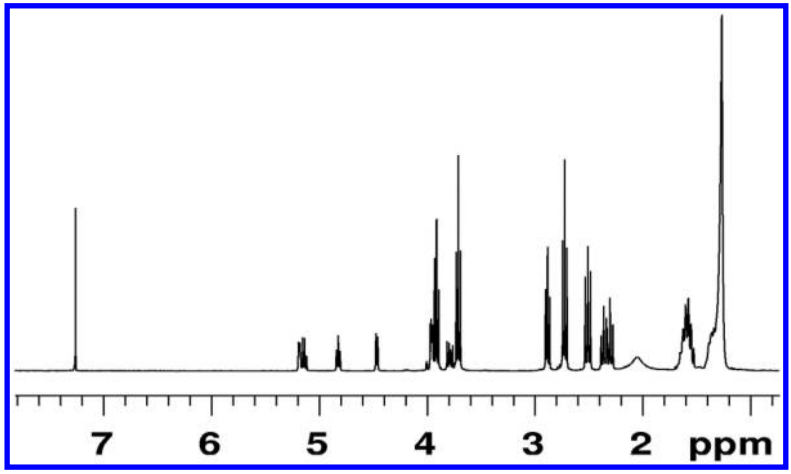

Figure 5. Proton NMR Spectrum of Isosorbide Di(14-hydroxy-12-thiatetradecanoate).

In Green Polymer Chemistry: Biobased Materials and Biocatalysis; Smith, et al.;
ACS Symposium Series; American Chemical Society: Washington, DC, 2015.

Publication Date (Web): June 18, 2015 | doi: 10.1021/bk-2015-1192.ch021

Publication Date (Web): June 18, 2015 | doi: 10.1021/bk-2015-1192.ch021

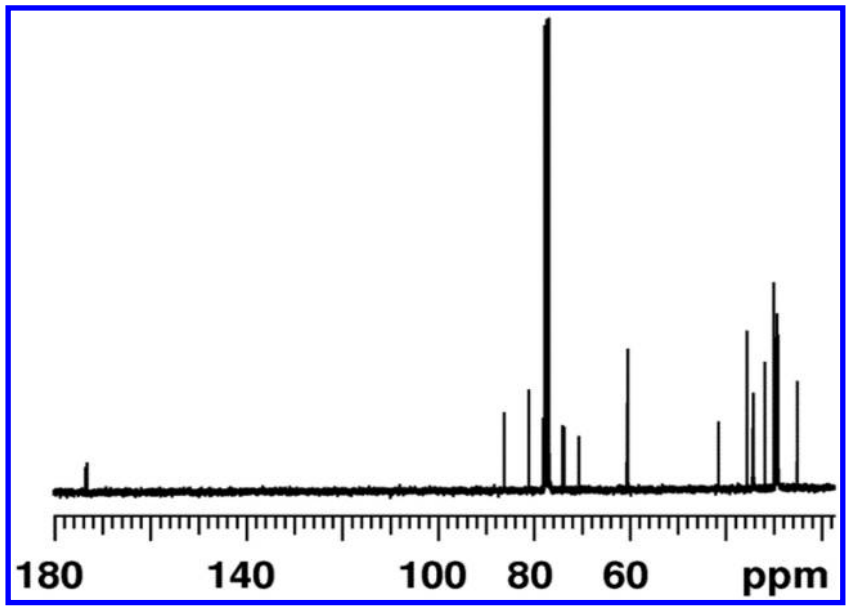

Figure 6. Carbon-13 NMR Spectrum of the Isosorbide Di(14-hydroxy-12-thiatetradecanoate).

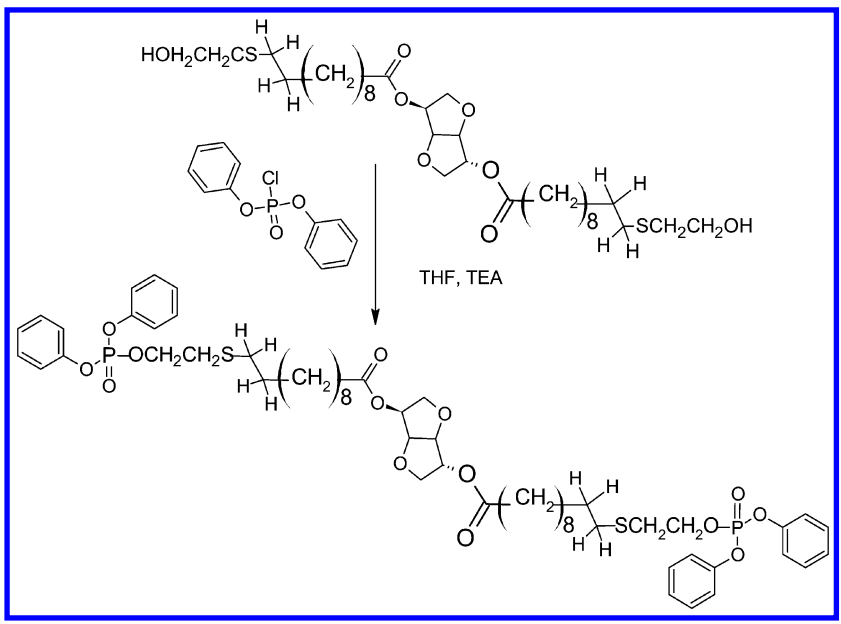

Scheme 6. Preparation of Isosorbide Di[14-(diphenylphosphonato)-12-thiatetradecanoate]

In Green Polymer Chemistry: Biobased Materials and Biocatalysis; Smith, et al.;
ACS Symposium Series; American Chemical Society: Washington, DC, 2015.

Publication Date (Web): June 18, 2015 | doi: 10.1021/bk-2015-1192.ch021

The diol could be converted to phosphorus esters in either of two ways: treatment of the diol with the appropriate phosphoryl chloride in the presence of an acid acceptor or by treatment of the diol with a phosphite in carbon tetrachloride (*32*). The first method is illustrated in Scheme 6 and the second in Scheme 7.

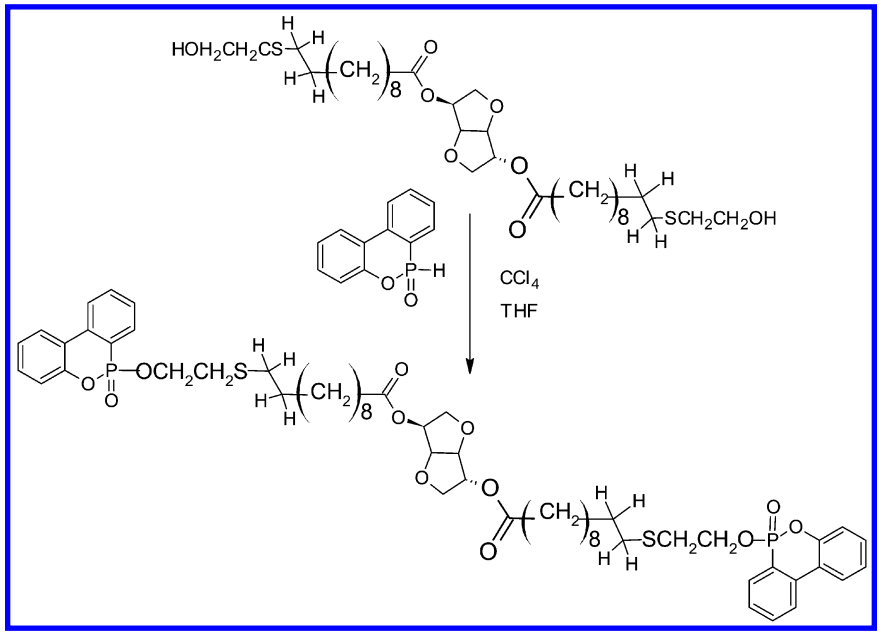

Scheme 7. Preparation of Isosorbide Di(14-dopyl-12-thiatetradecanoate)

Four phosphorus esters were prepared using these methods. Structures, names and abbreviations for these compounds are shown in Figure 7.

These compounds, DPPA, DPPE, DPPI, DPPD are solids melting (DSC) at 44, 48, 34, and 31 °C respectively. The infrared spectra of these compounds contain the bands expected for phosphorus esters (*33–35*). The proton and carbon-13 NMR spectra for these esters may be found in Figure 8. All contain the absorptions expected for the propsed structures.

Isosorbide Di[14-(diphenylphosphato)-12-thiatetradecanoate] [DPPA]

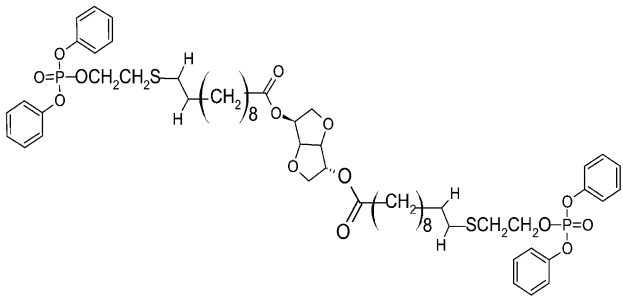

Isosorbide Di[14-(diethylphosphato)-12-thiatetradecanoate] [DPPE]

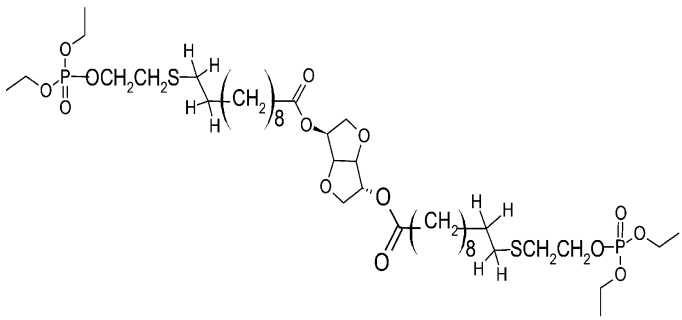

Publication Date (Web): June 18, 2015 | doi: 10.1021/bk-2015-1192.ch021

Publication Date (Web): June 18, 2015 | doi: 10.1021/bk-2015-1192.ch021

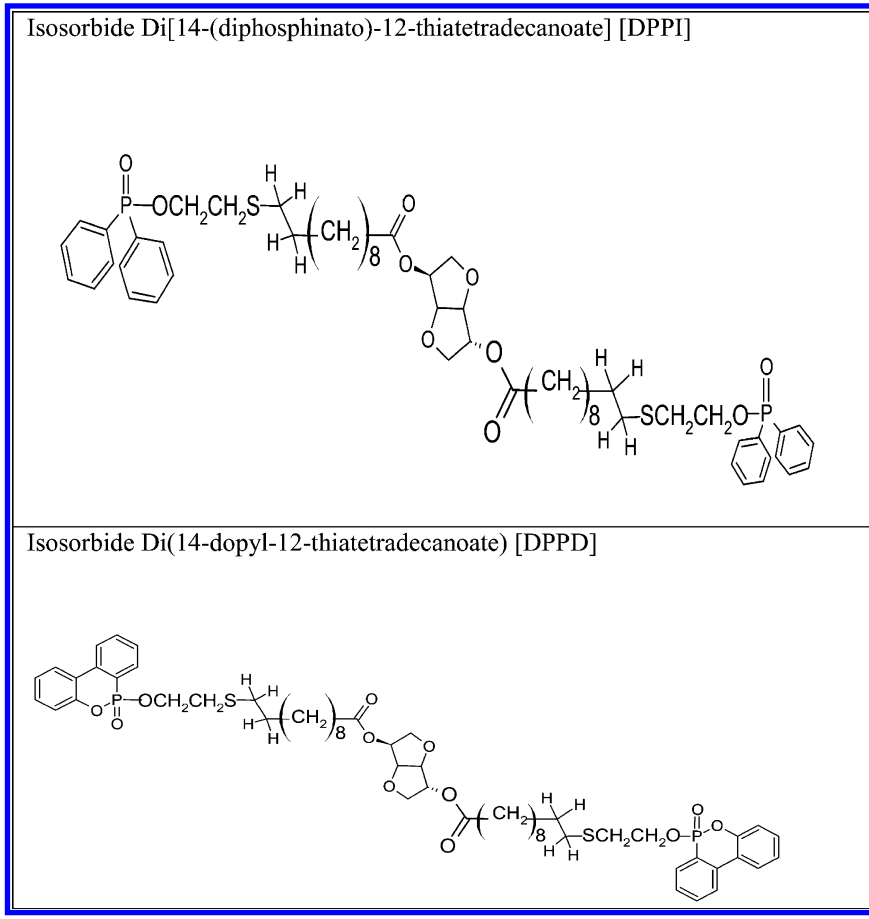

Figure 7. Phosphorus Esters Derived from Isosorbide Di(14-hydroxy-12-thiatetradecanoate).

Publication Date (Web): June 18, 2015 | doi: 10.1021/bk-2015-1192.ch021

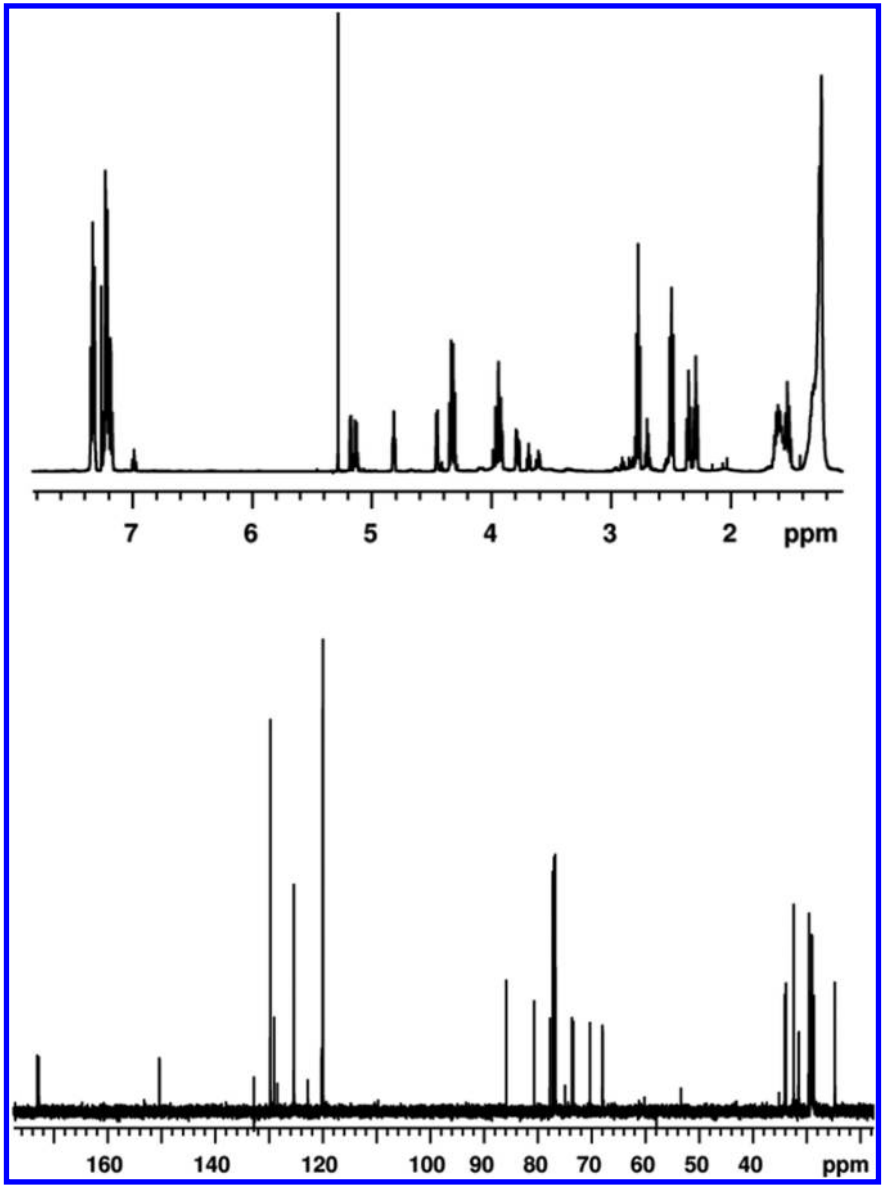

Publication Date (Web): June 18, 2015 | doi: 10.1021/bk-2015-1192.ch021

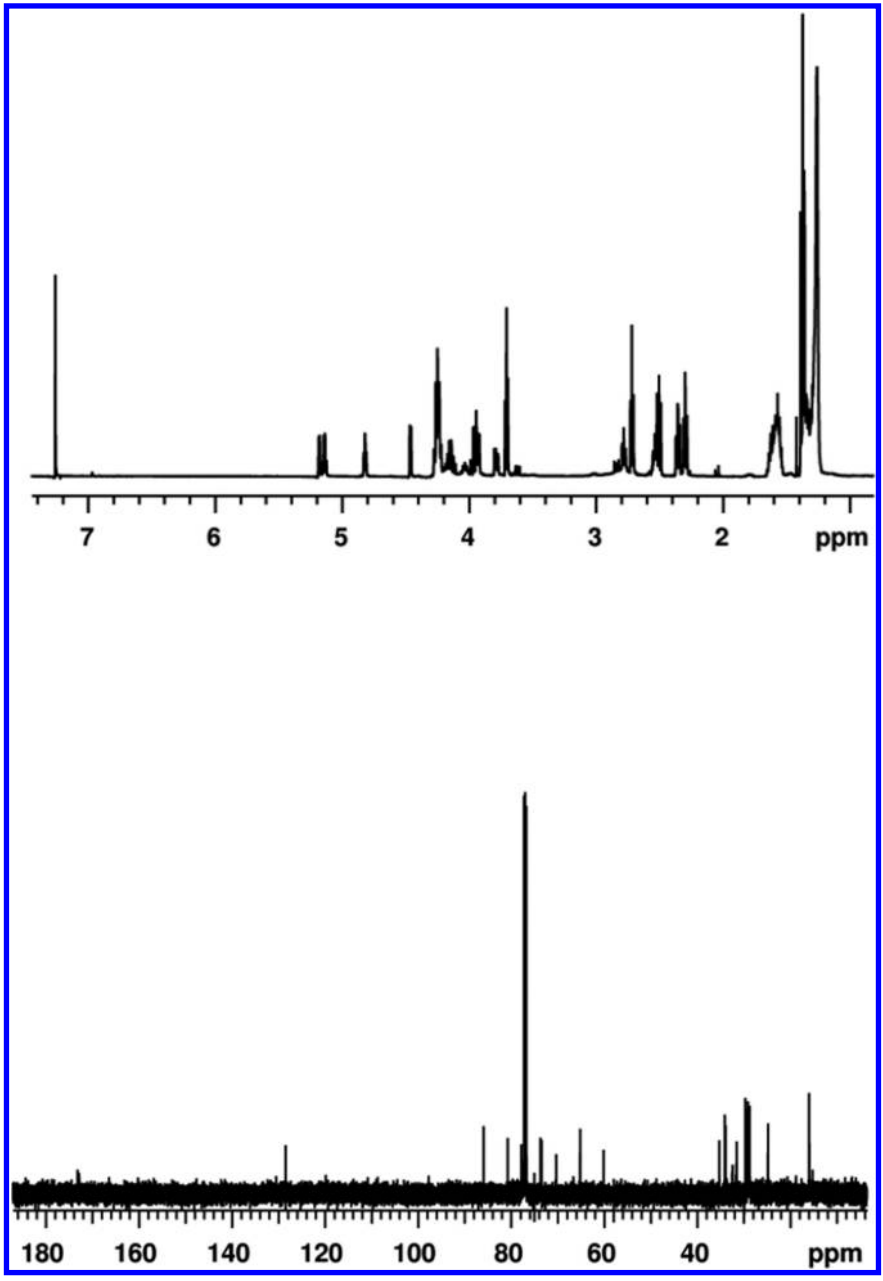

Publication Date (Web): June 18, 2015 | doi: 10.1021/bk-2015-1192.ch021

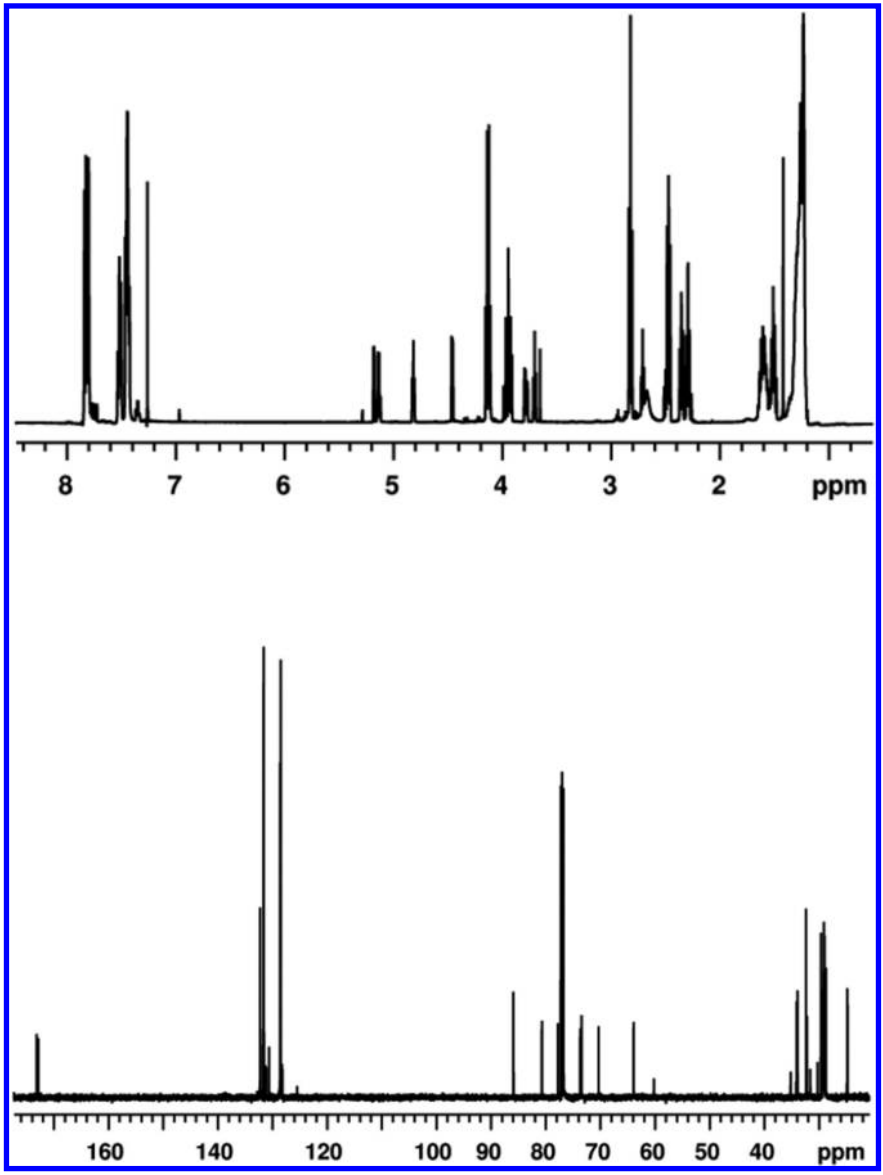

Publication Date (Web): June 18, 2015 | doi: 10.1021/bk-2015-1192.ch021

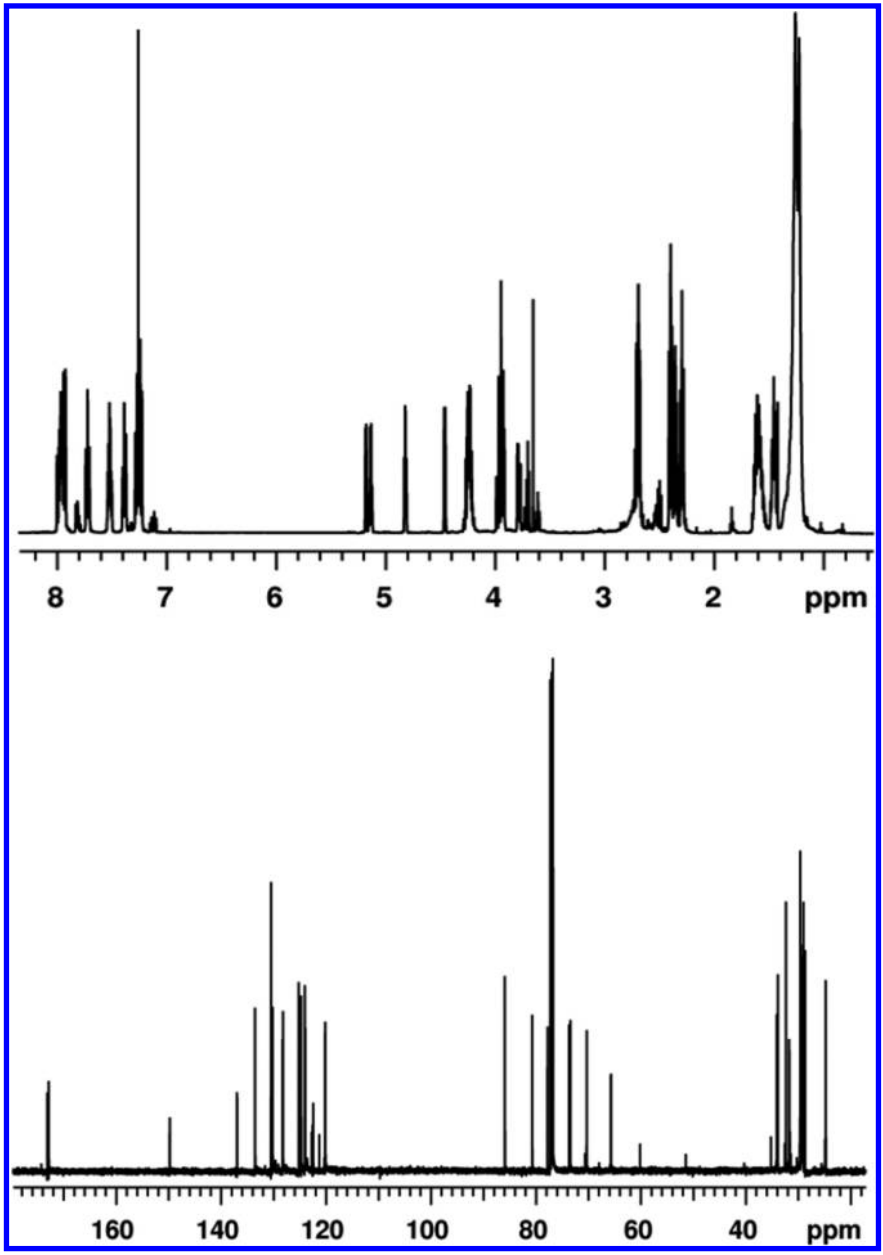

Figure 8. Proton and Carbon-13 NMR Spectra for Four Phosphorus Esters, DPPA, DPPE, DPPI and DPPD.

The thermal degradation behavior of the phosphorus esters has been examined using thermogravimetry and infrared spectroscopy (*36*). Decomposition of the esters as a function of temperature is displayed in Figure 9.

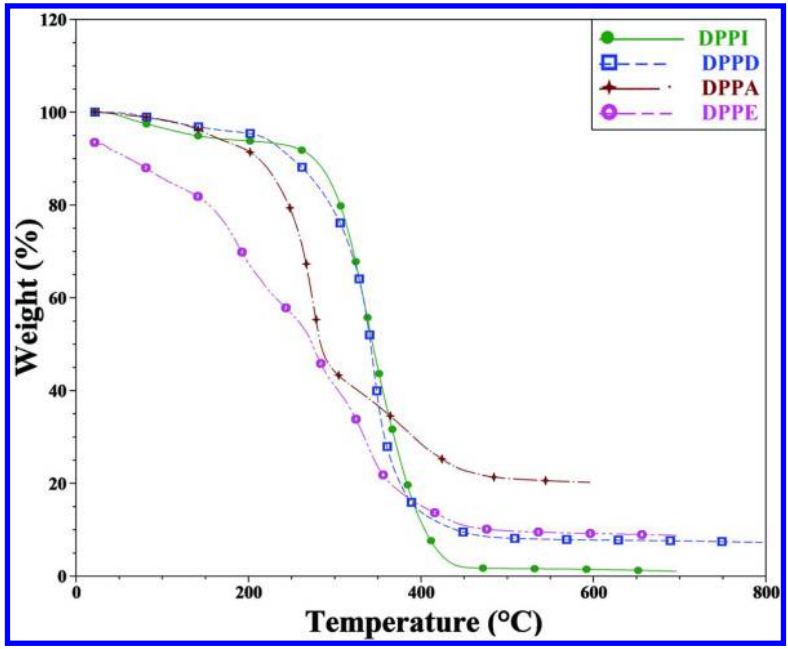

Figure 9. Thermal Degradation of Phosphorus Esters, DPPA, DPPE, DPPI, and DPPD, as a Function of Temperature.

Table 1. Thermal Decomposition of Phosphorus Esters, DPPA, DPPE, DPPI, and DPPD

Compound	*Onset Temperature (°C)*[a]	*Maximum Decomposition Temperature (°C)*[b]	*Decomposition Residue (%)*[c]
DPPA	262	293	22
DPPE	144	190	16
DPPI	278	337	8
DPPD	316	345	12

[a] Extrapolated onset temperature from the TGA derivative plot. [b] Temperature of maximum degradation rate. [c] Residue at 600 °C as a percentage of the initial sample mass.

As may be seen DPPE is the least stable and decomposes over a relatively wide temperature range and in several steps. DPPI and DPPD are the most stable. Details of the decomposition of all the esters are provided in Table 1.

In Green Polymer Chemistry: Biobased Materials and Biocatalysis; Smith, et al.;
ACS Symposium Series; American Chemical Society: Washington, DC, 2015.

Publication Date (Web): June 18, 2015 | doi: 10.1021/bk-2015-1192.ch021

Isothermal decomposition at 200°C is illustrated in Figure 10. Two of these, DPPE and DPPA, undergo rapid initial mass loss (about half of the initial sample mass is lost over the first three hours) to afford a residue stable at 200 °C.

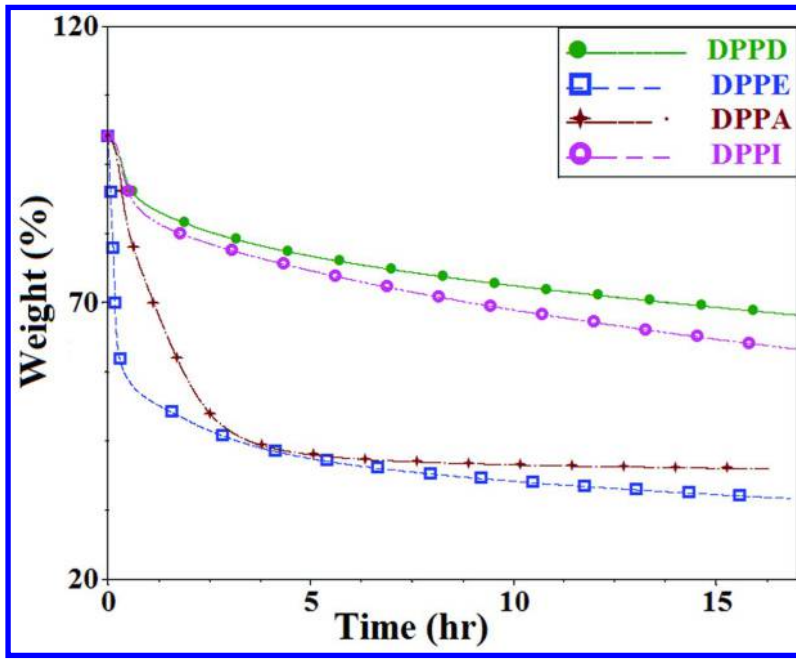

Figure 10. Thermal Degradation of Phosphorus Esters, DPPA, DPPE, DPPI, and DPPD at 200 °C.

Publication Date (Web): June 18, 2015 | doi: 10.1021/bk-2015-1192.ch021

Table 2. Thermal Degradation of Phosphorus Esters at 200 °C

Compound	*Residue at 4 hours (%)**	*Residue at 10 hours (%)**
DPPA	44	41
DPPE	43	38
DPPI	78	69
DPPD	80	73

* Residue as a percentage of the initial sample mass.

DPPI and DPPD degrade less readily with DPPD being the most stable at 200 °C (approximately 20% of the initial sample mass is lost over the first three hours). The mass loss is detailed in Table 2.

The mass loss would suggest that both DPPE and DPPA degrade by rapid loss of both phosphate groups probably by elimination of the corresponding phosphorus acid. The other two may degrade in the same way but at a much slower rate.

The thermal degradation of the phosphate esters was also monitored using infrared spectroscopy. Samples of the ester were placed in an oven maintained at 260 °C. Periodically, a sample was removed for analysis. Results for the degradation of DPPE are shown in Figure 11. As degradation proceeds several changes in the infrared spectrum become apparent.

Publication Date (Web): June 18, 2015 | doi: 10.1021/bk-2015-1192.ch021

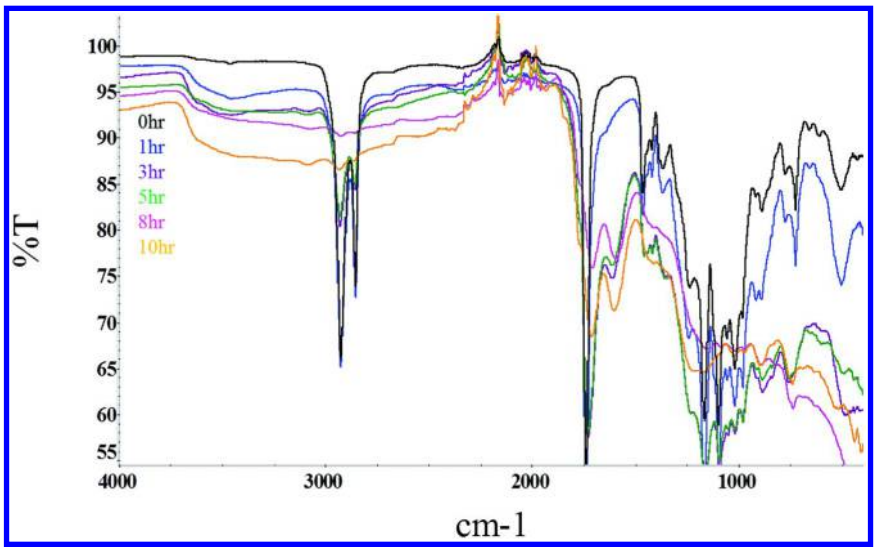

Figure 11. Thermal Degradation of DPPE at 260 °C.

Most of these occur in the molecular vibration region, 1400-700 cm^{-1}, but the most informative is the growth of a broad hydroxyl band, 3500-2500 cm^{-1}. This is probably reflective of the formation of a phosphorus acid (Scheme 8.)

In Green Polymer Chemistry: Biobased Materials and Biocatalysis; Smith, et al.;
ACS Symposium Series; American Chemical Society: Washington, DC, 2015.

Publication Date (Web): June 18, 2015 | doi: 10.1021/bk-2015-1192.ch021

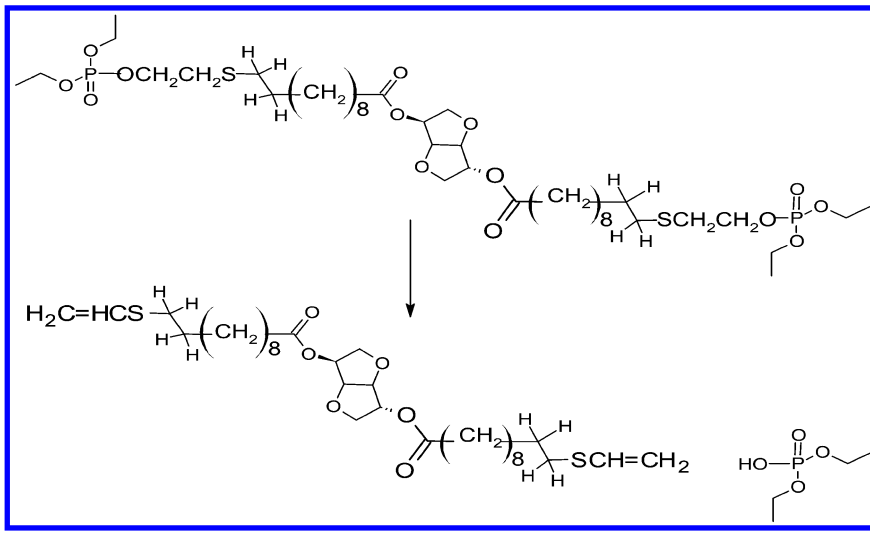

Scheme 8. Proposed Degradation Pathway for DPPE

Changes in the infrared spectrum of DPPA which accompany its degradation are shown in Figure 12.

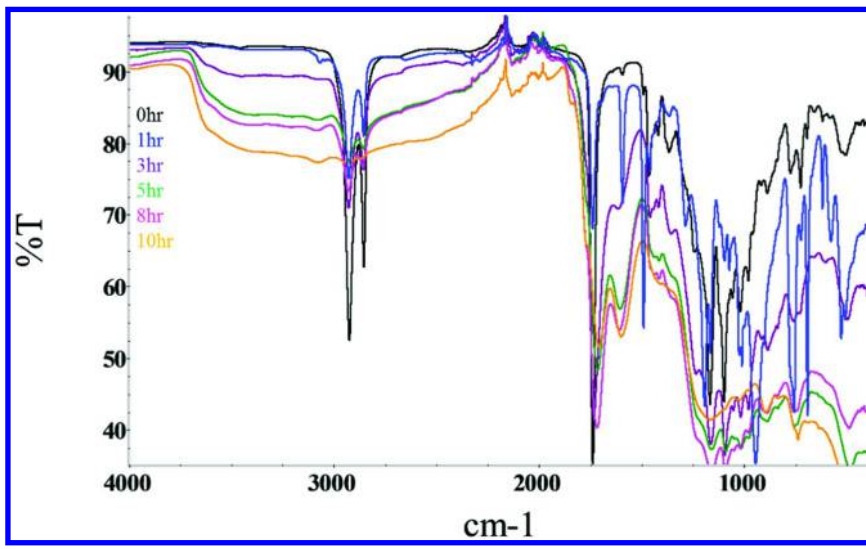

Figure 12. Thermal Degradation of DPPA at 260 °C.

The changes are similar to those observed for the degradation of DPPE and probably reflect a comparable elimination of a phosphorus acid.

In Green Polymer Chemistry: Biobased Materials and Biocatalysis; Smith, et al.;
ACS Symposium Series; American Chemical Society: Washington, DC, 2015.

Spectra detailing the degradation of DPPD are contained in Figure 13. Although the decomposition reaction is slower for this compound, it would appear to follow the same path. The primary reaction is again the elimination of a phosphorus acid (Scheme 9).

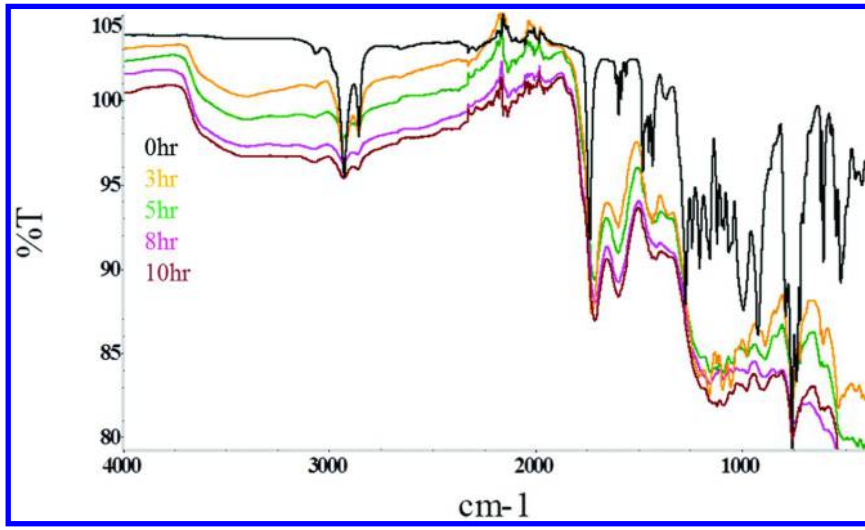

Figure 13. Thermal Degradation of DPPD at 260˚ C.

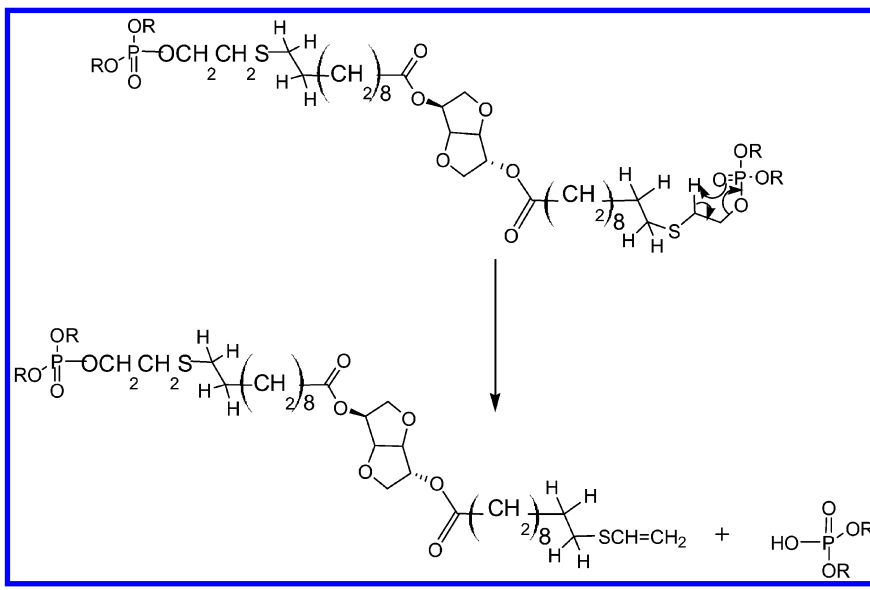

Scheme 9. Mode of Elimination of Phosphorus Acids from the Corresponding Esters

In Green Polymer Chemistry: Biobased Materials and Biocatalysis; Smith, et al.;
ACS Symposium Series; American Chemical Society: Washington, DC, 2015.

Publication Date (Web): June 18, 2015 | doi: 10.1021/bk-2015-1192.ch021

For assessment of the flame-retarding characteristics of phosphorus esters, isosorbide di(14-dopyl-12-thiatetradecanote) [DPPD] and isosorbide di[14-(diphenylphosphato)-12-thiatetradecanoate] [DPPA], blends of the ester in DGEBA epoxy resin were prepared. An amount of phosphorus ester required to provide one or two percent phosphorus in the blend was dissolved in DGEBA at 80° C. Hardner, 2-ethyl-4-methylimidazole was added. The mixture was rapidly stirred to ensure homogeneity and poured into Teflon molds of dimensions 3 x 12.7 x 127 mm. The samples were cured initially at 90°C for one hour and then at 120° C for one hour. The plaques generated could be used directly for LOI determination. Small amounts of the same material were used for PCFC.

The incorporation of the phosphorus esters into the polymer did not greatly impact physical properties. This is illustrated for DPPD blends in Table 3.

Publication Date (Web): June 18, 2015 | doi: 10.1021/bk-2015-1192.ch021

Table 3. Glass Transition Temperatures for DGEBA Epoxy Containing DPPD

Phosphorus Content	T_g (°C)
0% P	113
1% P	110
2% P	102

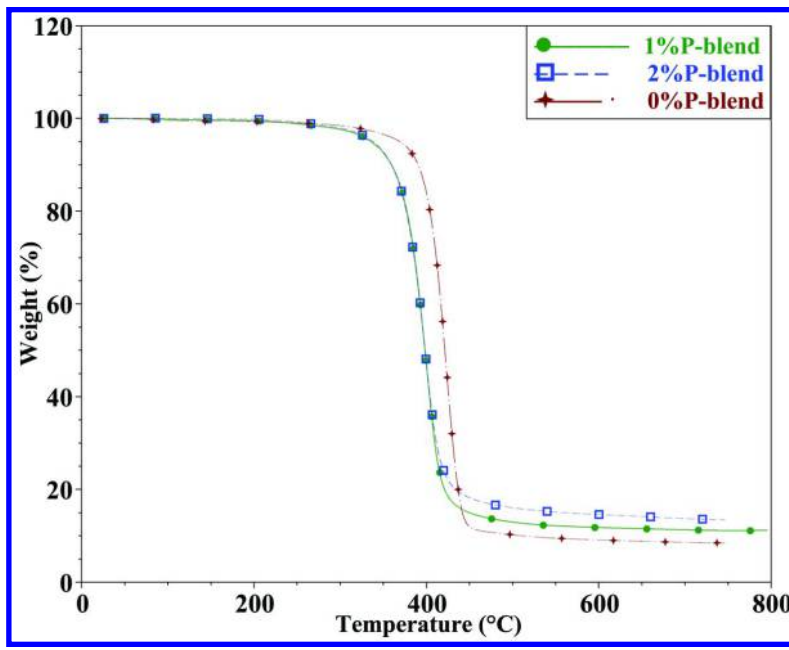

Figure 14. Thermal Decomposition of DGEBA Epoxy Containing DPPD.

In Green Polymer Chemistry: Biobased Materials and Biocatalysis; Smith, et al.;
ACS Symposium Series; American Chemical Society: Washington, DC, 2015.

Similarly, the degradation onset temperatures for the blends are not dramatically lower than that for the polymer containing no flame-retarding additive (Figure 14).

Data for decomposition onset and char formation are collected in Table 4.

Table 4. Degradation Onset Temperatures and Residual Mass for the Thermal Degradation of DGEBA Epoxy Resin Containing DPPD

Phosphorus Content	*Onset (°C)*[a]	*Char (750 °C)*[b]
0% P	390	8%
1% P	360	12%
2% P	330	15%

[a] Extrapolated onset temperature from the derivative plot of mass loss versus temperature. [b] Percent of initial sample mass.

It may be noted that char formation is enhanced by increasing amount of phosphorus in the polymer. The peak heat release rate values for these compositions are displayed in Figure 15. It may be seen that the presence of the DPPD ester in the polymer matrix greatly reduces the peak heat release rate (PHRR). The presence of 1% phosphorus reduces PHRR by 27% of the value for the polymer containing no additive. Increasing the phosphorus content to 2% in the polymer brings about a reduction in PHRR of nearly 60%. Limiting oxygen index data for these compositions are displayed in Table 5. As may be noted, the LOI values increase strongly with increasing levels of DPPD in the polymer. This is reflective of the robust flame-retarding influence of DPPD and is fully consistent with the PCFC results.

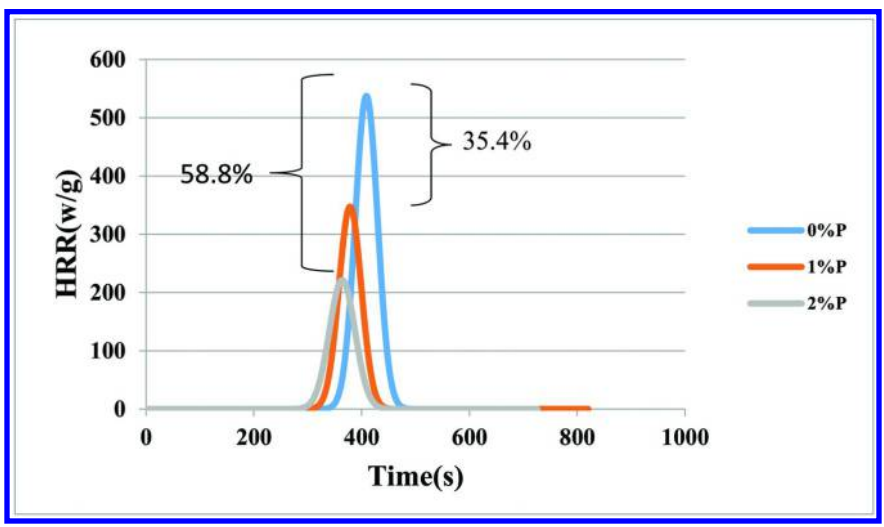

Figure 15. Peak Heat Release Rate for DGEBA Epoxy Containing DPPD.

Publication Date (Web): June 18, 2015 | doi: 10.1021/bk-2015-1192.ch021

Table 5. Limiting Oxygen Index for DGEBA Epoxy Samples Containing DPPD

Phosphorus Content	*LOI (%)*	*Percent Increase (%)*
0% P	18.0	0
1% P	23.7	26.1
2% P	28.8	53.2

Table 6. Glass Transition Temperatures for DGEBA Epoxy Containing DPPA

Phosphorus Content	T_g *(°C)*
0% P	113
1% P	110
2% P	70

Table 7. Degradation Onset Temperatures and Residual Mass for the Thermal Degradation of DGEBA Epoxy Resin Containing DPPA

Phosphorus Content	*Onset (°C)*[a]	*Char (750 °C)*[b]
0% P	390	8%
1% P	330	22%
2% P	303	21%

[a] Extrapolated onset temperature from the derivative plot of mass loss versus temperature. [b] Percent of initial sample mass.

Publication Date (Web): June 18, 2015 | doi: 10.1021/bk-2015-1192.ch021

The flammability behavior of similar compositions containing DPPA was also examined. The glass transition temperatures for the various formulations are presented in Table 6. While the impact on T_g is somewhat larger for DPPA formulations than for those containing DPPD, it is not overly large. Similary, the suppression of the degradation onset temperature (Figure 16) is somewhat larger for DPPD compositions. Decomposition data are summarized in Table 7. While the degradation onset temperature is suppressed somewhat by the presence of the DPPA ester char formation is strongly promoted.The peak heat release rate for these formulations is presented in Figure 17. Again, the presence of DPPA at a level sufficient to provide two percent phosphorus in the composition reduces the PHRR by almost 60%. Limiting oxygen index data for DPPA formulations are collected in Table 8.

Publication Date (Web): June 18, 2015 | doi: 10.1021/bk-2015-1192.ch021

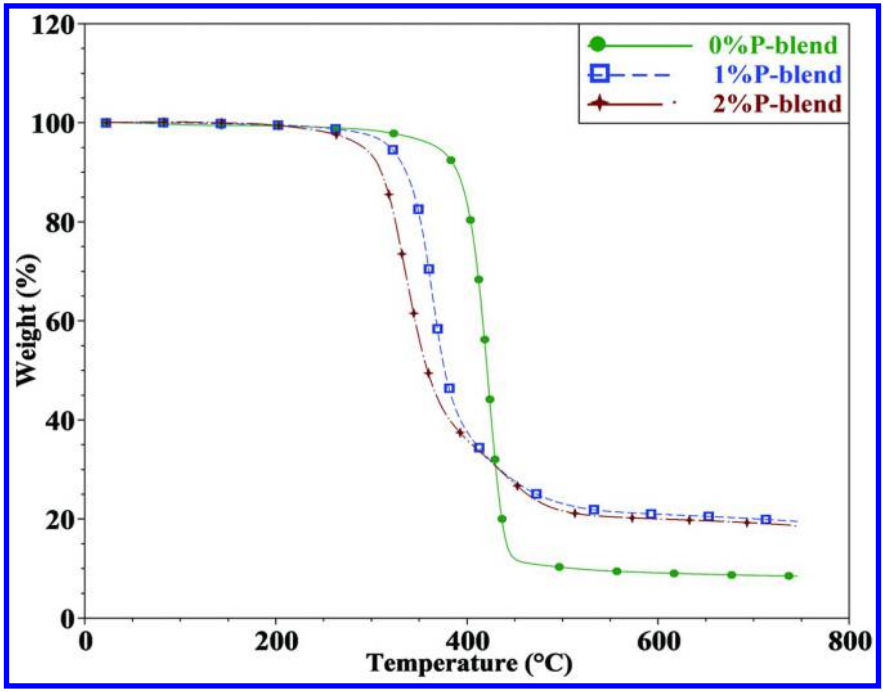

Figure 16. Thermal Decomposition of DEGBA Epoxy Containing DPPA.

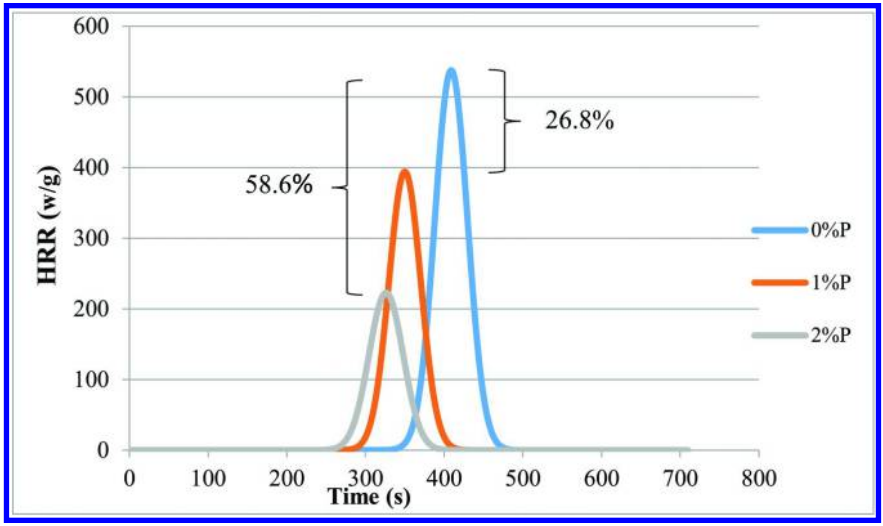

Figure 17. Peak Release Rate for DEGBA Epoxy Containing DPPA.

The influence of DPPA on the LOI for the epoxy polymer is not as great as that for DPPD. Nonetheless, the LOI is strongly improved by the presence of DPPA.

Table 8. Limiting Oxygen Index for DGEBA Epoxy Containing DPPA

Phosphorus Content	*LOI (%)*	*Percent Increase (%)*
0% P	18.0	0
1% P	23.4	26.7
2% P	24.9	32.4

Both LOI and PCFC results suggest that DPPA has good flame-retarding properties.

Publication Date (Web): June 18, 2015 | doi: 10.1021/bk-2015-1192.ch021

Conclusions

A series of phosphorus esters derived from the biomaterials, starch and castor oil, as the ultimate starting materials has been synthesized and fully characterized using spectroscopic and thermal methods. The thermal stability of these materials has been assessed using thermogravimetry and infrared spectroscopy. In the main, these compounds are stable to temperatures approaching 300° C and undergo decomposition via eliminative processes to form phosphorus acids. This suggests that the presence of these compounds in polymeric formulations might promote char formation at the surface of the polymer undergoing combustion. Incorporation of these compounds into an epoxy polymer at levels that introduce one to two percent phosphorus generates formulations with greatly reduced peak heat release rate and strongly enhanced limiting oxygen index values when compared with the corresponding parameters for the polymer containing no flame-retarding additives. Thus these compounds, derived from renewable biosources, show great potential as flame retardants for polymeric materials.

Acknowledgments

Support of this work by Chemtura Corporation/Great Lakes Solutions is gratefully acknowledged. A sample of diphenyl chlorophosphate was graciously provided by ICL-IP America. DGEBA was supplied by the Dow Chemical Company.

References

1. Reddy, M. R.; Vivekanandhan, S.; Misra, M.; Bhatia, S. K.; Mohanty, A. K. Biobased Plastics and Bionanocomposites: Current Status and Future Opportunities". *Prog. Polym. Sci.* **2013**, *38*, 1653–1689.
2. Malinconico, M.; Cerruti, P.; Santagata, G.; Immirzi, B. Natural Polymers and Additives in Commodity and Specialty Applications: A Challenge for the Chemistry of the Future. *Macromol. Symp.* **2014**, *337*, 124–133.

3. Soroudi, A.; Jakubowicz, I. Recycling of Bioplastics, their Blends and Biocomposites: A Review. *Eur. Polym. J.* **2013**, *49*, 2839–2858.
4. Doppalapudi, S.; Jain, A.; Khan, W.; Domb, A. J. Biodegradable Polymers – An Overview. *Polym. Adv. Technol.* **2014**, *25*, 427–435.
5. Chen, G. Q.; Patel, M. K. Plastics Derived from Biological Sources: Present and Future: A Technical and Environmental Review. *Chem. Rev.* **2012**, *112*, 2082–2099.
6. Tschan, M. J. L.; Brule, E.; Hapquette, P.; Thomas, C. M. Synthesis of Biodegradable Polymers from Renewable Resources. *Polym. Chem.* **2012**, *3*, 836–851.
7. Shen, L.; Haufe, J.; Patel, M. K. Product Overview and Market Projection of Emerging Bio-based Plastics;. In *PRO-BIP 2009*; Utrecht University: Utrecht, Netherlands, 2009.
8. van der Veen, I.; de Boer, J. Phosphorous Flame Retardants: Properties, Production, Environmental Occurance, Toxicity and Analysis. *Chemosphere* **2012**, *88*, 1119–1153.
9. Morris, P. J.; Medina-Cleghorn, D.; Heslin, A.; King, S. M.; Orr, J.; Mulvihill, M. M.; Krauss, R. M.; Nomura, D. M. Organophosphorus Flame Retardants Inhibit Specific Liver Carboxylesterases and Cause Serum Hypertriglyceridemia. *ACS Chem. Biol.* **2014**, *9*, 1097–1103.
10. Van den Eede, N.; Neels, H.; Jorens, P. G.; Covaci, A. Analysis of Organophosphate Flame Retardant Diester Metabolites in Human Urine by Liquid Chromatography Electrospray Ionization Tandem Mass Spectrometry. *J. Chromatogr., A* **2013**, *1303*, 48–53.
11. Meeker, J. D; Stapleton, H. M. House Dust Concentrations of Organophosphate Flame Retardants in Relation to Hormone Levels and Semen Quality Parameters. *Environ. Health Perspect.* **2010**, *118*, 318–323.
12. Salamova, A.; Ma, Y.; Venier, M.; Hites, R. A. High Levels of Organophosphate Flame Retardants in the Great Lakes Atmosphere. *Environ. Sci. Technol. Lett.* **2014**, *1*, 8–14.
13. Howell, B. A.; Dangalle, H. *Phosphorus-containing Tartrates and Hydroquinones as Flame Retardant Precursors*,. In Proceedings of the 39th Annual Technical Meeting of the North American Thermal Analysis Society, Des Moines, IA, August, 2011; Kessler, M. E., Ed.; XCD Technologies, Inc.: Toronto, ON, 2011.
14. Alace, M.; Wenning, R. J. The Significance of Brominated Flame Retardants in the Environment: Current Understanding, Issues and Challenges. *Chemosphere* **2002**, *46*, 579–582.
15. Darnerud, P. D. Brominated Flame Retardants as Possible Endocrine Disrupters. *Int. J. Androl.* **2008**, *31*, 152–160.
16. Herbstmann, J. B.; Sjödin, A.; Kurzon, M.; Lederman, S. A.; Jones, R. S.; Rauh, V.; Needham, L. L.; Tang, D.; Nieazwiecki, M.; Wang, R. Y.; Perera, F. Prenatal Exposure to PBDEs and Neurodevelopment. *Envrion. Health Perspect.* **2010**, *118*, 712–719.
17. Hess, G. Industry Drops Flame Retardant. *Chem. Eng. News* **2010**, *88*, 10.

Publication Date (Web): June 18, 2015 | doi: 10.1021/bk-2015-1192.ch021

18. Narayan, S.; Moore, M. Flame Retardants – A New, Versatile Flame Retardant for Olefinic and Styrenic Polymers. *Pop. Plast. Packag.* **2012**, *75*, 58–60.
19. Daniel, Y. G.; Howell, B. A. *Isosorbide as a Renewable Biosource for Phosphorus-based Flame Retardants*. In Proceedings of the 2012 IUPAC World Polymer Congress, Blacksburg, VA, June, 2012; Long, T. E., Ed., Blacksburg Press: Blacksburg, VA, 2012.
20. Feng, X.; East, A. J.; Hammond, W. B.; Zhang, Y.; Jaffe, M. Overview of Advances in Sugar-based Polymers. *Polym. Adv. Technol.* **2011**, *22*, 139–150.
21. Rose, M.; Palkovits, R. Isosorbide as a Renewable Platform Chemical for Versatile Applications-Quo Vadis? *ChemSusChem* **2012**, *5*, 167–176.
22. Fenouillot, F.; Rosseau, A.; Colomines, G.; Saint-Loup, R.; Pascault, J. P. Polymers from Renewable 1,4:1,6-Dianhydrohexitols (Isosorbide, Isomannide and Isoiodide): A Review. *Prog. Polym. Sci.* **2010**, *25*, 578–622.
23. von der Steen, M.; Stevens, C. V. Undecylenic Acid: A Valuable and Physiologically Active Renewable Building Block from Castor Oil. *ChemSusChem* **2009**, *2*, 692–713.
24. de Espinosa, L. M.; Meier, M. A. R. Plant Oils: The Perfect Renewable Resource for Polymer Science?! *Eur. Polym. J.* **2011**, *47*, 837–852.
25. Biermann, U.; Bornscheurer, U.; Meier, M. A. R.; Metzger, J. O.; Schafer, H. J. Oils and Fats as Renewable Raw Materials in Chemistry. *Angew. Chem., Int. Ed.* **2011**, *50*, 3854–3871.
26. Gilbert, E. E. The Unique Chemistry of Castor Oil. *J. Chem. Educ.* **1941**, *18*, 338–341.
27. Atabani, A. E.; Silitonga, A. S.; Ong, H. C.; Mahlia, T. M. I.; Masjuki, H. H.; Badruddin, I. A.; Fayaz, H. Non-edible Vegetable Oils: A Critical Evaluation of Oil Extraction, Fatty Acid Compositions, Biodiesel Production, Characteristics, Engine Performance and Emissions Production. *Renew. Sustain. Energy Rev.* **2013**, *18*, 211–245.
28. Howell, B. A.; Carter, K. E.; Dangalle, H. Flame Retardants Based on Tartaric Acid: A Renewable By-Product of the Wine Industry. In *Renewable and Sustainable Polymer*; Payne, G. F., Smith, P. B., Eds.; ACS Symposium Series 1063; American Chemical Society: Washington, D.C., 2011; Chapter 9, pp 133−152.
29. Lowe, A. B. Thiol-ene 'Click' Reactions and Recent Applications in Polymer and Materials Synthesis. *Polym. Chem.* **2010**, *1*, 17–36.
30. Grigor, B. B.; James, A. K.; Girma, B.; Moon, G. H. Free Radical Addition of Butanethiol to Vegetable Oil Double Bonds. *J. Agric. Food Chem.* **2009**, *57*, 1282–1290.
31. Maisonneuve, L.; Lebarb, T.; Nga Nguyen, T. H.; Cloutlet, E.; Gadenne, B.; Alfos, C.; Cramail, H. Hydroxyl Telechelic Building Blocks from Fatty Acid Methyl Esters for the Synthesis of Poly(ester/amide urethane)s with Versatile Properties. *Polym. Chem.* **2012**, *3*, 2583–2595.

Publication Date (Web): June 18, 2015 | doi: 10.1021/bk-2015-1192.ch021

32. Dumitrascu, A.; Howell, B. A. Flame-retarding Vinyl Polymers using Phosphorus-functionalized Styrene Monomers. *Polym. Degrad. Stab.* **2011**, *96*, 342–349.
33. Thomas, L. C. *Interpretation of the Infrared Spectra of Organophosphorus Compounds*; Academic Press, London, 1974.
34. Thomas, L. C.; Chittenden, R. A. Characteristic Infrared Absorption Frequencies of Organophosphorus Compounds I. The Phosphoryl Group. *Spectrochem. Acta* **1964**, *20*, 467–487.
35. Daasch, L. W.; Smith, D. C. Infrared Spectra of Phosphorus Compounds. *Anal. Chem.* **1951**, *23*, 853–868.
36. Daniel, Y. G.; Howell, B. A. Thermal Degradation of Phosphorus Esters Derived from Isosorbide and 10-Undecenoic Acid. *J. Therm. Anal. Calorim.* submitted for publication.

Publication Date (Web): June 18, 2015 | doi: 10.1021/bk-2015-1192.ch021

Publication Date (Web): June 18, 2015 | doi: 10.1021/bk-2015-1192.ch022

Chapter 22

Bio-Based Epoxy Resins from Diphenolate Esters—Replacing the Diglycidyl Ether of Bisphenol A

Anthony Maiorana, Stephen Spinella, and Richard A. Gross*

New York Center for Polymer Synthesis, Department of Chemistry and Chemical Biology, Rensselaer Polytechnic Institute, 110 8th Street, Troy, New York 12180, U.S.A.
***E-mail: grossr@rpi.edu.**

Bio-based epoxy monomers were synthesized from diphenolic acid (DPA) with the goal of producing a drop-in replacement for the diglycidyl ether of bisphenol A (DGEBA). A series of resins was prepared from alkyl diphenolate esters. The purity and properties of the resins were investigated through ^{1}H NMR and mass spectrometry, rheology, and differential scanning calorimetry. The bio-based resins were cured under identical conditions using the same crosslinker and the thermomechanical properties were compared by dynamic mechanical analysis (DMA), tensile testing, parallel plate rheology, and thermogravimetric analysis. The thermal properties of the diphenolate epoxy resins were tunable through the length of the ester chain.

Introduction

High performance polymer composites are an important class of materials. The low density of polymer composites allow for lightweight structural materials. The demand for suchI se materials may grow with new mandates for fuel efficient cars and construction of windmills (*1*).

In Green Polymer Chemistry: Biobased Materials and Biocatalysis; Smith, et al.;
ACS Symposium Series; American Chemical Society: Washington, DC, 2015.

Publication Date (Web): June 18, 2015 | doi: 10.1021/bk-2015-1192.ch022

The manufacture of advanced polymer composites typically involves the using high strength fillers in a thermosetting polymer matrix. A thermoset matrix is preferred for many reasons, but they allow for high glass transition temperatures, long service life, chemical resistance, and ease of processing (*2*). Epoxy resins mixed with an appropriate hardener represent the majority of thermoset polymers (not including polyurethanes). The epoxy resin that is most well-known is the diglycidyl ether of bisphenol A (DGEBA) and its oligomers. Epoxy resins are used for the manufacturing of composites but also find uses as adhesives and coatings. DGEBA thermosets are typically considered high performance and the thermomechanical properties are typically manipulated by changing the hardener. Liquid epoxy resins also allow for processing at low temperatures, reduction of voids, and ability to bind together high performance fillers at high filler loadings (*3*).

Bisphenol A has been highlighted as an endocrine disruptor and it has structural similarities to estrogens. Bisphenol A has also been discussed as increasing risk for reduced fertility, causing cancer, and the onset of disease (*4–6*). The US Federal Drug Administration has imposed a ban on Bisphenol A-based packaging baby products (*7*). Bisphenol A is also derived from petroleum and has a foreseeable limit.

There is already a growing body of work dedicated to bio-based epoxy resins. Bio-based feedstocks with rigid chemical structures offer suitable alternatives to DGEBA. Epoxidation of the double bonds in tree rosins offer allows for a resin that when cured yield properties that are comparable to DGEBA, but suffer from being solids at room temperature (*8*). Epoxy resins derived from the esters of 4-hydroxybenzoic acid and different polyols has been reported with the majority of the resins' mechanical properties as a formulation with DGEBA. The prepared resins had the effect of lowering the T_g or modulus and may also represent a challenge in processing because they are solids at room temperature (*9*). Epoxy resins from isosorbide exhibit excellent thermomechanical properties, but the synthesis is challenging and requires using allyl bromide with an epoxidation agent (*10*). Gallic acid have been used to make epoxy resins with the final materials yielding thermomechanical properties that surpass DGEBA. The epoxidized gallic acid requires allylation and then epoxidization due to the high reactivity of the carboxylic acid and the close proximity of the aromatic hydroxyls (*11*, *12*). Overall, a route to a bio-based alternative to DGEBA with similar processing conditions has yet to be achieved.

Our goal was to achieve a bio-based epoxy resin that could be synthesized and processed in similar fashion BPA-based resins. DGEBA is synthesized industrially through using a large excess of epichlorohydrin under alkaline conditions (*13*). A bio-based molecule that could be manufactured into an epoxy resin using a similar process to bisphenol A-based resins would allow for a drop-in replacement. Further, the use of lignocellulosic-based chemicals was desired so that the synthesis of the bio-based epoxy resins would not be dependent on food production.

Bio-based epoxy resins have the opportunity to become industrially prevalent with bio-based feedstocks becoming available at industrial and pilot levels. Solvay has introduced Epicerol a bio-based epichlorohydrin (*3*, *14*, *15*). Levulinic

In Green Polymer Chemistry: Biobased Materials and Biocatalysis; Smith, et al.;
ACS Symposium Series; American Chemical Society: Washington, DC, 2015.

acid is a platform chemical that is of great interest due to its ability to undergo chemical transformations (*16*) and it can be produced from cellulose (*17*). Lignin is thought to be a great source of bio-based phenolics. One method that has gained much attention is the fast pyrolysis of lignocellulose to produce phenol, guaiacol, vanillin, and other phenolic compounds (*18–20*). Condensation of levulinic acid with two equivalents of phenol yields diphenolic acid and has gained much attention as a replacement chemical for bisphenol A (*21*, *22*). The relative binding affinity of diphenolic acid to the estrogen receptor is an order of magnitude lower than BPA (*23*). Increases in conversion and selectivity for the desired *para, para* isomer of diphenolic acid have also been reported (*22*, *24*).

The use of diphenolic acid in benzoxazines, a high performance thermoset, has been well established to give excellent thermal and mechanical properties (*25*). The synthesis of diphenolic acid based polycarbonates has also been reported (*26*). There are currently no peer reviewed articles on the synthesis or structure property relationships of diphenolic acid based epoxies.

Due to structural similarities between diphenolic acid and bisphenol A we hypothesized the resulting epoxy resins and materials produced should have similar physical properties. Diphenolic acid has the advantage of having a free carboxylic acid allowing for a myriad of chemical modifications. These modifications may allow for manipulation of the thermomechanical properties. The most accessible modification is the synthesis of esters with relatively short chain alcohols (see Scheme 1). Furthermore, derivatives of diphenolic acid have the possibility of further inhibiting binding to the estrogen receptor.

Here, we report the synthesis of epoxy resins derived from esters of diphenolic acid that requires no complicated purification techniques with yields of 85% or higher. The prepared resins are liquid at room temperature and should have similar processability to DGEBA for composites. We cured our resins with isophorone diamine because it is a liquid and prevalent in industry. The cured bio-based epoxy resins exhibit the qualities of an engineering material and as the length of the ester chain increases, decreases in T_g (determined from the peak of the loss modulus) can be observed in a linear fashion without significant sacrifices in modulus (Storage and Young's). Epoxy resins based on diphenolate esters represent a bio-based alternative to DGEBA from synthesis and processability to performance.

Publication Date (Web): June 18, 2015 | doi: 10.1021/bk-2015-1192.ch022

Results and Discussion

Synthesis and Characterization of Epoxy Monomers

The epoxy monomers were prepared in a two-step process depicted in Scheme 1. Fischer esterification with a large excess of the desired alcohol led to the corresponding ester. Full conversion of the diphenolic acid was typically achieved. The glycidation proceeded through a reaction with excess epichlorohydrin, 20% sodium hydroxide, and 2-propanol as the solvent. Excess reactants and solvent were removed with conventional techniques (see experimental section).

In Green Polymer Chemistry: Biobased Materials and Biocatalysis; Smith, et al.;
ACS Symposium Series; American Chemical Society: Washington, DC, 2015.

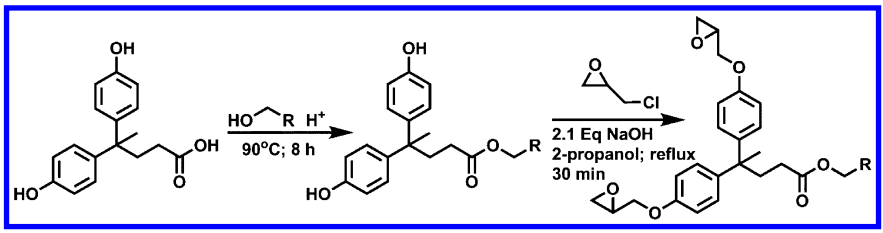

Scheme 1. Simple Two Step Synthetic Pathway for Synthesis of the Diglycidyl Ether of Alkyl Diphenolates

Publication Date (Web): June 18, 2015 | doi: 10.1021/bk-2015-1192.ch022

All prepared epoxy resins were liquid and exhibited Newtonian behavior under low sheer rates. Viscosities of the resins are reported in Table 1. The prepared resins exhibited sheer thinning at the higher sheer rates seen in Figure 1. The series of synthesized epoxy resins were observed to have different viscosities at room temperature with the longer chain esters being less viscous than the short chain esters (Table 1 and Figure 1). We believe that the origins of viscosity are due to a combination of side products and molecular interactions through the short chain esters. The length of the aliphatic ester chain appears to have a smaller effect on the viscosity in comparing the epoxy resins of butyl diphenolate (DGEBDP) and pentyl diphenolate (DGEPDP). No linear correlation between ester length and viscosity was observed.

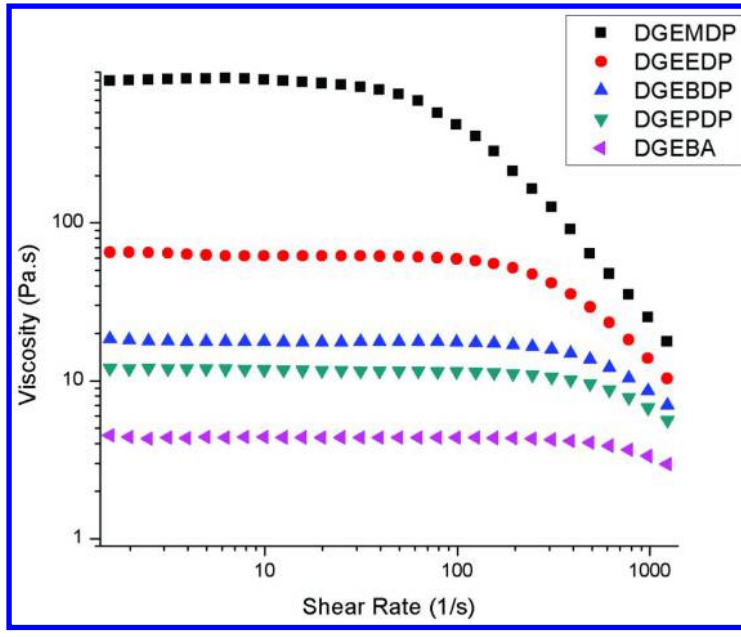

Figure 1. Parallel plate rotational rheology of synthesized epoxy resins compared to the DGEBA.

In Green Polymer Chemistry: Biobased Materials and Biocatalysis; Smith, et al.;
ACS Symposium Series; American Chemical Society: Washington, DC, 2015.

Table 1. Comparison of Viscosities and Epoxy Equivalent Weight Showing That the Presence of High Molecular Weight Fractions Is Minimal for All Resins Prepared

	Viscosity (Pa.s)	*Measured EEW*	*Theoretical EEW*[#]
DGEBA	4	175*	170
DGEMDP	792	215 ± 18	206
DGEEDP	63	222 ± 8.6	213
DGEBDP	18	243 ± 7.4	227
DGEPDP	12	265 ± 3.7	234

* From certificate of analysis supplied by vendor. # Determined from equations supplied by reference (*27*).

Publication Date (Web): June 18, 2015 | doi: 10.1021/bk-2015-1192.ch022

The large changes in viscosities are likely due to side reactions with the shorter chain aliphatic esters to produce a glycidyl ester *in-situ* by hydrolysis of the ester under alkaline conditions. Epoxy equivalent weight (EEW) was determined through the ASTM D1652 method. Each epoxy resin was run in triplicates to determine the average epoxy equivalent weight and values are reported in Table 1 against the theoretical EEW as determined from the literature (*27*). In comparing the measured EEW to the theoretical EEW the longer chain esters have higher values than the theoretical EEW, but the shorter chain esters are much closer to the theoretical values. Low epoxy equivalent weights indicate that the high viscosity is not due to oligomerization. If oligomers were formed they would show increase in epoxy equivalent weight above the theoretical EEW (*28*). Oligomers are more likely present in the longer chain esters due to their epoxy equivalent weights being above the theoretical values. Furthermore, if the glycidyl ester is being formed and mixtures of the two resins are present it would lower the epoxy equivalent weight.

To better understand if the shorter aliphatic esters would lead to side products due to hydrolysis under the alkaline conditions the ^{1}H NMR of the different epoxy resins were studied. The existence of a new set of peaks was observed to correspond to the side product depicted in Scheme 2.

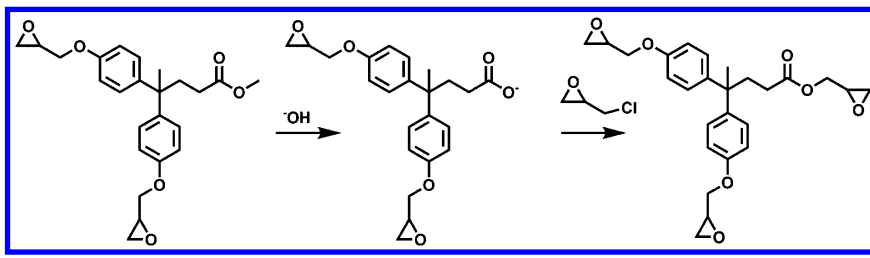

Scheme 2. Potential Pathway for a Side Reaction Resulting in the Glycidyl Ester

In Green Polymer Chemistry: Biobased Materials and Biocatalysis; Smith, et al.;
ACS Symposium Series; American Chemical Society: Washington, DC, 2015.

Publication Date (Web): June 18, 2015 | doi: 10.1021/bk-2015-1192.ch022

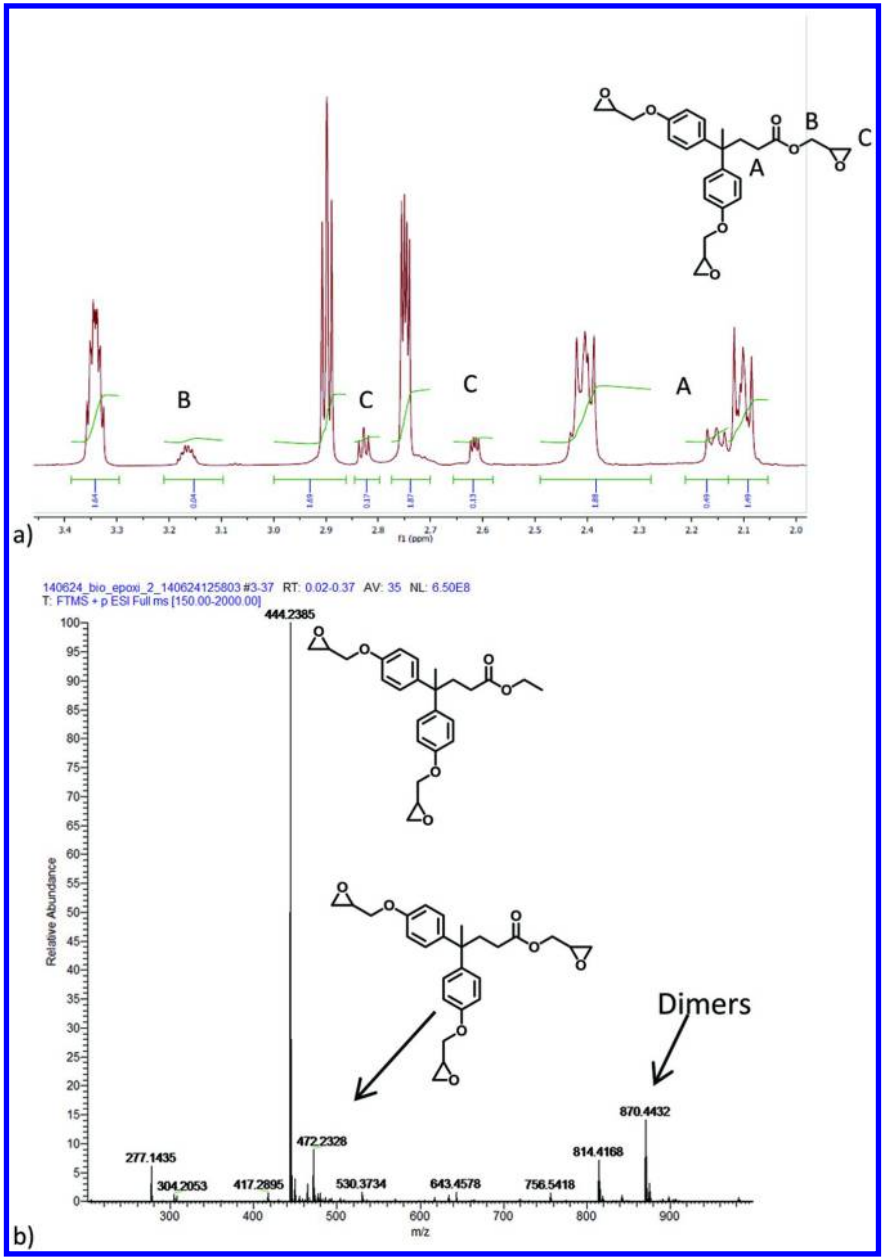

Figure 2. a) [1]H NMR of DGEMDP showing presence of a glycidyl ester with the ratio of peak A and peak 1 used to determine the amount of the side product. b) The mass ions of the major and side products in the direct infusion electron spray ionization for the DGEEDP. All m/z peaks contained NH_4^+.

In Green Polymer Chemistry: Biobased Materials and Biocatalysis; Smith, et al.;
ACS Symposium Series; American Chemical Society: Washington, DC, 2015.

Through integration, the peaks hypothesized to correspond to the glycidyl ester were compared to the peaks corresponding to the aliphatic ester. The relative quantity of the side product was estimated through the integration of the methylene hydrogens alpha to the glycidyl ester. We estimated that the diglycidyl ether of methyl diphenolate has about 15-20% of the glycidyl ester side product. Diglycidyl ether of ethyl diphenolate contains about 10% of the glycidyl ester side product. The diglycidyl ethers of butyl and pentyl diphenolate contained less than 3-4% (difficult to observe in the ^{1}H NMR). The mass for the glycidyl ester side product was confirmed through mass spectrometry at 472 m/z (glycidyl ester mass + NH_4) and can be seen in Figure 2. The abundances for the side products in the DGEBDP and DGEPDP were difficult to observe. The mass spectra indicated the existence of dimers for all epoxy resins, but were in low enough quantity that they could not be observed in the ^{1}H NMR. While mass spectrometry is not quantitative the relative counts of the glycidyl ester side products were extremely low for the DGEBDP and DGEPDP.

The different viscosities are important from a processing standpoint as higher viscosity resins will need higher temperatures to process for composites, but the high viscosity with relatively low epoxy equivalent weight may be suitable for other applications such as adhesives for foamed materials. The additional epoxy functionality of the glycidyl ester side product will also allow the resin to have an increased ability to crosslink.

Publication Date (Web): June 18, 2015 | doi: 10.1021/bk-2015-1192.ch022

Dynamic Mechanical Analysis and Parallel Plate Oscillatory Rheology

Samples for dynamic mechanical analysis (DMA) were run in triplicates and the values of the storage modulus and glass transition temperatures (determined from peak of loss modulus SI 5) can be seen in Table 2. The peaks of the tan δ (also related to T_g) can be seen in Figure 3c. All of the diglycidyl ethers of alkyl diphenolate resins (DGEADP) when cured under identical conditions to the DGEBA possessed comparable storage modulus values. The DGEMDP had a storage modulus that surpassed the DGEBA (Figure 3a) and a comparable glass transition temperature. The glass transition of the DGEMDP was only 7 °C lower than the DGEBA. The effect of the ester side chain on the storage modulus decreased moving from the methyl ester to the ethyl ester and remained constant for the butyl and pentyl esters. The relatively high storage modulus of the methyl ester epoxy may be due to higher concentrations of the glycidyl ester side product leading to increased crosslinking.

The glass transition temperatures (determined from peak of loss modulus) were observed to decrease in a linear fashion (Figure 3b). A similar shift in the peak of the tanδ is also observed (Figure 3c). The shifting of the T_g or T_α is likely due to the effect of the aliphatic side chain acting as an internal plasticizer by allowing movement of the main polymer chains at lower temperatures. The effect of the side chain is interesting because it represents a way to tune the glass transition temperature of the polymer without sacrificing the strength of the material.

Publication Date (Web): June 18, 2015 | doi: 10.1021/bk-2015-1192.ch022

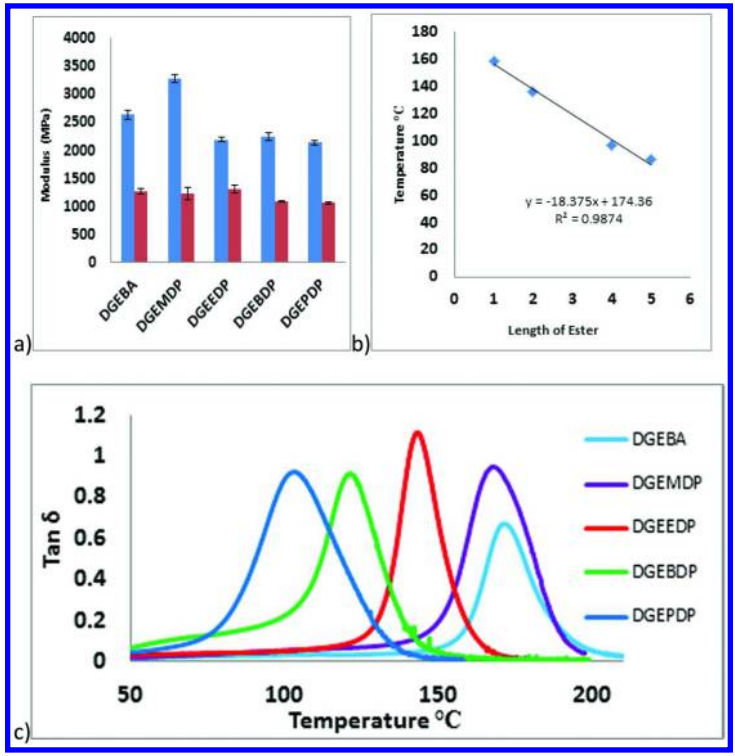

Figure 3. a) Storage (blue/left) and Young's modulus (red/right) as function of the ester length. b) Dependence of glass transition temperatures on ester chain length: a linear decrease as the length of the ester chain increases. c) The tanδ as function of the temperature: the tanδ of the DGEMDP overlaps well with DGEBA with only a slight shift in the peak and overall a broadening of the tanδ peaks when compared to DGEBA.

In order to determine if the side chains disrupted the three dimensional network of the thermosets we estimated the average molecular weight between crosslinks through oscillatory rheology. The following equation was used to determine the average molecular weight between crosslinks according to rubber elasticity theory (*29*):

$$M_x = \frac{\rho RT}{G_N}$$

Where M_x is equal to the average molecular weight between crosslinks, ρ is the density, G_N is the shear modulus (frequency independence of G′ storage modulus), R is the universal gas constant, and T is the temperature in kelvin. The

In Green Polymer Chemistry: Biobased Materials and Biocatalysis; Smith, et al.;
ACS Symposium Series; American Chemical Society: Washington, DC, 2015.

shear modulus was obtained with a frequency sweep from 0.1-100 rad/s of the cured samples at a temperature clearly above the tanδ peak (about tan δ + 50 °C), 0.1% strain, 15 N of normal force, and taking the average of the G' in the linear region. The densities of the cured samples were determined through the ASTM D792-13 method. The M_x values can be seen in Figure 4 in comparison to the DGEBA. Having a small amount of normal force was essential to ensure good adhesion/contact between the polymer sample and the rheometer. The prepared resins had M_x values that were comparable to the DGEBA. If the side chains severely interrupted the network formation there would most likely be drastic changes in the M_x values that would also be observable in storage modulus (E′) from dynamic mechanical analysis. The longer side chains appear to have small effect on network formation.

Overall the molecular weights between crosslinks are high when compared to molecular weights of epoxy resins determined by other methods (*30*, *31*). While the molecular weights are higher than other reported methods the shear parallel plate rheometer represents a method to explore the network of a thermoset material that minimizes clamping effects. Another method that is available is the in-situ curing on the rheometer. The curing of a high modulus polymer on a rheometer can be problematic during the cure due to high torques experienced during the cure cycle.

Publication Date (Web): June 18, 2015 | doi: 10.1021/bk-2015-1192.ch022

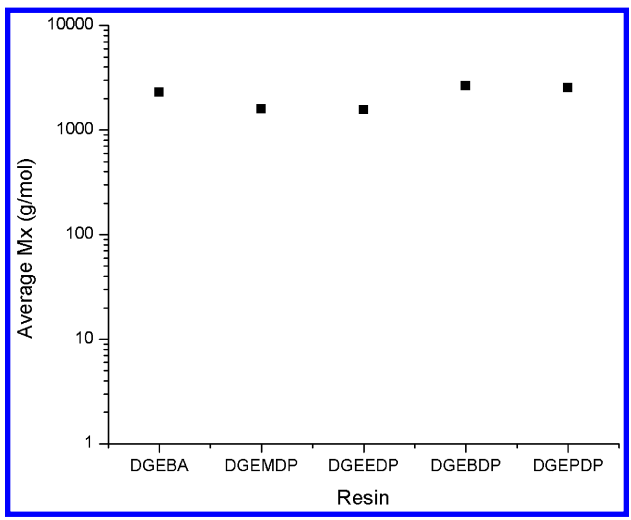

Figure 4. The average molecular weights between crosslinks as determined through parallel plate shear rheology using a normal force of 15 N to ensure good adhesion to the plates.

Publication Date (Web): June 18, 2015 | doi: 10.1021/bk-2015-1192.ch022

Tensile Testing

The tensile test revealed that all of the synthesized epoxy resins had similar properties to the DGEBA when cured under identical conditions. The stress-strain curves can be observed in Figure 5 with the Young's modulus being determined from the linear portion of the stress-strain curve. The tensile strength at break and percent strain at break are reported in Table 2. The trends seen in the Young's modulus data correlate with the storage modulus data from the dynamic mechanical analysis by not showing drastic changes due to the ester length. There is a small decrease in tensile strength with the increasing side chain length, but the values are very comparable to the DGEBA. The only drastic change that can be seen as an effect of the increasing side chain length is the glass transition temperature and in the longer esters.

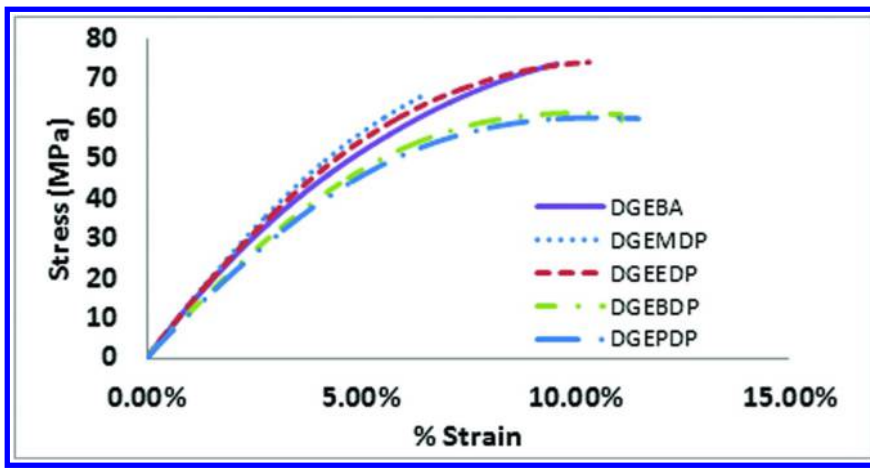

Figure 5. Stress strain curves of the prepared epoxy resins compared to the DGEB.

Thermal Stability

The effect of the ester length appeared to have no observable effect on thermal stability for the prepared epoxy resins under nitrogen. The onset of thermal degradation of DGEBA was 10 °C higher than the synthesized resins. A table depicting the thermal stability of the resins can be found in the SI 7. The use the DGEADP epoxy resins could be applicable to high temperature applications while being able to resist thermal degradation.

In Green Polymer Chemistry: Biobased Materials and Biocatalysis; Smith, et al.;
ACS Symposium Series; American Chemical Society: Washington, DC, 2015.

Table 2. DMA and Tensile Testing Results. Glass Transition Determined from Peak of the Loss Modulus (Alpha Transition)

	Storage Modulus at 25 °C (MPa)	*Glass Transition °C* (T_α) from peak of loss modulus*	*Youngs Modulus (MPa)*	*Tensile Strength (MPa)*	*% Strain at Break*
DGEBA	2640 ± 80	165	1263 ± 49	35 ± 3	8 ± 2
DGEMDP	3278 ± 63	158	1233 ± 107	41 ± 12	5 ± 2
DGEEDP	2186 ± 40	136	1306 ± 69	42 ± 4	9 ± 1
DGEBDP	2244 ± 76	96	1094 ± 10	36 ± 2	8 ± 2
DGEPDP	2141 ± 40	86	1058 ± 18	34 ± 0.4	11 ± 1

Publication Date (Web): June 18, 2015 | doi: 10.1021/bk-2015-1192.ch022

Conclusions

In summary, we have demonstrated an industrially relevant synthesis of bio-based epoxy resins that could act as drop-in replacements for the diglycidyl ether of bisphenol A. The diglycidyl ethers of alkyl diphenolates when cured under the same conditions as DGEBA gave similar modulus (both Young's and storage) values at room temperature. The effect of the ester side chain on the cured epoxy resins of DGEADP was found to correlate to a linear decrease in the glass transition temperature as the side chain increases in length. The short chain esters of DGEADP gave comparable glass transition temperatures to DGEBA, but the viscosities of the resins were significantly higher. The viscosity of the longer chain DGEADP was typical of a higher viscosity DGEBA resin and could be processed in a similar fashion. The origins of the high viscosity are potentially due to the concentration of side reaction products and intermolecular interactions that decrease as the length of the side chain increases. The length of the ester side chain did not significantly comprise the thermal stability of the bio-based epoxy resins and is comparable to the DGEBA. The epoxy resins of alkyl diphenolates are also liquids at room temperature allowing for low temperature processing for composite fabrication. The length of the ester gives a further control of the monomer viscosity with higher viscosity resins potentially being ideal for adhesives and the lower viscosity resins could be more suitable for composites. Additionally the thermosets produced from DGEADP have an ester side chain, which should assist in promotion of long service life of the material, but also allows for a potential pathway to assist in decomposition of the material.

In Green Polymer Chemistry: Biobased Materials and Biocatalysis; Smith, et al.;
ACS Symposium Series; American Chemical Society: Washington, DC, 2015.

Materials and Methods

Diphenolic Acid >98% from TCI America (D1274) was used as received. Epichlorohydrin, sodium hydroxide, methanol, ethanol, 1-butanol, and 1-pentanol were purchased from Sigma Aldrich and used as received. All reagents and solvents were purchased from Sigma Aldrich and used as received.

Synthesis of Diphenolate Esters and Epoxy Resins

Diphenolate Esters

50 g of diphenolic acid was charged to a 1 L round bottom flask with 400 mL of alcohol (ethanol or methanol), 1 mL of concentrated sulfuric acid, and refluxed overnight. The majority of the alcohol was removed by rotary evaporation with gentle heating. The ester was taken up in ethyl acetate and washed with distilled deionized water, 10% sodium bicarbonate, distilled deionized water, and dried over anhydrous magnesium sulfate. Magnesium sulfate was filtered off and ethyl acetate was removed by rotary evaporation till a white solid was obtained with 85% yield.

Methyl Diphenolate, ^{1}H NMR (500 MHz, DMSO-d_6):

ppm δ 1.45 (s, 3H), 2.00 (t, 2H), 2.20 (t, 2H), 3.50 (s, 3H), 6.60 (d, 4H), 6.90 (d, 4H), 9.10 (s, 2H)

Ethyl Diphenolate, ^{1}H NMR (500 MHz, DMSO-d_6):

ppm δ 1.11 (t, 3H), 1.45 (s, 3H), 2.00 (t, 2H), 2.20 (t, 2H), 4.00 (q, 2H), 6.60 (d, 4H), 6.90 (d, 4H), 9.10 (s, 2H)

50 g of diphenolic acid was charged to a 1 L round bottom flask with 400 mL of alcohol (1-butanol or 1-pentanol), 1 mL of concentrated sulfuric acid, and refluxed overnight. The ester was taken up in ethyl acetate and washed with distilled deionized water, 10% sodium bicarbonate, distilled deionized water, and dried over anhydrous magnesium sulfate. The magnesium sulfate was filtered off and ethyl acetate/alcohol mixture was removed by rotary evaporation. Trace amounts of alcohol were removed by vacuum distillation until a light orange/yellow glassy solid obtained with 85-97% yield.

Butyl Diphenolate, ^{1}H NMR (500 MHz, DMSO- d_6):

ppm δ 0.84 (t, 3H), 1.28 (m, 2H), 1.38 (m , 2H), 1.45 (s, 3H), 2.00 (t, 2H), 2.20 (t, 2H), 3.94 (q, 2H), 6.60 (d, 4H), 6.90 (d, 4H), 9.10 (s, 2H)

Pentyl Diphenolate, ^{1}H NMR (500 MHz, DMSO- d_6):

ppm δ 0.84 (t, 3H), 1.28 (m, 4H), 1.38 (m , 2H), 1.45 (s, 3H), 2.00 (t, 2H), 2.20 (t, 2H), 3.94 (q, 2H), 6.60 (d, 4H), 6.90 (d, 4H), 9.10 (s, 2H)

Synthesis of DGEADP

A three neck 1 L round bottom flask was equipped with overhead mechanical stirring, water condenser and pressure equalizing dropping funnel and charged with 25.00 grams of alkyl diphenolate, 15 equivalents of epichlorohydrin, 115

Publication Date (Web): June 18, 2015 | doi: 10.1021/bk-2015-1192.ch022

mL 2-propanol, and brought to reflux with stirring. A 20% solution of aqueous sodium hydroxide containing 2.1 equivalents of NaOH was added dropwise to the reaction and kept at reflux for 30 minutes after addition. The reaction mixture was cooled, filtered, and the majority of 2-propanol removed under rotary evaporation. Any remaining solids were filtered off. The reaction mixture was then neutralized with two portions of 3 M acetic acid, washed with 2 portions of distilled deionized water, and dried over anhydrous magnesium sulfate. Any remaining 2-propanol or epichlorohydrin was removed by rotary evaporation and vacuum distillation. The product obtained was a viscous light yellow liquid with 85-97% yield.

Diglycidyl Ether of Methyl Diphenolate and Proposed Glycidyl Ester Side Product ^{1}H NMR (500MHz, $CDCl_3$):

Glycidyl Ether Functionality: ppm δ 2.75 (dd, J = 5.10 Hz $2H_{\gamma b}$), 2.90 (observed triplet, J = Hz 4.48 $2H_{\gamma a}$), 3.34 (m, $2H_{\beta a}$), 3.94 (dd, J = 11.31 Hz $2H_{\alpha b}$), 4.19 (dd, J = 10.84 Hz $2H_{\alpha a}$)

Glycidyl Ester Side Product: ppm δ 1.45 (s, 3H), 2.15, (t, 2H), 2.20 (t, 2H), 2.61 (dd, J = 4.86 Hz, $2H_{\gamma b}'$), 2.83 (observed triplet, J = 4.32 Hz, $2H_{\gamma a}'$), 3.17 (m, $2H_{\beta a}'$), 3.85 (dd, J = 12.64 Hz $2H_{\alpha b}''$), 4.37 (dd, J = 12.10 Hz $2H_{\alpha a}'$), 6.60 (d, 4H), 6.90 (d, 4H)

Previously reported peaks corresponding to the methyl and ethyl ester remained consistent.

Diglycidyl Ether of Butyl and Pentyl Diphenolate ^{1}H NMR (500MHz, $CDCl_3$):

Glycidyl Ether Functionality: ppm δ 2.75 (dd, J = 5.10 Hz $2H_{\gamma b}$), 2.90 (observed triplet, J = Hz 4.48 $2H_{\gamma a}$), 3.34 (m, $2H_{\beta a}$), 3.94 (dd, J = 11.31 Hz $2H_{\alpha b}$), 4.19 (dd, J = 10.84 Hz $2H_{\alpha a}$)

Previously reported peaksc corresponding to the butyl and pentyl diphenolate esters remained consistent.

Preparation of samples for testing

The epoxy resins were mixed with near stoichiometric amounts of isophorone diamine (IPDA) by dividing the amine hydrogen equivalent weight (AHEW) of IPDA by the EEW of the desired epoxy and multiplied by 100 to give the amount of diamine per hundred parts of epoxy resin (*27*). This method was ideal as all the prepared resins contained small amounts of higher molecular weight fractions. The resins were mixed vigorously by hand with the appropriate amount of IPDA and degassed by centrifugation in a syringe. The resins were then syringed into stainless steel molds coated in a small amount of PTFE mold release agent. The three different mold geometries used were: ASTM type V tensile bars, rectangular dual cantilever bars (35 mm x 12 mm x 3 mm), and rheology discs (25 mm x 2 mm). The curing of the resins was adopted from literature (*32*) and were allowed to cure overnight at ambient conditions in the molds and then compression molded for four hours at 80 °C and four hours at 160 °C with 2 metric tons of pressure. The degree of cure was verified by modulated differential scanning calorimetry (m-DSC) and Fourier transform infrared spectroscopy (FTIR). The degree of cure was determined to be high through no significant changes in the non-reversible heat capacity and a significant decrease in the epoxide peak in the FTIR.

Publication Date (Web): June 18, 2015 | doi: 10.1021/bk-2015-1192.ch022

Dynamic Mechanical Analysis

A Thermal Analysis Q800 operating in dual cantilever mode with an amplitude of 10 um was used to determine the storage modulus and glass transition temperature (determined by peak of the loss modulus) by scanning from 0 °C to 200 °C. Samples were run in triplicates.

Rheology

The viscosity of the different resins was determined through rotational rheology at 25 °C using a Thermal Analysis AR-G2 rheometer equipped with 25 mm stainless steel parallel plate geometry. The sheer rate was swept from 1.25 - 1250 1/s under steady state flow with an equilibration time of 1 minute and a gap of 1000 mm. Viscosity was reported as an average from the Newtonian region.

To determine the average molecular weight between crosslinks a Thermal Analysis AR-G2 rheometer was employed and was equipped with 25 mm stainless steel parallel plate geometry and nitrogen flow. The testing was conducted under 15 N of normal force in order to ensure good contact between the plates and the sample and the frequency was swept from 0.1 rad/s to 100 rad/s with the shear modulus being determined from the average the storage modulus (G') that was frequency independent. Each sample was run at a temperature of 50 °C higher than the peak of the tan δ.

Tensile Testing

Tensile testing was conducted on compression molded samples using an Instron 4204 equipped with a 5 kN load cell following the ASTM D638 method with a crosshead speed of 1mm/min. Samples were of a ASTM type V geometry and only samples devoid of bubbles and defects were reported.

Thermal Gravimetric Analysis

The thermal stability of the prepared resins was studied by thermal gravimetric analysis using a Thermal Analysis Q50 with an alumina pan. The samples were of about 10 mg each and were run from room temperature to 800 °C at a rate of 20 °C per minute under constant N_2 flow.

Acknowledgments

The authors would like to thank National Science Foundation's PIRE program for supporting the research. We would also like to thank Professors Jim Crivello, Ica-Manas Zloczower, Chang Ryu, and Phillipe Dubois for their insight and suggestions.

In Green Polymer Chemistry: Biobased Materials and Biocatalysis; Smith, et al.;
ACS Symposium Series; American Chemical Society: Washington, DC, 2015.

Publication Date (Web): June 18, 2015 | doi: 10.1021/bk-2015-1192.ch022

Publication Date (Web): June 18, 2015 | doi: 10.1021/bk-2015-1192.ch022

References

1. Gal, J. *INSIGHT: Aerospace, light-weight cars to drive composite demand*; http://www.icis.com/resources/news/2012/10/24/9607060/insight-aerospace-light-weight-cars-to-drive-composite-demand/ (accessed Jun 6, 2014).
2. Pilato, L. A.; Michno, M. J. *Advanced Composite Materials*; Springer-Verlag: Berlin Heidelberg, 1994.
3. Auvergne, R.; Caillol, S.; David, G. *Chem. Rev.* **2014**, *114*, 1082–1115.
4. Maffini, M. V; Rubin, B. S.; Sonnenschein, C.; Soto, a M. *Mol. Cell. Endocrinol.* **2006**, *254*, 179–186.
5. Chen, M.-Y.; Ike, M.; Fujita, M. *Environ. Toxicol.* **2002**, *17*, 80–86.
6. O'Connor, J. C.; Chapin, R. E. *Pure Appl. Chem.* **2003**, *75*, 2099–2123.
7. U.S. Government F.D.A. *Indirect Food Additives: Adhesives and components of coatings*; United States, 2013; Vol. 78, pp 41840–41843.
8. Mantzaridis, C.; Brocas, A.-L.; Llevot, A.; Cendejas, G.; Auvergne, R.; Caillol, S.; Carlotti, S.; Cramail, H. *Green Chem.* **2013**, *15*, 3091–3098.
9. Fourcade, D.; Ritter, B.; Walter, P. *Green Chem.* **2013**, *15*, 910–918.
10. Łukaszczyk, J.; Janicki, B.; Kaczmarek, M. *Eur. Polym. J.* **2011**, *47*, 1601–1606.
11. Aouf, C.; Lecomte, J.; Villeneuve, P.; Dubreucq, E.; Fulcrand, H. *Green Chem.* **2012**, *14*, 2328–2336.
12. Aouf, C.; Nouailhas, H.; Fache, M.; Caillol, S.; Boutevin, B.; Fulcrand, H. *Eur. Polym. J.* **2013**, *49*, 1185–1195.
13. Green, M. M.; Wittcoff, H. A. *Organic Chemistry Principles and Industrial Practice*; Wiley-VCH: Weinheim, 2003; pp 45–63.
14. Gilbeau, P.; Balthasart, D. Glycerol-based product, process for obtaining same and use thereof in the manufacturing of dichloropropanol. U.S. Patent 8,314,205 B2, November 20, 2012.
15. Gilbeau, P. Method for Making an Epoxide. U.S. Patent 2012/0199786 A1, August 9, 2012.
16. Pan, T.; Deng, J.; Xu, Q.; Xu, Y.; Guo, Q.-X.; Fu, Y. *Green Chem.* **2013**, *15*, 2967–2974.
17. Habibi, Y.; Lucia, L. a; Rojas, O. J. *Chem. Rev.* **2010**, *110*, 3479–3500.
18. Demirbaş, a. *Energy Convers. Manage.* **2000**, *41*, 633–646.
19. Kawamoto, H.; Horigoshi, S.; Saka, S. *J. Wood Sci.* **2007**, *53*, 168–174.
20. Bu, Q.; Lei, H.; Ren, S.; Wang, L.; Zhang, Q.; Tang, J.; Ruan, R. *Bioresour. Technol.* **2012**, *108*, 274–279.
21. The, A.; Klohs, M. W.; Extraction, H. *J. Am. Chem. Soc.* **1954**, *5416*, 7–8.
22. Guo, Y.; Li, K.; Clark, J. H. *Green Chem.* **2007**, *9*, 839–841.
23. Blair, R. M.; Fang, H.; Branham, W. S.; Hass, B. S.; Dial, S. L.; Moland, C. L.; Tong, W.; Shi, L.; Perkins, R.; Sheehan, D. M. *Toxicol. Sci.* **2000**, *54*, 138–153.
24. Van de Vyver, S.; Geboers, J.; Helsen, S.; Yu, F.; Thomas, J.; Smet, M.; Dehaen, W.; Sels, B. F. *Chem. Commun.* **2012**, *48*, 3497–3499.
25. Zúñiga, C.; Bonnaud, L.; Lligadas, G.; Ronda, J. C.; Galià, M.; Cádiz, V.; Dubois, P. *J. Mater. Chem. A* **2014**, *2*, 6814–6822.

26. Zhang, R.; Moore, J. a. *Macromol. Symp.* **2003**, *199*, 375–390.
27. Pham, H. Q.; Marks, M. J. In *Ullmann's Encyclopedia of Industrial Chemistry, Electronic Release*; Elvers, B., Ed.; Wiley-VCH: Weinheim, 2012; pp 155–244.
28. Dorsey, J. G.; Dorsey, G. F.; Rutenberg, A. C.; Green, L. A. *Anal. Chem.* **1977**, *49*, 1144–1145.
29. Flory, P. J. *Principles of Polymer Chemistry*; Cornell University Press: New York, 1953; pp 432–493.
30. Chrysanthos, M.; Galy, J.; Pascault, J.-P. *Macromol. Mater. Eng.* **2013**, *298*, 1209–1219.
31. Amaral, C.; Rodriguez, R. *Polym. Eng. Sci.* **2013**, 1–7.
32. Garcia, F.; Soares, B. *J. Appl. Polym. Sci.* **2007**, *106*, 2047–2055.

Publication Date (Web): June 18, 2015 | doi: 10.1021/bk-2015-1192.ch022

Publication Date (Web): June 18, 2015 | doi: 10.1021/bk-2015-1192.ch023

Chapter 23

Influence of Furanyl Building Blocks on the Cure Kinetics of a Renewable Epoxy-Amine System

Fengshuo Hu, Majid Sharifi, and Giuseppe Palmese*,[1]

Department of Chemical & Biological Engineering, Drexel University, Philadelphia, Pennsylvania 19104, United States
[1]Present address: Department of Chemical & Biological Engineering, Drexel University, Philadelphia, Pennsylvania 19104, United States
***E-mail: grp27@drexel.edu.**

Recently, renewable furan-based epoxy systems containing furanyl building blocks in place of phenyl building blocks were reported by our group. Furan-based epoxy systems showed better mechanical properties compared with their phenyl analogues. In this work, an epoxy-amine cure kinetics study of analogous systems with furanyl and phenyl building blocks was conducted to evaluate the relative effect of the furan building block on the cure behavior. The reactivity rates of the epoxy-primary amine reaction (k_1) and epoxy-secondary amine reaction (k_2) were obtained, and the results suggest that hydrogen bonding on the furanyl ring potentially affects the reactivity and reactivity ratio thus influencing not only processing characteristics, but also the thermal and mechanical properties of furan-based epoxy systems relative to phenyl analogues.

Introduction

Currently, thermosetting materials produced with renewable sources have received attention due to the economic and environmental concerns of petroleum sources which are primarily used to prepare incumbent thermosetting resins. So

In Green Polymer Chemistry: Biobased Materials and Biocatalysis; Smith, et al.;
ACS Symposium Series; American Chemical Society: Washington, DC, 2015.

far, several types of biomass, including lignin (*1*), cellulose (*2*), hemicellulose (*3*), starch (*4*), chitin (*5*) and triglycerides (*6*), have been investigated for preparing thermosetting materials. These renewable sources are abundant and robust, and the bio-based thermosets derived from them are promising. Recently, we reported a study comparing the thermal and mechanical properties of thermosets prepared using two analogue epoxy monomers in which the sole structural difference was the central building block (*7*). Furan-based epoxy resins were shown to possess improved thermal and mechanical properties compared with phenyl-based analogues. For example, using 4,4′-methylene biscyclohexanamine (PACM) as the amine hardener, 2,5-bis[(2-oxiranylmethoxy)-methyl]-furan (BOF) not only possesses a glass transition temperature (T_g) of 71°C, 16°C higher than that of 2,5-bis[(2-oxiranylmethoxy)methyl]-benzene (BOB), but also a room temperature storage modulus (E'_{rt}) of 2.8GPa, 0.6GPa greater than that of BOB. These findings are promising because furanyl chemicals can be readily produced from several abundant biomasses including cellulose and hemicellulose, and they are now more likely to be considered as promising candidates to substitute petroleum-based phenyl chemicals currently used for producing high-performance thermosetting materials. Two hypotheses were proposed to explain the elevated T_g and E'_{rt} of BOF systems: first the presence of hydrogen bonding that associated with the furanyl building blocks and second the restricted rotational relaxation of furanyl building blocks in cured networks due to their asymmetric geometry. Cure kinetics studies of BOF-PACM, BOB-PACM and for comparison, DGEBA-PACM were conducted to elucidate the influence of the furanyl building block on the cure behavior as well as on the possible associated effects on the formation of network structure that could influence thermal and mechanical properties of these thermosetting materials.

Publication Date (Web): June 18, 2015 | doi: 10.1021/bk-2015-1192.ch023

Experimental Section

Materials

Epoxy resins and amine hardener used in this work are summarized in Figure 1. Difunctional epoxy resins, 2,5-bis[(2-oxiranylmethoxy)-methyl]-furan (BOF) and 2,5-bis[(2-oxiranylmethoxy)methyl]-benzene (BOB) were prepared by following reported methods (*7*); diglycidyl ether of bisphenol A (DGEBA, n = 0.13) was supplied by Miller-Stephenson chemical company, USA. Their epoxy equivalent weights (EEW) were determined by following ASTM epoxide titration technique, D 1652-97. The experimental results, 120.0 g/eq. for BOF, 125.0 g/eq. for BOB and 188.0 g/eq. for DGEBA, matched theoretical values. Tetrafunctional amine hardener, 4,4′-methylene biscyclohexanamine (PACM) with a 52.5 g/eq. amine hydrogen equivalent weight (AHEW), was provided by Air Products, USA. Cure kinetics were investigated with reaction mixtures having stoichiometric quantities of epoxy and amine on the basis of the EEW and AHEW values.

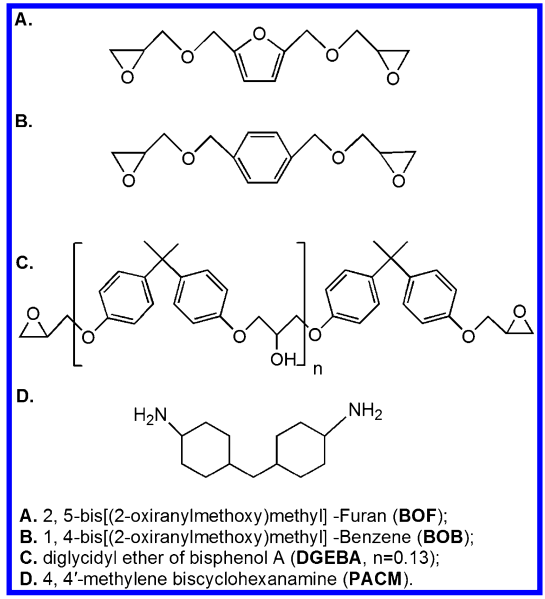

Figure 1. Epoxy resins and amine hardener used in this study.

Fourier Transform Infrared (FTIR) Spectroscopy

Cure kinetics studies of BOF-PACM, BOB-PACM and DGEBA-PACM were conducted using FTIR spectroscopy in the near-infrared (N-IR, 8000 – 4000 cm^{-1}) at 60°C. A Nexus 6700 FTIR spectrometer (Thermo-Nicolet Corp.) with a CaF_2 beam splitter and a DTGS KBr detector was used. Spectra were obtained at regular time intervals using 4 cm^{-1} resolution with 32 scans per spectrum. N-IR spectroscopy was used to monitor the concentrations of epoxy [EP] and primary amine [PA] in the resin mixture during reaction. Mass balance equations were employed to obtain the concentrations of secondary amines [SA] and tertiary amines [TA]. Epoxy peaks at 4529 cm^{-1} of DGEBA and 4527 cm^{-1} of BOF and BOB, respectively, were used to track the epoxy concentration. The primary amine peak at 4930 cm^{-1} of PACM was used for monitoring the primary amine concentration.

Experimental Setup

Low hydroxyl silica glass tubes with 1.60 ± 0.05 mm inside diameter and 65 mm length were employed as sample holders (*8*). Samples were prepared by mixing 1.000 gram of epoxy and the stoichiometric amount of PACM. The mixtures were then degassed and injected into a glass tube. To remove moisture, glass tubes were kept at 130°C overnight before use. A temperature controlled aluminum sample holder shown schematically in Figure 2 was used for the N-IR

In Green Polymer Chemistry: Biobased Materials and Biocatalysis; Smith, et al.;
ACS Symposium Series; American Chemical Society: Washington, DC, 2015.

experiments. This device allowed for control of temperature within ± 0.5°C of the 60°C set point. A background scan was conducted before each experiment using the glass tube before filling.

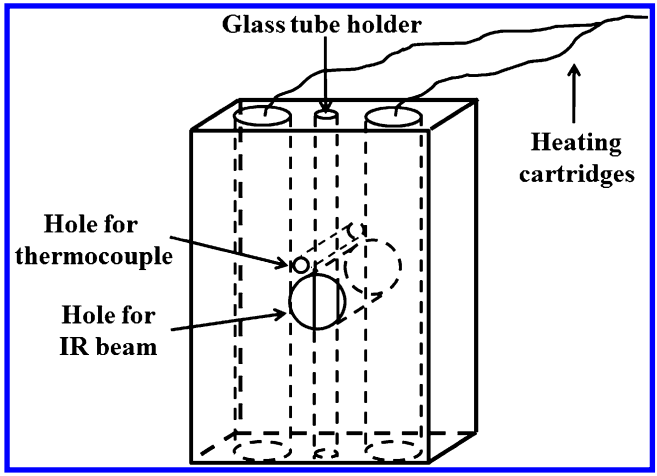

Figure 2. Sketch of the temperature controlled FTIR glass tube holder.

Publication Date (Web): June 18, 2015 | doi: 10.1021/bk-2015-1192.ch023

Numerical Procedure

The experimental concentrations of epoxy and primary amine were fitted to a two-parameter auto-catalytic model using a least-squares approach. A MATLAB code was generated and used for this purpose. The auto-catalytic rate equations were solved using MATLAB nonlinear ODE solver (ode45). Rate parameters for the set of numerical solutions that showed the least deviation from the experimental data points (epoxy and primary amine concentrations) were used as the rate constants for primary and secondary amine reactions.

Results and Discussion

The objective of this study was to evaluate cure behaviors of BOF-PACM, BOB-PACM and DGEBA-PACM in order to understand the influence of furanyl and phenyl building blocks on the cure reaction rates and network structure development. Epoxy-amine cure reactions include epoxy-primary amine addition, epoxy-secondary amine addition, epoxy-hydroxyl etherification and epoxy-epoxy etherification. The occurrence and the extent of these reactions are affected by the cure temperature, formulation, and the presence of impurities and solvents. In this study only the epoxy-amine reactions were considered, as previous work showed that etherification was minimal for the investigated conditions (*9*). Hydroxyl groups present in the epoxy-amine system are known to catalyze the epoxy-amine addition reactions and need to be considered. Thus in our analysis we were

interested in epoxy [EP], primary amine [PA], secondary amine [SA], tertiary amine [TA] and hydroxyl [OH] concentrations as a function of the reaction time.

Epoxy-amine reactions can proceed via an auto-catalytic pathway, given by Equations 1 and 2, or a non-catalytic pathway, Equations 3 and 4.

$$[PA] + [EP] + [OH] \overset{k_1}{\rightarrow} [SA] + 2 * [OH] \quad (1)$$

$$[SA] + [EP] + [OH] \overset{k_2}{\rightarrow} [TA] + 2 * [OH] \quad (2)$$

$$[PA] + [EP] \overset{k_1'}{\rightarrow} [SA] + [OH] \quad (3)$$

$$[SA] + [EP] \overset{k_2'}{\rightarrow} [TA] + [OH] \quad (4)$$

In these equations k'_1 and k'_2 were the kinetic parameters of epoxy-primary amine and epoxy-secondary amine addition reactions in the non-catalytic pathway, and k_1 and k_2 were those in the auto-catalytic pathway, respectively. The auto-catalytic pathway was selected due to the fact that DGEBA possessed a significant hydroxyl concentration, and BOF-PACM and BOB-PACM systems also possessed a comparable hydroxyl concentration as the DGEBA-PACM one because of the presence of small amounts of water despite drying.

As described in the experimental section, [EP] and [PA] were measured using N-IR. The concentrations [SA], [TA] and [OH] were obtained from mass balance relations as shown below. The initial epoxy concentration was related to epoxy, secondary amine and tertiary amine concentrations by Equation 5, and the initial primary amine concentration was related to primary amine, secondary amine and tertiary amine concentrations by Equation 6.

$$[EP]_0 = [EP] + [SA] + 2 * [TA] \quad (5)$$

$$[PA]_0 = [PA] + [SA] + [TA] \quad (6)$$

In these equations $[EP]_0$ and $[PA]_0$ are the concentrations (mol/L) of epoxy and primary amine in the system at $t = 0$, and [EP], [PA], [SA] and [TA] were corresponding concentrations at any time t. By re-arranging Equations 5 and 6, [SA] and [TA] concentrations, respectively, are expressed by Equations 7 and 8 below.

$$[SA] = 2 * ([PA]_0 - [PA]) - ([EP]_0 - [EP]) \quad (7)$$

$$[TA] = ([EP]_0 - [EP]) - ([PA]_0 - [PA]) \quad (8)$$

Using these equations, secondary and tertiary amine concentrations were calculated with the known and measured epoxy and primary amine concentrations.

Since the epoxy-amine reaction is catalyzed by the hydroxyl groups and as one hydroxyl group is formed for every epoxy-amine addition reaction, an expression is needed for the hydroxyl concentration as a function of conversion. The hydroxyl concentration [OH] is given by Equation 9.

$$[OH] = [OH]_{auto} + [OH]_0 \quad (9)$$

In Green Polymer Chemistry: Biobased Materials and Biocatalysis; Smith, et al.;
ACS Symposium Series; American Chemical Society: Washington, DC, 2015.

Publication Date (Web): June 18, 2015 | doi: 10.1021/bk-2015-1192.ch023

In this equation $[OH]_0$ and [OH] were the hydroxyl concentrations in the system at $t = 0$ and t, respectively. $[OH]_{auto}$ was the concentration of hydroxyl groups resulting from the epoxy-amine reaction at time t given by Equation 10.

$$[OH]_{auto} = [SA] + 2 * [TA] \quad (10)$$

$[OH]_0$ was predominately determined by the n value of DGEBA epoxy monomer in the DGEBA-PACM system, and by the initial hydroxyl concentration presumably from water in the BOF-PACM and BOB-PACM cases. In the DGEBA-PACM system, $[OH]_0$ was given by Equation 11, where $[OH]_0$ was proportional to $[EP]_0$ as indicated from the chemical structure of DGEBA.

$$[OH]_0 = \frac{0.13}{2} * [EP]_0 \quad (11)$$

In the BOF-PACM and BOB-PACM systems, $[OH]_0$ was calculated from the ratio between epoxy and hydroxyl peak heights in the N-IR spectrum taken at $t = 0$. As previously mentioned, these initial hydroxyl concentrations were possibly due to the trace moisture in the systems.

Figure 3 shows the evolution of N-IR spectra of BOF-PACM, BOB-PACM and DGEBA-PACM systems as the reactions proceed at 60°C for 3 hours. The spectra were normalized, and 10 representative spectra with an 18 minute interval between each are shown. Two epoxy peaks at 6075 and 4527 cm^{-1} for BOF, 6062 and 4527 cm^{-1} for BOB, 6063 and 4527 cm^{-1} for DGEBA can be used to track the epoxy concentration. However, the peak at 4527 cm^{-1} was preferred, since the one at the higher wavenumber typically overlapped with the aromatic peak in its neighborhood (*9*). The primary amine peak at 4929 cm^{-1} was used to track the primary amine concentration. The extent of cure, α, based on the consumption of the epoxy groups, was obtained from the ratio of the corresponding peak heights at times $t = t$ and $t = 0$. As shown in Figure 3, in these three systems, the epoxy and primary amine peaks disappeared and the hydroxyl peak (7099 cm^{-1}) appeared as cure progressed. The peak at 6507 cm^{-1} represented the combination of both primary and secondary amines, and it also disappeared over time. According to the spectra, primary amines were fully consumed; however, the epoxy peak and the primary-secondary amine peak were decreasing, signifying that the epoxy-amine reactions were still proceeding after 3 hours at 60°C. The reason for this was that the reactions became diffusion controlled as the systems reached vitrification, and this was particularly evident for the DGEBA-PACM system.

In cooperation with the N-IR data, the initial epoxy and primary amine concentrations, $[EP]_0$ and $[PA]_0$, were important for determining the rate constants. $[EP]_0$ and $[PA]_0$ were calculated using component weights, their densities at 60°C and the assumption that no volumetric change occurred at mixing. Densities of the components were measured using a 25 mL glass volumetric flask at both room temperature and 60°C, and the results are summarized in Table 1, together with the molecular weights, the EEW and AHEW values. These values were used to establish the formulations of the epoxy-amine systems and to calculate the initial conditions, i.e. $[EP]_0$ and $[PA]_0$, for the rate equations as summarized in Table 2.

Publication Date (Web): June 18, 2015 | doi: 10.1021/bk-2015-1192.ch023

Publication Date (Web): June 18, 2015 | doi: 10.1021/bk-2015-1192.ch023

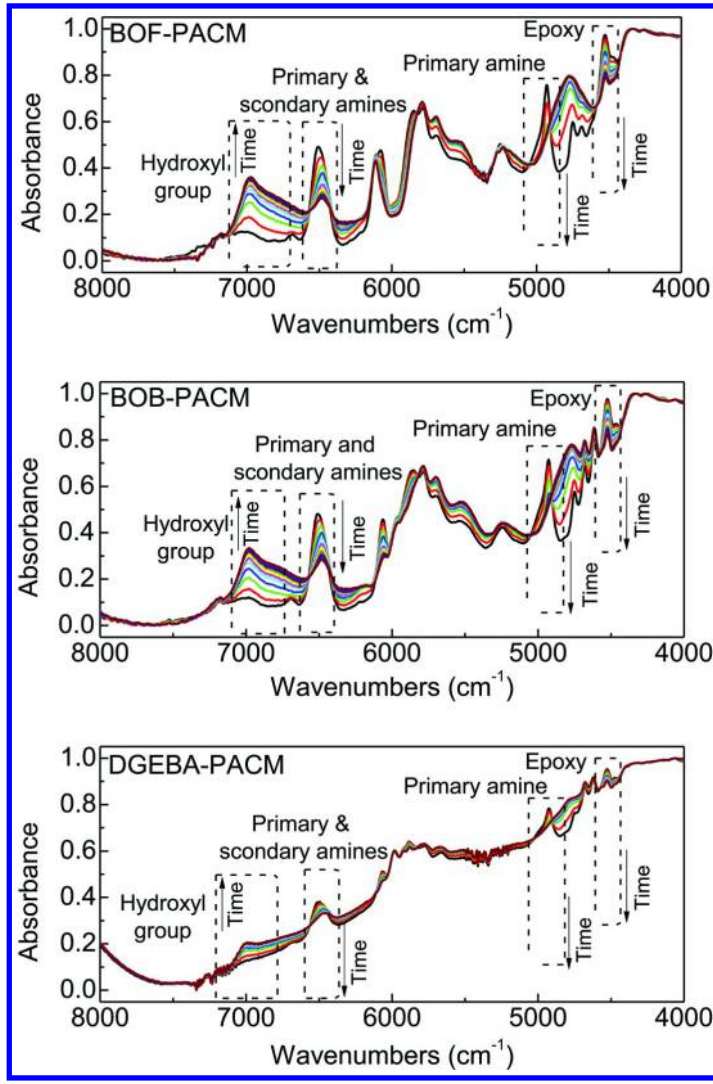

Figure 3. Selected spectra of BOF-PACM, BOB-PACM and DGEBA-PACM as the cure reactions occurred at 60°C for 3 hours. The interval of the present spectra was 18 minutes. The epoxy peak was present at 4527 cm-1 and primary amine peak was present at 4929 cm-1.The epoxy and amine peaks shrunk over time while the hydroxyl peak grew.

The epoxy and primary amine concentrations obtained from N-IR experiments were used in conjunction with Equations 7 and 8 to calculate the secondary and tertiary amine concentrations and resulting time dependent concentration profiles. Figures 4, 5 and 6 show representative profiles for the BOF-PACM, BOB-PACM,

and DGEBA-PACM systems, respectively. In all cases, the depletion of epoxy and primary amine, the formation and depletion of secondary amine and the formation of tertiary amines were observed.

Table 1. Molecular Weights of the Components, Their Densities at Room Temperature (rt) and 60°C, and the EEW and AHEW Values

Component	*Molecule Weight (g/mol)*	*Density @ rt (g/ml)*	*Density @ 60°C(g/ml)*	*EEW (g/eq.)*	*AHEW (g/eq.)*
BOF	240.3	1.1858	1.1634	120.0	-
BOB	250.3	1.1501	1.1214	125.0	-
DGEBA	377.1	1.1604	1.1344	188.0	-
PACM	210.4	0.9590	0.9380	-	52.5

Table 2. Resin Formulations of the Epoxy-Amine Systems and the Initial Concentrations of Epoxy and Primary Amine Groups

System	W_{epoxy} *(g)*	W_{amine} *(g)*	$[EP]_0$ *(mol/L)*	$[PA]_0$ *(mol/L)*
BOF-PACM	1.0000	0.4375	3.1384	1.5682
BOB-PACM	1.0000	0.4200	2.9826	1.4903
DGEBA-PACM	1.0000	0.2793	2.2488	1.1255

Differential equations describing the time dependent reaction behaviors of the systems, based on Equations 1, 2, 7, 8, 9, and 10 and 11, are given by Equations 12 and 13 below.

$$\frac{d[EP]}{dt} = -k_1 * [PA] * [EP] * ([OH]_{auto} + [OH]_0) - k_2 * [EP] * [SA] * ([OH]_{atuo} + [OH]_0) \quad (12)$$

$$\frac{d[PA]}{dt} = -k_1 * [PA] * [EP] * ([OH]_{auto} + [OH]_0) \quad (13)$$

The above set of ordinary differential equations was used to fit the experimental concentrations such as those shown in Figures 4, 5 and 6 and to obtain the best fit of k_1 and k_2 values as described previously. These values are reported in Table 3. Three experiments were conducted for the BOB and BOF systems, and all results are provided in Table 3 with averages. In addition, Figures 4, 5 and 6 show the best-fit curves corresponding to the k_1 and k_2 values obtained

In Green Polymer Chemistry: Biobased Materials and Biocatalysis; Smith, et al.;
ACS Symposium Series; American Chemical Society: Washington, DC, 2015.

Publication Date (Web): June 18, 2015 | doi: 10.1021/bk-2015-1192.ch023

for those sets of data. All reported kinetic parameters were obtained by solving the rate equations and minimizing the sum of square errors up to a certain stage of cure where the mixtures were still liquid, and the systems were in the "pre-gel" state. At higher concentrations above the gel point, a diffusion term would be needed to describe the cure behavior. Therefore, Figures 4, 5 and 6 only present the experimental data before gelation and demonstrate that the two-parameter model fits well with the experimental data during the initial stages of the cure.

One of the main purposes of this study was to measure the reactivity ratio, k_2/k_1. The epoxy-primary amine addition could potentially affect the reactivity of the secondary amine reaction, and this effect, often referred to as a substitution effect, can be measured by the reactivity ratio between the secondary amine reactivity rate to the primary amine, k_2/k_1. The substitution effect is critical since it can be used to provide insight into the structure of the developing network. A reactivity ratio of 0.5 indicates that both the primary and secondary amines react equally and form a completely random network. It should be noted that a primary amine has two reactive hydrogen atoms, and a secondary amine has one reactive hydrogen atom, thus an equal reactivity yields $k_2/k_1 = 0.5$. However, a ratio less than 0.5 shows that the reactivity of the secondary amine decreases due to the addition of an epoxy moiety to the primary amine group (*10*). In this case, a linear chain is formed first, and crosslinks will appear later in the reaction.

Publication Date (Web): June 18, 2015 | doi: 10.1021/bk-2015-1192.ch023

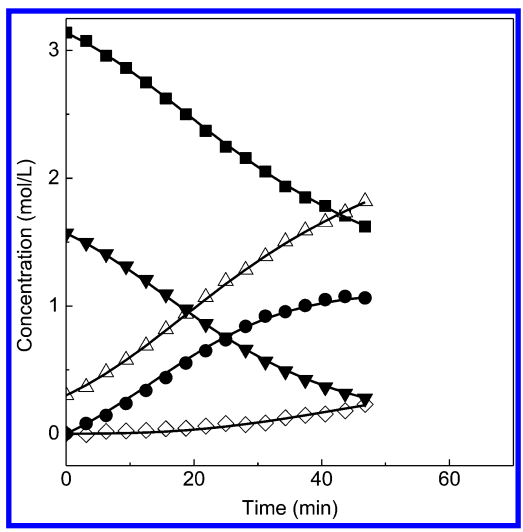

Figure 4. Experimental data (points) and the mode fits (lines) of the BOF-PACM system at 60°C. ■, ▼, ●, ◊ and Δ represent the experimental concentrations of epoxy, primary, secondary, tertiary amines and hydroxyl groups, respectively.

In Green Polymer Chemistry: Biobased Materials and Biocatalysis; Smith, et al.;
ACS Symposium Series; American Chemical Society: Washington, DC, 2015.

Publication Date (Web): June 18, 2015 | doi: 10.1021/bk-2015-1192.ch023

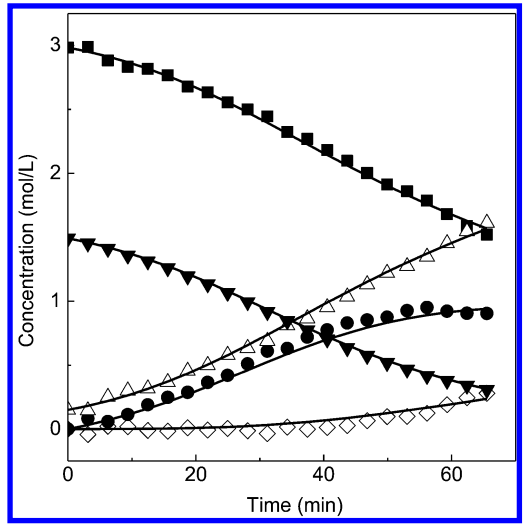

Figure 5. Experimental data (points) and the mode fits (lines) of the BOB-PACM system at 60°C. ■, ▼, ●, ◊ and Δ represent the experimental concentrations of epoxy, primary, secondary, tertiary amines and hydroxyl groups, respectively.

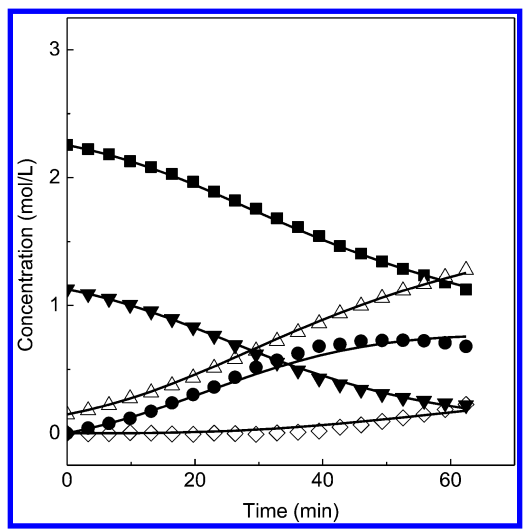

Figure 6. Experimental data (points) and the mode fits (lines) of the DGEBA-PACM system at 60°C. ■, ▼, ●, ◊ and Δ represent the experimental concentrations of epoxy, primary, secondary, tertiary amines and hydroxyl groups, respectively.

Table 3. Summary of the Kinetic Parameters of Auto-Catalytic Epoxy-Primary Amine Addition (k_1) and Epoxy-Secondary Amine Addition (k_2) at 60°C

Epoxy-amine system	*Entry*	k_1 ($L^2/(mol^2\ min)$)	k_2 ($L^2/(mol^2\ min)$)	k_2/k_1
BOF-PACM	expt 1	0.0082	0.0014	0.171
	expt 2	0.0075	0.0009	0.120
	expt 3	0.0075	0.0009	0.120
	average	0.00773±0.00040	0.00107±0.00029	0.137
BOB-PACM	expt 1	0.0074	0.0017	0.230
	expt 2	0.0056	0.0015	0.268
	expt 3	0.0056	0.0016	0.286
	average	0.00620±0.00104	0.00160±0.00010	0.261
DGEBA-PACM	expt 1	0.0072	0.0014	0.189
	average	0.00723	0.00137	0.189

Publication Date (Web): June 18, 2015 | doi: 10.1021/bk-2015-1192.ch023

Table 3 summarizes the epoxy-primary amine and epoxy-secondary amine addition kinetic parameters k_1 and k_2, respectively, for all three systems. With similar methods to the one used herein, Raman and Palmese reported reactivity ratios for a DGEBA-PACM system at 60°C with k_1 = 0.00607±0.00041 $L^2/(mol^2\ min)$, k_2 = 0.00123±0.00014 $L^2/(mol^2\ min)$ and k_2/k_1 = 0.203, which match our results closely (*9*). Overall, BOF possessed the highest epoxy-primary amine reactivity and the lowest epoxy-secondary amine reactivity compared with BOB and DGEBA. This interesting observation suggests that furanyl and phenyl building blocks have different influences in the epoxy-primary amine and epoxy-secondary amine reactions. Reasons for this could be the differences of (1) electron densities on the epoxy reactive groups and (2) intermolecular interactions on the amine reactive groups. For the first hypothesis, ^1H NMR results of BOF, BOB and DGEBA monomers showed minimal differences in epoxy peak positions (2.793 and 2.609 ppm for BOF, 2.797 and 2.621 ppm for BOB, and 2.894 and 2.743 ppm for DGEBA), and these indicated the electron density differences on the epoxy reactive groups were negligible. For the second hypothesis, the highly electronegative elements on the furanyl groups (oxygen atoms) would attract the electropositive elements (hydrogen atoms) on the amine hardener molecules, and the dipole-dipole interactions could activate the amine

groups, facilitate the epoxy-primary amine reactions and result in an elevated k_1 value for BOF. However, as shown by the lowest k_2 value of BOF compared with BOB and DGEBA, this effect is significantly weakened in the epoxy-secondary amine reaction. This can be explained since hydroxyl groups, a more favorable hydrogen bonding donor compared with primary and secondary amines, are generated and associated with furanyl groups through a more stable hydrogen bonding. The combination of these effects would explain the observation that BOF has the smallest k_2/k_1 value in comparison to the other systems as well as the highest k_1 constant. A comparison between DGEBA-PACM and BOB-PACM showed that DGEBA possessed a larger k_1 value and a smaller k_2 value. ^{1}H NMR results indicated that epoxy peaks of DGEBA presented at relatively higher positions compared with BOB. This indicates DGEBA epoxy groups are more electron-deficient, i.e. more electrophilic and favored to react with primary amines - resulting in a larger k_1 value compared with that of BOB. The structural difference between BOB and DGEBA which is responsible for this effect is the methylene linkage present in BOB between the phenyl group and oxygen atom. However, the secondary amine groups in the DGEBA-PACM network are perhaps more sterically hindered by the DGEBA than BOB, resulting in a smaller k_2 value.

Publication Date (Web): June 18, 2015 | doi: 10.1021/bk-2015-1192.ch023

Conclusion

The results of this investigation show clear differences in the reactivity of analogue diepoxy monomers prepared using furanyl (BOF) and phenyl building blocks (BOB). The overall reactivity of BOF was found to be significantly greater than that of BOB. More interestingly, the reactivity ratio k_2/k_1 of BOF with a standard amine curing agent was found to be about half that of BOB suggesting that the formation of the network structures in these two systems proceeds very differently during cure. In particular, in the early stages, BOF systems should possess a network that is characterized by more chain extension than that of analogue BOB thermosets. This behavior could lead to difference in mechanical properties such as strength and fracture toughness. Work is underway to characterize fracture behavior in these systems. Hydrogen bonding with the furanyl group in BOF before and during the course of the reaction was used to explain the reactivity differences with BOB systems for which hydrogen bonding with the phenyl ring is not possible.

Acknowledgments

The authors acknowledge financial support from SERDP under Project WP03-015 as well as from the U.S. Army Research Laboratory under the Army Materials Center of Excellence Program, contract W911NF-06-2-0013. Support to Fengshuo Hu from the China Scholarship Council is also acknowledged.

References

1. Fache, M.; Auvergne, R.; Boutevin, B.; Caillol, S. *Eur. Polym. J.* **2014**, http://dx.doi.org/10.1016/j.eurpolymj.2014.10.011
2. Wool, R. P.; Sun, X. S. *Bio-based Polymers and Composites*; Elsevier: Oxford, 2011; pp 7−8.
3. Belgacem, M. N.; Gandini, A. *Monomers, Polymers and Composites from Renewable Resources*; Elsevier: Oxford, 2011; pp 220-227.
4. Elchinger, P.-H.; Montplaisir, D.; Zerrouki, R. *Carbohydr. Polym.* **2012**, *87*, 1886–1890.
5. Kasaai, M. R. *Carbohydr. Polym.* **2008**, *71*, 497–508.
6. Lacerda, T. M.; Gandini, A. *J. Renewable Mater.* **2014**, *2*, 2–12.
7. Hu, F.; La Scala, J. J.; Sadler, J. M.; Palmese, G. R. *Macromolecules* **2014**, *47*, 3332–3342.
8. Sharifi, M.; Jang, C. W.; Abrams, C. F.; Palmese, G. R. *J. Mater. Chem. A* **2014**, *2*, 16071–16082.
9. Raman, V. I.; Palmese, G. R. *Macromolecules* **2005**, *38*, 6923–6930.
10. Mijovic, J.; Fishbain, A.; Wijaya, J. *Macromolecules* **1992**, *25*, 979–985.

Publication Date (Web): June 18, 2015 | doi: 10.1021/bk-2015-1192.ch023

Publication Date (Web): June 18, 2015 | doi: 10.1021/bk-2015-1192.ch024

Chapter 24

Polyesters from Bio-Aromatics

Ha T. H. Nguyen, Elizabeth R. Suda, Emma M. Bradic, Jessica A. Hvozdovich, and Stephen A. Miller*

The George and Josephine Butler Polymer Research Laboratory, Department of Chemistry, 318 Leigh Hall, University of Florida, Gainesville, Florida 32611-7200, United States
***E-mail: miller@chem.ufl.edu.**

Ferulic acid, a naturally occurring hydroxycinnamic acid possessing antioxidant properties, is abundantly available from lignin and lignocellulose. It is the starting material for the synthesis of acetylferulic acid and acetyldihydroferulic acid monomers. These monomers, when copolymerized at various feed ratios, produce copolymers with tunable thermal and physical properties. Some copolymers exhibit thermal properties comparable to commercially available fossil fuel-based packaging plastics—particularly polyethylene terephthalate (PET) and polystyrene (PS). For example, the glass transition temperature can be tuned from 78 °C to 153 °C and increases with increasing ferulic acid content and decreasing dihydroferulic acid content. With promising properties and scalable feedstock availability, copolyesters from substituted hydroxycinnamic acids could prove to be sustainable replacements for a variety of non-renewable and non-degradable commodity plastics.

Introduction

Polymer chemists have an increasing motivation to develop bio-based commodity plastics that are not built from fossil fuels and that degrade more readily in the natural environment into benign by-products. An overarching goal is to synthesize polymers from abundant and inexpensive biorenewable monomers, yielding materials with thermal and mechanical properties which mimic or excel those of commodity polymers.

In Green Polymer Chemistry: Biobased Materials and Biocatalysis; Smith, et al.;
ACS Symposium Series; American Chemical Society: Washington, DC, 2015.

Publication Date (Web): June 18, 2015 | doi: 10.1021/bk-2015-1192.ch024

Two polymers of interest to our research group are polyethylene terephthalate (PET) and polystyrene (PS) (*1*), which account for about 7% (*2*) and 9% (*3*) of the global plastics market, respectively. A primary driver for this interest is that these high-volume commodity plastics have thermal properties—specifically higher glass transition temperatures—in a range that bio-based polylactic acid (PLA, T_g = 55 °C) (*4*) cannot match. Since the key aromatic components of PET (terephthalic acid) and PS (styrene) derive from non-renewable petroleum, utilization of aromatic monomers from biorenewable feedstocks is a logical approach.

Lignin, which makes up about 30% of a typical tree, is the second most abundant organic polymer on earth and thus, appears to be the optimal source of renewable aromatics (*5*). It is the major by-product of the paper pulping industry, but nearly all of it is burned onsite for energy production. In addition to lignin, the bran of grains offers attractive opportunities to harvest potentially useful aromatic monomers (*6*). One such monomer, ferulic acid (4-hydroxy-3-methoxycinnamic acid), can be extracted from lignin or lignocellulose and is probably the most abundant hydroxycinnamic acid in the plant world (*7*). Besides being naturally occurring and abundantly available from non-food resources, ferulic acid also possesses antioxidant properties which protect against oxidative stress in cells, as well as the progression of age-related diseases (*8*). Accordingly, ferulic acid, derived from rice bran and rice bran oil, is sold in tablet form as a dietary supplement (*9*).

Our first successful ferulic acid-based PET mimic was poly(dihydroferulic acid) (PHFA), which exhibited a glass transition temperature (T_g = 73 ˚C) quite similar to that of PET (67 °C) and a melting temperature (T_m = 234 ˚C) about 30 °C lower than that of PET (*10*). In pursuit of further developing ferulic acid as a building block for sustainable polymers, herein we reveal a copolymerization strategy utilizing ferulic acid (FA) and dihydroferulic acid (HFA) at various feed ratios; this allows refinement of the glass transition temperature, including a match of the T_g value for polystyrene (95-100 ˚C) *en route* to values exceeding 150 ˚C (*11*, *12*). This control of the thermal properties—over a large temperature range—invites these copolymers to be polystyrene replacements, in addition to high temperature packaging applications such as pasteurized milk containment (70 °C) and other hot-fill bottling and canning processes. Moreover, the hydrolytic degradation products of the copolymers are ferulic acid and dihydroferulic acid, both of which are present in tea, coffee, whole grains, and other antioxidant rich foods.

Our previous synthesis of poly(dihydroferulic acid) (PHFA) began with vanillin and extended the carbon framework to that of ferulic acid via a Perkin reaction with acetic anhydride (*10*). Interestingly, Rhodia-Solvay performs the reverse conversion of ferulic acid to vanillin in their manufacture of bio-based, natural vanillin, trademarked as Rhovanil® (*13–15*). Thus, it seemed more direct and proper to use ferulic acid (FA) as the starting material. Accordingly, the monomers acetylferulic acid (AFA) and acetyldihydroferulic acid (AHFA) were synthesized as depicted in Figure 1.

In Green Polymer Chemistry: Biobased Materials and Biocatalysis; Smith, et al.;
ACS Symposium Series; American Chemical Society: Washington, DC, 2015.

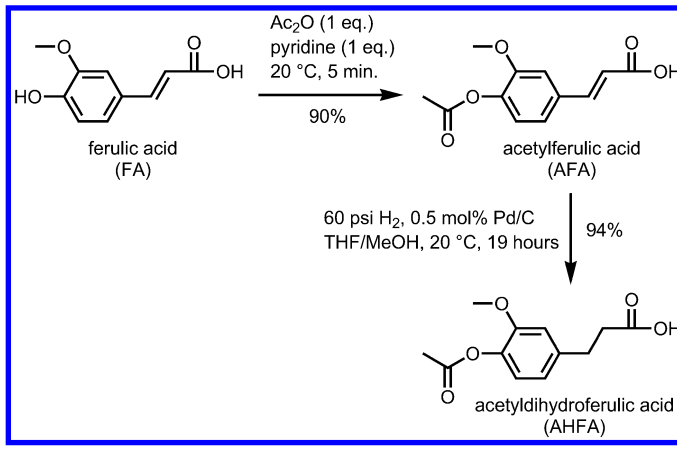

Figure 1. Synthesis of acetylferulic acid (AFA) and acetyldihydroferulic acid (AHFA) from ferulic acid (FA).

In a previous literature preparation, the acetylation of ferulic acid was accomplished with excess acetic anhydride (2.8 or 3.6 equivalents) (*16*) and a large excess of pyridine (15.8 or 18.6 equivalents) (*17*) over a long reaction time of 3 to 24 hours. The same product was successfully produced, in 90% yield, by using stoichiometric ratios (1:1:1) of ferulic acid:acetic anhydride:pyridine for a significantly shorter reaction time, about 5 minutes. The hydrogenation step to afford acetyldihydroferulic acid was optimized to employ only 0.5 mol% of Pd/C catalyst, yielding product in 94% yield.

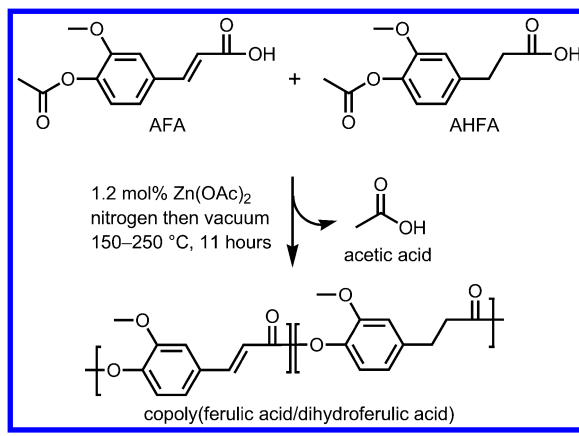

Figure 2. Transesterification copolymerization of acetylferulic acid and acetyldihydroferulic acid to yield copoly(ferulic acid/dihydroferulic acid).

Publication Date (Web): June 18, 2015 | doi: 10.1021/bk-2015-1192.ch024

Table 1. Polymerization and Characterization of Copoly(Ferulic Acid/Dihydroferulic Acid)

Entry	*AHFA (mol%)*	*AFA (mol%)*	*Inc. of AFA* [a] *(mol%)*	T_g [b] *(°C)*	T_m [b] *(°C)*	$T_{50\%}$ [c] *(°C)*	M_w [d] *(Da)*	M_n [d] *(Da)*	*PDI*	*Yield (%)*
1	100	0	0	78	243	408	9,400	3,400	2.8	85.6
2	90	10	9	80	223	408	22,600	6,300	3.6	85.3
3	80	20	18	80	212	412	18,600	5,200	3.6	80.4
4	70	30	32	79	n.o.	395	8,900	3,300	2.7	75.2
5	60	40	37	87	n.o.	414	9,200	3,000	3.0	77.0
6	50	50	46	98	n.o.	417	15,600	3,600	4.3	79.9
7	40	60	59	108	n.o.	420	13,900	3,500	3.9	81.4
8	30	70	71	118	n.o.	418	20,100	3,100	6.5	83.3
9	20	80	78	125	n.o	430	13,200	2,600	5.1	85.4
10	10	90	86	140	n.o.	442	20,000	3,500	5.8	86.6
11	0	100	100	153	n.o.	459	13,000	2,800	3.9	73.5

[a] Incorporation of acetylferulic acid in the copolymer determined by ^{1}H NMR. [b] T_g and T_m determined using Differential Scanning Calorimetry (DSC); n.o. = not observed. [c] Temperature at 50% weight loss of polymer determined using thermal gravimetric analysis (TGA) under nitrogen. [d] M_w and M_n determined by Gel Permeation Chromatography (GPC) in hexafluoroisopropanol (HFIP) *versus* poly(methyl methacrylate) (PMMA) standards.

Publication Date (Web): June 18, 2015 | doi: 10.1021/bk-2015-1192.ch024

A patent from 1980 reported that polyferulic acid (PFA) had a high glass transition temperature of 150 ˚C, but was rather intractable with no suitable solvents described (*18*). We reasoned that incorporation of more rigid ferulic acid units into a poly(dihydroferulic acid) (PHFA) polymer would augment the glass transition temperature, as well as improve the tractability and solubility—to the extent that a more random structure would result. Consequently, a series of copolymers, generalized in Figure 2, was targeted via transesterification copolymerization.

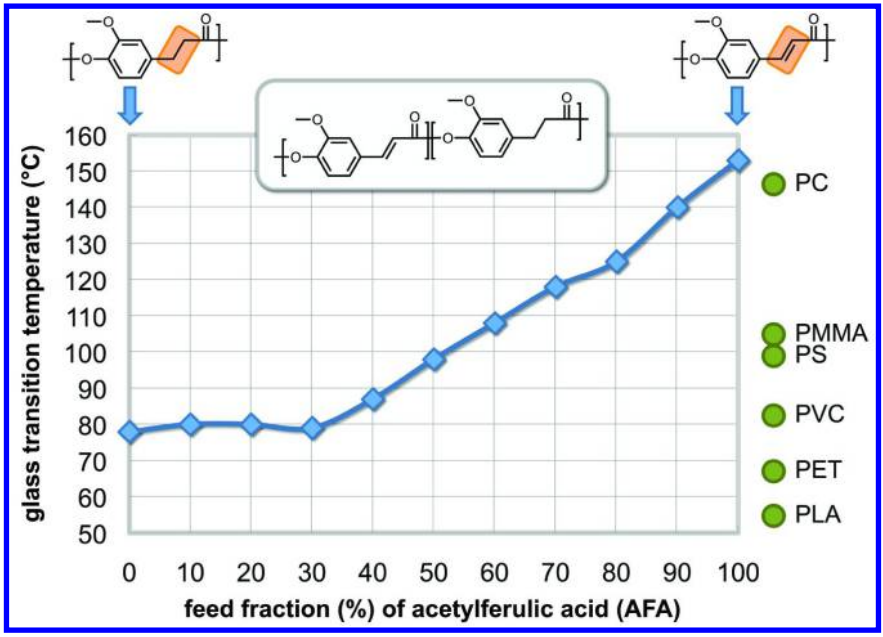

Figure 3. Glass transition temperatures observed and plotted for polydihydroferulic acid (0% AFA feed), polyferulic acid (100% AFA feed) and copolymers thereof, copoly(ferulic acid/dihydroferulic acid). T_g values for several common commodity plastics are given for comparison: polylactic acid (PLA), polyethylene terephthalate (PET), polyvinyl chloride (PVC), polystyrene (PS), polymethyl methacrylate (PMMA), and polycarbonate (PC).

Copolymerizations of acetylferulic acid and acetyldihydroferulic acid in feed ratios every decade (every 10%) from the homopolymer of acetyldihydroferulic acid to the homopolymer of acetylferulic acid were catalyzed by 1.2 mol% of anhydrous zinc acetate (Figure 2). These copolymerizations were performed under one atmosphere of nitrogen for 5 hours and vacuum was subsequently applied for 6 hours, which liberated acetic acid during a temperature ramp from 150 to 250 ˚C using an oil bath. As revealed in Table 1, the copolymers were obtained in good yields (73 to 87%) and with acceptable molecular weights. M_w

In Green Polymer Chemistry: Biobased Materials and Biocatalysis; Smith, et al.;
ACS Symposium Series; American Chemical Society: Washington, DC, 2015.

ranged from 9,200 to 22,600 with half of the samples above M_w = 15,000. The polydispersity values (PDI) were somewhat large for well-behaved step-growth polymerizations and ranged from 2.7 to 6.5. During these melt polymerizations, the reaction viscosity seemed especially high for those with larger acetylferulic acid feed fractions—possibly explaining the broader PDI values for entries 8, 9, and 10 (Table 1). The simple magnetic stir bar employed was likely inadequate and future studies with mechanical stirring and more efficient mixing are anticipated to increase molecular weights and corral the broad PDI values.

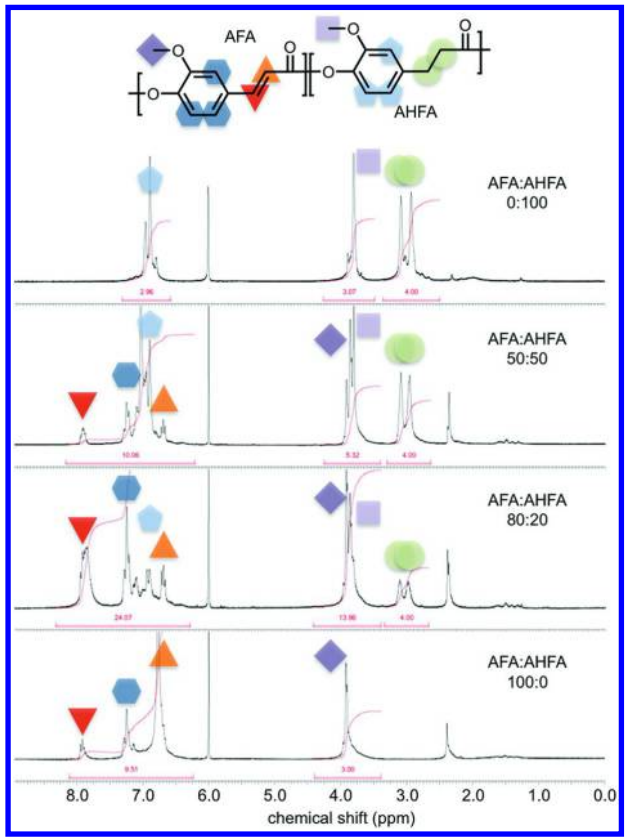

Figure 4. Proton Nuclear Magnetic Resonance (^{1}H NMR) spectra of copoly(dihydroferulic acid/ ferulic acid) with acetylferulic acid (AFA) feed fractions of 0%, 50%, 80%, and 100%.

Figure 3 plots the glass transition temperature values observed for copoly(ferulic acid/dihydroferulic acid) as the ferulic acid feed fraction increases from 0% to 100% with 10% increments. As predicted by the Fox equation (*19*), the glass transition temperatures followed a steady increase as the ferulic acid content increased, reaching a maximum with 100% ferulic acid feed fraction. Inspection of the Figure 3 plot reveals a minimal effect for the feed fraction

In Green Polymer Chemistry: Biobased Materials and Biocatalysis; Smith, et al.;
ACS Symposium Series; American Chemical Society: Washington, DC, 2015.

Publication Date (Web): June 18, 2015 | doi: 10.1021/bk-2015-1192.ch024

up to 30% of acetylferulic acid. The linear T_g relationship begins at 30% and extends to 100%. The thermal data collected confirmed the suspicion that increased unsaturation—and concomitant increased conformational rigidity—led to decreased chain flexibility and higher glass transition temperatures. It is clear from Figure 3 that this copolymer system can be tuned over a wide range of glass transition temperatures (range = 153 °C – 78 °C = 75 °C) that overlaps well with those of several common commodity plastics, including polyvinyl chloride (82 °C), polystyrene (100 °C), polymethyl methacrylate (105 °C), and polycarbonate (147 °C). Note from Table 1 that increased ferulic acid content decreases the melting temperature (T_m) from 243 °C (0% FA) to 212 °C (20% FA) but copolymers with FA contents above 20% did not display melting endotherms for various DSC trials.

The homopolymers and copolymers were analyzed by ^{1}H NMR spectroscopy (in a combination of 1,1,2,2,-tetrachloroethane-d_2 and trifluoroacetic acid) in order to quantify the relative abundance of the two monomers incorporated during polymerization. Figure 4 depicts exemplary ^{1}H NMR spectra for the polymers and copolymers with acetylferulic acid (AFA) feed fractions of 0%, 50%, 80%, and 100%. Of particular use are the peaks attributed to the methoxy hydrogens of both ferulic and dihydroferulic repeat units (3.8 and 3.9 ppm) and the methylene hydrogens of dihydroferulic repeat units (3.0 and 3.1 ppm). Relative integration provided the incorporation values reported in Table 1. Figure 5 plots the incorporation fraction of ferulic repeat units as a function of the acetylferulic acid (AFA) feed fraction. The linearity of this plot (see the dashed line) confirms that the incorporation fraction closely matches the feed fraction for these copolymerizations and thereby suggests a random copolymerization of the two comonomers.

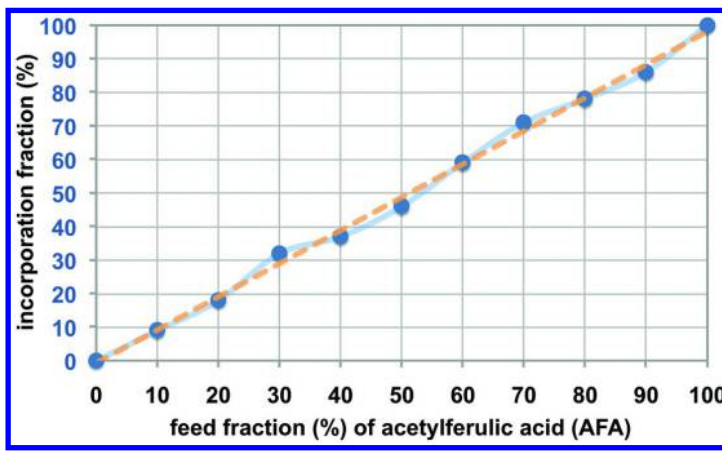

Figure 5. The incorporated ferulic content of the copolymers plotted as a function of the acetylferulic acid (AFA) feed fraction. The near linearity (shown by the dashed line) suggests a random copolymerization of acetylferulic acid (AFA) and acetyldihydroferulic acid (AHFA).

In Green Polymer Chemistry: Biobased Materials and Biocatalysis; Smith, et al.;
ACS Symposium Series; American Chemical Society: Washington, DC, 2015.

Publication Date (Web): June 18, 2015 | doi: 10.1021/bk-2015-1192.ch024

Conclusion

The naturally abundant phytochemical ferulic acid has been converted into acetylferulic acid and acetyldihydroferulic acid. The transesterification copolymerization of these monomers yields a novel series of biorenewable thermoplastics with tunable glass transition temperatures. Polydihydroferulic acid exhibited a T_g of 78 °C, polyferulic acid exhibited a T_g of 153 °C, and the copolymers exhibited intermediate T_g values. This broad glass transition temperature range suggests that these polymers might be sustainable mimics for important commodity polymers. For example, the copoly(ferulic acid/dihydroferulic acid) prepared with a 50:50 ratio of monomers has a T_g of 98 °C, an excellent match for that of polystyrene (PS). The prepared copolymers were of moderate molecular weight and somewhat broad polydispersity—likely because of the high melt viscosity encountered during polymerization. Future work will employ a polymerization autoclave with mechanical stirring and improved mixing during polymerization. Additionally, mechanical testing and hydrolytic degradation studies will be performed.

Ferulic acid is a noteworthy biorenewable feedstock because it is abundantly present in the non-edible components of the world's two largest crops, sugarcane and corn. Moreover, polyesters made from ferulic acid and dihydroferulic acid should readily undergo hydrolytic degradation yielding not just benign, but beneficial by-products which possess antioxidant properties important to human health.

Publication Date (Web): June 18, 2015 | doi: 10.1021/bk-2015-1192.ch024

Acknowledgments

This research was supported by the National Science Foundation (CHE-1305794), U.S. Bioplastics, Inc. (usbioplastics.com), and the Florida High Tech Corridor Council.

References

1. Miller, S. A. Degradable Biopolymers. *Chemistry Industry Magazine* **2013**, *7*, 20–23.
2. *Global PET Supply to Exceed 24.39 Mln Tonnes in 2015*; Merchant Research & Consulting, Ltd. http://mcgroup.co.uk/news/20140117/global-pet-supply-exceed-2439-mln-tonnes-2015.html; 19.8 million tons of PET produced were reported for 2012. In 2012, there were about 288 million tons of plastics produced globally. http://www.statista.com/statistics/282732/global-production-of-plastics-since-1950/.
3. *Global Styrene Production Exceeded 26.4 Million Tonnes in 2012*; Merchant Research & Consulting, Ltd. http://mcgroup.co.uk/news/20130830/global-styrene-production-exceeded-264-million-tonnes.html.
4. Becker, J. M.; Pounder, R. J.; Dove, A. P. *Macromol. Rapid Commun.* **2010**, *31*, 1923–1937.

5. Lebo, S. E., Jr.; Gargulak, J. D.; McNally, T. J. Lignin. In *Kirk-Othmer Encyclopedia of Chemical Technology*; John Wiley & Sons, Inc.: New York, 2001; Vol. 15, pp 1–32.
6. Gélines, P; McKinnon, C. M. *Int. J. Food Sci. Technol.* **2006**, *41*, 329–332.
7. Sindhu, M.; Abraham, T. E. *Crit. Rev. Biotechnol.* **2004**, *24*, 59–83.
8. Lee, C. Y.; Sharma, A.; Uzarski, R. L.; Cheong, J. E.; Xu, H.; Held, R. A.; Upadhaya, S. K.; Nelson, J. L. *Free Radical Biol. Med.* **2011**, *50*, 918–925.
9. *Source Naturals, trans-ferulic acid*; http://www.sourcenaturals.com/products/GP1298.
10. Mialon, L.; Pemba, A. G.; Miller, S. A. *Green Chem.* **2010**, *12*, 1704–1706.
11. Miller, S. A.; Mialon, L. Poly(dihydroferulic acid): A biorenewable polyethylene terephthalate mimic derived from lignin and acetic acid; U.S. Patent Application, PCT/US2011/36181, May 12, 2011.
12. Miller, S. A. *ACS Macro Lett.* **2013**, *2*, 550–554.
13. Solvay 2014; http://www.safevanillin.com/en/vanillin-and-ethyl-vanillin-range/index.html.
14. Gasson, M. J.; Kitamura, Y.; McLauchlan, W. R.; Narbad, A.; Parr, A. J.; Parsons, E. L. H.; Payne, J.; Rhodes, M. J. C.; Walton, N. J. *J. Biol. Chem.* **1998**, *13*, 4163–4170.
15. Rabenhorst, J.; Steinbüchel, A.; Priefert, H. *Appl. Microbiol. Biotechnol.* **2001**, *56*, 296–314.
16. Allais, F.; Martinet, S.; Ducrot, P. H. *Synthesis* **2009**, *21*, 3571–3578.
17. Barontini, M.; Bernini, R.; Carastro, I.; Gentili, P.; Romani, A. *New J. Chem.* **2014**, *2*, 809–816.
18. Charbonneau, L. F.; Morris, N. J. Thermotropic polyesters derived from ferulic acid and a process for preparing the polyesters. U.S. Patent 4,230,817. October 28, 1980.
19. Fox, T. G. *Bull. Am. Phys. Soc.* **1956**, *1*, 123–124.

Publication Date (Web): June 18, 2015 | doi: 10.1021/bk-2015-1192.ch024

Publication Date (Web): June 18, 2015 | doi: 10.1021/bk-2015-1192.ch025

Chapter 25

Development and Characterization of Pressure-Sensitive Adhesives from Dimer Acid and Epoxides

Anlong Li and Kaichang Li*

Department of Wood Science and Engineering, Oregon State University, Corvallis, Oregon 97331, U.S.A.
***E-mail: kaichang.li@oregonstate.edu. Tel.: +1 5417378421.**

A novel approach has been developed for the preparation of pressure-sensitive adhesive (PSA) films from renewable dimer acid (DA) and epoxides. DA was polymerized with various epoxides such as dimer acid diglycidyl ester (DADGE), neopentyl glycol diglycidyl ether, 1,4-butanediol diglycidyl ether, bisphenol A diglycidyl ether (BPAGE), trimethylolpropane triglycidyl ether (TMPGE), *N*,*N*-diglycidyl-4-glycidyloxyaniline, and tris(2,3-epoxypropyl) isocyanurate (TEPIC) under different conditions. The resulting polymers were evaluated for various PSA properties such as tack, peel strength, shear strength, and aging resistance. It was found that only the polymer from the DA-TMPGE mixture could serve as a PSA. Copolymerization of the aliphatic epoxides TMPGE and DADGE with DA did not generate a PSA with adequate cohesive strength. The replacement of the aliphatic epoxide DADGE with the phenylene-containing epoxide BPAGE resulted in PSAs with a peel strength of 1.5-2.6 N/cm, a loop tack of 2.7-6.9 N, a superior shear strength of more than 240 h, and a good aging resistance. Incorporation of a triazine ring into the polymers from DA-epoxide mixtures through the use of the triazine-containing epoxide TEPIC as a crosslinking agent also resulted in PSAs with a superior peel strength of 3.4-5.7 N/cm and a good loop tack of 12.8 N. The PSA properties of the polymers from the DA-epoxide mixtures could be tailored

In Green Polymer Chemistry: Biobased Materials and Biocatalysis; Smith, et al.; ACS Symposium Series; American Chemical Society: Washington, DC, 2015.

to meet requirements of different PSA products through the selection of the epoxides and their usages. This new class of PSAs can be fully based on renewable materials. The preparation of the PSAs did not require any organic solvent or toxic chemicals, thus being environmentally friendly.

Introduction

Publication Date (Web): June 18, 2015 | doi: 10.1021/bk-2015-1192.ch025

Pressure-sensitive adhesives (PSA) are also known as self-stick adhesives. They are typically coated onto paper and plastic films for the production of labels, package tapes, stamps and many other products. PSA-coated products can easily stick to various surfaces under light pressure and are indispensable in our everyday lives (*1*, *2*). At present, commercial PSAs are mainly derived from acrylate-based copolymers, styrene-based block copolymers, ethylene-vinyl acetate copolymers, natural rubber, and silicone-based polymers. In recent years, a lot of effort has been devoted to development of PSAs from bio-based polymers, especially those from vegetable oils (*3–11*).

Epoxides are organic compounds having at least one epoxy group. The most common application of epoxides is epoxy resins that can be polymerized and cured *via* ring-opening reactions of the epoxy groups with nucleophiles such as amines, carboxylates, and phenols. The epoxy resins are widely used in composites, coatings and thermosetting adhesives. However, there are only a relatively few reports describing the use of epoxides as starting materials for PSAs. It has been demonstrated that epoxidized methyl oleate after being acrylated can be polymerized or copolymerized with acrylates such as 1,4-butanediol diacrylate for the generation of PSAs (*3–6*). Another type of PSAs was recently developed from epoxidized soybean oil and phosphoric acid (*7–9*). It has also been reported that PSAs can be developed from the curing of polyesters from the condensation of dimer acid (DA) and diols with epoxidized plant oils (*10*, *11*). PSAs can also be developed from the polymerization of an AB-monomer, epoxidized oleic acid (*12*, *13*). It has been demonstrated that a mixture of epoxidized fatty acids (EFAs) can be efficiently produced from the selective hydrolysis of epoxidized soybean oils (*14*). Polymerizations of the EFA mixture in the presence or absence of a small amount of dicarboxylic acids readily afforded PSAs with superior properties (*14*). Reactions of dicarboxylic acids with epoxidized soybean oils were also found to generate superior PSAs (*15*). In this study, we investigated a new approach of developing PSAs from the direct polymerization of DA with various epoxides containing two or three epoxy groups. More specifically, DA was polymerized with each epoxide via the ring-opening reaction between a carboxylic acid (-COOH) group and an epoxy group. The resulting polymers were evaluated for their PSA properties and aging resistance.

Publication Date (Web): June 18, 2015 | doi: 10.1021/bk-2015-1192.ch025

Experimental Section

Materials

Dimer acid (DA) (hydrogenated, average M_n ~ 570, 99+%), dimer acid diglycidyl ester (DADGE) (epoxy equivalent weight (EEW), ~ 400), neopentyl glycol diglycidyl ether (NPGGE) (EEW, ~ 140), 1,4-butanediol diglycidyl ether (BDDGE) (95+%), bisphenol A diglycidyl ether (BPAGE) (EEW, ~172), trimethylolpropane triglycidyl ether (TMPGE) (EEW, ~ 140), *N*,*N*-diglycidyl-4-glycidyloxyaniline (DGGA) (EEW, ~ 100), and tris(2,3-epoxypropyl) isocyanurate (TEPIC) (EEW, ~ 100) were purchased from Sigma-Aldrich (St. Louis, MO) and used as received. The representative chemical structures of DA and DADGE, and the chemical structures of NPGGE, BDDGE, BPAGE, TMPGE, DGGA, and TEPIC are shown in Figure 1. AMC-2, a solution of 50% of chromium (III) 2-ethylhexanoate in a mixture of di(heptyl, nonyl, undecyl) phthalates, was kindly provided by Ampac Fine Chemical LLC (Rancho Cordova, CA) and used as received. The release paper (silicone coated paper) was obtained from ChemInstruments, Inc. (Fairfield, OH). The polyethylene terephthalate (PET) film (thickness, ~50 μm) was obtained from Henkel Corp. (Rochy Hill, CT) and was used as a backing material. PET-based release film and Fasson 54# Semi-Gloss Facestock (~ 68 μm) that was used as a paper backing were obtained from Avery Dennison Corp. (Pasadena, CA).

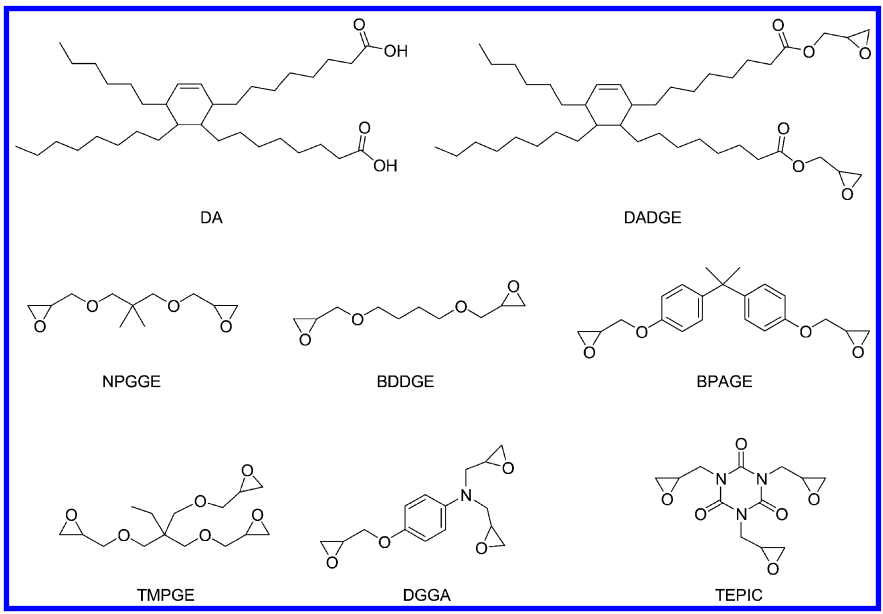

Figure 1. Chemical structures of DA, DADGE, NPGGE, BDDGE, BPAGE, TMPGE, DGGA, and TEPIC.

In Green Polymer Chemistry: Biobased Materials and Biocatalysis; Smith, et al.;
ACS Symposium Series; American Chemical Society: Washington, DC, 2015.

Analyses

FTIR spectra were recorded with a Thermo Nicolet Nexus 470 FTIR spectrometer (Thermo Nicolet Corp., Madison, WI) coupled with Smart Golden Gate diamond ATR accessory in a scanning range of 650–4000 cm^{-1} for 64 scans at a spectral resolution of 2 cm^{-1}.

Preparation of Polyesters Containing Two -COOH Groups

Preparation of PE-1

A mixture of DA (12.958 g, 0.0454 mol of -COOH groups) and AMC-2 (0.201 g) in a 50-mL, round-bottom flask was stirred with a magnetic stirrer at about 80 °C for 3 min, followed by addition of BPAGE (3.441 g, 0.0200 mol of epoxy groups). The resulting mixture was bubbled with nitrogen gas for 2 min and then stirred at 135 °C for 60 min to give a light green, homogeneous, and viscous resin. The resulting linear polyester contained two -COOH groups at the chain ends and was designated as PE-1. FTIR (neat, in cm^{-1}): 3450 (OH stretching), 2950 and 2870 (CH_3 stretching), 2922 and 2852 (CH_2 stretching), 1738 (ester carbonyl stretching), 1708 (carbonyl stretching of the -COOH group), 1608, 1582 and 1510 (benzene ring vibrations), 1460 (CH_2 bending), 1168 and 1110 (ester C-O stretching), 1245, 1180 and 1045 (ether C-O stretching), 828 (vibrations of the *para*-substituted benzene ring), 723 (CH_2 rocking motions, characteristic of at least four linearly connected CH_2 groups).

Preparation of PE-2

A mixture of DA (15.165 g, 0.0532 mol of –COOH groups) and AMC-2 (0.230 g) in a 50-mL, round-bottom flask was stirred with a magnetic stirrer at 80 °C for 3 min, followed by sequential additions of BPAGE (2.013 g, 0.0117 mol of epoxy groups) and NPGGE (1.639 g, 0.0117 mol of epoxy groups). The resulting mixture was bubbled with nitrogen gas for 2 min and then stirred at 135 °C for 60 min to give a light green, homogeneous, and viscous resin. The resulting polyester was designated as PE-2. FTIR (neat, in cm^{-1}): 3450 (OH stretching), 2950 and 2870 (CH_3 stretching), 2922 and 2853 (CH_2 stretching), 1739 (ester carbonyl stretching), 1709 (carbonyl stretching of the -COOH groups), 1609, 1583 and 1511 (benzene ring vibrations), 1460 (CH_2 bending), 1170 and 1110 (ester C-O stretching), 1246, 1181 and 1046 (ether C-O stretching), 828 (vibrations of the *para*-substituted benzene ring), 724 (CH_2 rocking motions).

Preparation of PE-3

A mixture of DA (12.800 g, 0.0449 mol of –COOH groups), DADGE (8.982 g, 0.0225 mol of epoxy groups) and AMC-2 (0.243 g) in a 50-mL, round-bottom flask was stirred with a magnetic stirrer at 80 °C for 3 min. The resulting

mixture was bubbled with nitrogen gas for 2 min and then stirred at 100 °C for 65 min to give a light green, homogeneous, and viscous resin. The resulting polyester was designated as PE-3. FTIR (neat, in cm^{-1}): 3450 (OH stretching), 2950 and 2870 (CH_3 stretching), 2922 and 2853 (CH_2 stretching), 1739 (ester carbonyl stretching), 1709 (carbonyl stretching of the -COOH groups), 1460 (CH_2 bending), 1170 and 1110 (ester C-O stretching), 724 (CH_2 rocking motions).

Prepolymerization of DA and an Epoxide

The following was a representivative procedure for the pre-polymerization of DA with TMPGE was the example for the epoxides. A mixture of DA (13.712 g, 0.0481 mol of –COOH groups), TMPGE (6.736 g, 0.0481 mol of epoxy groups) and AMC-2 (0.208 g) in a 50-mL, round-bottom flask was stirred at 70 °C for 3 min. The resulting mixture was bubbled with nitrogen gas for 2 min and then stirred at 70 °C for 45 min to give a light green, homogeneous, and viscous resin. FTIR (neat, in cm^{-1}): 3450 (OH stretching), 2950 and 2870 (CH_3 stretching), 2922 and 2853 (CH_2 stretching), 1736 (ester carbonyl stretching), 1710 (-COOH carbonyl stretching), 1460 (CH_2 bending), 1170 and 1100 (ester C-O-C stretching), 910 (epoxy ring vibrations), 723 (CH_2 rocking motions).

Prepolymerization of a Polyester Containing Two -COOH Groups and an Epoxide

The following was a typical procedure for the pre-polymerization of PE-1 as the example of the polyester containing two -COOH groups and TMPGE as the example of the epoxide. A mixture of PE-1 (16.399 g), AMC-2 (0.201 g), and TMPGE (3.565 g) was stirred at 75 °C for 16 min to afford a light green, homogeneous, and highly viscous resin. FTIR (neat, in cm^{-1}): 3450 (OH stretching), 2950 and 2870 (CH_3 stretching), 2922 and 2852 (CH_2 stretching), 1737 (ester carbonyl stretching), 1710 (-COOH carbonyl stretching), 1608, 1582 and 1510 (benzene ring vibrations), 1460 (CH_2 bending), 1168 and 1110 (ester C-O stretching), 1245, 1180 and 1045 (ether C-O stretching), 829 (vibrations of the *para*-substituted benzene ring), 723 (CH_2 rocking motions).

The Curing of the Prepolymers and the Preparation of PSAs

Each of the pre-polymers as prepared previously was coated onto a sheet of release paper at a coating thickness of 5.5±0.6 mg/cm² with a HLCL-1000 hot-melt coater/laminator (ChemInstruments, Inc., Fairfield, OH). The coating on the release paper was then mated with a sheet of PET film using the laminator, resulting in a "sandwich"-like laminate. The pre-polymer between the release paper and the PET film was cured in a forced air oven at 160 °C. The laminate was taken out of the oven after a pre-determined time. The release paper was peeled off to give a PSA tape with the PET film as the backing material. For preparation of a PSA tape with paper as the backing material, the pre-polymer coating on the release paper was mated with a sheet of a release film instead of the PET film. The release paper/pre-polymer/release film laminate was cured in the oven for a

Publication Date (Web): June 18, 2015 | doi: 10.1021/bk-2015-1192.ch025

pre-determined time. Afterwards, the release film was peeled off (no adhesive residue remained on the release film because the release film has better repellence against the adhesive than the release paper). The exposed adhesive layer on the release paper was then mated with a sheet of paper backing with the laminator to give a PSA tape.

Solubility Test of the Adhesive Film Obtained from the Polymerization of DA and TMPGE

The following is a typical procedure for the solubility test with ethyl acetate as an example solvent. After curing, the release paper/adhesive film/release film laminate was taken out of the oven, and the release film was peeled off. The adhesive film (2.2 g) on the release paper was carefully cut into small pieces, peeled off from the release paper, and carefully transferred to a 50-mL, round-bottom flask equipped with a magnetic stirrer. Ethyl acetate (30 mL) was then added to the flask. The resulting mixture in the flask was stirred at 200 rpm at room temperature for 3 days. After filtration, the remaining undissolved part was dried at 80 °C under reduced pressure, and weighed to be about 1.6 g, *i.e.*, ~ 73 wt% based on the dry weight (2.2 g) of the adhesive film.

Measurements of the Peel Strength, Loop Tack, and Shear Strength of the PSAs

The 90° peel, shear, and loop tack tests of the PSA samples were performed in accordance with the conditions and methods described in our previous studies (*14*, *15*).

Aging Test

For an accelerated aging test, samples of the PSA tapes were placed in an Isotemp 625D incubator (Thermo Fisher Scientific Inc., Waltham, MA) at 60 °C. After one or four weeks, the sample tapes were taken out of the incubator and conditioned at 23 ± 1 °C and 40 ± 5 % RH for 16 h. PSA specimens were then prepared from the aged sample tapes and measured for their peel strength and loop tack in accordance with the methods described previously (*14*, *15*).

Statistical Analysis

Peel strength, loop tack and shear strength data were statistically analysed with a two-sample t-test using Microsoft Excel (version 2010, Microsoft Corp., Redmond, WA). All comparisons were based on a 95% confidence interval.

In Green Polymer Chemistry: Biobased Materials and Biocatalysis; Smith, et al.;
ACS Symposium Series; American Chemical Society: Washington, DC, 2015.

Publication Date (Web): June 18, 2015 | doi: 10.1021/bk-2015-1192.ch025

Publication Date (Web): June 18, 2015 | doi: 10.1021/bk-2015-1192.ch025

Results and Discussion

Polymerization of DA and an Epoxide and the Preparation of PSAs

Theoretically, DA and a difunctional or polyfunctional epoxide can step-growth polymerize to form hydroxyl-functionalized polyesters *via* the ring-opening of the epoxy groups with the –COOH groups (Scheme 1). The chemical structure of the epoxide influences the reactivity of the epoxy groups and the rigidity/flexibility of its molecular chain, while the epoxy functionality, *i.e.*, the number of the epoxy groups per molecule of the epoxide, determines the topology of the resulting polymers that can be linear, branched, or crosslinked. The flexibility and topology of the resulting polymers may subsequently affect the T_g, modulus, adhesive and cohesive strengths, and crosslinking density (if any) of the polymers. The following epoxides with different flexibilities and/or epoxy functionalities of their backbones were investigated: DADGE, NPGGE, BDDGE, BPAGE, TMPGE, DGGA, and TEPIC (see Figure 1 for their chemical structures). A mixture of DA and each of the epoxides was polymerized and completely cured under the conditions described in Table 1. AMC-2 has been demonstrated to be an efficient catalyst for accelerating the reaction between a -COOH and an epoxy group in studies by our research group (*14*, *15*) and others (*4*), and was used as the catalyst for the polymerization of the DA-epoxide mixtures in this study.

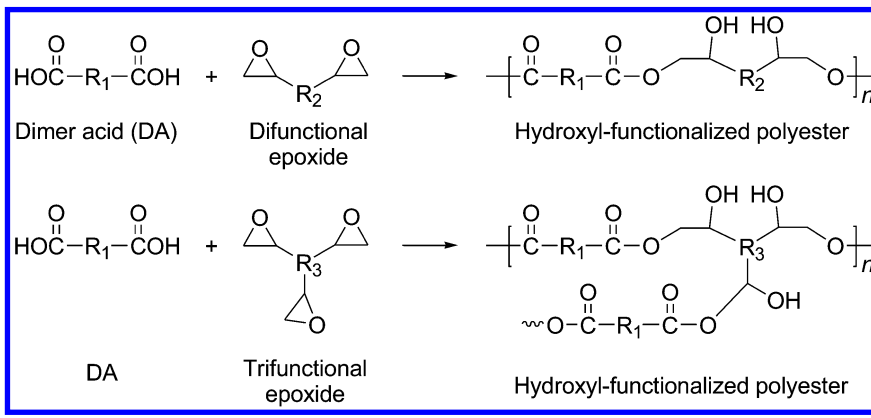

Scheme 1. Proposed polymerization of DA and a difunctional or trifunctional epoxide (see Figure 1 for the chemical structures of DA and epoxides used in this study).

DADGE, a long-chain aliphatic epoxide derived from DA, has two epoxy groups per molecule (Figure 1). Polymerization of DA and DADGE went smoothly at 110 °C. The viscosity of the reaction mixture increased with time; the mixture was too viscous to be magnetically stirred after about 20 min. Further heating for about 10 min without agitation resulted in a soft and weak gel. The gel was tacky, which was a good sign for potential PSA applications. However, the gel could not be spread onto a backing material for the evaluation of its

In Green Polymer Chemistry: Biobased Materials and Biocatalysis; Smith, et al.;
ACS Symposium Series; American Chemical Society: Washington, DC, 2015.

PSA properties because it did not melt at elevated temperature. Therefore, the following special procedure was designed and used for the preparation of an adhesive from a mixture of DA and DADGE (Table 1, entry 1). The DA-DADGE mixture was first pre-polymerized at 110 °C for 15 min to generate a pre-polymer that was still spreadable. The resulting pre-polymer was then coated on a sheet of release paper to form a uniform layer, and the coated paper was mated with a sheet of PET film to afford a "sandwich"-like laminate that was further cured in an oven at 160 °C for 90 min. After removal of the release paper, an adhesive film on the PET film was obtained and was directly used for 90º peel test. The film was tacky and easily wet the stainless steel panel, which was important to get good contact and adhesion to the panel. However, there was a lot of adhesive residues remaining on the panel after the peel test, which indicated that the cohesive strength of the adhesive film was insufficient for PSA applications. Further curing of the laminate at 160 °C for up to 150 min still did not improve the cohesive strength of the adhesive film.

Publication Date (Web): June 18, 2015 | doi: 10.1021/bk-2015-1192.ch025

Table 1. Polymerizations of DA and Epoxides, and the Properties of the Resulting Polymers[a]

Entry	*Pre-polymerization*			*Cure time (min)[b]*	*Peel strength (N/cm)[c]*	*Shear strength (h)[c]*
	Epoxides	*Temp (°C)*	*Time (min)*			
1	DADGE	110	15	90	tacky, insufficient cohesive strength	
2	NPGGE	125	25	150	tacky, insufficient cohesive strength	
3	BDDGE	125	25	120	tacky, insufficient cohesive strength	
4	BPAGE	70	23	25	Almost not tacky, slightly stiff	
5	TMPGE	70	45	20	1.2 ± 0.1 (1.8 ± 0.2[d])	> 240 (25 ± 23[d])
6	TMPGE	70	45	60	1.0 ± 0.2	> 240
7	DGGA	85	25	20	Not tacky, slightly stiff	
8	TEPIC	85	25	20	Not tacky, slightly stiff	

[a] The catalyst AMC-2, 1.0 wt% based on the weight of the reaction mixture; the -COOH/epoxy molar ratio of the reaction mixture, 1.0; the thickness of the PSA layer, 5.5±0.6 mg/cm^2; PET film (~ 50 μm thick) was used as the backing material unless otherwise noted. [b] The pre-polymers were cured in an oven at 160°C. [c] The failure mode in peel and shear tests was adhesive failure; n.m., not measured. [d] Paper (~ 68 μm thick) was used as the backing material for the PSA.

In Green Polymer Chemistry: Biobased Materials and Biocatalysis; Smith, et al.;
ACS Symposium Series; American Chemical Society: Washington, DC, 2015.

NPGGE and BDDGE are aliphatic epoxides, and have a shorter chain length between the epoxy groups than DADGE (Figure 1). Polymerization of DA and NPGGE (Table 1, entry 2) or BDDGE (Table 1, entry 3) also did not generate adhesive films with sufficient cohesive strength for a typical PSA application although both films were tacky.

It has been demonstrated that the incorporation of aromatic moieties into the flexible polymer chains can enhance the cohesive strength of the resulting polymers (*14*, *16*). BPAGE is an epoxide containing a phenylene moiety (Figure 1). Polymerization of DA with BPAGE (Table 1, entry 4) indeed generated a strong film. However, the film was slightly stiff and almost not tacky at room temperature, and could not readily wet the stainless steel panel, which suggested that the T_g of the adhesive film was too high for a PSA application. It is generally agreed that a polymer exhibits good tack only when its T_g is below the use temperature because the polymer chains are then able to easily deform under a light pressure (*1*, *2*). For the adhesive film from the DA-BPAGE mixture, the rigid phenylene moiety from BPAGE was incorporated into the flexible polymer chains, thus imparting the stiffness to the resulting polymer chains and increased the T_g of the polymer above room temperature.

Introduction of chemical crosslinks among polymer chains also significantly improves the cohesive strength of the resulting polymer. TMPGE has three epoxy groups per molecule. The polymerization of TMPGE with DA *via* the epoxy–COOH reaction could lead to formation of highly branched polymers with crosslinked networks. As expected, the polymerization of the DA-TMPGE mixture (Table 1, entry 5) generated a dry and tacky film. The film was infusible, and could only be swollen and partially dissolved in ethyl acetate, chloroform, tetrahydrofuran, toluene, acetone, ethyl ether, *N*,*N*-dimethylformamide, and hexane, which suggested the crosslinking nature of the film.

The pre-polymerization of the DA-TMPGE mixture and the subsequent curing of the pre-polymer were monitored with FTIR (Figures 2 and 3). The monitoring of the polymerization revealed that a new broad peak of hydroxyl groups at 3450 cm^{-1} and a new peak of ester groups at 1736 cm^{-1} appeared, and the peak of the epoxy groups at 910 cm^{-1} and that of -COOH at 1710 cm^{-1} decreased during the polymerization, which confirmed that the ring-opening of the epoxy groups with the –COOH groups took place and produced new ester linkages and hydroxyl groups. After curing for 20 min, the epoxy groups virtually disappeared, while a small amount of –COOH groups was still present (Figure 2, top). Increase in the curing time from 20 min to 60 min did not change the intensities of peaks of the unreacted –COOH groups, the remaining epoxy groups and other functional groups (Figure 3), which implied that the curing reactions were complete in 20 min. The monitoring of the polymerization with FTIR also revealed that the epoxy groups were consumed faster than the -COOH groups throughout the polymerization, which suggested that the epoxy groups also reacted with other functional groups in addition to the –COOH groups. The other functional groups might include the newly generated hydroxyl groups and water (*13*, *14*, *17*).

Publication Date (Web): June 18, 2015 | doi: 10.1021/bk-2015-1192.ch025

Publication Date (Web): June 18, 2015 | doi: 10.1021/bk-2015-1192.ch025

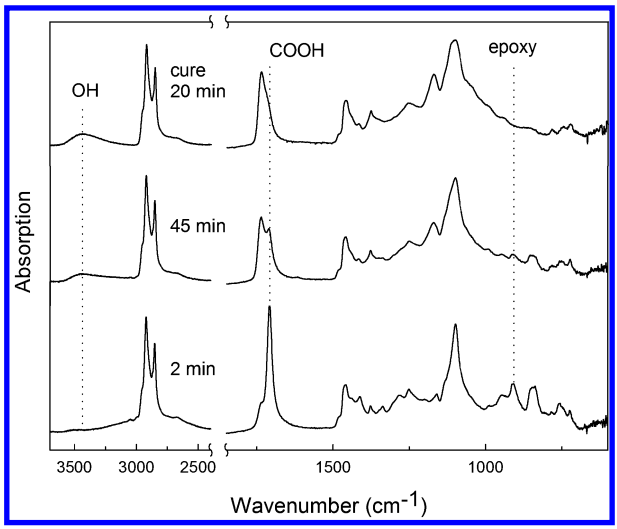

Figure 2. FTIR spectra of the pre-polymers from polymerization of the mixture of DA and TMPGE for 2 min (bottom) and 45 min (middle), respectively, and those (top) from the curing of the pre-polymers for 20 min.

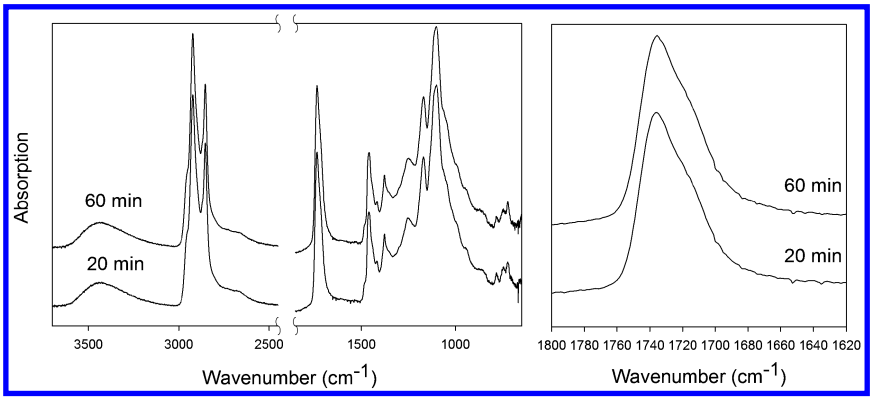

Figure 3. FTIR spectra of the products from the curing of the pre-polymer of the DA-TMPGE mixture for 20 min (left, bottom) and 60 min (left, top), respectively, and close-up views (right) of the peak of the ester carbonyl and the shoulder peak of the -COOH carbonyl groups.

The tacky film from the DA-TMPGE mixture on the PET backing exhibited a peel strength of 1.2 N/cm and a shear strength of more than 240 h (Table 1, entry 5). Its true shear strength was not known because the shear test was terminated at 240 h that was well above the typical value of 168 h for commercially available PSAs (*18*). Increase in the curing time from 20 min to 60 min (Table 1, entry 6) did not significantly change the peel and shear strengths of the tacky film. These

results revealed that polymerization of the DA-TMPGE mixture generated a PSA that had a decent peel strength and adequate cohesive strength for a typical PSA application. It should be noted that the PSA on a paper backing (Table 1, entry 5) had a higher peel strength of 1.8 N/cm but a lower shear strength of 25 h than that on the PET backing. The discrepancy between the two PSA tapes could be mainly due to the backing materials, since the peel and shear strengths of a PSA tape not only depend on the properties of PSA layer itself but are also strongly influenced by the properties of the backing materials such as their thickness and modulus (*2*).

DGGA and TEPIC also has three epoxy groups per molecule and could play the same role as TMPGE (Figure 1). Polymerization of a DA-DGGA (Table 1, entry 7) or DA-TEPIC mixture (Table 1, entry 8) generated a strong and slightly stiff film that was not tacky and could not wet adherends such as stainless steel well. The polymers were expected to have similar crosslinks from the reactions between the –COOH and epoxy groups to those from the DA-TMPGE mixture. In addition, the phenylene moiety from DGGA or the triazine ring from TEPIC had been incorporated into the flexible polymer backbones and could potentially pack together through π-electron stacking, thus providing physical crosslinks to the polymers. The additional physical crosslinks of the PSAs from the DA-DGGA and DA-TEPIC mixtures could result in a greater crosslinking density than that from the DA-TMPGE mixture. Our results are consistent with reports that an increase in the crosslinking density of a PSA can substantially decrease its tack and adhesive strength (*3*, *19*).

In summary, among the DA-epoxide mixtures (Table 1) investigated, only the polymer from the DA-TMPGE mixture had a decent peel strength and a sufficient cohesive strength for typical PSA applications. It was also concluded that the adhesive properties such as the tack, peel strength, and shear strength of the polymers from the DA-epoxide mixtures greatly depended on the properties of the starting epoxides such as the epoxy functionality and the rigidity/flexibility of their molecular chains. Therefore, extensive efforts were then devoted to copolymerization of DA with epoxides having different properties such as the epoxy functionality and/or the rigidity/flexibility of their molecular chains, hoping for achieving a good balance between the adhesive and cohesive strengths and improving the adhesive properties of the PSAs from DA-epoxide mixtures.

Publication Date (Web): June 18, 2015 | doi: 10.1021/bk-2015-1192.ch025

Copolymerization of DA with Epoxides and Preparation of PSAs

Copolymerization of a DA-DADGE-TMPGE mixture with a molar ratio of epoxy groups from DADGE vs. epoxy groups from TMPGE vs. -COOH groups of 0.5/0.5/1 was carried out, hoping that the partial replacement of the polyfunctional epoxide TMPGE with the difunctional epoxide DADGE could reduce the crosslinking density of the resulting polymers, thus increasing the adhesive strength of the resulting PSA over that from the DA-TMPGE mixture. The DA-DADGE-TMPGE mixture required a long curing time of about 1.5 h for the generation of a dry film. The film was tackier than that from the DA-TMPGE mixture, but left a small amount of adhesive residues on the stainless steel panel in the peel test, which indicated that it did not have adequate cohesive strength for PSA applications. Change in the addition sequence for the monomers, *i.e.*,

DA and DADGE were first polymerized at 100 °C for 65 min to form a mixture of polymers/oligomers containing two –COOH groups, followed by reacting with TMPGE, resulted in a shorter curing time of about 1 h for the generation of a dry and tacky film. The film left fewer adhesive residues on the stainless steel panel in the peel test than that obtained from the polymerization by adding the monomers all at once, which indicated that the cohesive strength was slightly improved. However, a commercially viable PSA is required to be cleanly removed from substrates without leaving any adhesive residues. Therefore, the cohesive strength of the film was still not desirable for PSA products.

As discussed previously in the polymerization of the DA-BPAGE mixture, the incorporation of phenylene moiety into the flexible polymer chains could significantly enhance the cohesive strength of the resulting polymers. Our attention was then turned to use of an epoxide containing a phenylene moiety as a comonomer for the replacement of the aliphatic epoxide DADGE, hoping for increasing the cohesive strength while maintaining good tack.

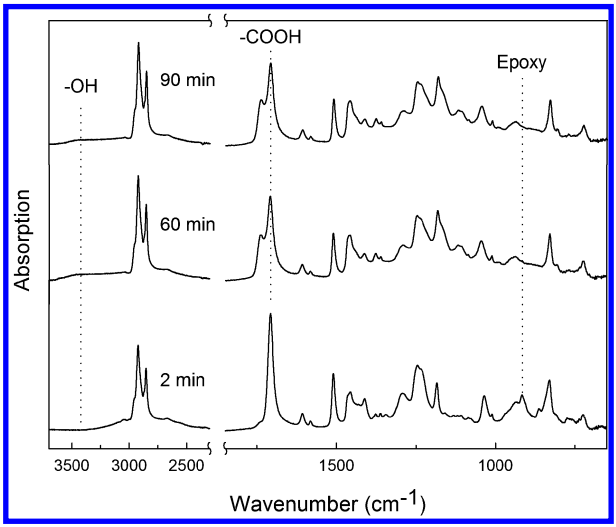

Figure 4. FTIR spectra of the pre-polymers from polymerization of the DA-BPAGE mixture for 2 min (bottom), 60 min (middle) and 90 min (top), respectively.

PE-1 was prepared from the polymerization of a DA-BPAGE mixture with a -COOH/epoxy molar ratio of 2.27. After the mixture was polymerized for 60 min, the epoxy groups of BPAGE were completely consumed as evidenced by disappearance of the characteristic peak of the epoxy groups at 916 cm^{-1} in the FTIR spectrum (Figure 4, middle), while a substantial amount of unreacted –COOH groups remained in the product. Increase in the reaction time from 60 min to 90 min (Figure 4, top) did not significantly change the intensities of the peaks of the remaining –COOH group and other functional groups in the FTIR spectrum, which implied that the reactions were complete in 60 min. Since

Publication Date (Web): June 18, 2015 | doi: 10.1021/bk-2015-1192.ch025

DA was present in excess in the reaction mixture and the epoxy groups were completely consumed by the –COOH groups of DA, the product was expected to be a mixture of polymers/oligomers containing two -COOH groups at the chain ends in addition to some unreacted DA.

Pre-polymerization of PE-1 with TMPGE and the subsequent curing of the resulting pre-polymer generated a PSA (Table 2, entry 1). The monitoring of the pre-polymerization and the curing with FTIR (Figure 5) revealed that the curing reactions completed in 23 min. The resulting PSA on the paper backing had a peel strength of 2.2 N/cm that was higher than that (1.8 N/cm) from the DA-TMPGE mixture (Table 1, entry 5), and had a shear strength of more than 240 h which was substantially higher than that (25 h) from the DA-TMPGE mixture. These results revealed that the incorporation of the phenylene-containing monomer BPAGE into the PSAs improved the adhesive properties, especially the shear strength of the resulting PSAs.

Publication Date (Web): June 18, 2015 | doi: 10.1021/bk-2015-1192.ch025

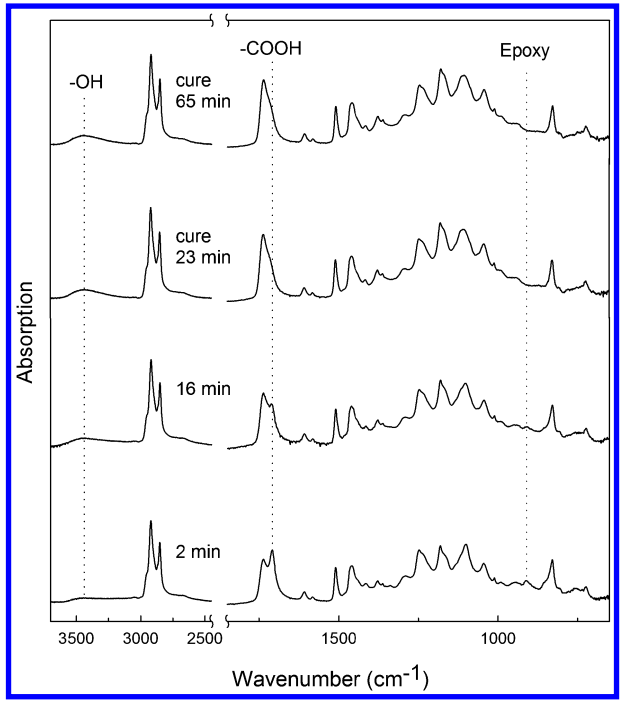

Figure 5. FTIR spectra of the pre-polymers from pre-polymerization of the mixture of PE-1 and TMPGE for 2 and 16 min, respectively, and those of the PSAs from the curing of the pre-polymer (that was pre-polymerized for 16 min) for 23 and 65 min, respectively.

In Green Polymer Chemistry: Biobased Materials and Biocatalysis; Smith, et al.;
ACS Symposium Series; American Chemical Society: Washington, DC, 2015.

Publication Date (Web): June 18, 2015 | doi: 10.1021/bk-2015-1192.ch025

Table 2. Preparation of PSAs from Polyesters Containing Two –COOH Groups and Epoxides, and the Properties of the PSAs[a]

Entry	*Pre-polymerization*			*Cure time (min)[b]*	*Peel strength (N/cm)[c]*	*Loop tack (N)[c]*	*Shear strength (h)[c]*
	Polyesters	*Epoxides*	*Time (min)*				
1	PE-1	TMPGE	16	23	2.2 ± 0.3	3.9 ± 0.7	> 240
2	PE-1	TMPGE	16	23	1.5 ± 0.3 1.2 ± 0.3[d]	2.7 ± 0.7 2.1 ± 0.8[d]	> 240
3	PE-2	TMPGE	16	28	2.6 ± 0.3	6.9 ± 1.8	> 240
4	PE-2	TMPGE	16	28	1.8 ± 0.2 1.5 ± 0.2[d] 1.3 ± 0.3[e]	5.3 ± 1.4 4.5 ± 1.3[d] 3.5 ± 1.2[e]	> 240
5	PE-3	TEPIC	12	38	5.7 ± 0.5	12.8 ± 2.6	0.6 ± 0.3
6	PE-3	TEPIC	12	38	3.4 ± 0.4	n.m.	8 ± 5

[a] Catalyst AMC-2, 1.0 wt% based on the weight of the reaction mixture; the -COOH/epoxy molar ratio of the reaction mixture, 1.0; the pre-polymerization took place at 75°C; thickness of the PSA layer, 5.5±0.6 mg/cm^2; paper (~ 68 μm thick) was used as the backing material in entries 1, 3, 5, and PET film (~ 50 μm thick) was used in entries 2, 4, and 6. [b] The pre-polymers were cured at 160°C. [c] The failure mode in peel and tack tests was adhesive failure; n.m., not measured. [d] The PSA samples were measured after one week of aging at 60°C. [e] Measured after four weeks of aging at 60°C.

The PSA on the PET backing (Table 2, entry 2) had a lower peel strength of 1.5 N/cm and a lower tack of 2.7 N than that on the paper backing (Table 2, entry 1), correspondingly. As discussed previously for the PSA tapes from the DA-TMPGE mixture, the discrepancy in the peel strength and the tack between the two PSA tapes was mainly due to the backing materials because the peel strength and the tack of PSA tapes were strongly influenced by the properties of the backing materials (*2*). After aging at 60 °C for 1 week (Table 2, entry 2), the peel strength and tack of the PSA were 1.2 N/cm and 2.1 N, respectively, which did not significantly change as compared to those without aging. The PSA left no adhesive residues on the stainless steel panel during the peel and tack tests, which revealed that the PSA did not disintegrate after an aging time of up to 1 week at 60 °C. As revealed by the aging studies on petrochemical-based PSAs, one week of aging at 60 °C is equivalent to about 9 months of aging at room temperature (*20*, *21*). If the aging results of petrochemical-based PSAs were applicable to the PSAs from this study, the PSA from the mixture of PE-1 and TMPGE was stable for at least 9 months.

PE-2 was prepared from copolymerization of a mixture of DA, BPAGE, and NPGGE with a molar ratio of epoxy groups from BPAGE vs. epoxy groups from NPGGE vs. -COOH groups of 0.22/0.22/1. The PSA obtained from polymerization of a mixture of PE-2 and TMPGE (Table 2, entry 3) had a higher peel strength of 2.6 N/cm and a much higher tack of 6.9 N than that from the mixture of PE-1 andTMPGE (Table 2, entry 1), while maintaining a very good shear strength of more than 240 h. The same amount of DA and the same –COOH/epoxy molar ratio were used in the preparation of PSAs from the mixture of PE-1 andTMPGE and the mixture of PE-2 and TMPGE, respectively, except that the rigid BPAGE that was used in the preparation of the former PSA was partially replaced with the flexible aliphatic epoxide NPGGE for the preparation of the latter PSA. Therefore, the PSA from the mixture of PE-2 and TMPGE had a smaller amount of BPAGE incorporated than that from the mixture of PE-1 and TMPGE. As demonstrated previously in the polymer from the DA-DGGA mixture, the phenylene moiety of BPAGE that had been incorporated into the flexible polymer backbones could provide physical crosslinks to the polymers. Therefore, the PSA from the mixture of PE-2 and TMPGE had a lower crosslinking density than that from the mixture of PE-1 and TMPGE. Our results are consistent with reports that a decrease in the crosslinking density of a PSA can increase its tack and peel strength (*3*, *19*).

The PSA on the PET backing (Table 2, entry 4) had a lower peel strength of 1.8 N/cm and a lower tack of 5.3 N than that on the paper backing (Table 2, entry 3). After aging at 60 °C for 1 week (Table 2, entry 4), the peel strength and tack of the PSA were 1.5 N/cm and 4.5 N, respectively, which did not significantly change as compared to those without aging. Even after 4 week aging (Table 2, entry 4), the peel strength and tack still did not significantly decrease. The PSAs after being aged left no adhesive residues on the stainless steel panel during the peel and tack tests, which revealed that the PSA did not disintegrate after an aging time of up to 4 week at 60 °C. If the aging results of petrochemical-based PSAs (*20*, *21*), were applicable to the PSA from this study, the PSA from the mixture of PE-2 and TMPGE was stable for at least 36 months.

Publication Date (Web): June 18, 2015 | doi: 10.1021/bk-2015-1192.ch025

It has been demonstrated previously that the cohesive strength of the PSAs from the DA-epoxide mixtures could be increased by incorporating of moieties such as phenylene and triazine rings into the PSAs through (co)polymerization of DA and epoxides containing these moieties. Alternatively, such moieties could also be incorporated into the PSAs by addition of polyfunctional epoxides containing these moieties as crosslinking agents. PE-3 was prepared from polymerization of a mixture of DA and aliphatic epoxide DADGE. Pre-polymerization of PE-3 and TEPIC containing a triazine group and three epoxy groups, and the subsequent curing of the resulting pre-polymer generated a PSA (Table 2, entries 5 and 6). The peel strengths of the PSA on the paper (Table 2, entry 5) and PET backings (Table 2, entry 6) were 5.7 and 3.4 N/cm, respectively, which were significantly higher than those from the mixture of PE-2 and TMPGE (Table 2, entries 3 and 4). The PSA also had a much higher tack of 12.8 N (Table 2, entry 5) than that (6.9 N) from the mixture of PE-2 and TMPGE. However, the shear strength of the PSA on the paper and PET backings were only 0.6 and 8 h, respectively, which were much lower than those from the mixture of PE-2 and TMPGE (Table 2, entries 3 and 4).

PSAs obtained from DA-TMPGE, (PE-1)-TMPGE, (PE-2)-TMPGE, and (PE-3)-TEPIC mixtures are tacky, soft and flexible, which was partly due to the inherent flexibility of long hydrocarbon chains from the starting monomers such as DA and DADGE (*22*). The flexible long hydrocarbon chains allowed the PSAs to readily deform and wet adherends under light pressure, thus facilitating establishment of an adhesive bond with the adherends (*2*). The crosslinks in the PSAs imparted the PSAs sufficient cohesive strength. In addition, the PSAs contained hydroxyl groups (-OH) and a small amount of unreacted –COOH groups. The -OH and -COOH groups could improve the wetting of the PSAs on various adherends such as paper, glass, and skin, thus facilitating the intimate contact between the PSAs and the adherends (*11*, *23–25*). These functional groups in PSAs could also significantly improve the adhesive strength of the PSAs through formations of hydrogen bonds between the PSAs and adherends (*23–26*). The -OH and –COOH groups also allowed formations of hydrogen bonds among molecular chains and within the same molecular chain of the PSA, thus increasing the cohesive strength of the PSA (*11*, *23–26*).

Commercially available office PSA tapes typically have a peel strength in the range of 3.5-8.8 N/cm, and labels such as Post-it® notes require a peel strength as low as 0.2 N/cm (*4*). The PSAs from this study could be tailored through the selection of epoxides and their usage for a peel strength ranging from 1.0 to 5.7 N/cm. They could potentially be used for office PSA tapes and labels. In addition, the PSAs described in this study could be solely based on renewable bio-materials because DA, DADGE, and TMPGE can be derived from renewable natural resources (TMPGE can be prepared from trimethylolpropane and epichlorohydrin; trimethylolpropane (*27*) and epichlorohydrin (*28*) can be derived from renewable sugars and glycerol, respectively). The process for the preparation of the PSAs did not require organic solvents or toxic chemicals, thus being very environmentally friendly.

Conclusions

Polymerization of DA with DADGE, NPGGE, BDDGE, BPAGE, TMPGE, DGGA, or TEPIC generated polymers with different properties. Only the polymer from the DA-TMPGE mixture could serve as a PSA that had a peel strength of 1.2-1.8 N/cm and an adequate shear strength. Copolymerization of the aliphatic epoxides DADGE and TMPGE with DA did not generate a PSA with adequate cohesive strength. The replacement of DADGE with the phenylene-containing monomer BPAGE resulted in PSAs with a peel strength of 1.5-2.6 N/cm, a loop tack of 2.7-6.9 N, a superior shear strength of more than 240 h, and a good aging resistance. Incorporation of triazine ring into the polymers from DA-epoxide mixtures by using the triazine-containing epoxide TEPIC as a crosslinking agent also resulted in PSAs with a superior peel strength of 3.4-5.7 N/cm and a good loop tack of 12.8 N. The PSA properties of the polymers from the DA-epoxide mixtures could be tailored to meet requirements of different PSA products through the selection of the epoxides and their usage. The new PSAs could be fully based on renewable materials. The process for the preparation of the PSAs was simple and environmentally friendly.

Publication Date (Web): June 18, 2015 | doi: 10.1021/bk-2015-1192.ch025

Acknowledgments

This research was supported by the royalty fee income of patented technologies from K. Li's research group. We thank Henkel Corp. (Rochy Hill, CT) for providing us with the polyethylene terephthalate (PET) film, and thank Avery Dennison Corp. (Pasadena, CA) for providing us with the PET-based release film and Fasson 54# Semi-Gloss Facestock.

References

1. Benedek, I.; Feldstein, M. M. *Handbook of Pressure-Sensitive Adhesives and Products: Fundamentals of Pressure Senitivity*; Taylor & Francis Group: Boca Raton, FL, 2009; Vol. 1, pp 1−2.
2. Chu, S. G. Viscoelastic Properties of Pressure Sensitive Adhesive. In *Handbook of Pressure Sensitive Adhesive Technology*, 2nd ed.; Satas, D., Ed.; Van Nostrand Reinhold: New York, 1989; pp 158−203.
3. Bunker, S. P.; Staller, C.; Willenbacher, N.; Wool, R. P. Miniemulsion polymerization of acrylated methyl oleate for pressure sensitive adhesives. *Int. J. Adhes. Adhes.* **2003**, *23*, 29–38.
4. Bunker, S. P.; Wool, R. P. Synthesis and characterization of monomers and polymers for adhesives from methyl oleate. *J. Polym. Sci., Part A: Polym. Chem.* **2002**, *40*, 451–458.
5. Klapperich, C. M.; Noack, C. L.; Kaufman, J. D.; Zhu, L.; Bonnaillie, L.; Wool, R. P. A novel biocompatible adhesive incorporating plant-derived monomers. *J. Biomed. Mater. Res.* **2009**, *91A*, 378–384.
6. David, S. B.; Sathiyalekshmi, K.; Raj, G. A. G. Studies on acrylated epoxydised triglyceride resin-co-butyl methacrylate towards the

development of biodegradable pressure sensitive adhesives. *J. Mater. Sci.: Mater. Med.* **2009**, *20*, S61–S70.
7. Ahn, B. K.; Kraft, S.; Wang, D.; Sun, X. S. Thermally stable, transparent, pressure-sensitive adhesives from epoxidized and dihydroxyl soybean oil. *Biomacromolecules* **2011**, *12*, 1839–1843.
8. Ahn, B. K.; Kraft, S.; Sun, X. S. Chemical pathways of epoxidized and hydroxylated fatty acid methyl esters and triglycerides with phosphoric acid. *J. Mater. Chem.* **2011**, *21*, 9498–9505.
9. Ahn, B. K.; Sung, J.; Sun, X. S. Phosphate esters functionalized dihydroxyl soybean oil tackifier of pressure-sensitive adhesives. *J. Am. Oil Chem. Soc.* **2012**, *89*, 909–915.
10. Vendamme, R.; Eevers, W. Sweet solution for sticky problems: chemoreological design of self-adhesive gel materials derived from lipid biofeedstocks and adhesion tailoring via incorporation of isosorbide. *Macromolecules* **2013**, *46*, 3395–3405.
11. Vendamme, R.; Olaerts, K.; Gomes, M.; Degens, M.; Shigematsu, T.; Eevers, W. Interplay between viscoelastic and chemical tunings in fatty-acid-based polyester adhesives: engineering biomass toward functionalized step-growth polymers and soft networks. *Biomacromolecules* **2012**, *13*, 1933–1944.
12. Wu, Y.; Li, A.; Li, K. Development and evaluation of pressure sensitive adhesives from a fatty ester. *J. Appl. Polym. Sci.* **2014**, *131*, 41143.
13. Wu, Y.; Li, A.; Li, K. Pressure sensitive adhesives based on oleic acid. *J. Am. Oil Chem. Soc.* **2014**, *92*, 111–120.
14. Li, A.; Li, K. Pressure-sensitive adhesives based on soybean fatty acids. *RSC Adv.* **2014**, *4*, 21521–21530.
15. Li, A.; Li, K. Pressure-Sensitive Adhesives Based on Epoxidized Soybean Oil and Dicarboxylic Acids. *ACS Sustainable Chem. Eng.* **2014**, *2*, 2090–2096.
16. White, J. E.; Brennan, D. J.; Silvis, H. C.; Mang, M. N. Epoxy-based thermoplastics: new polymers with unusual property profiles. In *Specialty Monomers and Polymers: Synthesis, Properties, and Applications*; Havelka, K. O., McCormick, C. L., Eds.; ACS Symposium Series 755; American Chemical Society: Washington, DC, 2000; pp 132−146.
17. Swern, D.; Billen, G. N.; Eddy, C. R. Chemistry of Epoxy Compounds. VI. Thermal Polymerization of the Isomeric 9,10-Epoxystearic Acids. *J. Am. Chem. Soc.* **1948**, *70*, 1228–1235.
18. Lligadas, G.; Ronda, J. C.; Galia, M.; Cadiz, V. Bionanocomposites from Renewable Resources: Epoxidized Linseed Oil-Polyhedral Oligomeric Silsesquioxanes Hybrid Materials. *Biomacromolecules* **2006**, *7*, 3521–3526.
19. Trenor, S. R.; Long, T. E.; Love, B. J. Development of a light-deactivatable PSA via photodimerization. *J. Adhes.* **2005**, *81*, 213–229.
20. ASTM D3611, Standard Practice for Accelerated Aging of Pressure-Sensitive Tapes; American Society for Testing and Materials,: West Conshohocken, PA, 2011.
21. PSTC-2 Appendages A and D, Test Methods for Pressure Sensitive Adhesive Tapes, 12th ed.; Pressure Senstitive Tape Council: Naperville, IL, 1996.

22. Hill, K. Fats and oils as oleochemical raw materials. *Pure Appl. Chem.* **2000**, *72*, 1255–1264.
23. Gay, C. Stickiness - some fundamentals of adhesion. *Integr. Comp. Biol.* **2002**, *42*, 1123–1126.
24. Bellamine, A.; Degrandi, E.; Gerst, M.; Stark, R.; Beyers, C.; Creton, C. Design of nanostructured waterborne adhesives with improved shear resistance. *Macromol. Mater. Eng.* **2011**, *296*, 31–41.
25. Dana, S. F.; Nguyen, D. V.; Kochhar, J. S.; Liu, X. Y.; Kang, L. UV-curable pressure sensitive adhesive films: effects of biocompatible plasticizers on mechanical and adhesion properties. *Soft Matter* **2013**, *9*, 6270–6281.
26. Gower, M. D.; Shanks, R. A. Acrylic acid level and adhesive performance and peel master-curves of acrylic pressure-sensitive adhesives. *J. Polym. Sci., Part B: Polym. Phys.* **2006**, *44*, 1237–1252.
27. Fleischer, M.; Blattmann, H.; Mülhaupt, R. R. Glycerol-, pentaerythritol- and trimethylolpropane-based polyurethanes and their cellulose carbonate composites prepared via the non-isocyanate route with catalytic carbon dioxide fixation. *Green Chem.* **2013**, *15*, 934–942.
28. Fourcade, D.; Ritter, B. S.; Walter, P.; Schönfeld, R.; Mülhaupt, R. Renewable resource-based epoxy resins derived from multifunctional poly(4-hydroxybenzoates). *Green Chem.* **2013**, *15*, 910–918.

Publication Date (Web): June 18, 2015 | doi: 10.1021/bk-2015-1192.ch025

Publication Date (Web): June 18, 2015 | doi: 10.1021/bk-2015-1192.ch026

Chapter 26

Structure-Property Relationships for Polycyanurate Networks Derived from Renewable Resources

Andrew J. Guenthner,*[,1] Benjamin G. Harvey,[2] Matthew C. Davis,[2] Michael D. Ford,[3] Heather A. Meylemans,[2] Michael E. Wright,[2] Andrew P. Chafin,[2] and Joseph M. Mabry[1]

[1]Air Force Research Laboratory, Aerospace Systems Directorate, 10 E. Saturn Boulevard, Edwards AFB, CA 93524, U.S.A.
[2]Naval Air Warfare Center, Weapons Division, 1 Administration Circle, China Lake, CA 93555, U.S.A.
[3]ERC Incorporated, Air Force Research Laboratory, 10 E. Saturn Boulevard, Edwards AFB, CA 93524, U.S.A.
***E-mail: andrew.guenthner@us.af.mil.**

The recent synthesis of a wide variety of cyanate ester monomers that may be derived from renewable resources has created a newly available set of chemical structures that, due to a wide range of chemical features, provide a unique opportunity for the development of quantitative structure-property relationships for dicyanate esters and their polymerized networks. Specific structure-property relationships for monomer melting point, glass transition temperature at full conversion, and char yields at 600 °C under nitrogen and air have been developed with the aid of partial least squares methods. The predictions inherent in these structure-property relationships are examined and compared to predictions based on ordinary least squares methods. Specific predictions for the properties of two as-yet unsynthesized dicyanate ester monomers derived from renewable resources are also presented.

In Green Polymer Chemistry: Biobased Materials and Biocatalysis; Smith, et al.;
ACS Symposium Series; American Chemical Society: Washington, DC, 2015.

Introduction

Polycyanurate networks, which are produced by cyclotrimerization of cyanate ester monomers, are a well-known class of high-performance thermosetting polymers that offer many unique advantages in demanding applications (*1–4*). For instance, in structures for space telescopes (*5*) and interplanetary space probes (*6*), the ease of polymerization with little or no generation of volatiles is especially advantageous for reliable long-term performance. Similarly, the unusually low dielectric constants, outstanding resistance to high-energy radiation, and low coefficients of thermal expansion of polycyanurate networks provide additional advantages in the harsh environments of outer space or on other planets. In terrestrial environments, the high mechanical strength and stiffness of polycyanurate networks at elevated temperatures are attractive for applications in micro-electronics and aircraft engines (*7*). From a fundamental standpoint, polycyanurates are advantageous for the study of structure-property relationships in thermosetting networks because the high selectivity of cyanurate formation results in networks with chemical structures that can be described with much greater precision than is possible with many other networks (*8*). The ease of network preparation, relatively low toxicity of monomers, and the ability to adjust reaction rates over a wide range through catalysis also greatly aid in carrying out studies of the relationship between network structure and properties.

At first glance, it may appear that polycyanurate networks are not an especially appealing class of polymers for replacement of petroleum-based sources with bio-based or other renewable sources, because traditionally, bio-based sources have been desired for their relatively low cost, with the expectation that significant declines in performance will be a necessary trade-off. Such reasoning, however, fails to take into account considerations of source variety. Cyanate ester monomers derived from petroleum sources have tended to fall into two distinct classes: bisphenol-type monomers that are derived from the coupling of phenol with ketones, or novolac-type monomers that are derived from the coupling of phenol and formaldehye (*1*). Because of its wide availability as a standard petroleum product, the use of phenol as a starting point for monomer synthesis has become an entrenched practice. In the realm of renewable sources, however, there is no bias toward phenol as a starting point. The plant kingdom offers a wide variety of phenolic compounds that may be obtained from essential oils, extracts, or from the decomposition of lignin.

From the perspective of performance, a wider variety of starting structures will enable the synthesis of networks with a wider variety of final properties. While some property combinations may offer lower performance, others will offer higher performance. For example, polycyanurate networks derived from the essential oil anethole have been shown to offer the lowest known water uptake near full conversion (1.1%) in networks that exhibit a glass transition temperature above 220 °C at full conversion and that can be produced from monomers that are stable liquids at room temperature (*9*). This combination of properties is particularly useful for production of structures by bulk molding for use in environments with both exposure to moisture and elevated temperature

In Green Polymer Chemistry: Biobased Materials and Biocatalysis; Smith, et al.;
ACS Symposium Series; American Chemical Society: Washington, DC, 2015.

Publication Date (Web): June 18, 2015 | doi: 10.1021/bk-2015-1192.ch026

From the perspective of developing structure-property relationships, the wide variety of structures afforded by renewable resources that can be converted into monomers is extremely useful. In most cases, the ultimate goal driving the development of structure-property relationships is the desire to rationally design a network at the molecular level to satisfy a given set of performance needs, based on the predicted properties of structures that have not yet been synthesized. The usefulness of such predictions depends on their reliability for structures that differ from those already available. The reliability in turn depends on the variety of available structures utilized to elucidate the structure-property relationships that enable prediction. The availability of a greater variety of structures from renewable resources will therefore translate into more robust structure-property relationships that can be used to generate more reliable predictions of performance. Thus, the development of polycyanurate networks based on renewable resources has afforded a unique opportunity to study structure-property relationships in a class of thermosetting polymers where both the structures are known with a high level of precision and a wide range of structures have been characterized.

In this chapter, the structure-property relationships in polycyanurate networks derived from renewable resources will be discussed with respect to four key properties: monomer melting point, glass transition temperature at full conversion, and char yields under nitrogen and air at 600 °C. These properties were chosen because they generally do not depend on the extent of conversion in the network. The first two are independent of conversion by definition, and the latter two, while they may show some conversion dependence, are the outcome of experiments in which the networks are heated to very high temperatures, thereby likely resulting in very high levels of conversion at the onset of degradation. The structure-property relationships, which are derived from partial least squares (PLS) regressions on the properties of interest as a function of quantitative structural parameters, are compared to more traditional linear regression analysis. We found the PLS technique to be effective in elucidating known structure-property relationships, even with a data set typically consisting of only around 15 samples. The majority of these relationships are known only because of the availability of bio-based monomers.

Publication Date (Web): June 18, 2015 | doi: 10.1021/bk-2015-1192.ch026

Experimental

Materials and Data Sources

The 19 monomers / networks chosen for analysis contain only the elements C, H, N, and O. All feature two aromatic rings containing one or more cyanate ester / cyanurate linkages, connected by a bridge containing only non-aromatic hydrocarbons. Two of the monomers are derived from petroleum; they are the well-known Primaset BADCy and Primaset LECy (dicyanate esters of bisphenol A and E, respectively); the remaining 17 have been derived from a variety of plant compounds. Figure 1 shows the chemical structure of all monomers, along with the nomenclature used to identify them. The networks chosen for comparison have all been analyzed using either identical or nearly identical protocols in our laboratories, thereby helping to ensure that comparisons reflect meaningful

differences. Table 1 lists the properties of interest for all of these materials, along with the original source publications (*9–15*), where available. In some cases, as noted in the table, publication is in progress.

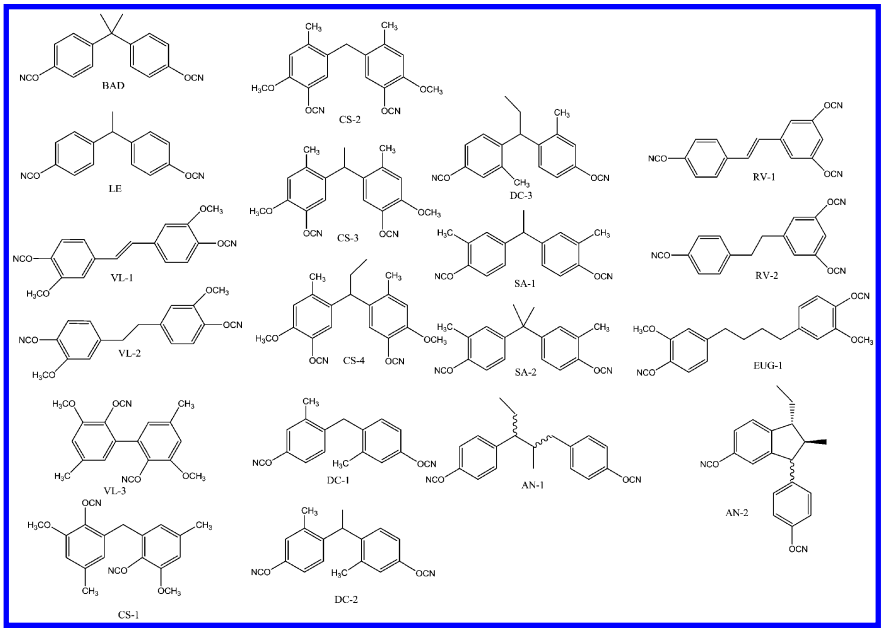

Figure 1. Structures of monomers included in correlations, with labels.

Publication Date (Web): June 18, 2015 | doi: 10.1021/bk-2015-1192.ch026

Methods of Analysis

An advantage of PLS regression is that there is no need to try and guess which structural parameters are of importance ahead of time, nor is there a need to try and combine parameters judiciously so as to produce mechanistically relevant independent variables or to limit correlations in the structural parameters. Instead, all that is necessary is to produce a consistent scheme of non-duplicative parameters that are capable of describing the structure. It might be assumed that because of the highly similar nature of the monomers, that the number of structural parameters would be small. However, as Figure 2 shows, we found that a minimum of ten parameters was necessary to describe these systems. Five parameters describe the subsituttion patterns around the aromatic rings, which are usually but not always the same for both rings in each monomer. The other five describe the architecture of the bridge. Six of the parameters take on values

from 0 to 1, while four (all associated with the bridge) can take on any number larger than 0. Table 2 provides extended definitions for each parameter, while Figure 2 provides a convenient graphical way to visualize the meaning of each parameter. We could have included additional parameters, however, we chose not to include parameters which were unique to a single monomer because these parameters simply become correction factors that are unique to that particular monomer. Thus, for instance, with regard to methyl groups on aromatic rings, we do distinguish between *–ortho* substitution and other substitution patterns, but not between *–meta* and *–para* substitution.

Publication Date (Web): June 18, 2015 | doi: 10.1021/bk-2015-1192.ch026

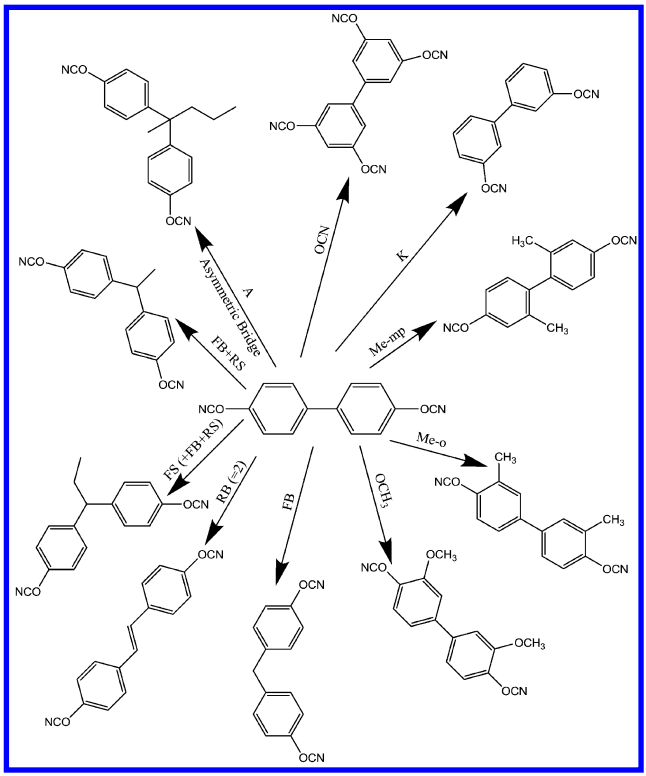

Figure 2. Illustration of the structural parameters used in developing structure-property correlations. The "baseline monomer" structure is shown in the center, with the arrows describing the unit changes to parameters that result in the modified structures shown on the outer circle. For instance, changing the parameter K from 0 to 1 results in the structure shown in the upper right corner. Note that in some case, sensible structures result only from multiple simultaneous changes if starting with the "baseline" monomer.

In Green Polymer Chemistry: Biobased Materials and Biocatalysis; Smith, et al.;
ACS Symposium Series; American Chemical Society: Washington, DC, 2015.

Table 1. Physical Property Data Used in Structure-Property Correlations

Monomer/network	*T_m (°C)*[a.]	*$T_{G\text{-}fc}$ (°C)*[b.]	*Char Yield (N_2, %)*	*Char Yield (Air, %)*	*Source*
BAD	83	323	47	25	9
LE	Liquid[c.]	295	54	24	9
AN-1	Liquid[c.]	223	31	9	9
AN-2	72	313	48	6	9
CS-1	151	236	33	8	10
CS-2	125	240	35	11	10
CS-3	98	206	28	11	10
CS-4	120	238	27	11	10
DC-1	88	259	53	30	11[d.]
DC-2	105	283	43	4	11[d.]
DC-3	Liquid[c.]	273	43	3	11[d.]
EUG-1	104	167	31	1	12
RV-1	156	>340	74	71	13
RV-2	123	334	70	66	13
SA-1	73	236	48	11	14
SA-2	82	237	43	8	14
VL-1	237	n/a	n/a	n/a	15
VL-2	190	n/a	n/a	n/a	15
VL-3	205	n/a	n/a	n/a	15

[a.] Melting point as observed by differential scanning calorimetry [b.] Glass transition temperature as determined by peak in loss component of stiffness in oscillatory thermomechanical analysis after heating to 350 °C [c.] No differential scanning calorimetry melting point was observed [d.] Publication in progress. Numbers in the "source" column refer to the number of the reference given at the end of this chapter in which the data are located.

Publication Date (Web): June 18, 2015 | doi: 10.1021/bk-2015-1192.ch026

Table 2. Explanation of Structural Parameters

Parameter	*Explanation*
OCN	Additional -OCN groups per monomer (e.g. 1 for tricyanates)
K	"Kinked" -OCN groups (that is, -OCN groups -*ortho* or -*meta* to bridge junction); 1 if any such groups are present on a cyanated aromatic ring; 0 if not present on a cyanated ring; averaged over all cyanated aromatic rings in monomer (e.g. 0 for the typical 4,4′ –OCN substitution pattern in dicyanate monomers)
Me-mp	Methyl groups in positions -*meta* or -*para* to -OCN groups; 1 if any such groups are present on a single aromatic ring; 0 if not present; averaged over all cyanated aromatic rings in monomer
Me-o	Methyl groups in positions -*ortho* to -OCN groups; counting / averaging rules are the same as for Me-mp.
OCH_3	Methoxy groups on cyanated aromatic rings; counting / averaging rules are the same as for Me-mp
FB	"Flexible" non-hydrogen atoms in bridge "backbone" structure; the "backbone" of the bridge is defined as the set of non-hydrogen atoms bonded along the shortest possible path connecting two cyanated aromatic rings; if more than one such path exists, atoms in all such paths count, if more than one bridge exists, the total number of flexible non-hydrogen atoms in all bridge structures is counted, with each counted only once; "flexible" is defined as having sp^3 hybridization and being bonded to at least two other atoms (e.g. not a chain terminus) not in a ring; sp^3 atoms in ring structures considered on a case by case basis.
RB	"Rigid" non-hydrogen atoms in bridge "backbone" structure. "Rigid" is defined as any non-hydrogen atom not meeting the criteria for "flexible", with sp^3 atoms in ring structures considered on a case by case basis. Non-hydrogen atoms that terminate chains, such as methyl carbons, and hydroxyl oxygens, count as "rigid". Rules for backbones and bridges are the same as for FB.
FS	"Flexible" non-hydrogen atoms in bridge "side group" structures. "Flexible" is defined as in FB, and the rules for counting paths and bridges are the same as in FB. A "side group" atom is any non-hydrogen atom in a structure bridging cyanated aromatic rings that is not counted as part of the "backbone"
RS	"Rigid" non-hydrogen atoms in "side group" bridge structures; definitions and rules are the same as for FB, RB, and FS (e.g. an isopropylidene bridge will have FB=1 and RS=2).
A	Asymmetric bridge. 1 if a bridge group is symmetrically substituted along its backbone(s), 0 if not, averaged over all bridge structures. Bridge and backbone are defined as in FB.

Publication Date (Web): June 18, 2015 | doi: 10.1021/bk-2015-1192.ch026

Publication Date (Web): June 18, 2015 | doi: 10.1021/bk-2015-1192.ch026

Table 3. Structural Parameter Values for All Monomers

Monomer	*OCN*	*K*	*Me-mp*	*Me-o*	*OCH3*	*FB*	*RB*	*FS*	*RS*	*A*
BAD	0	0	0	0	0	1	0	0	2	0
LE	0	0	0	0	0	1	0	0	1	1
AN-1	0	0	0	0	0	3	0	1	2	1
AN-2	0	0	0	0	0	0.5	0.5	1.5	3.5	1
CS-1	0	1	1	0	1	1	0	0	0	0
CS-2	0	1	1	0	1	1	0	0	0	0
CS-3	0	1	1	0	1	1	0	0	1	1
CS-4	0	1	1	0	1	1	0	1	1	1
DC-1	0	0	1	0	0	1	0	0	0	0
DC-2	0	0	1	0	0	1	0	0	1	1
DC-3	0	0	1	0	0	1	0	1	1	1
EUG-1	0	0	0	0	1	4	0	0	0	0
RV-1	1	0.5	0	0	0	0	2	0	0	0
RV-2	1	0.5	0	0	0	2	0	0	0	0
SA-1	0	0	0	1	0	1	0	0	1	1
SA-2	0	0	0	1	0	1	0	0	2	0
VL-1	0	0	0	0	1	0	2	0	0	0
VL-2	0	0	0	0	1	2	0	0	0	0

Monomer	*OCN*	*K*	*Me-mp*	*Me-o*	*OCH3*	*FB*	*RB*	*FS*	*RS*	*A*
VL-3	0	1	1	0	1	0	0	0	0	0
AN-U	0	0	0	0	0	1	2	1	2	1
EUG-U	0	0	0	0	1	2	0	0	0	0

Publication Date (Web): June 18, 2015 | doi: 10.1021/bk-2015-1192.ch026

For monomers containing different structures on each ring, the values were averaged. For instance, in resveratrol, one but not both rings have an additional –OCN group, therefore the "additional –OCN" parameter has a value of 0.5, just as the "kinked chain" parameter also takes on a value of 0.5. Note that for the bridge groups, in accordance with a method described by Bicerano (*16*), we assume that aliphatic rings have intermediate flexibility between that of aromatic rings and linear aliphatics, with fused rings biased toward increased rigidity. For AN-2, this required that the bridge atoms be partitioned among the various parameters. For the single atom in the backbone, we apportioned 0.5 to the flexible backbone parameter FB and the remaining 0.5 to the rigid backbone parameter. Similarly, for the side groups, taking into account that only one atom clearly meets the definition of "flexible:", we partitioned 1.5 atoms to the flexible side group parameter and 3.5 to the rigid side group parameter, which includes terminal methyl group carbons. Table 3 lists the values of these parameters for all of the monomers / networks studied. It is worth noting that, like all structural parameterizations, the one developed for this study has limitations. CS-1 and CS-2, for instance, have exactly the same structural parameters, despite differing in the type of "kink" found in the chain. This limitation stems from the decision not to include structural parameters that were unique to a single monomer.

For each property of interest, a partial least squares regression was done on all samples with measured data (typically 14 to 17 of the 19 available monomers). The PLS regressions were carried out using the SIMPLS algorithm (*17*) in MATLAB. This algorithm automatically centers the input data but does not require normalization. The regressions were repeated while varying the number of PLS components from 0 to 9, and, in each case, the mean squared error of the regression was estimated using "leave one out" cross-validation. The number of PLS components was then chosen so as to minimize the estimated mean squared error, and detailed information was gathered on the selected regression. More traditional linear regressions were also carried out, first using all structural parameters, and then using only those parameters that were found to be significant in some cases The latter approach represents a more traditional means of reducing the effects of overfitting, which would likely be attempted if PLS were not available.

Publication Date (Web): June 18, 2015 | doi: 10.1021/bk-2015-1192.ch026

Results and Discussion

Monomer Melting Point

Of the 19 monomers studied, melting points were measured for 16. The remaining three had melting points that were near or below room temperature, making measurement difficult. In the case of LECy, the melting point is known to be 29 °C, a value likely depressed significantly due to the presence of two co-crystalline forms (*18*), however, we did not include this melting point in the data set for reasons of consistency. It is not known whether the other "liquid" cyanate ester monomers are also simply supercooled liquids with melting points near room temperature, so only those melting points that were observed in a standard DSC experiment were included. In general, we have found that melting

In Green Polymer Chemistry: Biobased Materials and Biocatalysis; Smith, et al.;
ACS Symposium Series; American Chemical Society: Washington, DC, 2015.

points of cyanate esters vary widely and do not conform to simple structural rules, therefore a model based on PLS regression may be quite useful. In this section, the melting point model is examined in some detail in order to illustrate the concepts underlying all of the PLS models described in this chapter.

Figure 3 shows that with just three components, PLS regression provides the minimum error according to cross-validation. In contrast, the root-mean-squared ("rms") error of the regression itself continues to decrease as more components are added. Note that the use of 10 components yields a model equivalent to ordinary least squares regression. The three component model explains about 83% of the variation in melting point. Although the 10-component model can explain 95% of the variation, this comes at the cost of over-prediction, as expected for a data set with just 16 samples.

Publication Date (Web): June 18, 2015 | doi: 10.1021/bk-2015-1192.ch026

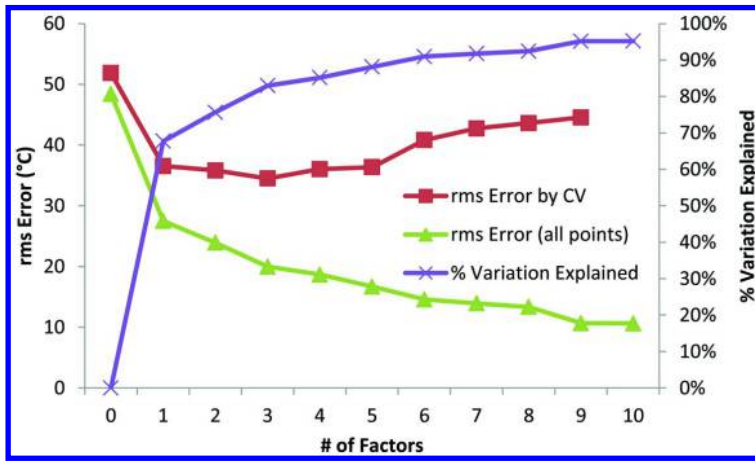

Figure 3. Partial least squares regression characteristics as a function of the number of regression components present.

In order to understand how over-prediction affects the data set, Figure 4 shows the predicted melting points for each of the samples as a function of the number of PLS components added. The PLS regression process can be thought of generating a set of successively corrected predictions for the observed results. As Figure 4 shows, the first two or three components (which can be considered iterations in successive prediction) affect nearly all of the predictions, whereas later iterations affect only a few. Note that the shaded area in Figure 4 indicates where over-prediction takes place according to cross-validation experiments. In more colorful terms, the first three components can be thought of as "catering to the masses", whereas the additional components can be envisioned as "catering to special interests".

In Green Polymer Chemistry: Biobased Materials and Biocatalysis; Smith, et al.;
ACS Symposium Series; American Chemical Society: Washington, DC, 2015.

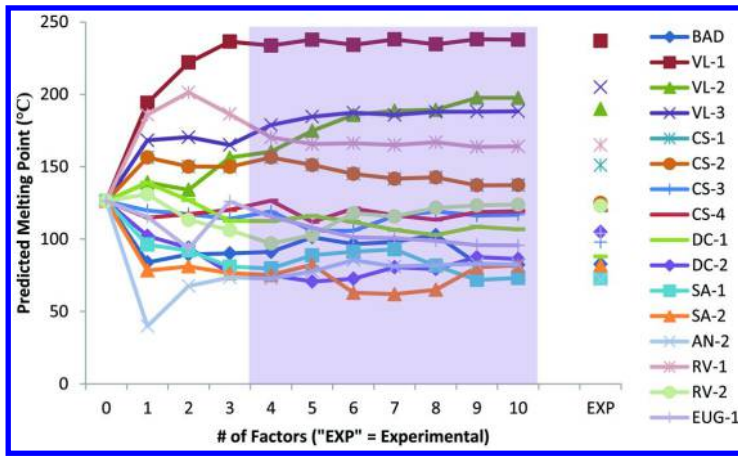

Figure 4. Predicted melting point values as a function of the number of partial least squares regression components.

The effect of "catering to special interests" on the quantitative model for monomer melting point can be seen in Figure 5. The values plotted reflect the relative effect of a unit change in each of the structural parameters on the predicted melting point. Note that "const." refers to the model intercept. With few components, the model generally features a cluster of features that tend to depress the melting point, with the presence of flexible backbone linkages in the bridge and rigid or terminal side groups on the bridge having the largest relative effects. In contrast, the presence of rigid backbone linkages and methoxy groups *ortho*- to the cyante ester groups tend to result in a significant increase in melting point. However, as more components are added, many of the coefficients "blow up". For instance, the predicted effect of methoxy groups triples in magnitude, while the effect of having one additional –OCN linkage per aromatic ring is transformed from insignificant to an almost 150 °C increase, and the effect of "kinked" –OCN groups is transformed from insignificant to an over 100 °C decrease. In fact, Figure 5 makes clear that the most significant effects indicated by ordinary linear regression are actually just those effects that have been "blown up" the most by over-prediction.

For prediction of melting points, then, it can be seen that ordinary least squares leads to over-prediction, in which "catering to special interests" by the model (that is, reducing the errors in predicting the values of a few select data points) leads to estimates of structural effects that are wildy different than those found in models that reduce prediction errors across the entire sample set. These results demonstrate that the typical advantages of PLS regression are realized when constructing structure-property models on relatively small data sets.

In Green Polymer Chemistry: Biobased Materials and Biocatalysis; Smith, et al.;
ACS Symposium Series; American Chemical Society: Washington, DC, 2015.

Publication Date (Web): June 18, 2015 | doi: 10.1021/bk-2015-1192.ch026

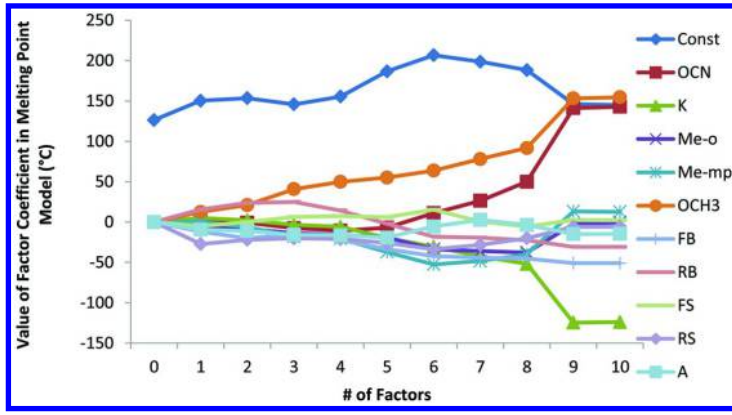

Figure 5. Melting point regression coefficients as a function of the number of partial least squares regression components.

Publication Date (Web): June 18, 2015 | doi: 10.1021/bk-2015-1192.ch026

Having established the model, it is important to consider the actual predictive capabilities it provides. Cross-validation indicates that the PLS regression should predict melting points to within about 35 °C. As a result, for samples (such as LECy) not included in the model, the predicted melting points should be not much greater than about 50 °C. Figure 6 shows the predicted melting points (Table 4 provides the model coefficients) according to both ordinary least squares (OLS) and PLS regressions for LECy, DC-3, and AN-1, the three "room temperature liquid" monomers. Both models predict that only AN-1 should be liquid at room temperature. As mentioned earlier, the melting points of monomers such as LECy appear to be anomalously low due to the ease of producing disorder in the crystalline structure. Other studies of cyanate esters have shown the monomers may be liquid at room temperature due to the presence of multiple stereoisomers (*19*), as would be the case for AN-1. Thus, although the models may be able to quantify the expected value of the melting point, many complex physical and chemical factors will also play a role.

In Figure 6, the predicted melting points according to OLS and PLS regressions for two as-yet unsynthesized monomers are given. These are the unsaturated forms of the AN-1 and EUG-1 monomers. The synthesis of both monomers involves a hydrogenation step that may be skipped in order to produce the structures AN-U and EUG-U (shown in Figure 7). As of this writing, these monomers have not been made, thus the predicted melting points shown in Figure 6 cannot have been influenced by any experimental findings to date. The OLS model predicts that AN-U should be a liquid like AN-1, while the PLS model predicts that AN-U will be a solid with a melting point in the 100-150 °C range. These contrasting predictions will provide an interesting test of these models should the compound AN-U be synthesized.

In Green Polymer Chemistry: Biobased Materials and Biocatalysis; Smith, et al.;
ACS Symposium Series; American Chemical Society: Washington, DC, 2015.

Publication Date (Web): June 18, 2015 | doi: 10.1021/bk-2015-1192.ch026

Table 4. Linear Regression Model Coefficients for Melting Point

Factor	*PLS*	*OLS*
Constant	145.88	144.97
OCN	-7.64	142.86
K	-3.44	-123.97
Me-o	-13.73	-0.42
Me-mp	-18.07	12.73
OCH3	40.74	154.55
FB	-15.17	-50.97
RB	24.92	-30.87
FS	6.21	2.37
RS	-20.27	-5.86
A	-15.69	-14.60

Regression types: PLS = partial least squares; OLS = ordinary least squares.

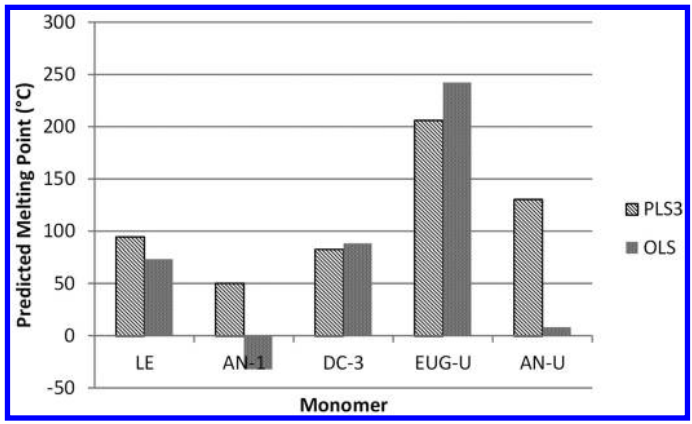

Figure 6. Predicted melting points of monomers not included in regression models; comparison of ordinary least squares and partial least squares predictions.

Glass Transition Temperature at Full Cure

Figure 8 shows the error characteristics of the PLS model of the glass transition temperature at full cure. In this case, 15 of the 19 samples were used for the model. RV-1 was excluded because its glass transition temperature at full cure was too high to be measured reliably, while degradation of the networks

interfered with the measurement of the glass transition temperature at full cure for the systems with monomers derived from vanillin. With six components, the rms error based on cross-validation is minimized, and over 95% of the variation is accounted for. Similar to the regression for melting point, the minimum rms error is around 30 °C.

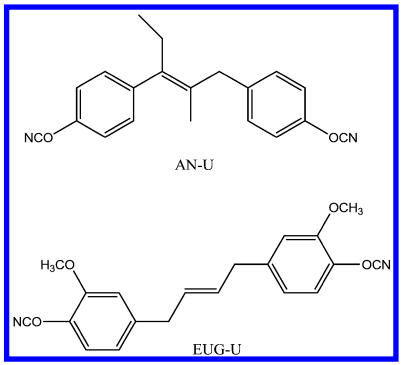

Figure 7. Chemical structures of the as-yet unsynthesized monomers AN-U and EUG-U.

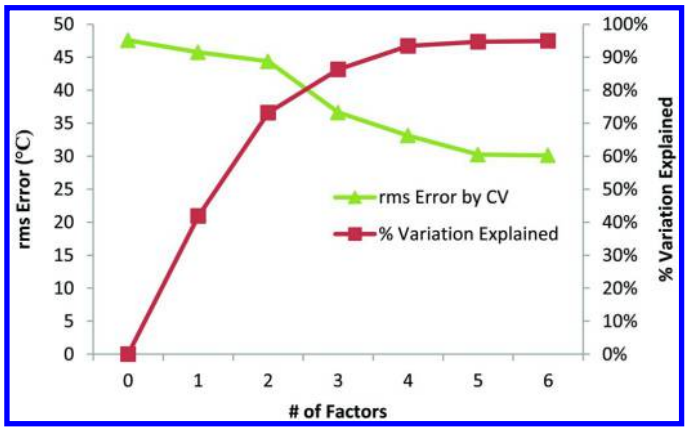

Figure 8. Error characteristics of partial least squares model for glass transition temperature at full cure.

Figure 9 shows the predicted glass transition temperature values as a function of the number of PLS components. Unlike the case with melting point, as more components are added, the adjustments become finer but remain spread out more or less evenly over at least five different samples. This result indicates that the PLS regression algorithm is still "catering to the masses" as errors are reduced, rather than "catering to special interests".

In Green Polymer Chemistry: Biobased Materials and Biocatalysis; Smith, et al.;
ACS Symposium Series; American Chemical Society: Washington, DC, 2015.

Publication Date (Web): June 18, 2015 | doi: 10.1021/bk-2015-1192.ch026

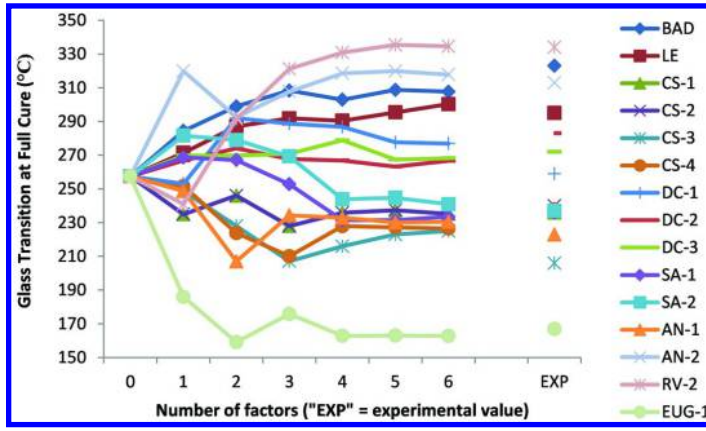

Figure 9. Predicted glass transition temperature values as a function of the number of partial least squares components utilized in the model.

Publication Date (Web): June 18, 2015 | doi: 10.1021/bk-2015-1192.ch026

In order to examine the predictive capabilities of the models, the glass transition temperature at full cure was predicted for RV-1, and the as-yet unsynthesized monomers AN-U and EUG-U. The PLS regression was compared to ordinary least squares (OLS), and ordinary least squares in which only statistically significant factors were retained (OLS-r). The OLS-r model represents an alternative means of avoiding the pitfalls of over-prediction. For RV-1, which is known to have a glass transition temperature at full cure significantly exceeding 340 °C (not to be confused with the "as cured" glass transition temperature, which is lower due to incomplete conversion), the PLS model predicts a glass transition temperature near 410 °C, while the OLS and OLS-r models predict much lower values of 280 °C and 300 °C, respectively. Table 5 lists the coefficients and Figure 10 shows the predicted values. In contrast, for the closely related RV-2, both PLS and OLS predict a glass transition temperature near 350 °C, which agrees well with the experimental value of 334 °C, while the OLS-r model predicts a much lower glass transition temperature of 250 °C. The PLS model thus does a good job of "extrapolating" the model to predict the properties of a structure that is not included in the model but is closely related, while the OLS model "extrapolates" poorly, predicting that the more rigid RV-1 will have a significantly lower glass transition temperature compared to RV-2, in contrast to both conventional heuristics and the available qualitative observations.

Both OLS models therefore contradict known experimental data. The PLS model shows that increased cyanate ester density increases the glass transition temperature, as does the OLS model. All three models show that adding a methyl group *–ortho* to the cyanate ester decreases the glass transition by about 35 °C

In Green Polymer Chemistry: Biobased Materials and Biocatalysis; Smith, et al.;
ACS Symposium Series; American Chemical Society: Washington, DC, 2015.

compared to the addition of a methyl group either *–meta* or *–para* to the cyanate ester, an observation noted earlier by us (*15*). All models also agree that adding flexible linkages in the bridge lowers the glass transition temperature, a prediction that is in general agreement with observed glass transition temperature trends in polymers. The PLS model indicates that the addition of methoxy groups to the aromatic rings decreases the glass transition temperature, a sensible result given the known effects of methyl group subsitution.

For AN-U and EUG-U, both PLS and OLS-r models predict higher glass transition temperature values, of 250 – 300 °C at full cure, compared to the OLS model, which predicts values of 170 °C and 110 °C, respectively, for AN-U and EUG-U. Significantly, the OLS model predicts that the glass transition temperatures of AN-U and EUG-U will be substantially lower than those of the more flexible, hydrogenated analogues. These predictions seem highly counter-intuitive, and are likely the result of the "RB" coefficient experiencing a "blow up" due to over-prediction in the OLS model.

Publication Date (Web): June 18, 2015 | doi: 10.1021/bk-2015-1192.ch026

Char Yields in Nitrogen and Air

Char yield data was available on 16 out of the 19 networks (all but the vanillin-based systems). The char yields measured were at 600 °C after heating at 10 °C/min. in both nitrogen and air. Generally, the thermal degradation behavior of cyanate esters in nitrogen and air is quite similar. However, additional degradation in air often begins at temperatures just under 600 °C. As a result, the char yields in air can be quite sensitive to the onset of this secondary degradation, which in turn is sensitive to the details of the primary degradation process. As a result, it can be difficult to correlate char yields in air to specific structural features.

For the char yields in nitrogen, a two-component PLS model minimized the prediction error according to cross-validation experiments, while for char yields in air, seven components were required. In general, the prediction errors were larger for char yields in air, likely due to the greater sensitivity of this variable to the specific details of the decomposition process, as explained earlier. Figure 11 shows the characteristic errors obtained by cross-validation as well as the amount of variation explained by PLS models for char yields in nitrogen and in air as a function of the number of PLS components.

Figures 12 and 13 show the predicted char yield values as a function of the number of PLS components for both nitrogen and air, respectively. Note how, although major changes take place in the first few components, they are distributed among several samples rather than just one or two. Note also how, in Figure 13, the subtle changes in the predictions caused by addition of the sixth and seventh factors do not appear to be significant, however, when vieweing the rms error according to cross-validation shown in Figure 11, the addition of these factors does result in a 20% reduction in prediction error by cross-validation. This apparent difference is an indication that the predictive model for char yields in air may be sensitive to the exclusion of a single data point.

In Green Polymer Chemistry: Biobased Materials and Biocatalysis; Smith, et al.;
ACS Symposium Series; American Chemical Society: Washington, DC, 2015.

Table 5. Linear Regression Model Coefficients for Glass Transition Temperature at Full Cure

Factor	*PLS*	*OLS*	*OLS-r*
Constant	345.45	355.59	297.61
OCN	58.52	90.519	0
K	1.13	-38.66	0
Me-o	-66.72	-72.50	-35.17
Me-mp	-33.56	-36.40	0
OCH3	-42.84	-3.04	0
FB	-34.95	-46.39	-25.94
RB	2.48	-73.01	0
FS	1.53	10.50	0
RS	-1.41	3.52	0
A	-8.81	-10.98	0

Regression types: PLS = partial least squares; OLS = ordinary least squares; OLS-r = ordinary least squares re-calculated with only signficiant factors included.

Publication Date (Web): June 18, 2015 | doi: 10.1021/bk-2015-1192.ch026

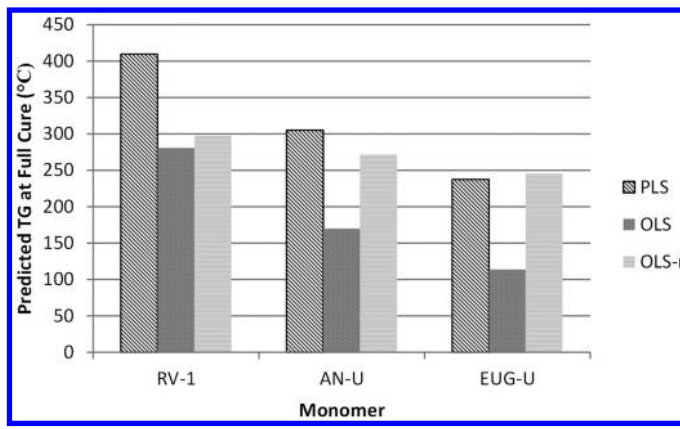

Figure 10. Predicted glass transition temperature values for networks not included in models; comparison of predictions by model type.

The predictive capabilities of the models are illustrated in Figure 14. (Table 6 provides model coefficients). Although char yields at 600 °C were not available for VL-1 and VL-2, some TGA experiments have been done. These show ~80% and ~60% char yields at about 400 °C under nitrogen after accounting for the loss

of trapped solvent, values which are roughly consistent with the predicted char yields at 600 °C. The predicted char yields of AN-U and EUG-U are also shown. In general, the model coefficients indicate that aromatic substitution patterns and the density of cyanate ester linkages are key factors controlling char yields, with methoxy group substitution having a particularly negative effect. The negative effect of methoxy group substitution on thermo-chemical stability in general has been noted in studies of cyanate esters.

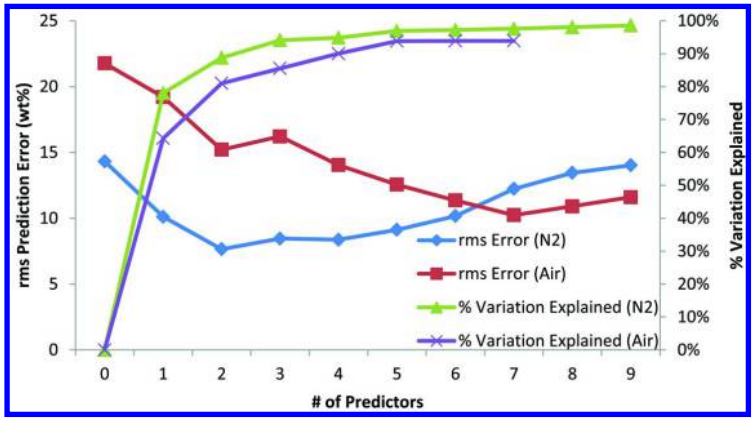

Figure 11. Error characteristics of partial least squares regressions for char yield.

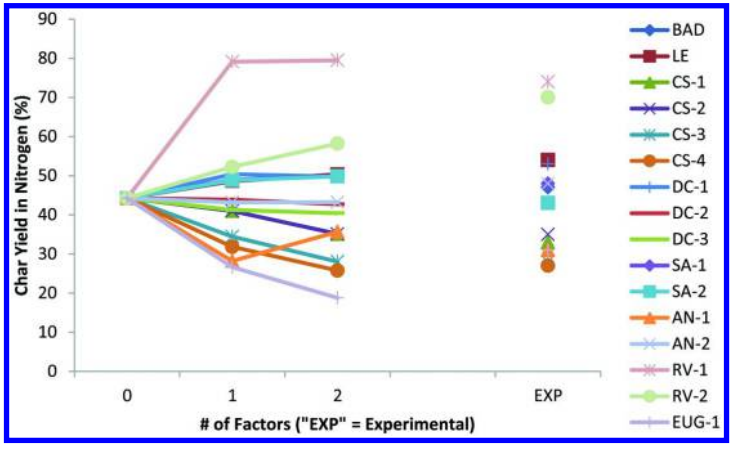

Figure 12. Predicted char yield values as a function of the number of partial least squares regression components, for char yields in nitrogen.

In Green Polymer Chemistry: Biobased Materials and Biocatalysis; Smith, et al.;
ACS Symposium Series; American Chemical Society: Washington, DC, 2015.

Publication Date (Web): June 18, 2015 | doi: 10.1021/bk-2015-1192.ch026

Publication Date (Web): June 18, 2015 | doi: 10.1021/bk-2015-1192.ch026

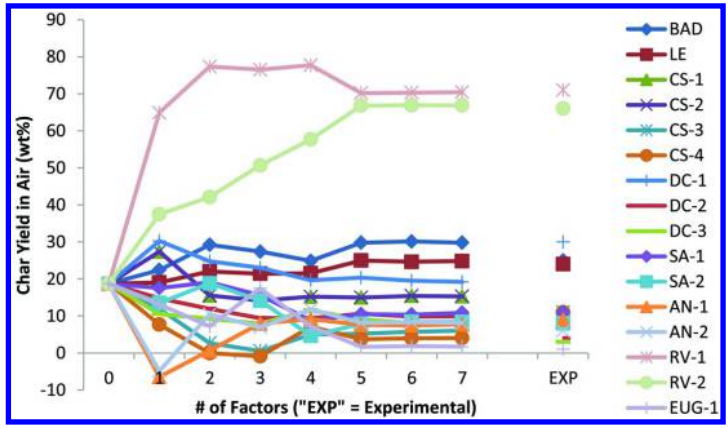

Figure 13. Predicted char yield values as a function of the number of partial least squares regression components, for char yields in air.

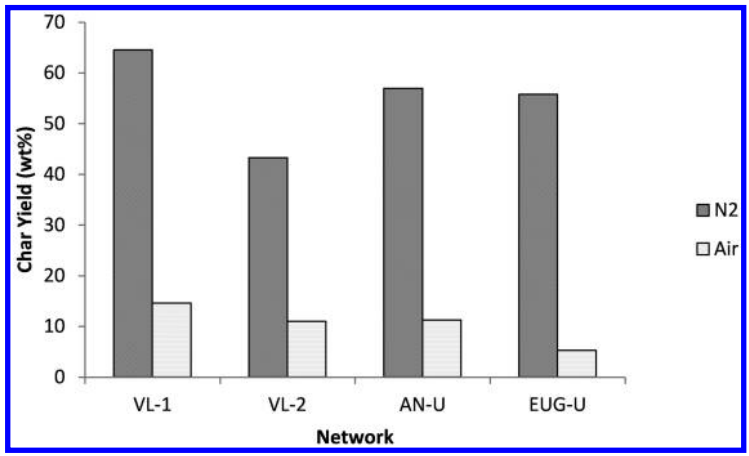

Figure 14. Predicted char yields of networks not included in models.

In Green Polymer Chemistry: Biobased Materials and Biocatalysis; Smith, et al.;
ACS Symposium Series; American Chemical Society: Washington, DC, 2015.

Table 6. PLS Linear Regression Model Coefficients for Char Yield

Factor	*Char Yield (N_2, %)*	*Char Yield (Air, %)*
Constant	61.77	38.73
OCN	7.62	30.20
K	-4.88	14.49
Me-o	-0.38	-13.97
Me-mp	-7.62	-14.87
OCH3	-9.77	-18.42
FB	-4.38	-4.65
RB	6.26	-2.87
FS	-2.30	-1.95
RS	-3.59	-5.86
A	-3.50	-3.40

Publication Date (Web): June 18, 2015 | doi: 10.1021/bk-2015-1192.ch026

Conclusions

Using a set of 19 cyanate ester monomers, 17 of which may be derived from renewable sources, structure property relationships, in the form of partial linear regression models, have been produced for the monomer melting point, glass transition temperature at full cure, and char yield at 600 °C under nitrogen and in air. The partial least squares method was able to provide linear models based on a set of 10 structural parameters that predicted melting points to within about 35 °C, glass transition temperatures at full cure to within about 30 °C, and char yields to within about 10%, based on "leave one out" cross-validation analysis. The predictive power of the patial least squares models was compared to that of ordinary least squares and shown to be at least as good. Moreover, analysis of ordinary least squares models for the monomer melting point clearly showed that such models suffer from over-prediction. The models have been used to predict the properties of two cyanate ester systems that have not yet been synthesized, but could easily be produced for future validation experiments.

Acknowledgments

The authors wish to thank the Strategic Enrivonmental Research and Development Program (project WP-2214), Air Force Office of Scientific Research, the Office of Naval Research, and the Air Force Research Laboratory for their support of these efforts.

References

1. Hamerton, I. In *Chemistry and Technology of Cyanate Ester Resins*; Hamerton, I., Ed.; Chapman & Hall: London, 1994; pp 1−6.
2. Fang, T.; Shimp, D. A. *Prog. Polym. Sci.* **1995**, *20*, 61–118.
3. Nair, C. P. R.; Mathew, D.; Ninan, K. N. In *New Polymerization Techniques and Synthetic Methodologies*, Abe, A., Albertsson, A.-C., Cantow, H. J., Eds.; Springer-Verlag: Berlin, 2001; Vol. 155, pp 1−99.
4. Hamerton, I.; Hay, J. N. *High Perform. Polym.* **1998**, *10*, 163–174.
5. Chen, P. C.; Bowers, C. W.; Content, D. A.; Marzouk, M.; Romeo, R. C. *Opt. Eng.* **2000**, *39*, 2320–2329.
6. Wienhold, P. D.; Persons, D. F. *SAMPE J.* **2003**, *39*, 6–17.
7. Shivakumar, K. N.; Chen, H.; Holloway, G. *J. Reinf. Plast. Compos.* **2009**, *28*, 675–689.
8. Fyfe, C. A.; Niu, J.; Rettig, S. J.; Burlinson, N. E.; Reidsema, C. M.; Wang, D. W.; Poliks, M. *Macromolecules* **1992**, *25*, 6289–6301.
9. Davis, M. C.; Guenthner, A. J.; Groshens, T. J.; Reams, J. T.; Mabry, J. M. *J. Polym. Sci., Part A: Polym. Chem.* **2012**, *50*, 4127–4136.
10. Meylemans, H. A.; Harvey, B. G.; Reams, J. T.; Guenthner, A. J.; Cambrea, L. R.; Groshens, T. J.; Baldwin, L. C.; Garrison, M. D.; Mabry, J. M. *Biomacromolecules* **2013**, *14*, 771–780.
11. Harvey, B. G.; Guenthner, A. J.; Lai, W. W.; Meylemans, H. A.; Davis, M. C.; Cambrea, L. R.; Reams, J. T.; Lamison, K. R. *Macromolecules* submitted for publication.
12. Harvey, B. G.; Sahagun, C. M.; Guenthner, A. J.; Groshens, T. J.; Cambrea, L. R.; Reams, J. T.; Mabry, J. M. *ChemSusChem* **2014**, *7*, 1964–1969.
13. Cash, J. J.; Davis, M. C.; Ford, M. D.; Groshens, T. J.; Guenthner, A. J.; Harvey, B. G.; Lamison, K. R.; Mabry, J. M.; Meylemans, H. A.; Reams, J. T.; Sahagun, C. M. *Polym. Chem.* **2013**, *4*, 3859–3865.
14. Guenthner, A. J.; Wright, M. E.; Chafin, A. P.; Reams, J. T.; Lamison, K. R.; Ford, M. D.; Kirby, S. P. J.; Zavala, J. J.; Mabry, J. M. *Macromolecules* **2014**, *47*, 7691–7700.
15. Harvey, B. G.; Guenthner, A. J.; Meylemans, H. A.; Haines, S. R. L.; Lamison, K. R.; Groshens, T. J.; Cambrea, L. R.; Davis, M. C.; Lai, W. W. *Green Chemistry* **2015** DOI: 10.1039/C4GC01825G.
16. Bicerano, J. *Prediction of Polymer Properties*, 3rd ed.; Marcel Dekker, Inc.: New York, 2002; p 113.
17. de Jong, S. *Chemom. Intell. Lab. Syst.* **1993**, *18*, 251–263.
18. Guenthner, A. J.; Reams, J. T.; Lamison, K. R.; Ramirez, S. M.; Swanson, D. D.; Yandek, G. R.; Sahagun, C. M.; Davis, M. C.; Mabry, J. M. *ACS Appl. Mater. Interfaces* **2013**, *5*, 8772–8783.
19. Cambrea, L. R.; Davis, M. C.; Groshens, T. J.; Guenthner, A. J.; Lamison, K. R.; Mabry, J. M. *J. Polym. Sci., Part A: Polym. Chem.* **2010**, *48*, 4547–4554.

Publication Date (Web): June 18, 2015 | doi: 10.1021/bk-2015-1192.ch027

Chapter 27

Bio-Based Sources for Terephthalic Acid

Patrick B. Smith*

Michigan Molecular Institute, 1910 West St. Andrews Road, Midland, Michigan 48640
***E-mail: smith@mmi.org.**

There is a growing consumer demand for bio-based plastics and chemicals that is being fueled by the public's attitude toward environmental responsibility. One plastic in particular, poly(ethylene terephthalate) (PET), is the fastest growing bio-based plastic as a result of significant market demand for bio-based PET from the "Plant PET Technology Collaborative" made up of Coca Cola, Ford, Heinz, Nike and Proctor&Gamble. This consortium and other retailers are assisting several pre-commercial enterprises to develop commercial processes for bio-based terephthalic acid. Most of these processes target *p*-xylene (pX), the petrochemical precursor for terephthalic acid. They include three thermochemical processes, those of Anellotech, Virent and Ensyn, which produce the benzene, toluene and xylenes (BTX) fraction. Gevo uses a carbohydrate fermentation process to isobutylene which it converts to pX and there are chemical processes including those of Micromidas and Avantium. These latter processes dehydrate carbohydrate feedstocks to furan intermediates from which Micromidas produces pX and Avantium produces 2,5-furandicarboxylic acid (FDCA). FDCA is used to make poly(ethylene furanoate) which has some advantaged properties relative to those of PET. Techno-economic evaluations have shown that some of these companies have achieved economics that are competitive with those of petro-based pX. Most of these have operating pilot facilities and are anticipating scale up to larger production capacity.

In Green Polymer Chemistry: Biobased Materials and Biocatalysis; Smith, et al.;
ACS Symposium Series; American Chemical Society: Washington, DC, 2015.

Publication Date (Web): June 18, 2015 | doi: 10.1021/bk-2015-1192.ch027

Introduction

There is a growing realization that the public's tastes are changing, desiring more products from bio-based rather than petrochemical sources. Many factors are driving this change, including increasing concerns for the environment which promote a desire for greener products (*1*). According to a recent global survey, 94% of consumers would buy a product that has an environmental benefit and 76% have already purchased an environmentally favored product in the past 12 months (*2*). Environmental sustainability is a major strategic initiative with many OEMs and retailers who have initiated programs to provide more bio-based offerings to consumers, companies such as Walmart, Ford, Whole Foods, Starbucks, Target and many others. These trends will continue to support the growth of the bioplastics industry. While these trends are genuine, it is also generally accepted that the majority of customers are not willing to pay a significant premium for a bio-based offering.

One polymer of particular commercial interest is bio-based poly(ethylene terephthalate) (PET), a copolymer of ethylene glycol and terephthalic acid (Scheme 1). A consortium made up of Coca Cola, Ford, Heinz, Nike and Proctor&Gamble, the "Plant PET Technology Collaborative", has announced that they "are committed to supporting and championing research, expanding knowledge and accelerating technology development to enable commercially viable, more sustainably sourced, 100% plant-based PET plastic while reducing the use of fossil fuels" (*3*). The collaboration builds on Coke's "PlantBottle" packaging technology which today is up to 30% bio-based, as a result of incorporating only bio-based ethylene glycol which is derived from bio-ethanol. The terephthalic acid component is petro-based. Heinz has already licensed the technology from Coke for some Heinz ketchup bottles (*4*). PepsiCo has indicated a similar commitment.

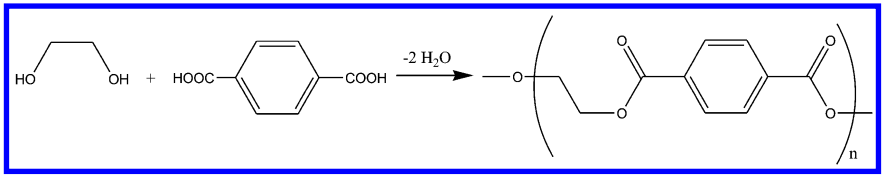

Scheme 1. The Esterification of Ethylene Glycol and Terephthalic Acid to Yield Poly(ethylene terephthalate)

The source of petro-based terephthalic acid is primarily from the oxidation of *p*-xylene (pX). The petrochemical source for pX is the catalytic reforming of naphtha yielding the BTX aromatics stream (benzene, toluene and mixed xylene isomers). The xylene fraction is separated from the other BTX components by

In Green Polymer Chemistry: Biobased Materials and Biocatalysis; Smith, et al.;
ACS Symposium Series; American Chemical Society: Washington, DC, 2015.

distillation but purification of the individual isomers within the xylene fraction is difficult due to their similar boiling points. This purification is done by a series of distillation and adsorption steps, usually with zeolites, or crystallization processes to separate the pX from the other xylene isomers and ethylbenzene (*5*). p-Xylene's melting point is the highest of the xylene isomers, but eutectic mixtures prevent purification by crystallization from being highly efficient. Greater than 98% of the p-xylene produced globally is converted to terephthalic acid (TA) and the global demand for purified TA in 2006 exceeded 30 million metric tons and is expected to exceed 60 million tons by 2020 (*6*). TA is primarily used to produce poly(ethylene terephthalate) (PET). As a result of the expressed demand for cost-competitive, bio-based TA detailed above, bio-based TA made at equal purity and cost as petro-TA would have a clear market advantage over petro-TA. Another advantage for bio-based TA from pX is the fact that it will have significantly lower price volatility than petro-based pX. The recent selling price for petro-pX has varied between 55 and 70¢/lb during which time the price of a barrel of oil was near $100 (*7*).

Publication Date (Web): June 18, 2015 | doi: 10.1021/bk-2015-1192.ch027

Market Growth

The size of the existing PET market for soda and water bottles is immense. About 8% of Coca Cola's PET plastic bottles in 2013 used "PlantBottle" technology. This accounted for about 4 billion bottles or about 210 million pounds of PET (*8*). Avantium CEO, Tom van Aken, stated "The global PTA market represents great potential for bio-based alternatives - more than 50 million tonnes/year. PET bottles are a 15 million tonne/year market based on resin volume with a strong pull for green materials." (*9*). As discussed earlier, only the ethylene glycol component of the PET used in Coca Cola's "PlantBottle" technology is bio-based. The terephthalic acid component is not. If a bio-based TA were available at similar quality and price as petro-based TA, it would have an immediate market for Coke's PlantBottle PET. Coke has expressed the goal of making all of its bottles using PlantBottle technology by 2020. The bio-based market would rapidly grow incorporating the other members of the PlantBottle consortium, as well as PepsiCo.

The major markets for PET include polyester fiber for applications such as carpet, apparel and upholstery, accounting for 66% of the PET market, and packaging films and containers which account for the majority of the rest. The European Bioplastics Institute published recent analyses defining the current market size for the bioplastics industry globally and projected the growth of 600% for this industry between 2010 and 2017 (*10*, *11*), from 1.0 MMT/A in 2010 to 6.2 MMT/A in 2017. The bioplastic that will dominate this growth is bio-based PET, as can be seen from the graphic of Figure 1, accounting for 80% of the total bioplastic capacity by 2016. These forecasts indicate an explosive growth for bio-based PET, with the European Bioplastics Institute projecting that bio-PET will actually grow to 5.2 MMT/A, almost 10% of the total PET market. The PET of this forecast is up to 30% bio-based, coming from the bio-ethylene glycol component. This explosive growth provides significant and direct opportunity for bio-terephthalic acid.

In Green Polymer Chemistry: Biobased Materials and Biocatalysis; Smith, et al.;
ACS Symposium Series; American Chemical Society: Washington, DC, 2015.

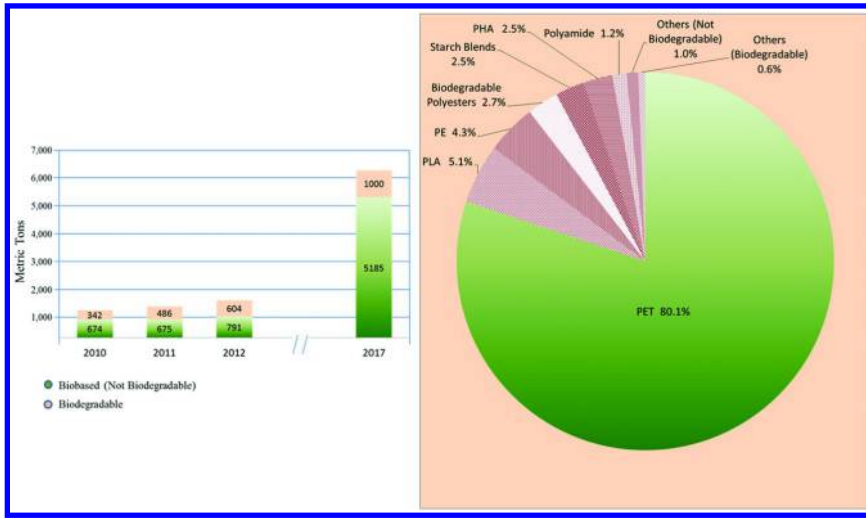

Figure 1. Projected bioplastic production capacity growth from 2010 to 2017 and bioplastic production capacity in 2016.

As the bio-based industry grows, focusing on chemicals rather than fuels is advantageous because chemical products are of significantly higher value than fuels such as ethanol. In particular, furan building blocks are expected to be a platform from which other chemicals will emerge, especially higher value specialty intermediates.

Commodity and specialty chemicals from bio-based feedstocks provide several additional benefits. They lessen dependence on foreign oil, have a smaller carbon footprint, provide domestic jobs, as well as enhance the value to farmers and other biomass suppliers. Consumer products companies and retailers who use bio-based PET view it as a market advantage.

Bio-Based Processes for *p*-Xylene

There are many bio-based processes being developed for the production of pX, terephthalic acid, or 2,5-furandicarboxylic acid (FDCA). Many of the predominant processes are described below and listed in Table 1.

1) Thermochemical (pyrolysis) routes:

   a) Virent - BioForming™ catalytic aqueous phase reforming
   b) Anellotech - catalytic fast pyrolysis to BTX
   c) Ensyn - Rapid Thermal Process™ pyrolysis process

   These processes generate the benzene, toluene, xylenes (BTX) fraction through the catalytic pyrolysis of biomass. These thermochemical approaches produce mixed xylene isomers.

In Green Polymer Chemistry: Biobased Materials and Biocatalysis; Smith, et al.;
ACS Symposium Series; American Chemical Society: Washington, DC, 2015.

Publication Date (Web): June 18, 2015 | doi: 10.1021/bk-2015-1192.ch027

2) Fermentation routes:

    a) Gevo - isobutanol (from fermentation) is dehydrated to isobutylene which is then catalytically dimerized and dehydrocyclized to p-xylene.
    b) Draths (now owned by Amyris) - muconic acid (from fermentation) is converted to TA using a Diels-Alder [4+2] cycloaddition with ethylene.

3) Chemical catalysis:

    a) Coca Cola - patented process to produce bio-based pX from bioethanol.
    b) Avantium - fructose dehydration to HMF which is oxidized to FDCA.
    c) BP – patented process for the conversion of 2,5-furandicarboxylic acid directly to pX using Diels-Alder chemistry with ethylene with low yield of pX.
    d) Professor George Kraus, Iowa State University - chemical process to convert methyl coumalate and methyl pyruvate (from fermentation) directly to TA.
    e) Micromidas - process to dehydrate C6 carbohydrates to 5-chloromethylfurfural which is hydrogenolized to 2,5-dimethylfuran and then converted to pX through a [4+2] Diels-Alder cycloaddition with ethylene.

None of these bio-based processes to produce pX are truly commercial today. Several are being practiced at the pilot scale. Gevo has announced the construction of a 1 million gallon/year pilot facility in St. Joseph, MO, to produce isobutanol from a yeast-based fermentation (*12*). It is also building a pilot facility in Silsbee, TX to convert isobutanol to pX. Isobutanol is catalytically dehydrated to isobutylene, dimerized and dehydrocyclized to xylenes. Gevo has collaborations with Cargill, ICM and Lanxess. The main challenge for this process is to bring the manufacturing cost of isobutanol down.

Anellotech is a start-up using technology developed by Professor George Huber at the University of Massachusetts, Amherst (*13*). It uses a catalytic fast pyrolysis process to convert lignocellulosic biomass to bio-oil, a component of which is the benzene, toluene, xylene (BTX) fraction. The biomass is dried, ground and then conveyed into a fluidized bed reactor charged with a zeolite catalyst. The biomass is pyrolyzed (heated in an oxygen-starved environment) where the resulting pyrolysis gases are catalytically converted to aromatic and olefinic hydrocarbons and other products. Anellotech has built a pilot facility in Pearl River, New York.

The Virent process, trade named BioForming™, is based on catalytic aqueous phase reforming (APR) technology (*14*). APR includes several processes to convert biomass to hydrocarbons, similar to those found in petroleum refineries, including reforming to generate hydrogen which is used to hydrogenolyze

In Green Polymer Chemistry: Biobased Materials and Biocatalysis; Smith, et al.;
ACS Symposium Series; American Chemical Society: Washington, DC, 2015.

Publication Date (Web): June 18, 2015 | doi: 10.1021/bk-2015-1192.ch027

(deoxygenate) biomass, cyclization reactions to form BTX, etc. The product is a mixture of hydrocarbons typically found in conventional petroleum-based fuels. Virent has partnered with Cargill and Coca Cola in the chemicals market and Shell and Honda in the fuels market. Shell built a pilot facility in Houston, TX based on Virent technology.

Table 1. Bio-Based Processes for *p*-Xylene and 2,5-Furandicarboxylic Acid

Company	***Process***	***Commercial Milestones***
Gevo	Isobutanol fermentation	Partnerships with Cargill, ICM and Lanxess, pilot facility in operation
Anellotech	Catalytic fast pyrolysis to BTX	Pilot facility in operation
Virent	Aqueous catalytic reforming to BTX	Partnerships with Cargill, NREL, Coke, Shell and Honda, pilot facility in operation
Micromidas	Chemo-catalytic to CMF	Pilot facility in operation
Ensyn	Rapid Thermal Process, pyrolysis to BTX	Partnerships with UOP, Chevron Technology Ventures, Fibria, pilot scale in operation
Coca-Cola	Bioethylene oligomerization	
Amyris	Muconic acid fermentation	
BP	FDCA Diels-Alder with ethylene	
Avantium	FDCA	Coca Cola, Solvay, Danone and ALPHA, pilot facility in operation
Iowa State University	Coumalate, methyl pyruvate Diels-Alder	

Publication Date (Web): June 18, 2015 | doi: 10.1021/bk-2015-1192.ch027

Ensyn was incorporated in 1984 to commercialize a fast pyrolysis process, tradenamed Rapid Thermal Process™ (RTP), to convert biomass to liquid fuels (*15*). Ensyn has built seven commercial RTP plants in the United States and Canada; the largest being located in Renfrew, Ontario, with a capacity to process 100 tonnes/day of dry wood. Ensyn is planning to significantly expand beyond the Renfrew plant. It produces primarily renewable transportation fuels. Ensyn is also exploring a catalytic route to BTX (benzene, toluene, xylene).

These thermochemical processes use catalytic conversion technologies to enhance the yield of aromatics to up to 40% based on carbon. The yield of pX is normally considerably less than 20% and the aromatics are a mixture of many compounds which present separation challenges. These processes also have high capital costs because materials of construction must be corrosion-proof and able to withstand high temperatures and pressures.

In Green Polymer Chemistry: Biobased Materials and Biocatalysis; Smith, et al.;
ACS Symposium Series; American Chemical Society: Washington, DC, 2015.

2,5-Furandicarboxylic acid (FDCA) which is being marketed by Avantium, is also of interest to the PlantBottle consortium. It is the building block for poly(ethylene furanoate) (PEF), shown in Scheme 2, which has better barrier characteristics than those of PET. Avantium introduced FDCA-based PEF as their premier product because the improved barrier properties would increase the shelf life of soda packaged in plastic bottles as well as potentially creating a new market for beer packaging. The barrier properties of PET are not adequate to package beer but those of PEF appear to be good enough for this application. Fructose or glucose can be used as feedstocks for FDCA which is dehydrated to HMF and oxidized to FDCA (*16*). Avantium is commercializing PEF and polyamides from FDCA. A large hurdle for commercializing PEF for soda and water bottles is that it may contaminate the PET recycle stream. Avantium has constructed a pilot facility in Geleen, the Netherlands. It has developed collaborations with Coca Cola, Danone, Solvay and ALPHA Werke Alwin Lehner GmbH.

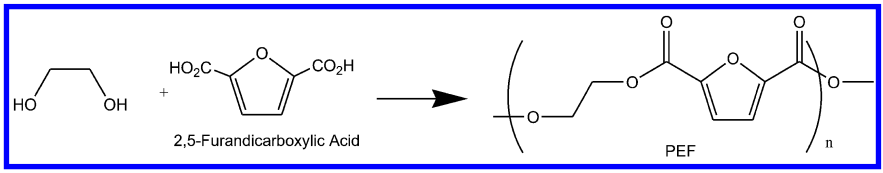

Scheme 2. The Esterification of Ethylene Glycol and FDCA to Yield Poly(ethylene furanoate)

The Micromidas process will be described in more detail later. The other companies of Table 1 have not announced commercial intent thus far.

Advantages of Chemical Processes

The chemical conversion of biomass to furan intermediates has some important advantages over fermentation and thermochemical processes, especially for lignocellulosic biomass. The processing of lignocellulosic biomass by fermentation requires that the biomass first be pretreated with acid or base at elevated temperature to isolate the carbohydrate fraction from the lignin and other plant wall substituents (*17*). The carbohydrate fraction must be recovered and purified and then saccharified to sugars which are fermented to products. This is a multi-step process using corrosive materials in the pretreatment step. The mass yield for the fermentation to ethanol and butanol, for example, is under 50%. The feedstocks for fermentation processes are usually limited because the fermentation organism is often optimized for each substrate type.

Thermochemical processes are able to utilize a variety of feedstocks, although catalyst poisons can be feedstock dependent. Thermochemical processes normally give a broad distribution of products and the yield of any one product is low. These processes give a BTX (benzene, toluene, xylenes) fraction which requires a challenging separation process to yield pure pX.

In Green Polymer Chemistry: Biobased Materials and Biocatalysis; Smith, et al.;
ACS Symposium Series; American Chemical Society: Washington, DC, 2015.

Publication Date (Web): June 18, 2015 | doi: 10.1021/bk-2015-1192.ch027

The chemical conversion of biomass to HMF or CMF is a single step process, similar to the biomass pretreatment process used in a fermentative conversion, but directly providing the HMF product in high yield. Further, the chemical process is able to effectively convert a broad variety of carbohydrate feedstocks with high yields. These include starch, sugar, municipal wastes, corn stover, cardboard, chitin, woody biomass and many others. HMF must be converted to DMF and then to pX and the process gives only one xylene isomer, the para isomer, in high yields, so separation costs are reduced relative to thermochemical processes.

HMF from Biomass

The volume of reports on the production of HMF from biomass has exploded in recent years. It is not within the scope of this manuscript to review all of these, especially because several recent reviews have appeared. Several reviews are of particular interest (*18–22*). The synthesis, toxicity, process chemistry and applications of HMF were described (*19*). This review provides one of the most thorough treatments of HMF chemistry to date. HMF is present in the human diet as a result of food preparation whenever carbohydrates are thermally decomposed, specifically through carmelization and Maillard reactions. These reactions occur in roasting processes and are often responsible for flavor ingredients. The evidence described in the review indicates that the human toxicity of HMF is quite low.

The mechanistic aspects of the dehydration chemistry of fructose, mono, di and polysaccharides were also reviewed. It was concluded that even though there have been numerous studies concerning hexose dehydration, they were largely inconclusive as to the specific glucose to fructose conversion process. However, several conclusions can be drawn:

1) The dehydration of fructose (ketose) is much faster and more selective for HMF than for glucose (aldose). Isomerization of glucose to fructose (Scheme 3) appears to be a rate limiting step for dehydration to HMF.
2) Solvents appear to play a large role in the stabilization of the activated complexes, thereby improving rates and yields for the conversion of hexoses to HMF. Solvents such as dimethylsulfoxide (DMSO), dimethylfomaldehyde (DMF), tetrahydrofuran (THF) and ionic liquids (ILs), especially acidic ILs, have been shown to be quite effective.
3) HMF is unstable in aqueous acid, rehydrating and decomposing to levulinic acid and formic acid. It also condenses to form humins. Performing the dehydration in organic solvents and ILs is one method to limit these side reactions but since water is produced during carbohydrate dehydration, it is difficult to completely isolate HMF from water.
4) The most effective way to isolate and stabilize HMF appears to be through the use of biphasic processes where the hexose is dehydrated in aqueous acid and extracted into an organic phase for its stabilization and recovery. Organic solvents such as methylisobutylketone, DMSO, THF, toluene, 2-butanol and dichloroethane have been used. The carbohydrate is dehydrated in the aqueous phase to HMF which then

Publication Date (Web): June 18, 2015 | doi: 10.1021/bk-2015-1192.ch027

In Green Polymer Chemistry: Biobased Materials and Biocatalysis; Smith, et al.;
ACS Symposium Series; American Chemical Society: Washington, DC, 2015.

partitions into the organic phase. The HMF selectivity in this type of process has been shown to correlate with the partition coefficient of HMF between the 2 phases. The organic phase serves the dual purposes of stabilizing the HMF and providing an effective means for HMF recovery. HMF has a boiling point of about 115°C but is difficult to recover by distillation due to its poor thermal stability. HMF can also be recovered by crystallization.

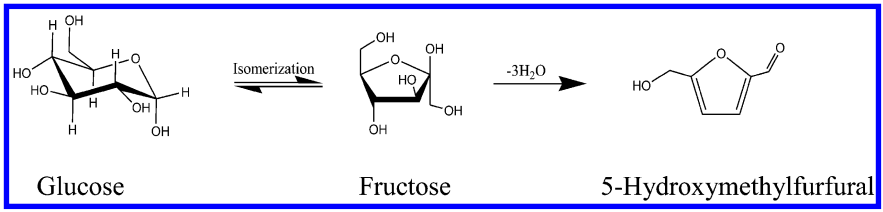

Scheme 3. The Isomerization of Glucose to Fructose and Its Dehydration to HMF

There is vast literature concerning ILs as solvents for the dehydration of hexoses to HMF. ILs have several important advantages for this process: they are able to dissolve high concentrations of sugars and biomass, they are able to catalyze the dehydration without added catalyst, high conversions and selectivities are achieved and rehydration reactions are suppressed. There are also several barriers to their commercial application which include their high cost, necessitating effective recovery schemes, toxicity, the ability to recover HMF from them (neither IL or HMF can be effectively distilled so solvent extraction methods are usually used), the build-up of humins and other impurities which limit IL recycling and issues with IL purity giving rise to irreproducible dehydration yields and rates. Impurities in the ILs which have catalytic effects on HMF formation have been implicated in the irreproducibilities.

The stability problems associated with the conversion of carbohydrates in aqueous media have been documented (*20*). A compelling case was made for the use of biphasic reactors to minimize HMF rehydration reactions. An effective organic phase in terms of HMF yield was identified, 2-*sec*-butylphenol, but the fact that its boiling point is higher than that of HMF made recovery of HMF difficult. It was also shown that both Lewis and Brønsted acid catalysts are important for the conversion of carbohydrates to HMF. Lewis acids such as $AlCl_3$, $InCl_3$, $CrCl_3$, $YbCl_3$ and $SnCl_4$ were shown to catalyze the isomerization of glucose to fructose while Brønsted acids catalyzed its dehydration. Heterogeneous, bifunctional catalysts having large pore diameter and surface area, such as Sn-beta zeolites, performed well.

Fructose is the monosaccharide most readily converted to HMF. As an example, fructose was catalytically converted to HMF at 100°C in under 1 hour in DMSO with yields over 90% (*19*). In comparison, glucose was catalytically converted to HMF in DMSO at 100°C in 3 hours with a yield of 44%. Similarly, the best cellulose conversions were in DMF at 120°C with fairly high catalyst

In Green Polymer Chemistry: Biobased Materials and Biocatalysis; Smith, et al.;
ACS Symposium Series; American Chemical Society: Washington, DC, 2015.

Publication Date (Web): June 18, 2015 | doi: 10.1021/bk-2015-1192.ch027

loadings in 3 hours with a yield of 35%. The rates and yields for conversion of lignocellulosic materials were much lower still. It is not surprising that most of the recent work on processes to convert carbohydrates to HMF has used simple sugars such as fructose and glucose as substrates. The conversion of disaccharides such as sucrose and cellobiose to HMF has been evaluated in a limited number of studies. Still fewer studies have used microcrystalline cellulose as a substrate and a very few have attempted real lignocellulosic biomass.

Techno-Economic Analysis for HMF Manufacture

Potential processes for the conversion of biomass to HMF with associated techno-economic analyses have been presented (*18*, *19*). The cost to produce HMF is closely tied to raw material costs. Fructose at 25¢/lb was the substrate for the most attractive process. The process incorporated a fructose dehydration section using a biphasic reactor, HMF purification, recycle of solvent and fructose, and recovery of byproducts such as levulinic acid. The minimum selling price to produce HMF at the scale of 100 kton/yr fructose utilization was roughly 50¢/lb. This cost was also dependent on yield, byproduct price, catalyst cost and capital costs (scale), in that order. An HMF selling price of about 45¢/lb seemed to be a reasonable selling price for commodity applications but a plant size of at least 100 kton/yr would be required. In order to justify a plant of this size, the products would require markets of this size such that the plant is able to run near capacity. A plant of this size would also create challenges for supply of biomass if unconventional sources, such as corn stover, were to be used.

5-Chloromethylfurfural from Biomass

A process for biomass conversion in which concentrated hydrochloric acid was used to convert simple sugars, starch, cellulose and even chitin to 5-chloromethylfurfural (CMF) was described (*23*, *24*). CMF is more stable than HMF (*19*). Yields of CMF using this process are similar to that for HMF from fructose and glucose but are significantly higher than that from lignocellulosic biomass substrates. A biphasic process with aqueous HCl and dichloroethane (DCE) as the organic phase was used. The partition coefficient for CMF in this system was also quite high. The drawback of this process is the high capital costs due to the use of corrosive aqueous HCl.

HMF Conversion to 2,5-Dimethylfuran

HMF may be converted to DMF by hydrogenolysis of the hydroxymethyl group and reduction of the aldehyde as shown in Scheme 4. Two methods to accomplish this reduction of HMF to DMF in a one step process have recently been reported. In one, a ruthenium-cobalt oxide catalyst for the conversion was used (*25*). The HMF was dissolved in THF at roughly 3 wt%, the ratio of HMF to catalyst being equal to 2.5 by weight. The reaction was carried out at 130°C and 0.7 MPa hydrogen pressure, achieving DMF yields as high as 93.4%. It was shown

In Green Polymer Chemistry: Biobased Materials and Biocatalysis; Smith, et al.;
ACS Symposium Series; American Chemical Society: Washington, DC, 2015.

Publication Date (Web): June 18, 2015 | doi: 10.1021/bk-2015-1192.ch027

that it is possible to recycle the catalyst at least 5 times with no loss of activity. This conversion at atmospheric hydrogen pressure using a Pd-Au/C bimetallic catalyst has also been demonstrated (*26*). The reaction was carried out at 60°C in THF with an HMF concentration of about 1.4 wt%, an HMF to catalyst ratio equal to 2 by weight, with a 6 hour reaction time. Conversions of HMF of greater than 99% were achieved with yields of over 95% DMF.

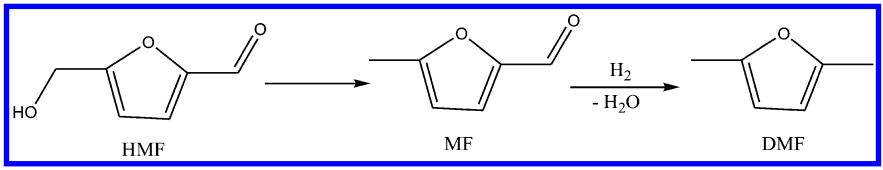

Scheme 4. The Conversion of HMF to DMF

The effect of promoters on the selectivity of palladium on carbon catalysts for the conversion of HMF to products was evaluated (*27*). These promoters could alter the chemical pathway in order to obtain decarbonylated products, hydrogenolyzed products (DMF) or completely hydrogentated products (2,5-dimethyltetrahydrofuran). It was found that formic acid could play multiple roles in this reaction. It could act as a mild hydrogen source and it suppresses decarbonylation; CO_2 and carboxylic acids suppress ring hydrogenation.

The hydrogenolysis of HMF to DMF was found to be very selective using Pd/C in supercritical CO_2-water (*28*). Very high yields were obtained at 80°C in 2 hours. It was found that the products of the reaction were strongly dependent on pressure and the concentration of water in the fluid. Furfural was also converted to 2-methylfuran very effectively using this process.

The hydrogenolysis of HMF to DMF using a platinum-cobalt nanoparticle catalyst produced 98% yields in 2 hours (*29*). The chemoselective hydrogenation of HMF to DMF and other analogues was reviewed (*30*).

Conversion of 2,5-Dimethylfuran to *p*-Xylene

The last step in the process is the conversion of DMF to pX via a Diels-Alder [4+2]-cycloaddition with ethylene (Scheme 5). Furans are known to possess significant dienic character which gives them a high reactivity toward Diels-Alder [4+2]-cycloadditions (*31*). This catalytic conversion has been actively studied with the best selectivity to pX being about 90% at high conversion (*32–34*). Reaction times were about 24 hours at 250°C and 62 bar ethylene pressure using an H-BEA zeolite as catalyst. DMF concentrations of 1.2 M and lower in heptane were used for the reactions. The products of the Diels-Alder reaction of DMF and ethylene using zeolite catalysts were characterized (*35*). The oxa-norbornene intermediate, shown in Scheme 5, was identified using GC-MS.

In Green Polymer Chemistry: Biobased Materials and Biocatalysis; Smith, et al.;
ACS Symposium Series; American Chemical Society: Washington, DC, 2015.

Publication Date (Web): June 18, 2015 | doi: 10.1021/bk-2015-1192.ch027

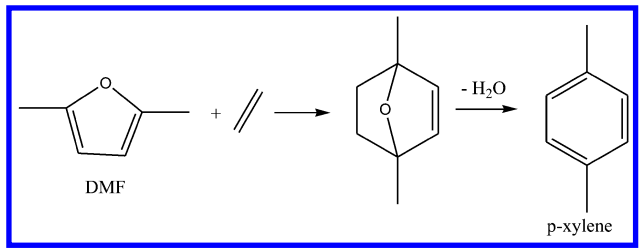

Scheme 5. The conversion of DMF to pX via a Diels-Alder [4+2]-Cycloaddition with Ethylene

Publication Date (Web): June 18, 2015 | doi: 10.1021/bk-2015-1192.ch027

High pX yields (greater than 90%) in the presence of carboxylic acid anhydrides that apparently play a dual role as catalysts and dehydrating agents have been achieved (*36*). The reaction was carried out at 84 bar pressure at 280°C for 8 hours.

The Micromidas process also produces a series of furan intermediates from the dehydration of lignocellulosic biomass using aqueous HCl. The polysaccharide feedstock is first saccharified using hydrochloric acid (HCl) and dehydrated to 5-chloromethylfurfural (CMF). CMF is hydrogenolyzed to form 2,5-dimethylfuran (DMF). This process involves the hydrodechlorination of CMF to 5-methylfurfural (MF) and the hydrogenation of the aldehyde to DMF, similar to that shown in Scheme 4. Finally, DMF is converted to pX by the Diels-Alder [4+2]-cycloaddition with ethylene, which can be done with yields in excess of 90% (*37*). Furfural is converted to toluene through a 2-methylfuran intermediate.

2,5-Hexanedione (HDO) is often observed as a by-product in the conversion of HMF to DMF and DMF to pX (*38*). It is formed from the hydrolysis of DMF under acidic conditions. It has been shown that the 2,5-hexanedione is actually in equilibrium with DMF and when the DMF is predominantly converted to pX in the Diels-Alder cycloaddition reaction with ethylene, the HDO is also converted to pX presumably through a DMF intermediate. In fact, when HDO was used as a substrate for this reaction, the yield of pX was nearly as high as that for a DMF substrate.

Techno-Economic Analysis for the Production of *p*-Xylene from HMF

There have been several recent techno-economic analyses for the bio-based processes for producing pX. Techno-economic analyses using previously reported processes (*39*, *40*) for the conversion of biomass to HMF to 2,5-dimethylfuran (DMF) and another (*32*) for the conversion of DMF to pX, have been carried out (*41*, *42*). These analyses concluded that the minimum pX selling price was $1.31/lb. The Gevo process was also evaluated and it was found to require a minimum selling price of $1.58/lb (*42*, *43*). These minimum selling prices are significantly higher than the recent selling price of petro-based pX of 55 to 70¢/lb for oil at around $100 per barrel (*7*).

A techno-economic analysis of several of the processes described in Table 1, including the Micromidas process has recently been published (*44*). This analysis showed that several of these processes are competitive with petro-pX under circumstances of reasonably priced feedstocks and in certain geographies. The Micromidas process was found to be the most competitive in the US market.

HMF as a Platform Chemical

HMF is being described as a platform chemical from which many other compounds, some of which are commodities, can be produced. Many of these compounds, most of which have significantly higher value than fuel value, are shown in Figure 2. They include 1,6-hexanediol, p-xylene, adipic acid, 2,5-dimethylfuran, caprolactone and caprolactam. Several pharmaceuticals, natural products, macrocycles and other compounds which can be derived from HMF have been described (*19*). These products have considerably higher value than fuel value.

The synthesis of ranitidine (Zantac), an anti-ulcer medication, *δ*-aminolevulinic acid, a herbicide, and Prothrin insecticides have been described (*45*). Their structures are given in Figure 3.

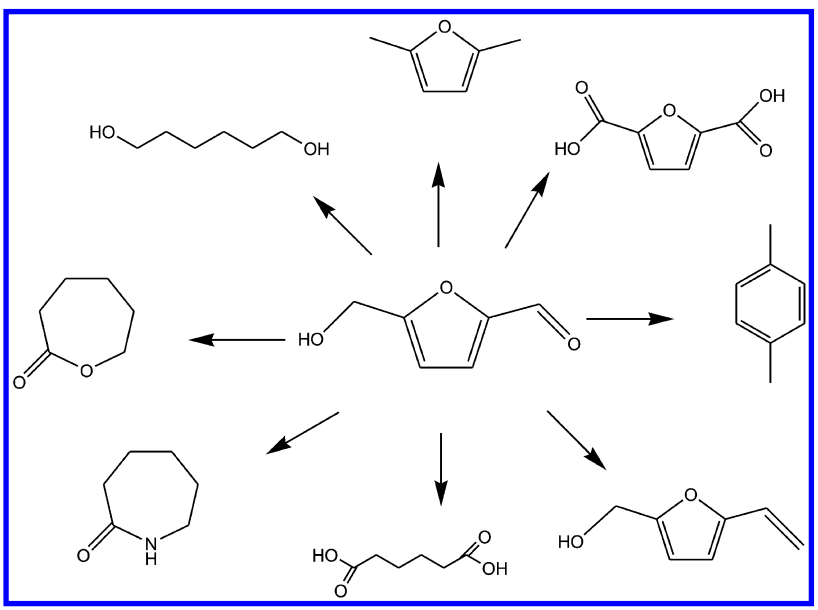

Figure 2. Chemical products that can be derived from the HMF platform.

Publication Date (Web): June 18, 2015 | doi: 10.1021/bk-2015-1192.ch027

Publication Date (Web): June 18, 2015 | doi: 10.1021/bk-2015-1192.ch027

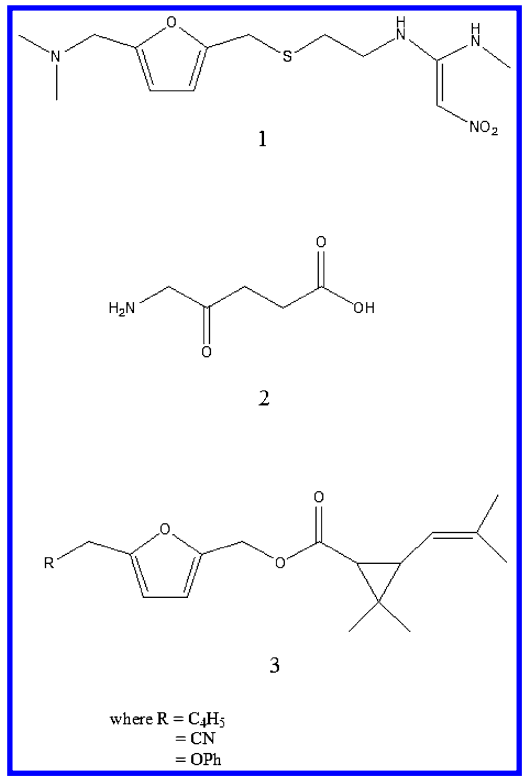

Figure 3. Chemical structures for ranitidine (1), δ-aminolevulinic acid (2) and prothrin analogues (3).

Conclusions

The demand for bio-based materials is growing both in the US and globally. There are many reasons for this growth which include a reduced carbon footprint for these materials, reduced dependence on limited fossil fuels and consumers' desire to be more environmentally responsible. However, while these trends are real, it is generally accepted that their green attributes do not afford significant pricing value to bio-based products. If they are to be competitive broadly in the market, they must compete on a cost/performance basis.

Poly(ethylene terephthalate) (PET) is the fastest growing bio-based plastic primarily as a result of significant market demand. The most visible source of market demand for bio-based PET has come from the "Plant PET Technology Collaborative" made up of Coca Cola, Ford, Heinz, Nike and Proctor&Gamble. Coke's so-called "PlantBottle" is composed of up to 30% bio-based material, the ethylene glycol component which is made from bio-based ethylene. The terephthalic acid component is petro-based. This consortium and other retailers are assisting several pre-commercial enterprises to develop a competitive commercial process for bio-based terephthalic acid. Most of these processes

target *p*-xylene (pX), the petrochemical precursor for terephthalic acid. They include several thermochemical processes yielding the benzene, toluene, xylenes (BTX) fraction, namely, those of Anellotech, Virent and Ensyn. Gevo has developed a fermentation route to isobutylene which it converts to pX. There are also chemical processes including those of Micromidas and Avantium. These processes dehydrate carbohydrate feedstocks to furan intermediates from which Micromidas produces pX and Avantium produces 2,5-furandicarboxylic acid (FDCA). FDCA is used to make poly(ethylene furanoate) which has some advantaged properties relative to those of PET. Techno-economic evaluations have shown that several of these companies have achieved economics competitive with those of petro-based pX and are in the process of building production capacity. The commercial prospects for this technology are quite promising.

Publication Date (Web): June 18, 2015 | doi: 10.1021/bk-2015-1192.ch027

References

1. The Society of the Plastics Industry Bioplastics Council home page, article online only: *Bioplastics Industry Overview Guide, Executive Summary*; http://www.plasticsindustry.org/files/about/BPC/Industry%20Overview%20Guide%20Executive%20Summary%20--%200912%20-%20Final.pdf (accessed Feb 17, 2015).
2. General webpage: Cone Communications home page, www.coneinc.com/globalCRstudy (accessed Feb 17, 2015).
3. General webpage: Plastics Today, plasticstoday.com; Caliendo, H. *Five major U.S. brands collaborating on plant-based PET*; http://www.plasticstoday.com/articles/Five-major-US-brands-collaborating-on-plant-based-PET-0605201202 (accessed Feb 17, 2015).
4. Article online only: Schut, J. H. *The Race to 100% Bio PET*; http://plasticsengineeringblog.com/2012/08/13/the-race-to-100-bio-pet/ (accessed Feb 17, 2015).
5. Vermoortele, F.; Maes, M.; Moghadam, P. Z.; Lennox, M. J.; Ragon, F.; Boulhout, M.; Biswas, S.; Laurier, K. G.; Beurroies, I.; Denoyel, R.; Roeffaers, M.; Stock, N.; Düren, T.; Serre, C.; De Vos, D. E. *J. Am. Chem. Soc*. **2011**, *13*, 18526–18529.
6. Global Business Intelligence Research webpage, article online only: *China and India to Lead Global Purified Terephthalic Acid Demand Growth by 2020*; www.gbiresearch.com/pressreleasedetails.aspx?title=Chemicals&prid=240 (accessed Feb 17, 2015).
7. General webpage: ICIS; http://www.icis.com/chemicals (accessed Feb 17, 2015).
8. Article online only: Moye, J. *15 Billion and Counting*; http://www.coca-colacompany.com/15-billion-and-counting (accessed Feb 17, 2015).
9. Article online only: www.icis.com/resources/news/2012/03/12/9539959/development-of-bio-paraxylene-and-pta-on-the-rise/ (accessed Feb 17, 2015).

10. Biomass Magazine webpage, article online only: http://biomassmagazine.com/articles/8183/european-bioplastics-releases-2016-market-forecast (accessed Feb 17, 2015)
11. European Bioplastics webpage, "*Bioplastics Facts and Figures*", article online only: http://en.european-bioplastics.org/wp-content/uploads/2013/publications/EuBP_FactsFigures_bioplastics_2013.pdf (accessed Feb 17, 2015). Biomass Magazine webpage, article online only: http://biomassmagazine.com/articles/8183/european-bioplastics-releases-2016-market-forecast (accessed Feb 17, 2015).
12. Plastics News webpage, article online only: http://www.plasticsnews.com/article/20130827/NEWS/130829938/on-the-way-to-bio-based-pet-gevo-opens-paraxylene-plant-in-texas (accessed Feb 17, 2015).
13. General webpage: Anellotech home page, http://anellotech.com/ (accessed Feb 17, 2015).
14. General webpage: Virent home page, http://www.virent.com/technology/bioforming/ (accessed Feb 17, 2015).
15. *General webpage: Ensyn home page*. http://www.ensyn.com/technology/overview/ (accessed Feb 17, 2015).
16. Gruter, G.-J. M.; Dautzenberg, F. Method for the Synthesis of 5-Alkoxymethyl Furfural Ethers and Their Use. World Patent 2007/104514, Sept 20, 2007.
17. Wyman, C. E.; Dale, B. E.; Elander, R. T.; Holtzapple, M. T.; Ladisch, M. R.; Lee, Y. Y. *Bioresource Technol.* **2005**, *96*, 1959–1966.
18. van Putten, R.-J., Dias, A. S., de Jong, E. *Catalytic Process Development for Renewable Materials*; Imhof, P., van der Waal, J. C., Eds.; Wiley-VCH Publishers: Weinheim, Germany, 2013; pp 81−111.
19. van Putten, R.-J.; van der Waal, J. C.; de Jong, E.; Rasrendra, C. B.; Heeres, H. J.; de Vries, J. G. *Chem. Rev.* **2013**, *113*, 1499–1597.
20. Saha, B.; Abu-Omar, M. M. *Green Chem.* **2014**, *16*, 24–38.
21. Nakagawa, Y.; Tamura, M.; Tomishiga, K. *ACS Catal.* **2013**, *3*, 2655–2668.
22. Wang, T.; Nolte, M. W.; Shanks, B. H. *Green Chem.* **2014**, *16*, 548–572.
23. Mascal, M.; Nikitin, E. *Angew. Chem.* **2008**, *47*, 7924–7926.
24. Mascal, M.; Nikitin, E. *ChemSusChem.* **2009**, *2*, 859–861.
25. Zu, Y.; Yang, P.; Wang, J.; Liu, X.; Ren, J.; Lu, G.; Wang, Y. *Appl. Catal., B* **2014**, *146*, 244–248.
26. Nishimura, S.; Ikeda, N.; Ebitani, K. *Catal. Today* **2014**, *232*, 89–98.
27. Mitra, J.; Zhou, X.; Rauchfuss, T. *Green Chem.* **2015**, *17*, 307–313.
28. Chatterjee, M.; Ishizaka, T.; Kawanami, H. *Green Chem.* **2014**, *16*, 1543–1551.
29. Wang, G.-H.; Hilgert, J.; Richter, F. H.; Wang, F.; Bongard, H.-J.; Spliethoff, B.; Weidenthaler, C.; Schueth, F. *Nat. Mater.* **2014**, *13*, 293–300.
30. Hu, L.; Lin, L.; Liu, S. *Ind. Eng. Chem. Res.* **2014**, *53*, 9969–9978.
31. Gandini, A.; Belgacem, M. N. *Prog. Polym. Sci.* **1997**, *22*, 1203–1379.
32. Williams, C. L.; Chang, C.-C.; Do, P.; Nikbin, N.; Caratzoulas, S.; Vlachos, D. G.; Lobo, R. F.; Fan, W.; Dauenhauer, P. J. *ACS Catal.* **2012**, *2*, 935–939.

33. Nikbin, N.; Do, P. T.; Caratzoulas, S.; Lobo, R. F.; Dauenhauer, P. J.; Vlachos, D. G. *J. Catal.* **2013**, *297*, 35–43.
34. Chang, C.-C.; Green, S. K.; Williams, C. L.; Dauenhauer, P. J.; Fan, W. *Green Chem.* **2014**, *16*, 585–588.
35. Do, P. T. M.; McAtee, J. R.; Watson, D. A.; Lobo, R. F. *ACS Catal.* **2013**, *3*, 41–46.
36. Wang, B.; Gruter, G. J.; Dam, M. A.; Kreigle, R. M.; Zeestraten, A. W. J. Process for the Preparation of Benzene Derivatives from Furan Derivatives. World Patent 2014/065657 A1, May 1, 2014.
37. Masuno, M. N.; Cannon, D.; Bissell, J.; Smith, R. L.; Foster, M.; Wood, A. B.; Smith, P. B.; Hucul, D. A. Methods of Producing Para-Xylene and Terephthalic Acid. World Patent 2013/040514 A1, March 21, 2013.
38. Masuno, M. N.; Bissell, J.; Smith, R. L.; Foster, M.; Smith, P. B.; Hucul, D. A.; Stark, E. J.; Henton, D. R.; Dumitrascu, A. Methods of Producing Para-Xylene and Terephthalic Acid. World Patent 2014/043468A1, March 20, 2014.
39. Roman-Leshkov, Y.; Barrett, C. J.; Liu, Z. Y.; Dumesic, J. A. *Nature* **2007**, *447*, 982–985.
40. Nikolla, E.; Román-Leshkov, Y.; Moliner, M.; Davis, M. E. *ACS Catal.* **2011**, *1*, 408–410.
41. Lin, Z.; Nikolas, V.; Ierapetritou, M. *Ind. Eng. Chem. Res.* **2014**, *53*, 10688–10699.
42. Swanson, R. M.; Satrio, J. A.,; Brown, R. C.; Platon, A.; Hsu, D. D. NREL Technical Report NREL/TP-6A20-46587, 2010.
43. Klein-Marcuschamer, D.; Blanch, H. W. *AIChE J.* **2013**, *59*, 4454–4460.
44. Dhanik, N.; Critelli, C. Biorenewable Insights, Bio-based BTX and PX, Technical Report A01392.0014.4003, Nexant: White Plains, New York, 2014.
45. Chang, F.; Dutta, S.; Becnel, J. J.; Estep, A. S.; Mascal, M. *J. Agric. Food Chem.* **2014**, *62*, 476–480.

Publication Date (Web): June 18, 2015 | doi: 10.1021/bk-2015-1192.ch027

Publication Date (Web): June 18, 2015 | doi: 10.1021/bk-2015-1192.ch028

Chapter 28

Green Polymer Aerogels

David A. Schiraldi*

Department of Macromolecular Science and Engineering, Case Western Reserve University, 2100 Adelbert Road, Cleveland, OH 44106, U.S.A.
***E-mail: das44@case.edu.**

A wide range of sustainable, bio-based polymers can be converted into low density aerogels, in essentially quantitative yields. The freeze drying process employed is somewhat energy intensive, but generates no appreciable chemical waste. These aerogels exhibit useful mechanical properties which span six orders of magnitude, and perhaps most importantly low flammability. The future of these materials could indeed bright, as they are considered for commercialization.

Aerogels are a fascinating class of emerging materials noted for their ultra-low densities and in many cases exceptionally low thermal conductivities. First described by Kistler (*1*, *2*), an aerogel is defined as a former gel whose liquid has been replaced with air (hence "aero gel"). The term aerogel is most often associated with silica-based materials, which dominated the field from Kistler to the work of NASA, Hoechst AG, and others to about the year 2000. The image of a diaphanous silica aerogel seemingly hovering in air has been shown extensively, and illustrates how little solid matter can be packed into a unit of volume, often producing materials with bulk densities as low as 0.003 g/cm^3. As striking as such materials might be, they completely lack mechanical integrity, crumbling into dust when touched (*3*, *4*). The other major limitation of such materials is the environmental impact of their production. The standard method for producing silica (or other metal oxide) aerogels starts with an acid or alkaline hydrolysis of the associated orthoester. The hydrolysis of tetraethyl orthosilicate or tetramethyl orthosilicate then produces four moles of ethanol or methanol per mole of silicon atoms incorporated into the final aerogel structure. That these alcohol molecules

In Green Polymer Chemistry: Biobased Materials and Biocatalysis; Smith, et al.;
ACS Symposium Series; American Chemical Society: Washington, DC, 2015.

Publication Date (Web): June 18, 2015 | doi: 10.1021/bk-2015-1192.ch028

are produced in dilute, alkaline aqueous solution represents a significant economic and environmental problem, which is compounded by the next step, a slow solvent exchange with ethanol or acetone to remove water from the structure. This process has to be carried out in a slow, controlled manner in order to prevent collapse of the gel structure (*5*, *6*). The organic solvent-based gel then is most typically dried using supercritical carbon dioxide extraction, a chemically-benign, but energy intensive process. All in all, from orthoester to aerogel, significant handling of organic solvents, production of low concentration organic solvent-contaminated water, and a high use of energy are required in order to produce a very low mass of product. The mechanical properties of the silica aerogels have been shown to be dramatically improved by the addition of isocyanates or epoxides, enabling the launch of commercial aerogel products, but then the environmental footprint of these still low density products (these chemically-modified aerogels typically exhibit densities in the 0.2 – 0.4 g/cm^3 range) are even greater than that of the pure silica materials (*7–9*).

Organic aerogels have been produced from thermoset polymers, such as the phenolic resins, producing robust, high temperature materials that can in turn be carbonized (*10–12*). These aerogels do not produce the large volumes of sol-gel waste associated with silica aerogels, but they still require the handling of a large amount of volatile organic solvents per unit weight of final product, and still use large amounts of energy in supercritical extraction. Carbonization of these thermoset aerogels can produce interesting substrates for energy storage systems, for example. Polyimides have more recently become the focus of significant efforts, especially those of workers at NASA, who polymerize aromatic monomers then supercritically dry the *in situ* produced polymer to produce light weight, high temperature and strength aerogels. Again, these organic aerogels do require the handling of organic solvents contaminated by reaction residues, and supercritical drying processing, but overall represents a large step forward environmentally (*13–16*).

Freeze drying of aqueous polymer or polymer/clay gels has been extensively evaluated over the past decade, especially by our group at Case Western Reserve University (*17–19*). The process, which will be described in greater depth below, takes advantage of ~100% conversion of solids into aerogel product, and the use of water as a more benign processing fluid. The use of freeze drying does, however, represent significant energy use per weight of finished goods, similar to that of supercritical drying. We propose a hierarchy of "greenness" for the various families of aerogels as is illustrated in Figure 1.

The freeze drying process for producing aerogels has in common with the supercritical process the conversion of a gel into a dried material. The supercritical process under ideal conditions carefully retains the gel structure, whereas the freeze drying process modifies the aqueous gel structure by superimposing the structure of ice upon the finished product. The gel structure is forced into the grain boundaries of ice crystals as the water freezes, producing materials whose solid state structure resemble a house of cards, with solid struts composed of polymer or polymer/filler composites which retain only some of their hydrogel structure. The use of smectite clays, such as bentonite or montmorillonite, in most cases significantly improves the freeze dried aerogel structural regularity

In Green Polymer Chemistry: Biobased Materials and Biocatalysis; Smith, et al.;
ACS Symposium Series; American Chemical Society: Washington, DC, 2015.

and mechanical properties, as these clays gel at levels as low as 2 wt% in water, enabling the formation of stable gel phases (*17*). The basic process steps for freeze drying of gels into aerogels is given in Figure 2. Water and clay (normally present in these products) are blended at high shear rates to produce an aqueous gel. In the laboratory, this is accomplished using a blender, whereas in a commercial operation, this likely would make use of a mixer similar to those used in the production of bread dough and other food products (one example of such a machine is the family of Hobart® mixers used throughout the food industry). The polymer component of the aerogel is generally mixed at low shear rates, to minimize air bubble entrainment into the mixture; this is carried out using a kitchen mixer in the laboratory, and likely would use a paint production mixer commercially. After combining all of the components under low shear conditions, the gel is poured into a mold, whose dimensions will determine the shape and size of the finished aerogel, the material is frozen then ice removed by sublimation in the freeze drier. Scale up of this step should be straight forward, as flash freezing of materials was optimized by the frozen food industry during the past century, and large scale freeze drying is used for the production of pharmaceuticals, instant coffee, and other dried food products. ***The entire process, therefore, can be scaled up using commercially available processing equipment, converting ~100% of raw materials into product, with water vapor as its only effluent – truly this is in line with the goal of green product and process development.***

Publication Date (Web): June 18, 2015 | doi: 10.1021/bk-2015-1192.ch028

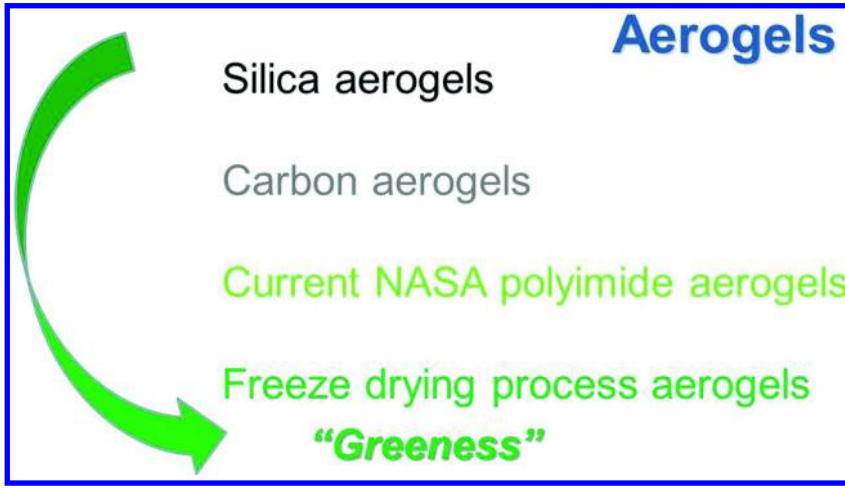

Figure 1. Hierarchy of "greeness" of aerogel products.

In Green Polymer Chemistry: Biobased Materials and Biocatalysis; Smith, et al.;
ACS Symposium Series; American Chemical Society: Washington, DC, 2015.

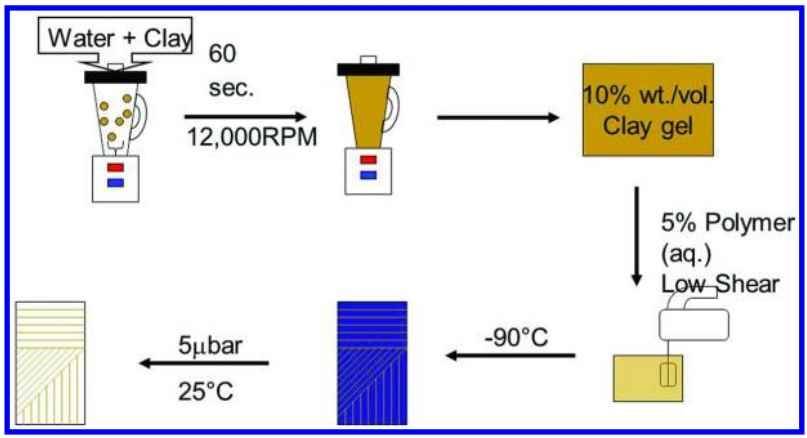

Figure 2. Freeze drying process for aerogel production.

Publication Date (Web): June 18, 2015 | doi: 10.1021/bk-2015-1192.ch028

Another useful attribute of the freeze drying process is flexibility in mold design. While commercial injection molds used in the plastics industry can cost tens or hundreds of thousands of dollars each, the molds used in the freeze drying process for aerogels are essentially ice cube trays. Figure 3 illustrates such a mold, wherein a penguin-shaped ice cube tray was used to produce an ice cube (left) and an aerogel (right). Hence a mold purchased for less than $10 produced finished goods with high fidelity and detail, at virtually no added cost. The whimsical penguin aerogel is not of significant marketplace value, but shows how easily aerogels of complex and custom shapes can be produced. In addition to custom shapes needed for components in manufactured goods, one can imagine very soon in the future, the combination of emerging technologies producing exceedingly import products. An example that our group is currently working on is the production of bone replacement scaffolds using aerogels produced from collagen. In as of yet unpublished work, we have shown that collagen hydrogels can be mineralized using electrophoresis to produce hydroxyapatite composite materials that can be freeze dried to produce aerogels. One can imagine that in the wake of disease or accident, a medical imaging procedure would produce a CAD-CAM drawing of missing bone tissue. This image would then drive a 3D printer to produce a plastic replica of the missing bone; embedding the replica bond into a silicone molding compounding would produce a negative “ice cube tray” of the desired bone geometry, which upon mineralization and freeze drying would result in a near perfect fit, collagen/hydroxyapatite part that could be implanted for bone repair.

In Green Polymer Chemistry: Biobased Materials and Biocatalysis; Smith, et al.;
ACS Symposium Series; American Chemical Society: Washington, DC, 2015.

Publication Date (Web): June 18, 2015 | doi: 10.1021/bk-2015-1192.ch028

Figure 3. Penguin-shaped ice cube (left) and aerogel (right).

Over 50 different polymer and polymer/clay materials have been freeze dried into aerogels in our laboratory over the past decade; increasing activity in this area is now being seen by a number of groups throughout the world. Of interest to the present work is the use of bio-based polymers, thereby increasing the sustainability of the finished group, compared to petrochemical polymers, such as poly(vinyl alcohol). The processing requirements are the same for biological or petrochemical polymers: the system to be converted into an aerogel needs to remain homogeneous throughout the rapid freezing process, so that homogeneous products can be produced. This process has proven to be successful for polymer solutions, suspension, emulsions and latexes, in materials ranging from ultrahigh molecular weight polyethylene to natural rubber. Biopolymers successfully converted into aerogels include proteins (including casein (*20–22*) and whey protein isolate (*23*)), carbohydrates (including pectin, alginate, and xanthan gum (*24*)), natural rubber (*25*, *26*), and tree-based structural polymers (cellulose (*27–29*) and lignin (*30*)).

Casein has proven to be a very useful biopolymer for aerogel production. Used as a purified polymer starting material, casein produces an aerogel which closely matches the properties of poly(vinyl alcohol) aerogels. As such the casein aerogels will slowly redissolve in water, limiting their utility. Enzymatic or chemical crosslinking significantly reduces this moisture susceptibility (*19*), yet the aerogel remains highly biodegradable even when buried in a landfill, losing approximately 30% of its organic content per month (*20*). Since casein is the

In Green Polymer Chemistry: Biobased Materials and Biocatalysis; Smith, et al.;
ACS Symposium Series; American Chemical Society: Washington, DC, 2015.

predominant milk protein, we examined the use of milk directly, eliminating the separation and purification steps – we found that milk, before or after its "sell by" date can be used directly as a 10% protein solution, producing aerogels equivalent to those produced from chemically purified casein, Figure 4. Casein aerogels lose approximately 8% of their mass around 100° C, corresponding to the absorbed water typically associated with biopolymers, but do not further degrade until an onset at 215° C, making them suitable for a number of consumer applications, Figure 5. Density scales linearly with concentration of solids in the aqueous mixture to be frozen, but mechanical properties increase geometrically (*20*). For a 2.5% clay content series of solutions, compressive moduli for increasing casein levels are 0.5, 3.0, 12, and 35MPa for 5, 10, 15, and 20% casein solutions, these values double with crosslinking (*21*); casein aerogel compressive stress/strain curves, typical of polymer foams, are given in Figure 6. Specific moduli in the range of 5-100 MPa-cm^3/g are thereby obtained, and are equivalent to many of the petrochemical polymers that have been similarly processed.

Publication Date (Web): June 18, 2015 | doi: 10.1021/bk-2015-1192.ch028

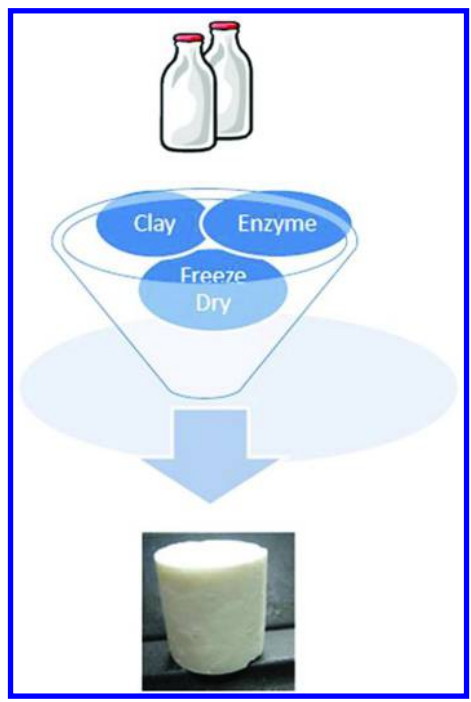

Figure 4. Conversion of milk into aerogels.

In Green Polymer Chemistry: Biobased Materials and Biocatalysis; Smith, et al.;
ACS Symposium Series; American Chemical Society: Washington, DC, 2015.

Publication Date (Web): June 18, 2015 | doi: 10.1021/bk-2015-1192.ch028

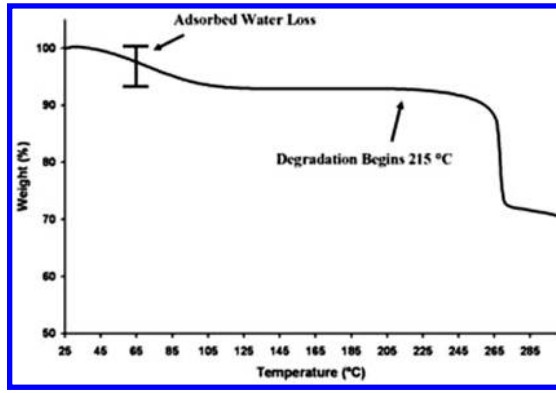

Figure 5. Thermogram of a casein aerogel.

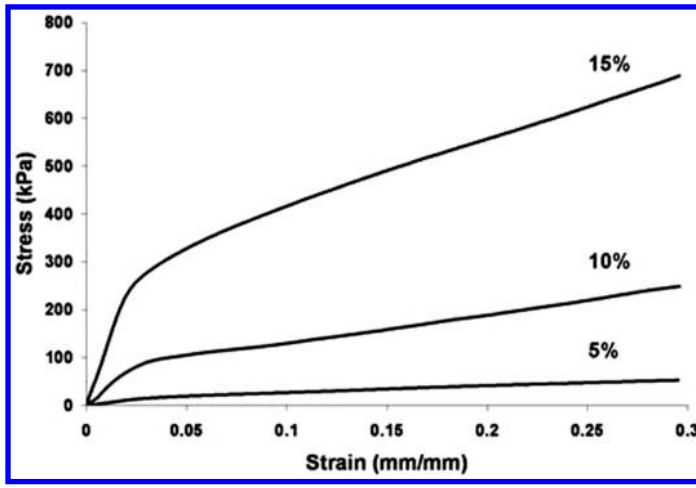

Figure 6. Typical compressive stress-strain curves for casein aerogels (% casein in starting solution indicated on curves).

Carbohydrate pectin and alginate polymer aerogels are capable of having their physical and mechanical properties tuned by replacing some of their monovalent sodium or ammonium ions with Ca^{2+} ions, bringing about ionic crosslinks with the structures. A digital photograph of pectin aerogel monoliths is given in Figure 7, and scanning electron micrograph of these materials, produced under a range of concentrations and added metal ions, is given in Figure 8. Aerogels produced from 5% pectin solutions can exhibit compressive moduli in the range of 70 KPa, but can be tuned to as high as 2 MPa by the simple addition of Ca^{2+} ions. Utilizing 10% or 15% pectin solutions results in 10x and 100x amplification of the compressive moduli compared to those obtained with 5% solutions (*31*). A range of five orders of magnitude in compressive moduli can therefore be, by simple manipulation of starting solution concentrations, and the resultant products biodegrade in landfills

even faster than does wheat starch (*31*). Alginate is similarly tunable by Ca^{2+} or Al^{3+} ion exchange; these aerogels exhibit higher modui than are observed with pectin, as well as the lowest flammability (fully self-extinguishing) of any aerogel tested by us (*24*, *30*, *32*). An example of an aerogel after being subjected to a propane torch for 2 minutes is given in Figure 9.

Figure 7. Pectin aerogel monoliths.

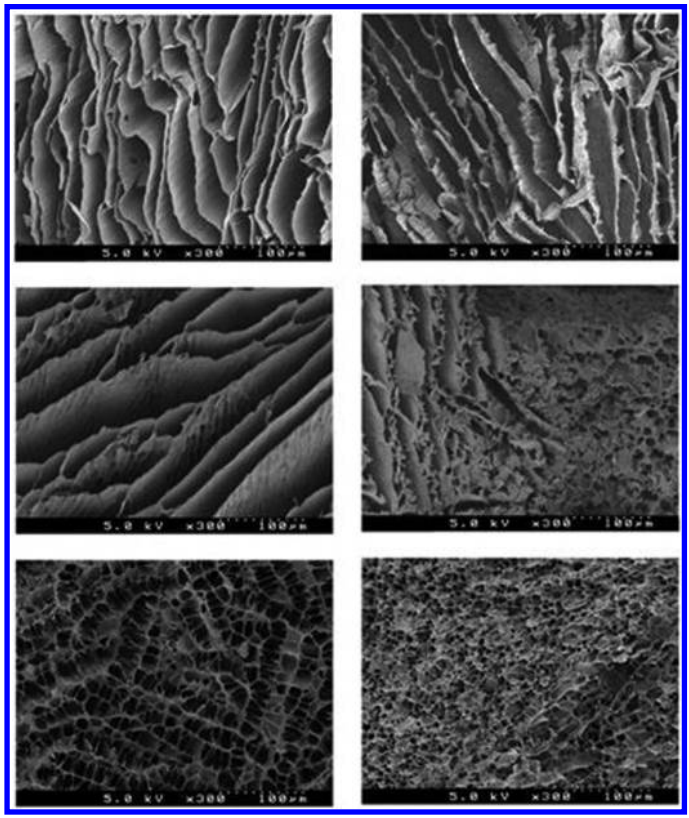

Figure 8. Pectin aerogel SEM images produced under a variety of concentrations.

In Green Polymer Chemistry: Biobased Materials and Biocatalysis; Smith, et al.;
ACS Symposium Series; American Chemical Society: Washington, DC, 2015.

Publication Date (Web): June 18, 2015 | doi: 10.1021/bk-2015-1192.ch028

Publication Date (Web): June 18, 2015 | doi: 10.1021/bk-2015-1192.ch028

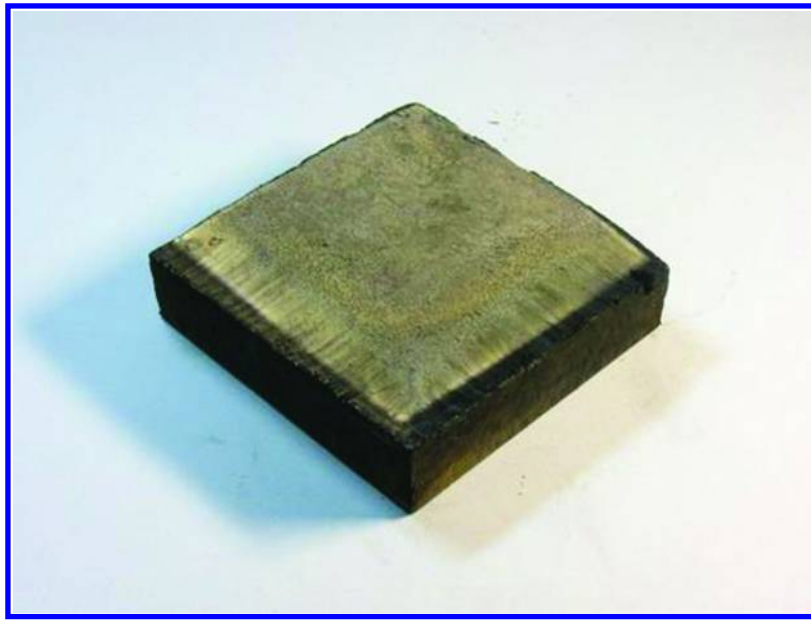

Figure 9. Alginate aerogel after treatment with a propane torch.

Cellulosic polymers have been evaluated as aerogel feedstock by ourselves and other groups (*33*, *34*). Processing of cellulose poses a particular difficulty in that this polymer is insoluble in most solvents, and is dispersed only with some difficulty. A common approach of authors producing cellulose gels for supercritical drying makes use of ionic liquids, which can solubilize the polymer, but unfortunately introduce other components which then have to be separated from the product, once again adding cost and environmental problems. *Berglund* simplified this process by producing aqueous dispersion of cellulose, which could be solvent exchanged with *tert*-butanol, then supercritically dried (*35*). Compressive moduli of 35-2800 KPa were obtained in this manner for flexible aerogels of 0.015-0.105 g/cm^3 (specific moduli of 2-27 MPa-cm^3/g). Using the freeze drying approach to aerogel production, we found that by chemically modifying cellulose, we could indeed produce low density structures sufficiently strong to be handled, but possessing otherwise unremarkable properties. In some current work, we are finding that wood-based lignin also can be converted into aerogels, that these products possess mechanical properties somewhat superior to those of their cellulose analogs, but these too are not especially useful. Related to lignin, we became interested in tannins as feedstocks for aerogels. The tannin-based aerogels are dramatically-improved by the addition of alginate as a co-matrix polymer, and these low density materials show very low flammabilities. Perhaps more importantly, we discovered that tannins can

be used as a coating material for other aerogels, improving both mechanical and flammability properties. The most striking example of this effect is when epoxy aerogels are dip coated with tannins, increasing their compressive moduli 40x, and drastically reducing their flammability, as measured by cone calorimetry (a patent application was recently filed on this).

Finally, natural rubber as also been shown to produce aerogels which exhibit the classic house of cards structure, Figure 10. In our hands, these rubber aerogels, produced directly from the latex as received from their producers, are very gummy and do not recover elastically. As is the case with rubber used in automobile tires, rubber aerogels require vulcanization. Our first effort in this area used a highly toxic vulcanizing agent, sulfur monochloride, which proved the point without being highly attractive as a commercial approach (*25*). We currently are exploring the use of vulcanizing agents which are considerably less toxic.

Publication Date (Web): June 18, 2015 | doi: 10.1021/bk-2015-1192.ch028

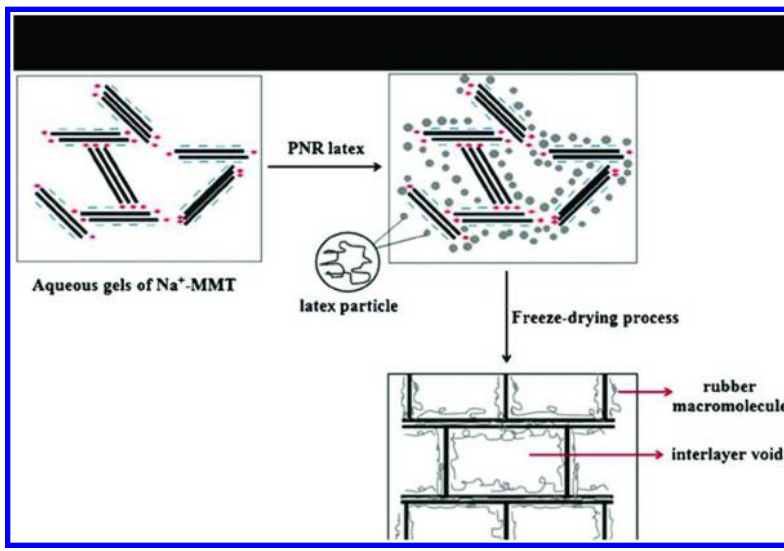

Figure 10. Natural rubber aerogels.

In summary, a wide range of sustainable, bio-based polymers can be converted into low density aerogels, in essentially quantitative yields, into low density aerogel materials. The freeze drying process employed is somewhat energy intensive, but generates no appreciable chemical waste. These aerogels exhibit useful mechanical properties which span six orders of magnitude, and perhaps most importantly low flammability. The future of these materials could indeed be bright, as they are considered for commercialization.

Publication Date (Web): June 18, 2015 | doi: 10.1021/bk-2015-1192.ch028

References

1. Kistler, S. S. *Nature* **1931**, *127*, 741.
2. Kistler, S. S. *J. Phys. Chem.* **1932**, *36*, 52–64.
3. Pajonk, G. M. *J. Non-Cryst. Solids* **1998**, *225*, 307–314.
4. Wagh, P. B.; Pajonk, G. M.; Haranath, D.; Venkateswara Rao, A. *Mater. Chem. Phys.* **1997**, *50*, 76–81.
5. Smith, D. S.; Stein, D.; Anderson, J. M.; Ackermann, W. *J. Non-Cryst. Solids* **1995**, *186*, 104–112.
6. Kanamori, K. *Adv. Porous Mater.* **2013**, *1*, 147–163.
7. Meador, M. A. B.; Fabrizio, E. F.; Ilhan, F.; Dass, A.; Zhang, G.; Vassilaras, P.; Johnston, J. C.; Leventis, N. *Chem. Mater.* **2005**, *17*, 1085–1098.
8. Meador, M. A.; Scherzer, C. M.; Vivod, S. L.; Quade, D.; Nguyen, B. N. *ACS Appl. Mater. Interfaces* **2010**, *2*, 2162–2168.
9. Capadona, L. A.; Meador, M. A. B.; Alunni, A.; Fabrizio, E. F.; Vassilaras, P.; Leventis, N. *Polymer* **2006**, *47*, 5754–5761.
10. Yang, J.; Li, S.; Yan, L.; Liu, J.; Wang, F. *Microporous Mesoporous Mater.* **2010**, *133*, 134–140.
11. Peikolainen, A.-L.; Volobujeva, O.; Aav, R.; Uibu, M.; Koel, M. *J. Porous Mater.* **2012**, *19*, 189–194.
12. Mahadik-Khanolkar, S.; Donthula, S.; Sotiriou-Leventis, C.; Leventis, N. *Chem. Mater.* **2014**, *26*, 1303–1317.
13. Guo, H.; Meador, M. A. B.; McCorkle, L.; Quade, D. J.; Guo, J.; Hamilton, B.; Cakmak, M. *ACS Appl. Mater. Interfaces* **2012**, *4*, 5422–5429.
14. Randall, J. P.; Meador, M. A. B.; Jana, S. C. *ACS Appl. Mater. Interfaces* **2011**, *3*, 613–626.
15. Meador, M. A. B.; Malow, E. J.; Silva, R.; Wright, S.; Vivod, S. L.; Guo, H. *ACS Appl. Mater. Interfaces* **2012**, *4*, 536–544.
16. Chidambareswarapattar, C.; Larimore, Z.; Sotiriou-Leventis, C.; Mang, J. T.; Leventis, N. *Mater. Chem.* **2010**, *20*, 9666–9678.
17. Somlai, L. S.; Bandi, S. A.; Schiraldi, D. A.; Mathias, L. J. *AICHE J.* **2006**, *52*, 1162–1168.
18. Bandi, S.; Schiraldi, D. A. *Macromolecules* **2006**, *39*, 6537–6545.
19. Wang, Y.; Gawryla, M. D.; Schiraldi, D. A. *J. Appl. Polym. Sci.* **2013**, *129*, 1637–1641.
20. Pojanavaraphan, T.; Magaraphan, R.; Chiou, B. S.; Schiraldi, D. A. *Biomacromolecules* **2010**, *11*, 2640–2646.
21. Gawryla, M. D.; Nezamzadeh, M.; Schiraldi, D. A. *Green Chem.* **2008**, *10*, 1078–1081.
22. Wang, Y.; Schiraldi, D. A. *Green Mater.* **2013**, *1*, 11–15.
23. Chen, H.-B.; Wang, Y.; Schiraldi, D. A. *Eur. Polym. J.* **2013**, *49*, 3387–3391.
24. Wang, L.; Schiraldi, D. A.; Sánchez-Soto, M. *Ind. Eng. Chem. Res.* **2014**, *53*, 7680–7687.
25. Pojanavaraphan, T.; Liu, L.; Ceylan, D.; Okay, O.; Magaraphan, R.; Schiraldi, D. A. *Macromolecules* **2011**, *44*, 923–931.

26. Pojanavaraphan, T.; Schiraldi, D. A.; Magaraphan, R. *Appl. Clay Sci.* **2010**, *50*, 271–279.
27. Hoepfner, S.; Ratke, L.; Milow, B. *Cellulose* **2008**, *15*, 121–129.
28. Liang, C.; Sha, G.; Guo, S. *J. Non-Cryst. Solids* **2000**, *271*, 167–170.
29. Surapolchai, W.; Schiraldi, D. A. *Polym. Bull* **2010**, *65*, 951–960.
30. Viggiano, R. P., III; Schiraldi, D. A. *Green Mater.* **2014**, *2*, 153–158.
31. Chen, H.-B.; Chiou, B.-S.; Wang, Y.-Z.; Schiraldi, D. A. *ACS Appl. Mater. Interfaces* **2013**, *5*, 1715–1721.
32. Chen, H.-B.; Wang, Y-Z.; Sánchez-Soto, M.; Schiraldi, D. A. *Polymer* **2012**, *53*, 5825–5831.
33. Hoepfner, S.; Ratke, L.; Milow, B. *Cellulose* **2008**, *15*, 121–129.
34. Surapolchai, W.; Schiraldi, D. A. *Polym. Bull* **2010**, *65*, 951–960.
35. Sehaqui, H.; Zhou, Q.; Berglund, L. A. *Compos. Sci. Technol.* **2011**, 1593–1599.

Publication Date (Web): June 18, 2015 | doi: 10.1021/bk-2015-1192.ch028

Subject Index

In Green Polymer Chemistry: Biobased Materials and Biocatalysis; Smith, et al.;
ACS Symposium Series; American Chemical Society: Washington, DC, 2015.

Publication Date (Web): June 18, 2015 | doi: 10.1021/bk-2015-1192.ix002

C

D

E

Publication Date (Web): June 18, 2015 | doi: 10.1021/bk-2015-1192.ix002

In Green Polymer Chemistry: Biobased Materials and Biocatalysis; Smith, et al.;
ACS Symposium Series; American Chemical Society: Washington, DC, 2015.

F

G

I

In Green Polymer Chemistry: Biobased Materials and Biocatalysis; Smith, et al.;
ACS Symposium Series; American Chemical Society: Washington, DC, 2015.

L

M

Publication Date (Web): June 18, 2015 | doi: 10.1021/bk-2015-1192.ix002

In Green Polymer Chemistry: Biobased Materials and Biocatalysis; Smith, et al.;
ACS Symposium Series; American Chemical Society: Washington, DC, 2015.

N

O

P

In Green Polymer Chemistry: Biobased Materials and Biocatalysis; Smith, et al.;
ACS Symposium Series; American Chemical Society: Washington, DC, 2015.

R

Publication Date (Web): June 18, 2015 | doi: 10.1021/bk-2015-1192.ix002

In Green Polymer Chemistry: Biobased Materials and Biocatalysis; Smith, et al.;
ACS Symposium Series; American Chemical Society: Washington, DC, 2015.

S

T

In Green Polymer Chemistry: Biobased Materials and Biocatalysis; Smith, et al.;
ACS Symposium Series; American Chemical Society: Washington, DC, 2015.

V

W

Publication Date (Web): June 18, 2015 | doi: 10.1021/bk-2015-1192.ix002